The Dissertation Committee for Nabijan Nizamidin Certifies that this is the approved version of the following dissertation:

Optimized Heavy Oil-in-Water Emulsions for Flow in Pipelines

Committee:

Gary A. Pope, Supervisor

Upali P. Weerasooriya

Kishore Mohanty

Matthew Balhoff

Roger Bonnecaze

Optimized Heavy Oil-in-Water Emulsions for Flow in Pipelines

by

Nabijan Nizamidin, BE; MSE

Dissertation

Presented to the Faculty of the Graduate School of

The University of Texas at Austin

in Partial Fulfillment

of the Requirements

for the Degree of

Doctor of Philosophy

The University of Texas at Austin

May 2016

Dedication

To my father, mother, sister, and grandparents

for their hard work, perseverance, and unwavering support.

Acknowledgements

I would like to, first and foremost, extend my sincerest gratitude to my supervisor, Dr. Gary A. Pope for his guidance and encouragement on my journey here at The University of Texas at Austin. I would also like to extend my gratitude to my dissertation committee members Dr. Upali Weerasooriya, Dr. Kishore Mohanty, Dr. Matthew Balhoff, and Dr. Roger Bonnecaze for their helpful comments and suggestions.

I want to acknowledge my colleagues and research group members in the Petroleum and Geosystems Engineering Department. Thanks to my fellow graduate students Donghee Song, Stefan Szlendak, Jun Lu, Robert Fortenberry, Vincent Lee, Mike Unomah, Leonard Chang, Heesong Koh, Sean Li, Moslem Taghavifar, Himanshu Sharma, Joseph Tansey, Roman Shor, and Kyle Smith for their help, both professionally and personally. I would not have enjoyed such a memorable, productive, and educational time at UT without them. Thanks to Dr. Pope's current and former research staff members Do Hoon Kim, Chris Britton, Stephanie Adkins, Sung Hyun Jang, Nadeeka Upamali, Jith Liyanage, Erin Shook, Gayani Pinnawala. Gayani Kennedy, Erandimala Kulawardana, Dharmika Lansakara-P, Pradeep Wickremasiri, Austin Lim, Patrick Lim, and Arnob Bhyuan for all their help. I would like to acknowledge the contribution of undergraduate research assistants Richard Hernandez, Pearson Suniga, Gibson Strickland, Reda Ayoubi, Sean Li, George Song, and Lauren Churchwell to my research.

Special thanks to the Morphodynamics Laboratory in the Jackson School of Geosciences at The University of Texas at Austin for the use of the Malvern Mastersizer 3000. I would like to thank Dr. Raissa Ferron from the Civil, Architectural, and Environmental Engineering Department at The University of Texas at Austin for allowing me the use of the Malvern Mastersizer 2000 in her laboratory.

I was very fortunate to have had three internships with Chevron during my graduate school education at The University of Texas at Austin. Thanks to my Chevron supervisors Greg Winslow, Rusty Mathis, Dwarakanath Varadarajan, Taimur Malik, Sophany Thach, and Art Inouye, and Chevron co-workers Vincent Lee, Matt Dean, Dustin Walker, Will Slaughter, Behdad Aminzadeh, Dinara Dussenova for an incredible learning experience. I look forward to working with you guys for many years to come.

I would like to express my gratitude to Esther Barrientes, Joanna Castillo, Frankie Hart, Glen Baum, and Gary Miscoe for their administrative and personal support from the first day of my graduate studies to the very end.

Last but not least, I would like to thank Enakshi Wikramanayake for making my stay in Austin memorable.

This research was partially supported by the National Science Foundation Graduate Research Fellowships Program (Grant #: 2011128365). Any opinions, findings, and conclusions or recommendations expressed in this material are those of the author and do not necessarily reflect the views of the National Science Foundation. The work was also supported by the industrial sponsors of The University of Texas at Austin Chemical Enhanced Oil Recovery Industrial Affiliates Project, who lent important financial support for this research.

Optimized Heavy Oil-in-Water Emulsions for Flow in Pipelines

Nabijan Nizamidin, Ph.D.

The University of Texas at Austin, 2016

Supervisor: Gary A. Pope

Oilfield operations such as drilling, reservoir management, and production require the injection and/or production of complex fluids to improve the extraction of crude oils. Some of these complex fluids such as drilling muds, fracking fluids, foams, emulsions, surfactants, and polymers, fall under the classification of colloidal suspensions which is one substance of microscopically dispersed insoluble particles suspended throughout another substance. These colloidal suspensions show complex rheological properties that are dependent on the suspension properties, flow conditions, and flow conduit dimensions. Rheology of colloidal suspensions is a complex subject that is still being investigated.

The focus of this study is on heavy oil-in-water emulsions. Heavy oil and bitumen resources account for approximately 70% of the remaining oil discovered to date in the world. Heavy crude oils are costly to produce, transport, and refine compared to light crude oils due to the high viscosity of heavy crude oils. To improve the economic viability of producing heavy oils, especially in a time with low crude oil prices, operational expenses must be reduced. One of the main areas to improve is the cost associated with transporting produced heavy oils from production wells to refineries. Currently, heavy oils are diluted with low viscosity diluents such as condensates and light crude oils to lower the mixture viscosity below 350 cSt before heavy oils can be

transported through pipelines. The diluted mixtures require up to 50% (vol.) diluents to lower the heavy oil viscosity. High demand and low supply of condensates and constrained pipeline capacities have resulted in pipeline transportation costs of up to $22/bbl of diluted heavy oil from Canada to refineries in the U.S. An alternative method of transporting heavy oils is to transport heavy oils in an emulsified form, heavy oil-in-water emulsions, which can show orders of magnitude lower viscosities compared to the viscosity of heavy oils.

In this study, a simple, one-step method of preparing heavy oil-in-water emulsions was developed. The physical properties of heavy oil-in-water emulsions are controlled and modified by optimizing the chemical formulation used to prepare emulsions. Stable heavy oil-in-water emulsions can be prepared with chemical formulations that are tailored to the type of heavy oils and available water sources which can range from freshwater to softened seawater.

The rheology of heavy oil-in-water emulsions has been characterized with a rotational viscometer. Heavy oil-in-water emulsions, especially concentrated emulsions, showed complex rheological properties such as shear thinning behavior, two-step yield stresses, two-step wall slips, and rheopexy. A rheological equation and a wall slip equation have been developed to model the rheology of heavy oil-in-water emulsions over a range of shear rates and flow conduit dimensions.

Heavy oil-in-water emulsions characterized with capillary tube viscometers showed drastically different viscosity measurements compared to the viscosity measurements obtained with a rotational viscometer. This is important because the flow of emulsions in pipelines are similar to the flow of emulsions in capillary tube viscometers, not rotational viscometers. The lower viscosities measured with capillary tube viscometers are attributed to oil droplet migration away from the tube walls due to

the shear heterogeneity observed in Poiseuille (tube) flow. A scaling equation was proposed to relate the viscosity measurements of emulsions with a rotation viscometer to the viscosity measurements of emulsions with capillary tube viscometers.

The rheological measurements of heavy oil-in-water emulsions are used to estimate the flow of emulsions in crude oil pipelines with various radii. Viscosity measurements of optimized heavy oil-in-water emulsions with a rotational viscometer showed that heavy oil-in-water emulsions with up to 75% dispersed heavy oil can be successfully transported in crude oil pipelines. Adding the effect of oil droplet migration measured with capillary tube viscometers, heavy oil-in-water emulsions with up to 85-90% dispersed heavy oil can be successfully transported in crude oil pipelines. The cost of chemicals used to prepare 85% heavy oil-in-water emulsion is approximately $1-3/bbl of emulsion. Heavy oil-in-water emulsions also showed drag reduction properties which can significantly increase the maximum flow capacity of crude oil pipelines

Transporting heavy oils as concentrated heavy oil-in-water emulsions appeared to be a competitive if not a better method of lowering heavy oil viscosity compared to the diluent method in terms of cost and flow performance in pipelines.

Table of Contents

List of Tables

List of Figures

Chapter 1: Introduction

1.1 MOTIVATION

Oilfield operations such as drilling, reservoir management, and production have steadily been increasing in complexity in the last 20 years to increase the recoverable reserves from new or producing oil fields. Due to the declining recoverable reserves of the so called conventional crude oil, exploration and production of unconventional oils such as shale oil and heavy oil/bitumen have been increasing in the United States and the world. Furthermore, to offset the declining production rate of conventional oil and to meet the global demand for petroleum, many national oil companies (NOCs) and international oil companies (IOCs) have been performing enhanced oil recovery (EOR) operations in their existing conventional oilfields. EOR operations improve and increase the fields' oil production rate and ultimate oil recovery of the original oil in place (OOIP) compared to the primary production operation (5-15% of OOIP) and conventional secondary (waterflood) production operation (~25-30% of the OOIP) with ultimate oil recovery of 30-45% of the OOIP [Laherrere (2001); Lake et al. (2014)]. Figure 1.1 shows the source of the worldwide crude oil production (data + projection) from 1990-2030. The general trend is decreasing production from conventional producing fields and increasing production from EOR and unconventional reservoirs in the future.

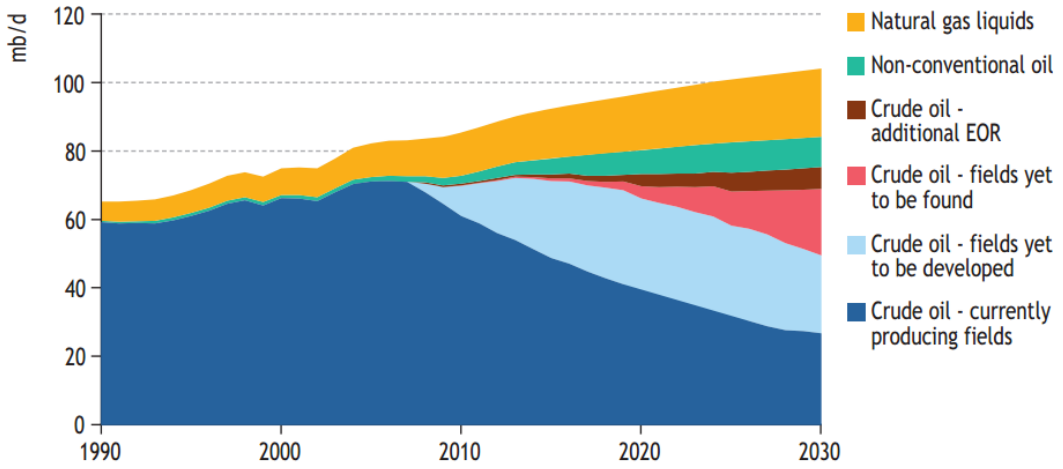

Fig. 1.1: World oil production by source from World Energy Outlook 2008

One common theme for all of the unconventional and EOR operations is the necessity for technological advances which allow for economically viable extraction of the remaining oil in the fields which otherwise would not have been produced based on the crude oil price at the time. In almost all the cases, these operations require the injection of specialized complex fluids and/or production of specialized complex fluids as the result of the operations. The proper design and optimization of these fluids are critical to the success of all the operations. Some of these complex fluids are listed:

- Drilling: Drilling muds, fracking fluids
- Reservoir/EOR: Surfactants, polymers, foams, nanoparticles, polymer gels
- Production: Oil-in-water (O/W) emulsions, water-in-oil (W/O) emulsions, sand/fines suspensions
- Surface transportation to/from fields: Concentrated chemicals (surfactants, polymers, emulsion polymers), O/W, and W/O emulsions

All the complex fluids fall under the classification of colloidal suspensions which is defined as one substance of microscopically dispersed insoluble particles suspended

throughout another substance. The dispersed and continuous phases can be any combination of gases, liquids, and solids except for gas and gas which are miscible in all cases.

Table 1.1: Colloidal suspension classification

		Dispersed Phase		
		Gas	Liquid	Solid
Continuous Phase	Gas	N/A	Aerosol	Solid aerosol
	Liquid	Foam Ex: CO_2/N_2 in brine for EOR	Emulsion Ex: Oil-in-water, Water-in-oil	Sol Ex: drilling mud, polymer solution, sand/fine/nanoparticle in oil/water
	Solid	Solid foam	Gel	Solid Sol

Almost all oilfield colloidal suspensions have liquids as the continuous phase with gases/liquids/solids as the dispersed phase.

Some of the concentrated colloidal suspensions utilized in the oil industry are shown in Fig. 1.2.

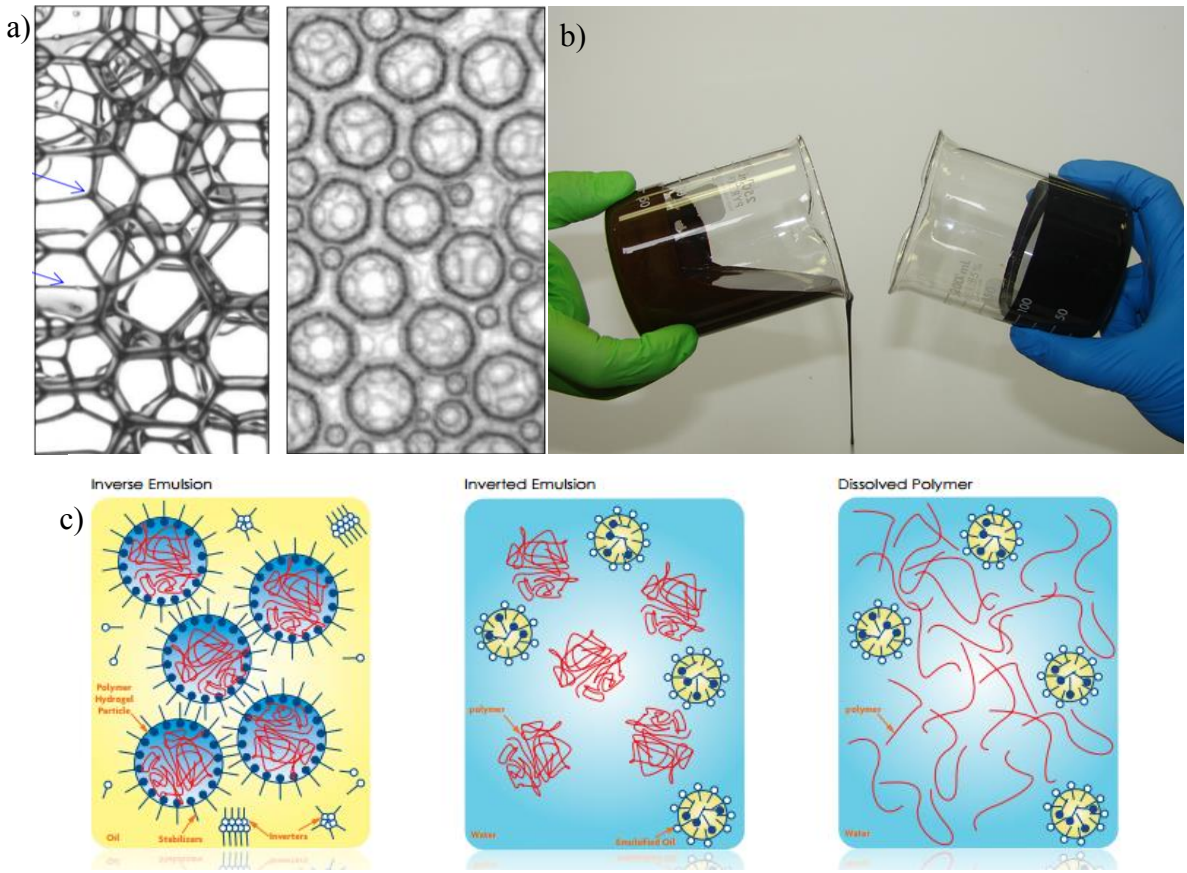

Fig. 1.2: (a) Dry (left) and wet (right) foam under microscope [Höhler and Cohen-Addad (2005)] b) Heavy oil-in-water emulsion (left) and heavy oil (right) c) Emulsion polymer illustrations of W/O to W/O inversion process [SNF Floerger (2014)]

The concentrated colloidal suspensions in Fig. 1.2 are described in detail below.

1. Foam

Foam is a colloidal suspension with gas as the dispersed phase and liquid as the continuous phase. The composition of foam in oil industry is usually gas ($\varphi > 0.7$) dispersed in continuous phase of brine. Very high gas concentration ($\varphi > 0.9$), dry foam, and moderate gas concentration ($\varphi < 0.7$), wet foam, microscope images are shown in Fig. 1.2a. The dispersed phase can be N_2, CO_2, or hydrocarbon gases. The foam stability is improved by appropriate surfactants and in recent cases, nanoparticles. Foam viscosity is very high compared to either of the pure phases, gas or water. Thus,

foam has been utilized as a secondary/tertiary EOR injection method to improve oil displacement efficiency in oil reservoirs. It is especially useful in low permeability reservoirs where polymer flooding is not possible. Foam exhibits shear thinning property and yield stress which can best be described by Herschel-Bulkley model and its viscosity increases exponentially with higher dispersed gas concentration [Bonilla and Shah (2000)]. Foam injection into porous media requires careful optimization and tuning. Lower than required foam viscosity results in poor oil displacement efficiency and higher than required viscosity results in very low oil production rates.

2. Drilling mud [Caenn and Chillingar (1996)]

Drilling mud is a complex fluid used to lubricate drill bit/pipe, prevent wellbore collapse, prevent mud loss to the reservoir, prevent gas kick, and transport cuttings to the surface. To accomplish all these tasks, drilling mud has to be designed and optimized to each well being drilled to possess the right density, viscosity, yields stress, and shear-thinning behavior. The composition of drilling mud consists of any combination of brine, minerals/clay, alkane/oil, polymers, and surfactants (concentrated dispersed phase of solid and/or liquid in liquid continuous phase). Drilling mud rheology is also described properly with Herschel-Bulkley rheological model [Kelessidis et al. (2006)].

3. Emulsion polymer [SNF Floerger (2014)**]**

Emulsion polymer usually describes concentrated aqueous polymer solution-in-oil emulsions. Low concentration (<~2,000 ppm) aqueous polymer solutions such as hydrolyzed polyacrylamide (HPAM) are often used as a secondary/tertiary EOR injection method to improve oil displacement efficiency similar to foam. Ideally, dry HPAM powders are mixed into the injection brine with the required mixing procedure in the field [Levitt (2012)]. However, large polymer mixing facilities are not available on offshore

platforms where space is extremely limited. That is where, emulsion polymer becomes very valuable. Concentrated HPAM aqueous solution consisting of 50-95% (wt) HPAM is prepared offsite. Such solution viscosity is on the order of millions of cP which makes transportation to the injection sites very difficult. Thus, to reduce the apparent viscosity of the aqueous polymer solution, the concentrated HPAM aqueous solution is emulsified in some type of alkane/oil using surfactants. These W/O emulsions show only a fraction of the viscosity of the concentrated HPAM aqueous solution. Financially, it is prudent to prepare and transport as highly concentrated W/O emulsion as possible while still maintaining transport viscosity to the injection sites. Once at the injection site the emulsion polymer can be inverted to O/W emulsion and further diluted to the required polymer injection concentration with the injection brine without the need for large mixing equipment (Fig. 1.2c).

4. Heavy oil-in-water emulsions

Heavy oil and bitumen resources account for approximately 70% of the remaining oil discovered to date in the world. However, only 3 billion barrels of the 25 billion barrels of crude oil produced worldwide in 2000 was heavy oils/bitumen [Meyer and Attanasi (2003)]. Compared to light crude oils, heavy oils and bitumen are more costly to produce, transport, and refine. The viscosity of heavy oils and bitumen is usually too high to be produced by the natural energy of the reservoir and/or secondary production methods such as waterflood and gas flood. If the heavy oil/bitumen reservoirs are shallow, surface mining is used. Otherwise, thermal EOR methods such as steam and combustion are used to lower the oil viscosity.

A key challenge of transporting heavy oils/bitumen from production sites to refineries is also their viscosity which can be ~10^3-10^7 cP at standard conditions.

Regulations limit the operation of crude oil pipelines to oils with <~350 cSt at the transport temperature. The most common method of reducing heavy crude oil viscosity below the regulation limit is to dilute the heavy oils with low viscosity hydrocarbon diluents such as condensate. The required volume of diluents can be up to 50%v [Saniere et al. (2004)]. Once transported to a refinery, heavy oil and bitumen must be upgraded by lowering the carbon content and increasing the hydrogen content before the traditional refining processes can take place. The diluent cost and increased cost of transporting a larger volume of diluted heavy oil are as significant a challenge in exploiting heavy oil/bitumen resources as the higher costs of producing and refining heavy oils/bitumen.

An alternative method to transport heavy oil/bitumen from the production sites to refineries is to prepare concentrated heavy O/W emulsions such as the commercial emulsion pipelines in Indonesia [Simpson (1963)] and Venezuela [Salager et al. (2001)]. The viscosity of such heavy oil emulsions can be orders of magnitude lower than the heavy oil viscosity. Concentrated heavy oil-in-water emulsions composed of up to 98% vol. heavy oil are possible [Chirinos et al. (1990)], but a higher emulsion viscosity is observed for higher dispersed oil concentrations. The ultimate goal is to transport as little water in the emulsion as possible while still maintaining viscosity below the pipeline limit of <350 cSt. viscosity.

The rheological properties of concentrated heavy oil-in-water emulsions are very complex and an extensively studied subject in the literature [Abdurahman et al. (2012); Ahmed et al. (1999a); Ashrafizadeh and Kamran (2010); Gutierrez et al. (2003); Hoshyargar and Ashrafizadeh (2013); Núñez et al. (1996); Nuñez et al. (2000)]. Shear-thinning behavior and yield stress are two of the many reported non-Newtonian properties of concentrated heavy oil emulsions.

Understanding the flow properties of colloidal suspensions is essential since all fluids are transported through porous media and/or pipes of varying dimensions during oil field operations. The flow rate of fluids is a function of flow conduit dimensions, pressure gradient, fluid density, and fluid viscosity. Pressure gradient is controlled by independent variables in most operations such as the downhole pressure and the capacity of pumps as well as the stress failure limit of the flow conduits. Flow conduit dimensions can seldom be varied since the rock properties and pipeline dimensions are fixed. To optimize the flow rate of colloidal suspensions, the only parameter that can typically be controlled is the viscosity of colloidal suspensions. To be able to tune the rheological properties of concentrated colloidal suspensions utilized in the oil industry, better understanding of the relationship between their rheological properties and physicochemical properties is needed.

1.2 Objectives of the Research

The main objective of this research was to develop a deeper knowledge of the properties of concentrated colloidal suspensions utilized in the oil industry. The experimental focus was on understanding how the rheological properties of concentrated colloidal suspensions are affected by the sample properties, as well as the flow conduit dimensions and flow conditions. To achieve the main objective, the research focus was on one specific type of colloidal suspension utilized in the oil industry, concentrated heavy oil-in-water emulsions. The idea is that the microstructures of all colloidal suspensions show fundamental similarities. Understanding the underlining connections between the physical and rheological properties of concentrated heavy oil-in-water emulsions should translate to the understanding of the basic properties of most concentrated colloidal suspensions. Finally, the physical properties of concentrated

heavy oil emulsions were tuned to possess the desired rheological properties for pipeline transportation.

The major objectives of this research are listed below:

1. To develop a simple method of preparing low viscosity, high dispersed phase concentrations of heavy oil-in-water emulsions with viscosity below the pipeline operation limit (<350 cSt).
2. To understand and characterize the rheological properties of concentrated heavy oil-in-water emulsions as a function of their physicochemical properties, flow conduit dimensions, and operating conditions.
3. Lastly, using experimental laboratory measurements (capillary tube viscometers and parallel plate viscometer), flow of concentrated heavy oil emulsions is up-scaled to full-scale pipeline dimensions as well as flow conditions. Sensitivity analysis of pipeline dimensions, flow conditions, as well as emulsion physicochemical properties are performed to find the optimal conditions and emulsion properties for pipeline transportation of heavy oil emulsions. The goal is to prepare concentrated heavy oil emulsions with the highest dispersed phase while still maintaining the pipeline viscosity limit (<350 cSt).

1.3 DESCRIPTION OF THE CHAPTERS

The dissertation is organized into 7 chapters.

Chapter 2 is an in-depth literature review of heavy oils and many methods of transporting heavy oils/bitumen from the production sites to refineries. The focus is on the heavy oil-in-water emulsion method. Rheological models for emulsions of varying dispersed phase concentrations are reviewed and discussed.

Chapter 3 describes a new, one-step procedure for preparing concentrated heavy oil-in-water emulsions. A chemical formulation method was used to prepare concentrated emulsions with varying physical properties. The goal was to prepare concentrated emulsions with specific physical properties that show lower emulsion viscosity at pipeline operating conditions.

Chapter 4 presents the photomicrographs of heavy oil-in-water emulsions taken using a fluorescent microscope. The energy of interaction between oil droplets in the emulsions are analyzed.

Chapter 5 presents a systematic experimental study on the rheology of concentrated heavy oil emulsions. Concentrated emulsion samples were prepared with the new procedure mentioned in Chapter 3. Smooth and roughened parallel plate geometry were used to perform a full analysis of concentrated emulsions using steady state, oscillatory, and transient measurements. Non-Newtonian properties of concentrated emulsions with varying physical properties were examined and characterized. Modeling equations were used to describe the rheology of concentrated emulsions.

Chapter 6 presents experimental rheology data of heavy oil-in-water emulsions using capillary tube viscometers of varying dimensions. Tube viscometers were used to simulate pipe flow of heavy oil-in-water emulsions. Capillary tube viscometer measurements make it possible to study the effects of high shear rate flow, laminar to turbulent flow transition, and flow conduit dimensions on the flow of emulsions.

Chapter 7 presents the methods and equations that were used to up-scale laboratory viscosity measurements of heavy oil-in-water emulsions to flow in crude oil pipelines of various dimensions. A sensitivity analysis was conducted to obtain the optimal flow conditions, flow dimensions, and physicochemical properties of concentrated heavy oil-in-water emulsions for large scale pipeline flow.

Chapter 8 presents the major findings of this research as well as recommendations for future research.

Chapter 2: Literature Review of Heavy Oil Emulsions

2.1 HEAVY CRUDE OILS

Petroleum liquids are classified as either light, medium or heavy based on their API gravity, a type of inverse specific gravity commonly used in the oil and gas industry, referenced to water properties at standard conditions of 60 °F and atmospheric pressure. API gravity of 10 corresponds to the same density as water. API>10 and API<10 correspond to less dense than water, and more dense than water, respectively. Heavy crude oils are classified further into subgroups based on both API gravity and viscosity. Table 2.1 summarizes the crude oil classifications based on API gravity and viscosity:

Table 2.1: Crude oil classification based on API gravity and viscosity defined by the USGS

Classification of Oils/Oil Property		**API Gravity**	**Viscosity (cP) at reservoir conditions**
Light Oils		API>20°	μ<100
Heavy Oils	Heavy	10°<API<20°	100<μ<10,000
	Bitumen	API<10°	10,000<μ

Light crude oils can be produced at economically viable flow rates mainly from the pressure gradient between the initial reservoir pressure and the bottom-hole pressure when wells are drilled (primary production). Factors such as oil compressibility, solution gas, and presence of water aquifer also contribute to the rate of production. When the reservoir pressure declines and leads to lower production rates of oil, water/gas injection wells can be drilled to inject water/gas into the oil reservoirs (secondary production). Water/gas injection helps to increase or maintain the reservoir pressure, resulting in longer duration of sustained oil production rates. The relationship between the flow rate (q), pressure gradient (∇P), oil viscosity (μ), and porous media permeability (k) is expressed simply and elegantly by Darcy's law:

$$q = -\frac{kA\nabla P}{\mu} \tag{2.1}$$

where A is the cross-sectional area to flow. For flow of oil, k is the permeability of oil and μ the oil viscosity.

As shown in Fig. 1.1, the production rate of currently producing conventional oil reservoirs of the world are expected to decline in the future. Yet to be produced and undiscovered conventional oil reservoirs in the world are expected to replace some of the oil production from producing oil reservoirs to satisfy the energy demand of the world. Unconventional resources also make up a significant portion of the future world oil production. A vast source of mostly untapped unconventional oil that exists in the world is heavy crude oils and bitumen.

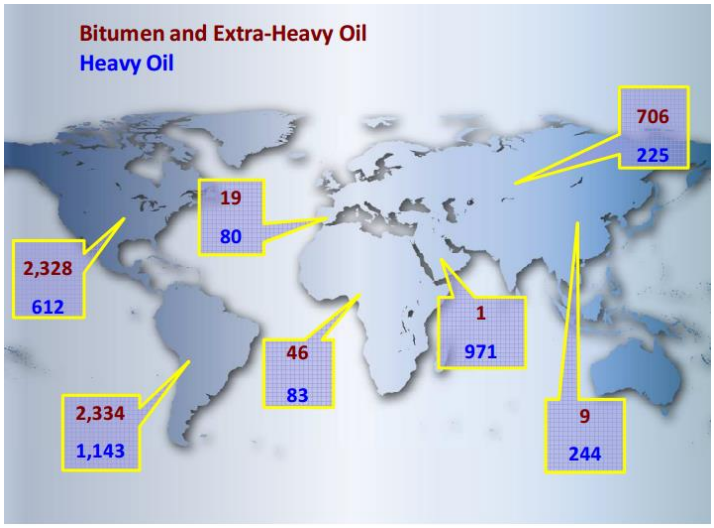

Fig. 2.1: Global heavy crude oil resources (billion barrels of oil) [Klavers and Atkins (2011)]

It has been estimated that over seven trillion barrels of heavy oils and bitumen exist in the world (Fig. 2.1). One of the challenges of economically producing large quantities of heavy crude oils is their high viscosity. Since the viscosity of heavy oils is significantly higher than that of light oils, the production rates are extremely low and

uneconomical for most heavy oil fields as Eq. 2.1 demonstrates. Thermal EOR production methods are utilized to decrease the viscosity of heavy oils to improve the production rates. It is estimated that the in-situ recovery factor of heavy oils/bitumen are approximately 10-20% of the OOIP [Meyer and Attanasi (2003)]. That is 10-25% less ultimate recovery of OOIP compared to light oil reservoirs with secondary recovery methods.

EOR of heavy oil reservoirs are necessary to fill the gap between the demand and supply of petroleum liquids now and in the future. The most common EOR method utilized to produce oil from heavy oil reservoirs is thermal EOR, where steam is injected into the heavy oil reservoirs. Hot waterflood, steam flood, cyclic steam stimulation (CSS), steam assisted gravity drainage (SAGD), and in-situ combustion are some of the common thermal EOR techniques used. The primary purpose of thermal EOR methods is to reduce the oil viscosity by increasing the temperature. Fig. 2.2 demonstrates the extreme viscosity sensitivity of heavy crude oils to temperature.

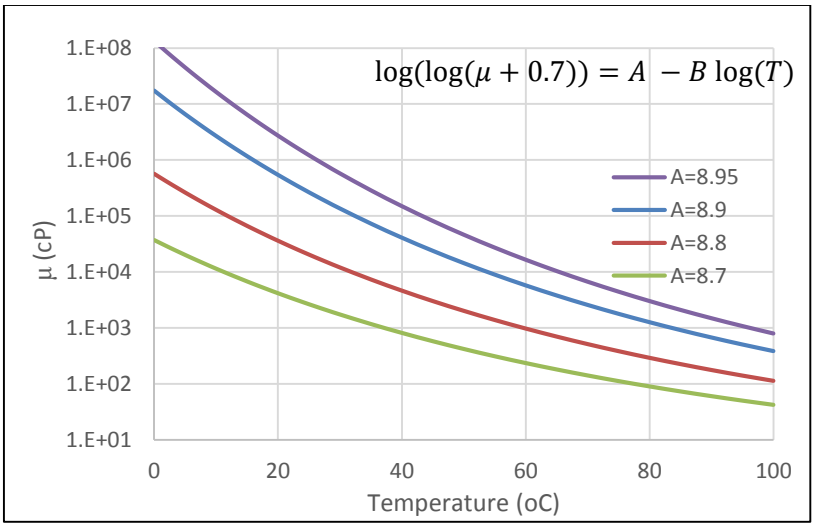

Fig. 2.2: Effect of temperature on heavy crude oil viscosity. Lines are modified Walther's equation with B=3.3

Modified Walther's equation was used in Fig. 2.2 to estimate the effect of temperature on heavy oil/bitumen viscosity. Modified Walther's equation models heavy oil viscosity vs. temperature more accurately than a power law model or an exponential model. Constant, *A*, represents the heavy oil/bitumen of varying viscosity. Constant, *B*, in the equation represents the effect of temperature on viscosity and was estimated from the experimentally measured heavy oil data presented in Chapter 3. Orders of magnitude change in heavy oil viscosity is observed compared to 6-7 fold change in water viscosity when the temperature changes from 0-100 ^{o}C. The temperature effect on heavy crude oil viscosity is even more dramatic at steam flood operating temperatures.

As more and more heavy oils are produced globally to meet energy demand, heavy oils must be transported from the production sites to refineries around the world. The obvious solution is to use the existing crude oil pipeline infrastructure and oil tankers to transport heavy crude oils. However, high crude oil viscosity, the same heavy oil property that makes subsurface heavy oil production so challenging, also translates to surface transportation difficulties. It is impossible to transport unmodified heavy crude oil above a certain viscosity through pipelines at a reasonable flow rate. Heavy crude oil viscosities can be modified with methods that use the unique properties of heavy crude oils such as viscosity lowering effect of higher temperature, miscibility with light hydrocarbons, and a presence of a large quantity of acidic components in the oil. The heavy crude oil transportation methods used in the oil industry have met with varying commercial success.

2.2 CRUDE OIL PIPELINE OPERATING CONDITIONS

Crude oil pipeline dimensions as well as the number of pump stations that provide the necessary pressure for flow are designed to transport crude oils within a certain range

of flow rates, crude oil densities, and crude oil viscosities. In the U.S.A., the Federal Energy Regulatory Commission (FERC) regulates pipeline transmission of crude oils and has a strict specification: the kinematic viscosity shall not exceed 350 cSt at the pipeline reference line temperature. The specifications are also equivalent to the ones imposed by the Canadian National Energy Board (CNEB). Operating conditions of most of the major crude oil pipelines in the world are summarized in Table A1 in Appendix A. The range of operating conditions of major crude oil pipelines, a summary of Table A1, is listed in Table 2.2. A viscosity of 20 cP and a density of 0.8 g/cm^3 were assumed in the calculation of Reynold's number and pressure drop given in Table 2.2.

Table 2.2: The typical range of maximum operating conditions of major crude oil pipelines

	Range	Average
Pipe Diameter (inch)	18-48	33
Velocity (miles/hr)	2-11	6
Shear Rate (s^{-1})	9-40	20
Reynold's Number	40,000-200,000	100,000
Pressure Drop (psi/mile)	3-36	11

With crude oil kinematic viscosity of 350 cSt, the flow rate and thus shear rate would drop to a range of 5-20 s^{-1} within the same range of maximum pressure drops.

2.3 Pipeline Transportation of Heavy Oils

To maintain pipeline transportability, heavy and extra heavy crude oils must be treated or altered to meet the pipeline viscosity specifications. Many methods exist that manipulate the physical and chemical properties of heavy crude oils to meet the pipeline viscosity specifications. Some recent reviews of the most common methods used to transport heavy crude oils are discussed in the studies by Saniere et al. (2004), Martínez-

Palou et al. (2011), and Wylde et al. (2012). A thorough literature review of the most prevalent and promising methods is conducted and discussed below.

2.3.1 Diluted Heavy Oils (Dilbit)

Perhaps, the most widely used method of lowering the heavy and extra heavy crude oil viscosity is by blending heavy crude oils with a low viscosity diluent that is miscible with heavy crude oils. Classical diluents are condensates, naphtha, light crudes, and synthetic crudes. The resulting viscosity of the mixtures depends on the dilution rate, and on the respective viscosities and densities of the heavy crude oil and the diluent. Depending on the heavy crude oil viscosity, diluents such as condensates and synthetic crudes of up to 30-50% vol. of the diluted heavy oils have been reported to be necessary in the literature to satisfy the pipeline viscosity regulations [Saniere et al. (2004); Wylde et al. (2012)]. The following equation by Miadonye et al. (2000) is used to estimate the mass fraction of diluent necessary to reduce the various heavy oil/bitumen viscosities to the pipeline transport limit of 350 cSt.

$$X_D = e^{\left[\frac{\ln\left(\frac{a-\ln(lnv_m - lnv_D+1)}{a}\right)}{n}\right]} \tag{2.2}$$

where X_D is the mass fraction of diluent, v_O the kinematic viscosity of crude oil, v_D the kinematic viscosity of diluent, v_m the kinematic viscosity of the mixture, $a = \ln(\ln(v_O) - \ln(v_D) + 1)$, and $n = v_D/(0.9029v_D + 0.1351)$. Literature densities and viscosities of toluene and hexane were used in the calculation. Heavy oil density was assumed to be 1 g/cm^3. Light hydrocarbon/synthetic crude oil viscosities and densities were assumed to be 2 cP and 0.85 g/cm^3 at 25 ^{o}C and 3 cP and 0.88 g/cm^3 at 0 ^{o}C. Eq. 2.2 was converted to a volume fraction of diluent based on the densities and plotted in Fig. 2.3 for temperatures of 0 and 25 ^{o}C.

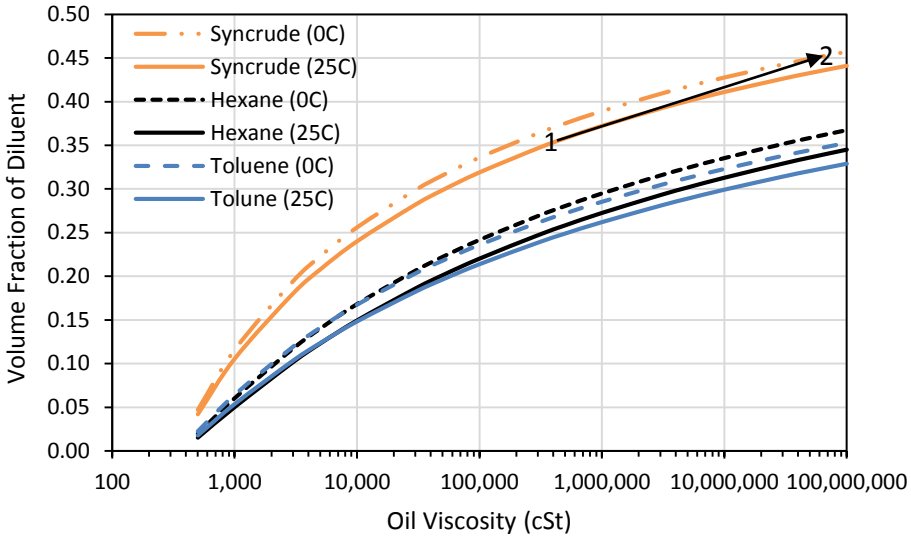

Fig. 2.3: Volume fraction of diluent required to reach diluted heavy oil viscosity of 350 cSt vs. the pure heavy oil viscosity. Example: Black arrow indicates the path of a heavy oil viscosity from 25 ºC (1) to 0 ºC (2) and the increase in the diluent volume required to reach ν_m=350 cSt.

Miadonye et al. (2000) did not observed more than 15% error with their model when compared to experimental data of diluted heavy oil viscosities with all three types of diluent. Aromatic solvents such as toluene appear to be better viscosity reducing diluents per volume followed by straight chain alkanes such as hexane and light crude/Syncrude. For a temperature of 25ºC, up to 30-35% toluene, ~35% hexane, and ~45% Syncrude are necessary. For a temperature of 0ºC, up to ~35% toluene, 35-40% hexane, and 45-50% Syncrude/light crude are necessary. A good rule-of-thumb is approximately 10-15% (vol) extra diluent/Syncrude is required to reach ν_m=350 cSt for the same heavy oil/bitumen when the pipeline operating temperature changes from 25 to 0 ºC, not an unreasonable seasonal temperature change. Recent studies have been conducted to improve the efficiency of viscosity reduction by using a mixture of classical diluents with polar solvents such as alcohols and methylethylketone (MEK) [Argillier et al. (2005)].

The biggest disadvantage of the diluent method of reducing heavy crude oil viscosity is the large quantity of diluent needed to create a blend that meets the pipeline viscosity specification. While necessary for facilitating transport, diluted heavy oils create additional load on the strained pipeline infrastructure by consuming valuable pipeline capacity. Increased distillation cost downstream is another add-on cost. Perhaps, the most expensive and pressing problem with diluted heavy oil method is the strained supply of diluents. Lack of diluents or high premium diluents can bottle-neck the production of heavy oils and bitumen. Condensates have been selling up to $13/bbl over U.S. benchmark futures because of this disparity between supply and demand in Canada [Fomitchev-Zamilov (2015)]. Kinder Morgan estimated in 2013 that the diluent demand in Canada is forecasted to be approximately 1 million bpd by 2025 [Lindley (2013)]. Also, the demand for diluent in Canada in 2013 was approximately 300,000 bpd while the local Canadian supply was only 150,000 bpd [Lindley (2013)] The difference between the demand and local supply has been satisfied with imports from the U.S., as far away as the Gulf Coast. The added costs of recycling and transportation of the diluent from the refineries back to the heavy oil and bitumen production sites can be enormous. The cost of transporting diluted heavy oil and bitumen is estimated to be up to $18/bbl of diluted heavy oil/bitumen because of constrained pipeline capacities [Fomitchev-Zamilov (2015)].

The transportation of heavy crude oils and bitumen from production sites in Canada to the refineries in the U.S. can cost up to $22/bbl of diluted heavy oil/bitumen assuming 30% diluent in the mixture. The diluted bitumen normally sells at ~20% discount to WTI. All the extra transportation costs as well as the discount of diluted heavy oils compared to WTI also hurt the producers of heavy oil/bitumen producers who are limited to only producing economically feasible fields. While the diluent

transportation method is the most popular and dominant choice, the high costs associated with this method provide incentives for alternative, cheaper methods of heavy oil and bitumen transportation.

2.3.2 Upgrading Before Transportation

Another method of achieving a low heavy crude oil viscosity, closely associated with the diluent method, is the partial upgrading of the heavy crude oils before transportation. A portion of the heavy crude oil produced is partially upgrade in an upgrading unit at the production site or nearby, resulting in a lower viscosity crude oil called synthetic crude (Syncrude). The synthetic crude is used as a type of diluent and blended with heavy crude oils. A major disadvantage of this method, on top of the disadvantages of the diluent method, is the major capital investment required to build an upgrading unit close to the production sites [Saniere et al. (2004)].

2.3.3 Core-Annular Flow

Core annular flow is a unique method of transporting heavy crude oils in pipelines. Unlike the previous methods, core annular flow works by reducing the drag by the pipe wall on the heavy crude oils instead of reducing the oil viscosity. On average, 10-30% water is injected with heavy crude oils and a layer of water forms between the crude oil core and the pipelines, with the water layer acting as a slip layer, resulting in a significantly reduced pumping power [Wylde et al. (2012)]. Fig. 2.4 shows an illustration of the core-annular flow method.

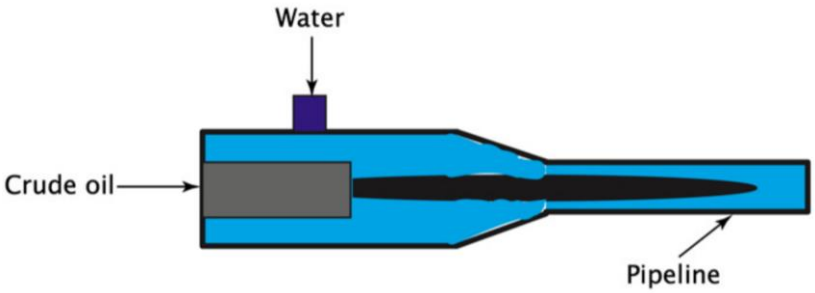

Fig. 2.4: Core-annular method of transporting heavy oils/bitumen. Illustration is from Martínez-Palou et al. (2011)

Some success have been achieved in lab-scale and pilot-scale runs with limited implementation in two commercial operations [Guevara et al. (1997)]. The main problem associated with core annular flow occurs during pipeline shutdowns. The density difference between the oil and water causes gravity separation, resulting in the destruction of the annular water layer, and eventual blockage of the pipelines by the heavy crude oils [Saniere et al. (2004)].

2.3.4 Heating and Insulating Pipeline

The heavy crude oil viscosity decreases dramatically with increasing temperature. The effect of temperature on heavy crude oil viscosity is demonstrated in Fig. 2.2. Pipelines can be heated/insulated with the use of insulation and heating stations, taking advantage of this heavy crude oil physical property, to transport heavy crude oils. One example of a heated pipeline is the Trans Alaska Pipeline System in Alaska which operates at ~50°C to transport heavy crude oils [Saniere et al. (2004)]. The method requires high utility costs to keep the pipelines heated, large capital investments on installing insulation for the pipelines, building multiple heating stations, and causes greater corrosion of the pipelines [Guevara et al. (1997)].

According to Fig. 2.2, the heating and insulating method is limited to heavy oils with viscosity of less than ~2,500-3,000 cP, ~20,000 cP, and ~250,000 cP at 25 ^{o}C for heated temperatures of 60 ^{o}C, 80 ^{o}C, and 100 ^{o}C respectively. A hybrid method of heating/insulation and one of the other methods such as the diluent method is a very interesting idea that may enable the use of the heating/insulation method with higher viscosity heavy oils at lower heated temperature. A hybrid method may also result in a synergistic viscosity reduction where economically superior transportation of heavy crude oils/bitumen would be possible compared to an application of a single method.

2.3.5 Heavy Oil-in-Water Emulsions

Emulsified heavy crude oil/bitumen can show significantly lower apparent viscosity compared to the heavy crude oil/bitumen viscosity. Fig. 2.5 illustrates the types of common emulsions found in the oil industry.

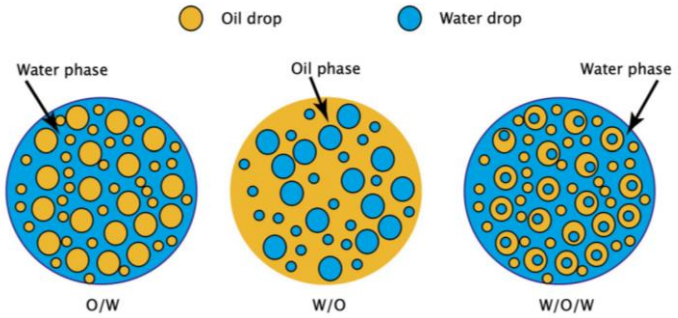

Fig. 2.5: Types of common emulsions found in petroleum production and transport. Obtained from Martínez-Palou et al. (2011)

The preferred type of emulsion to transport heavy crude oils is oil-in-water (O/W) emulsions. O/W emulsions have been shown to possess orders of magnitude lower viscosity than heavy crude oils. On the other hand, W/O emulsions have higher viscosity than the crude oil used in the emulsion mixture.

The advantages of the emulsion method of transporting heavy oils are numerous. First, the oil industry is very familiar with handling emulsions, which are often observed in produced heavy oils. Instead of demulsifying produced emulsions, concentrated O/W emulsions can be prepared for heavy oil transportation purposes. The source of the water used in the emulsification process is one of the main concerns. Freshwater use is regulated locally in many locations and are necessary in large quantities to produce steam for thermal EOR of heavy oils as well as for hydraulic fracturing of shale formations. Between 2-4.5 bbl of water is necessary to produce 1 bbl of oil in a mining operation in Canada [National Energy Board (2006)]. To not be dependent on freshwater supply, readily available and cheap seawater or produced water from the wells may be used with the right combination of co-solvents and surfactants to emulsify heavy oils. Once heavy oil emulsions reach the refineries, the emulsion must be demulsified before conventional heavy oil refinery processes can proceed. The main costs associated with the emulsion method are the chemical/surfactant costs and the cost associated with demulsification.

Heavy oil emulsions have been transported in major pipelines at least three times. Literature is available on only two of the three cases.

Indonesia [Simpson (1963)]

Tandjung Pipeline in Indonesia was placed into operation in 1962 to transport heavily paraffinic crude oil with a high pour point. The high paraffin content resulted in crude oil with a very high yield stress at the transport temperature. After evaluation heating, diluent, pour point depressor, and O/W emulsion methods for heavy oil transportation, Shell Indonesia chose the O/W emulsion transport method which showed the most promising results in laboratory and pilot-scale tests. The pipeline dimension had a diameter of 20 inches and a length of 238 km. The heavy oil emulsion consisted of 70% dispersed oil phase. Non-Newtonian properties such as shear-thinning and

thixotropy were observed with the Tandjung O/W emulsion during transport. A start-up pressure drop of up to 14 psi/mile and a steady state pressure drop of about 10 psi/mile were observed. A peculiar observation was made during the operation. The pressure drop was almost constant within the range of flow rates during the operation. The effective viscosity vs. calculated shear rate is shown in Fig. 2.6.

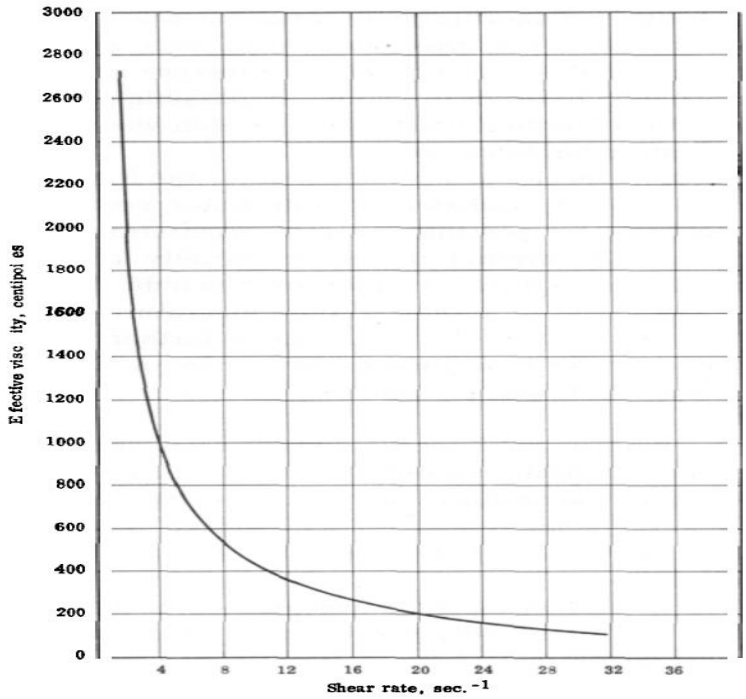

Fig. 2.6: Effective viscosity vs. shear rate observed during the pipeline operation of 70% O/W emulsion transportation. Obtained from Simpson (1963)

At the operating temperature and shear rate of 10 s^{-1}, a viscosity reduction from ~100,000 to 400 cP was achieved for 70% O/W emulsion.

Venezuela (Orimulsion) [Salager et al. (2001)]

Venezuela was one of the first countries to seriously explore the production of heavy oil in the late 1970's. The motivation is very simple. Venezuela holds the largest heavy oil reserves in the world. The surface transportation problem of heavy oils was

recognized early. INTEVEP, the research subsidiary of Petroleos de Venezuela, S.A. (PDVSA), spent over a decade trying to solve the heavy oil transportation problem. PDVSA came to the conclusion that the most cost effective method of transporting heavy oils was the use of O/W emulsions. In mid 1980's, after over a decade of research and development, a trademarked heavy O/W emulsion composition, Orimulsion®, was developed. The composition of Orimulsion® was 70-73% heavy oil emulsion stabilized with a low concentration of nonionic surfactants. Orimulsion® showed viscosity of ~350-570 cP at 30 ºC and 100 s^{-1} in the laboratory.

Orimulsion® was transported in a 350 km pipeline with a residence time of 3-4 days. The observed flow conditions were a shear rate of less than 10 s^{-1} and laminar flow with Reynold's number <1,000. At these operating conditions, the apparent viscosity of the Orimulsion® was ~2,000 cP. The same peculiar, constant pressure drop readings, similar to the Indonesian emulsion pipeline, were observed when the flow rate was increased four-fold (Fig.2.7).

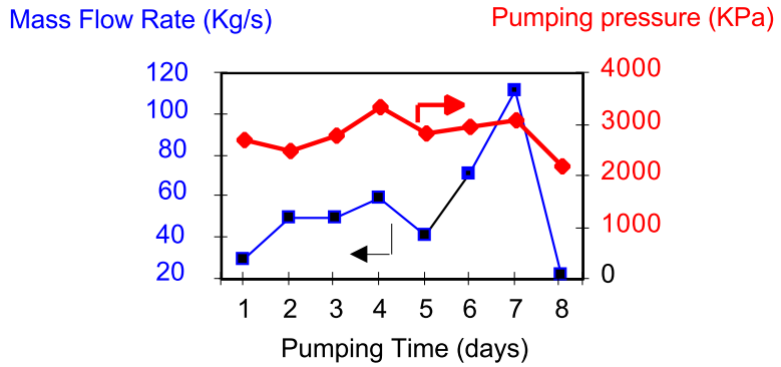

Fig. 2.7: Mass flow rate and pumping pressure vs. pumping time for Orimulsion®. The figure is from Revista Tecnica INTEVEP, vol. 10, Nº 1, page. 13, 1990 but obtained from Salager et al. (2001)

It was speculated that migration of heavy oil droplets away from the pipe walls created a thin slip layer of water which caused the peculiar pressure drop readings instead

of the shear thinning property of concentrated emulsions [Núñez et al. (1996)]. The unusual and unexpected pressure drop readings resulted in an apparent viscosity lower than what was predicted from laboratory rheometer measurements.

The original journal articles that published the Orimulsion data presented in this section were all written in Spanish. Salager et al. (2001) summarized the Orimulsion data in Chapter 20 of *Encyclopedic Handbook of Emulsion Technology* published in 2001. Original article citations can be found at the end of the book chapter.

Surfactants

Normally, crude oil and water are immiscible. When mixed together, the immiscible phases separate in a matter of seconds. However, when surface active agents are added to a mixture of crude oil and water, interfacial tension is lowered and an emulsion is created where one liquid is the dispersed phase and the other is the continuous phase. The stability of emulsions is improved and can be stable for >months, depending of the preparation procedure and emulsion composition. Since the residence time of emulsions in pipelines is days, stability of emulsions is a critical component of emulsion transportation method.

Surfactants are organic molecules that possess both a hydrophilic group (head) and a lipophilic group (tail). Bancroft rule states that the liquid in which an emulsifier is more soluble constitutes the continuous phase. Solubility preference of surfactants can be quantified by the concept of hydrophilic-lipophilic balance (HLB), where high HLB surfactants are more soluble in water than in oil, thus forming O/W emulsions, and low HLB surfactants are the opposite, resulting in W/O emulsions. The HLB is a function of the surfactant structure, surfactant concentration, brine composition, oil composition and, temperature.

The stability and rheological properties of concentrated heavy O/W emulsions are affected critically by the type and concentration of the surfactants utilized in the process of preparing emulsions. There are three main types of surfactants that are commercially available with distinct advantages and disadvantages associated with each. They are nonionic, cationic, and anionic surfactants

Nonionic Surfactants

The most common type of surfactants used in preparation of heavy crude O/W emulsions is nonionic surfactants. Nonionic surfactants consist of a hydrocarbon chain as the lipophilic group and a polar group with no charge such as ethylene oxide as the hydrophilic head. The most common type of nonionic surfactants, used for preparation of heavy O/W emulsions, is alkylphenol ethoxylates. Orimulsion® is prepared with nonylphenol ethoxylate. The structure is shown below.

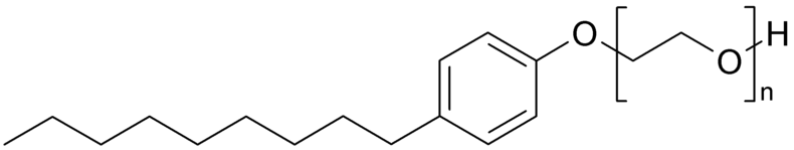

Fig.2.8: Structure of nonylphenol ethoxylate. n represents the number of ethylene oxides.

Nonionic surfactants are relatively insensitive to salt concentrations in water compared to ionic surfactants. Thus, nonionic surfactants can readily be used with seawater or high salinity brine to prepare O/W emulsions. No precipitation of nonionic surfactants is observed with divalent cations. The HLB of nonionic surfactants does not vary a lot as a function of salinity. However, nonionic surfactants are very sensitive to temperature. Higher temperature changes the HLB of nonionic surfactants to be more lipophilic and may result in formation of viscous W/O emulsions. The cost of non-ionic surfactants is moderate, but the stability of the emulsions is poor compared to emulsions

prepared using ionic surfactants. Wylde et al. (2012) screened dozens of nonionic surfactants to create and optimize heavy O/W emulsions with great success.

Cationic Surfactants

Cationic surfactants are ionic surfactants that contain a positively charged hydrophilic head group with a lipophilic tail. Cationic surfactants are the most expensive and typically the least used type of surfactants for preparation of heavy O/W emulsions because of the cost. Cationic surfactant are often sensitive to water salinity as well as the electrolyte composition, resulting in precipitation of surfactants with divalent anions in the brine. Cationic surfactants are not as sensitive to temperature as nonionic surfactants. O/W and W/O emulsions form below and above an optimal water salinity, respectively. An optimum salinity is defined as the salinity at which the surfactant molecules are equally attracted to both water and hydrocarbon phases (HLB=10).

Anionic Surfactants

Anionic surfactants contain a negatively charged hydrophilic head group with a lipophilic tail. Anionic surfactants have the same properties as cationic surfactants except anionic surfactant may precipitate in the presence of a high concentration of divalent cations in water. Anionic surfactants form very stable and homogenous emulsions. Recent advances have been made with synthesis of new anionic surfactant groups that can tolerate higher salinity and hardness for chemical enhanced oil recovery purpose [Adkins et al. (2010)].

Studies have also been conducted that show synergetic effect of combining nonionic surfactants with anionic surfactants to prepare heavy crude O/W emulsions with lower viscosity than possible with just individual surfactant types [Ahmed et al. (1999a); Zaki et al. (2001)].

Natural Anionic Surfactants

Crude oil is a highly complex mixture of thousands of different components. A component found in most heavy oils and bitumen is naphthenic acids. Naphthenic acids are isomeric mixtures of carboxylic acids containing one or more saturated fused alicyclic rings. Very fortunate for preparing very stable heavy O/W emulsions, the naphthenic acids present in heavy oils can be deprotonated with the use of alkali to generate "natural anionic surfactants" commonly called soap. Heavy crude oils can be tested for the presence and quantity of the naphthenic acid by a titration method detailed in ASTM D974. Common alkalis are extremely inexpensive compared to synthetic surfactants, making this the lowest cost method of stabilizing heavy O/W emulsions. Examples of common inorganic alkalis are sodium hydroxide, sodium carbonate and sodium metaborate. Ammonia and organic alkalis such as alkyl amines have also been shown to increase the pH and generate natural surfactants from heavy crude oils and provide unique advantages compared to the common alkali [Gutierrez et al. (2003); Verzaro et al. (2002)].

The key disadvantages of the natural surfactant O/W emulsion method are:

- Unknown combination of surfactants as well as surfactants of unknown molecular weight are generated.
- Surfactant concentration is very sensitive to alkali concentration and pH.
- High hydrophobicity of the natural soap results in inversion of O/W emulsions to W/O emulsions at very low salinity. Freshwater is usually required.

Advances in chemical EOR, with the concept and application of alkali-surfactant polymer-flooding (ASP) [Nelson et al. (1984)] and the more recent alkali co-solvent polymer flooding (ACP) [Fortenberry et al. (2013)], have overcome some of the limitations listed above. By adding hydrophilic surfactants and/or co-solvents, heavy

O/W emulsions can be prepared with high salinity alkaline water without inverting to W/O emulsions.

2.4 HEAVY OIL EMULSION RHEOLOGY

Extensive studies have been published on the preparation, stability, and rheology of colloidal suspensions. The key problem of all these studies is how to relate the viscosity of colloidal suspensions (μ_{sus}) to the physicochemical properties of colloidal suspensions such as dispersed phase concentration (φ), dispersed phase particle size, particle size distribution, interaction potential between the dispersed phase particles, as well as the viscosities of dispersed (μ_d) and continuous (μ_c) phases to the viscosity of the colloidal suspensions.

2.4.1 Dilute

Einstein (1906) was the first to show that the viscosity of a dilute suspension of spherical particles is a function of dispersed phase concentration and continuous phase viscosity:

$$\frac{\mu_{sus}}{\mu_c} = 1 + 2.5\varphi + O(\varphi^2) \quad (2.3)$$

where μ_c is the continuous phase viscosity and φ the dispersed phase concentration. Taylor (1932) derived the viscosity equation for very dilute emulsions which included the dispersed phase viscosity (μ_d) and reduced to Eq. 2.3 when $\mu_d \to \infty$.

$$\frac{\mu_{emul}}{\mu_c} = 1 + \left(\frac{\mu_c + 2.5\mu_d}{\mu_c + \mu_d}\right)\varphi \quad (2.4)$$

Eqs. 2.3-2.4 are only accurate for very dilute colloidal suspensions which show negligible interaction between dispersed particles/droplets ($\varphi \ll 0.05$).

2.4.2 Moderate

A vast literature exists on how to extend the dispersed phase concentration range of Eq. 2.3 to higher φ [Batchelor (1977); Krieger (1972); Krieger and Dougherty (1959); Maron and Pierce (1956); Mooney (1951)] and Eq. 2.4 [Pal (2001), (2000a); Phan-Thien and Pham (1997)]. The Pal (2001) equation reduces to the Krieger and Dougherty equation when the viscosity ratio of the dispersed phase to continuous phase approaches infinity ($K \to \infty$):

$$\mu_r \left[\frac{2\mu_r+5K}{2+5K}\right]^{3/2} = \left(1-\frac{\varphi}{\varphi_m}\right)^{-2.5\varphi_m} \quad (2.5)$$

where μ_r is the viscosity ratio of the emulsion (μ_{emul}) to the continuous phase(μ_c) and φ_m the maximum packing volume fraction of the particles. Equations 2.3-2.4 are only accurate for very dilute colloidal suspensions that show negligible interaction between dispersed particles/droplets ($\varphi \ll 0.05$). Equation 2.5 and thus also the Krieger and Dougherty equation have been shown to be only accurate up to moderate dispersed particle/droplet concentrations ($\varphi < \sim 0.5-0.6$) with accurate φ_m values. As $\varphi \to 0$, Equation. 2.5 reduces to 1. Shewan and Stokes (2015) plotted the relative viscosity of hard sphere suspensions using data from the literature as a function of normalized dispersed phase concentration. The hard sphere suspensions varied in size from colloidal to non-colloidal and φ_m varied from 0.58-0.81. The curves in Fig. 2.9 are calculated using Eq. 2.5 (Krieger-Dougherty) with $\varphi_m = 0.64$, and from the Mason and Pierce equation (MPQ) with estimated φ_m values.

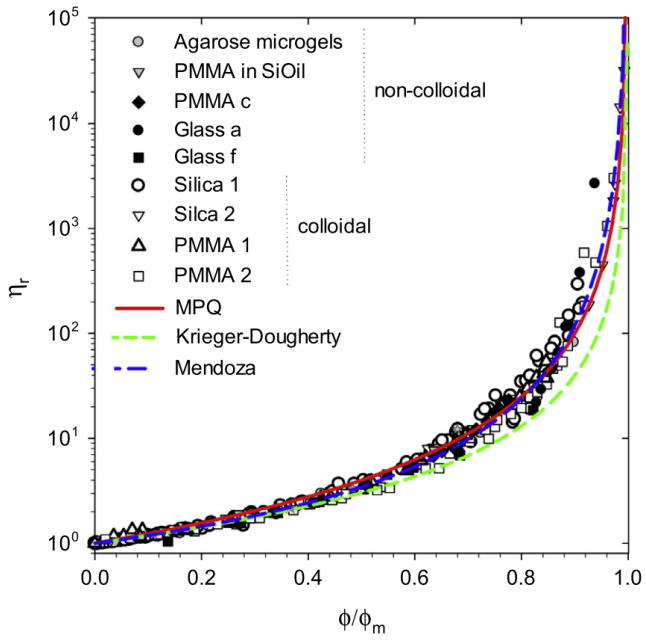

Fig. 2.9: Relative viscosity of colloidal suspensions vs. φ/φ_m [Shewan and Stokes (2015)].

The MPQ equation appears to fit the data the best out of the three models shown in Fig. 2.9. μ_r approaches infinity as φ/φ_m approaches 1 using Eq. 2.5 and MPQ. The implication is that colloidal suspensions cannot pack tighter than φ_m and flow, which is true for solid/rigid dispersed phases but not for a soft dispersed phases such as a liquid

2.4.3 Concentrated

Equations 2.3-2.5 are more than adequate for describing the rheological properties of repulsive colloidal suspensions with dilute and moderate dispersed phase concentrations. However, a large fraction of the colloidal suspension products utilized in oil field operations require 1) rheological properties observed only in concentrated colloidal suspensions ($\varphi > \sim 0.7$) and/or 2) as highly concentrated colloidal suspensions as possible to reduce the volume required to transport to and from the injection/production sites. Since emulsions and foams are soft, studies have shown that emulsion and foam droplets can deform at the sites of droplet contact to pack a lot denser

than the random close packing of uniform spheres (φ>0.64). See the photomicrograph of concentrated and compressed O/W below (Fig. 2.10).

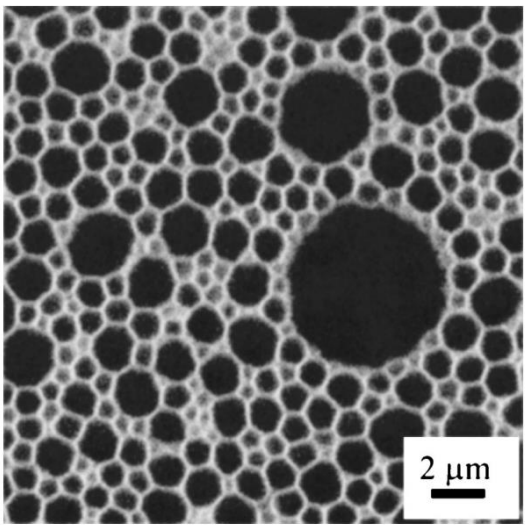

Fig. 2.10: Concentrated O/W emulsion, $\varphi = 0.77$, obtained by confocal microscopy [Meeker et al. (2004)].

Stable emulsions up to 98% dispersed phase concentration have been prepared [Chirinos et al. (1990)]. Eq. 2.5 is not suitable for concentrated emulsions since a solution doesn't exist when $\varphi_m < \varphi$. The deformation of the droplets has been observed to result in concentrated emulsions/foams possessing unique non-Newtonian properties such as shear-thinning, yield stress, thixotropy, and slip at the flow surface. The most commonly used model to describe the rheological properties of concentrated emulsions is the Herschel-Bulkley (HB) model.

$$\tau = \tau_y + k\dot{\gamma}^n \tag{2.6}$$

where τ is the shear stress, τ_y the yield stress, $\dot{\gamma}$ the shear rate, k the consistency index, and n the flow index. However, the limitation of HB model is that k is simply a fitting parameter and does not hold a physical explanation.

Princen (1983, 1985) and later Princen and Kiss (1986, 1989) published a set of four groundbreaking papers on rheology of concentrated emulsions and foams, relating shear stress vs. shear rate, elasticity, and yield stress to physicochemical properties; Sauter mean diameter (d_{32}), interfacial tension (Γ), and φ. The viscosity equation they used for concentrated unimodal oil-in-water emulsions ($\varphi > 0.74$) is:

$$\mu_{emul} = \frac{\tau_y}{\dot{\gamma}} + C(\varphi)\left[\frac{\mu_c \Gamma}{d_{32}\dot{\gamma}}\right]^{1/2} \tag{2.7}$$

where τ_y is the yield stress and $\dot{\gamma}$ the shear rate. Princen and Kiss (1989) estimated $C(\varphi)$ to be a simple function of φ, $C(\varphi) = 32(\varphi - 0.73)$. The strain and frequency independent storage modulus, G, of concentrated emulsions can be approximated with the equation:

$$G \cong 1.77\frac{\Gamma}{R_{32}}\varphi^{1/3}(\varphi - \varphi_m) \tag{2.8}$$

where φ_m is the volume fraction of the close-packed-spheres configuration and Princen and Kiss estimated it to be 0.73. Mason et al. (1995) found Eq. 2.8 was in sharp disagreement with results from an extensive series of experiments and came up with the following relationship:

$$G \sim \frac{\Gamma}{R_{32}}\varphi(\varphi - \varphi_m) \tag{2.9}$$

$C(\varphi) \cong 32(\varphi - 0.73)$ is very similar to $C \cong A\varphi(\varphi - \varphi_{rcp})$ where $A \cong 25.5$ and $\varphi_m = 0.67$ for $\varphi > 0.75$. When Eq. 2.7 is rearranged to include G with the assumption that $C(\varphi) \sim \varphi(\varphi - \varphi_m)$, the following equations is obtained:

$$\tau = \tau_y + BG\left[\frac{\mu_c d_{32}\dot{\gamma}}{\Gamma}\right]^{1/2} \tag{2.10}$$

where B is a constant.

Seth et al. (2011) developed a micromechanical model to predict the flow curve of soft particle glasses by using the concept of elastohydrodynamic phenomena.

$$\tau = \tau_y + c\tau_y \left[\frac{\mu_c \dot{\gamma}}{{\gamma_y}^2 E^*}\right]^{1/2} \quad (2.11)$$

where c is a numerical coefficient, γ_y the yield strain, and E^* the contact modulus. Using the expressions, $\tau_y = \gamma_y G$ and $E^* = 9.92\Gamma/R$ [Seth et al. (2006)], Eq. 2.11 can be expressed:

$$\tau = \tau_y + 0.2245cG \left[\frac{\mu_c d_{32} \dot{\gamma}}{\Gamma}\right]^{1/2} \quad (2.12)$$

The modified Princen and Kiss equation (Eq. 2.10) is very similar to the micromechanical model derived by Seth et al. (2011) (Eq. 2.12).

Note the similarities of HB equation (Eq. 2.6), Princen and Kiss equation (Eq. 2.10), and Seth et al. (2011) equation (Eq. 2.12). The Princen and Kiss equation and Seth et al. (2011) equation have no fitting parameters and eliminated the limitation of HB model, which has fitting parameters. The consistency index, k, in HB model equals $BG[\mu_c d_{32}/\Gamma]^{1/2}$ where B is a constant.

2.5 UNSOLVED ISSUES TO BE ADDRESSED

There are four main issues that have not been addressed in the literature about heavy O/W emulsion transportation. These issues are the main focus of this research.

A simple method of optimizing Heavy O/W emulsion physicochemical properties

A simple method of tuning the physicochemical properties of heavy O/W emulsions such as the interfacial tension, droplet size distribution, and average droplet size needs to be developed. Heavy O/W emulsions with optimized physicochemical properties that result in low viscosity need to be identified.

Application of existing rheology models for heavy O/W emulsions

One of the key questions in this study is whether Eqs. 2.5 and 2.7 can be used to accurately describe the rheological properties of moderate and concentrated dispersed phase heavy O/W emulsions.

Accurate rheological characterization of heavy O/W emulsions

Concentrated emulsions show very complex rheological properties that must be measured accurately using the right equipment and procedure. How the following variables affect the rheological properties of heavy O/W emulsions are investigated

1. Flow conduit dimensions (flow radius and length)
2. Flow types (drag flow and pressure driven flow)
3. Flow surface properties (smooth and rough)

Upscaling rheological properties of O/W emulsions to various flow conduit dimension

Some laboratory viscosity measurements seem to indicate that up to 75-85% heavy oil-in-water emulsions show low emulsion viscosity of <350 cP [Abdurahman et al. (2012); Hasan et al. (2010); Nuñez et al. (2000); Zaki (1997)]. However, transportation of 70% heavy oil Orimulsion ® in a pipeline showed apparent emulsion viscosity of ~2,000 cP which is six times the viscosity limit of most crude oil pipelines. Emergence of slip layer and/or lubrication layer appears to be the common explanation for the difference in the emulsion viscosity observed between laboratory measurements and pipeline scale operations. A systematic study of how heavy O/W emulsions slip, as well as development of an upscaling model which takes into account various rheological properties of heavy O/W emulsions is needed.

NOMENCLATURE

A Cross-sectional area of flow
φ Dispersed-phase volume fraction
n Flow behavior index
k Flow consistency index
Γ Interfacial tension
v_i Kinematic viscosity where $i = O, D, m$ represent oil, diluent, and mixture
φ_m Maximum close packing fraction possible for solid spheres
k Permeability
∇P Pressure gradient
d_{32} Sauter mean diameter
τ Shear stress
G Strain and frequency independent storage modulus
K Viscosity ratio of dispersed-phase to continuous-phase
μ_i Viscosity where $i = sus, d, c, emul$ represent suspension, dispersed, continuous, and emulsion
q Volumetric flow rate
τ_y Yield stress

ABBREVIATIONS

$CNEB$ Canadian national energy board
CSS Cyclic steam stimulation
EOR Enhanced oil recovery
$FERC$ Federal energy regulatory commission
HB Herschel-Bulkley
$HPAM$ Hydrolyzed polyacrylamide
HLB Hydrophilic lipophilic balance
IOC International oil company
NOC National oil company
O/W Oil-in-water
$OOIP$ Original oil in place
$SAGD$ Steam assisted gravity drainage
W/O Water-in-oil

Chapter 3: Preparation of Heavy Oil-in-Water Emulsions

3.1 INTRODUCTION

The focus of this chapter is the method used to prepare tailored stable, concentrated heavy oil-in-water (O/W) emulsions with low viscosity. Heavy oils mixed with just brine show a tendency to form viscous water-in-oil (W/O) emulsions because of the presence of hydrophobic polar molecules present in the oil such as asphaltenes and resins. Typically, the phases in the O/W emulsion separate within minutes if not seconds unless a surfactant is added or created by saponification to stabilize it. The emulsions must be stable for the duration of pipeline transport (residence time of days).

Many heavy oils and bitumen contain significant quantities of naphthenic acid components [Speight (2014)] Such oils can be reacted with an alkaline solution to generate soap and reduce interfacial tension. The quantity and type of soap are dependent on the composition of the heavy crude oil and the pH of the alkaline solution [Speight (2014)]. Alkali is used for this purpose in enhanced oil recovery (EOR) methods. The most common EOR process is to use alkali with a surfactant and a water-soluble polymer (ASP flooding). More recently, Fortenberry et al. (2013) found that heavy oil emulsions had a lower viscosity when co-solvents were used with the alkali instead of surfactants and this was advantageous, with respect to EOR. Fortenberry et al. (2013) used several novel co-solvents such as IBA-5EO and phenol-16EO.

Chapter 3 is based on a previously published article of the author. The author conducted all the experiments and wrote the journal article.
Nizamidin, N., Weerasooriya, U.P. and Pope, G.A., 2015. Systematic Study of Heavy Oil Emulsion Properties Optimized with a New Chemical Formulation Approach: Particle Size Distribution. Energy & Fuels, 29(11), pp.7065-7079.

These and other novel ethoxylated co-solvents used in this study to optimize heavy oil emulsions have shown superior performance, compared to conventional alcohol co-solvents [Fortenberry et al. (2013); Taghavifar (2014)]. One of the major advantages of these ethoxylated co-solvents is their ability to be easily tailored to the crude oil and brine by modifying the ethylene oxide (EO) number, which affects their hydrophilic-lipophilic balance.

Rheological scaling equations presented in Chapter 2 can be analyzed to quantify the effect of the physicochemical properties of emulsions on emulsion viscosity. For moderate dispersed-phase emulsions, Pal's model (Eq. 2.5) shows that only three parameter, continuous phase viscosity (μ_c), dispersed phase concentration (φ), and the maximum packing parameter of the dispersed phase (φ_m), control the viscosity of repulsive emulsions. Since the goal is to increase the oil concentration (dispersed-phase) in heavy oil emulsions, φ cannot be lowered. The continuous phase viscosity (μ_c) cannot be changed unless the pipeline operating temperature is increased or a liquid with a lower viscosity than water can be used for the continuous phase. Thus, the only parameter that can be realistically modified is φ_m.

For concentrated dispersed-phase emulsions, the Princen and Kiss equation (Eq. 2.7), modified with Mason's expression (Eq. 2.9), predicts that four additional parameters, yield stress (τ_y), shear rate ($\dot{\gamma}$), Sauter mean diameter (d_{32}), and interfacial tension (Γ), affect the emulsion viscosity. Table 3.1 shows the effect of each parameter on the emulsion viscosity and stability.

Table 3.1: Physicochemical properties of emulsions necessary for low emulsion viscosity

	Lower viscosity of moderate O/W emulsion (Eq. 2.5)	Lower viscosity of concentrated O/W emulsion (Eq. 2.7)	Better emulsion stability
$\boldsymbol{\varphi}$	↓	↓	
$\boldsymbol{\varphi_m}$	↑	↑	
$\boldsymbol{\mu_c}$	↓	↓	↑
$\dot{\boldsymbol{\gamma}}$		↑	
$\boldsymbol{\tau_y}$		↓	↑
$\boldsymbol{d_{32}}$		↑	↓
Γ		↓	

The yield stress, τ_y, can also be expressed as a function of other parameters [Princen and Kiss (1989)]:

$$\tau_y = \frac{2\Gamma}{d_{32}}\varphi^{\frac{1}{3}}Y(\varphi) \tag{3.1}$$

where $Y(\varphi)$ is an experimentally determined function that increase sharply as φ increass. To prepare concentrated emulsions with low viscosity, higher $\dot{\gamma}$, d_{32}, φ_m and lower Γ and μ_c are necessary. φ_m, Γ, and d_{32} of emulsions are three parameters that can be modified by tuning the chemical formulation used in the preparation of heavy O/W emulsions.

φ_m is a fitting parameter in Eq. (2.5). Its value ranged from 0.55-0.74 for the experimental data fit by Pal. When $\varphi << \varphi_m$, the viscosity of repulsive emulsions is Newtonian and insensitive to mean droplet size [Pal (2003), (2001), (2000b)], whereas when $\varphi > \varphi_m$, emulsion viscosity is shear-thinning and is dependent on d_{32} for unimodal emulsions [Foudazi et al. (2012); Malkin et al. (2004); Masalova et al. (2011); Nuñez et al. (2000); Pal (2006), (2000b), (1996)]. These observations are consistent with experimental data in the literature.

The change in the regime for unimodal emulsion rheological properties modeled by Eq. (2.5) and Eq. (2.7) occurs at φ of ~0.55-0.65 and this is also when the emulsions become more viscous and have non-Newtonian behavior such as yield stress and shear-

thinning behavior [Nuñez et al. (2000); Pal (2000b)]. The observed range of φ is close to φ_m for monodisperse hard sphere suspensions. The parameter φ_m is defined as the glass-transition point (φ_g = 0.58), the random loose packing point ($\varphi_{rlp} = 0.60$), or the random close packing point ($\varphi_{rcp} = 0.64$) for monodisperse spheres [Mewis and Wagner (2009)]. The term φ_g is used when a hard sphere is only able to relax within a cage formed by its nearest neighbors, thus limiting diffusion and flow [Sollich et al. (1997)]; φ_{rlp} is the packing volume fraction of uniform hard spheres packed in a random manner; and φ_{rcp} is the highest packing volume fraction of uniform hard spheres packed by the vibration method in a random manner. φ_m is a function of the particle size distribution of droplets/spheres. Larger φ_m values are obtained for polydisperse size distributions compared to narrow uniform size distributions.

Since the high viscosity, yield stress and shear-thinning behavior of concentrated emulsions are caused by increasing particle-to-particle interactions as the result of the deformation of the droplets when $\varphi > \varphi_m$, physicochemical properties of the emulsions can be tuned to mitigate the increase in viscosity of concentrated emulsions in two ways: (1) increase φ_m which keeps the dispersed-phase droplets from deforming and (2) if $\varphi > \varphi_m$, increase d_{32} and decrease Γ while maintaining emulsion stability.

One of the main objectives of this research was to prepare concentrated heavy O/W emulsions with low viscosity by optimizing the co-solvents, surfactants, alkali, and electrolytes with respect to the droplet size distribution. Núñez et al. (1996, 2005) described a two-step method of preparing two concentrated unimodal emulsions, one with smaller mean droplet diameter and one with larger droplet diameter, and then mixing the two emulsions at the optimum ratio to obtain concentrated bimodal emulsions of lower viscosity. Lower emulsion viscosities are achieved using this method because of the higher φ_m values of bimodal emulsions compared to unimodal emulsions. The

procedure used in this research offers the advantage of one-step preparation of concentrated low viscosity emulsions (multimodal droplet size distribution) with optimized chemical formulations, which requires only one mixing tank, whereas the two-step method requires three mixing tanks.

The φ_m value of the emulsions was calculated using the method of Farr and Groot (2009) to compare and contrast the effectiveness of the various chemical formulations used to prepare concentrated emulsions from a purely droplet size distribution point of view. Section 3.2 describes the chemicals, the concentrated emulsion preparation procedure, and the equipment and procedures used to measure and analyze particle size distributions, as well as the method used to measure oil rheological properties. Section 3.3 reviews the theories related to the mean diameter, standard deviation, and polydispersity of the particle size distribution and how they affect φ_m of concentrated emulsions. A literature review of experimental data of concentrated emulsions and the relationship between phase behavior studies of oil/surfactant/water systems and particle size distributions is presented. Section 3.4 discusses the results of the experiments based on the effects the chemical formulations have on d_{32} and φ_m, in terms of the heavy oils, co-solvents, alkali, electrolytes, and synthetic surfactants. Section 3.5 presents the conclusions of this study.

3.2 EXPERIMENTAL SECTION

3.2.1 Materials

The chemicals used in the preparation of heavy O/W emulsions are presented in this section.

3.2.1.1 Crude Oils.

Four heavy crude oils were used in this study. The properties of the oils are illustrated in Table 3.2. The crude oil samples are identified using the letters A, B, C, and D. The crude oils were selected to represent a broad range of viscosities from a variety of geological settings.

Table 3.2: Heavy Crude Oil Properties

	TotalC (A)	**Zuata (B)**	**PRB (C)**	**Ugnu (D)**
Origins	unknown	Venezuela	Canada	Alaska
Dynamic viscosity (mPa s) at 25ºC and 10 s^{-1}	310,000	93,000	62,500	9,000
Specific gravity at 25ºC	1.01	0.99	1.02	0.97
API gravity at 25ºC	8-9	10-11	7-8	14-15
Total acid number (mg KOH/g oil)	6.40±0.1	3.85±0.2		

The viscosities of the heavy crude oil samples, as a function of temperature, are shown in Fig. 3.1.

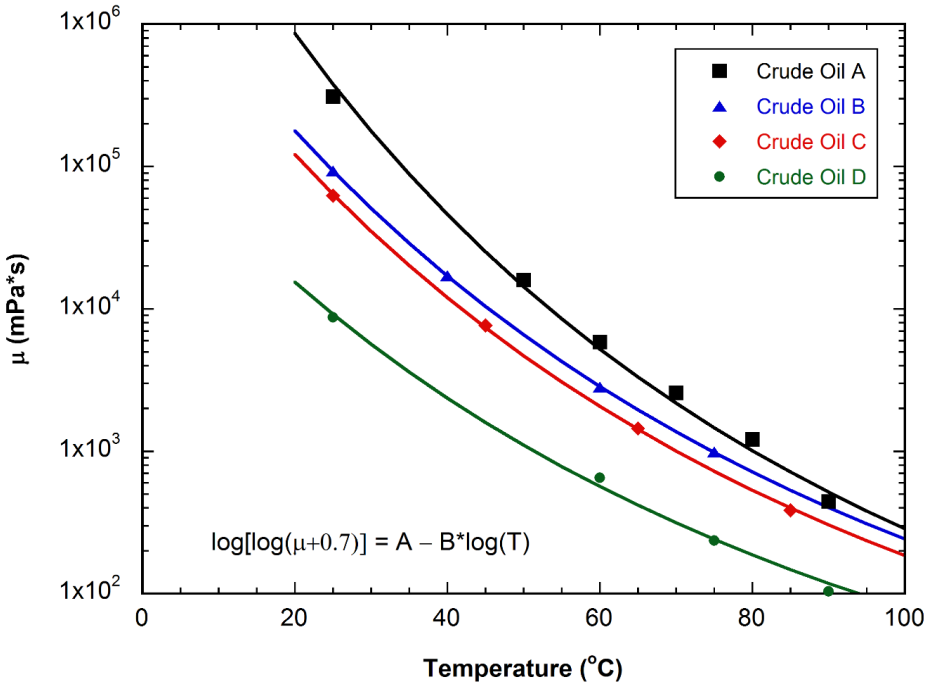

Fig. 3.1: Viscosity of four heavy crude oils at a shear rate of $10s^{-1}$. The lines represent the modified Walther equation

The viscosities of the heavy crude oils were measured using an advanced rheometric expansion system (ARES) (TA Instruments, Model LS-1). A cone-and- plate geometry was used to measure the heavy crude oil samples, because of the extremely high viscosity of the oils at low temperature, and the Couette geometry was used for high temperature. The modified Walther equation [Mehrotra et al. (1989)] fit the data better for all four heavy crude oil samples compared to power law or exponential fits. Table 3.3 shows the fitting parameters for the modified Walther equation for all four oils.

Table 3.3: Modified Walther equation fitting parameters for oils

Oil	Oil A	Oil B	Oil C	Oil D
A	9.786	8.786	8.955	9.058
B	3.653	3.269	3.344	3.277

3.2.1.2 Co-solvents and Surfactants.

A variety of co-solvents were tested. The co-solvents were ethoxylated isobutyl alcohol (IBA-nEO), triethylene glycol monobutyl ether (TEGBE), alkoxylated phenol (Ph-mPO-nEO), and ethoxylated diisopropylamine (DIPA-nEO). The chemical structures are shown in Fig. 3.2. The chemicals were obtained from Harcros Chemicals, Taminco, Aldrich Chemicals, and Huntsman Corporation.

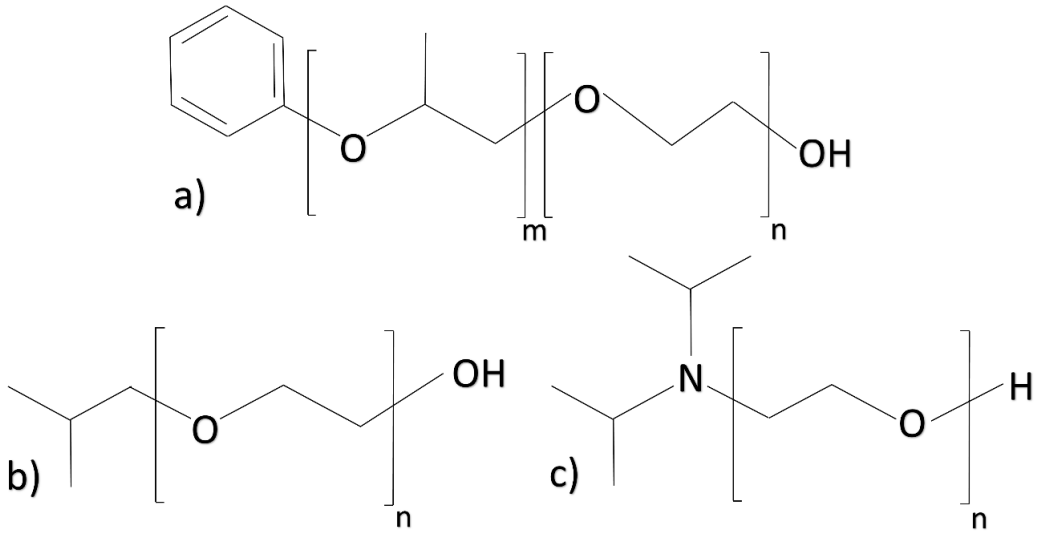

Fig. 3.2: Structures of (a) alkoxylated phenol (ph-mPO-nEO, (b) ethoxylated isobutyl alcohol (IBA-nEO), and (c) ethoxylated diisopropylamine (DIPA-nEO)

The most commonly used nonionic surfactant used to prepare heavy crude oil emulsions is nonylphenol-ethoxylate (NPE). In this study, it was used to prepare oil-in-water (O/W) emulsions as a reference point for the emulsion samples prepared using co-solvents. NPE was obtained from Harcros Chemicals.

3.2.1.3 Salts and Alkali.

Aqueous solutions of sodium hydroxide (NaOH), sodium carbonate (Na_2CO_3), and sodium metaborate ($NaBO_2$) were used to saponify the naphthenic acids and precursors in the heavy crude oils. Sodium chloride (NaCl) was used to adjust the salinity of the water. These chemicals were obtained from Fisher Scientific.

3.2.2 Preparation Procedure of Heavy Crude Oil-in-Water Emulsions

All emulsion samples were prepared using the following procedure unless otherwise noted.

1. The aqueous solution consisting of deionized water (DI), NaCl, co-solvents, alkali and surfactants is mixed at room temperature. All chemicals are measured and reported as a weight percent of the aqueous solution (w/w).
2. A mixture of the aqueous solution and a heavy crude oil is poured into a volumetric vial to prepare emulsions with different concentrations of oil (i.e., 20%, 40%, 60%, 80%, 85%, and 90%). The concentration of the crude oil in an emulsion is reported as a volume percent of the total volume of an emulsion at room temperature (v/v).
3. The mixture is sealed and placed in a 95-100^{o}C oven. No light end losses were observed.
4. After heating to the oven temperature, the sample is vigorously hand-shaken for 10 seconds every 30 minutes for several hours.
5. The sample is taken out of the oven and cooled down to a room temperature of 23^{o}C ±2^{o}C overnight before experiments are conducted.

The compositions of the emulsions are given in the figure descriptions. The droplet size distributions of all concentrated emulsions were best described by log-normal distributions. However, unlike the data reported in the literature, most of the concentrated emulsions formed polydisperse distributions that can be best described with bimodal or trimodal log-normal droplet size distributions, instead of narrow unimodal droplet size distributions. A likely explanation for the observed difference with the droplet size distribution of the emulsions, compared to those described in the literature, is the different method of concentrated emulsion preparation used in this study and the optimization of the chemical formulations. The high internal phase ratio (HIPR) method [Chirinos et al. (1990)] is a commonly used method of preparing concentrated emulsions

($\varphi > 0.7$). The HIPR method uses continuous low shear (10-100 s^{-1}) mixing for <5 min to create emulsions with a very narrow droplet size distribution at <60°C [Chirinos et al. (1990)]. These emulsions were prepared with brief, high shear (100-1,000 s^{-1}) vigorous hand mixing at a higher temperature of 95-100°C.

3.2.3 PARTICLE SIZE DISTRIBUTION

Two methods were used to ascertain the droplet particle size and shape of the emulsion samples.

3.2.3.1 Fluorescent Light Microscopy

A fluorescent light microscope (Zeiss Axiovert) was used to take photomicrographs of the emulsion samples. The samples were doped with a water-soluble fluorescent dye, fluorescein. Fluorescein has peak excitation at 494 nm and peak emission at 521 nm. Very low dye concentrations of fluorescein (10-20 ppm) were used to minimize the effects of dyes on emulsion properties. Borosilicate chambered coverglasses obtained from Thermo Scientific were used to contain the emulsion samples. The 63x oil immersion objective was used to take the photomicrographs. The photomicrographs provide visual evidence of the range of the emulsion droplet size for each sample.

3.2.3.2 Static Light Scattering

The particle size distribution of the emulsion samples were measured using static light scattering equipment (Malvern Mastersizer 2000 and 3000). After mixing the samples thoroughly, the emulsion samples were diluted to the necessary concentration using 0.2% NaOH and 0.1% NaCl solution. The alkali is necessary to maintain the pH and to keep the naphthenic acids deprotonated. All measurements were conducted under

ambient conditions. The theory proposed by Mie (1908) was used to calculate the oil droplet size distribution based on how light is scattered by the spherical particles.

Refractive indices of both dispersed and continuous phases were required for the application of Mie theory. The indices were measured using a refractometer. However, since heavy oils are opaque, refractive indices of pure heavy oils cannot be measured. Heavy oils were diluted with toluene at various volume fractions and the refractive indices of diluted oils were measured. Refractive indices of mixtures with up to 60% vol. oil were successfully measured with the refractometer. The refractive indices of pure heavy oils were estimated from the extrapolation of the refractive indices of mixtures using the Lorentz-Lorenz mixing rule [Yarranton et al. (2015)]. The refractive index of a fluid is defined using the function:

$$FRI = \frac{n_D^2 - 1}{n_D^2 + 2} \tag{3.2}$$

where n_D is the refractive index at the sodium D-line. The FRI mixture rule is used to estimate the FRI of pure oils [Evdokimov and Losev (2007); Taylor et al. (2001)].

$$FRI_{mix} = \varphi_{oil} FRI_{oil} + (1 - \varphi_{oil}) FRI_{toluene} \tag{3.3}$$

where φ is the volume fraction. Ideal mixing is assumed for the mixtures which while not true is accurate enough for the extrapolation [Yarranton et al. (2015)]. Fig. 3.3 shows the measured FRI_{mix} of the oil-toluene mixtures for all four oils.

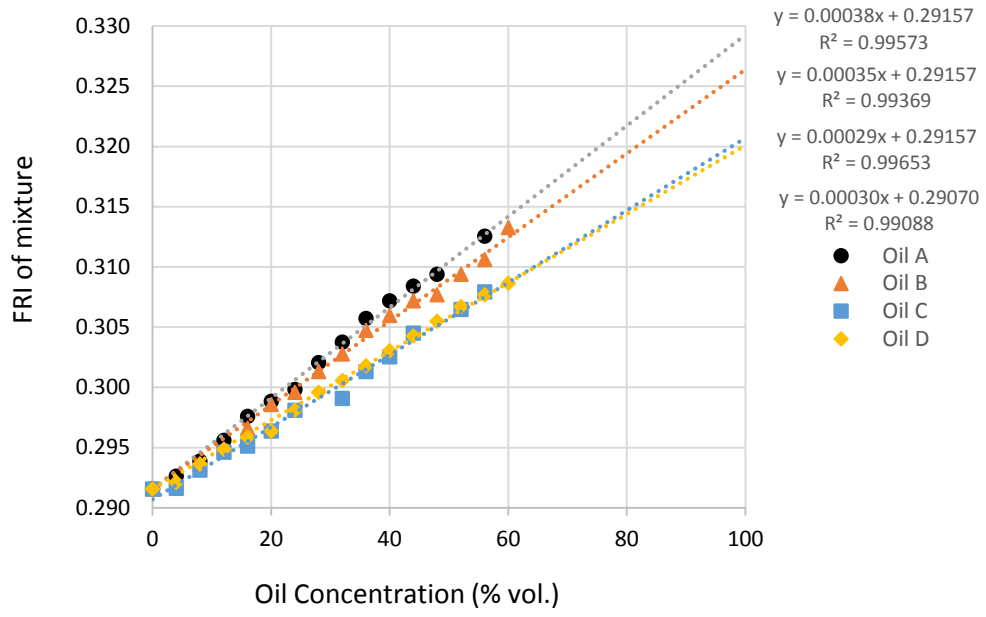

Fig. 3.3: FRI of oil-toluene mixtures vs. the oil concentration (vol. %)

For Mie theory, both real and imaginary refractive indices of the fluids are required ($n_{complex} = n_{real} - in_{imaginary}$). The n_{real} is the refractive index n_D measured while $n_{imaginary}$ represents the absorption of light by opaque liquids. The $n_{imaginary}$ of the heavy oils were estimated according to the user's manual of Malvern Mastersizer 3000. $n_{imaginary}$ values of oils can be estimated by matching the volume fraction of oil droplets measured using Mastersizer 3000 and the known volume fraction of oil droplets by varying the $n_{imaginary}$ value in the equipment software. Table 3.4 shows the estimated refractive indices of the liquids at standard room temperature of 22 ºC ±1.

Table 3.4: Real and imaginary refractive indices of four heavy oils and toluene

	n_{real}	$n_{imaginary}$
Oil A	1.5745	0.003
Oil B	1.5685	0.003
Oil C	1.5555	0.003
Oil D	1.5548	0.003
Toluene	1.4949	0
Dilution water	1.33	0

The n_D values of all four heavy oils varied from 1.555-1.57 which matched the refractive index values reported in the literature for heavy oils and bitumen of similar densities [Evdokimov and Losev (2007); Taylor et al. (2001)]. The $n_{imaginary}$ values for all oils were ~0.003.

Since such low concentrations of diluted emulsions (0.01-0.05 vol%) are required to accurately measure the particle size distribution, the Mastersizer 3000 accessory with a sample volume of 600 mL was used. The large volume accessory necessitates a larger quantity of concentrated emulsion samples to be diluted, resulting in a more accurate representation of the particle size distribution of the entire samples in case of sample inhomogeneity. The samples were mix at 1,500-2,000 rpm during the particle size measurements to assure that droplets were fully separated from any aggregating structures caused by droplet-droplet interactions.

To calculate the φ_m value of emulsions, the droplet size distributions must be accurately fitted to a distribution model. Emulsion droplet size distributions can be modeled accurately by a log-normal distribution for unimodal distributions and a combination of log-normal distributions for multimodal distributions:

$$fv(d;\ \mu,\sigma) = \prod_1^n \left[f_n \left(\frac{1}{d\sigma_n\sqrt{2\pi}} e^{-(ln[d]-\mu_n)^2/2{\sigma_n}^2} \right) \right], \tag{3.4}$$

where f_v is the probability density function of volume, n the number of peaks in the distribution, d the diameter of droplets, σ the natural logarithm standard deviation of the droplet diameters, μ the natural logarithm of the mean of the droplet diameters, and f the volume fraction of a peak in the distribution over the entire droplet volume $\varphi_n/\sum_1^n \varphi_n$. The droplet size distributions are fitted to the log-normal probability density function of volume with the least-square method weighted toward larger diameters, since the larger droplets contribute significantly more to the volume fraction of the droplets.

A closed analytical equation that calculates the φ_m value of spheres modeled by a unimodal log-normal distribution has recently been derived by Brouwers (2014). However, the equation cannot handle a multimodal log-normal distribution and the authors have no knowledge of an analytical equation that is capable of calculating the random close packing fraction of spheres with a bimodal lognormal distribution. The only method of calculating the φ_m value of polydisperse spheres is to directly simulate the packing of spheres using numerical simulations. Farr and Groot (2009) used a fast one-dimensional (1D) algorithm for accurately estimating the φ_m value of polydisperse hard spheres and compared it to the more computationally expensive 3D algorithms with favorable results [Hopkins et al. (2013); Spangenberg et al. (2014)]. The Farr and Groot algorithm was used to estimate the φ_m value of concentrated emulsions in this paper from the log-normal distribution model parameters. Note that we estimated φ_m from the φ_{rcp} of the droplet size distribution, since the φ_{rcp} can be estimated relatively easily for polydisperse emulsions. While we do not claim that φ_{rcp} represents φ_m better than φ_g or φ_{rlp}, Spangenberg et al. (2014) showed that φ_m=~0.93±0.005 φ_{rcp} in Eq. (3.1) gave the best fit of experimental data from the literature. Note that, for the sake of simplicity, we assumed that φ_m= φ_{rcp}.

3.3 THEORY

The theory section is divided into three main parts: (1) parameters that influence the φ_m value of spherical droplets; (2) literature review of experimental results of concentrated bimodal emulsions of varying d_L/d_S and $\varphi_s/(\varphi_s + \varphi_L)$ on the emulsion rheology; and (3) phase behavior study of oil/surfactant/brine mixtures and particle size distribution.

3.3.1 Parameters that Influence the φ_m Value of Spherical Droplets

The goal of this study was to ascertain the optimal droplet size distribution of emulsions that results in large φ_m values.

The φ_m value of monodisperse hard spheres is dependent on the method of packing, random (φ_{rlp}=0.60 or φ_{rcp}=0.64) or ordered (~0.74). The value of φ_m= ~0.58-0.64 is exactly the range of φ observed with emulsions where the emulsion viscosity starts to increase dramatically for narrow unimodal emulsions [Nuñez et al. (2000); Pal (2000b)], suggesting emulsion rheology is best described by random packing of droplets [Spangenberg et al. (2014)]. How do polydisperse hard spheres pack?

Two parameters affect the packing fraction of binary solid spheres where two monodisperse spheres of varying sizes are mixed in varying ratios. The variables are the sphere diameter ratio (d_L/d_S), where d is the sphere diameter and the subscripts "S" and "L" respectively correspond to the small and large component of the binary mixture and the volume fraction of the small monodisperse spheres, with respect to the total monodisperse sphere volume ($\varphi_s/(\varphi_s + \varphi_L)$). Furnas (1928) introduced the concept of saturated, noninteracting binary monodisperse spheres, which is defined as the smaller spheres filling the void created by the larger spheres without affecting the packing of the larger spheres, expressed as $d_L/d_S=\infty$ and $\varphi_s/(\varphi_s + \varphi_L)$=0.36 (Fig. 3.4).

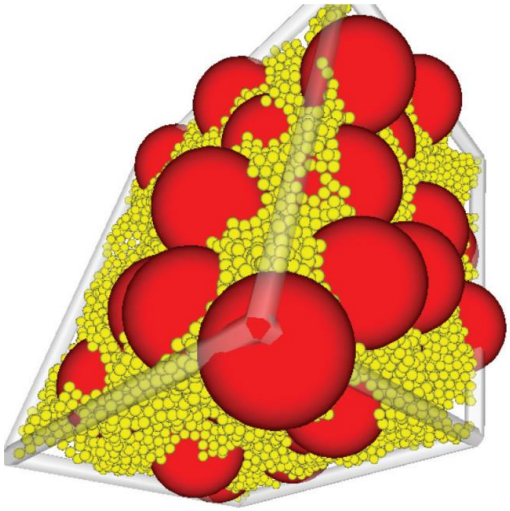

Fig. 3.4: Depiction of binary sphere packing, $\varphi = 0.83$. Obtained from Hopkins et al. (2013).

Brouwers (2014) summarized Furnas' observations and concluded that the φ_m value of combined mixtures of saturated noninteracting monodisperse spheres can be described by Eq. (3.5):

$$\varphi_n^{sat} = 1 - (1 - \varphi_{rcp})^n \,, \tag{3.5}$$

where n is the number of noninteracting monodisperse size groups, φ_n^{sat} the φ_m value of saturated noninteracting spheres of n monodisperse size groups, and φ_{rcp} the random close packing fraction of monodisperse spheres (~0.64). For a binary mixture of saturated noninteracting monodisperse spheres where n=2 and 3, the theoretical value of φ_2^{sat} = ~0.87 and φ_3^{sat} = ~0.95. Experiments have revealed that noninteracting binary monodisperse spheres are approximated when d_L/d_S is >7-10, since realistic experimental emulsion samples with $d_L/d_S=\infty$ are not possible [Furnas (1928); McGeary (1961)]. Recent numerical simulation studies by Hopkins et al. (2013) show that, for d_L/d_S=3-10, the maximum packing density is observed at $\varphi_s/(\varphi_s + \varphi_L)$=~0.20-0.25.

The φ_m value of theoretical unimodal log-normal distributions estimated using the Farr and Groot model, as a function of the standard deviation, is depicted in Fig. 3.5 to show how the standard deviation affects the φ_m.

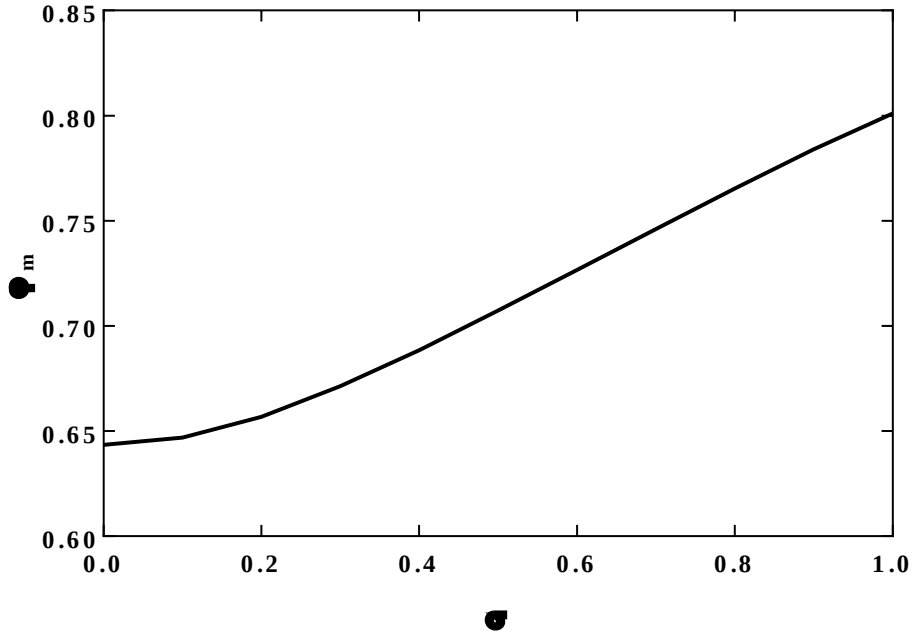

Fig. 3.5: φ_m of an unimodal lognormal distribution vs. σ. σ is the natural logarithm standard deviation in Eq. 3.4.

Polydisperse emulsions showed standard deviations in the range of 0.4-1. The benefit of emulsions with a higher standard deviation of the particle size distribution becomes apparent when Eq. (3.5) is modified to include the effect of standard deviation on the φ_m value of emulsions:

$$\varphi_n^{sat} = 1 - \prod_1^n (1 - \varphi_{m,n}) \ , \qquad (3.6)$$

where n is the number of noninteracting unimodal groups, φ_n^{sat} the φ_m of saturated noninteracting spheres of n unimodal size groups, and $\varphi_{m,n}$ the φ_m of individual unimodal groups estimated based on the standard deviation. Table 3.5 shows the φ_n^{sat} as

a function of σ_L, σ_M, and σ_S for theoretical noninteracting saturated spheres. Very broad bimodal emulsions can have even higher φ_n^{sat} value than narrow trimodal emulsions.

Table 3.5: Saturated noninteracting φ_n^{sat} estimated as a function of standard deviation using the Groot and Farr model (Assumed $\sigma_L = \sigma_M = \sigma_S$)

σ	Unimodal, φ_1^{sat}	Bimodal, φ_2^{sat}	Trimodal, φ_3^{sat}
0	0.64	0.87	0.96
0.1	0.65	0.88	0.97
0.5	0.71	0.91	0.98
1.0	0.80	0.96	0.99

3.3.2 Literature Review of Experimental Data of Concentrated Bimodal Emulsions

The rheological benefits of increasing the φ_m value of concentrated emulsions by preparing mixtures of two narrow unimodal emulsions of varying mean diameter have been explored extensively [Foudazi et al. (2012); Nuñez et al. (2000); Otsubo and Prud'homme (1994); Pal (2006), (1996); Romero et al. (2002)]. This is the commonly used two-step method of preparing concentrated bimodal emulsions with lower viscosity compared to concentrated unimodal emulsions (Fig. 3.6).

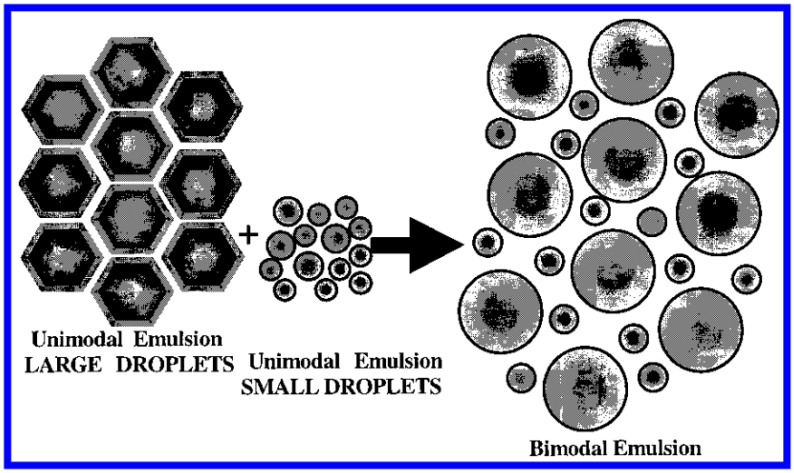

Fig. 3.6: Schematic representation of the formation of a bimodal emulsion from the two-step method of preparing 2 unimodal emulsions and mixing them. Obtained from Nuñez et al. (2000)

Narrow unimodal concentrated emulsions of varying d_{32} were prepared using the "High Internal Phase Ratio" (HIPR) method developed by Chirinos et al. (1990) and mixtures of d_L/d_S = 1.5-15 with $\varphi_s/(\varphi_s + \varphi_L)$ = 0-1 were prepared and tested in the literature [Nuñez et al. (2000); Pal (2006), (1996)]. A summary of the literature data is displayed in Table 3.6.

Table 3.6: Bimodal emulsions are prepared by mixing unimodal emulsions of varying $d_{0.5}$ at various volume fractions in the literature. [a]Parameters d_L, d_S, φ, experimental optimum $\varphi_S/(\varphi_L + \varphi_S)$, and μ are reported in the literature. φ_m and calculated optimum $\varphi_S/(\varphi_L + \varphi_S)$ are estimated using the Farr and Groot model with standard deviation of σ_L=σ_S=0.3. [b]Obtained at a shear stress of 0.9 Pa. [c]Obtained at a shear rate of 10 s^{-1}

Surfactants	$d_{0.5}$ (um)	d_L/d_S	φ	φ_m	$\varphi_{optimum} = \varphi_s/(\varphi_s + \varphi_L)$			μ (mPa·s) at 20 s^{-1}	Ref.
					Range tested	Experimental optimum	Calculated optimum		
Dispersed Phase: Mineral Oil; Continuous Phase: Water									
Octylphenol ethoxylate (10EO)	d_L = 1.95 d_S = 1.28	1.50	0.94	~0.68	0-1.00	0	~0.35-0.50	$\mu_L = \mu_{optimum}$	Pal (2006)
Dispersed Phase: Light Crude Oil; Continuous Phase: Water									
Octylphenol ethoxylate (10EO)	d_L = 18 d_S = 5	3.60	0.75	~0.76	0-1.00	~0.36	~0.20-0.35	μ_L=~1,500[b] μ_S=>10,000,000[b] $\mu_{optimum}$=~100[b]	Pal (1996)
Dispersed Phase: Heavy Crude Oil; Continuous Phase: Water									
Nonylphenol ethoxylate (17.5EO)	d_L = 20 d_S = 4	5.00	0.70	~0.80	0-1.00	0.25-0.30	~0.20-0.30	μ_L=~1,000 $\mu_{optimum}$=~100	Nuñez et al. (2000)
	d_L =20 d_S = 2	10.00	0.70	~0.85	0-1.00	0.25-0.30	~0.20-0.30	μ_L=~1,000 μ_S=~4,000 $\mu_{optimum}$=~70	Nuñez et al. (2000)
	d_L = 30 d_S = 2	15.00	0.70	~0.86	0-1.00	0.25-0.30	~0.20-0.30	μ_L=~550 μ_S=~4,000 $\mu_{optimum}$=~30	Nuñez et al. (2000)
	d_L = 20 d_S = 2	10.00	0.80	~0.85	0-1.00	0.25-0.30	~0.20-0.30	μ_L=~2,200 μ_S>7,000 $\mu_{optimum}$=~900	Nuñez et al. (2000)
	d_L = 30 d_S = 2	15.00	0.80	~0.86	0-1.00	0.25-0.30	~0.20-0.30	μ_L=~1,400 μ_S>7,000 $\mu_{optimum}$=~500	Nuñez et al. (2000)
Dispersed Phase: Saturated Solution of NH_4NO_3 in Water; Continuous Phase: Hydrocarbon Oil									
PIBSA-Urea	d_L = 16.9 d_S = 8.2	2	0.85	~0.71	0-1.00	0	~0.20-0.40	μ_L=~4,000[c] μ_S>10,500[c] $\mu_{optimum}$=μ_L	Foudazi et al. (2012)
	d_L = 16.9 d_S = 5.6	3	0.85	~0.74	0-1.00	0	~0.20-0.30	μ_L=~4,000[c] μ_S>19,000[c] $\mu_{optimum}$=μ_L	Foudazi et al. (2012)
	d_L = 16.9 d_S = 2.7	6	0.85	~0.83	0-1.00	0.15-0.20	~0.20-0.30	μ_L=~4,000[c] μ_S>57,000[c] $\mu_{optimum}$=~2,800[c]	Foudazi et al. (2012)

Fig. 3.7 shows the estimated φ_m and theoretical optimum $\varphi_s/(\varphi_s + \varphi_L)$ values calculated using the Farr and Groot model, assuming standard deviations of σ_L=σ_S=0.3 for the d_L/d_S in Table 3.6.

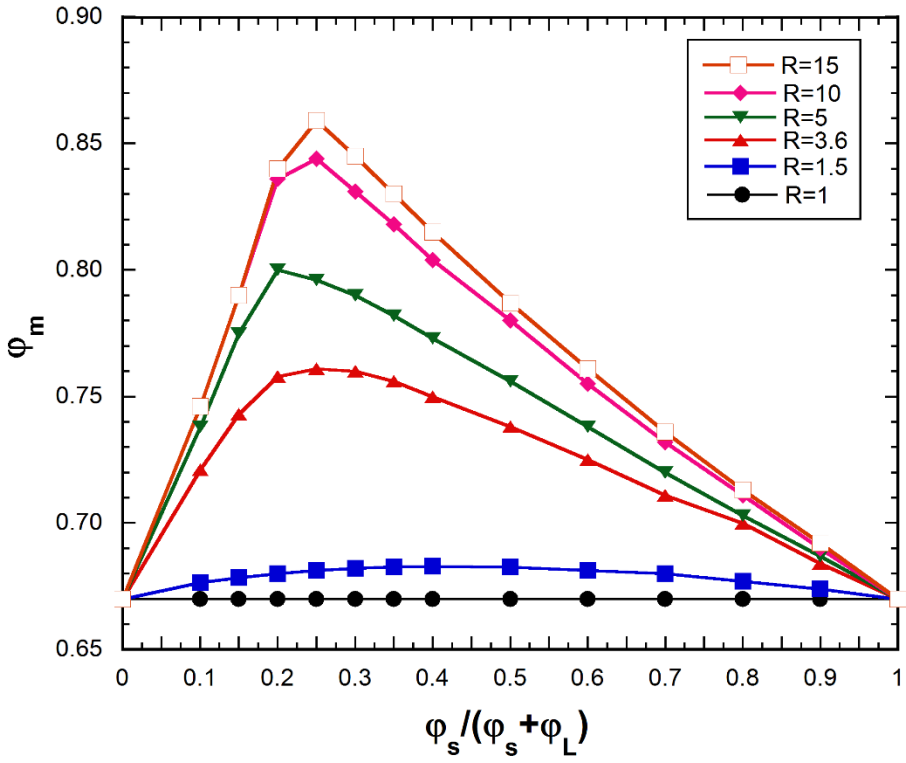

Fig. 3.7: The φ_m binary log-normal distribution, as a function of theoretical ratio $R=d_L/d_S$ and $\varphi_S/(\varphi_L + \varphi_S)$. A value of $\sigma_{S=}$ σ_L=0.3 used in the Farr and Groot model to calculate the points. The lines are in place only to guide the eyes.

Table 3.6 shows that a concentrated bimodal emulsion with d_L/d_S = 1.5 did not lower the emulsion viscosity, compared to the unimodal emulsion with d_L [Pal (2006)]. Fig. 3.7 supports this finding by showing that the φ_m value only increases by 0.01 for d_L/d_S = 1.5 compared to d_L/d_S = 1. A value of d_L/d_S = 3.6 showed a 15-fold reduction in emulsion viscosity at the optimum $\varphi_s/(\varphi_s + \varphi_L)$ value of 0.36, compared to the unimodal emulsion of the large component at τ=0.9 Pa, but no minimum in emulsion viscosity was observed at τ=30 Pa [Pal (1996)]. Fig. 3.7 supports this finding by

showing that the φ_m value increases by 0.09 for d_L/d_S = 3.6 compared to d_L/d_S = 1. For φ=0.7, as the value of d_L/d_S increased from 5 to 10, the emulsion viscosity decreased from 100 mPa·s to 70 mPa·s at the optimum $\varphi_s/(\varphi_s + \varphi_L)$, which can be explained by the increase in φ_m, from ~0.8 to ~0.85 (see Fig. 3.7), compared to the unimodal coarse emulsion viscosity of 1,000 mPa·s [Nuñez et al. (2000)]. When the value of d_L/d_S increased from 10 to 15 the emulsion viscosity decreased from 70 mPa·s to 30 mPa·s, while the value of φ_m only increased from ~0.85 to ~0.86 (See Fig. 3.7); thus, the decrease in the viscosity can be attributed mainly to the increase in d_L from 20 μm from 30 μm [Nuñez et al. (2000)]. The effect of emulsion mean diameter was observed as the unimodal emulsion viscosity decreased from ~4,000 mPa·s to 550 mPa·s when the mean diameter increased from 2 μm to 30 μm for φ=0.7. Foudazi et al. (2012) also observed similar effects of d_L/d_S and $\varphi_s/(\varphi_s + \varphi_L)$ on emulsion viscosity for water-in-oil (W/O) emulsions of φ=0.85. The experimental data in Table 3.6 show that, when $\varphi > \varphi_m$ for bimodal emulsions, larger d_L/d_S values, larger d_{32} values, and optimum $\varphi_s/(\varphi_s + \varphi_L)$ significantly lowered the emulsion viscosity of bimodal emulsions, compared to unimodal emulsions of the same φ. The experimental findings are in agreement with the trends observed in Table 3.1 from Eq. 2.7.

Shewan and Stokes (2015) used Eq. (2.5) to calculate the hard sphere suspension viscosity for a range of materials, fluids, and φ from the data available in the literature, as well as their own experiments. The value of φ_m was estimated using the Farr and Groot model, instead of being a fitting parameter from the particle size distribution of both monodisperse and bimodal suspensions of d_{43} = 0.3-250 μm, d_L/d_S = 0.002-7, and $\varphi_s/(\varphi_s + \varphi_L)$ = 0-1, and the data collapsed into one curve when the relationship of $\mu_r \; vs. \; \varphi/\varphi_m$ was plotted [Shewan and Stokes (2015)]. Calculating the φ_m value of colloidal suspensions from the droplet size distribution and incorporating it into Eq. (2.5)

appeared to accurately describe the effects of the droplet size distribution on the hard sphere packing viscosity when $\varphi < \varphi_m$ and in the presence of purely repulsive interdroplet interactions.

High φ_m values are obtained for multimodal emulsions with high d_L/d_S values at optimum $\varphi_s/(\varphi_s + \varphi_L) = 0.2 - 0.3$. How can heavy O/W emulsions with such physicochemical properties be prepared with a simple one-step mixing procedure?

3.3.3 Phase Behavior Study of Oil/Surfactant/Brine Mixtures and Particle Size Distribution

The composition of the chemical formulations used to prepare O/W emulsions influences the particle size distribution as well as d_{32}. Phase behavior studies of oil/surfactant/brine mixtures are often performed to test surfactants in chemical EOR research to identify ultra-low interfacial tension at the desired electrolyte concentration and temperature [Flaaten et al. (2009); Levitt et al. (2009); Lu et al. (2014); Taghavifar (2014)]. Baldauf et al. (1982) conducted phase behavior experiments to study the relationship between microemulsions and concentrated macroemulsions. The optimum condition of a Winsor type III bicontinuous microemulsion is defined as the point where the interfacial tension is equal at the oil/microemulsion interface and the water/microemulsion interface (Fig. 3.8). Observations show that, under these same conditions, the volumes of water and oil solubilized in the microemulsion are also equal and the coalescence rate is a maximum [Bourrel et al. (1979)].

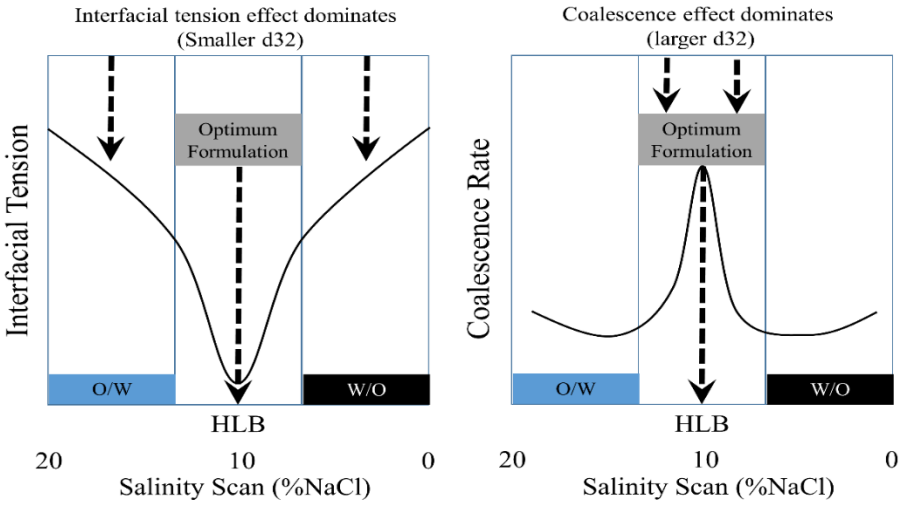

Fig. 3.8: Interfacial tension (left) and coalescence rate (right) of emulsions. Modified from Perez et al. (2002)

A minimum in the average droplet diameter was found near but not at the optimum condition for some emulsions [Perez et al. (2002); Salager et al. (1996); Tolosa et al. (2006)]. Tolosa et al. (2006) showed in Fig. 3.9 that this minimum in average droplet size is only found when co-solvent is added to the chemical formulation to increase the coalescence rate. Co-solvents change the interfacial properties of the micelles by disrupting the ordered packing of surfactant molecules, resulting in a more fluid interface and lower interfacial viscosity [Taghavifar (2014)]. Thus, the time needed for crude oil/surfactant/brine mixtures to reach thermodynamic equilibrium decreases dramatically when co-solvent is added to the mixture (higher coalescence rate). Without co-solvents in the chemical formulation, no minimum in droplet diameter was observe at the formulation approached optimum salinity/condition.

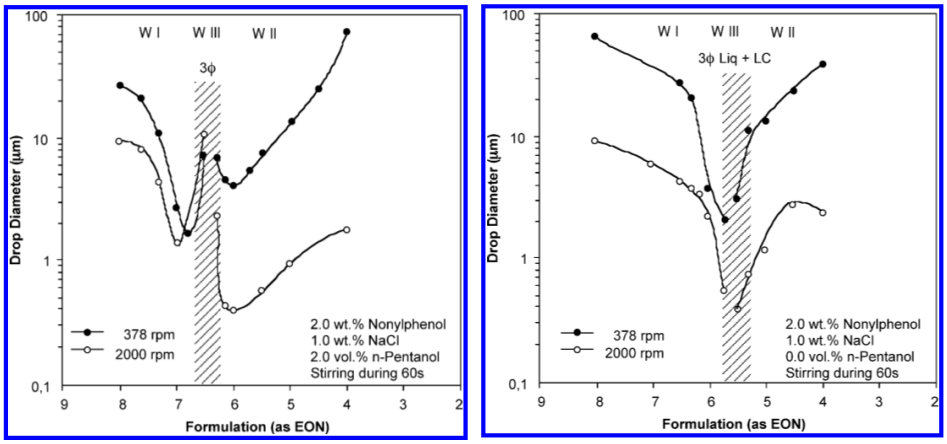

Fig. 3.9: Average droplet diameter of two emulsions prepared with (left) and without (right) co-solvent (n-Pentanol). Figures obtained from Tolosa et al. (2006)

Perez et al. (2002) observed that, along with minimum in average particle diameter, a bimodal droplet size distribution formed a small distance from the optimum conditions when alcohol was used with a surfactant. dos Santos et al. (2011) also recently reported that the addition of light/medium alcohol co-solvents to surfactants resulted in a bimodal distribution of emulsion droplets. Thus, to form concentrated emulsions with high φ_m, emulsions should be prepared with optimized chemical formulations containing a co-solvent near the optimum conditions. We expanded upon the observations of both Perez et al. (2002) and dos Santos et al. (2011) and quantified the effects of co-solvent, surfactant, electrolyte, and crude oil on the particle size distribution, represented by φ_m, with a simplified one-step mixing process instead of mixing multiple unimodal emulsions of varying d_{32} and combining them at an optimal ratio to generate bimodal/trimodal emulsions. The characterization of multimodal concentrated emulsions in terms of φ_m when prepared with the one-step chemical formulation approach similar to chemical EOR phase behavior scans, has not previously been published .

3.4 RESULTS AND DISCUSSIONS

Photomicrographs of two 80% Oil D emulsions as wells as the particle size distributions of the two emulsions are shown in Fig. 3.10.

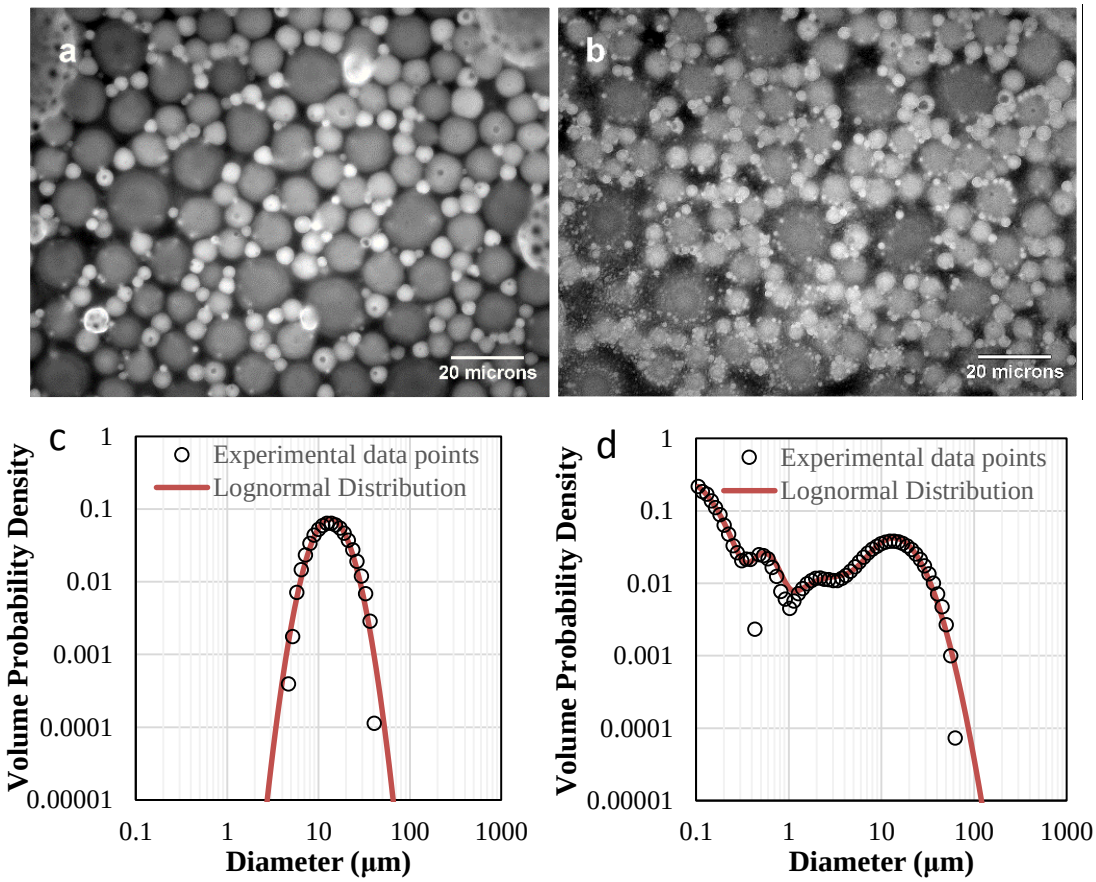

Fig. 3.10: Photomicrographs of 80% Oil D emulsions: (a) d_{32}=14.4 µm, φ_m=0.68, and aqueous composition (1.6% Ph15EO, 0.2% NaOH, 0% NaCl); (b) d_{32}=14.1 µm, φ_m=0.78, and aqueous composition (1.6% Ph15EO, 0.2% NaOH, 1% NaCl). Volume probability density function of the emulsion samples measured with the static light scattering equipment: (c) Emulsion sample from Fig. 3.10a; (d) Emulsion sample from Fig. 3.10b

The only difference between the two emulsions is the NaCl concentration of 0% and 1%. The photomicrograph of the emulsion sample with 0% NaCl (Fig. 3.10a), showed a unimodal droplet size distribution and spherical droplet shapes with the bigger droplets, showing a slight deformation under static conditions, reflected by a low φ_m value

(φ_m=0.68). The photomicrograph of the emulsion sample with 1% NaCl (Fig. 3.10b), showed a multimodal droplet size distribution with no observable deformation of the droplets, reflected by a higher φ_m value (φ_m =0.78). Fig. 3.10b shows that the smaller droplets surround the bigger droplets. We have observed that emulsion samples with φ_m>0.75 do not cause significant deformation of the oil droplets under static conditions when φ=0.8. Visual inspection of the emulsion droplet size distributions from the photomicrographs (Fig. 3.10a-b) agrees with the droplet size distribution measurements from the Malvern Mastersizer 2000/3000 (Fig. 3.10c-d).

3.4.1 Effect of Mixing Conditions (mixing speed, frequency, and temperature)

The conditions that we used to prepare the emulsions were varied to observe the effects of mixing temperature, speed, and duration on the particle size distributions. The modified capillary number (Ca) has been shown to control the mechanism of droplet breakup and droplet diameter for concentrated emulsions [Jansen et al. (2001)].

$$Ca = \mu_{emul}\dot{\gamma}R/\Gamma \qquad (3.7)$$

where μ_{emul} is the viscosity of the emulsion at the mixing shear rate, $\dot{\gamma}$ the shear rate of mixing, R the radius of droplets, and Γ the interfacial tension. The Grace Curve and the concept of a critical capillary number ($Ca_{critical}$) vs $\lambda=\mu_d/\mu_{emulsion}$ has been used to accurately predict if droplets in a concentrated emulsion will break apart into smaller droplets or not [Grace (1982); Jansen et al. (2001)]. If $Ca_{critical}$ is above the Grace Curve, the droplet will break apart into smaller droplets and a new, smaller $Ca_{critical}$ value is obtained because of a smaller droplet radius.

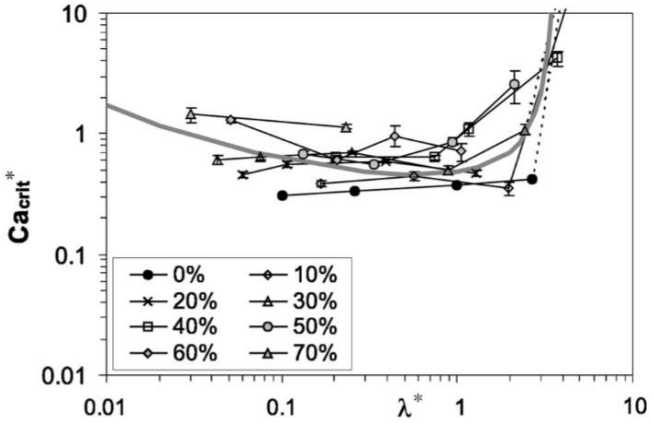

Fig. 3.11: Ca_{crit} vs. the λ for emulsions of varying dispersed phase concentration. The grey solid line is the Grace curve. Obtained from Jansen et al. (2001)

The key limitation of the Grace Curve and $Ca_{critical}$ is the assumption of a very slow coalescence rate. Average droplet diameters from Fig. 3.9 with no co-solvent (right) are accurately described with Fig. 3.11 but not Fig. 3.9 with co-solvent (left) because of fast coalescence rate. Table 3.7 is created according to Eq. 3.7 which shows how the mixing conditions affect Ca and λ.

Table 3.7: How the mixing conditions affect the Ca and λ assuming constant R

	μ_{emul}	$\dot{\gamma}$	Γ	μ_d	Ca	λ
Higher Mixing Temperature	↓	?	↓	↓	?	?
Higher Mixing Speed (rpm)	↓	↑	N/A	N/A	↑	↓
Higher Mixing frequency (min/mix)	N/A	N/A	N/A	N/A	N/A	N/A

Mixing Speed

While not the focus of this dissertation, we conducted a brief study of mixing speed on the particle size distribution of concentrated emulsions. Data in the literature [Ahmed et al. (1999b); Jansen et al. (2001); Perez et al. (2002); Tolosa et al. (2006)] agree that higher mixing speed always results in a smaller average droplet diameter as

well as the analysis in Table 3.7. The capillary number analysis showed that, with the shear-thinning behavior of a concentrated emulsion viscosity (n=0.5) [Foudazi et al. (2012); Meeker et al. (2004); Seth et al. (2011)], a 2-orders-of-magnitude change in $\dot{\gamma}$ (1-100 s^{-1}) resulted in only a 1-order-of-magnitude change in Ca (Ca($\dot{\gamma}$=100s^{-1})/Ca($\dot{\gamma}$=1s^{-1}) = ~10) and a 1-order-of-magnitude changed in λ (λ ($\dot{\gamma}$=100s^{-1})/ λ ($\dot{\gamma}$=1s^{-1}) = ~10). The effect of $\dot{\gamma}$ on d_{32} is dampened because of the shear-thinning behavior of concentrated emulsions.

Mixing Temperature

Fig. 3.12 depicts the effects of mixing temperature on the φ_m and d_{32} values of 80% Oil B emulsions with two different chemical formulations.

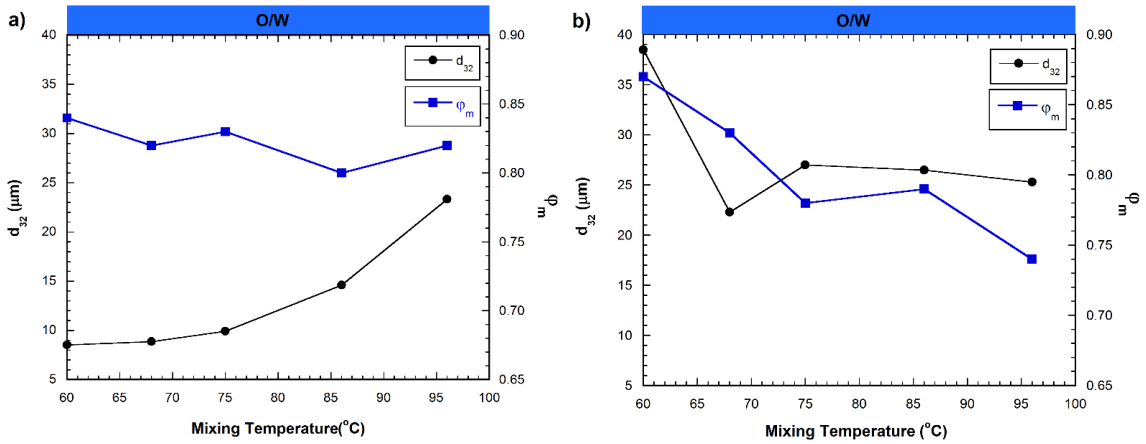

Fig. 3.12: (a) d_{32} of the entire lognormal distribution (primary axis) and φ_m (secondary axis) of emulsions made from 80% oil B and 20% aqueous solution (0.4% NaCl and 0.2% NaOH) vs the mixing temperature of the samples hand-shaken for 10 s every 30 min for 4 h. (b) d_{32} of the entire lognormal distribution (primary axis) and φ_m (secondary axis) of emulsions made from 80% oil B and 20% aqueous solution (1.6% phenol-15EO, 0.4% NaCl and 0.2% NaOH) vs the mixing temperature of the samples hand-shaken for 10 s every 30 min for 4 h. O/W stands for oil-in-water emulsions, and pH =9.14-9.16. In both panels, the lines are present only to guide the eyes.

While the mixing temperature and speed significantly impacts d_{32} as other researchers have noted, we also observed that the addition of co-solvent influenced how the mixing conditions affected d_{32} as well as φ_m. In Fig. 3.12a, the φ_m value of the emulsions prepared without co-solvent showed no dependence on the mixing temperature within the experimental uncertainty for the range of temperatures tested. The d_{32} value of the emulsions increased as the mixing temperature increased. In Fig. 3.12b, the emulsions with co-solvent showed a decreasing trend of φ_m from 0.87 to 0.74 and a decreasing trend of d_{32} from 38.5 to 25 μm with increasing mixing temperature. The change in d_{32} cannot be explained with only the capillary number concept, because of the change in φ_m, which indicates change in the coalescence rate. The samples prepared at 60-68°C with co-solvents showed the lowest viscosity based on visual observations, which can be explained by the highest φ_m and d_{32} values.

The change in d_{32} and φ_m with mixing temperature (Fig. 3.12b) is also caused by the change in the interfacial properties of the emulsions, depending on EO number of the co-solvents. Ethoxylated co-solvents are less hydrophilic at high temperature. For example, the water solubility of phenol-15EO co-solvent decreases as the temperature increases, because of decreasing interaction between the EO chain and water molecules at higher temperature. This behavior of ethoxylated co-solvents is very similar to the temperature sensitive interfacial tensions property of nonionic surfactants. It also means that at higher mixing temperature, the interfacial tension of O/W emulsions with co-solvents are lower compared to the lower transport/test temperature (room temperature). Thus, it is extremely difficult to predict how mixing temperature affect the droplet size distribution of concentrated emulsions prepared with optimized chemical formulation. All emulsion samples in Fig. 3.12 were best modeled by bimodal/trimodal log-normal distributions.

Mixing Frequency

We explored the effects of the frequency of mixing on the parameters φ_m and d_{32} of emulsions, as illustrated in Fig. 3.13.

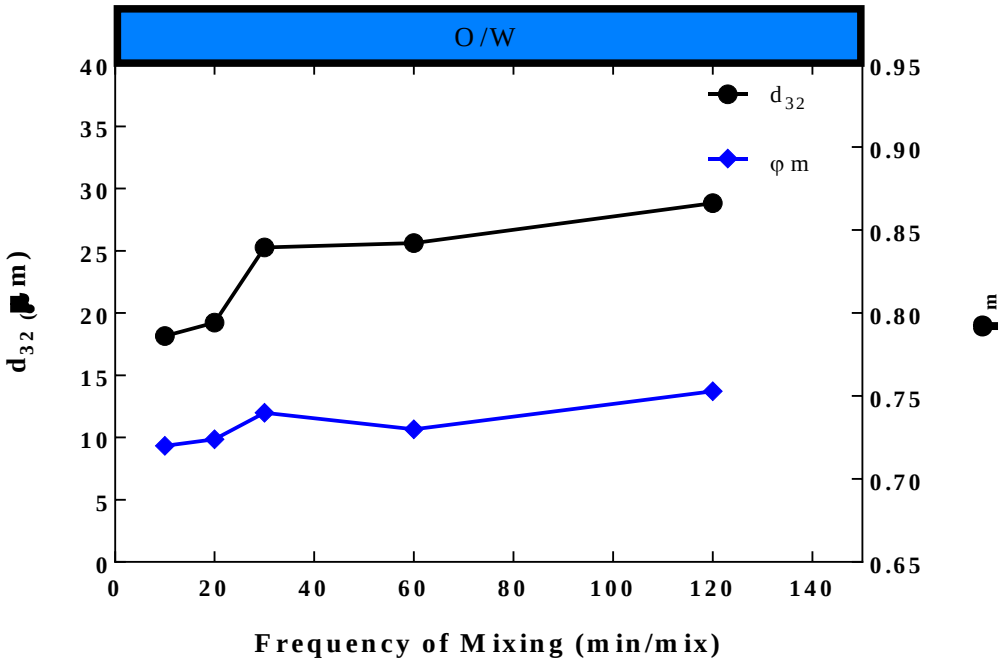

Fig. 3.13: The d_{32} of the entire lognormal distribution (primary axis) and φ_m (secondary axis) of emulsions made from 80% oil B and 20% aqueous solution (1.6% phenol-15EO, 0.4% NaCl and 0.2% NaOH) vs. the frequency of the sample mixing. Frequency of mixing at 10 minutes means the sample was mixed for 10 seconds every 10 minutes over a period of 4 hours at 96°C.

As stated in Table 3.7, mixing frequency doesn't affect any of the critical capillary number variables significantly. What is affected by mixing frequency is the competition between mixing, which results in smaller droplets, and coalescence, which results in bigger droplets. Mixing the samples more frequently resulted in the same φ_m values within experimental uncertainty and a smaller d_{32} when the mixing frequency was <30 min/mix. This suggests that the effect of interfacial tension (mixing) is dominant at mixing frequencies of <30 min/mix and the effect of coalescence is dominant at mixing

frequencies of >30 min/mix. With high coalescence rates, the particle size distribution of concentrated emulsions should be relatively insensitive to mixing speed. To illustrate this, the effect of mixing speed was observed by making optimized emulsions from 80% Oil B and 20% of an aqueous phase with 1.6% phenol-15EO, 0.2% NaOH, and 1.4% NaCl. The emulsions are very close to inversion salinity of O/W to W/O emulsions where coalescence rate is high. The emulsions were mixed at 60 ^{o}C by gently tilting the sample vial upside down (~1-10 s^{-1}) and by vigorously shaking (~100-1,000 s^{-1}) the samples for 10s every 30min for 4h. Both procedures resulted in values of d_{32}=15±0.2 μm and φ_m=0.8±0.01.

Using optimized co-solvents and the preparation procedure described in this study helped us achieve our goal of polydisperse emulsions with higher values of φ_m.

3.4.2 Effect of Heavy Crude Oil Types

Concentrated oil-in-water emulsions with φ=0.8 were prepared using the same aqueous formulation with four heavy crude oils (Table 3.2). The particle size distribution of the four heavy oils are shown in Fig. 3.12 for an aqueous formulation with 1.6% phenol-15EO, 0.2% NaOH, and 0.8% NaCl.

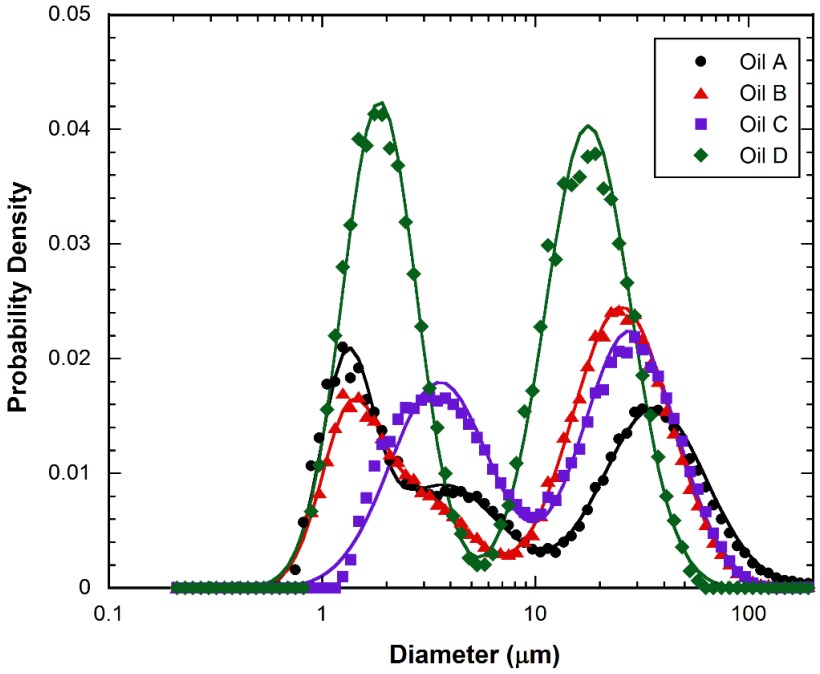

Fig. 3.14: Log-normal distribution fitting of particle size distribution of emulsions prepared with 80% oil and 20% aqueous solution (1.6% phenol-15EO, 0.8% NaCl, 0.2% NaOH). Volume probability density (volume fraction/diameter vs. diameter) is plotted.

All four oils formed bimodal/trimodal distributions and the φ_m values of all four samples were ~0.77±0.02 (see Appendix for fitting parameter). Although the same aqueous formulation was used for the heavy crude oils, the droplet size distributions of the emulsions, as well as the d_{32} values, showed some noticeable differences. The viscosity of the heavy oils varied over a range of ~100-400 mPa·s at a mixing temperature of 95°C (see Fig. 3.1). Oil A with the highest viscosity showed the largest d_{32} value, while Oil D with the lowest viscosity showed the lowest d_{32} value. Oils B and C had similar viscosities and d_{32} values.

Fig. 3.15 depicts the d_{32} and φ_m values of 80% oil emulsions with phenol-15EO co-solvent concentrations of 0-3.2% in the aqueous phase for the same four heavy oils.

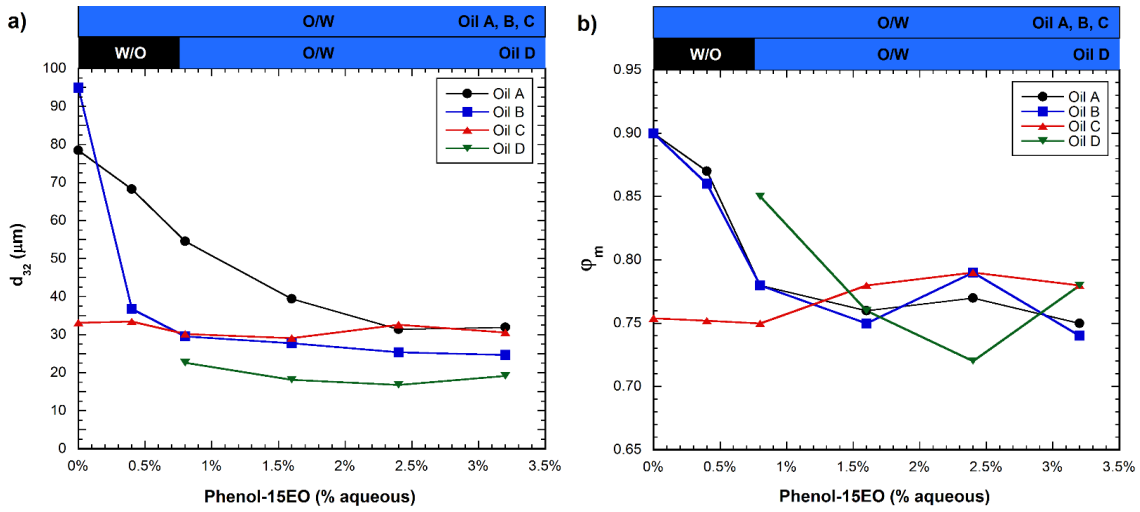

Fig. 3.15: (a) d_{32} and (b) φ_m of the entire lognormal distribution of emulsions made from 80% oil and 20% aqueous solution (0.8% NaCl, 0.2% NaOH, and 0-3.2% phenol-15EO) vs the weight percentage of phenol-15EO in the aqueous solution. The sample was mixed for 10 s every 30 min over a period of 4 h at 96°C. (In both panels, O/W and W/O stand for oil-in-water and water-in-oil emulsions, respectively. The lines are present only to guide the eyes.)

Oils A, B, and D showed a strong dependence on phenol-15EO concentration. Higher phenol-15EO concentrations resulted in lower d_{32} and φ_m values until a plateau is reached, while Oil C showed negligible changes in d_{32} and slightly higher φ_m values for the range of phenol-15EO concentration tested. The difference observed is most likely a property of the soap generated by each oil. The soap generated from Oil C is significantly more hydrophilic and, thus, is further away from the inversion point of O/W to W/O, compared to the other three oils. Oils A and B are very close to the inversion point with 0% phenol-15EO, while Oil C can tolerate a further increase of ~0.4% NaCl to 1.2% NaCl before the emulsion inverts to W/O. W/O emulsions formed with Oil D until the concentration of phenol-15EO exceeded 0.8%. Two significant observations about the φ_m values of concentrated emulsions can be made from Fig. 3.15b. First, φ_m increased as the emulsion approached the inversion point of O/W to W/O without inverting but showed extremely high d_{32} values and visual observation of the samples

showed worse stability, compared to the emulsions with co-solvents. Second, φ_m decreased with increasing phenol-15EO concentration, except for a bump in the φ_m value observed at a specific phenol-15EO concentration. The amplitude and the position of the bumps on Fig. 3.10b appear to vary, based on the composition of the heavy oil, but collapse into one curve with similar trends when normalized to the inversion point with the bumps appearing at ~2.5% phenol-15EO from the inversion point.

3.4.3 Effect of Co-solvent Types and Co-solvent Concentrations

Co-solvents are frequently mixed with surfactants to develop optimum chemical formulations for chemical enhanced oil recovery [Sahni et al. (2010)]. The most common types of co-solvents used for EOR are small-chain alcohols (six carbons or less). Faster equilibration time, which is directly related to the rate of coalescence, lower microemulsion viscosity, low IFT over a wider range of salinity, improved solubility of the surfactants at optimum salinity, and a more favorable activity diagram are some of the benefits of using co-solvents to make microemulsions used for EOR [Chang (2014); Fortenberry et al. (2013); Taghavifar (2014)]. The literature on the effect of co-solvents on the droplet size distribution and rheological properties of concentrated O/W emulsions is limited. dos Santos et al. (2014), (2011) observed that the addition of medium straight-chain alcohols to concentrated heavy oil emulsions led to a sharp decrease in d_{32} and the formation of bimodal emulsions, compared to unimodal emulsions without any alcohols and had a direct impact on the emulsions' stability and apparent viscosity. However, as shown below, the co-solvent type and concentration can be used to great advantage to optimize the emulsion properties.

The droplet size of emulsions is dictated by a dynamic equilibrium between two opposite phenomena: breakup and coalescence of the droplets [Coulaloglou and

Tavlarides (1976)]. Thus, any process that affects the droplet breakup and coalescence of emulsions results in variation in the value of d_{32}. For phase behavior studies of crude oil-surfactant-water mixtures, it was found that the coalescence rate was the highest with the type III microemulsions at ultralow IFT under optimum conditions. Thus, as the chemical formulation approaches the optimum formulation, with respect to electrolyte, temperature, co-solvent, or surfactant, competition occurs between decreasing interfacial tension that generates smaller droplets and increasing rate of coalescence that generates bigger droplets, resulting in a minimum in d_{32} and a multimodal droplet size distribution near the optimum [Tolosa et al. (2006)].

Fig. 3.16 shows the effects of various co-solvents on the d_{32} and φ_m values of 80% Oil B emulsions.

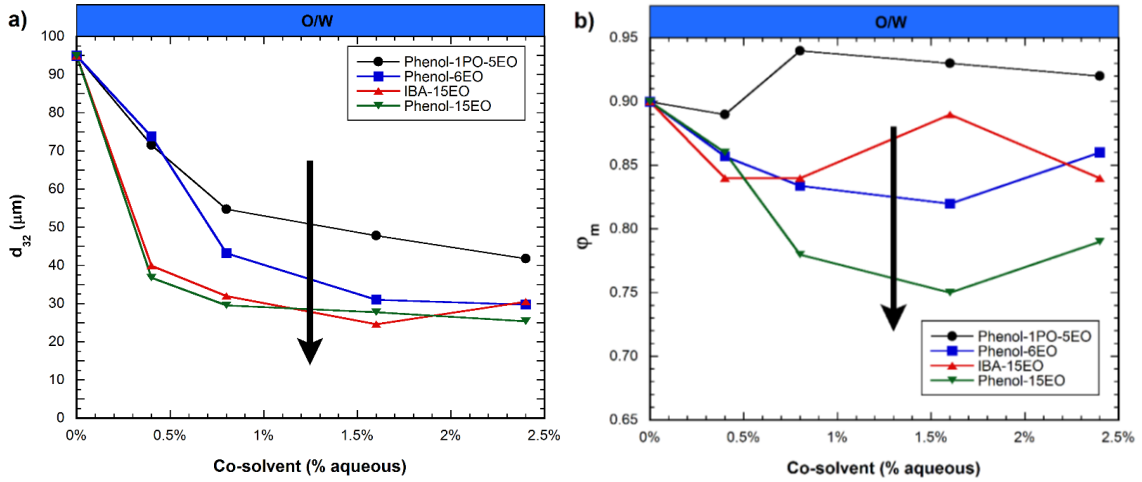

Fig. 3.16: (a) d_{32} and (b) φ_m of the entire lognormal distribution of emulsions made from 80% oil B and 20% aqueous solution (0.8% NaCl, 0.2% NaOH, and 0-2.4% co-solvent) vs the weight percentage of co-solvent in the aqueous solution. (In both panels, the co-solvents are phenol-1PO-5EO, phenol-6EO, IBA-15EO, and phenol-15EO from the least hydrophilic to most hydrophilic as indicated by in direction of the arrow. The sample was mixed for 10 s every 30 min over a period of 4 h at 96°C. The lines are present only to guide the eyes.)

A similar trend of decreasing and plateauing of d_{32} is observed for all co-solvents, with some co-solvents showing slightly increasing d_{32} at high co-solvent concentrations. The

amplitude and concentration of the co-solvent at which the bump in φ_m is observed showed a dependence on the co-solvent structure. At any co-solvent concentration, d_{32} and φ_m correlate inversely with the hydrophilicity of the co-solvents with the least hydrophilic co-solvent (phenol-1PO-5EO) showing the highest d_{32} and φ_m values and the most hydrophilic co-solvents (phenol-15EO) showing the lowest d_{32} and φ_m values. The bump in φ_m is observed because of changing d_L/d_S and $\varphi_s/(\varphi_s + \varphi_L)$ caused by the co-solvent concentration. The bumps in φ_m shown on Fig. 3.16b happened to coincide with the maximum φ_m observed at the optimum $\varphi_s/(\varphi_s + \varphi_L)$ shown in Fig. 3.7 for the d_L/d_S. The bumps are observed at ~0.75% phenol-1PO-5EO, ~1.5% IBA-15EO, and ~2.5% phenol-6EO and phenol-15EO. Co-solvents of varying structures and concentrations can be used to optimize the values of d_{32} and φ_m.

3.4.4 Effect of Electrolytes

A decreasing trend in d_{32} as the NaCl concentration increased was observed until the O/W to W/O transition point. This trend is consistent with the data reported in the literature [Acevedo et al. (2001); dos Santos et al. (2011); Gutierrez et al. (2003)]. Fig. 3.17 shows NaCl scans of 80% Oil B emulsions with 0 and 1.6% phenol-15EO.

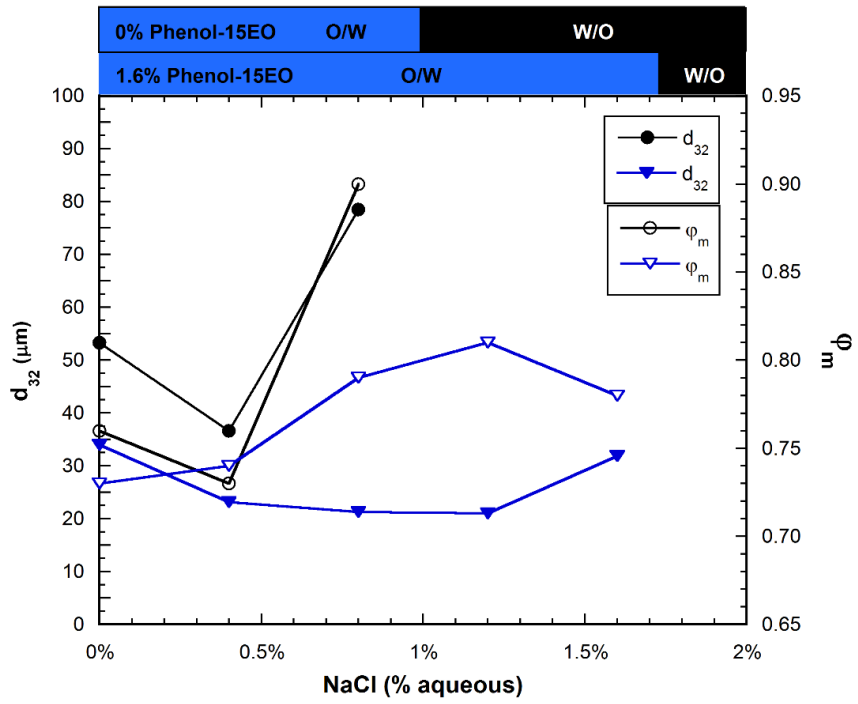

Fig. 3.17: d_{32} of the entire log-normal distribution (primary axis) and φ_m (secondary axis) of emulsions made from 80% oil B and 20% aqueous solution (0-0.8% NaCl, 0.2% NaOH, and 0 & 1.6% phenol-15EO) vs the weight percentage of NaCl in the aqueous solution. (The sample was mixed for 10 s every 30 min over a period of 4 h at 96°C. pH = 9.9-10.1 for all emulsion samples. The lines are present only to guide the eyes.)

The addition of co-solvent increased the salinity where the emulsion inverted from ~1% NaCl with 0% phenol-15EO to ~1.7% NaCl with 1.6% phenol-15EO. Thus, co-solvents with different hydrophilicity can be used to tune the chemical formulation to the available water sources with different salinities. $\varphi_s/(\varphi_s + \varphi_L)$ increased as the NaCl increased for emulsions with 1.6% phenol-15EO with the optimum $\varphi_s/(\varphi_s + \varphi_L)$ and φ_m observed near the O/W to W/O transition salinity (Fig. 3.7). The d_{32} of the emulsion with no co-solvent showed a very high value of ~80 μm, compared to ~32 μm for the emulsion with co-solvent near the transition point. The emulsion with no co-solvent near the inversion point showed poor stability.

Since the Na^+ counterion is provided by both the alkali and the electrolyte, a better method of analyzing the effect of electrolytes with varying alkali concentration is to plot the d_{32} and $\varphi_m/\varphi_{m,0}$ of emulsions versus the total Na^+ concentration normalized to the Na^+ concentration at the O/W to W/O inversion point, $Na_{inversion}^+$, instead of the NaCl concentration (Fig. 3.18). $\varphi_{m,0}$ is the φ_m at the lowest salinity (highest IFT) where the φ_m is relatively constant.

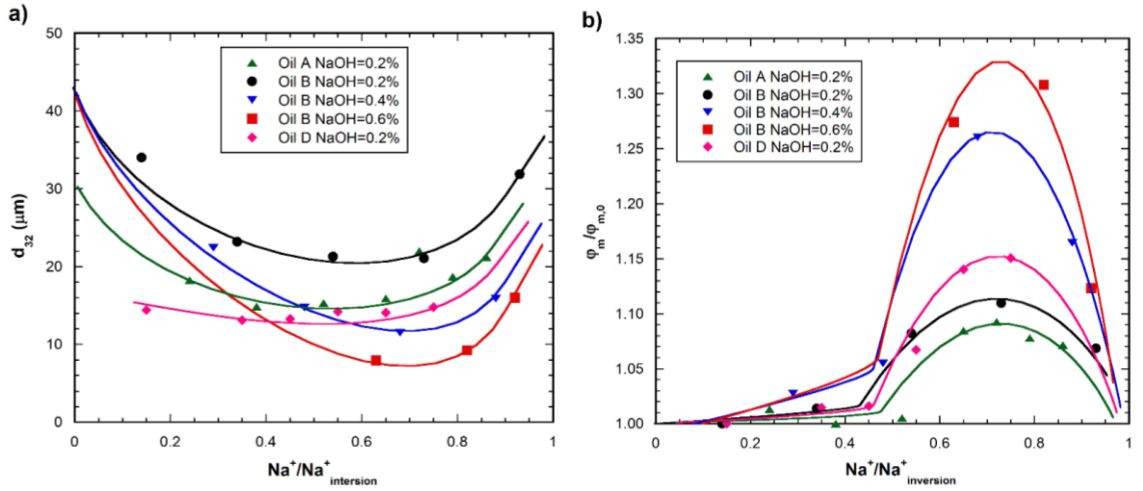

Fig. 3.18: (a) d_{32} and (b) $\varphi_m/\varphi_{m,0}$ of the entire lognormal distribution of emulsion made from 80% oil and 20% aqueous solution (0.2/0.4/0.6% NaOH, and 1.6% phenol-15EO) vs $Na^+/Na^+_{inversion}$ in the aqueous solution. NaCl was used to vary the Na^+. Oil A emulsions were prepared with 0.2% NaOH and 3% phenol-15EO. $\varphi_{m,0}$=0.755, 0.73, and 0.685 for oils A, B, and D respectively. (The sample was mixed for 10 s every 30 min over a period of 4 h at 96°C. pH = 9.9-10.1 for 0.2% NaOH, 10.3-10.5 for 0.4% NaOH and 10.9-11.1 for 0.6% NaOH for oil B emulsions. The lines are present only to guide the eyes.)

The effect of Na^+ seems to be dependent on the concentration of NaOH, which controls the quantity of soap generated from the heavy oil. The d_{32} values of the 0.2%, 0.4%, and 0.6% NaOH Oil B emulsions showed a minimum in d_{32} as the Na^+ increased. The d_{32} values of all emulsions made using Oil B appear to be converging to the same value near the transition point. Emulsions made with Oils A and D showed similar trends, suggesting that the one-step preparation method used in this study is applicable to a

variety of heavy oils with different compositions and viscosities. Note that Oil A emulsions required 3% instead of 1.6% phenol-15EO in Fig. 3.16 to observe φ_m going through a maximum since 1.6% phenol-15EO was not sufficient to increase the coalescence rate of the oil/aqueous mixture. The φ_m of all emulsions with varying NaOH concentration increased as the Na^+ increased with φ_m going through a maximum until converging to the same φ_m value just near the transition point. The effect of Na^+ on d_{32} and φ_m seems to be amplified when the surfactant concentration is increased via higher NaOH concentration. The maximum φ_m value is observed at ~0.75 $Na^+/Na^+_{inversion}$. The effects of alkali are further explored in the next section.

3.4.5 Effect of Alkali Type and Alkali Concentrations

Alkalis such as NaOH, Na_2CO_3, and $NaBO_2$ perform two functions: (1) increase the pH and (2) increase the electrolyte concentration. Acevedo et al. (2001) discussed the mechanism of naphthenic acid deprotonation from active crude oils. They showed that the quantity of carboxylate ions generated is a function of the pH, with increasing pH resulting in higher carboxylate ion concentration at the interface, thus resulting in lower interfacial tension and smaller d_{32} of O/W emulsions [Acevedo et al. (2001); dos Santos et al. (2011); Verzaro et al. (2002)]. Fig. 3.19 shows the pH of alkali at various concentrations in water.

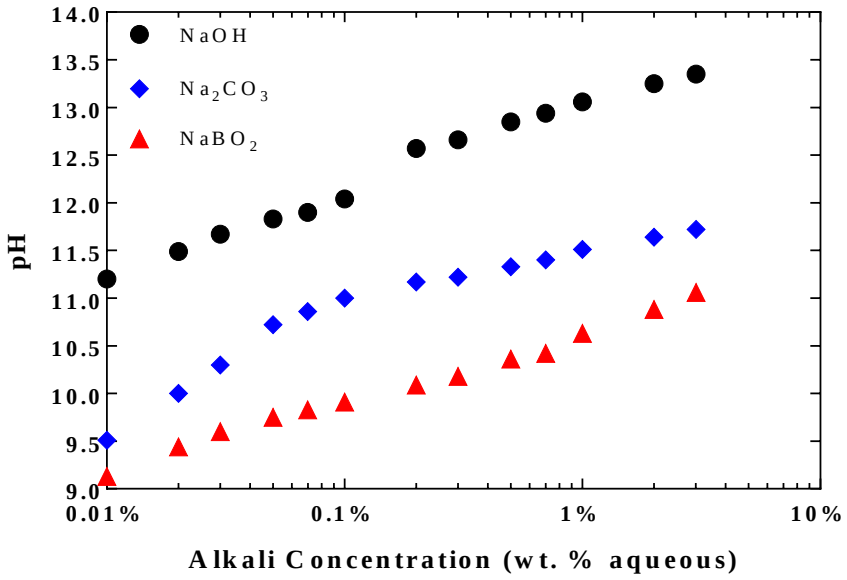

Fig. 3.19: The pH of various alkali in DI water vs. the alkali concentration.

The emulsions with various alkali and alkali concentrations are compared on the Na^+ basis in Fig. 3.20.

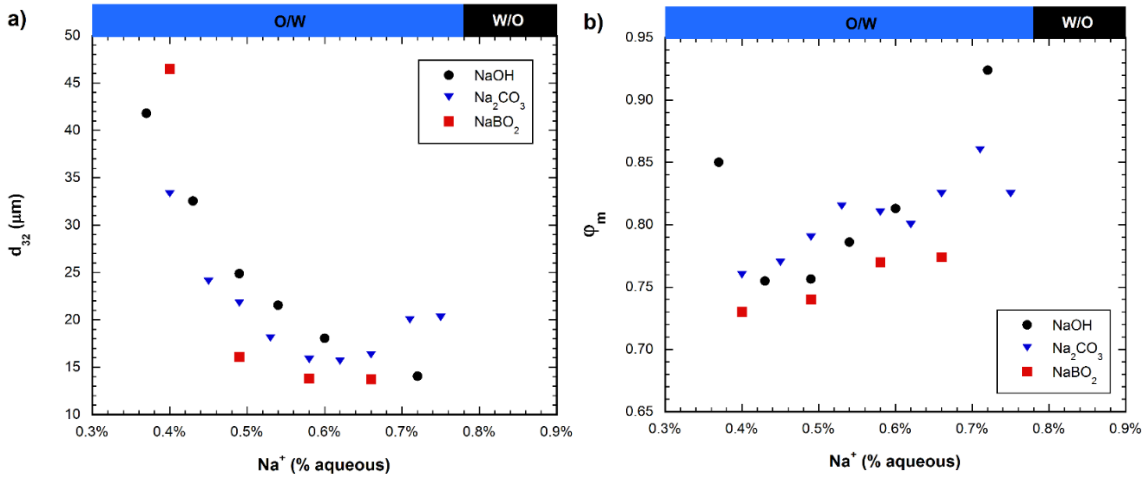

Fig. 3.20: (a) d_{32} and (b) φ_m of the entire log-normal distribution of emulsions made from 80% oil B and 20% aqueous solution (0.8% NaCl, alkali, and 1.6% phenol-15EO) vs the weight percentage of N^+ in the aqueous solution. (In both panels, the sample was mixed for 10 s every 30 min over a period of 4 h at 96°C.)

The scan of NaOH from 0.1%-0.7% showed that d_{32} decreased and $\varphi_s/\varphi_s + \varphi_L$ increased as the NaOH concentration increased. This resulted in higher φ_m values, with the highestφ_m value of ~0.93 being observed with 0.7% NaOH, which is just below the transition salinity of 0.8% NaOH. These trends are in agreement with the effect of electrolyte concentration described in Section 3.4.4, except for the lower d_{32} values observed at high NaOH concentration. Higher-concentration NaOH emulsions also generated trimodal distributions with a significant volume fraction of particles showing particle diameters of <1μm. The scan of Na_2CO_3 from 0.2%-1.0% showed that the d_{32} decreased and passed through a minimum before increasing as the concentration of Na_2CO_3 increased. The φ_m value of the Na_2CO_3 scan showed an increasing trend as the Na_2CO_3 concentration increased and reached the optimum $\varphi_s/(\varphi_s + \varphi_L)$ value at 0.9% Na_2CO_3, as observed by the bump in φ_m, which is similar to the bumps observed in the co-solvent scans in Fig. 3.16b. $NaBO_2$ emulsions showed behaviors similar to that of the Na_2CO_3 emulsions.

No conclusive results about the effect of varying alkali/pH on d_{32} and φ_m were found within the experimental uncertainty, suggesting that, if enough alkali is present to generate enough soap to create stable emulsions, the type of alkali used does not affect the droplet size distributions of concentrated emulsions significantly.

3.4.6 Effect of Ethoxylated Amines as Both a Co-solvent and Alkali

Amines, with a pH of 11.5-12.5, depending on the amine type and concentration, have been utilized successfully as organic alkaline agents in place of inorganic alkalis such as NaOH and Na_2CO_3 to emulsify and stabilize acidic heavy O/W emulsions [Gutierrez et al. (2003)]. Some fraction of the amines gain a positive charge and contribute as counterions to the anionic surfactants, as well as increase the pH of the

aqueous solution, as is the case with traditional inorganic alkalis. Alkyl amines are attractive because the chemical formulation containing an alkali and a co-solvent would be reduced to just one chemical, since alkyl amines function as both a co-solvent and an alkali. Also, alkyl amines have been used as effective steel corrosion inhibitors at low concentrations [Rihan et al. (2014)]. However, the combined effects of alkyl amines as alkalis, electrolyte, and co-solvent on the droplets size distribution has not been investigated until this study.

As shown in Fig. 3.17, the inversion point increased from ~1% to ~1.75% NaCl when 1.6% phenol-15EO co-solvent was added to the formulation. The increase in salinity shows that the co-solvent made the formulation more hydrophilic. With 1.0% DIPA-15EO in the formulation shown in Fig. 3.21, the transition point decreased to ~0.4% NaCl from ~1% NaCl with 0.2% NaOH and no co-solvent. With 2.2% DIPA-15EO in the formulation, the transition point decreased from ~1% NaCl to ~0.8% NaCl.

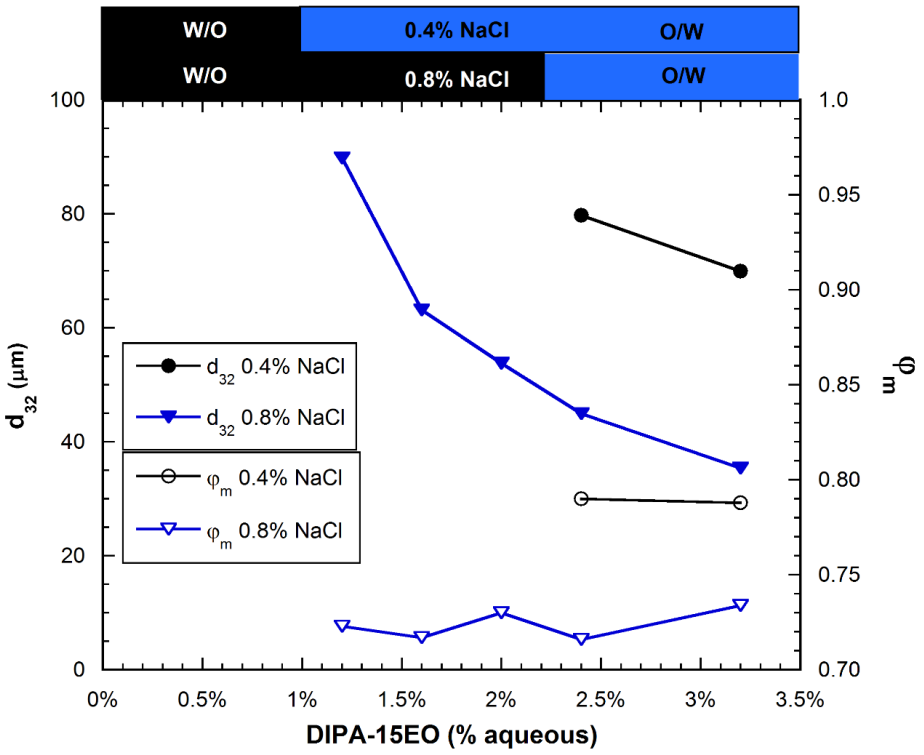

Fig. 3.21: d_{32} of the entire log-normal distribution (primary axis) and φ_m (secondary axis) of emulsions made from 80% oil B and 20% aqueous solution (up to 3.2% DIPA-15EO, 0.4 & 0.8% NaCl) vs. the weight percentage of DIPA-15EO in the aqueous solution. (The sample was mixed for 10 s every 30 min over a period of 4 h at 96°C. The lines are present only to guide the eyes.)

As shown in Fig. 3.21 for 0.4% NaCl, an almost constant value of $\varphi_m = 0.72 \pm 0.01$ was observed for the range of DIPA-15EO concentrations tested. The low value of φ_m observed is due to the unimodal droplet size distribution of the emulsions. The results in Fig. 3.21 for 0.8% NaCl show a bimodal droplet size distribution, with $\varphi_m = 0.79 \pm 0.01$ over the entire range of DIPA-15EO concentrations tested. A possible explanation for the constant φ_m observed with DIPA-15EO, compared to the other co-solvents, could be that the soaps with bulky DIPA counterion interfer with the packing of surfactants, compared to Na^+ soaps [Gutierrez et al. (2003)]. The high d_{32} values and lack of fine droplets for the emulsions shown in Fig. 3.21 support this interpretation. The

parameter d_{32} followed the same decreasing trend observed in Fig. 3.16a as the formulation progressed further away from the transition point of O/W to W/O.

3.4.6 Co-solvent/Soap versus Nonionic Surfactant

Octylphenol/nonylphenol ethoxylates are common nonionic surfactants used to prepare oil-in-water emulsions [Abdurahman et al. (2012); Ahmed et al. (1999a); Ashrafizadeh and Kamran (2010); dos Santos et al. (2014), (2011); Hasan et al. (2010); Meeker et al. (2004); Núñez et al. (1996); Nuñez et al. (2000); Pal (2006), (1996); Romero et al. (2002), (2000); Seth et al. (2012)]. Nonylphenol-12EO was used as a reference point, compared to 80% oil emulsions prepared with the method described in Section 3.2.2. The particle size distributions of emulsions made with and without nonylphenol-12EO were compared. The cloud point of nonylphenol-12EO is 78 ^{o}C. Therefore, the emulsions with nonylphenol-12EO were prepared at 75 ^{o}C. The 80% Oil B emulsions prepared with only nonylphenol-12EO required an aqueous concentration of >1.5% to create stable emulsions that did not phase separate for times greater than 1 day. φ_m=0.81 and d_{32}=102 μm were obtained with 1.5% nonylphenol-12EO, suggesting that a much higher concentration than 1.5% is needed to create stable concentrated emulsions since the IFT is much higher for emulsions made using only nonylphenol-12EO (as seen by very high d_{32} values) than for emulsions made using the anionic surfactants used in this study.

A scan of over 100 surfactants and surfactant combinations have been tested with the preparation of O/W emulsions [Wylde et al. (2012)], as well as combinations of nonionic and anionic surfactants [Ahmed et al. (1999a); Zaki et al. (2001)], to explore the effects of surfactant types on emulsion viscosity and stability. However, only a brief mention of how the combination of nonionic/natural surfactants and anionic/natural

surfactant at various mass ratios affected the d_{32} of emulsions has been published [Zaki et al. (2001)]. We explored the idea further.

Synergy between nonionic surfactants and soaps was tested, and the results are shown in Fig. 3.22.

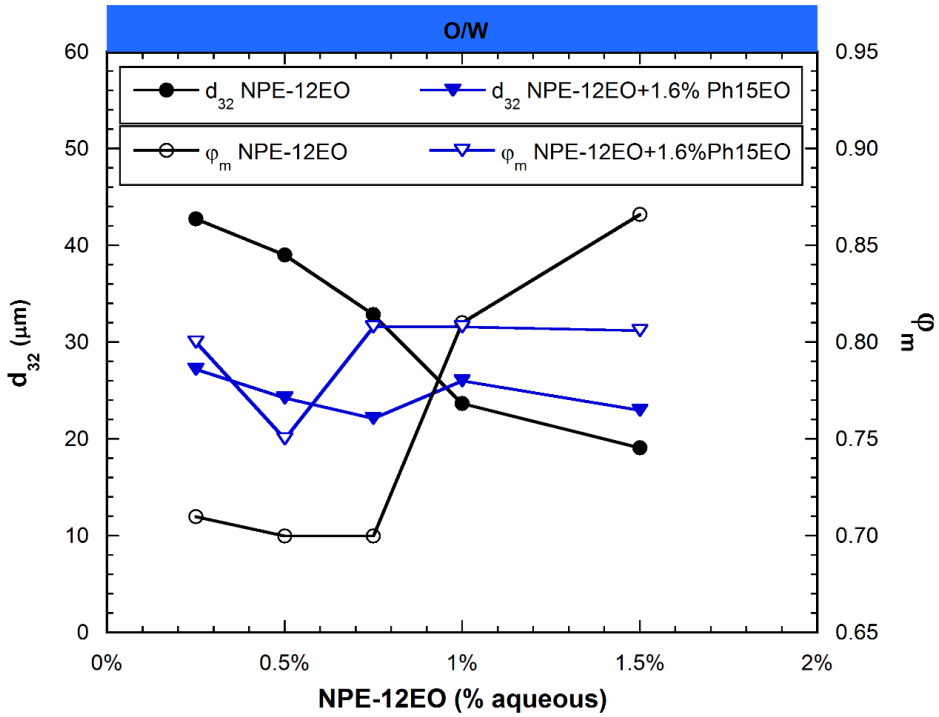

Fig. 3.22: d_{32} of the entire log-normal distribution (primary axis) and φ_m (secondary axis) of emulsions made from 80% oil B and 20% aqueous solution (0.25-1.5% NPE-12EO, 0.8% NaCl, 0.2% NaOH, 0 & 1.6% phenol-15EO) vs the weight percenrage of NPE-12EO in the aqueous solution. (The sample was mixed for 10 s every 30 min over a period of 4 h at 75°C. The lines are present only to guide the eyes.)

The mixture of NPE-12EO + phenol-15EO increased the cloud point (>95 °C). As shown in Fig. 3.22, the addition of nonionic surfactant to the chemical formulation without co-solvent decreased the d_{32} value of droplets as the NPE-12EO concentration was increased while an almost constant value of φ_m = 0.70 was obtained at low NPE-12EO concentration, but φ_m increased sharply to 0.86 at 1.5% NPE-12EO. The high value of

φ_m at high NPE-12EO concentration seems to be due to the shifting of the transition point of O/W to W/O as the concentration of NPE-12EO increased. The behavior of emulsions with 1.6% phenol-15EO shown in Fig. 3.22 supports this interpretation of the data. When the chemical formulation was made more hydrophilic by adding phenol-15EO, φ_m remained relatively constant at 0.8 for the entire range of NPE-12EO concentration tested.

3.5 CONCLUSIONS

A new chemical formulation method was used to prepare polydisperse bimodal and trimodal concentrated heavy oil-in-water (O/W) emulsions (high oil content). This chemical formulation approach is similar to the well-known method used to optimize microemulsions used for enhanced oil recovery, but with several significant differences. Several novel co-solvents were used, in addition to the more commonly used surfactants and alkalis. This is the first time that the φ_m of emulsions prepared with this new chemical formulation method have been characterized. Stable emulsions with broad bimodal and trimodal particle size distributions were achieved with a maximum packing parameter (φ_m) as high as 0.95 and a larger Sauter mean diameter in the range of d_{32} = 10-50 μm. These emulsions were prepared using a new one-step mixing procedure. Three conditions were found to be necessary for emulsions with these characteristics: (1) a low interfacial tension; (2) a fast coalescence rate, and (3) sufficient amounts of interfacially active chemicals (surfactants). The conditions needed for polydisperse heavy O/W emulsions occur at ~75% of the Na^+ concentration required for oil-in-water to water-in-oil (O/W to W/O) inversion point, with φ_m going through a maximum as a scan of electrolyte concentration in the presence of alkali only with the addition of a sufficient quantity of co-solvents. These results show that ethoxylated co-solvents such as phenol-

nEO and IBA-nEO interact favorably with heavy oils and perform better at disrupting the ordered packing of naphthenic soaps than small alcohols that were used as co-solvents in previous studies by other investigators. Concentrated heavy oil emulsions with $\varphi_m > 0.90$ exhibited significantly lower viscosity, compared to unimodal emulsions with $\varphi_m < 0.75$. This is essential for the transport of heavy oil emulsions in pipelines.

Millions of combinations of surfactants, co-solvents, alkali, and electrolytes over a wide range of concentrations can be used to make heavy oil emulsions using different preparation methods and variables. Most of these emulsions do not have the desired properties for emulsion transport. For the purposes of this study, it was essential to develop a systematic procedure for selecting and testing the best chemical formulations. Concentrated (φ>0.64) heavy O/W emulsions with φ_m values as high as 0.95 were prepared in a simplified one-step mixing process by optimizing the particle size distribution based on fundamental principles of interfacial activity and rheology. The viscosity of multimodal concentrated emulsions ($\varphi_m > 0.85$) prepared with our method showed comparable, if not lower, viscosity than the heavy oil emulsions prepared via the common two-step process (mixing two unimodal emulsions) reported in the literature. Extensive rheological characterization of the optimized emulsions prepared by this method is presented in Chapters 5 and 6.

NOMENCLATURE

Ca	Capillary number
E^*	Contact modulus
μ_c	Continuous-phase viscosity
$Ca_{critical}$	Critical capillary number at which droplet breakup occurs
d_L	Diameter of the group of droplets with larger d_{32} in a bimodal/binary mixture
d_S	Diameter of the group of droplets with smaller d_{32} in a bimodal/binary mixture
μ_d	Dispersed-phase viscosity
φ	Dispersed-phase volume fraction of emulsions
R	Droplet radius
μ_{emul}	Emulsion viscosity
φ_g	Glass transition point
Γ	Interfacial tension (IFT)
φ_m	Maximum packing volume fraction (φ_m) of dispersed-phase possible without deformation of the spherical dispersed-phase
$\varphi_{m,0}$	Maximum packing volume fraction (φ_m) at the low salinity (high interfacial tension) where the φ_m doesn't vary much as a function of salinity
φ_n^{sat}	Maximum packing volume fraction (φ_m) of saturated non-interacting spheres of n monodisperse size groups
σ	Natural logarithm standard deviation of droplet diameter
μ	Natural logarithm mean diameter of droplets
d	Mean diameter of droplets within a bin width from histogram data
n	Number of non-interacting monodisperse size groups
k	Numerical coefficient
f_v	Probability density function of volume
φ_{rcp}	Random close packing of monodisperse, hard spheres
φ_{rlp}	Random loose packing of monodisperse, hard spheres
λ	Ratio of dispersed-phase viscosity to emulsion viscosity, $\mu_d/\mu_{emulsion}$
μ_r	Ratio of emulsion viscosity to μ_c
K	Ratio of μ_d to μ_c
d_{32}	Sauter mean droplet diameter
G	Shear modulus
$\dot{\gamma}$	Shear rate
γ	Strain
γ_y	Critical strain
τ	Shear stress
φ_L	Volume fraction of the group of droplets with larger d_{32} in a bimodal/binary mixture with respect to the total dispersed-phase volume

φ_S	Volume fraction of the group of droplets with smaller d_{32} in a bimodal/binary mixture with respect to the total dispersed-phase volume
f_S	Volume fraction of smaller droplet volume to total droplet volume, $\varphi_S/(\varphi_L + \varphi_S)$
d_{43}	Volume-weighed mean diameter
τ_y	Yield stress

ABBREVIATIONS

ASP	Alkali surfactant polymer
EOR	Enhanced oil recovery
EO	Ethylene oxide
HIPR	High internal phase ratio
O/W	Oil-in-water
PO	Propylene oxide
Na^+	Sodium concentration in wt. % in aqueous solution
$Na^+_{inversion}$	Sodium concentration in wt. % in aqueous solution at the O/W to W/O transition sodium concentration
W/O	Water-in-oil

Chapter 4: Interdroplet Interaction between Heavy Oil Droplets in Heavy Oil-in-Water Emulsions

4.1 INTRODUCTION

The term "soft matter" describes materials that display both solid-like properties and liquid-like properties. Concentrated heavy oil-in-water emulsions, like many other concentrated colloidal suspensions, fall into the category of "soft matter" based on the presence of a yield stress. Soft matter can be categorized into two sub-category, a soft-glass or gel. Fig. 4.1 shows illustrations of soft-glass and gel materials.

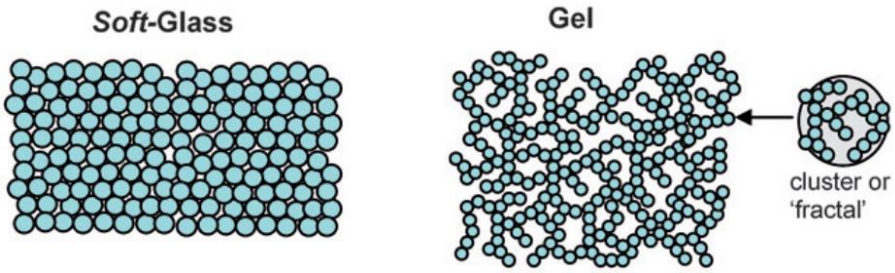

Fig. 4.1: Cartoon illustrations of soft matter microstructure: Soft-glass and gel [Stokes and Frith (2008)]

A gel is generally a material with an interconnected network of the dispersed-phase. The percolating structure causes the solid-like properties, which can be observed at much lower value than the maximum packing fraction (φ_m) of the dispersed-phase. The percolating structure arises due to the attractive interactions between the dispersed-phase droplets. The solid-like properties of a soft-glass primarily arises from caging effects observed at high volume fraction of the soft dispersed-phase above the maximum packing fraction, φ_m. A soft-glass can further be categorized into two sub-categories, attractive and repulsive. A repulsive soft-glass is a soft-glass with repulsive interaction between the dispersed-phase droplets. An attractive soft-glass is a soft matter that contains elements of both a soft glass and gel; a material with high dispersed-phase concentration

that forms interconnected, percolating structures. The percolating structures are caused by both the attractive interactions between the dispersed-phase droplets and caging effect of high dispersed-phase concentration.

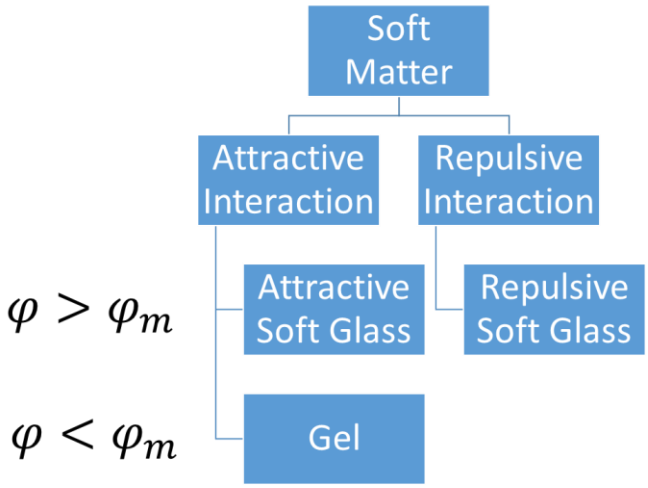

Fig. 4.2: Classification of soft matter materials based on dispersed-phase concentration and interdroplet interaction

The rheological models of colloidal suspensions mentioned in Chapter 2 are derived with the assumption of repulsive or no interactions between the dispersed-phase particles/droplets. An attractive interaction between the dispersed-phase particles/droplets results in a deviation of the rheological behavior modeled by the equations in Chapter 2. Yield stress and shear thinning behavior, not usually observed with repulsive colloidal suspensions for $\varphi < \varphi_m$, have been observed with attractive colloidal suspensions below $\varphi < \varphi_m$ [Datta et al. (2011); Grenard et al. (2014); Laurati et al. (2011)]. For concentrated colloidal suspensions, a change in the interparticle interaction from repulsive to attractive while keeping everything else the same resulted in a transition from a single-step yielding behavior (repulsive) to a two-step yielding behavior (attractive) [Koumakis and Petekidis (2011); Pham et al. (2008)]. The Princen

and Kiss equation (Eq. 2.7) and Seth's micromechanical model (Eq. 2.12) assumed repulsive interactions between droplets and cannot accurately model the rheological properties of attractive soft glass materials.

Whether or not the rheological equations in Chapter 2 can be used accurately to model the rheological properties of heavy O/W emulsions depend on the type of interaction between the heavy oil droplets. Are heavy oil droplets in heavy oil-in-water emulsions attractive or repulsive in nature?

4.2 PHOTOMICROGRAPHS OF HEAVY O/W EMULSIONS

Photomicrographs of heavy O/W emulsions can provide a variety of information about the microstructures, interaction potentials, and particle size distribution of the emulsions. It is important to note that the photomicrographs only provide information about emulsions in static conditions. Fluorescent light microscope is an ideal piece of equipment for taking photomicrographs of opaque samples. Photomicrographs of heavy oil-in-water emulsions can be taken without dilution with a fluorescent light microscope.

4.2.1 Experimental Procedure

A fluorescent light microscope (Zeiss Axiovert) was used to take photomicrographs of the emulsion samples. The samples were doped with a water-soluble fluorescent dye, fluorescein. Fluorescein has a peak excitation at 494 nm and a peak emission at 521 nm. Very low dye concentrations of fluorescein (10-20 ppm) were used to minimize the effects of the dye on emulsion properties. Borosilicate chambered coverglasses obtained from Thermo Scientific were used to contain the emulsion samples. The 63x oil immersion objective was used to take the photomicrographs. The photomicrographs provide visual evidence of the range of the emulsion droplet sizes for each sample.

Limitations of a light microscope:

1. Cannot identify objects smaller than the wavelength of the light (~500 nm).
2. Cannot focus on multiple objects with an order of magnitude difference in size at the same time.

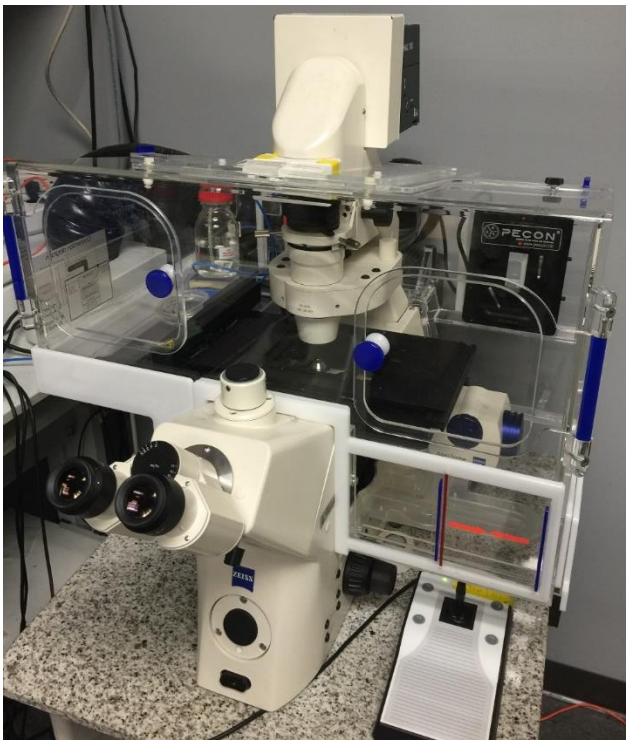

Fig. 4.3: A picture of the fluorescent light microscope (Zeiss Axiovert) used to take the emulsion photomicrographs.

4.2.2 Photomicrographs

Photomicrographs of oil D emulsions prepared with 1.6% phenol-15EO, 0.2% NaOH, and 0% NaCl with dispersed oil concentration of φ=40-85% are shown in Fig. 4.4.

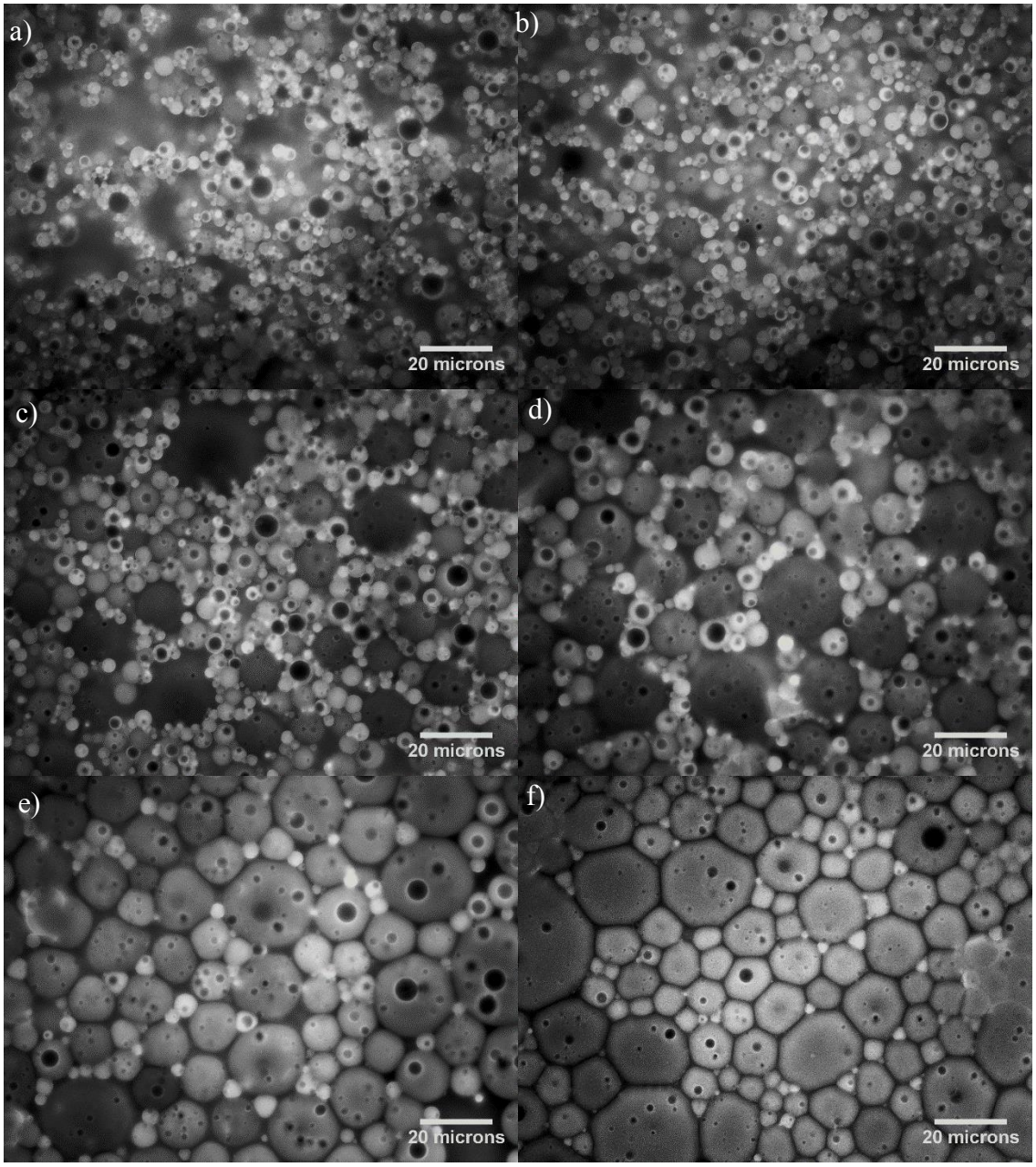

Fig. 4.4: Microscope pictures of oil D in water emulsions (a) φ=40% d_{43}=11.9µm d_{32}=6.1µm φ_m=0.79, (b) φ=50% d_{43}=13.5µm d_{32}=8.0µm φ_m=0.78, (c) φ=60% d_{43}=20.2µm d_{32}=14.5µm φ_m=0.80, (d) φ=70% d_{43}=22.2µm d_{32}=16.4µm φ_m=0.73, (e) φ=80% d_{43}=18.5µm d_{32}=15.6µm φ_m=0.69, (f) φ=85% d_{43}=19.1µm d_{32}=16.2µm φ_m=0.69. Aqueous phase formulation (1.6% ph15EO 0.2% NaOH, 0% NaCl)

Fig. 4.4 showed that an increasing emulsion d_{32} is observed as the oil concentration φ increased from 40% to 85%. This can be explained by the higher ratio of the mass of alkali per volume of oil available for emulsions with lower φ which generates a larger quantity of natural surfactants from the heavy oil. Oil droplets begin to deform away from the spherical shape for ≥80% oil D emulsions in Fig. 4.4 which coincided with $\varphi > \varphi_m$. Clear polyhedron shaped droplets are observed with 85% oil D emulsion (Fig. 4.4f). The droplet size distribution of the emulsions in Fig. 4.4 appeared to be relatively uniform with low polydispersity at high φ.

The chemical formulation in Fig. 4.4 was modified according to the method mentioned in Chapter 3 to achieve ~0.75 $Na^+/Na^+_{inversion}$ in the aqueous formulation where the highest φ_m is observed. $Na^+_{inversion}$ is the sodium concentration needed to invert the emulsion from O/W to W/O. This is at 1% NaCl. Fig. 4.5 shows the photomicrographs of optimized oil D emulsions of varying φ. The aqueous chemical composition and measured φ_m and d_{32} values are listed in the figure descriptions.

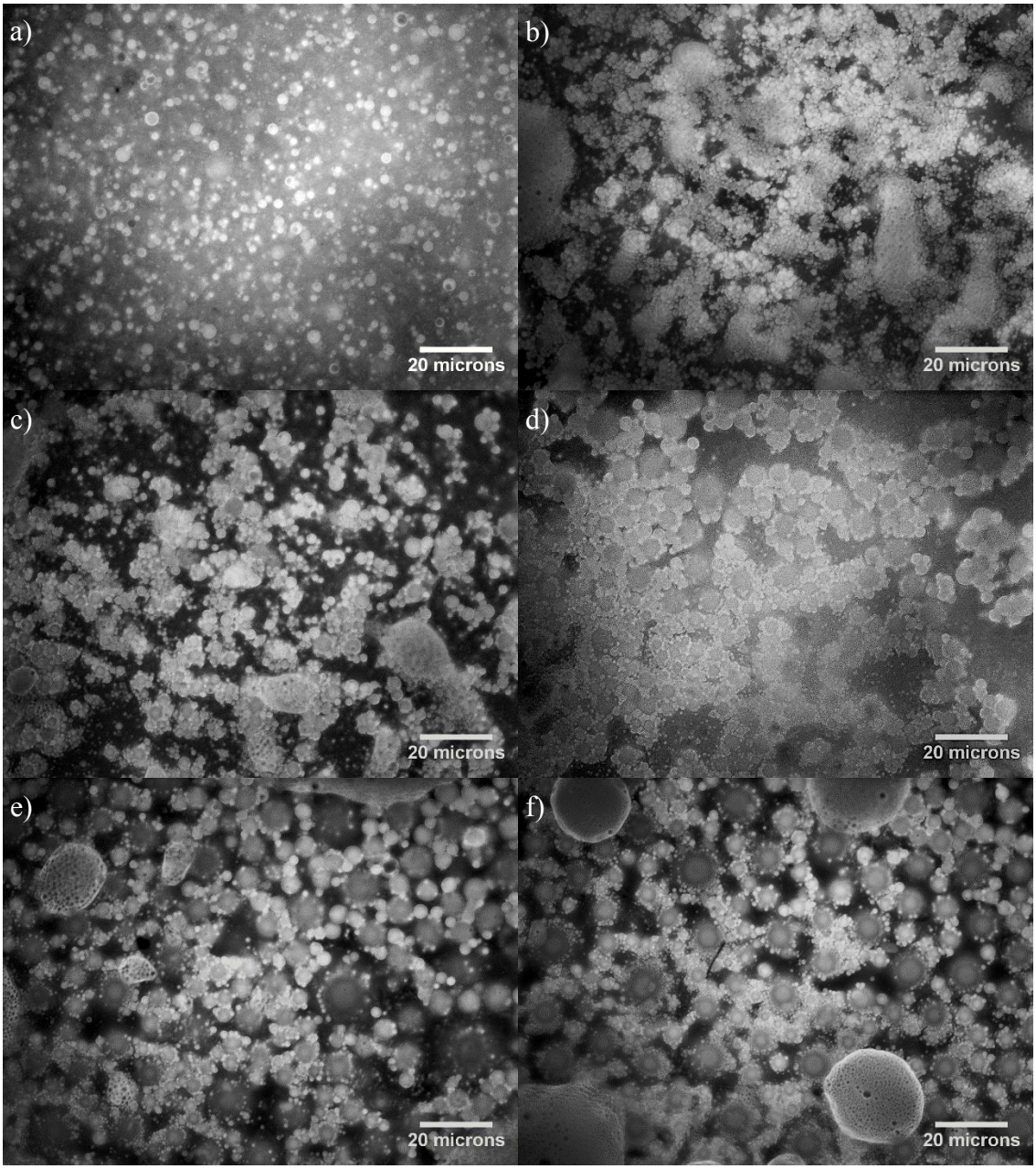

Fig. 4.5: Microscope pictures of oil D in water emulsions. (a) φ=40% d_{43}=2.9µm d_{32}=1.9µm φ_m=0.83, (b) φ=50% d_{43}=6.1µm d_{32}=4.8µm φ_m=0.76, (c) φ=60% d_{43}=13.6µm d_{32}=9.2µm φ_m=0.81, (d) φ=70% d_{43}=21.3µm d_{32}=12.3µm φ_m=0.81, (e) φ=80% d_{43}=19.8µm d_{32}=14.1µm φ_m=0.76, (f) φ=85% d_{43}=20.7µm d_{32}=14.6µm φ_m=0.75. Aqueous phase (1.6% ph15EO 0.2% NaOH, 1% NaCl)

Compared to Fig. 4.4, Fig. 4.5 showed a significantly larger volume fraction of small oil droplets, an indication of the multimodal droplet size distributions and high φ_m values of the emulsions. The smaller droplets are generated because of the lower interfacial tension of the chemical formulation used to prepare the emulsions. The smaller droplets appeared to surround the bigger droplets. Aggregating structures can be observed with 50-85% oil D emulsions (Fig. 4.5b-f) indicating attractive interaction between the oil droplets. Hardly any deformation of spherical oil droplets are observed even up to 85% oil D emulsion with the optimized formulation (Fig. 4.5f) unlike the emulsion with the compressed droplets (Fig. 4.4f). The volume fraction of oil droplets in the emulsions in Fig. 4.5 appeared to be a lot less than in Fig. 4.4. This is because it was not possible to focus on both the very small droplets and large droplets in Fig. 4.5. Also, a thin layer of liquid with lower concentration of oil droplets could have formed at the bottom of the sample due to the gravitational migration of oil droplets to the top. Since the images are taken at the bottom of the samples, artificially lower concentration of oil droplets could be observed.

Similar observations are made with heavy oil A emulsions (Fig. 4.6) and oil B emulsions (Fig. 4.7), suggesting the microstructures of heavy oil emulsions are similar for most heavy oils when the chemical formulation used to prepare emulsions are the same.

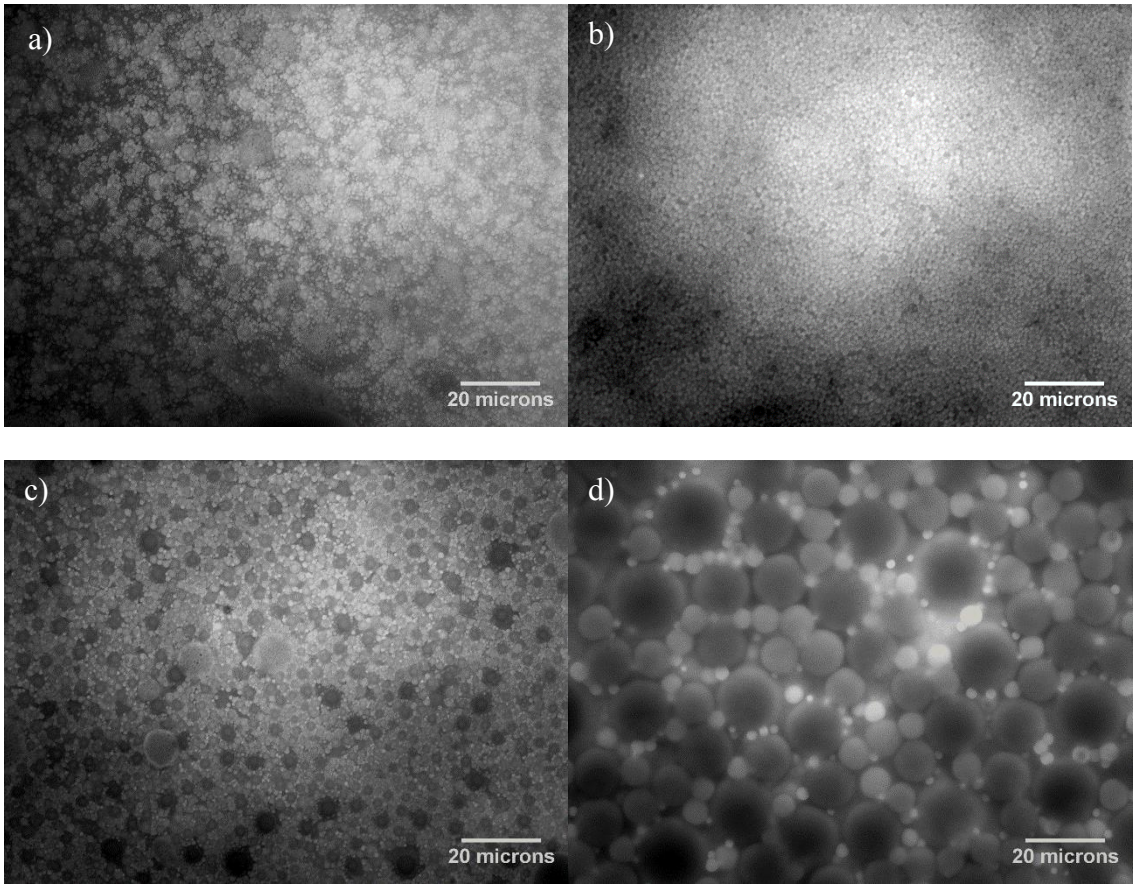

Fig. 4.6: Microscope pictures of oil A in water emulsions. (a) φ=20% d_{43}=2.1µm d_{32}=1.7µm φ_m=0.71, (b) φ=40% d_{43}=1.6µm d_{32}=1.4µm φ_m=0.86, (c) φ=60% d_{43}=6.4µm d_{32}=4.5µm φ_m=0.75, (d) φ=80% d_{43}=22µm d_{32}=15.9µm φ_m=0.74. Aqueous phase formulation (1.6% ph15EO 0.2% NaOH, 0.8% NaCl).

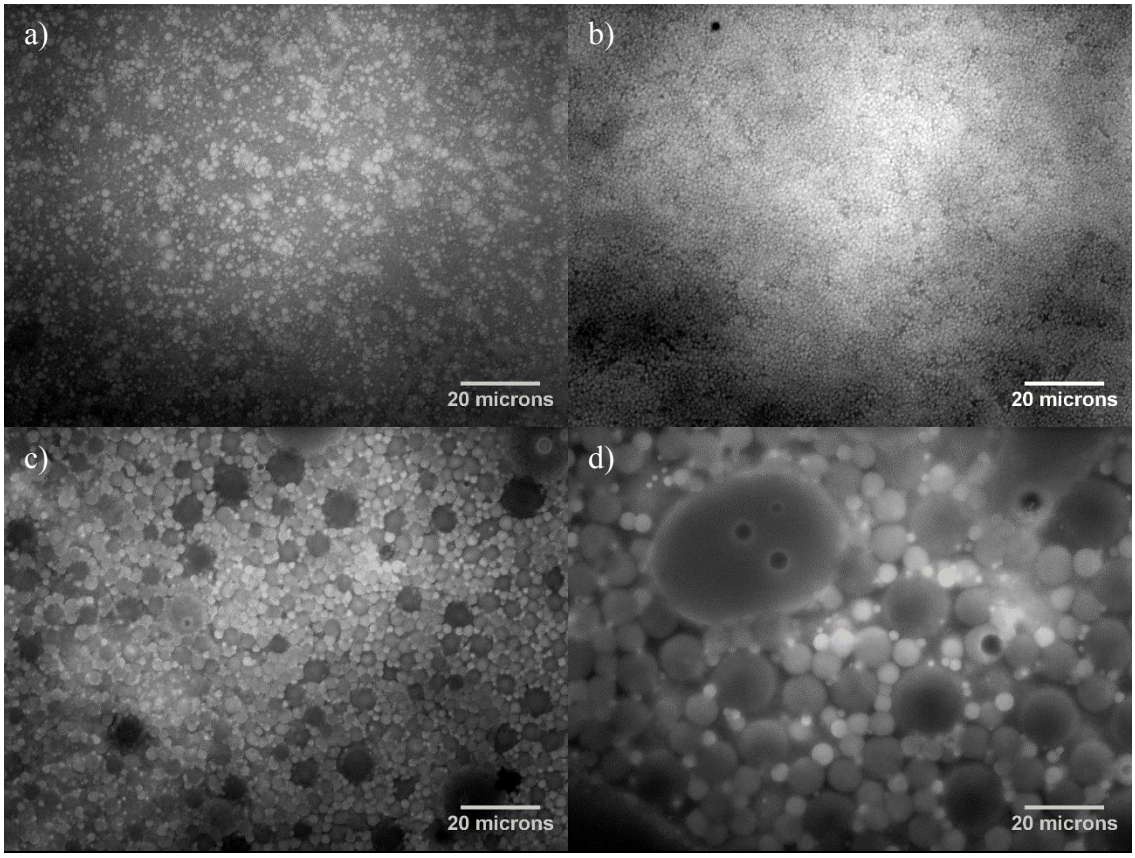

Fig. 4.7: Microscope pictures of oil B in water emulsions. (a) φ=20% d_{43}=3.4μm d_{32}=2.7μm φ_m=0.72, (b) φ=40% d_{43}=3.2μm d_{32}=2.3μm φ_m=0.76, (c) φ=60% d_{43}=8.0μm d_{32}=5.1μm φ_m=0.78, (d) φ=80% d_{43}=20.9μm d_{32}=14.9μm φ_m=0.77. Aqueous phase formulation (1.6% ph15EO 0.2% NaOH, 0.8% NaCl).

At the edge of the chambered coverglass used to contain the emulsion samples for photomicrography, a region with very low oil concentrations can be observed. With a low oil concentration, a better visual inspection of the interdroplet interaction can be made. This method is superior to the method of diluting heavy oil emulsions with the aqueous phase used to prepare emulsions. Dilution may modify the heavy O/W emulsion physicochemical properties (salinity, pH, surfactant concentration, soap concentration) and may not be a good representation of concentrated emulsions. Fig. 4.8 shows the photomicrographs of oil D emulsions, the same samples shown in Fig. 4.4, at the edge of the coverglasses.

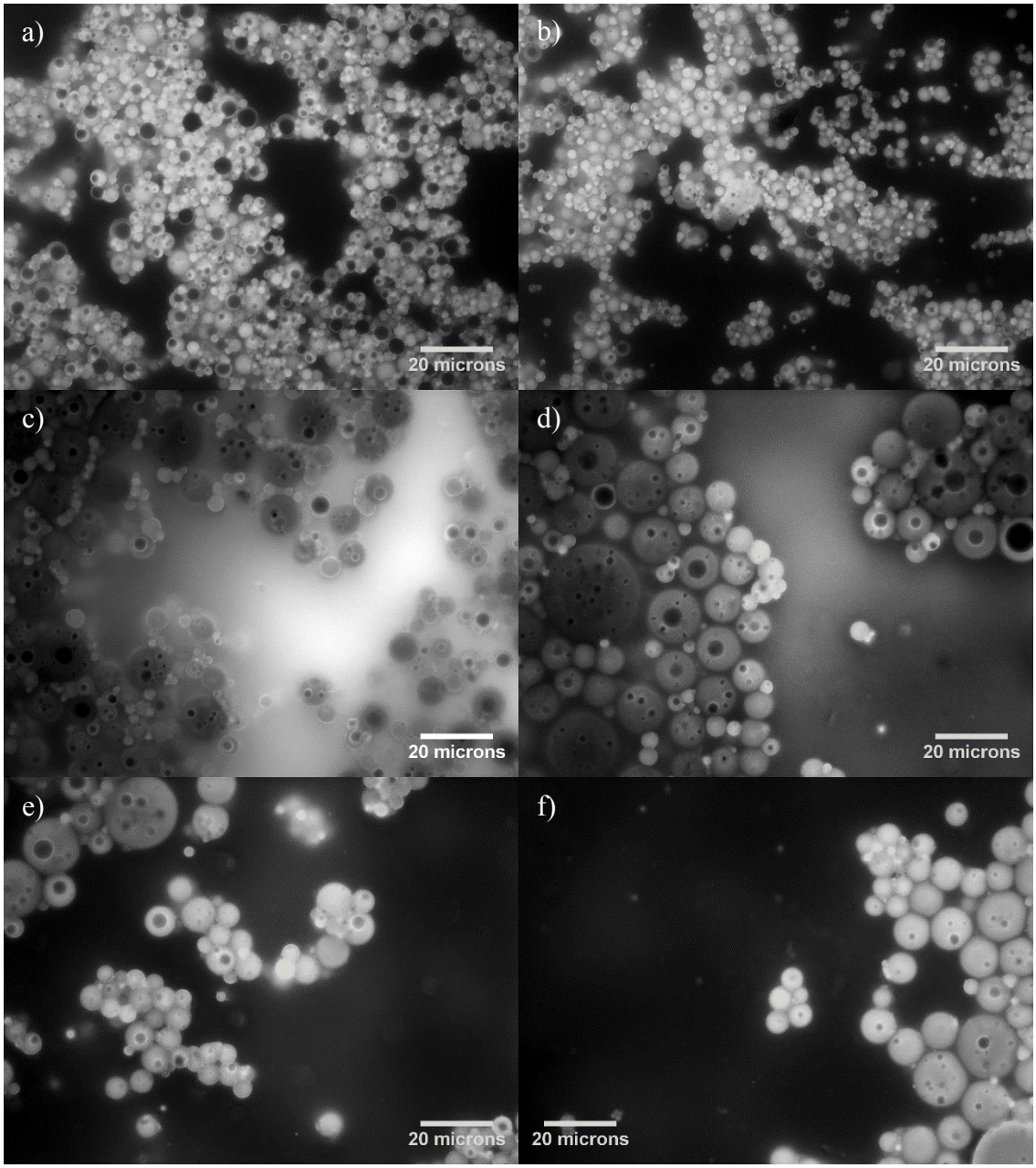

Fig. 4.8: Microscope pictures of oil D in water emulsions. (a) φ=40% d_{43}=11.9µm d_{32}=6.1µm φ_m=0.79, (b) φ=50% d_{43}=13.5µm d_{32}=8.0µm φ_m=0.78, (c) φ=60% d_{43}=20.2µm d_{32}=14.5µm φ_m=0.80, (d) φ=70% d_{43}=22.2µm d_{32}=16.4µm φ_m=0.73, (e) φ=80% d_{43}=18.5µm d_{32}=15.6µm φ_m=0.69, (f) φ=85% d_{43}=19.1µm d_{32}=16.2µm φ_m=0.69. Aqueous phase formulation (1.6% ph15EO 0.2% NaOH, 0% NaCl). The pictures were taken at the edge of the borosilicate chambered coverglass where a higher concentration of water is observed.

The photomicrographs of emulsion samples at the edge of the coverglasses showed formation of aggregating structures due to the attractive interactions between the oil droplets. An importance point to note is a slight deformation of spherical droplets at the point of contact observed clearly in Fig. 4.8f. It appeared that the attractive strength between large oil droplets are strong enough to deform the oil droplets at the point of contact. Fig. 4.9 shows the photomicrographs of optimized oil D emulsions, the same samples shown in Fig. 4.5, at the edge of the coverglasses.

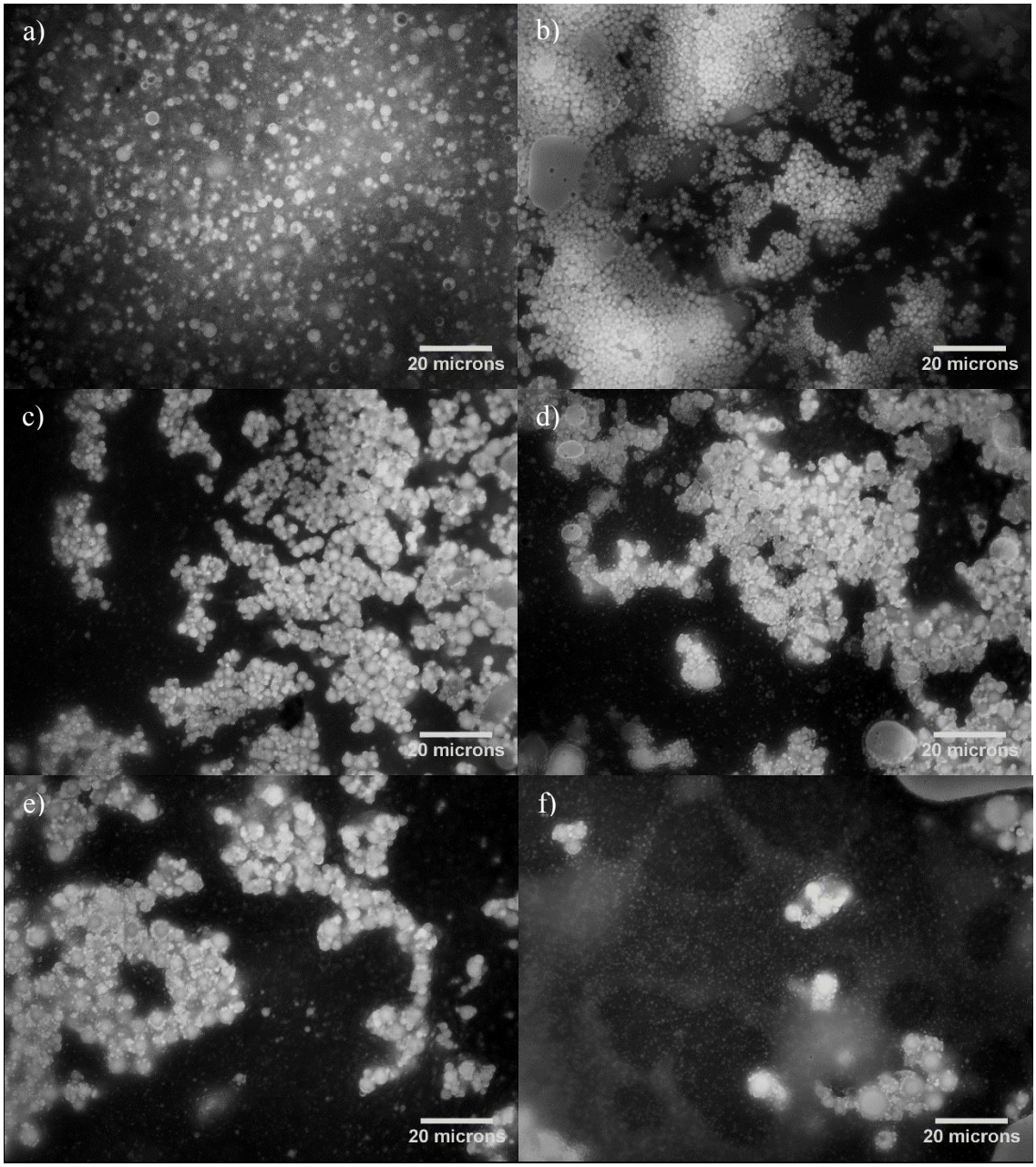

Fig. 4.9: Microscope pictures of oil D in water emulsions. (a) φ=40% d_{43}=2.9µm d_{32}=1.9µm φ_m=0.83, (b) φ=50% d_{43}=6.1µm d_{32}=4.8µm φ_m=0.76, (c) φ=60% d_{43}=13.6µm d_{32}=9.2µm φ_m=0.81, (d) φ=70% d_{43}=21.3µm d_{32}=12.3µm φ_m=0.81, (e) φ=80% d_{43}=19.8µm d_{32}=14.1µm φ_m=0.76, (f) φ=85% d_{43}=20.7µm d_{32}=14.6µm φ_m=0.75. Aqueous phase formulation (1.6% ph15EO 0.2% NaOH, 1% NaCl). The picture were taken at the edge of the borosilicate chambered coverglass where a higher concentration of water is observed.

The photomicrographs of optimized oil D emulsion at the edge of the coverglasses also showed aggregating structures caused by the attractive interaction between oil droplets. Attraction between big-big droplets and big-small droplets are observed. However, very small droplets are observed to be floating individually, suggesting repulsive interaction between very small-very small droplets (d<1μm).

Similar observations were made with oil A and oil B emulsions at the edge of the coverglasses (Fig. 4.10-4.11).

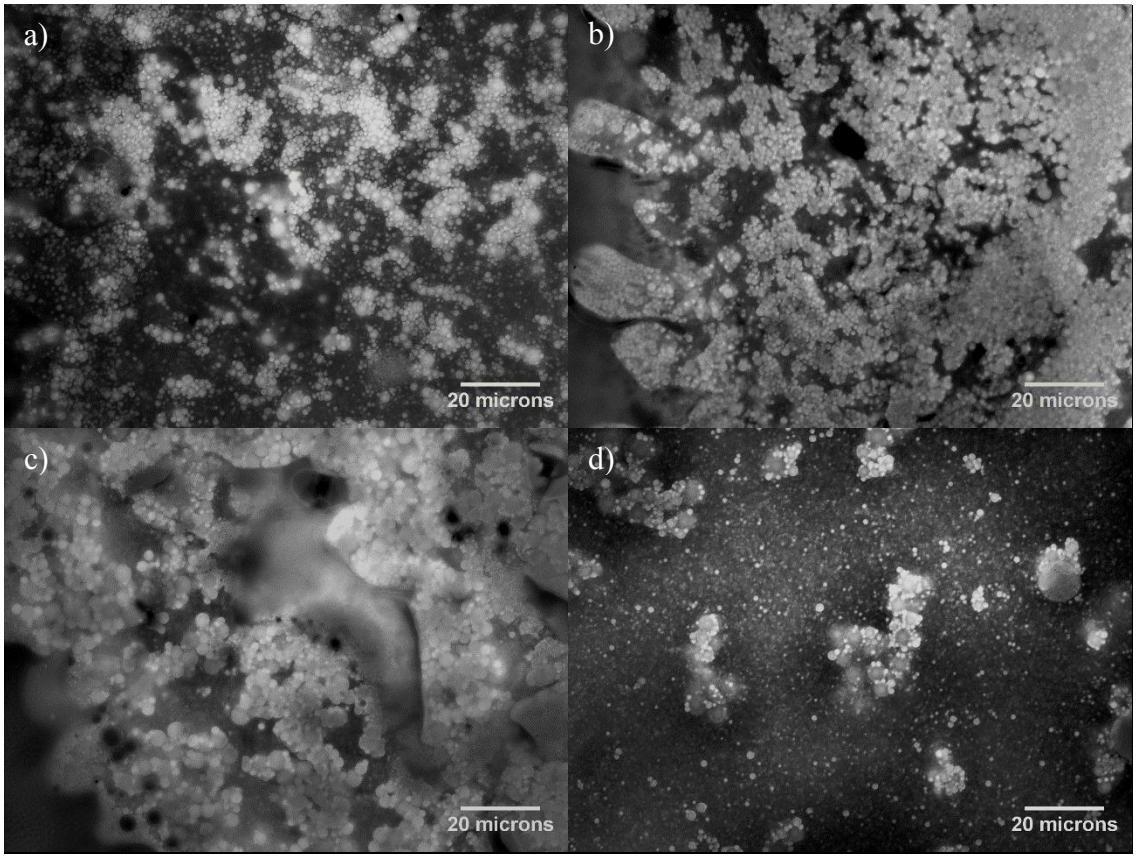

Fig. 4.10: Microscope pictures of oil A in water emulsions. (a) φ=20% d_{43}=2.1μm d_{32}=1.7μm φ_m=0.71, (b) φ=40% d_{43}=1.6μm d_{32}=1.4μm φ_m=0.86, (c) φ=60% d_{43}=6.4μm d_{32}=4.5μm φ_m=0.75, (d) φ=80% d_{43}=22μm d_{32}=15.9μm φ_m=0.74. Aqueous phase formulation (1.6% ph15EO 0.2% NaOH, 0.8% NaCl). The picture taken at the edge of the borosilicate chambered coverglass where a higher concentration of water is observed.

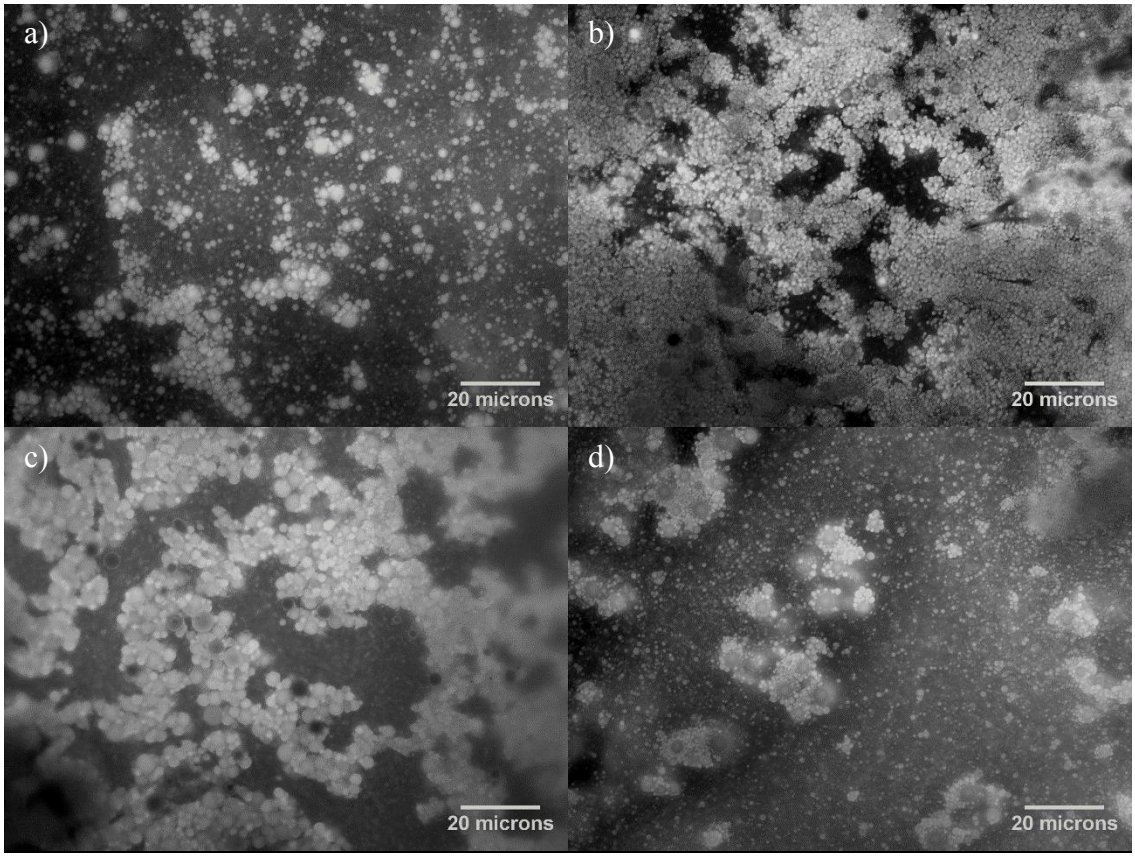

Fig. 4.11: Microscope pictures of oil B in water emulsions. (a) φ=20% d_{43}=3.4µm d_{32}=2.7µm φ_m=0.72, (b) φ=40% d_{43}=3.2µm d_{32}=2.3µm φ_m=0.76, (c) φ=60% d_{43}=8.0µm d_{32}=5.1µm φ_m=0.78, (d) φ=80% d_{43}=20.9µm d_{32}=14.9µm φ_m=0.77. Aqueous phase formulation (1.6% ph15EO 0.2% NaOH, 0.8% NaCl). The picture were taken at the edge of the borosilicate chambered coverglass where a higher concentration of water is observed.

The chemical formulations used to prepared emulsions are changed to observe the effect of chemical formulations on the droplet interaction potential.

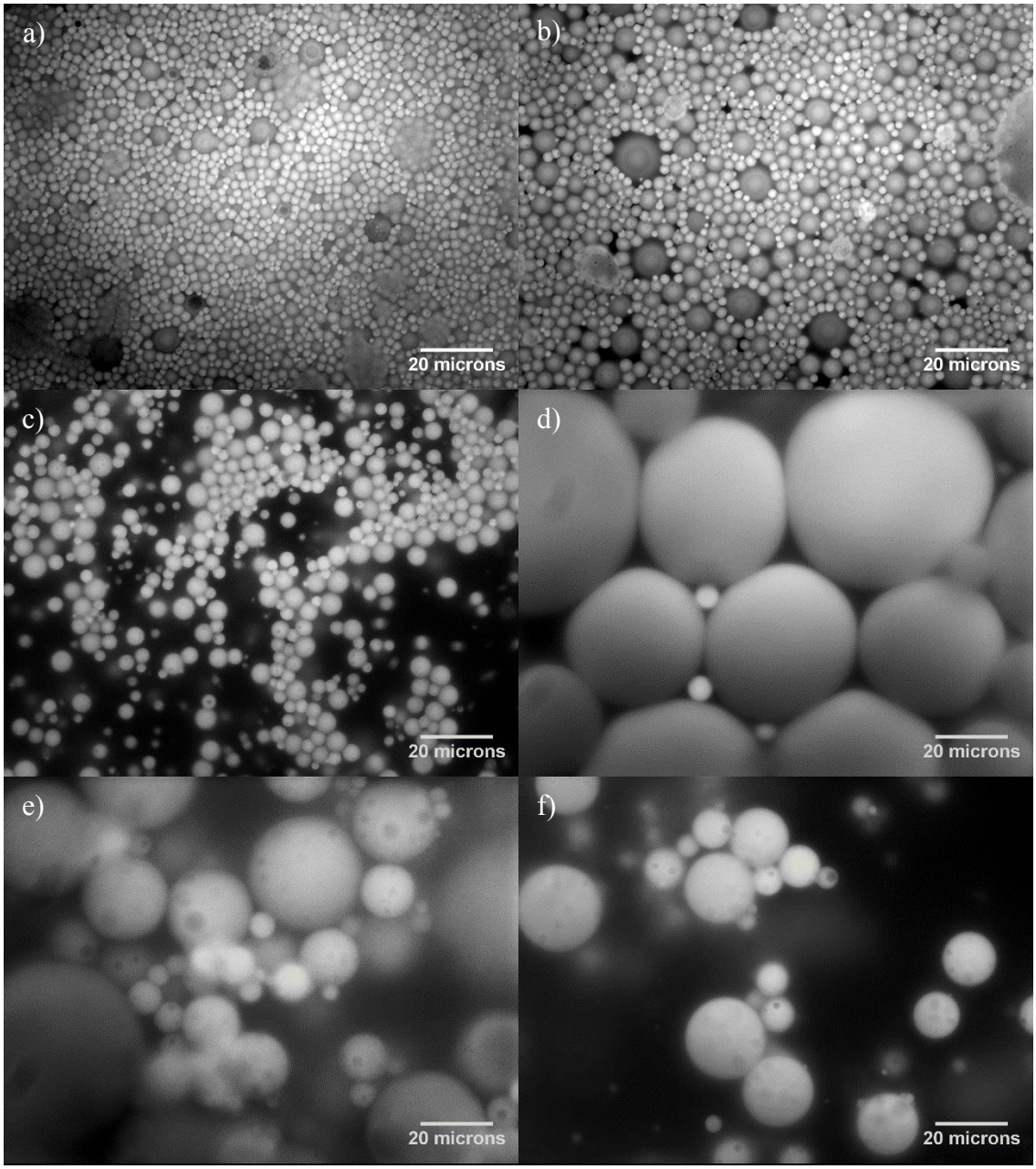

Fig. 4.12: Microscope pictures of (a) 60% oil A emulsion prepared with 2% DMHPA 0.1% NaCl, (b) 60% oil A emulsion prepared with 2% TETA 0.1% NaCl, (c) 60% oil A emulsion prepared with 2% TETA 0.1% NaCl, (d) 85% oil A emulsion prepared with 3% DIPA-15EO 0.2% NaCl, e) 60% oil A emulsion prepared with 1.6% NPE-12EO 0.8% NaCl, f) 60% oil A emulsion prepared with 1.6% NPE-12EO 0.8% NaCl. (c) and (f) are taken at the edge of the coverglasses.

Emulsions prepared with alkyl amines (DMHPA, TETA, and DIPA-15EO) as an alkali and a co-solvent formed stable emulsions with attractive droplets. Emulsions prepared with a non-ionic surfactant, NPE-12EO, showed similar behaviors. The following conclusions can be made from the photomicrographs of heavy O/W emulsions:

1. Oil droplets deformed into polyderal shapes when $\varphi > \varphi_m$
2. Heavy O/W emulsions showed attractive interaction between oil droplets with all chemical formulations used to prepare emulsions in this study.
3. The interaction potential of oil droplets appeared to be a function of droplet diameter.
    a. Big droplets (d>1μm) showed attractive interactions
    b. Very small droplets (d<1μm) showed repulsive interactions
4. A slight deformation of the spherical oil droplets at the point of contact caused by attractive oil droplet interactions was observed for some emulsion even when $\varphi < \varphi_m$.
5. The attractive interdroplet interactions resulted in the formation of aggregating structures and perhaps percolating networks of oil droplets for heavy O/W emulsions.

Heavy O/W emulsions prepared with the method stated in Chapter 3 fall under the category of gels and attractive soft glasses because of the attractive interdroplet interactions.

4.3 CALCULATION OF DROPLET INTERACTION POTENTIAL

The interdroplet interaction potential between oil droplets can be modeled using the physicochemical properties of the emulsions. Forces such as the van der Waals attraction force, steric repulsion force, electrostatic repulsion force, oscillatory structural force [Kralchevsky and Denkov (1995); Wasan et al. (2004)], and interfacial deformation force [Danov et al. (1993)] affect the interdroplet interaction potential of oil droplets in

emulsions. However, all the interdroplet forces between oil droplets cannot be calculated due to either the lack of key parameter needed in the calculations or the lack of analytical equations. To capture the qualitative overall picture of oil droplet interactions, the following assumptions are made about the oil droplets in the emulsions to simplify the interaction potential calculations:

1. Solid spheres (no oil droplet deformation)
2. No oscillatory structural forces or depletion attraction force. If depletion attraction force is present due to the presence of surfactant micelles, the contribution is negligible compared to the van der Waals and electrostatic forces.
3. Steric repulsion is ignored. However, steric repulsion force may be present due to the presence of large ethoxylated co-solvents in the chemical formulations. Co-solvents adsorb at the interface along with soaps and may increase the repulsion force between oil droplets.

For dispersions of solid particles in liquid medium, the potential interaction energy between colloids are satisfactorily explained in the framework of the Derjaguin-Landau-Verwey-Overbeek (DLVO) theory. The DLVO theory describes the combined effects of van der Waals forces and Coulombic forces. While only considering the two forces may be too simplistic for heavy oil droplets, it should be enough to qualitatively observe the effects of droplet diameter and aqueous electrolyte concentration on the interaction potential of oil droplets.

The total interaction energy $W_t(r)$ between two oil droplets can be estimated as a sum of two different contributions according to the DLVO theory:

$$W_t(r) = W_{vdW}(r) + W_e(r) \tag{4.1}$$

where $W_{vdW}(r)$ is the van der Waals energy, $W_e(r)$ the electrostatic energy, and r the center-center separation distance between the two droplets. The theories and equations for each of these forces for heavy O/W emulsions are discussed below.

4.3.1 van der Waals Attraction

The energy of interaction per unit area between two hard spheres of different diameter at a distance *D* apart is given by Hamaker (1937):

$$W_{vdw} = -\frac{A_{ret}}{6}\left[\frac{2R_1R_2}{(2R_1+2R_2+D)D} + \frac{2R_1R_2}{(2R_1+D)(2R_2+D)} + \ln\left(\frac{2R_1+2R_2+D)D}{(2R_1+D)(2R_2+D)}\right)\right] \quad (4.2)$$

where A_{ret} is the retarded Hamaker constant of heavy oil droplets in brine, R_1 the radius of the first sphere, R_2 the radius of the second sphere, and D the distance between two spheres ($D = 0$ is when two spheres are in contact). A_{ret} is given by Israelachvili (2011):

$$A_{ret} = A_{non-ret}/(1 + \frac{pD}{100\ nm}) \quad (4.3)$$

where $A_{non-ret}$ is the nonretarded Hamaker constant and $p = 11$ for interactions between spheres. $A_{non-ret} = 3 \times 10^{-21}\ J$ is appropriate for bitumen in water emulsions [Rodríguez-Valverde et al. (2003); Salou et al. (1998); Wu et al. (1999)].

4.3.2 Electrostatic Repulsion

The repulsive energy between two spheres can be calculated by [Rosen and Kunjappu (2012)]:

$$W_R = \frac{\varepsilon_r R \Psi_0^2}{2} \ln(1 + e^{-\kappa D}) \quad (4.4)$$

where Ψ_0 is the surface potential, ε_r the dielectric constant of the dispersing liquid, $1/\kappa$ the effective thickness of the electrical double layer:

$$\frac{1}{\kappa} = \left(\frac{\varepsilon_r \varepsilon_0}{4\pi F^2 \sum_i C_i Z_i^2}\right)^{1/2} \quad (4.5)$$

where ε_r is the dielectric constant of the solution, ε_0 the permittivity of a vacuum, F the Faraday constant, C_i the molar concentration of any ion in the solution, and Z_i the

valence of the ions. $\varepsilon_0 = 8.854 \times 10^{-12}\ F$, $\varepsilon_r = 80.1$ for water, and $F = 96485.33\ C/mol$ are used. An effective radius of two spheres can be calculated for two spheres of different diameter:

$$R_{eff} = \frac{2R_1R_2}{R_1+R_2} \tag{4.6}$$

where R_1 is the radius of the first sphere and R_2 the radius of the second sphere.

The Ionizable Surface Group Model (ISG) proposed by Healy and White (1978) is used to calculate the surface potential of the heavy oil droplets. ISG model assumes that the surface charge of the heavy oils or bitumen is derived from the dissociation of acidic groups on the surface of the droplets. The following equation is used to relate the pH, pKa, and Ψ_0 [Buckley et al. (1989); Healy and White (1978); Takamura and Chow (1985)]:

$$pH_b = -\frac{e\Psi_0}{2.303kT} + pK_a - log\left(\frac{\theta}{\sinh\frac{ze\Psi_0}{2kT}} - 1\right) \tag{4.7}$$

where pH_b is the bulk pH, e the electron charge, k the Boltzmann constant, T the absolute temperature, pK_a the dissociation constant of the naphthenic acids in the heavy oils, z the valency of ions, and θ:

$$\theta = \frac{-eN_s}{(8n\varepsilon kT)^{1/2}} \tag{4.8}$$

where n is the number of counter ions per unit volume, N_s the total surface density of functional groups, and ε the permittivity of the medium.

Three variables are needed to calculate Ψ_0 using Eq. 4.7, pH_b, pK_a, and N_s. The pK_a of naphthenic acids have been found to be ~4-5 [Buckley (1996); Havre et al. (2003); Pauchard et al. (2008)] and N_s can be approximated as $N_s \approx 2 \times 10^{18} - 5 \times 10^{18}$ carboxylic acid cites/m^2 [Buckley (1996); Healy and White (1978); Takamura and Chow (1985)]. $pK_a = 4.5$ and $N_s = 5 \times 10^{18}$ carboxylic acid cites/m^2 were used in this study.

The total surface area of the oil droplets per volume of the emulsion can be estimated as $A_H = 6\varphi/(d_{32})$. Assuming $OH^- + HA \leftrightarrows A^- + H_2O$ where HA is the naphthenic acid and A^- the deprotonated soap, the total moles of NaOH needed to cover the entire surface of oil droplets in an emulsion with soaps can be estimated as $A_H \times V_{emul} \times N_s/N_A$ where V_{emul} is the volume of the emulsion and N_A the Avogadro constant. In all emulsions prepared in this study, the concentration of NaOH was sufficient to generate enough soaps to cover the entire surface of oil droplets.

pH_b of 80% oil B emulsions were measured to be just a fraction of the original aqueous phase pH at moderate alkali concentrations.

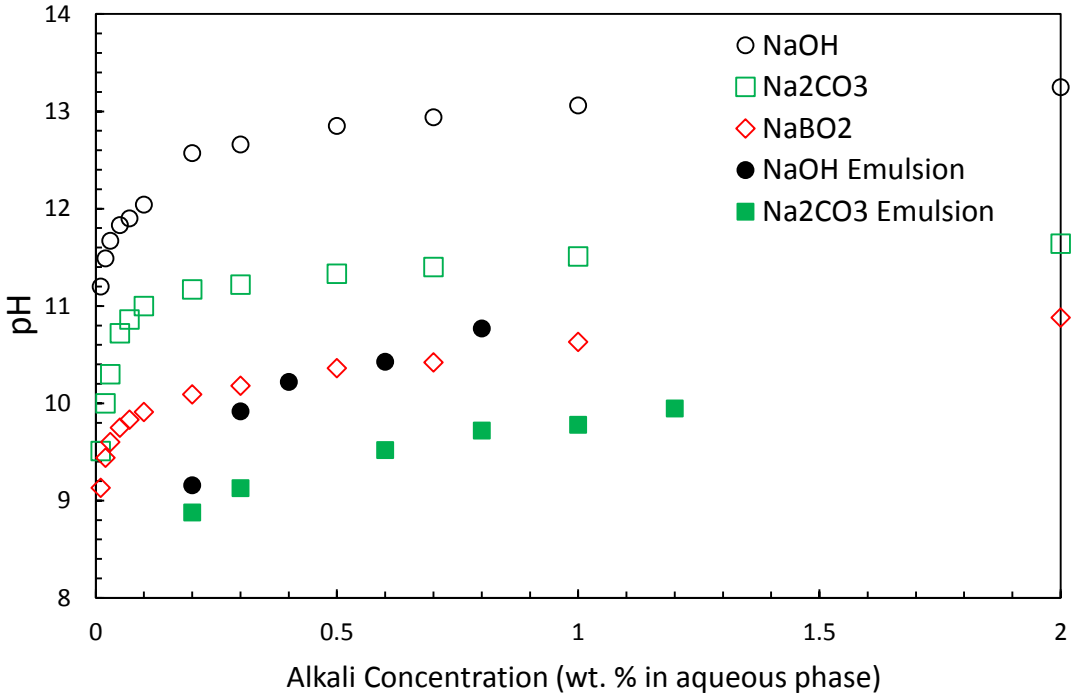

Fig. 4.13: pH of pure aqueous solutions with various alkali and 80% oil B emulsions prepared with 1.6% phenol-15EO, 0.4% NaCl and 0.2-1.2% alkali.

For the ISG model, the bulk pH of the emulsions was estimated to be 1% of the original aqueous phase pH. Very low pH are observed because the total moles of NaOH in most

chemical formulations are a lot less than the total moles of naphthenic acids present in heavy oils. Since Buckley (1996) and Takamura and Chow (1985) showed that Ψ_0 is relatively insensitive when $pH_b > 9$ for moderate electrolyte concentrations, the pH_b of the emulsions should not affect Ψ_0 significantly.

4.3.3 Non-DLVO forces

The non-DLVO forces that were ignored in the calculations are summarized. The accuracy of the interdroplet interaction calculations would improve if these forces can be calculated for heavy oil-in-water emulsions.

Deformable spheres

Soft oil droplets behave differently from hard spheres. Oil droplet can deform at the point of contact and increase the area of contact from a point to a plane. The potential energy of interaction between the two deformed droplets becomes a sum of interactions between two spheres and two planes. Danov et al. (1993) derived expressions to calculate the potential energy of interaction between two deformed droplets. The expressions are very complex and require knowledge of the thickness of the water film that forms between two deformed droplets. They also included a term called surface deformation energy which accounts for the energy required to increase the interfacial area of droplets. Because all the variables needed for these expressions were not available in this study or the literature for heavy O/W emulsions, the expressions derived by Danov et al. (1993) could not be used.

Steric repulsion force

Another type of repulsion force that can stabilize emulsion droplets is the steric repulsion force. Large molecules such as non-ionic surfactants or polymers adsorb at the interface between oil and water and provide a physical barrier against coalescence. The

co-solvents, especially large ethoxylated co-solvents, included in the chemical formulations used to prepare heavy oil-in-water emulsions may provide an additional repulsive force against oil droplet coalescence on top of the electrostatic repulsion effect of the soaps.

Depletion attraction force

An attractive force can arise when large particles such as oil droplets and solid particles are suspended in a solution with much smaller molecules (depletants) such as polymers and surfactant micelles. Asakura and Oosawa (1958) explained the mechanism of depletion attraction force as entropic in nature. Attraction arises when large particles are close enough that the depletants are excluded between them. Thus, depletion attraction force are only relevant at a distance less than the depletant size between the particles. Surfactant micelles and very small oil droplets in polydisperse heavy oil-in-water emulsions can act as depletants to generate an attraction force between the oil droplets. When the concentration of depletants is high, oscillatory structural forces can arise between oil droplets [Kralchevsky and Denkov (1995); Wasan et al. (2004)].

4.4 Results and Discussions

The total energy of interactions for the emulsions in the photomicrographs (Chapter 4.2) are analyzed using the equations in Chapter 4.3 to see if the attractive interdroplet interactions can be modeled. The purpose is quantify the trend of attractive strength as a function of mean droplet diameters and electrolyte concentrations.

The energy of interaction of 80% oil emulsions prepared with 1.6% phenol-15EO, 0.2% NaOH, and 0.8% NaCl is analyzed.

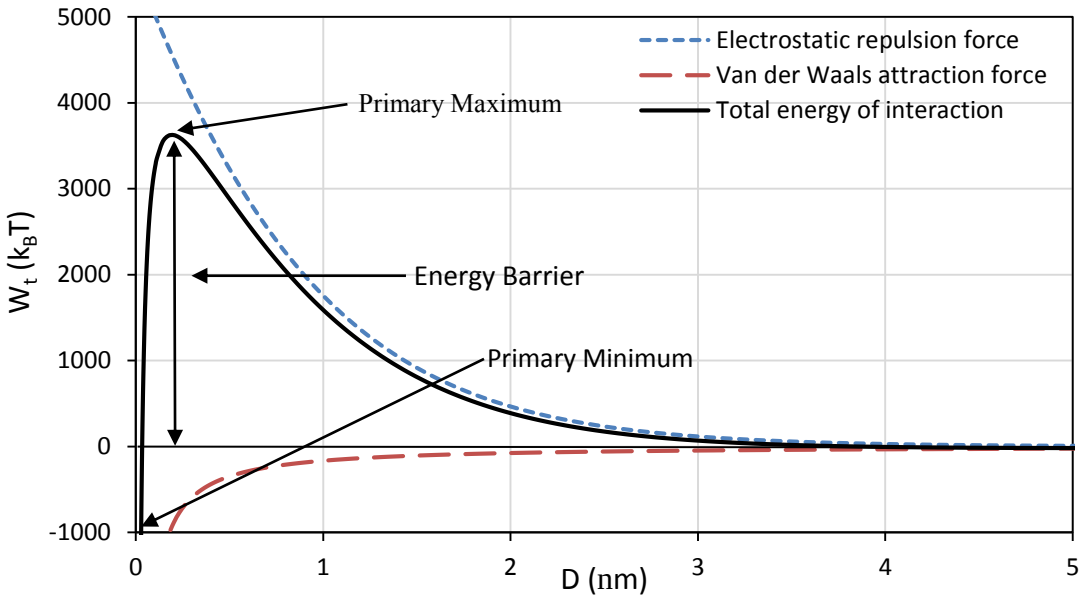

Fig. 4.14: Total energy of interaction of oil D droplets of d_{32}=6μm vs. distance between two droplets. Aqueous formulation of 0.2% NaCl and 0.8% NaCl. Na^+=0.185M. W_t is normalized to k_BT (Thermal energy).

Fig. 4.14 showed W_t vs. D relationship between two oil droplets that is typically observed for heavy O/W emulsions [Salou et al. (1998)]. Positive W_t represents repulsion and negative W_t represents attraction between oil droplets. A primary maximum of W_t is observed near D=0 and represents the energy barrier required for colliding oil droplets to overcome for droplet coalescence to occur. Irreversible droplet coalescence occurs at the primary minimum. The height of the energy barrier indicates the stability of the emulsions. Fig. 4.14 is plotted with a smaller y-axis in Fig. 4.15.

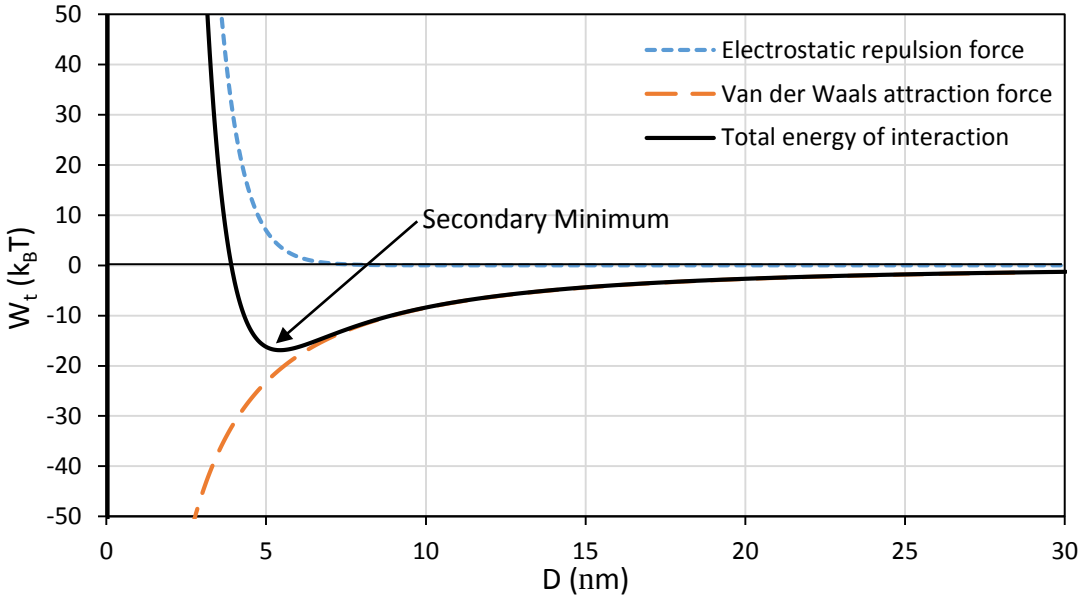

Fig. 4.15: Total energy of interaction of oil D droplets of d_{32}=6μm. Aqueous formulation of 0.2% NaCl and 0.8% NaCl. Na^+=0.185M. W_t is normalized to k_BT.

A secondary minimum of the total energy of interaction is observed when the distance between the two oil droplets is ~5nm. The secondary minimum represents an attractive force much weaker than the primary minimum. If the secondary minimum is $W_t > -1k_BT$, aggregating structures will not form. If the secondary minimum is $W_t < -1k_BT$, a reversible aggregation of droplets will occur. The DLVO analysis of the energy of interaction between the oil droplets with d_{32}=6μm agreed with the photomicrograph observation of aggregating heavy oil droplets. The two values of importance are the primary maximum (stability against coalescence) and secondary minimum (oil droplet aggregation).

The effect of droplet size on the total energy of interaction is analyzed in Fig. 4.16.

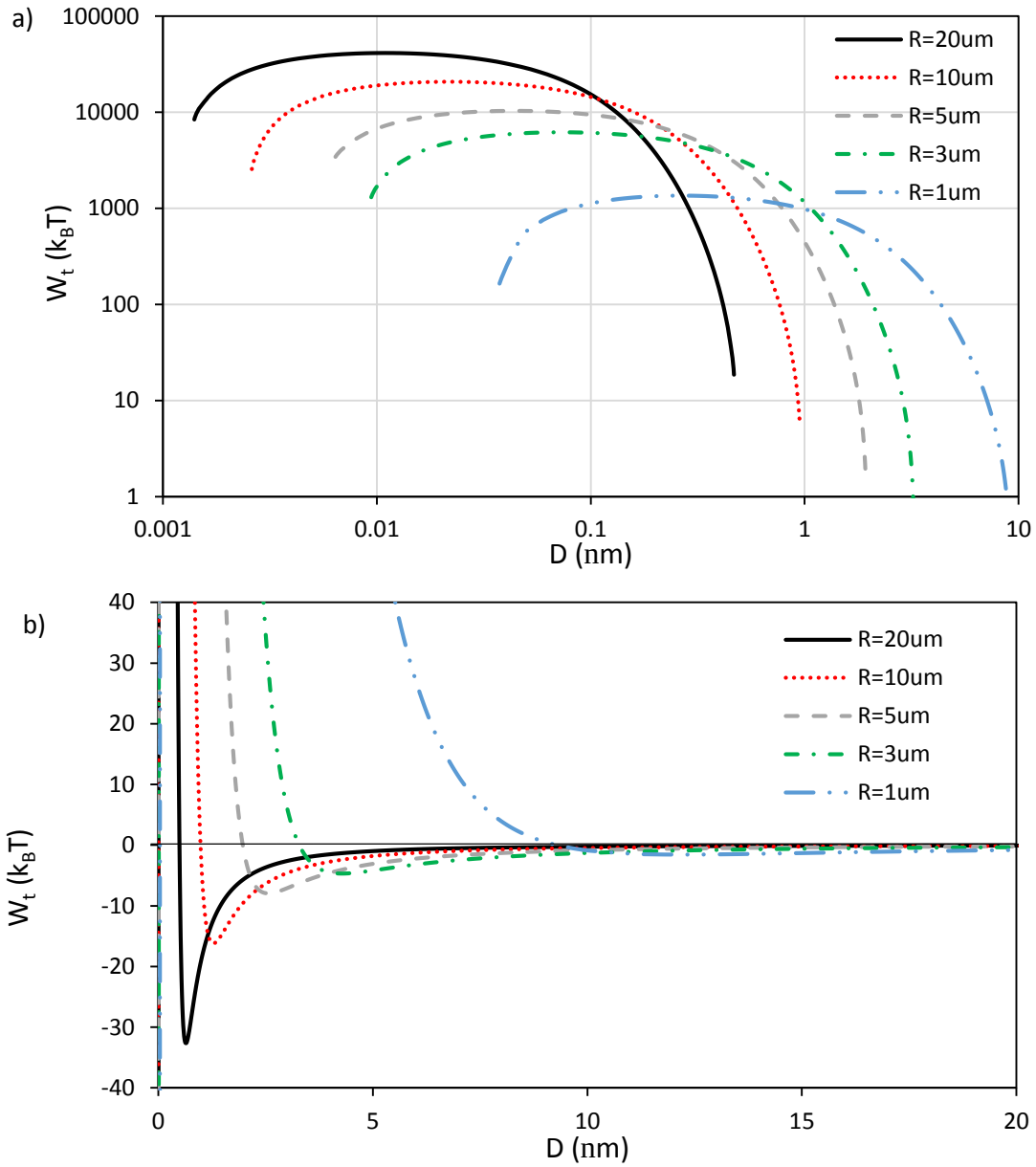

Fig. 4.16: Total energy of interaction of oil droplets with an aqueous formulation of 1.6% phenol-15EO, 0.2% NaOH and 0.0% NaCl. Na^+=0.05M. The radius of the oil droplets are varied from 1-20μm. a) A plot of the primary maximum. b) A plot of the secondary minimum.

The primary maximum (energy barrier) increased as the oil droplet size increased. The secondary minimum was the lowest for the droplets with the largest size and biggest for the droplets with the smallest size. Droplets with R=1μm showed a secondary minimum

of $W_t \approx -1.5k_BT$. The analysis of the effect of droplet size on the interaction energy of droplets agreed with the photomicrographs of emulsions. Big droplets form aggregates and very small droplets with $R \ll 1\mu m$ show repulsive interactions and resist aggregation.

The effect of electrolyte concentration on the total energy of interaction is analyzed in Fig. 4.16.

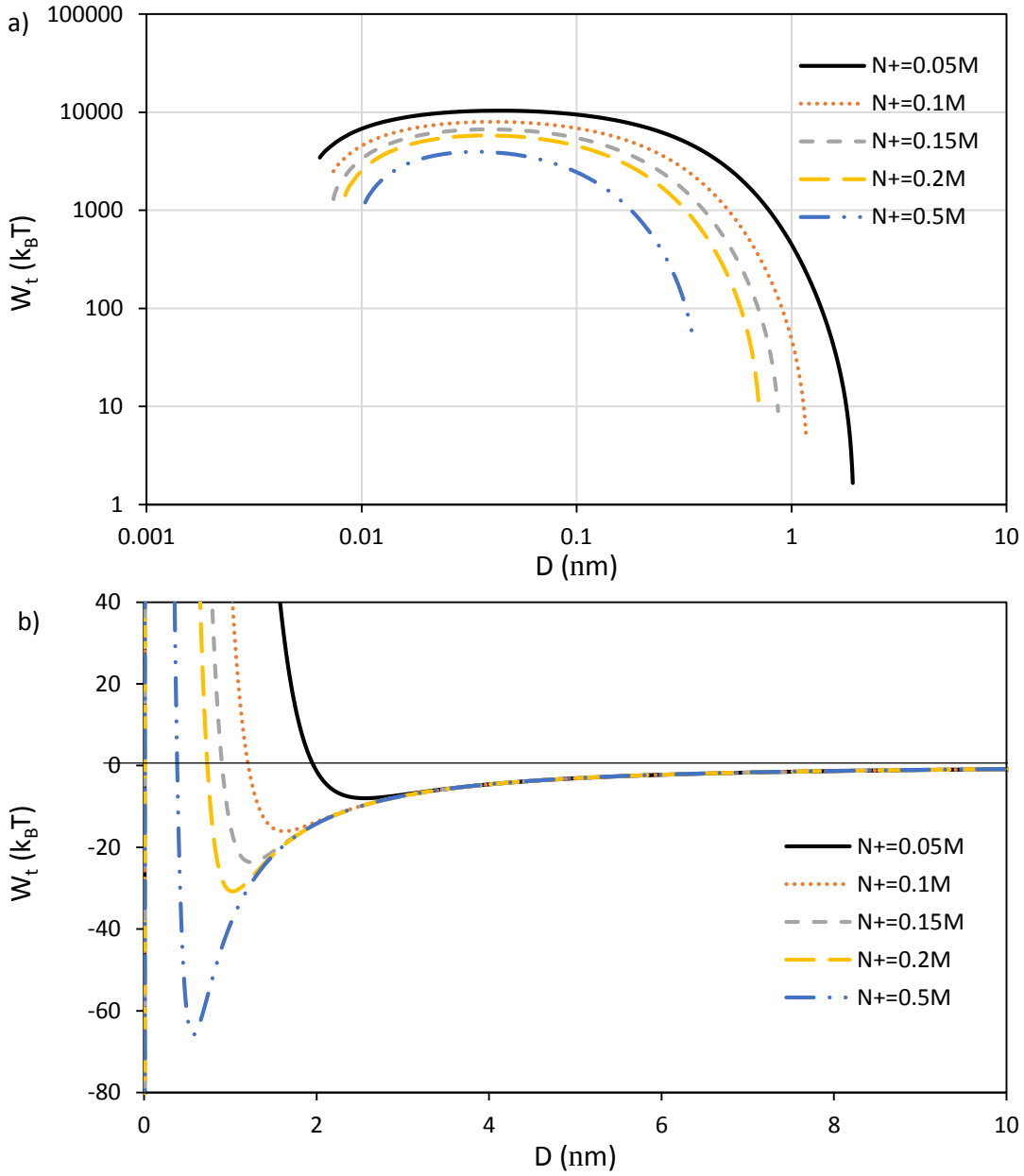

Fig. 4.17: Total energy of interaction of oil droplets with an aqueous formulation of 1.6% phenol-15EO and 0.2% NaOH. R=5 μm. The electrolyte concentration in the aqueous phase are varied from Na^+=0.05-0.5M. a) A plot of the primary maximum. b) A plot of the secondary minimum.

Both the primary maximum and secondary minimum decreased when the electrolyte concentration increased. This is due to the decrease in the electrical double layer thickness (κ^{-1}) caused by higher electrolyte concentrations. Smaller κ^{-1} translates to a

weaker electrostatic repulsive force between oil droplets and stronger secondary minimum.

The interaction potential between two droplets of different radii are calculated. The first droplet radius is a constant of R_1=5 μm. The second droplet radius is varied from R_2=0.25-5 μm.

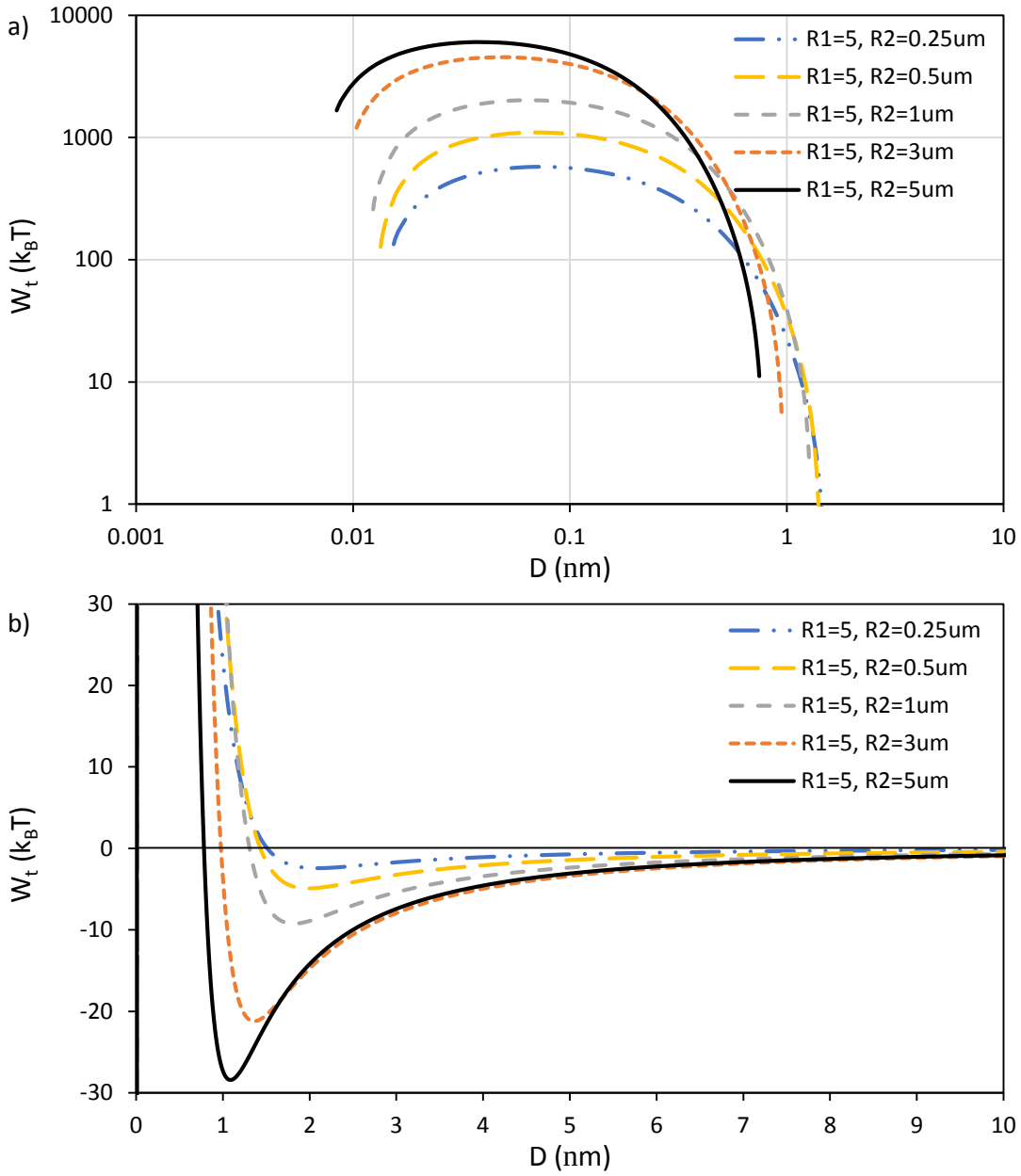

Fig. 4.18: Total energy of interaction of oil droplets with an aqueous formulation of 1.6% phenol-15EO and 0.2% NaOH, and 0.8% NaCl. Na^+=0.2M. Oil droplets of different radius were analyzed. R_1=5 µm and R_2=0.25-5 µm. a) A plot of the primary maximum. b) A plot of the secondary minimum.

The primary maximum decreased and secondary minimum increased when R_2 decreased.

Small droplets (R_2=0.25 µm) that do not form aggregating structures with each other will

be attracted to big droplets (R_1=5 μm). However, if R_2 is very small (R_2<0.25 μm), the aggregate structures of very small droplets and big droplets will not form.

4.5 CONCLUSIONS

The DLVO analysis and photomicrographs of heavy oil-in-water emulsions both agreed on the following points:

1. All heavy oil-in-water emulsions prepared with a chemical formulation of alkali, co-solvent, and electrolyte formed reversible aggregate structures with
    a. A very large energy barrier against droplet coalescence.
    b. A secondary minimum where a weak attraction between oil droplets is observed at some distance between the droplets.
2. The interaction potential of heavy oil droplets is a function of droplet diameter. Oil droplets with a larger diameter showed a stronger interdroplet attractive force.
    a. Two big droplets (d>1μm) showed attractive interactions.
    b. Two small droplets (d<1μm) showed repulsive interactions.
    c. A big droplet (d>1μm) and a small droplet (d<1μm) showed attractive interactions unless the diameter of the small droplet was d<<1μm.
3. The interaction potential of heavy oil droplets is a function of the aqueous electrolyte concentration. Higher electrolyte concentration increased the attractive force between the oil droplets.
4. The attractive inter-droplet interactions resulted in the formation of aggregating structures and perhaps percolating networks of oil droplets for heavy oil-in-water emulsions. The presence of yield stress for emulsions with $\varphi < \varphi_m$ is an indiction of percolating networks of oil droplets.

The heavy oil-in-water emulsions prepared in this study fall under the category of soft matter that form attractive soft glasses when $\varphi > \varphi_m$ and gels when $\varphi < \varphi_m$ due to the attractive forces between the oil droplets. The formation of reversible aggregate structures composed of heavy oil droplets may impart unique rheological properties to heavy oil-in-water emulsions that are not typically observed with emulsions that show repulsive interdroplet interactions.

NOMENCLATURE

pK_a	Acid dissociation constant
N_A	Avogadro constant
k_B	Boltzmann constant
r	Center-to-center distance between two spheres
φ	Dispersed-phase volume fraction of emulsions
R_{eff}	Effective radius of two spheres with different radius
$1/\kappa$	Effective thickness of the electrical double layer
e	Electron charge
W_e	Electrostatic energy
F	Faraday constant
A	Hamaker constant
φ_m	Maximum packing volume fraction (φ_m) of dispersed-phase possible without deformation of the spherical dispersed-phase
C_i	Molar concentration of ion *i*
$A_{non-ret}$	Nonretarded Hamaker constant
n	Number of counter ions per volume
ε_0	Permittivity of a vacuum
pH_b	pH of the bulk solution
R_i	Radius of sphere i
ε_r	Relative dielectric constant of the solution
A_{ret}	Retarded Hamaker constant
d_{32}	Sauter mean droplet diameter
Ψ_0	Surface potential
D	Surface-to-surface distance between two spheres
T	Temperature
W_t	Total interaction energy
A_H	Total surface area of oil droplets per volume of emulsion
N_S	Total surface density of functional groups
Z_i	Valence of ion i
W_{vdW}	van der Waals energy
V_{emul}	Volume of emulsion

ABBREVIATIONS

DLVO	Derjaguin-Landau-Verwey-Overbeek
ISG	Ionizable Surface Group

Chapter 5: Rheology of Concentrated Heavy Oil-in-Water Emulsions

5.1 INTRODUCTION

Concentrated emulsions with dispersed phase concentration higher than the sphere random close packing limit deform the dispersed phase into non-spherical shapes [Foudazi et al. (2012); Meeker et al. (2004); Princen (1983)]. These concentrated emulsions show complex non-Newtonian fluid behaviors, shear thinning behavior, yield stress, slip at the surface [Meeker et al. (2004); Seth et al. (2012)], and viscoelasticity, not observed with dilute and moderate dispersed phase emulsions. Princen and Kiss (1989) and Seth et al. (2011) derived models that accurately described the rheological properties of concentrated emulsions with repulsive interdroplet interactions.

Princen and Kiss (1989) and Seth et al. (2011) made two assumptions in the derivation of the model: 1) repulsive interaction between the dispersed-phase particles/droplet and 2) fairly uniform unimodal droplet size distribution. However, heavy oil-in-water emulsions are polydisperse in nature and showed attractive interactions between the oil droplets, forming gels or attractive soft glasses based on the dispersed-phase concentration. Datta et al. (2011) showed that attractive interactions between oil droplets dramatically influenced the emulsion rheology compared to repulsive emulsions. Foudazi et al. (2012) showed that the micromechanical model proposed by Seth et al. failed to accurately model the rheological properties of concentrated W/O emulsions with bimodal droplet size distributions.

Repulsive soft glasses, such as microgels and concentrated emulsions, showed wall slip behavior on smooth surfaces at stresses below and just above the yield stress of the material [Meeker et al. (2004); Seth et al. (2008)]. Wall slip can significantly improve the flow rate of emulsions below and above the yield stress in pipelines.

There are two main objectives for studying the rheology of heavy oil-in-water emulsions for pipeline transportation purpose:

1) Characterize all the rheological properties of heavy oil-in-water emulsions. Investigate whether heavy oil-in-water emulsions with attractive droplet interactions show wall slip behavior similar to concentrated emulsions with repulsive droplet interactions. Accurately upscaling and predicting the flow of emulsions in crude oil pipelines from laboratory measurements can only be accomplished by fully understanding the rheology of heavy-oil-water emulsions.

2) Optimize concentrated heavy oil-in-water formulation to prepare emulsions with low viscosity. Quantify how the physicochemical properties of emulsions such as average droplet diameter, droplet size distribution, and dispersed phase and continuous phase viscosities affect the rheological properties of concentrated heavy oil-in-water emulsions.

5.2 LITERATURE REVIEW

The literature review of the rheological properties of colloidal suspensions, especially soft glasses with attractive interaction between the dispersed phase, are discussed below. Refer to Appendix A2 for the background on the rheological measurement techniques, procedures, and calculations used to characterize colloidal suspensions.

5.2.1 Effect of physicochemical properties of emulsions on rheology

The effect of physicochemical properties of emulsions on rheology can be analyzed using the rheological models. Rheological models for repulsive emulsions are readily available in the literature. However, there is a lack of rheological models for attractive emulsions.

Repulsive emulsions

There are several models that can be used to describe the rheology of repulsive emulsions.

For emulsions with $\varphi < \varphi_m$, the equation introduced by Pal (2001) works very well:

$$\mu_r \left[\frac{2\mu_r+5K}{2+5K}\right]^{3/2} = \left(1-\frac{\varphi}{\varphi_m}\right)^{-2.5\varphi_m} \quad (5.1)$$

where μ_r is the viscosity ratio of the emulsion (μ) to the continuous phase (μ_c), K the viscosity ratio of the dispersed phase to continuous phase, and φ_m the maximum packing volume fraction of the particles. Neither the mean droplet diameter d_{32} nor the interfacial tension Γ affected the emulsion viscosity [Pal (2001)].

For emulsions with $\varphi > \varphi_m$, the micromechanical model proposed by Seth et al. (2011) and modified with $\tau_y = \gamma_y G$ and $E^* = 9.92\Gamma/R$ [Seth et al. (2006)] accurately modeled the rheology of concentrated emulsions with repulsive interactions :

$$\tau = \tau_y + cG\left[\frac{\mu_c d_{32}\dot{\gamma}}{\Gamma}\right]^{1/2} \quad (5.2)$$

where τ_y is the yield stress, c a constant, G the strain and frequency independent storage modulus, $\dot{\gamma}$ the shear rate, Γ the interfacial tension, d_{32} the Sauter mean diameter, and μ_c the continuous phase viscosity. Eq. 5.2 can be modified using the expression $G_0 \sim \Gamma\varphi(\varphi-\varphi_m)/R_{32}$ [Mason et al. (1995)] and $\tau_y = \Gamma\varphi^{\frac{1}{3}}Y(\varphi)/d_{32}$ [Princen and Kiss (1989)] where $Y(\varphi)$ is obtained from experiments and lower $Y(\varphi)$ is obtained for lower φ:

$$\tau = \frac{\Gamma\varphi^{\frac{1}{3}}Y(\varphi)}{d_{32}} + c\varphi(\varphi-\varphi_m)\left[\frac{\Gamma\mu_c\dot{\gamma}}{d_{32}}\right]^{1/2} \quad (5.3)$$

Eq. 5.3 suggests that lower τ and thus μ are obtained for concentrated emulsions with $\downarrow \varphi$, $\downarrow \Gamma$, $\downarrow \mu_c$, $\uparrow \varphi_m$, $\uparrow \dot{\gamma}$, and $\uparrow d_{32}$. Heavy oil-in-water emulsions with the physicochemical properties that result in low emulsion viscosities can be prepared using the chemical formulation method proposed in Chapter 3.

Attractive emulsions

A model for rheology of attractive emulsions has not been developed in the literature. The difficulty of developing a model for attractive emulsions may be because of the formation of networks and aggregates/clusters. The mean effective diameter of aggregates/clusters is a function of $\dot{\gamma}$ ($d_{eff}(\dot{\gamma})$) and is hard to predict because aggregates/clusters breakup under shear. Also the φ of attractive emulsions is a function of $\dot{\gamma}$ ($\varphi_{eff}(\dot{\gamma})$) because of water inclusions in the aggregates/clusters which increase the effective dispersed-phase volume φ_{eff} (see Fig. 5.1).

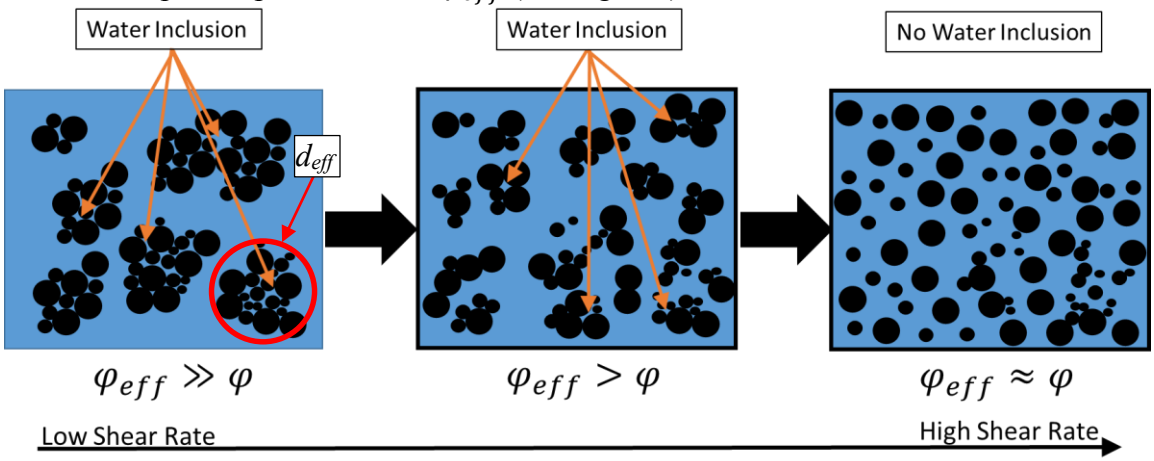

Fig. 5.1: Illustration of aggregate structures breaking down with increasing magnitude of shear. Water inclusion results in higher dispersed-phase volume than the total particle/droplet volume.

The effect of attractive interactions between the dispersed phase particles/droplets on the rheological properties of colloidal suspensions have been reviewed.

5.2.2 Yield Stress

Two yield stresses have been observed for attractive colloidal suspensions; 1) a conventional yield stress necessary to start flow (τ_{y1}) and 2) a flow induced yield stress (τ_{y2}). This behavior is termed "two-step yielding" in the literature. Since the concentrated heavy oil-in-water emulsions prepared in this study are observed to be all

attractive from the photomicrographs, whether heavy oil-in-water emulsions show two-step yielding behavior needs to be verified and characterized.

Extensive literature review suggested the following theory for the appearance of a two-step yielding behavior with concentrated colloidal suspensions; two different length scales and/or relaxation times. Pham et al. (2006) observed that repulsive spheres showed a single yield stress and attractive spheres showed a two-step yielding behavior. The degree of attraction between the repulsive hard spheres was adjusted by adding small quantities of non-adsorbing polymer which caused depletion attraction between the spheres. Subsequent studies of the same attractive samples by Koumakis and Petekidis (2011) and Pham et al. (2008) suggested that the first yielding is caused by the inter-particle bond breaking process between the aggregates and the second yielding is caused by cage breaking of the aggregates. Two different length scales/relaxation times can be created by two methods: 1) creating optimal bimodal particle size distribution of repulsive dispersed phase as observed by Sentjabrskaja et al. (2013) or 2) creating colloidal suspensions with attractive interparticle interactions such as attraction-dominated hard colloidal glasses [Pham et al. (2008), (2006) and Koumakis and Petekidis (2011)], polymer microgel suspensions [Balmforth et al. (2014); Coussot et al. (2009); Shao et al. (2013); Zhou et al. (2014)], attraction dominated soft particle glasses such as concentrated emulsions [Datta et al. (2011); Foudazi et al. (2012), (2011)], and magnetic iron particle suspensions [Fernández-Toledano et al. (2014); Segovia-Gutiérrez et al. (2012)]. Two step yielding behavior is observed by Foudazi et al. (2012) as humps in the flow curves for concentrated W/O emulsions measured with cross-hatched parallel plates even though it is not explicitly stated as such. The attraction between the dispersed spheres/droplets can be created by depletion mechanism [Koumakis and Petekidis (2011); Pham et al. (2008), (2006)], varying the van der Waals attraction and electrostatic

repulsion forces by changing the temperature, concentration of surfactants, and salinity of the continuous phase [Berli (2007); Shao et al. (2013)], having oppositely charged colloidal particles [Zong et al. (2013)], and having particles with varying size and surface functionality in surfactant suspension paste [Shukla et al. (2015)].

The two yield stresses in two-step yielding are defined as follows: (1) a dynamic yield stress, τ_{y1}, as the yield stress when the shear rate approaches zero and (2) a flow induced yield stress, τ_{y2}, as the yield stress observed at some critical shear rate, $\dot{\gamma}_c$. The τ_{y1} value can be measured either with 1) dynamic methods such as extrapolating τ vs. $\dot{\gamma}$ flow curves to zero $\dot{\gamma}$ and oscillatory measurements with the use of Hooke's law $\tau = G\gamma_y$ or 2) static methods such as a stress ramp test and stress growth test. The presence of the flow induced yield stress observed in attractive colloidal suspensions are usually inferred from 1) observations of a hump from a flow curve of τ vs. $\dot{\gamma}$ at some critical shear rate [Foudazi et al. (2012, 2011)] and more commonly, 2) oscillatory measurements of G', G'', and τ vs. γ. The strain overshoot of G', G'' vs. γ and a stress maximum were observed at γ=~1-10 for attractive suspensions [Koumakis and Petekidis (2011); Pham et al. (2008); Zong et al. (2013)].

The literature published on two-step yielding of colloidal suspensions is summarized below.

Table 5.1: A brief summary of literature on two-step yielding. Updated and expanded on the table from Shukla et al. (2015)

Paper	Colloidal Suspension	Description	Dispersed-phase vol. frac.	Method of analysis
Pham et al. 2006, 2008	Sterically stabilized PMMA particles, in decalin. Depletion attraction induced by using PS	Hard sphere repulsive glasses and attractive glasses are formed. Two-step yielding attributed to breaking of attractive bonds, while second yield stress is attributed to cage breaking	$\varphi = 0.6$	Dynamic Oscillatory Rheology
Koumakis & Petekidis 2011	Same as above	Attractive colloidal gels and attractive colloidal glasses are formed. For $\varphi < 0.2$, single-step yielding. For $0.2 < \varphi < 0.58$, attractive gels are formed while for $\varphi > 0.58$, attractive glasses are formed. As volume fraction is increased, two-step yielding becomes more prominent. In glasses: bond breaking followed by cage breaking. In gels: bond breaking following by cluster breaking.	$\varphi = 0.1 - 0.6$	Dynamic Oscillatory Rheology
Laurati et al. 2011	Same as above	Attractive colloidal gels are formed. First yielding is attributed to bond breaking. Second yielding is attributed to cluster breaking. Both yield stresses showed power-law dependence on polymer concentration. Higher polymer concentration equals stronger attraction.	$\varphi = 0.4$	Dynamic Oscillatory Rheology
Kramb & Zukoski 2011	Anisotropic particles of PS, stabilized by PEG suspended in 0.03 M NaCl solution	Hard colloidal glasses are formed. Two-step yielding is shown by heterodicolloid and symmetric homodicolloid shaped particles. Two steps attributed to two relaxation mechanisms by virtue of anisotropy in the particles. First yielding is attributed to particles rotating within the cage and second to particles' center of mass moving within the cage.	$\varphi: = 0.579 - 0.704$ for various shapes	Dynamic Oscillatory Rheology
Datta et al. 2011	Silicone oil dispersed in formamide. Emulsifier: Pluronic P101 nonionic amphiphilic copolymer. Depletion attraction induced by micelles	Repulsive and attractive O/W emulsions are formed. Repulsive emulsions showed only a single yield stress while attractive emulsions showed two-step yielding behavior. First yield stress is attributed to bond breaking and second yield stress is attributed to cluster breaking.	$\varphi = 0.25 - 0.96$	Dynamic Oscillatory Rheology
Chan & Mohraz 2012	Sterically stabilized PMMA particles, in mixed organic system. Depletion attraction induced by PS	Depletion-induced dilute colloidal gels are formed. First yielding event is attributed to unwinding of gel network by bond rotation and rearrangements, and second is attributed to bond breaking	$\varphi = 0.05$	Dynamic Oscillatory Rheology

Continuation of Table. 5.1: A brief summary of literature on two-step yielding. Updated and expanded on the table from Shukla et al. (2015)

Segovia-Gutierrez et al. 2012	Carbonyl iron particle in silicone oil	Magneto-rheological fluids are studies. Two-step yielding is shown at intermediate magnetic fields (~10 kA) for $\varphi > 0.1$. Mechanism is similar to that of attractive gels. First yielding is attributed to breaking of gel network into clusters. Second yielding is attributed to breaking clusters.	$\varphi = 0.05 - 0.5$	Dynamic Oscillatory Rheology
Foudazi et al. 2012	Saturated solution of NH_4NO_3 dispersed in hydrocarbon oil. Emulsifier: polyisobutylen succinic anhydride-urea (PIBSA-Urea)	Bimodal W/O emulsion with size ratios of 2-6 are formed. Volume fraction of the smaller droplets from 0-100% were tested for size ratios of 2-6. Two-step yielding is observed and a steady-state $\sigma\ vs.\dot{\gamma}$ model proposed for two-step yielding emulsions.	$\varphi = 0.85$	Steady-State Rheology
Koumakis et al. 2013	Sterically stabilized PMMA particles, in mixed organic system	Hard sphere glasses are formed. Two-step yielding is shown at intermediate Peclet number. At intermediate Peclet number, both Brownian motion aided yielding and shear induced diffusion act, resulting in two peaks in G"	$\varphi = 0.6 - 0.639$	Dynamic Oscillatory Rheology
Sentjabrskaja et al. 2013	Same as above	Binary hard sphere mixtuers, with size ratio up to 0.2 are formed. Two-step yielding has been linked with the presence of two equally dominant different length scales. Presence of two length scales leads to cages of different sizes. Although two length scales are present in all mixtures, in most samples, one dominates, thus leaving the second one less significant.	$\varphi = 0.55 - 0.61$	Dynamic Oscillatory Rheology
Shao et al. 2013	Aqueous carbopol microgel, with attraction induced by adding salt	Soft jammed repulsive glass and attractive colloidal gel are formed. As attractive strength is increased, the two-step yielding becomes more prominent. First yielding is attributes to network breaking followed by cluster formation. Second yielding is due to breaking of clusters.	Weight %=0.5	Dynamic Oscillatory Rheology
Zong et al. 2013	Oppositely charged colloidal particles, with equal size and PS core and a thin PNIPAM shell, but have oppositely charged end groups. Mixed in equimolar ratio	Low φ gel and high φ glass are formed. Samples with $\varphi < 0.46$ show one-step yielding, $\varphi > 0.46$ show two-step yielding. The first yielding is linked to bond breakage between cages/clusters. The second yielding event is attributed to breaking of cages/clusters themselves. Cages appear in high volume fraction glasses, while clusters are found in low volume fraction gels.	$\varphi = 0.18 - 0.53$	Dynamic Oscillatory Rheology
Shukla et al. 2015	Pastes containing anionic surfactants, clay, and abrasive particles of calcite	Surfactant pastes that contain particles and clay are formed. Two-step yielding is observed. First yielding is attributed to rupture of network. Second yielding is attributed to breaking of aggregates/clusters.	$\varphi = \sim 0.36$	Dynamic Oscillatory Rheology

PMMA: polymethylmethacrylate, PS: polystyrene, PEG: polyethylene glycol, PANIPAM: N-isopropyl acrylamide

The consensus in the literature is that the first yielding event is attributed to breaking of gel network into aggregates/clusters. The second yielding event is attributed to breaking of aggregates/clusters themselves into individual particles/droplets. For $\varphi < \varphi_m$, only the first yielding event results in a yield stress and for $\varphi > \varphi_m$, both yielding events results in yield stresses.

5.2.3 Wall Slip

Using elastohydrodynamic theory, Meeker et al. (2004) and Seth et al. (2012, 2008) were able to relate the physicochemical properties of repulsive soft matter to their wall slip behavior. They showed that wall slip for repulsive soft glasses was tied directly to the bulk fluid yield stress and identified three regimes of slip. *Regime I* is observed at high shear stresses ($\tau/\tau_y > X \; where \; X > 1$), where slip is negligible compared to the bulk flow. *Regime II* is observed above the τ_y ($1 < \tau/\tau_y < X$), where slip becomes significant and the total flow is a combination of slip and bulk flow. *Regime III* is observed below the τ_y ($\tau/\tau_y < 1$), where bulk flow is negligible and flow is due to pure slipping of soft matter. They theorized the X value to be dependent on the type of soft matter with X~1.5 measured for microgel paste.

Meeker et al. (2004) also identified that a yield stress exists for sliding soft matter on smooth surfaces, referred to as the sliding yield stress τ_{sy}. Seth et al. (2008) considered various interaction between the dispersed-phase droplets and the smooth wall surfaces (van der Waals, electrostatic, steric forces) and showed that the τ_{sy} observed for sliding soft matter is controlled by the short-range interactions. They modified the interactions between the droplets and the surfaces by modifying the surface chemistry of the measurement geometries. Repulsive interactions between the droplets and the surfaces resulted in negligible τ_{sy}while strong attractive interactions resulted in the τ_{sy}

value equal to or higher than the τ_y value of the bulk fluid, completely suppressing wall slip even with smooth walls. This is another method of eliminating wall slip without the use of roughened surfaces.

Meeker et al. (2004) derived the following slip velocity model according to the elastohydrodynamic theory for slip *Regime III*:

$$\frac{V_S}{V_y} = \left[\frac{\tau-\tau_{sy}}{\tau_y-\tau_{sy}}\right]^2, \tau/\tau_y < 1 \quad (5.4)$$

where V_S is the slip velocity and V_y the slip velocity at $\tau/\tau_y = 1$. Seth et al. (2012) visually confirmed wall slip of soft glasses using fluorescent microscopy and particle tracking velocimetry. They showed experimentally that the slip velocity varied linearly with the stress τ for wall slip in slip *Regimes II*:

$$\frac{V_S}{V_y} = \left[\frac{\tau-\tau_{sy}}{\tau_y-\tau_{sy}}\right], \tau/\tau_y > 1 \quad (5.5)$$

Meeker et al. (2004) showed that the V_y of repulsive soft glasses scaled linearly according to $V_y \sim G_0 R/\mu_c$, where G_0 is the strain and frequency independent storage modulus, R the radius of the dispersed-phase particles/droplets, and μ_c the continuous phase viscosity. Seth et al. (2012) expanded on the equation and derived the following relationship for the V_y:

$$V_y = \frac{\gamma_y^2 G_0 R}{\mu_c}, \quad (5.6)$$

where γ_y is the yield strain. With the emulsion properties in Eq. 5.6, the $V_S\ vs.\ \tau$ relationship of repulsive soft glasses can be modeled and predicted for any measurement geometry and dimension.

Experimental study of the slip behavior of repulsive soft glasses exist in the literature. However, no comprehensive study on the slip behavior of attractive soft gels/glasses have been conducted in the literature until now. The wall slip behavior of

heavy oil-in-water emulsions with attractive interdroplet interactions have been characterized in this study.

5.2.4 Viscoelasticity

Viscoelasticity of soft matter, both repulsive and attractive, have been studied extensively in the literature using dynamic oscillatory measurements. The oscillatory motion is controlled by a sinusoidal function of sine described as follows:

$$\gamma(t) = \gamma_0 \sin \omega t \tag{5.7}$$

where $\gamma(t)$ is the strain as a function of time, γ_0 the strain amplitude, ω the angular frequency of oscillation, and t the time. The resultant torque data are used to calculate the elastic and viscous properties of the materials. G' is defined as the storage modulus, and $G"$ the loss modulus. G' and $G"$ values are materials functions (ratios of stress and strain) and represent the elastic (solid) and viscous (fluid) properties of the material, respectively. Refer to Appendix A2.5.2 for a detail explanation on oscillatory rheology.

Repulsive soft glasses

All repulsive soft glasses show similar oscillatory behaviors. Fig. 5.2 shows the typical G', G" vs. γ and G', G" vs. ω data of unimodal O/W emulsions with varying dispersed-phase concentrations. Analysis of repulsive emulsions showed the classical Type III behavior outlined by Hyun et al. (2002) for viscoelastic materials. The type III behavior is characterized by a weak strain overshoot of G" with strain sweep test (Fig. 5.2a). The overshoot is a function of φ with stronger overshoot observed for higher φ. Frequency sweep tests at a constant strain within the linear viscoelastic region showed G' that is independent of ω and G" that goes through a minimum for the range of φ tested (Fig. 5.2b). The yield strain of $\gamma_y \approx 10\%$ is observed for all emulsions in Fig. 5.2.

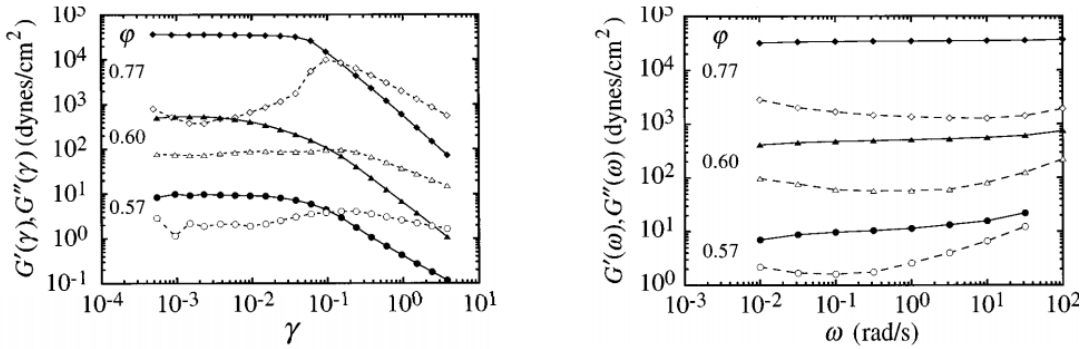

Fig. 5.2: (a) Strain γ and (b) frequency ω dependence of the storage modulus G' (solid symbols) and loss modulus G" (open symbols) for monodisperse silicone O/W emulsions of varying dispersed-phase volume φ. Obtained from Mason et al. (1997)

The γ and ω independent G', G_0, is scaled according to the relationship $G_0 \sim \Gamma f(\varphi)/R_{32}$ where $f(\varphi)$ is a function of φ and is found to be well represented by $G_0 \sim \Gamma\varphi(\varphi - \varphi_m)/R_{32}$ for monodisperse, repulsive O/W emulsions [Mason et al. (1995)].

Attractive soft glasses

Attractive colloidal suspensions show distinctively different dynamic oscillatory rheology compared to repulsive colloidal suspensions. Analysis of attractive soft glasses in the literature showed a combination of Type I & IV behaviors outlined by Hyun et al. (2002) for viscoelastic materials. The Type IV behavior is characterized by a strong strain overshoot of G' and G" with strain sweep tests which indicates attractive interdroplet interactions. Fig. 5.3 shows oscillatory strain sweep measurements of sterically stabilized attractive PMMA particles suspended in decalin obtained from Koumakis and Petekidis (2011). Depletion attraction is induced by polystyrene polymer.

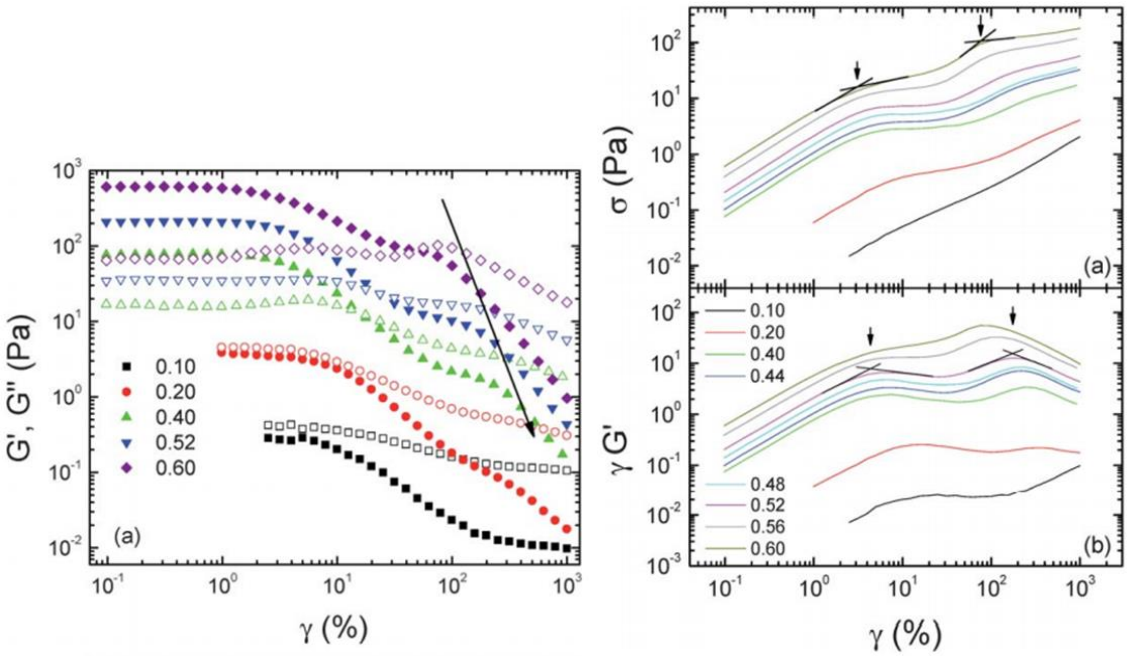

Fig. 5.3: Dynamic strain sweep for suspensions with equal attraction strength and different φ. (a) G',G" vs γ are plotted. The arrow shows the G" peaks. (b) $\tau, \gamma G'$ vs. γ are plotted. The arrows indicate the yield strains and yield stresses. Figures obtained from Koumakis and Petekidis (2011)

The combination of Type I and IV behaviors appeared similar to a combination of two repeating Type I behavior (repulsive). The $\sigma, \gamma G'$ vs. γ plots showed two maximums that indicate the yield strains and stresses. The attractive interdroplet interaction affected the strain independent G' and $G"$ of emulsions significantly compared to emulsions with repulsive interaction when all other parameters were the same. Experimental results from Datta et al. (2011) and Mason et al. (1997) showed that G' and $G"$ vs. φ_{eff} varied significantly for attractive and repulsive emulsions (Fig. 5.4)

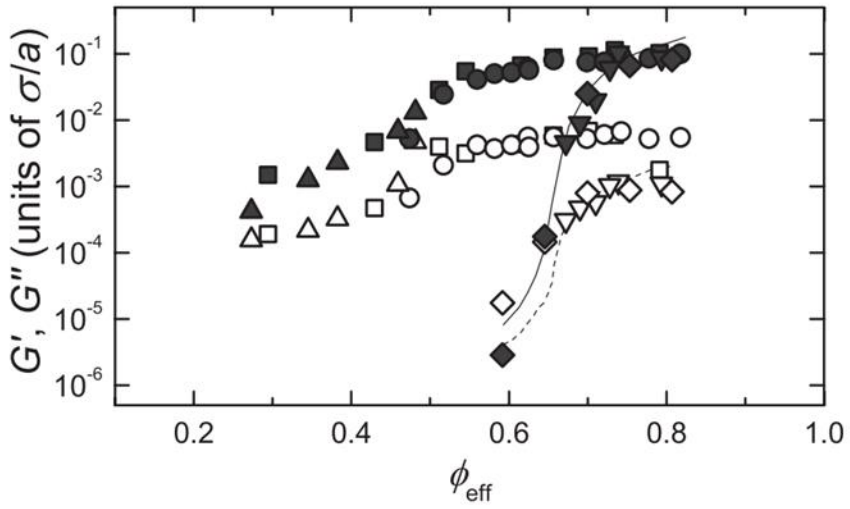

Fig. 5.4: Linear viscoelastic storage and loss moduli G'(solid symbols) and G"(open symbols) vs. φ_{eff} for attractive and repulsive emulsions. Attractive emulsions are circles, upward-pointing triangles, and squares. Repulsive emulsions are diamonds and downward-pointing triangles. Attractive emulsions all have same interaction potential energy. $\varphi_m \approx 0.68 - 0.72$. Figure obtained from Datta et al. (2011). The lines are measurements from Mason et al. (1997)

Datta et al. (2011) showed that for repulsive emulsions, G' and G" values decreased orders of magnitude for $\varphi_{eff} < \varphi_m$, suggesting negligible yield stress. For attractive emulsions, higher G' and G" values are observed for $\varphi_{eff} < \varphi_m$ compared to repulsive emulsions. G' values for attractive emulsions suggested yield stress for $0.25 < \varphi_{eff}$ which are well below the φ_m values. G' values for both attractive and repulsive emulsions converged for high φ_{eff} values, suggesting the interdroplet interactions provide a negligible effect on G' for emulsions that are significantly deformed. The G" values are higher for attractive emulsions compared to the repulsive emulsions at all φ_{eff} values. This suggests that the viscosity of attractive emulsions are higher than the repulsive emulsions at all φ_{eff} values.

The yield strain of emulsions showed a significant variation for attractive emulsions compared to repulsive emulsions (see Fig. 5.5). Repulsive emulsions with

$\varphi_{eff} > \varphi_m$ showed a single yield strain γ_y. The γ_y value appeared to be a constant and not a function of φ_{eff}. The attractive emulsions displayed one yield strain γ_{y1} for $\varphi_{eff} < \varphi_m$ and two yield strains, γ_{y1} and γ_{y2}, for $\varphi_{eff} > \varphi_m$. The two yield strains observed at higher φ_{eff} support the two-step yielding behavior of attractive emulsions.

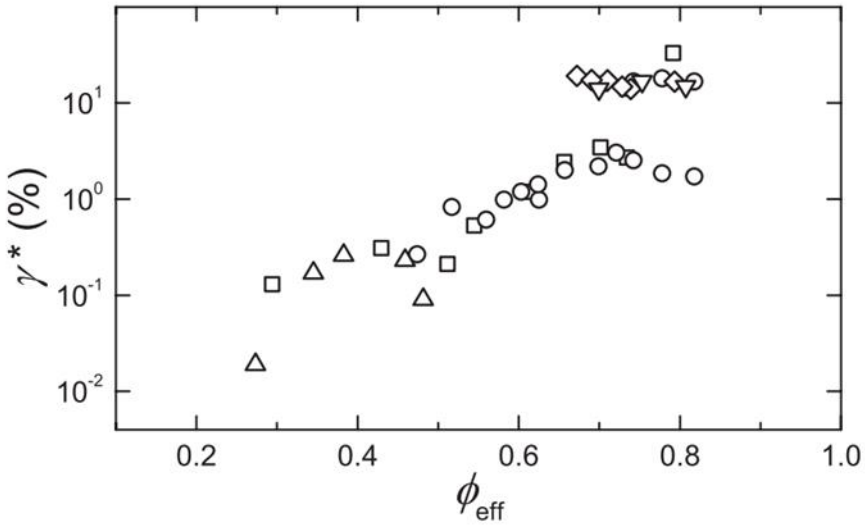

Fig. 5.5: Volume fraction dependent behavior of O/W emulsions. Yield strains of attractive (circles, upward-pointing triangles, and squares) and repulsive (diamonds and downward-pointing triangles) emulsions vs. φ_{eff} are plotted. The lower symbols are the first yield strain of attractive emulsions, γ_{y1}. The top symbolss are the second yield strain of attractive emulsions, γ_{y2} and the yield strain of repulsive emulsions, γ_y. Figure obtained from Datta et al. (2011)

5.2.5 Time-Dependent Flow Property

Concentrated colloidal suspensions showed strong time-dependent properties. The time-dependence is attributed to the microstructural rearrangement of the particles/droplets. At low shear rates, concentrated W/O emulsions showed rheopectic behavior where stress/viscosity increased as the material was sheared longer [Masalova et al. (2005)]. The rheopectic behavior can be identified with two methods; (1) comparison of upward and downward shear rate sweeps of the emulsion (Fig. 5.6a), and (2) transient (time) testing of stress at constant shear rates (Fig. 5.6b).

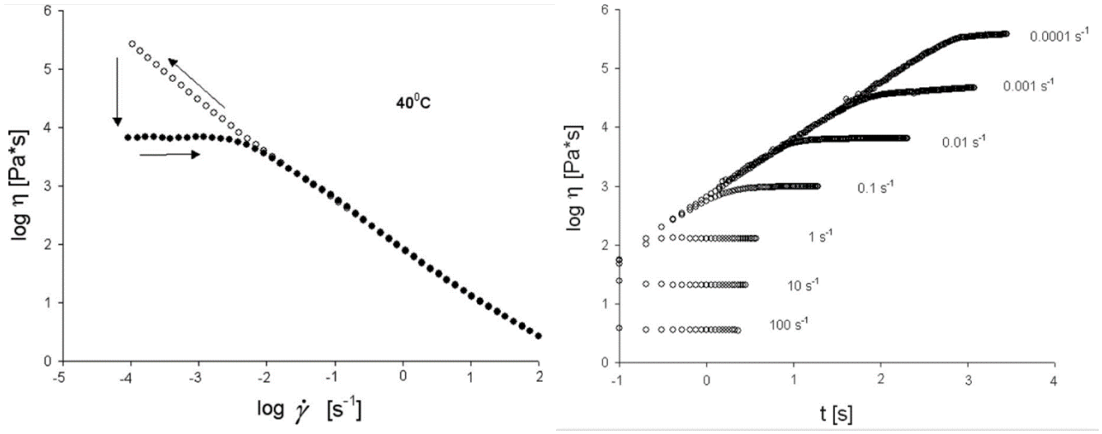

Fig. 5.6: (a) Upward and downward strain sweeps of W/O emulsion ($\varphi = 0.9$) and (b) transient measurement of viscosity at constant shear rates. The x-axis is in log(t). Figures obtained from Masalova et al. (2005)

Fig. 5.6a showed that viscosity hysteresis is observed for a W/O emulsion when upward and downward shear rate sweep tests are performed. The hysteresis is only observed at very low shear rates, confirmed by the transient measurements of viscosity vs. time at constant shear rates (Fig. 5.6b). Less than 1 s is needed to reach steady-state viscosity for $\dot{\gamma} = 1 - 100\ s^{-1}$ while $t > 1{,}000\ s$ is needed to reach steady-state viscosity for $\dot{\gamma} = 10^{-4}\ s^{-1}$.

5.2.6 Shear banding

Attractive colloidal suspensions showed shear banding behavior in measurement geometries with a homogeneous stress field [Bécu et al. (2006); Fall et al. (2010); Møller et al. (2008); Ragouilliaux et al. (2007)]. Shear banding is where the globally imposed shear rate is not distributed homogeneously. This results in thin regions of highly sheared bands while the remaining part of the fluid is not sheared at all. Shear banding can interfere with the analysis and measurements of the emulsion rheological properties.

The direct method of validating the occurrence of shear banding is to measure the velocity profiles of fluids under shear. An indirect evidence of shear banding can be observed from steady-state flow curves of attractive emulsions measured with both strain

controlled and stress controlled viscometers. For emulsions that shows shear banding behavior, the shear rate jumps discontinuously to zero below a critical shear rate with a stress controlled viscometer, unlike with a strain controlled viscometer [Fall et al. (2010); Møller et al. (2008); Ragouilliaux et al. (2007)]. Fig. 5.7 shows the steady-state flow curves of a repulsive emulsion (Fig. 5.7a) and an attractive emulsion (Fig. 5.7b) measured with shear controlled and stress controlled viscometers.

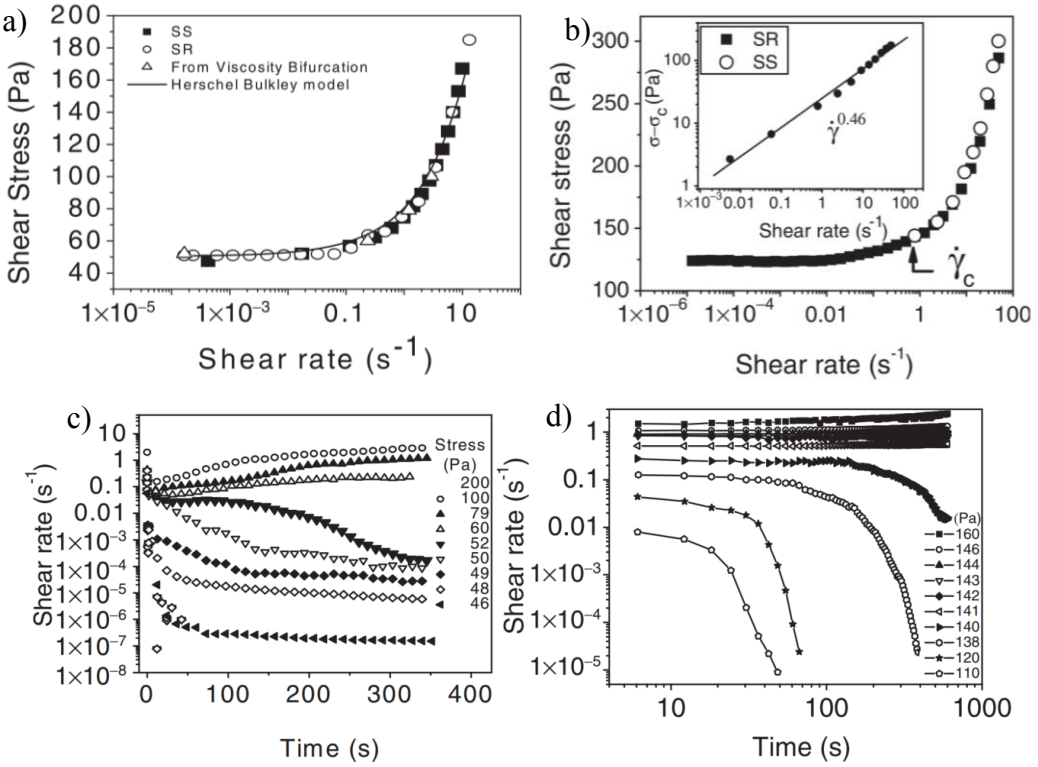

Fig. 5.7: (a) Steady-state flow curve of repulsive emulsion. The diamonds are shear rate controlled (SR) and the squares are stress controlled (SS) measurements. (b) Steady-state flow curve of attractive emulsion. The squares are shear rate controlled (SR) and the circles are stress controlled (SS) measurements. (c) Transient measurements of shear rate vs. time with stress controlled measurements for repulsive emulsion. (d) Transient measurements of shear rate vs. time with stress controlled measurements for attractive emulsion. Figures obtained from Fall et al. (2010).

Fig. 5.7a showed the flow curves of a repulsive emulsion measured with shear controlled and stress controlled viscometers. Both measurements overlapped. However, while an

attractive emulsion showed a typical flow curve behavior when measured with a strain controlled viscometer, no flow below a critical shear rate $\dot{\gamma}_c$ was observed when measured with a stress controlled viscometer (Fig. 5.7b). The discontinuous jump of shear rate to zero below $\dot{\gamma}_c$ for an attractive emulsion can be observed with the transient measurements in Fig. 5.7d.

5.3 EXPERIMENTAL SECTION

The heavy O/W emulsion samples are prepared and their droplet size distribution are characterized according to the procedures outlined in Chapter 3. The rheological properties of the emulsions were measured using TA Instruments advanced rheometric expansion system (ARES LS1) at ambient conditions of 22.25 ^{o}C ±0.25. The parallel plate geometry was used with smooth plates which promotes slip at the wall and cross-hatched parallel plates which eliminates slip at the wall (50 mm diameter and 1 mm gap between plates). The pictures of the parallel plates are shown in Fig. 5.8.

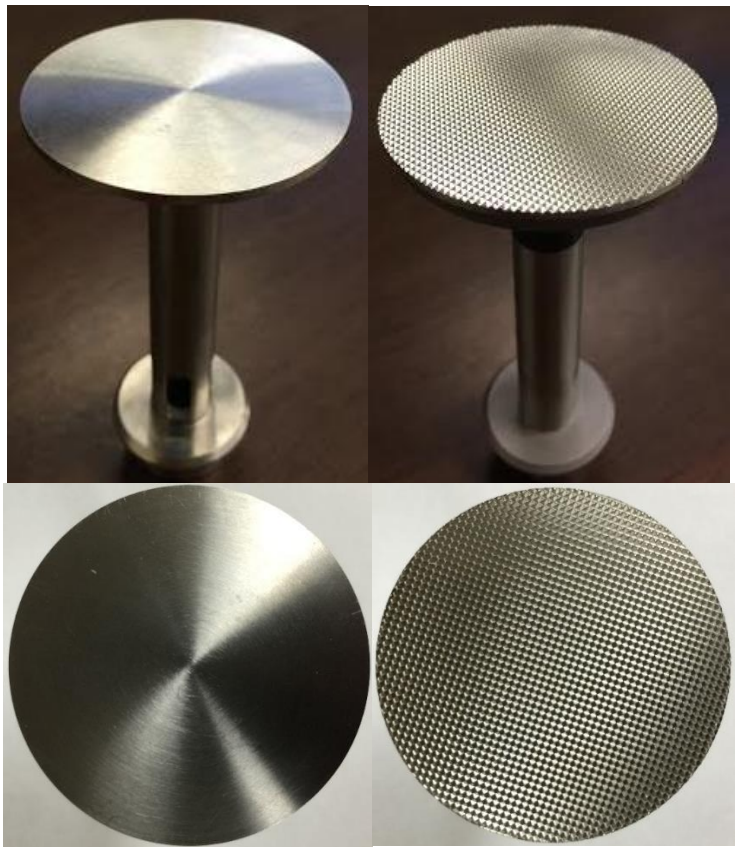

Fig. 5.8: Pictures of parallel plates: Side and top view of a smooth parallel plate (left) and a cross-hatched parallel plate (right).

Appendix A2 has detailed explanations on the following topics as a reference:

1. Basics of fluid mechanics
2. Types of measurement geometries available for viscometers
3. Measurement problems encounters with the viscometer geometries for colloidal suspensions
4. Selection of a measurement geometry for heavy O/W emulsions
5. Rheological measurement techniques and procedures used to characterize heavy O/W emulsions

All measurement scans, steady and oscillatory, are performed from high shear rate/strain/frequency to low. Some of the samples were measured with varying gap widths to verify the elimination of slip at the wall. Since the parallel plate measurements apply heterogeneous shear rates over the radius of the plates, non-Newtonian shear correction must be manually applied to the torque vs. $\dot{\gamma}$ measurement to obtain accurate shear stresses at the edge of the plates. We utilized the Weissenberg-Rabinowitsch correction method [Rabinowitsch (1929)].

$$\tau_R = \frac{2M}{\pi R^3}\left[\frac{3}{4} + \frac{1}{4}\frac{d\ln M}{d\ln \dot{\gamma}_R}\right] \tag{5.8}$$

where τ_R is the shear stress at the edge of the plate, M the torque, and $\dot{\gamma}_R$ the shear rate at the edge of the plate. de Souza Mendes et al. (2014) found that the Weissenberg-Rabinowitsch correction method can also be used to correct the effects of heterogeneous shear rates with oscillatory parallel plate measurements. The only difference is the replacement of the shear rate in Eq. 5.8 with the strain rate. The corrected stresses at the edge of the place are used to calculate the G' and G".

5.3.1 Steady State Measurement

The emulsion samples are loaded onto the bottom parallel plate and the top plate is lowered on the sample slowly until the gap width is reached. Any excess emulsion sample is wiped off. Shear rate sweep tests are conducted in a downward direction from high shear rates to low shear rates. The shear rate range of measurement is 10^{-4}-10^{2} s^{-1}. At each shear rate, the parallel plate rotates for 30 s before 10 s of torque measurements and the torque measurements are averaged. The steps are repeated for subsequent shear rates. Upward shear rate sweep is conducted along with downward shear rate sweep to test for any hysteresis and transient behavior. The same procedure is used with both

smooth and cross-hatched parallel plates to characterize both the bulk emulsion rheological properties and wall slip properties.

5.3.2 Oscillatory Measurements

Only cross-hatched parallel plates are used for oscillatory measurements to measure the bulk emulsion properties. After loading the emulsions sample with a gap width of 1mm, the sample is pre-sheared at 50-100 s^{-1} for 60s prior to the dynamic oscillatory measurements. The first test performed is the strain sweep test at a constant frequency of 1 Hz. A downward sweep of strain from 1,000 to 0.1% is used. The linear viscoelastic region which is below the yield strain of the sample is identified. The second test performed is a frequency sweep test at a constant strain rate within the linear viscoelastic region. A downward sweep of frequency from 100 to 0.1 rad/s is used.

The oscillatory torque measurements of attractive colloidal suspensions using most commercial rheometers introduce error to the measurements because the equation used to analyze the torque readings ignored the higher harmonic contributions. Higher harmonic contributions are observed at large amplitude strain rates above the yield strain. However, Hyun et al. (2005) (Fig. 5.6) and Heymann et al. (2002a, 2002b) showed that the two-step yielding attractive colloidal suspensions do not behavior similar to repulsive suspensions. They showed that the error introduced to the torque measurement by the higher harmonic contributions is highest between the two yield strains. However, the contribution of higher harmonic near the second yield strain γ_{y2} is small (<15%). We assumed that the $\tau, \gamma G'$ vs. γ values obtained near γ_{y2}at higher strain amplitudes are fairly accurate even with the assumption of negligible higher harmonic contribution based on the studies of Hyun et al. (2005) and Heymann et al. (2002a, 2002b).

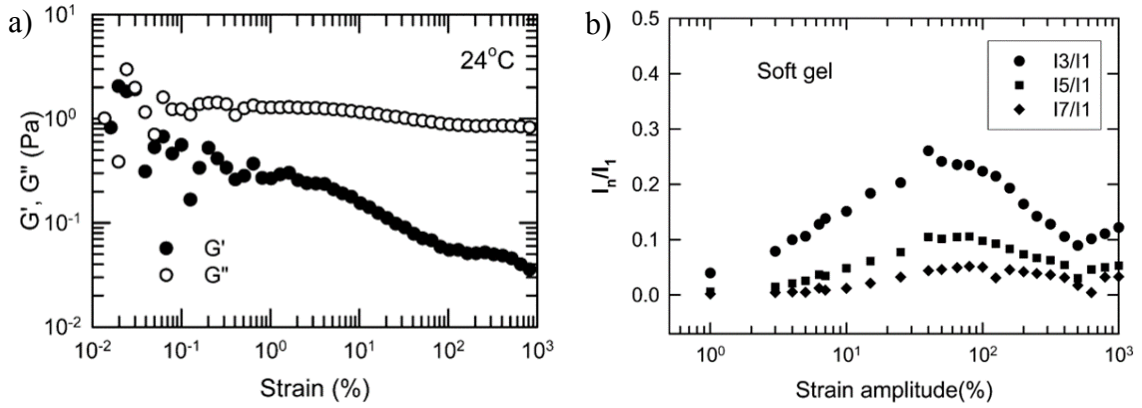

Fig. 5.9: (a) Oscillatory strain sweep measurement of polymer solution (soft gel). Shows a combination of Type I and IV behavior of attractive colloidal suspensions. (b) Nonlinear odd higher harmonic ($n \geq 3$) stresses normalized to the linear viscoelastic stress ($n = 1$) for strain sweep measurements. Fourier transform used to analyze the data. Figures obtained from Hyun et al. (2005)

5.3.3 Transient Measurements

Transient measurements can be performed using either a strain-controlled or a stress-controlled setting. Most of the measurements were conducted with a strain-controlled setting. After loading the emulsion sample with a gap width of 1mm, transient measurements of τ vs. t at constant shear rates for the strain-controlled setting and $\dot{\gamma}$ vs. t at constant stresses for the stress-controlled setting are performed. Samples are rested for 3 min between each constant shear rate/stress measurements.

5.4 RESULTS

The physicochemical properties, the rheological modeling parameters, and the wall slip modeling parameters of the characterized heavy O/W emulsions are summarized in Appendix (Table A5). Each figure has the sample name of the emulsions in the figure descriptions. The naming convention is xAA-B where x represents the oil (oil A, B, D), AA the concentration of oil in the emulsion, and B the number of the sample.

5.4.1 Transient Measurements

The time dependent measurements of heavy O/W emulsions are performed to develop the steady-state shear rate sweep procedure. The time-dependent measurements are also used to quantify whether heavy O/W emulsions show thixotropic or rheotropic behaviors. The constant shear setting for the ARES LS1 Rheometer is used to measure τ vs. t of a 80% oil D emulsion at constant shear rates.

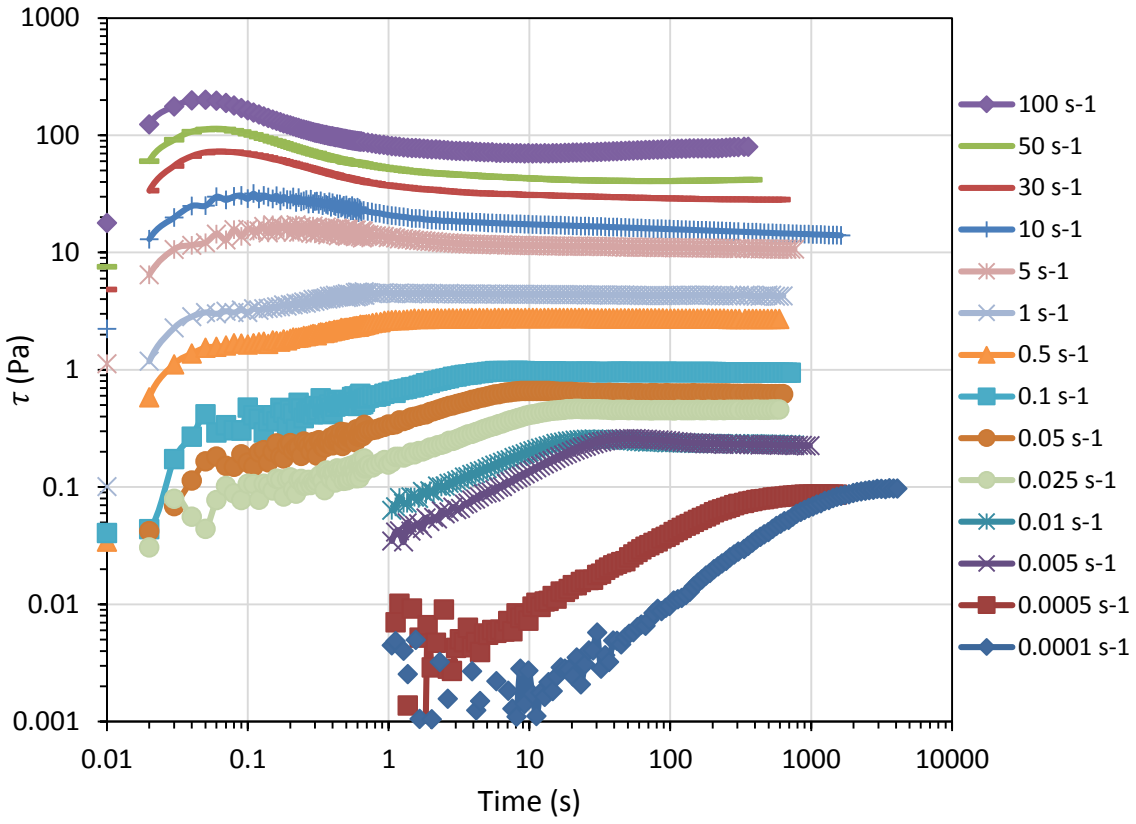

Fig. 5.10: τ vs. t at constant shear rates. 80% oil D emulsion prepared with 1.6% phenol-15EO, 0.2% NaCl, 1.0% NaCl (D80-4). 50 mm cross-hatched parallel plate with 1mm gap at 22.25°C ±0.25. Shear stress was not corrected using the Weissenberg-Rabinowitsch correction method.

The measurement time required for the emulsion flow to reach steady state in parallel plates depended on the shear rate. At $\dot{\gamma} > 5\ s^{-1}$, τ went through a maximum at

the start of flow and reached steady state after $\sim 10\ s$. At $0.01 < \dot{\gamma} < 5\ s^{-1}$, τ did not go through a maximum and reached steady state after $\sim 10 - 30\ s$. At $\dot{\gamma} < 0.001\ s^{-1}$, τ did not reached steady state until $> 1{,}000\ s$. This increase in τ as a function of time at low $\dot{\gamma}$ indicated rheopectic behavior similar to what Masalova et al. (2005) observed with concentrated W/O emulsions.

The constant stress setting for the ARES LS1 rheometer is used to measure $\dot{\gamma}$ vs. t of a 80% oil D emulsion at constant stresses.

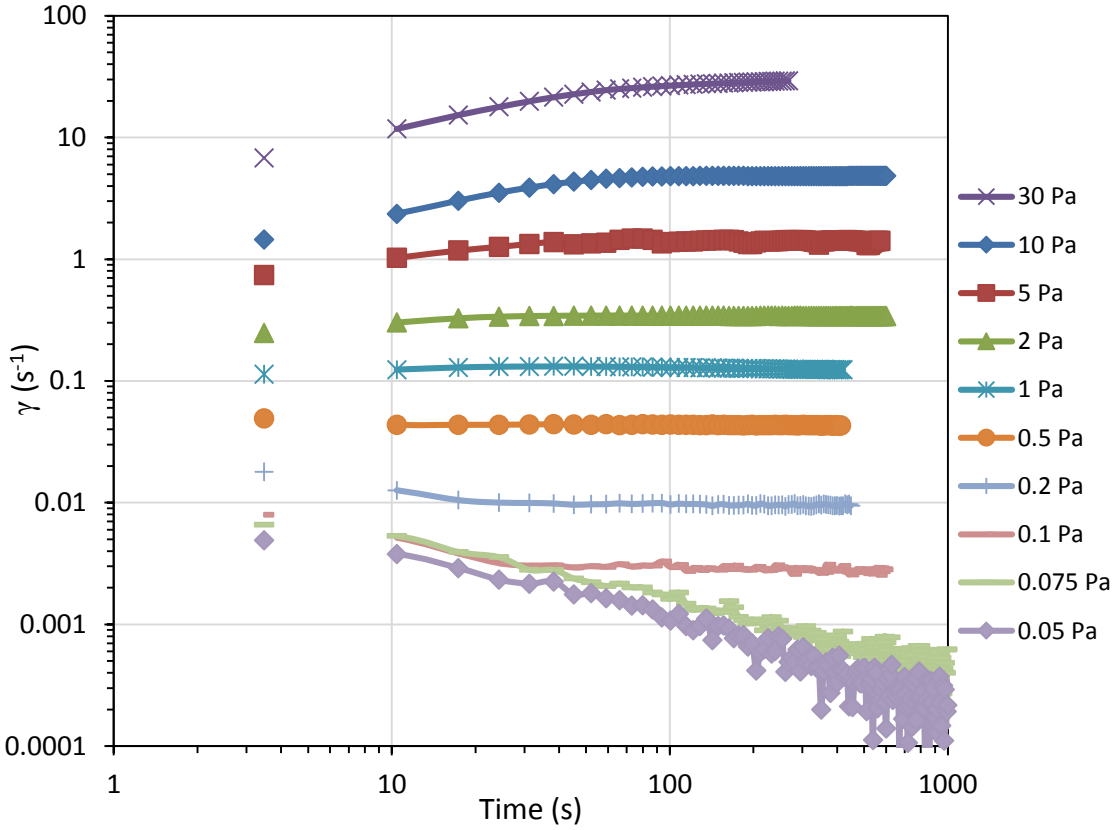

Fig. 5.11: $\dot{\gamma}$ vs. t. 80% oil D emulsion prepared with 1.6% phenol15EO, 0.2% NaCl, 1.0% NaCl (D80-4). 50 mm cross-hatched parallel plate with 1mm gap at 22.25°C ±0.25. Shear stress was not corrected using the Weissenberg-Rabinowitsch correction method.

It took $\sim 50\, s^{-1}$ for the 80% oil D emulsion to develop a steady state flow with the constant shear rate measurements. For $\tau \leq 0.075\, Pa$, the $\dot{\gamma}$ decreased steadily and did not reach steady state even for $> 1{,}000\, s$. The constant declined of $\dot{\gamma}$ may be an indication that the yield stress of the 80% oil D emulsion is at $0.05 \leq \tau \leq 0.075\, Pa$.

Downward and upward shear rates sweeps of the 80% oil D emulsions is performed according to the experimental procedure and the constant shear rate and constant stress measurements at steady state are plotted over the shear rate sweep measurements in Fig. 5.12.

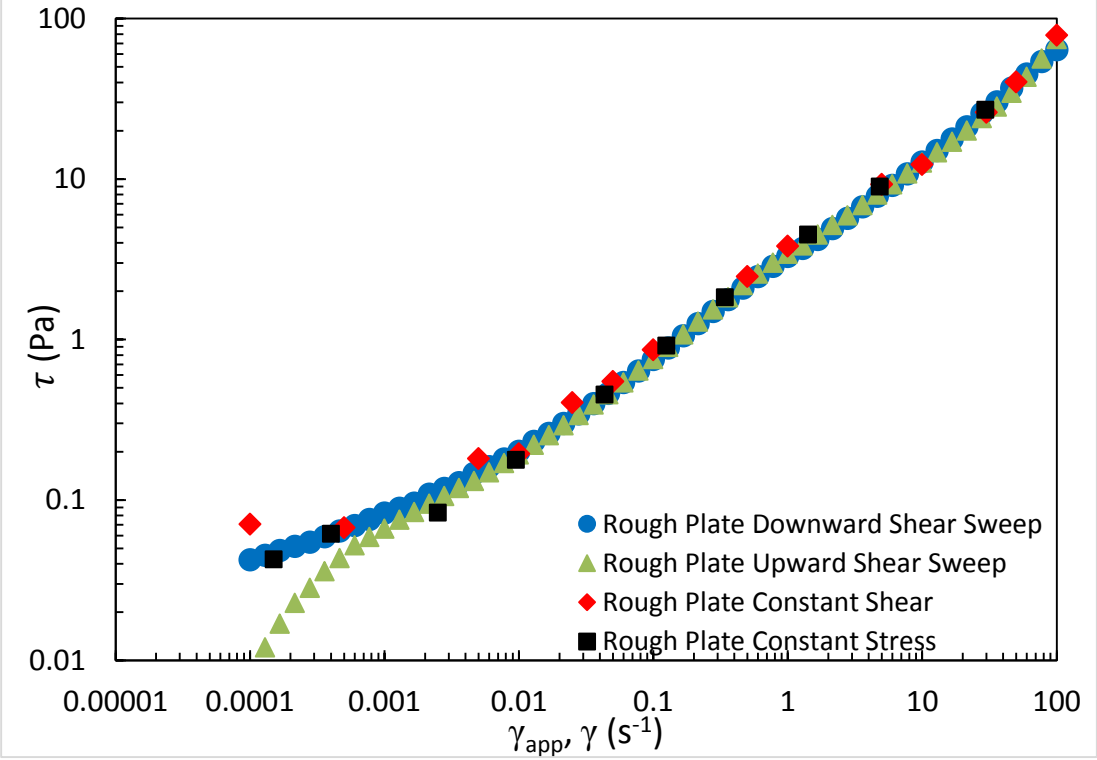

Fig. 5.12: τ vs. γ. 80% oil D emulsions 1.6% phenol-15EO, 0.2% NaOH, 1.0% NaCl (D80-4). 50 mm cross-hatched parallel plates with 1mm gap at 22.25°C ±0.25. Shear stress was corrected using the Weissenberg-Rabinowitsch correction method. Filled circle is downward shear rate scan. Green triangle is upward shear rate scan. Black square is shear rate obtained from the constant shear stress transient measurements in Fig. 5.11. Red diamond is shear stress obtained from the constant shear rate transient measurements in Fig. 5.10.

The downward and upward shear sweeps of the 80% oil D emulsion as well as all concentrated heavy O/W emulsions tested showed hysteresis at very low shear rates of $\dot{\gamma} < 0.005\ s^{-1}$. This is another indication of a rheopectic material. The steady state transient measurements performed with constant shear rate and constant stress settings (Figs. 5.10-5.11) agreed well with the downward shear sweep measurements even at $\dot{\gamma} < 0.005\ s^{-1}$. Fig. 5.12 showed that downward shear sweep measurements should be performed when characterizing heavy O/W emulsions over the upward shear sweep measurements to obtain data at steady state flow. Oscillatory measurements are also performed with downward sweeps of strain and frequency for this reason.

A lot of attractive colloidal suspensions showed shear banding at low shear rates [Fall et al. (2010); Møller et al. (2008); Ragouilliaux et al. (2007)]. Even though the 80% oil D emulsion showed attractive interdroplet interaction, the characteristic behavior of shear banding where the shear rate jumps discontinuously to zero below a critical shear rate with a stress controlled viscometer, unlike with a strain controlled viscometer [Fall et al. (2010); Møller et al. (2008); Ragouilliaux et al. (2007)], was not observed. While not a definitive proof, this may indicate that shear banding does not occur with the flow of attractive heavy O/W emulsions.

5.4.2 Oscillatory Measurements

Oscillatory measurements of concentrated heavy O/W emulsions showed a combination of Type I & IV behaviors outlined by Hyun et al. (2002) for viscoelastic materials. The type I behavior is characterized with a plateau of $G', G" vs. \gamma$ which declines with an increase in γ. The Type I behavior represents a shear thinning property of the material. The Type IV behavior is characterized by a strong strain overshoot of $G' \ and \ G"$ with strain sweep tests and indicates attractive interdroplet interactions and a

yielding event. Fig. 5.13 shows the typical oscillatory measurements of $G', G"vs.\gamma$ and $G', G"\ vs.\omega$ observed with concentrated heavy O/W emulsions.

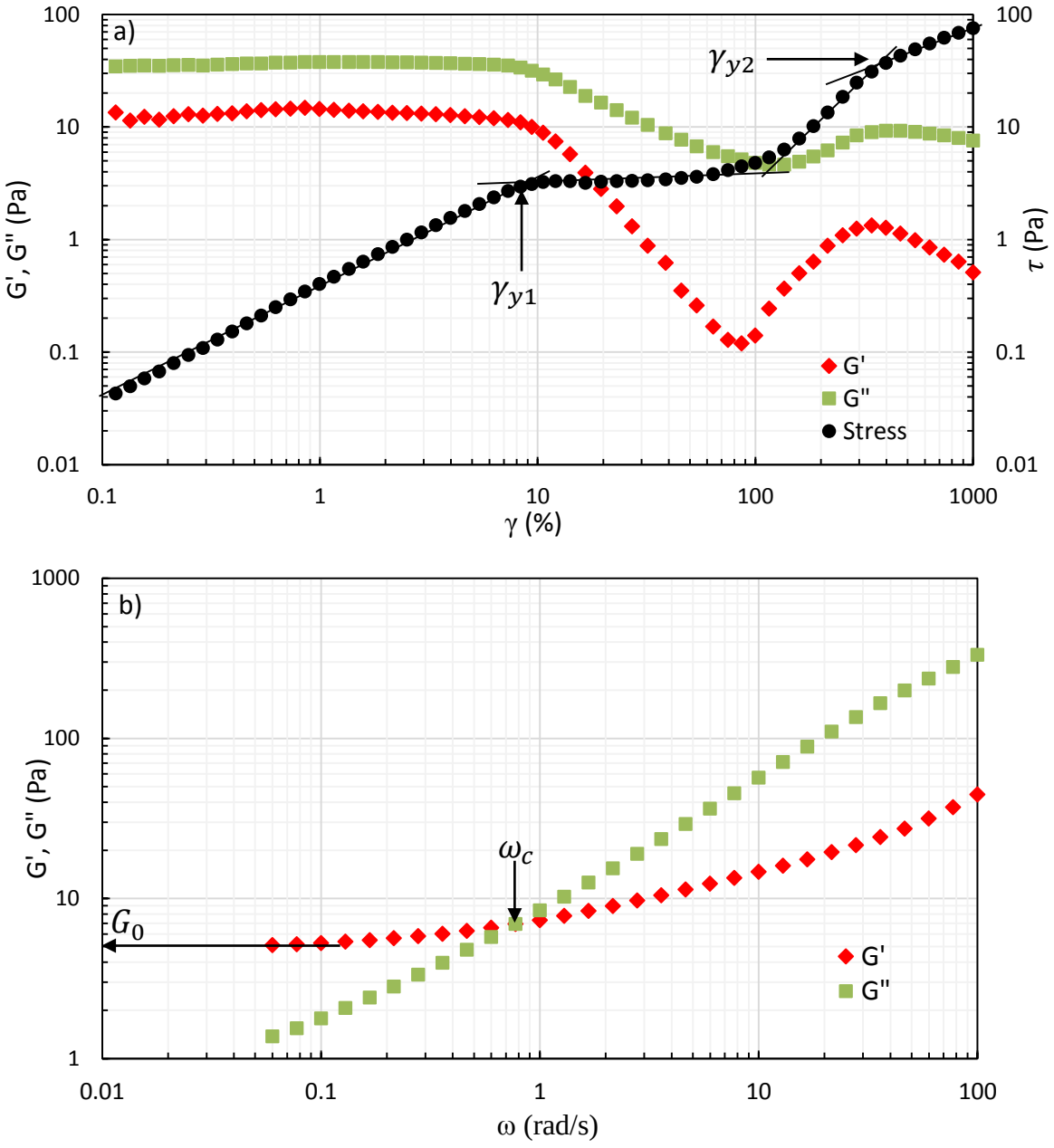

Fig. 5.13: 80% oil D emulsion prepared with 1.6% phenol-15EO 0.4% NaOH and 0.4% NaCl (D80-7). a) $G', G", \tau\ vs.\gamma$ relationship at constant $\omega = 1\ Hz$. The arrows represent the yield strains of the sample. b) $G', G"\ vs.\omega$ relationship at constant $\gamma = 5\%$. The arrows point to the ω and γ independent ${G_0}'$ and material relaxation time ω_c.

Fig. 5.13a showed that the oscillatory measurements of heavy O/W emulsions are similar to the oscillatory measurements of attractive colloidal suspensions reported by Koumakis and Petekidis (2011). Two yielding events are observed. The first yield strain γ_{y1} represents the breaking of networks created by attractive interactions between oil droplets and the second yield strain γ_{y2} represents the breaking of clusters/aggregates into individual droplets. The strain overshoot of G' and $G"$ at $\gamma = 100 - 1000\%$ is an indication of the flow induced yielding event. Concentrated heavy O/W emulsions showed a two-step yielding behavior according to the oscillatory measurements.

Fig. 5.14 shows the oscillatory measurements of 80% oil D emulsions prepared with different chemical formulations. NaCl concentration is varied in the chemical formulations.

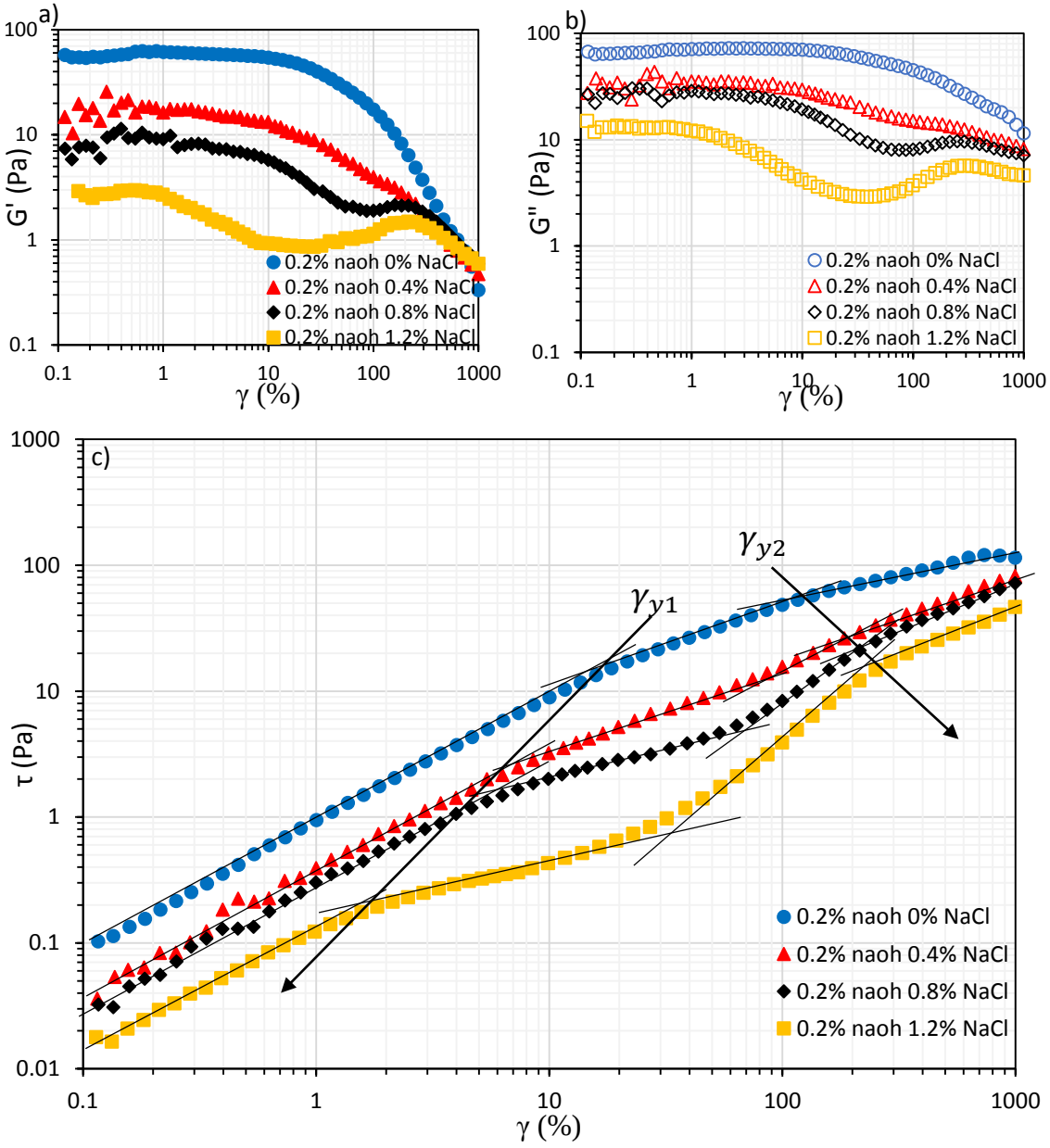

Fig. 5.14: 80% oil D emulsion prepared with 1.6% phenol-15EO 0.2% NaOH and 0-1.2% NaCl (D80-1 to D80-5). a) $G'\ vs.\gamma$ relationship, b) $G"\ vs.\gamma$ relationship, and c) $\tau\ vs.\gamma$ relationship measured at constant $\omega = 1\ Hz$. The arrows represent how the yield strains moved when NaCl concentration was increased in the chemical formulation.

Fig. 5.14a-b showed the $G', G"\ vs.\gamma$ relationships where lower G' and $G"$ were observed for emulsions when prepared with higher NaCl concentrations. Higher φ_m and lower Γ

are observed with emulsions prepared with optimized chemical formulations which results in lower G_0 according to the relationship $G_0 \sim \Gamma\varphi(\varphi - \varphi_m)/R_{32}$ [Mason et al. (1995)].

Table 5.2: Properties of 80% oil D emulsions in Fig. 5.14 prepared with 1.6% phenol-15EO, 0.2% NaOH, and 0-1.2% NaCl (D80-1 to D80-5).

NaCl	d_{32} (um)	φ_m	W_t at secondary minimum (k_BT)
0%	14.4	0.68	-11
0.4%	13.1	0.695	-24
0.8%	14.2	0.73	-40.5
1.2%	14.6	0.79	-55

Fig. 5.14a-b also showed that the strain overshoot of G' and $G"$ at $\gamma = 100 - 1000\%$ was minimal for the emulsion prepared with 0% NaCl and largest with the emulsion prepared with 1.2% NaCl. The magnitude of the overshoot is an indication of the attractive interaction strength of emulsions where no overshoot is observed for repulsive emulsions and a large overshoot is observed for emulsions with strong interdroplet attractions [Hyun et al. (2002)]. The calculation of the interaction potential of the emulsions agreed that 0% NaCl emulsion had the weakest attraction between droplets and the 1.2% NaCl emulsion had the strongest attraction between droplets at the secondary minimum (Table 5.2).

` Fig. 5.14c showed the $\tau\ vs.\gamma$ relationships. The magnitude of the yield strains changed as the NaCl concentration increased in the chemical formulations used to prepare emulsions. γ_{y1} decreased and γ_{y2} increased as the NaCl concentration increased. This behavior is similar to what Pham et al. (2008) observed with 60% colloidal suspensions when the particle interaction potential was changed from repulsive to

attractive. The yield strains appeared to be converging to a single yield point as the attraction strength became weaker. The ratio of γ_{y2}/γ_{y1} may be an indication of the interdroplet interaction strength.

Fig. 5.15 shows the $G', G"\ vs.\ \omega$ relationship of the 80% oil D emulsions in Table 5.2.

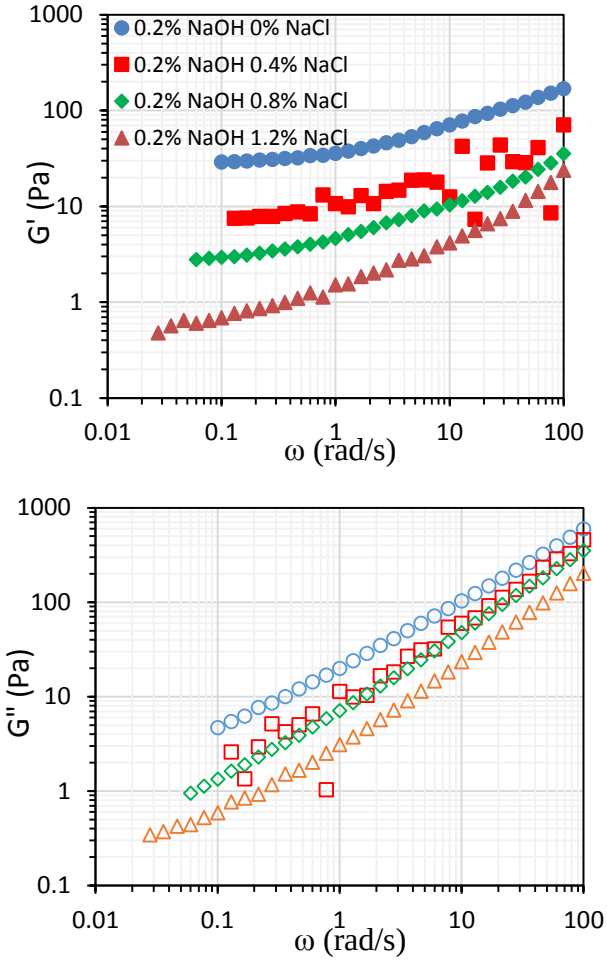

Fig. 5.15: 80% oil D emulsion prepared with 1.6% phenol-15EO 0.2% NaOH and 0-1.2% NaCl (D80-1 to D80-5). $G', G"\ vs.\ \omega$ at constant γ. Filled symbols are G' and empty symbols are $G"$.

Similar to the $G', G"\ vs. \gamma$ relationships, lower $G', G"$ are observed as a function of ω when the NaCl concentration is higher in the chemical formulation used to prepare emulsions. For emulsions with a small yield stress, the $G', G"\ vs. \omega$ relationship cannot be measured at very low ω due to the lower torque limit of the rheometer transducer. This makes it hard to accurately estimate G_0 which is observed as ω approaches 0. However, G_0 can be extrapolate from the measured data using rheological models similar to how the dynamic yield stress is extrapolated from the steady-state flow curves of $\tau\ vs. \dot{\gamma}$. $G', G"\ vs. \omega$ is normalized and plotted as $G'/G_0, G"/G_0\ vs. \omega/\omega_c$ to collapse all the $G', G"\ vs. \omega$ measurements from emulsions into one master curve.

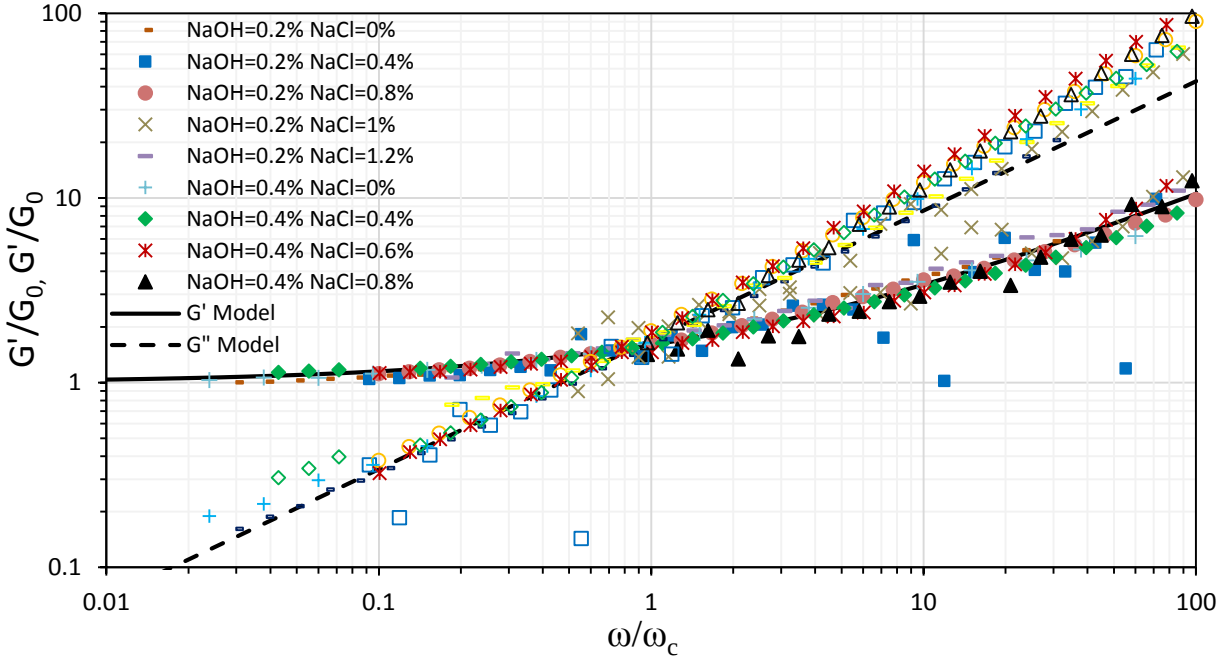

Fig. 5.16: 80% oil D emulsion prepared with 1.6% phenol-15EO 0.2-0.4% NaOH and 0-1.2% NaCl (D80-1 to D80-9). $G'/G_0, G"/G_0\ vs. \omega/\omega_c$ at constant γ. Filled symbols are G'/G_0 and empty symbols are $G"/G_0$. Solid line is $G'/G_0 = 1 + 0.6(\omega/\omega_c)^{0.6}$ and the dashed line is $G"/G_0 = 1.7(\omega/\omega_c)^{0.7}$

The solid line for G' and dashed line for $G"$ in Fig. 5.16 modeled the normalized frequency sweep data of concentrated heavy O/W emulsions accurately for $\omega/\omega_c < 5$.

γ_{y1}, γ_{y2}, G_0, and ω_c of heavy O/W emulsions are measured with the oscillatory measurements. Using Hooke's law, the yield stress can be calculated $\tau_{y1} = G_0\gamma_{y1}$. Qualitatively, the interdroplet interaction strength of emulsions can be inferred from the $G', G", \tau\ vs.\gamma$ data based on the magnitude of $G', G"$ overshoots. However, τ_{y2} could not be measured or calculated from the oscillatory measurements. The yield strains and stresses are used to model the rheological properties of attractive heavy O/W emulsions.

5.4.3 Rheology and Wall Slip

The $\tau\ vs.\dot{\gamma}$ flow curves of oil D emulsions prepared with 1.6% phenol-15EO, 0.2% NaOH, and 0% NaCl are presented in Fig. 5.17. The dispersed heavy oil concentrations are varied from 40-85%.

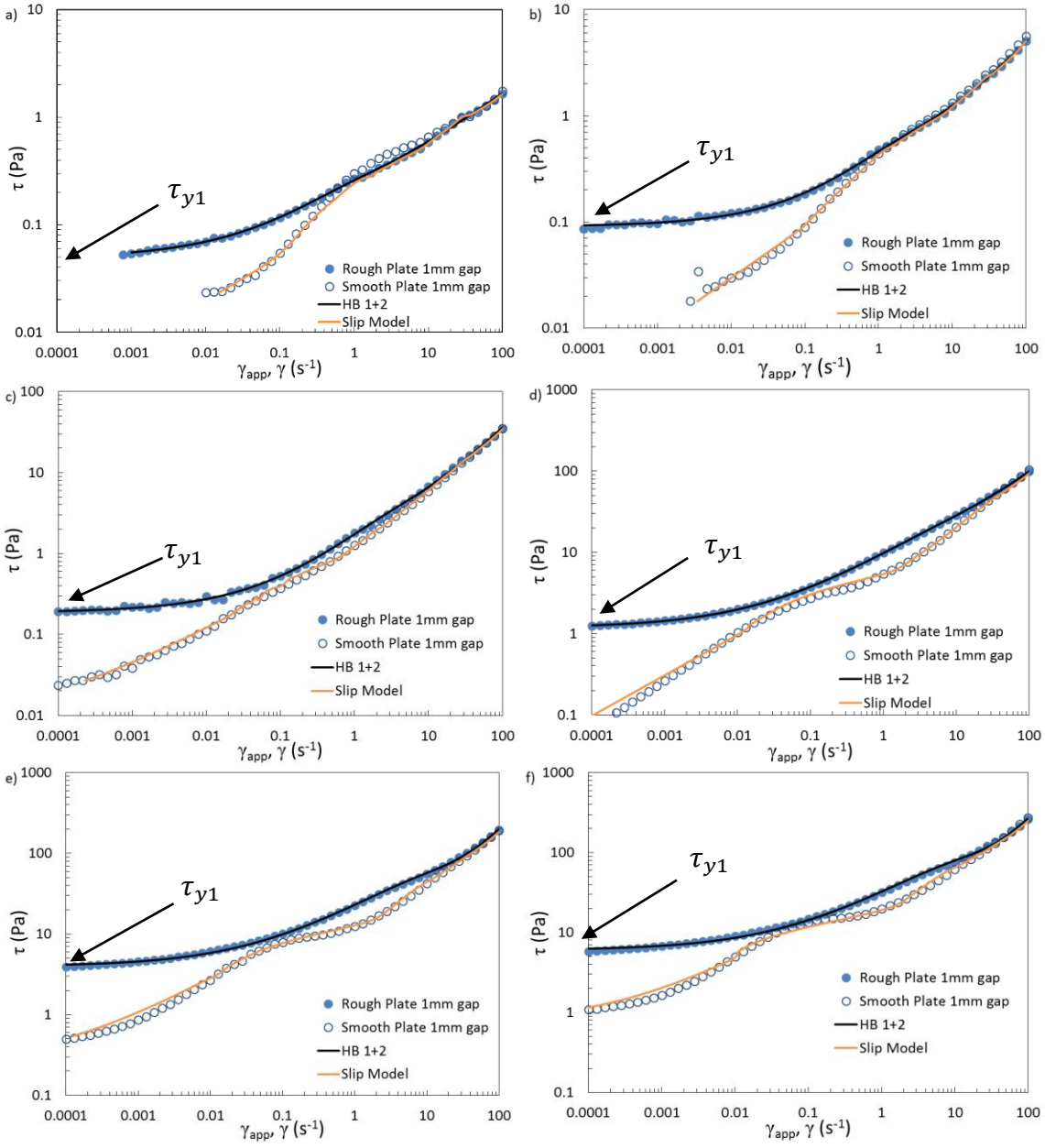

Fig. 5.17: $\tau\ vs.\dot{\gamma}$ of oil D emulsions prepared with 1.6% phenol-15EO, 0.2% NaOH, and 0% NaCl. a) D40-10: $\varphi = 40\%$, $\varphi_m = 0.79$, b) D50-11: $\varphi = 50\%$, $\varphi_m = 0.78$, c) D60-12: $\varphi = 60\%$, $\varphi_m = 0.8$, d) D70-13: $\varphi = 70\%$, $\varphi_m = 0.73$, e) D80-14: $\varphi = 80\%$, $\varphi_m = 0.69$, f) D85-15: $\varphi = 85\%$, $\varphi_m = 0.69$. The black line is the modified Herschel-Bulkley model. The orange line is the wall slip model. The arrows indicate the yield stress τ_{y1}.

A yield stress τ_{y1} is observed for emulsions with oil concentration as low as $\varphi = 40\%$ in Fig. 5.17. The presence of a yield stress at $\varphi/\varphi_m \ll 1$ is an indication of a percolating network formed by attractive oil droplets. τ_{y1} increased as the oil concentration increased. The presence of τ_{y1} is supported by the oscillatory measurements and the wall slip observed with smooth parallel plates. Wall slip indicates the presence of a yield stress [Meeker et al. (2004)].

Wall slip is observed with all emulsions in Fig. 5.17 at $\tau \leq \tau_{y1}$ similar to the wall slip observed with repulsive microgel pastes and repulsive concentrated emulsions [Meeker et al. (2004); Seth et al. (2012, 2008)]. Unlike repulsive emulsions, wall slip is observed for attractive emulsions with $\varphi/\varphi_m < 1$. A second region of wall slip appeared for heavy O/W emulsions with $\varphi \geq 60\%$ at higher shear rates of $0.1 < \dot{\gamma} < 10\ s^{-1}$. The emergence of the wall slip at higher shear rates indicates the presence of a flow induced yield stress that is collaborated by the oscillatory measurements of two yield strains. The region where the second wall slip appeared is accompanied by a hump in the rough parallel plate measurements. While oscillatory measurements could not be used to quantify the flow induced yield stress τ_{y2}, τ_{y2} can be estimated by analyzing the wall slip behavior.

The rheological models for concentrated emulsions, Herschel-Bulkley model, Seth et al. (2011) model, and Princen and Kiss (1989) model, cannot accurately model the rheological properties of concentrated heavy O/W emulsions because of the presence of the hump caused by the flow induced yield stress. Also, the wall slip regimes developed by Meeker et al. (2004) and Seth et al. (2012) do not account for the second region of wall slip observed at high shear rates.

Equations that model the flow curves of heavy O/W emulsions are very useful when analyzing the measured data and designing the flow of heavy O/W emulsions in

flow conduits of varying dimensions. The two lines in Fig. 5.17 represent the new equations developed in this chapter to model the rheological properties and wall slip behavior of heavy O/W emulsions.

The heavy O/W emulsion measurements in Fig. 5.18 were used to design the new equations.

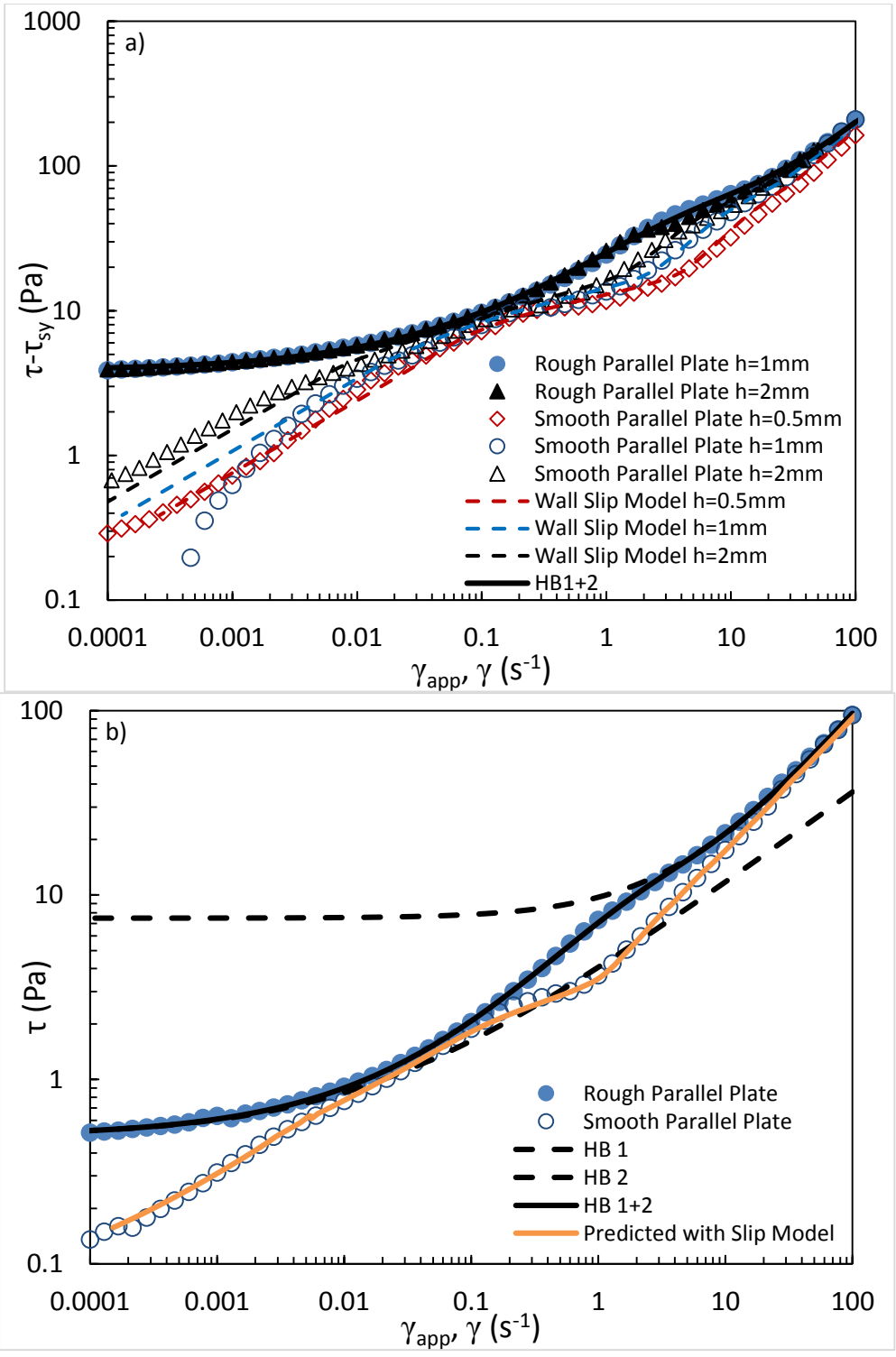

Fig. 5.18 continued.

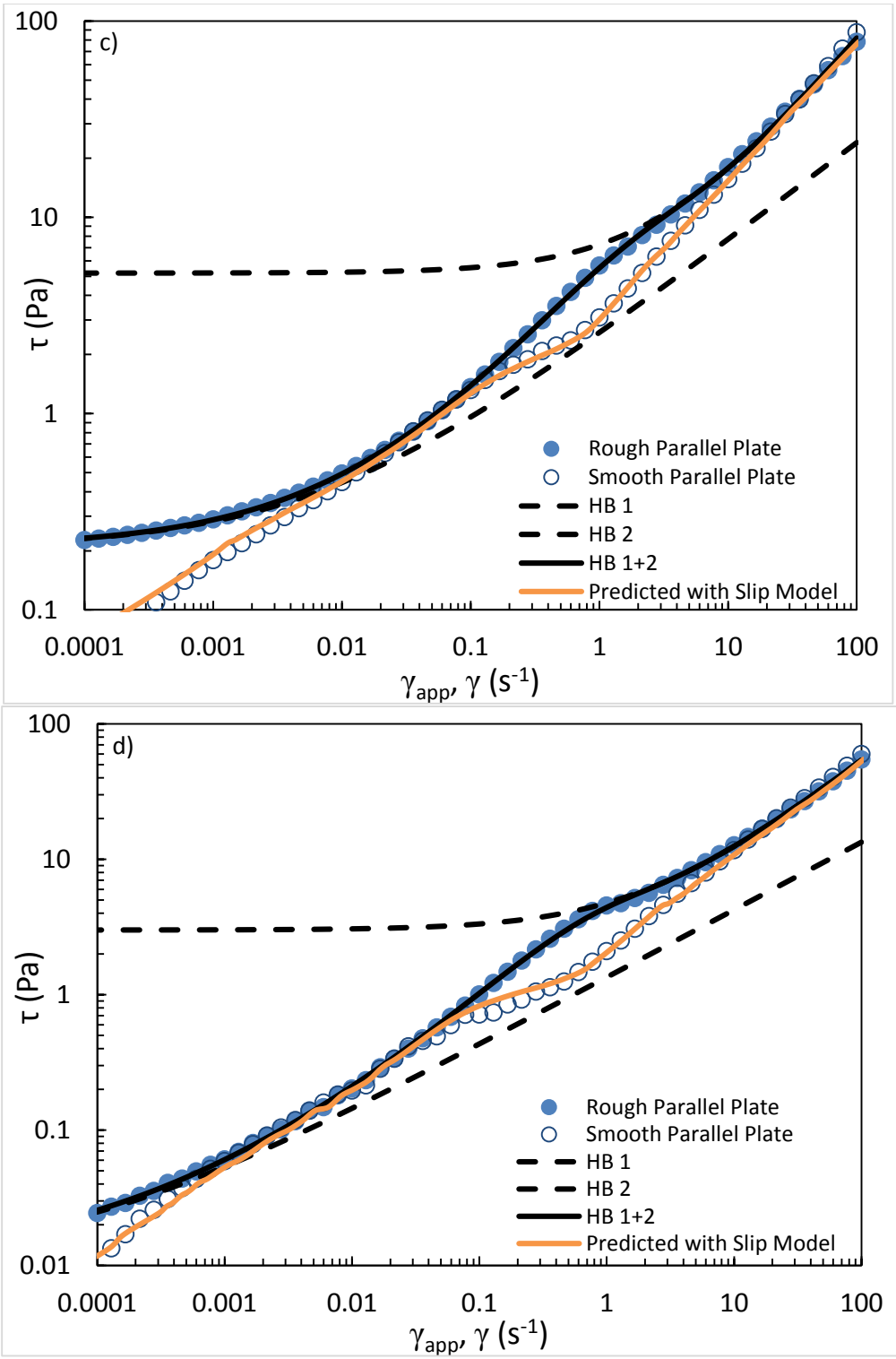

Fig. 5.18 continued.

Fig. 5.18: $\tau\ vs.\dot{\gamma}$ of 80% oil D emulsions prepared with a chemical formulation of 1.6% phenol-15EO, 0.4% NaOH, and a) D80-6: 0%, b) D80-7: 0.4%, c) D80-8: 0.6%, and d) D80-9: 0.8% NaCl. The solid black line is the modified Herschel-Bulkley model. The dotted black lines are the two Herschel-Bulkley models that were combined to form the solid black line. The colored lines are the wall slip model.

The new equations modeled both the flow curves of $\tau\ vs.\dot{\gamma}$ and the effect of wall slip very well. Fig. 5.18a showed that varying the gap width of the rough parallel plates from h=1-2mm did not have any effect on $\tau\ vs.\dot{\gamma}$. This suggests that wall slip was completely eliminated by using the rough parallel plates. The $\tau\ vs.\dot{\gamma}_{app}$ varied significantly when the gap width of the smooth parallel plates were changed from h=0.5-2mm. The smallest gap showed the largest wall slip. The slip model was able to capture the effect of the plate gap width on the wall slip. Wall slip can be scaled up to flow conduits of varying dimensions using the slip model.

5.4.3.1 Model for $\tau\ vs.\dot{\gamma}$ flow curves (No Wall Slip)

All concentrated heavy oil emulsions measured with rough parallel plates showed steady state flow curves similar to Fig. 5.18. To model the flow curves of concentrated heavy O/W emulsions in Fig. 5.18, two rheological models, the micromechanical model proposed by Seth et al. (2011) and Herschel-Bulkley (HB) model, were considered.

The micromechanical model is desirable compared to the Herschel-Bulkley model because all variables are measurable physical properties of emulsions, unlike the Herschel-Bulkley model. Foudazi et al. (2012) modified the micromechanical model for polydiserse samples

$$\tau = \tau_y + 18G_0\left(\frac{\dot{\gamma}\mu_c d_{32}}{\Gamma}\right)^n \tag{5.9}$$

where G_0 is the strain and frequency independent storage modulus, Γ the interfacial tension, and μ_c the continuous phase viscosity. Since the Γ of the emulsion samples

could not be measured, the Γ in the equation was used as a fitting parameter. The micromechanical model proposed by Seth et al. (2011) for concentrated emulsions proved not to be suitable for the flow curves of concentrated heavy O/W emulsions. The short comings of the micromechanical model were:

1. Unrealistically low Γ values ($\Gamma \approx 10^{-3} - 10^{-4}\, mN/m$) were necessary to fit the flow curves before the hump.
2. The hump in the flow curves could not be modeled.

The unrealistically low Γ values needed as a fitting parameter may be because of the very large size of the oil droplet aggregates. Since $d_{aggregate} \gg d_{indivisual}$, very low Γ fitting values are necessary to satisfy the relationship $\frac{d_{individual}}{d_{aggregate}}\Gamma = \Gamma_{fitting}$.

The Herschel-Bulkley equation faced the same problem where the flow curves could not be accurately modeled because of the presence of a hump. Since concentrated heavy O/W emulsions showed two yield stresses, a combination of two Herschel-Bulkley models was used to model the flow curves of concentrated heavy O/W emulsions similar to Foudazi et al. (2012, 2011).

Foudazi et al. (2012, 2011) observed that a combination of two Herschel-Bulkley equations adequately described the flow curves of concentrated emulsions which showed "a hump" at a certain critical shear rate.

$$\tau = \tau_{y1} + k_1\dot{\gamma}^{n_1} + \left[\left(\tau_{y2} + k_2\dot{\gamma}^{n_2}\right) - \left(\tau_{y1} + k_1\dot{\gamma}^{n_1}\right)\right]\left[1 - e^{-\dot{\gamma}/\dot{\gamma}_c}\right] \quad (5.10)$$

where τ_{y1} is the traditional dynamic yield stress obtained from extrapolation, τ_{y2} the flow induced yield stress, k_i the consistency index, n_i the flow index, and $\dot{\gamma}_c$ the critical shear rate. The curve smoothening function $\left[1 - e^{-\dot{\gamma}/\dot{\gamma}_c}\right]$ is used to combine the two Herschel-Bulkley models into a continuous function at $\dot{\gamma}_c$.

The flow regimes of the two Herschel-Bulkley equations used to model the flow curves of concentrated heavy O/W emulsions are theorized from the yielding events of

two-step yielding materials. The first yielding event of concentrated heavy O/W emulsions represents the breaking of percolating networks into clusters/aggregates and the second yielding event represents the breaking of clusters/aggregates. The first Herschel-Bulkley equation models the flow of clusters/aggregates between the two yielding events and the second Herschel-Bulkley equation models the flow of individual droplets after the second yielding event. Energy from shearing the emulsions is necessary for the yielding events and the process is illustrated in Fig. 5.1.

A key assumption is made that the two Herschel-Bulkley equations describe the two extremes of flow regimes: 1) The first Herschel-Bulkley equation describes flow of aggregate emulsion droplets with a constant aggregate size when the emulsions first yield, and 2) the second Herschel-Bulkley equation describes flow of emulsions with individual droplets. The region between the two Herschel-Bulkley equations is a gradual transition from the first Herschel-Bulkley equation to the second Herschel-Bulkley equation where the breaking of clusters/aggregates occurs. The flow regimes are illustrated below.

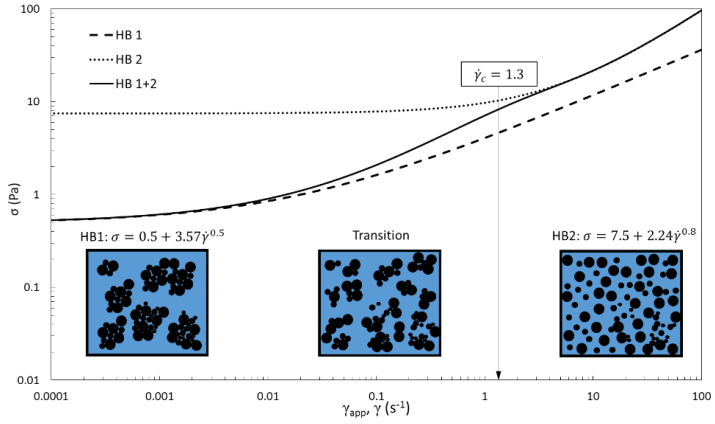

Fig. 5.19: Illustration of flow regimes modeled by Herschel-Bulkley equations. The dotted lines are the individual HB equations. The solid line is Eq. 5.10. The drawings represent the state of droplet aggregation as a function of shear. The dispersed-phase concentrations are not drawn to scale.

Eq. 5.10 has 7 fitting parameters to fit the measured flow curves. A challenge with such a large number of fitting parameters is the existence of multiple solutions. Some of the fitting parameters are replaced by measured values to reduce the number of available solutions with Eq. 5.10.

1. τ_{y1} calculated from oscillatory measurements of G_0 and γ_{y1}
2. $n = 0.5$ for concentrated emulsions with repulsive interactions [Foudazi et al. (2011); Meeker et al. (2004); Princen and Kiss (1989); Seth et al. (2006)]. $n_1 = 0.5$ is assumed because of the assumption of a constant aggregate diameter for the HB1 model and $\varphi_{eff} > \varphi$ caused by inclusion of water to the dispersed-phase volume in the aggregates.
3. τ_{y2} is estimated from the analysis of wall slip behavior based on the relationship between the wall slip behavior and yield stress [Meeker et al. (2004); Seth et al. (2012)].

The 7 fitting parameters of Eq. 5.10 are reduced to 4 fitting parameters with 3 measurable and known parameters, significantly limiting the number of possible solutions. Eq. 5.10 modeled the flow curves of emulsions in Fig. 5.18 and other emulsions very well.

5.4.3.2 Model for Wall Slip

The $\dot{\gamma}$ at the edge of the parallel plates can be converted to bulk fluid velocity with $V = \dot{\gamma}_R h$ ($\dot{\gamma}_R$: shear rate at the edge of the cross-hatched plates, h: gap between the plates) and bulk+slip velocity $V_0 = \dot{\gamma}_{R,app} h$ ($\dot{\gamma}_{R,app}$: apparent shear rate at the edge of the smooth plates, h: gap between the plates). At constant τ, the slip velocity $V_S = V_0 - V$ can be calculated. Note that V_S is the sum of wall slip velocity at both the top and bottom plates as illustrated in Fig. A4 in the Appendix. Each plate has wall slip velocity of $V_S/2$. The V_S/V_0 vs. τ for the 80% oil D emulsions in Fig. 5.18 are plotted in Fig.5.20.

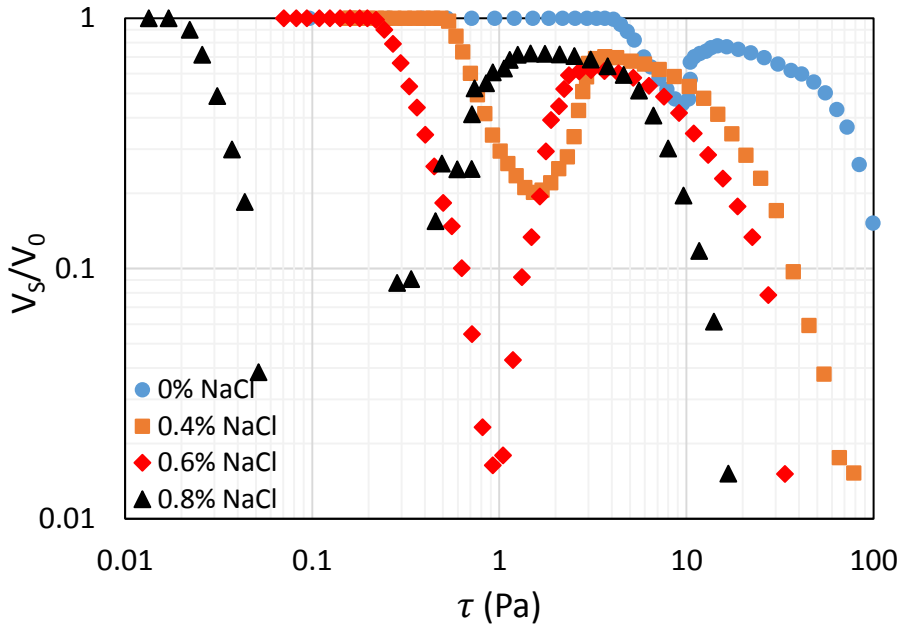

Fig. 5.20: V_S/V_0 vs. τ of 80% oil D emulsions with 1.6% ph15EO, 0.4% NaOH, and 0-0.8% NaCl (D80-6 to D80-9). Measured with 50 mm cross-hatched and smooth parallel plates with 1mm gap at 22.25°C ±0.25.

V_S/V_0 represents the contribution of wall slip to total flow with $V_S/V_0 = 0$ and $V_S/V_0 = 1$ representing flow with no wall slip and flow with only wall slip and no bulk flow, respectively. $V_S/V_0 = 1$ was observed for $\tau < \tau_{y1}$. The trend for V_S/V_0 vs. τ can be analyzed when τ is normalized with τ_y (See Fig. 5.21).

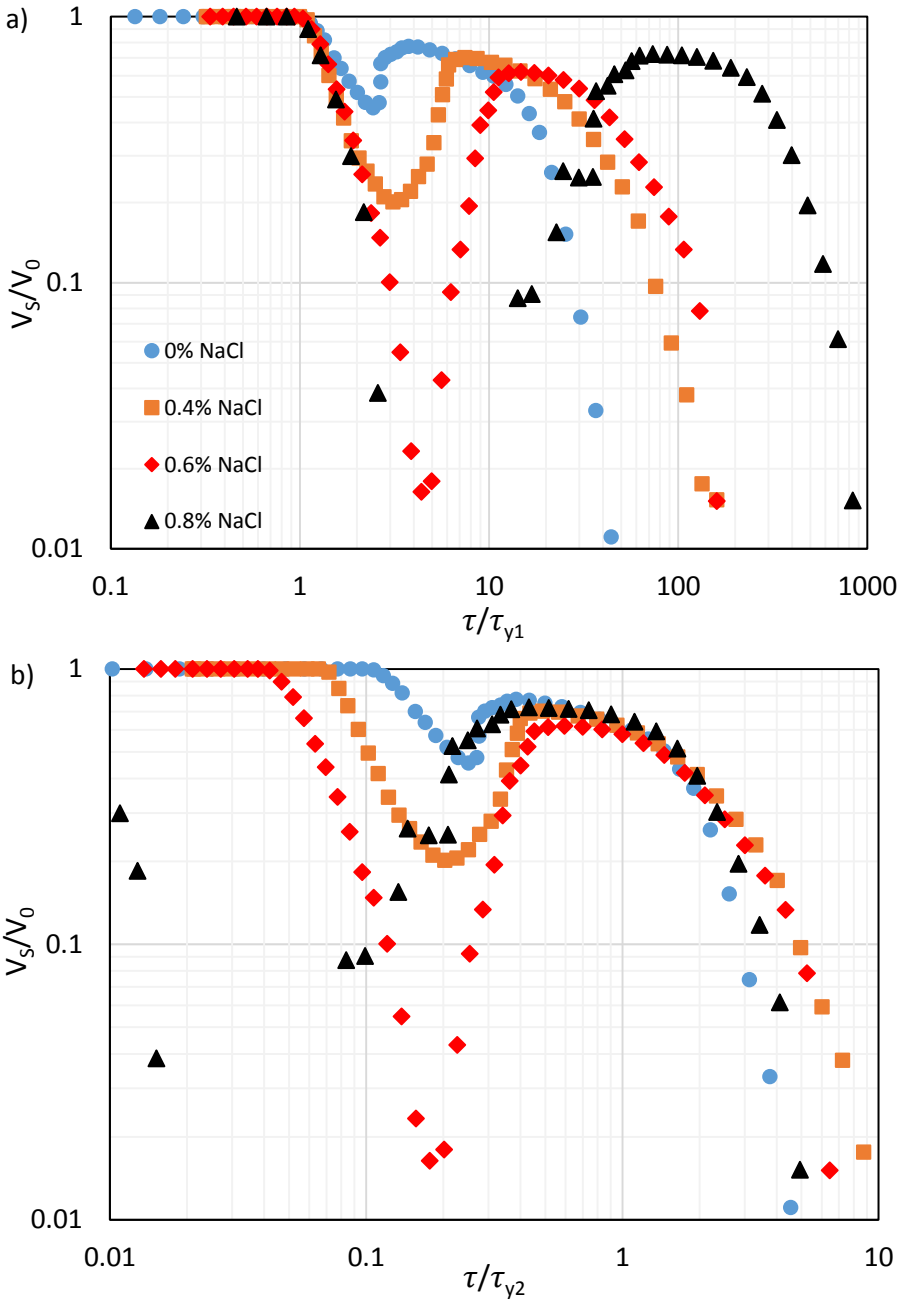

Fig. 5.21: V_S/V_0 vs. a) τ/τ_{y1} and b) τ/τ_{y2} of 80% oil D emulsions with 1.6% ph15EO, 0.4% NaOH, and 0-0.8% NaCl (D80-6 to D80-9). Measured with 50 mm cross-hatched and smooth parallel plates with 1mm gap at 22.25°C ±0.25.

Fig. 5.20a showed that V_S/V_0 vs. τ/τ_{y1} collapsed the four sets of data well for $\tau/\tau_{y1} < 1$. The V_S/V_0 decreased significantly for $\tau/\tau_{y1} > 1$. τ_{y1} was estimated using

the extrapolation method of the flow curves with the Herschel-Bulkley model. The wall slip behavior observed in Fig. 5.21a followed the slip mechanism proposed by Meeker et al. (2004) with the transition of slip *Regime II* to *Regime I* happening at $\tau/\tau_{y1} \approx 1$.

What is not observed in the works of Meeker et al. (2004) and Seth et al. (2012) is the presence of significant wall slip appearing at $\tau/\tau_{y1} \gg 1$. The V_S/V_0 increased to a constant value of 0.6-0.7 at $\tau/\tau_{y1} \gg 1$ and decreased significantly in Fig. 5.21a. Because wall slip occurs as a result of yield stress, it can be inferred from the V_S/V_0 vs. τ/τ_{y1} that a flow induced yield stress is present for the emulsions. Two repeating patterns of wall slip are occurring at two different yield stresses. Using the same concept of V_S/V_0 vs. τ/τ_{y1} observed in Fig. 5.21a, the V_S/V_0 vs. τ data in Fig. 5.20 is normalized at the flow induced yield stress τ_{y2} (see Fig. 5.21b). The τ_{y2} is estimated so that the wall slip at τ_{y2} followed the slip Regimes proposed by Meeker et al. (2004) with transition of slip *Regime II* to *Regime I* occurring at $\tau/\tau_{y2} \approx 1$.

We defined the start of shear induced yield stress as τ_{y2S} and end of shear induced yield stress as τ_{y2}. The main difference between the contributions of two yield stresses to slip velocity is $V_S/V_0 = 1$ for $\tau < \tau/\tau_{y1}$ and $V_S/V_0 < 1$ for $\tau_{y2S} < \tau < \tau_{y2}$. The values of $V_S/V_0 < 1$ for $\tau_{y2S} < \tau < \tau_{y2}$ suggest that bulk flow is present to some degree for $\tau_{y2S} < \tau < \tau_{y2}$, unlike the flow at $\tau < \tau/\tau_{y1}$ which is due entirely to wall slip. The flow induced yield stress τ_{y2} obtained from the wall slip analysis was found to be slightly below the stress at which the hump in the flow curves measured with rough parallel plates were observed in Fig 5.18. The τ_{y2} obtained from the analysis of the wall slip behavior is used in the modified Herschel-Bulkley equation (Eq. 5.10) as a measurable parameter instead of a fitting parameter.

The V_S vs. V_0 relationship can be analyzed further to obtain information about the slip behavior of heavy O/W emulsions.

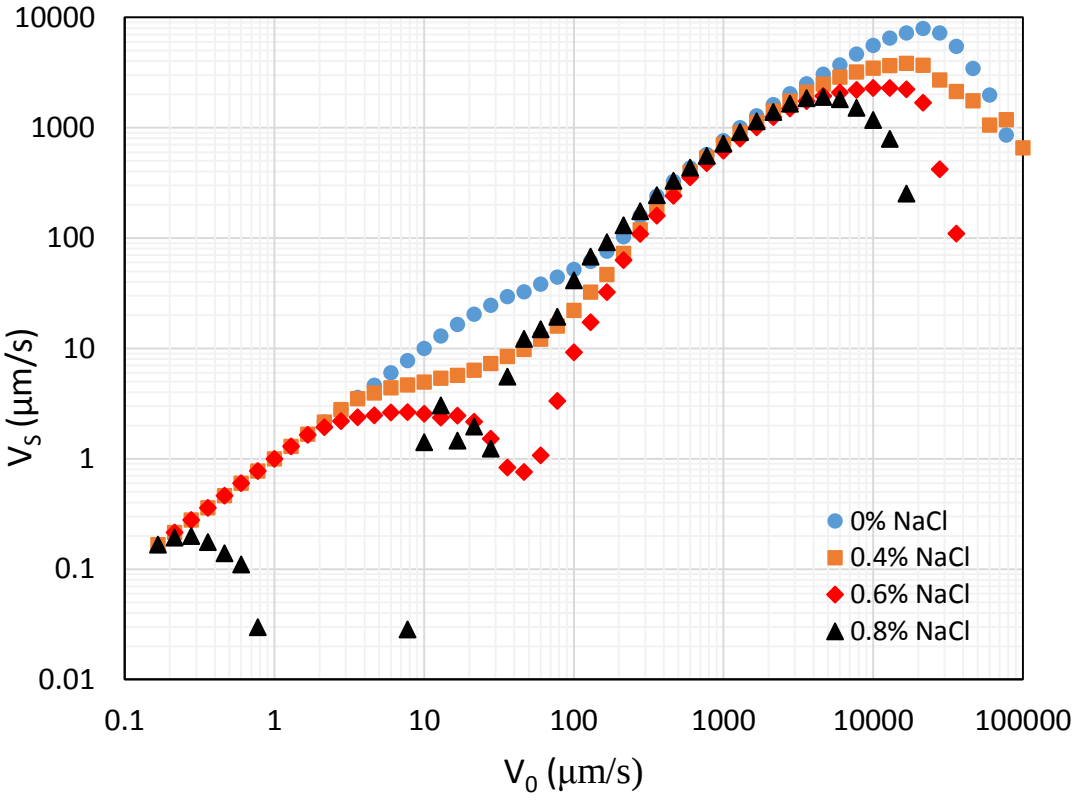

Fig. 5.22: V_S vs. V_0 of 80% oil D emulsions with 1.6% ph15EO, 0.4% NaOH, and 0-0.8% NaCl (D80-6 to D80-9). Measured with 50 mm cross-hatched and smooth parallel plates with 1mm gap at 22.25°C ±0.25.

The V_S vs. V_0 relationship can be non-dimensionalized with the characteristic slip velocity V_{yi} which is defined as V_S at $\tau = \tau_{y1}$ (V_{y1}) and $\tau = \tau_{y2}$ (V_{y2}). To normalized both V_S and V_0 at $\tau = \tau_{y2}$, variable C is defined where $C = V_S/V_0$ at the yield stresses. $C = 1$ at τ_{y1} and C is a constant less than 1 at τ_{y2} (obtained from Fig. 5.20). The normalized V_S vs. V_0 with respect to both V_{y1} and V_{y2} is plotted in Fig. 5.23

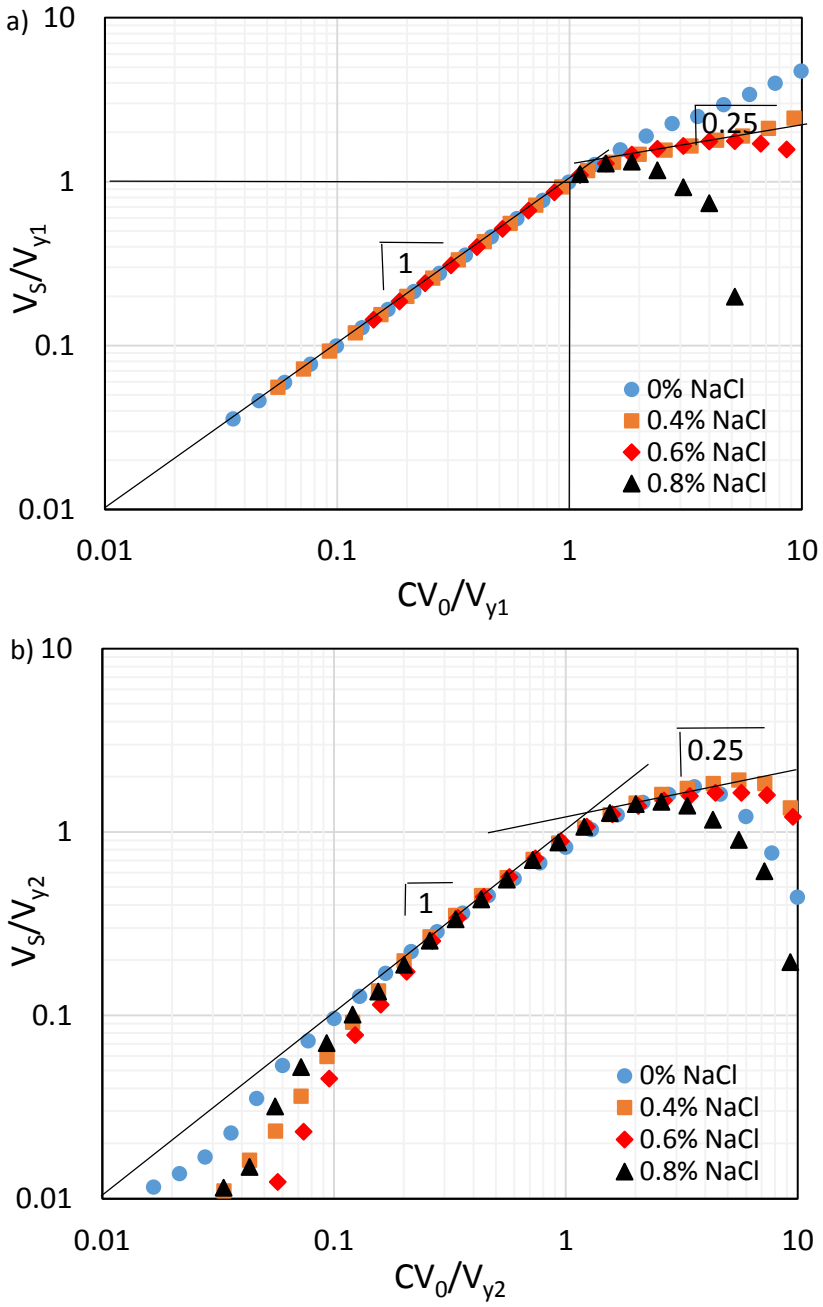

Fig. 5.23: a) V_S/V_{y1} vs. CV_0/V_{y1} and b) V_S/V_{y2} vs. CV_0/V_{y2} of 80% oil D emulsions with 1.6% ph15EO, 0.4% NaOH, and 0-0.8% NaCl (D80-6 to D80-9). Measured with 50 mm cross-hatched and smooth parallel plates with 1mm gap at 22.25°C ±0.25.

Fig. 5.23 showed that $V_S/V_y = CV_0/V_y$ for $\tau < \tau_y$ and $V_S/V_y = a(CV_0/V_y)^{0.25}$ for $\tau \gg \tau_y$, similar to what Seth et al. (2012) observed for repulsive concentrated emulsions showing only a single yield stress with $n \approx 0.5$. The variable a is a constant.

Since the slip velocity is negligible compared to bulk fluid velocity ($V_S/V \approx 0$) at high shear rate, we can estimate that $V_0 \approx V$ at $\tau \gg \tau_y$. Substituting in $\dot{\gamma} \sim V_0$ to the Hershel-Bulkley equation, $V_0 \sim \tau^{1/n}$ is obtained for $\tau \gg \tau_y$. Because $V_S/V_y = a(CV_0/V_y)^{0.25}$ for $\tau \gg \tau_y$, the relationship $V_S \sim {V_0}^{0.25} \sim \tau^{1/4n}$ is obtained. Based on these analysis, the following model is derived for V_S vs. τ:

$$\frac{V_S}{V_y} = \frac{CV_0}{V_y} = \left[\frac{\tau - \tau_{sy}}{\tau_y - \tau_{sy}}\right]^{1/n}, \qquad \tau \leq \tau_y \tag{5.11}$$

$$\frac{V_S}{V_y} = a\left[\frac{CV_0}{V_y}\right]^{0.25} = a\left[\frac{\tau - \tau_{sy}}{\tau_y - \tau_{sy}}\right]^{1/4n}, \qquad \tau \gg \tau_y \tag{5.12}$$

where a is a constant and τ_{sy} the sliding yield stress. Sliding yield stress is observed when there is an attraction between emulsion droplets and the smooth flowing surface [Seth et al. (2008)]. Seth et al. (2012) showed that for concentrated emulsions with n = 0.5, $V_S/V_y = \left(\frac{\tau - \tau_{sy}}{\tau_y - \tau_{sy}}\right)^2$ and $V_S/V_y = \left(\frac{\tau - \tau_{sy}}{\tau_y - \tau_{sy}}\right)^1$ were obtained for $\tau < \tau_y$ and $1 \leq \tau/\tau_y \leq 2.5$, respectively. The exponent of 1 obtained by Seth et al. (2012) is based on slip velocity measurements up to $2.5\tau/\tau_y$ and may represent the transition from the exponent of 2 to 0.5 at $\tau \gg \tau_y$.

The V_S vs. τ relationship of 80% oil D emulsions normalized to V_S/V_y vs. $(\tau - \tau_{sy})/(\tau_y - \tau_{sy})$ at both yield stresses are plotted in Fig. 5.24.

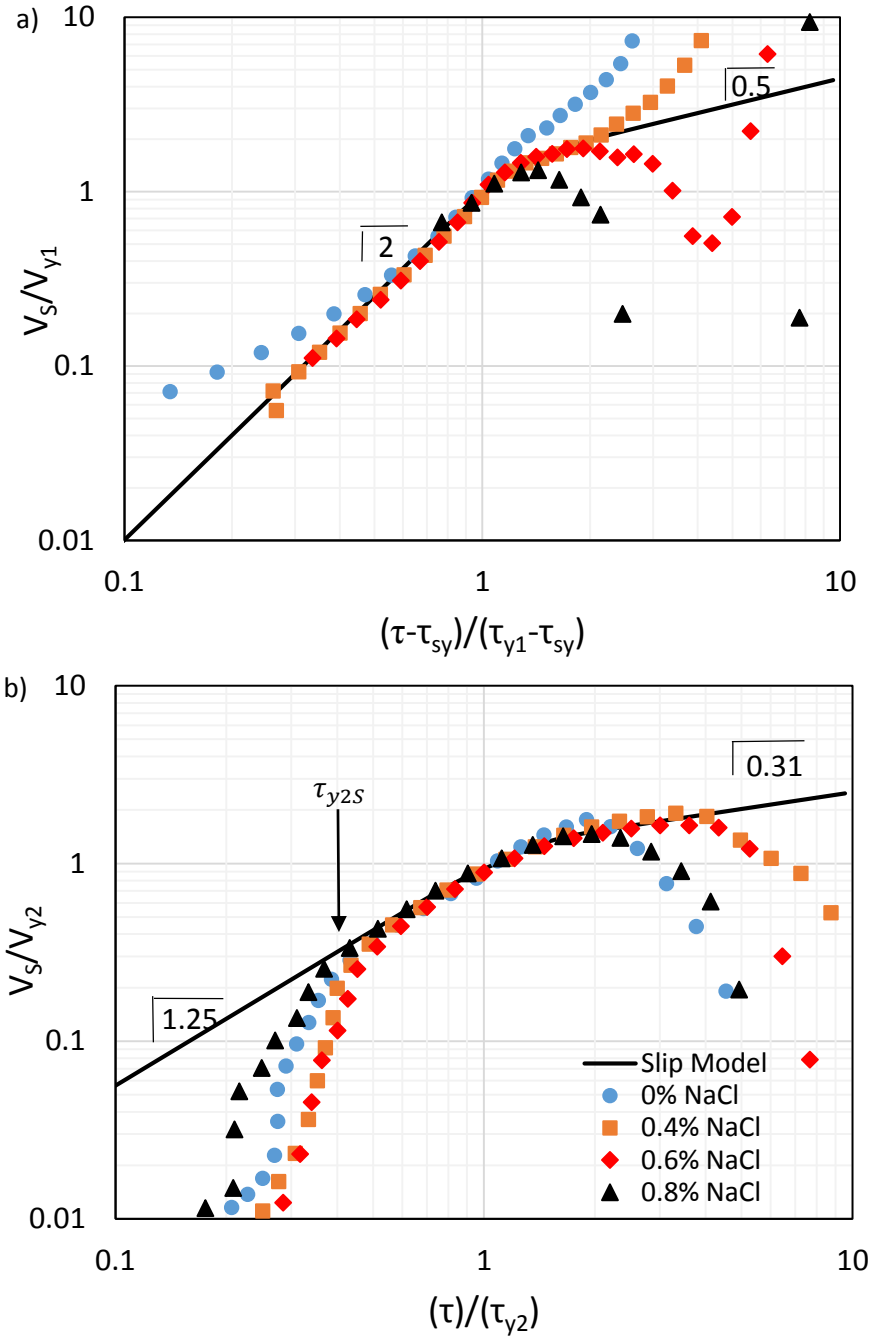

Fig. 5.24: a) V_S/V_{y1} vs. $(\tau-\tau_{sy})/(\tau_{y1}-\tau_{sy})$ and b) V_S/V_{y2} vs. τ/τ_{y2} of 80% oil D emulsions with 1.6% ph15EO, 0.4% NaOH, and 0-0.8% NaCl (D80-6 to D80-9). The τ_{y2S} represents the start of the flow induced yield stress. The black line represents the wall slip model (Eqs. 5.11-12)

Fig. 5.24a showed that $V_S/V_{y1} = \left[(\tau - \tau_{sy})/(\tau_{y1} - \tau_{sy})\right]^2$ for $(\tau - \tau_{sy})/(\tau_{y1} - \tau_{sy}) \leq 1$ and $V_S/V_{y1} = \left[(\tau - \tau_{sy})/(\tau_{y1} - \tau_{sy})\right]^{0.5}$ for $(\tau - \tau_{sy})/(\tau_{y1} - \tau_{sy}) \gg 1$ fit the data well. As $(\tau - \tau_{sy})/(\tau_{y1} - \tau_{sy}) \gg 1$, the error from the measurements of very small V_S resulted in a significant scatter of data compared to the slip model. Fig. 5.24b showed that $V_S/V_{y2} = \left[\tau/\tau_{y2}\right]^{1.25}$ for $\left[\tau/\tau_{y2}\right] \leq 1$ and $V_S/V_{y2} = \left[\tau/\tau_{y2}\right]^{0.3}$ for $\left[\tau/\tau_{y2}\right] \gg 1$ fit the data well. The slip model indicated that the flow behavior index of 80% oil D emulsions are $n_1 \approx 0.5$ and $n_2 \approx 0.8$ near τ_{y1} and τ_{y2}, respectively. This supports the assumption of $n_1 \approx 0.5$ for the modified Herschel-Bulkley equation. $n_2 \approx 0.8$ from the wall slip analysis are very similar to the fitted n_2 values used in the modified Herschel-Bulkley equation to model the flow curves of the emulsions in Fig. 5.18. At $\tau/\tau_{y2} > 4$, the contribution of V_S is negligible compared to the bulk fluid velocity for heavy O/W emulsions. Thus, the deviation of V_S data at high τ/τ_{y2} compared to the slip model becomes insignificant.

The slip model in Fig. 5.23 is a product of combining Eqs. 5.11-12 with a smooth transition between the two equations for $1 < \tau/\tau_y < 2$. The mathematical expression used to smoothly transition between the two equations is the tanh method. For τ_{y1} and τ_{y2}, the V_S expression as a function of τ is:

$$V_{S\mathrm{i}} = V_{yi}\left[\left(\frac{\tau-\tau_{sy}}{\tau_{yi}-\tau_{sy}}\right)^{1/\mathrm{n}} + \left(\frac{1+\tanh\left[A\left(\frac{\tau-\tau_{sy}}{\tau_{yi}-\tau_{sy}}-1\right)\right]}{2}\left(a\left(\frac{\tau-\tau_{sy}}{\tau_{yi}-\tau_{sy}}\right)^{1/4n} - \left(\frac{\tau-\tau_{sy}}{\tau_{yi}-\tau_{sy}}\right)^{1/\mathrm{n}}\right)\right)\right]$$

for $\mathrm{i} = 1$ and 2 (5.13)

where $A = 5$ and a equals

$$a = \left[D + \left(\frac{1+\tanh\left[E\left(\frac{\tau}{\tau_{yi}} - 1\right)\right]}{2} \left(2^{1/4n} - D\right) \right) \right] \tag{5.14}$$

where $D = 0.5$ and $E = 2.5$. Fig. 5.25 plots Eq. 5.13 for $n = 0.5$ and $n = 0.8$.

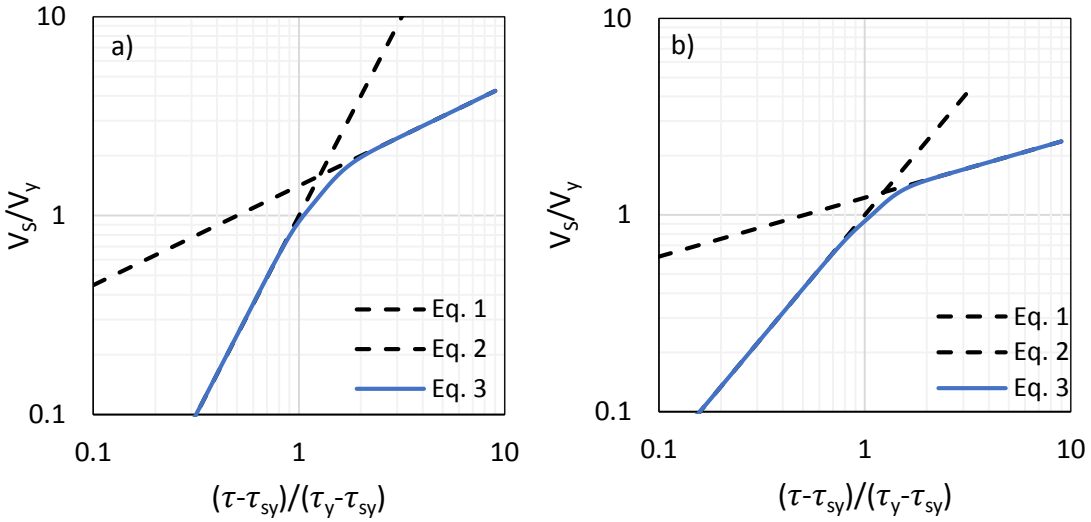

Fig. 5.25: V_S/V_y vs. $(\tau - \tau_{sy})/(\tau_y - \tau_{sy})$ for a) $n = 0.5$ and b) $n = 0.8$ with slip model (Eq. 5.13).

The flow induced yield stress appeared at some stress below τ_{y2} based on the emergence of second wall slip regime. Fig. 5.24 showed that the start of flow induced yield stress τ_{y2S} occurred at $\sim\tau_{y2}/2.5$ for 80% oil D emulsions. Eq. 5.13 can be combined to describe the entire range of V_S for heavy O/W emulsions that showed two-step yielding behavior by using the same method used to combine two Herschel-Bulkley equations (Eq. 5.10).

$$V_{S,tot} = V_{S1} + (V_{S2} - V_{S1})\left(1 - e^{\left(-\left(\frac{\tau}{\tau_{y2S}}\right)^6\right)}\right) \tag{5.15}$$

For concentrated emulsions samples that exhibit more than two yield stresses, the slip behavior of multi-step yielding emulsions can be modeled by adding further repeating V_S terms to Eq. 5.15

$$V_{S,tot} = V_{S1} + \sum_2^n \left[\left(V_{S\mathrm{n}} - V_{S(\mathrm{n}-1)} \right) \left(1 - e^{\left(-\left(\frac{\tau}{\tau_{y\mathrm{n}S}} \right)^6 \right)} \right) \right] \tag{5.16}$$

where n is the number of yield stresses.

The wall slip model for concentrated emulsions that show two-step yielding behavior (Eq. 5.15) is fitted to the measured V_S vs. τ data from Fig. 5.18.

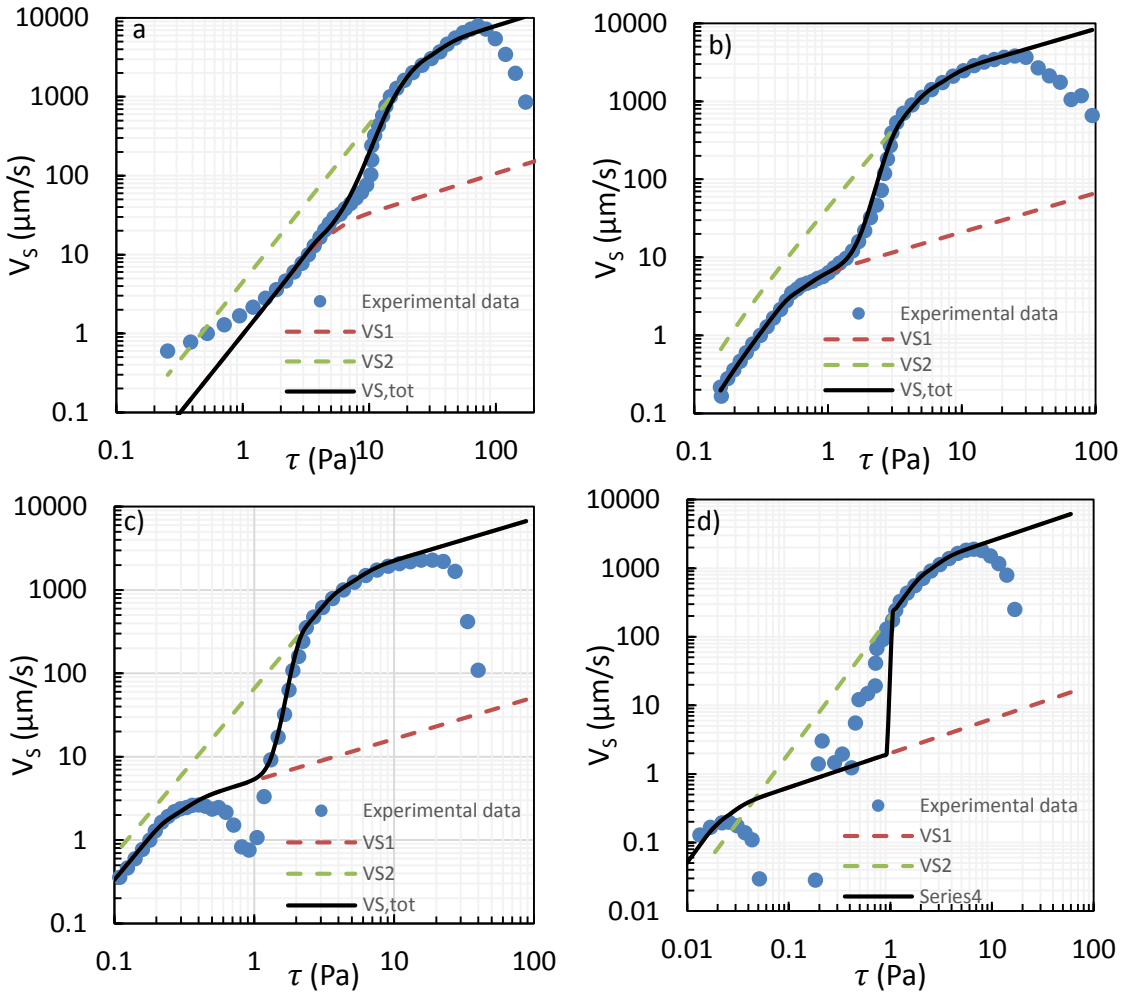

Fig. 5.26: V_S vs. τ of 80% oil D emulsions with 1.6% ph15EO, 0.4% NaOH, and 0-0.8% NaCl (D80-6 to D80-9). a) 0% b) 0.4% c) 0.6% d) 0.8% NaCl emulsions.

Fig. 5.26 showed three regions of experimental uncertainty. At very low τ, the sensitivity of the viscometer transducers created some noise with the torque readings (Fig. 5.26a). It should be physically impossible to have slip when τ is extrapolated to 0. Figs. 5.26c-d data showed a lot of scatter compared to the slip model between the two individual slip models. There is a large error in calculating V_S because of very low V_S/V_0 observed at the transition between the two slip models. The same explanation is applied to the lower experimental V_S data points observed at high τ compared to the slip model (Fig. 5.26a-d).

The regions of τ where a significant deviation compared to the slip model are observed is where the V_S/V_0 ratio is very small and the contribution of V_S to V_0 is negligible. The slip models of V_S vs. τ for 80% oil D emulsions are used to predict the smooth parallel plate flow curves of τ vs. $\dot{\gamma}$ from the roughened parallel plate flow curve measurements (see Fig. 5.18).

Based on Fig. 5.24, two sets of wall slip Regimes for attractive heavy O/W emulsions have been identified. Regime 1 and Regime 2 identify the slip behavior near τ_{y1} and τ_{y2}, respectively.

Regime 1

- 1.1: Slip dominated flow for
- 1.2: Combination of Slip and bulk fluid flow for $1 < \tau/\tau_{y1} < 4$
- 1.3: Bulk fluid flow with negligible slip for $\tau/\tau_{y1} > 4$

Regime 2

- 2.1: Slip dominated flow for $S \leq \tau/\tau_{y2} \leq 1$ with $S < 1$
- 2.2: Combination of Slip and bulk fluid flow for $1 < \tau/\tau_{y2} < 4$
- 2.3: Bulk fluid flow with negligible slip for $\tau/\tau_{y2} > 4$

Fig. 5.27: Slip flow regimes for concentrated heavy O/W emulsions that show two-step yielding behavior

There are six variables that are utilized in Eq. 5.15 to estimated V_S vs. τ: τ_{y1}, τ_{y2s}, τ_{y2}, τ_{sy}, V_{y1}, and V_{y2}. The variables τ_{y1} and τ_{y2} can be measured using roughened parallel plates. τ_{sy} can be estimated based on the interaction potential between the droplets and the flow surfaces [Seth et al. (2008)]. Seth et al. (2012) proposed the relationship $V_y = {\gamma_y}^2 G_0 R/\mu_0$ for repulsive soft glasses. The variables γ_y and G_0 are

measurable emulsion properties using oscillatory measurements. Using Hooke's Law $\tau_y = \gamma_y G_0$, $V_y = {\gamma_y}^2 G_0 R/\mu_0$ was modified and the a constant of 1/100 was included based on the rheological characterization of over 60 heavy O/W emulsions:

$$V_{yi} = \frac{1}{100}\frac{\gamma_{yi}\tau_{yi}d_{32}}{2\mu_0} \tag{5.17}$$

where $\gamma_{yi}d_{32}/2$ is the distortion of the emulsion droplets and i the yield number.

The measured V_{y1} and V_{y2} of over 60 heavy O/W emulsions were compared to the calculated V_{y1} and V_{y2} using Eq. 5.17.

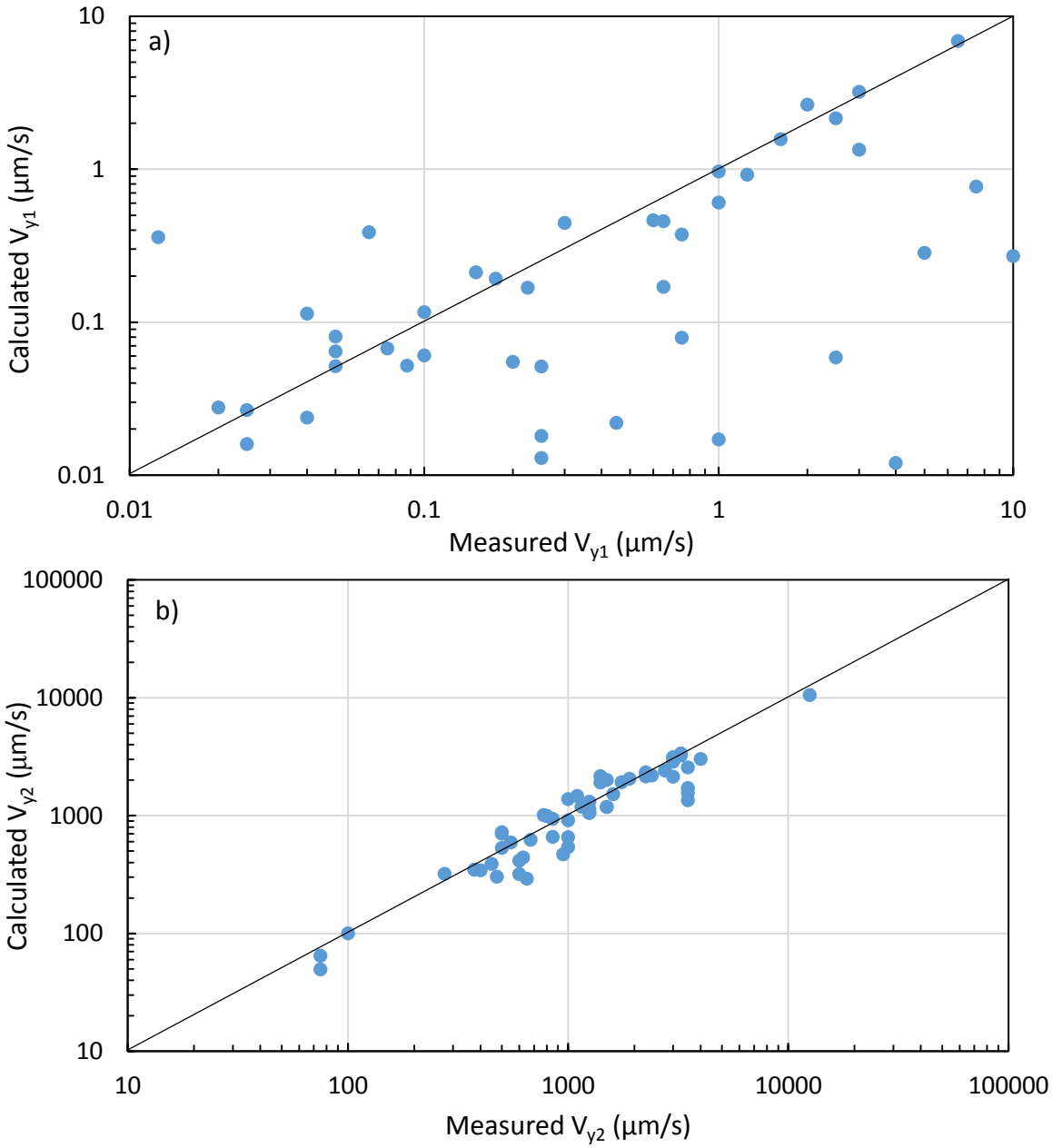

Fig. 5.28: Calculated V_{yi} vs. measured V_{yi}. a) V_{y1} and b) V_{y2}.

Fig. 5.28 showed a good agreement between the measured and calculated V_y values. Experimental errors are introduced in every step of experiments such as the measurement of mean droplet diameter using a static light scattering equipment, oscillatory

measurements of γ_y and τ_y, and measurements of V_y. Error is also introduced by using the d_{32} value to describe the mean droplet size of emulsions samples with broad droplet size distributions. The measurement errors are higher at the first yield point because the torque measurements are near the accuracy limit of the torque transducers used by the ARES LS1 Rheometer. This is reflected in the larger scatter of data in Fig. 5.28a compared to the data in Fig. 5.28b. The same d_{32} was used to calculate both V_y values, suggesting that the wall slip is controlled by the individual droplet size and not the aggregate size.

The only fitting parameter necessary to use the wall slip model (Eq. 5.15) is τ_{y2s} which often equaled to $\tau_{y2}/2.5$ but values as low as $\tau_{y2}/20$ were measured. $\tau_{y2s} < \tau_{y2}/2.5$ may indicate the presence of multiple flow induced yield stresses due to the stepwise breaking of the clusters/aggregates.

5.4.4 Effect of Physicochemical Properties on the Rheology of Heavy O/W Emulsions

The effect of the physicochemical properties of the heavy O/W emulsions on the rheological properties are explored in this section. The type of heavy oil, oil concentration, NaOH concentration, NaCl concentration, and co-solvent type are varied in the chemical formulations used to prepare the emulsions.

5.4.4.1 Effect of Heavy Oil

The effect of the type of heavy oils used to prepare heavy O/W emulsions is explored in Fig. 5.29. Viscosities of oil A, oil B, and oil D are ~310,000 cP, ~91,000 cP, and ~9,000 cP at 10 s^{-1} and 25°C, respectively.

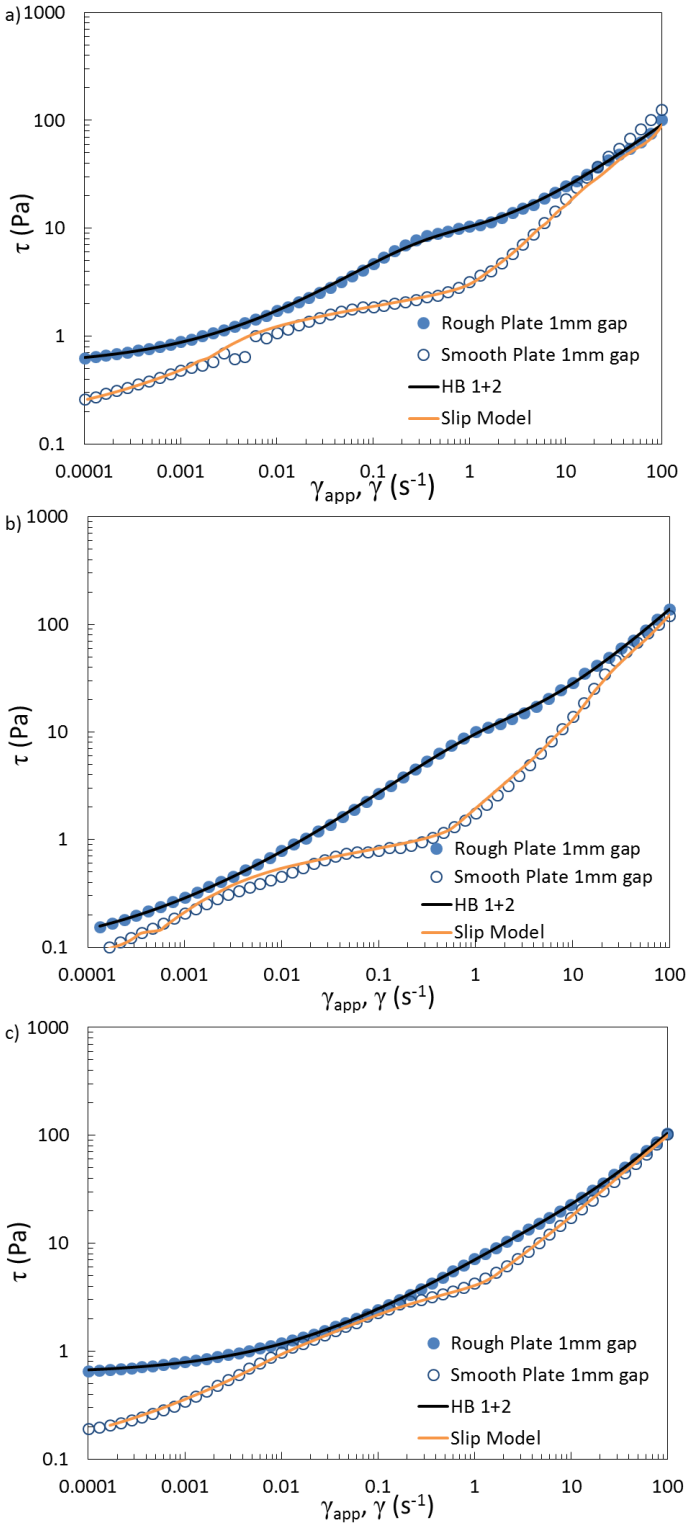

Fig. 5.29 continued.

Fig. 5.29. $\tau\ vs.\dot{\gamma}, \dot{\gamma}_{app}$ of 80% O/W emulsions prepared with 1.6% phenol-15EO, 0.2% NaOH, and 0.4% NaCl. a) A80-1: Oil A, d_{32}=17.3μm, $\varphi_m = 0.79$, b) B80-3: Oil B, d_{32}=26.7μm, $\varphi_m = 0.78$, c) D80-2: Oil D, d_{32}=13μm, $\varphi_m = 0.7$.

The flow curves of $\tau\ vs.\dot{\gamma}$ measured with the rough parallel plates did not show a significant difference between the emulsions prepared with heavy oils of varying viscosities. Emulsions prepared with oil A and oil B showed more distinct humps at the site of the flow induced yield stress compared to the emulsion prepared with oil D. Also, the contribution of wall slip to total flow at the sites of the flow induced yield stress were significantly higher for oil A and oil B emulsions ($V_S/V_y \approx 0.95$) compared to oil D emulsion ($V_S/V_y \approx 0.65$). The hump in the flow curves and wall slip due to the flow induced yield stress are more significant when emulsions are prepared with heavy oils with higher viscosities.

5.4.4.2 Effect of Heavy Oil Concentration

The concentration of heavy oil in the emulsions is the variable that has the biggest effect on the emulsion viscosities. Fig. 5.30 shows the $\mu\ vs.\dot{\gamma}$ of 40-85% oil D emulsions prepared with two different chemical formulations.

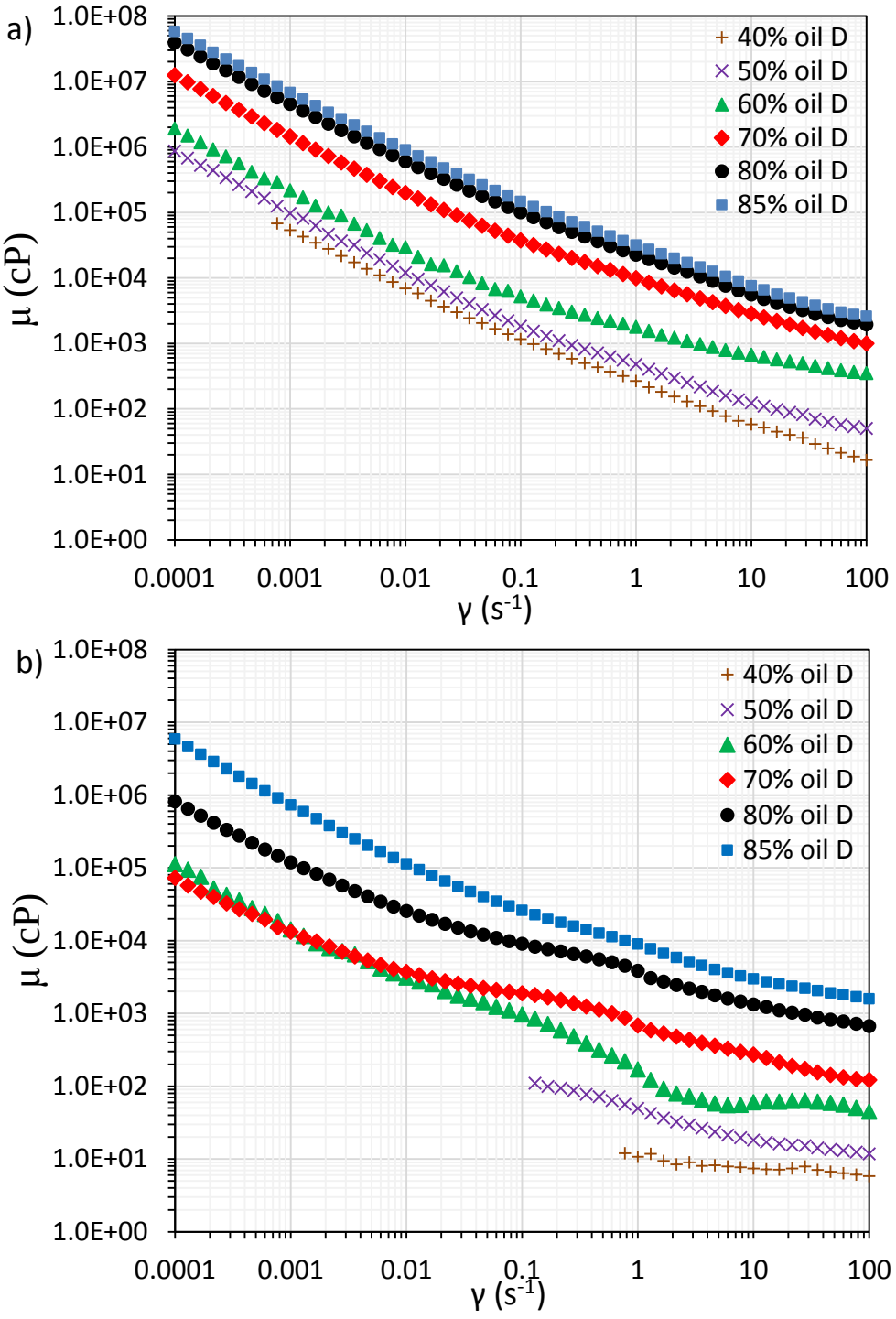

Fig. 5.30: $\mu \; vs. \dot{\gamma}$ of 40-85% oil D emulsions prepared with 1.6% phenol-15EO, 0.2% NaOH, and a) 0% NaCl (D40-10 to D85-15) and b) 1% NaCl (D40-16 to D85-21). Measured with 50 mm cross-hatched parallel plates with 1mm gap at 22.25°C ±0.25.

Emulsions with higher viscosities were prepared when the oil concentration in the emulsion was higher. Changed in the oil concentration from 40% to 85% resulted in over two orders of magnitude increase in the emulsion viscosities. Similar trend was observed with oil B emulsions in Fig. 5.31.

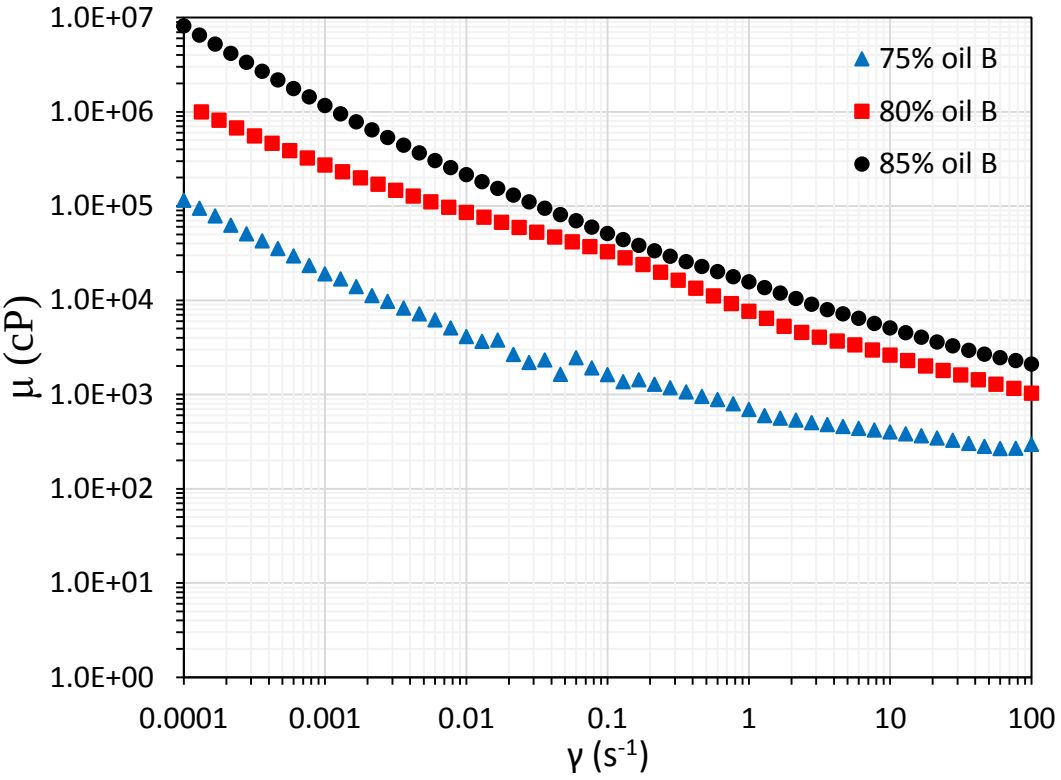

Fig. 5.31. $\mu\ vs.\dot{\gamma}$ of 75-85% oil B emulsions prepared with 1.6% phenol-15EO, 0.4% NaOH, and 0.8% NaCl. B75-5: 75% emulsion (d_{32}=28.8μm, $\varphi_m = 0.81$). D80-26: 80% emulsion (d_{32}=6.6μm, $\varphi_m = 0.94$). D85-42: 85% emulsion (d_{32}=20.5μm, $\varphi_m = 0.87$). Measured with 50 mm cross-hatched parallel plates with 1mm gap at 22.25°C ±0.25

Oil D emulsions prepared with the low salinity chemical formulation (1.6% phenol-15EO, 0.2% NaOH, and 0% NaCl) showed higher viscosities compared to the emulsions prepared with the higher salinity chemical formulation (1.6% phenol-15EO, 0.2% NaOH, and 1% NaCl) at all oil concentrations. Up to an order of magnitude lower viscosities were observed when the NaCl concentration was increased from 0-1% in the

chemical formulation. The effect of the chemical formulation used to prepare emulsions on emulsion rheology is explored further.

5.4.4.2 Effect of Chemical Formulation

The effect of the chemical formulation composition used to prepare heavy O/W emulsions is explored in Fig. 5.32. 80% oil B emulsions are prepared with 1) only NaOH of varying concentrations 2) NaOH and phenol-15EO, and 3) NaOH, NaCl, and phenol-15EO.

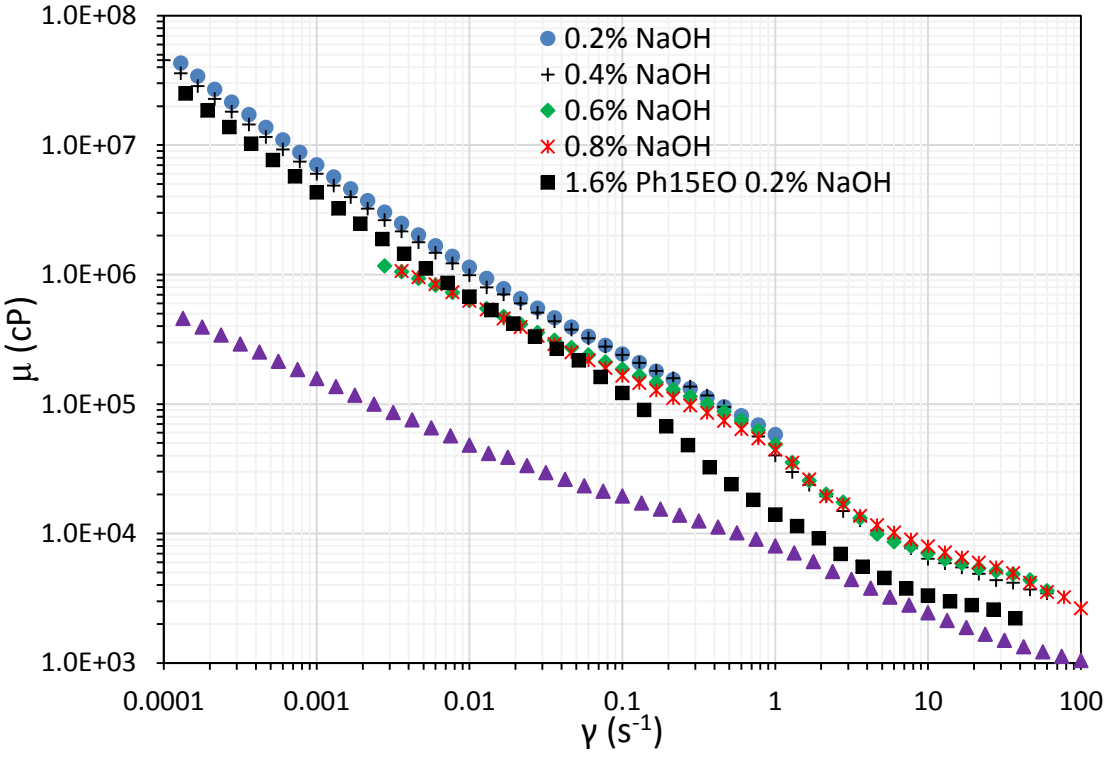

Fig. 5.32: $\mu\ vs.\dot{\gamma}$ of 80% oil B emulsions prepared with different chemical formulations. Blue circle: 0.2% NaOH (B80-5: d_{32}=30μm, $\varphi_m = 0.765$), Black cross: 0.4% NaOH (B80-6: d_{32}=15μm, $\varphi_m = 0.8$), Green diamond: 0.6% NaOH (B80-7: d_{32}=6.8μm, $\varphi_m = 0.73$), Red star: 0.8% NaOH (B80-8: d_{32}=5μm, $\varphi_m = 0.75$), Black square: 1.6% Ph15EO 0.2% NaOH (B80-9: d_{32}=33.5μm, $\varphi_m = 0.73$), Purple triangle: 1.6% Ph15EO 0.2% NaOH 1.2% NaCl (B80-30: d_{32}=21.3μm, $\varphi_m = 0.81$). Measured with 50 mm cross-hatched parallel plates with 1mm gap at 22.25°C ±0.25.

80% oil B emulsions prepared with chemical formulations that consisted of only NaOH showed very similar behavior regardless of the NaOH concentration (0.2-0.8%). Also, some of the emulsions were expelled from the parallel plates at shear rates higher than the critical shear rate where the τ_{y2} appeared. Even through d_{32} varied from 5 to 30μm and φ_m varied from 0.73 to 0.8, no significant difference in rheological properties were observed when the chemical formulation consisted of only NaOH in deionized water.

The addition of 1.6% phenol-15EO to 0.2% NaOH in the chemical formulation drastically changed the rheological properties while the physical properties did not change significantly. At low shear rates of $\dot{\gamma} < 0.1\ s^{-1}$, both the emulsion prepared with 0.2% NaOH and the emulsions prepared with 1.6% phenol-15EO to 0.2% NaOH showed similar behavior. However, at higher shear rates of $\dot{\gamma} > 0.1\ s^{-1}$, the emulsion prepared with 1.6% phenol-15EO and 0.2% NaOH showed viscosities that were up to three times lower than the viscosities of emulsions prepared with only 0.2% NaOH. Because ethoxylated co-solvents partition preferentially to the interface between oil and water [Chang (2014)] and make the interface more flexible [Taghavifar (2014)], the heavy oil droplets may be able to deform at high shear rates with less energy, resulting in lower viscosities and a lower shear induced yield stress. Fortenberry et al. (2013) observed that the interfacial viscosities between heavy oil and alkaline brine decreased by an order of magnitude when 3% IBA-10EO co-solvent was added to the alkaline brine.

While the co-solvent alone with the NaOH did not significantly affect the emulsions viscosity at low shear rates of $\dot{\gamma} < 0.1\ s^{-1}$, adding 1.2% NaCl to the chemical formulation of 1.6% phenol-15EO and 0.2% NaOH drastically reduced the emulsion viscosities at low shear rates of $\dot{\gamma} < 1\ s^{-1}$. Emulsions with up to 100 times lower viscosities at low shear rates and 10 times lower viscosities at high shear rates were

observed when both phenol-15EO and NaCl were added to the chemical formulation used to prepare 80% heavy O/W emulsions.

The effect of NaCl concentration with 1.6% phenol-15EO and 0.2% NaOH on the rheological properties of 80% oil B and 80% oil D emulsions is explored in Fig. 5.33.

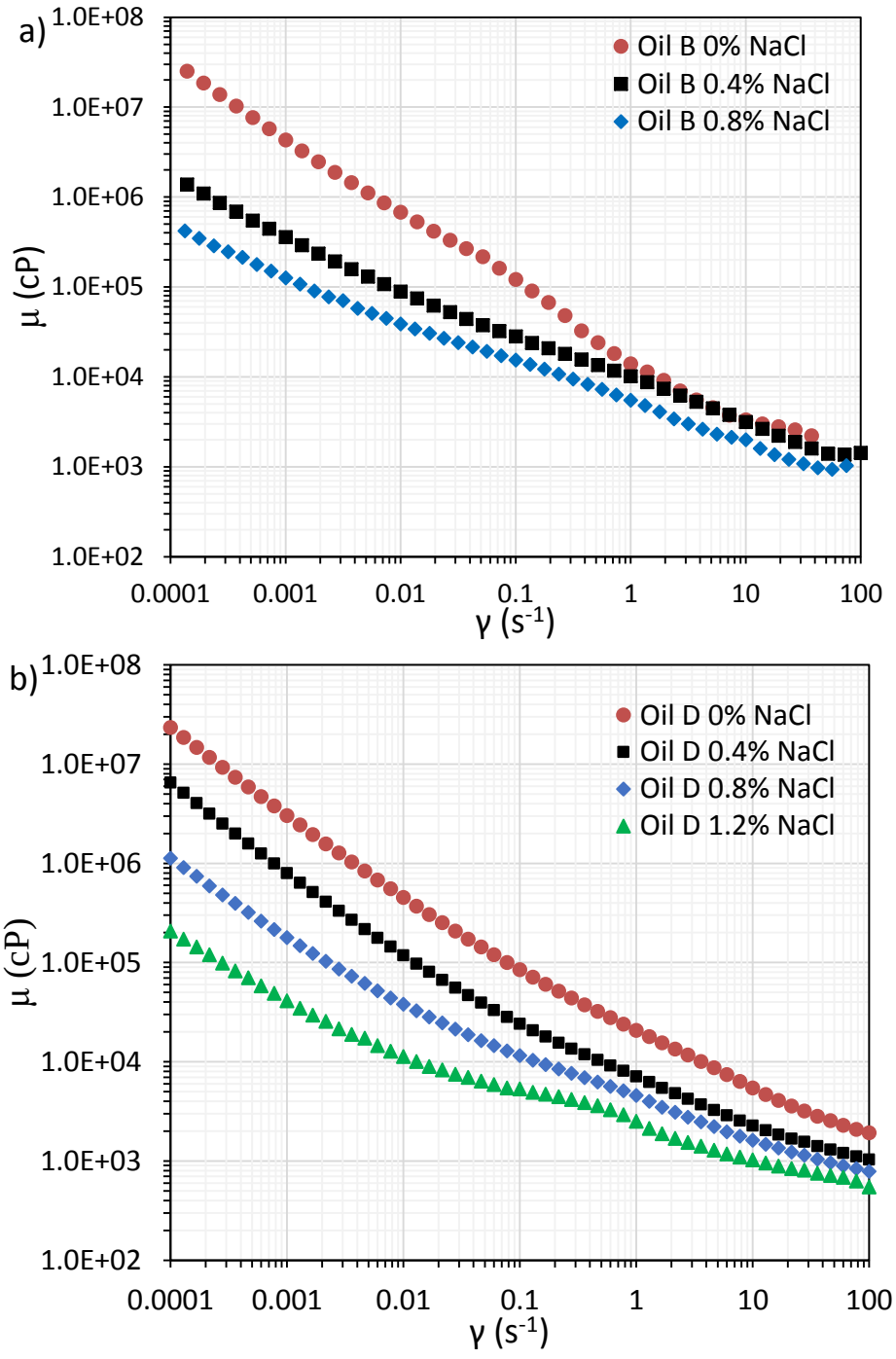

Fig. 5.33: $\mu \, vs. \dot{\gamma}$ of a) 80% oil B emulsions prepared with 1.6% phenol-15EO 0.2% NaOH, and 0-0.8% NaCl (B80-9, B80-12, and B80-21). b) 80% oil D emulsions prepared with 1.6% phenol-15EO 0.2% NaOH, and 0-1.2% NaCl (D80-1 to D80-5). Measured with 50 mm cross-hatched parallel plates with 1mm gap at 22.25°C ±0.25.

Higher NaCl concentration in the chemical formulation lowered the emulsion viscosities at all shear rates. The viscosity reduction was more significant at lower shear rates. Emulsions prepared with higher NaCl concentration increased φ_m which may have contributed to the lower viscosities of the emulsions. However, the increase in φ_m is not enough to explain the drastic decrease in emulsion viscosities with higher NaCl concentration observed in Fig. 5.33. Lower interfacial tension may also contribute to the lower viscosities of emulsions prepared with a higher NaCl concentration. The interfacial tension of the heavy O/W emulsions are lower as the NaCl concentration approaches the inversion salinity from O/W to W/O with ultra-low interfacial tension achieved at the inversion point.

The d_{32} and φ_m of 80% oil B emulsions before and after 3 hours of rheological measurements (steady state, oscillatory, and transient) are measured to test the stability of emulsions against shear.

Table 5.3: Physical properties of 80% oil B emulsions before and after rheological measurements. Emulsions are prepared with 1.6% phenol-15EO, 0.4% NaOH, and 0.1-1.4% NaCl.

	Before rheological measurements		**After rheological measurements**	
NaCl concentration	d_{32} (μm)	φ_m	d_{32} (μm)	φ_m
0.1%	14.3	0.8	13.8	0.81
0.4%	13	0.81	9.8	0.82
0.8%	8.9	0.92	8.2	0.94
1.2%	8.9	0.9	12.5	0.91
1.4%	20.7	0.92	20.6	0.9

The d_{32} and φ_m of 80% oil B emulsions in Table 5.3 did not change significantly after rigorous rheological measurements. This suggests that the emulsions were stable against shear for the rheological tests outlined in Experimental Procedures Section.

Changing the type of ethoxylated co-solvents in the chemical formulation used to prepare heavy O/W emulsions did not have a significant effect on the rheological properties. Flow curves of 80% oil B emulsions prepared with 1.6% IBA-15EO and 1.6%Phenol-15EO and mixed in 60ºC and 96ºC oven are shown in Fig. 5.34.

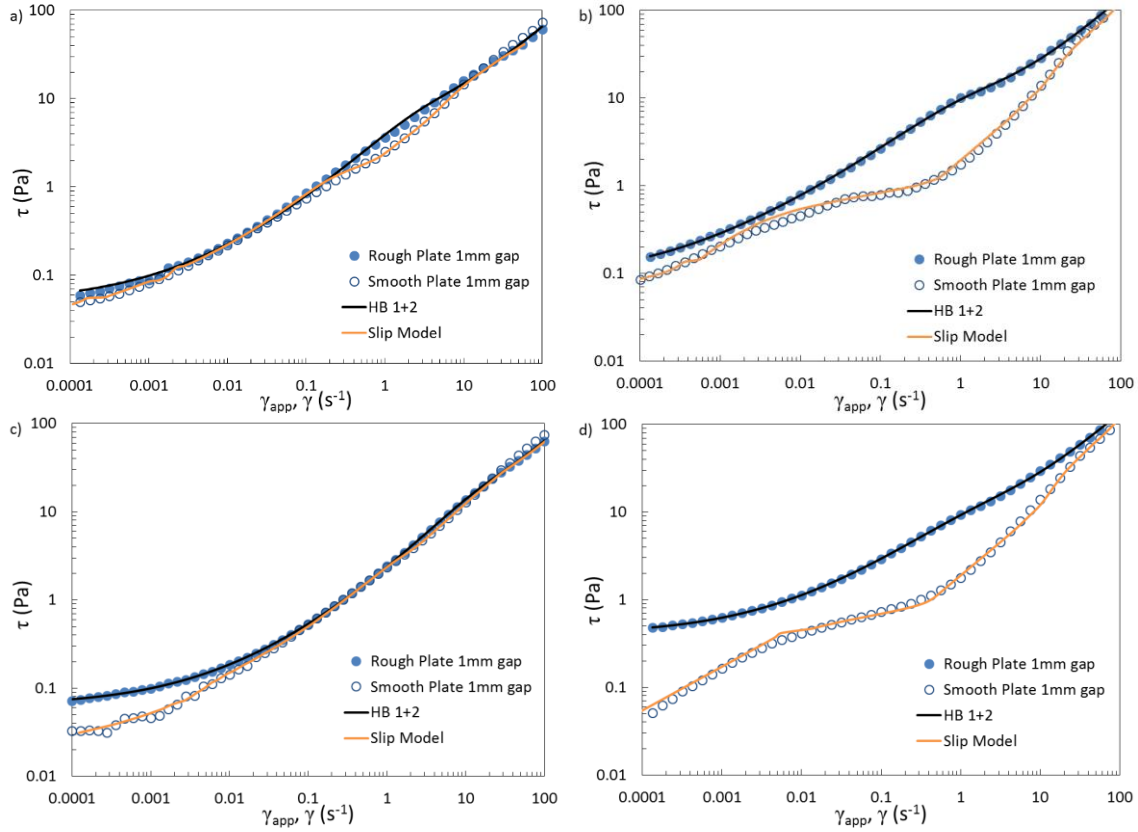

Fig. 5.34. $\tau\ vs.\dot{\gamma}$ of 80% oil B emulsions prepared with 1.6% phenol-15EO 0.2% NaOH 0.4% NaCl. a) B80-14: d_{32}=11.9µm, $\varphi_m = 0.805$, b) B80-13: d_{32}=26.7µm, $\varphi_m = 0.78$ and prepared with 1.6% IBA-15EO 0.2% NaOH 0.4% NaCl c) B80-1: d_{32}=17.8µm, $\varphi_m = 0.81$, d) B80-04: d_{32}=26.9µm, $\varphi_m = 0.75$. Emulsions in a) and c) were mixed in a 60ºC oven and emulsions in b) and d) were mixed in a 96ºC oven.

The type of ethoxylated co-solvent used to prepare heavy O/W did not affect the emulsion rheology significantly. The mixing temperature of the emulsions significantly affected the emulsion rheology with lower emulsions viscosities observed when mixed in an oven with a lower temperature. Emulsions that were mixed in a 60ºC oven compared

to a 96°C oven showed lower d_{32} and higher φ_m. The flow induced yield stress was negligible for emulsions mixed in a 60°C oven which resulted in a negligible or a very small wall slip.

5.5 CONCLUSIONS

Heavy oil-in-water emulsions showed complex rheological properties such as yield stresses, shear thinning behavior, time-dependent property, and wall slip. The rheological properties of the emulsions are different depending on the dispersed oil concentration.

Emulsions with dispersed phase heavy oil concentrations of $\varphi < 60\%$ showed the following properties due to the percolating networks and clusters/aggregates formed by attractive heavy oil droplets:

1. Shear thinning behavior
2. Higher viscosity than what Pal (2001) equation predicts for emulsions.
3. A yield stress
4. Wall slip was observed just above and below the yield stress.

The non-Newtonian fluid properties observed with attractive heavy oil emulsions with $\varphi < 60\%$ are not usually observed with repulsive emulsions.

Concentrated emulsions with attractive interdroplet interactions showed rheological properties not observed with concentrated emulsions with repulsive interdroplet interactions and attractive heavy oil-in-water emulsions with lower oil concentrations ($\varphi < 60\%$).

1. Time-dependent rheological property at low shear rates where emulsion viscosity increased as it was sheared longer (rheopectic).

2. Two-step yielding behavior with a traditional yield stress and a flow induced yield stress.
3. Two-step wall slip behavior observed near the two yield stresses.

The two-step yielding and two-step wall slip behaviors of concentrated heavy oil-in-water emulsions with attractive interdroplet interactions were observed for the first time in the literature.

A modified Herschel-Bulkley equation accurately modeled the viscosity of heavy oil-in-water emulsions as a function of shear rate. The equation can be used for heavy oil-in-water emulsions of all dispersed phase concentration.

A wall slip equation was derived to model the wall slip behavior of heavy oil-in-water emulsions. The equation can model the wall slip velocity of heavy oil emulsions with two-step yielding behavior. The second region of wall slip is due to the presence of the flow induced yield stress. The shear induced yield stress can be measured by analyzing the wall slip velocity.

Heavy oil-in-water emulsions showed lower viscosity when prepared with a chemical formulation that included:

1. An alkali
2. A ethoxylated co-solvent such as IBA-xEO and phenol-xEO
3. A high NaCl concentration

The effect of the heavy oil viscosity on the emulsion viscosity was found to be small. With an optimized chemical formulation, heavy O/W emulsions with up to 75% dispersed oil phase showed emulsion viscosities less than 350 cP at the operating conditions for crude oil pipelines. Emulsions prepared with a chemical formulation that was not optimized showed viscosities of ~350 cP with 55-60% dispersed oil phase. Optimizing the chemical formulations used to prepare heavy oil-in-water emulsions

improved the volume fraction of heavy oils that can be transported in an emulsified form from 55-60% to 75% in pipelines.

NOMENCLATURE

ω Angular frequency of oscillation
$\dot{\gamma}_{app}$ Apparent shear rate
ω_c Critical angular frequency
$\dot{\gamma}_c$ Critical shear rate
φ Dispersed-phase volume fraction
n Flow behavior index
k Flow consistency index
Γ Interfacial tension
$G"$ Loss modulus
φ_m Maximum close packing fraction possible for solid spheres
R_{32} Sauter mean radius of the droplets
d_{32} Sauter mean diameter of the droplets
$\dot{\gamma}$ Shear rate
$\dot{\gamma}_R$ Shear rate at the edge of the parallel plate
τ Shear stress
τ_{sy} Sliding yield stress
V_y Slip velocity at $\tau/\tau_y = 1$
G, G_0 Strain and frequency independent storage modulus
γ Strain rate
τ_{y2s} Stress where the flow induced yield stress emerges
G' Storage modulus
M Torque
W_t Total interaction energy between oil droplets
V_0 Total velocity of emulsion
K Viscosity ratio of dispersed-phase to continuous-phase
μ_r Viscosity ratio of the emulsion to the continuous phase
μ_i Viscosity where $i = sus, d, c, emul$ represent suspension, dispersed, continuous, and emulsion
V Velocity of bulk emulsion with no wall slip
V_S Wall slip velocity
γ_y Yield strain
τ_y Yield stress

ABBREVIATIONS

O/W Oil-in-water
W/O Water-in-oil
HB Herschel-Bulkley Equation

Chapter 6: Viscosity Measurements of Concentrated Heavy O/W Emulsions using Capillary Tube Viscometers

6.1 INTRODUCTION

Crude oil is transported under a pressure gradient through pipelines of varying diameter and length. The rheological characterization of concentrated heavy oil-in-water emulsions with the rotational shear viscometer works on the principal of a drag flow between two plates. In Chapter 5, the rheological properties of heavy oil-in-water emulsions were characterized and shown to depend on both the shear rate and flow conduit dimensions. In this chapter, the rheology of heavy oil-in-water emulsions measured with capillary tube viscometers is compared to the rotational viscometer measurements. Various tube diameters and lengths were used to test the effect of tube dimensions on the emulsion rheology.

The rheological properties of heavy oil-in-water emulsions were also found to be extremely sensitive to the type of flow, a drag flow in a rotational viscometer and a pressure driven flow in tubes. The apparent viscosity of concentrated heavy oil-in-water emulsions were significantly lower in capillary tube viscometers compared to the rotational viscometer measurements. While wall slip on the tube wall contributed to the lower than expected pressure gradients, they were still significantly lower when wall slip was eliminated. The lower than expected pressure gradients of heavy oil-in-water emulsions in capillary tube viscometers may be caused by migration of oil droplets away from the tube wall. Heavy oil-in-water emulsions showed up to ten times lower viscosity in capillary tube viscometers than in rotational viscometers. Flow rates of concentrated heavy oil-in-water emulsions in capillary tube viscometers (pressure driven flow) cannot be predicted based only on the rheological properties measured with a rotational viscometer (drag flow).

6.2 LITERATURE REVIEW

A majority of the studies on heavy oil-in-water (O/W) emulsions used one of the two flow types, drag flow or pressure driven flow, to characterize the emulsion rheological properties. The rheological properties of concentrated heavy O/W emulsion were measured with either a rotational viscometer with a Couette geometry [Acevedo et al. (2001); Ahmed et al. (1999a), (1999b); Gutierrez et al. (2003); Hoshyargar and Ashrafizadeh (2013); Romero et al. (2002), (2000); Sanchez and Zakin (1994); Zaki (1997)], a rotational viscometer with a parallel plate/cone-and-plate geometry [dos Santos et al. (2011); Hasan et al. (2010); Pal (1996)], or a capillary tube viscometer [Sanchez and Zakin (1994); Wylde et al. (2012)]. Measurement geometries with smooth surfaces were used in all these studies. Thus, the contribution of wall slip to the viscosity measurements cannot be ignored. Rotational viscometers (drag flow) appeared to be the preferred method for viscosity measurements of heavy O/W emulsions over tube viscometers. Accurate viscosity measurements using tube viscometers require a significantly longer time and more effort compared to using rotational viscometers.

Several key studies have been conducted that compared the rheological properties of concentrated heavy O/W emulsions measured using a rotational Couette viscometer and a tube viscometer [Gillies and Shook (1992); Layrisse et al. (1985); Núñez et al. (1996); Sumner et al. (1998); Wyslouzil et al. (1987)]. The studies indicated that some heavy O/W emulsions showed lower pressure gradients in tube viscometers than the values predicted using measured viscosities from a Couette viscometer. Sumner et al. (1998) summarized the experiments and concluded that the heavy O/W emulsions that showed lower pressure gradients than expected in tube viscometers were due to oil droplet migration away from the tube wall.

Experiments have shown that particles in colloidal suspensions experience shear – induced migration if exposed to inhomogeneous stress or shear fields. Gadala-Maria and Acrivos (1980) first noticed a decrease in concentrated sphere suspension viscosity over a period of time when measured with a Couette viscometer. Leighton and Acrivos (1987) demonstrated that this phenomenon of transient viscosity behavior of a neutrally buoyant, non-Brownian, concentrated suspension was due to shear-induced migration of particles out of the sheared Couette gap into the fluid reservoir at the bottom where shear rates are lower compared to the gap. The observed migration direction is from regions of high to low shear rates/stresses. Hookham (1986) and Koh et al. (1994) showed experimental evidence that a pressure-driven flow of sphere suspensions in rectangular channels also show particle migration away from the walls accompanied by flattening of the velocity profile compared to Newtonian fluids. Particle migrations in a pressure-driven flow of Brownian colloidal suspensions have also been experimentally observed by Frank et al. (2003). Particle migration resulted in lower viscosity for Couette geometry over time because of a lower particle concentration within the gap compared to the initial particle concentration.

The topic of particle migration in rotational flow between parallel plate and cone-and-plate geometries is more complex. Chow et al. (1994) observed particle migration of neutrally buoyant spherical particle suspension in a Couette geometry, but they observed no particle migration in a parallel-plate geometry regardless of its inhomogeneous shear field. However, experimental studies of particle migrations in parallel plate geometries have been published. Krishnan et al. (1996) proposed that in plate geometries, such as parallel plates and a cone-and-plate, the curved streamlines caused particle migration toward regions of lower curvature. The shear rate inhomogeneity in parallel plates results in particle migration toward the center of the plates while the curved streamlines result in

particle migration away from the center of the plates. If both forces are equally strong, no particle migration is observed in parallel plates. Merhi et al. (2005) showed experimental evidence of outward particle migration in concentrated suspensions measured with a parallel plate geometry. They showed that the curved streamline effect is stronger than the shear rate inhomogeneity effect, resulting in a higher concentration of particles away from the center of the plates. They also reported that a significantly longer migration time was required to reach a steady state particle concentration profile with a lower particle concentration gradient observed in a parallel plate geometry compared to a Couette geometry. This could be a possible explanation as to why Chow et al. (1994) didn't observe any particle migration in a parallel plate geometry for his experiments.

King and Leighton (2001) and Hudson (2003) demonstrated that emulsion droplets also migrate when exposed to a heterogeneous shear/stress field similar to hard sphere suspensions. Norman et al. (2005) demonstrated that buoyancy (relative density of dispersed to continuous phase) also has a significant effect on particle migration in a pressure-driven flow through tubes.

The bulk dispersed-phase concentration φ_{bulk} as well as the ratio of particle radius to the flow dimension radius a/R influenced the magnitude of particle migrations. Hampton et al. (1997) demonstrated experimentally that particle migration in pressure-driven tube flow of neutrally buoyant sphere suspensions is a strong function of φ_{bulk}. They observed that negligible particle migration occurred for $\varphi_{bulk} = 0.1$. For $\varphi_{bulk} \geq 0.2$, particle migration was observed with the magnitude of $\varphi(r)$ gradient increasing with higher φ_{bulk} values. NMR images of particle concentration profiles in the tube flow experiments from Hampton et al. (1997) are shown in Fig. 6.1.

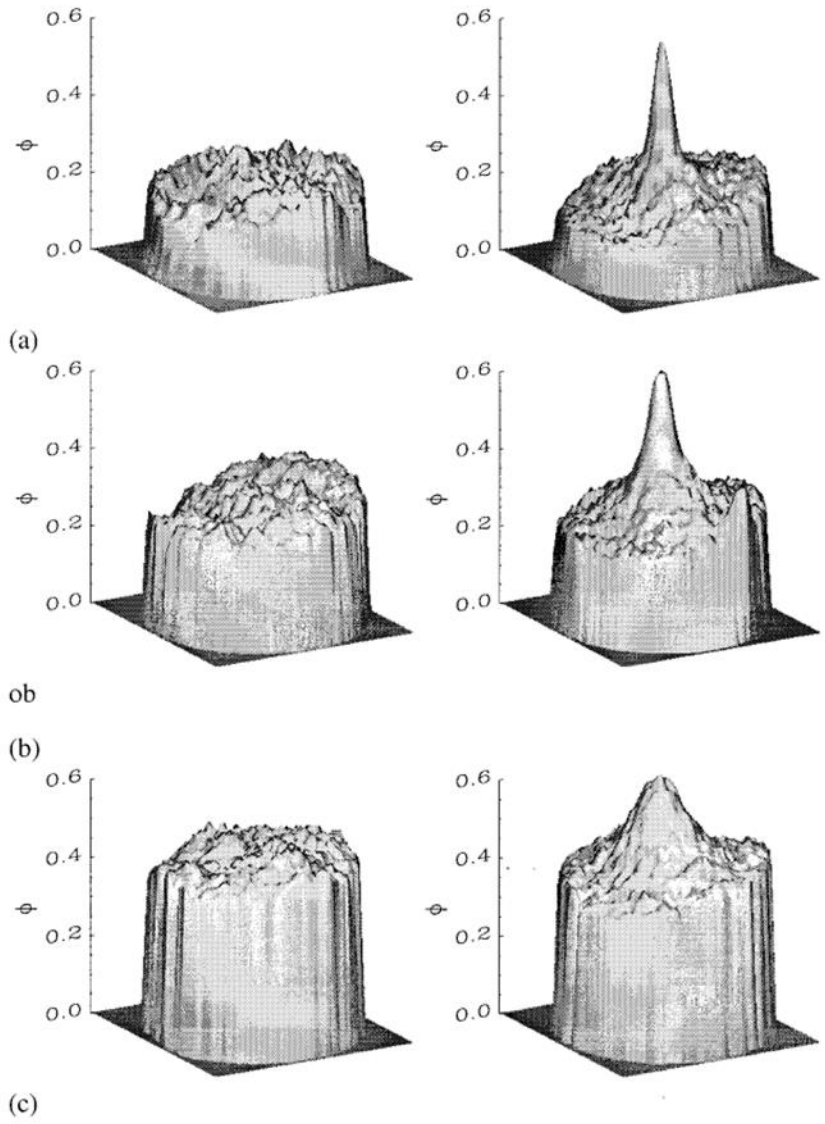

Fig. 6.1: NMR $\varphi(r)$ images of initial (left) and fully developed (right) flows for $a/R = 0.0256$ and φ_{bulk} of (a) 0.2, (b) 0.3, and (c) 0.45. a is the particle radius and R the tube radius. No particle migration observed for $\varphi_{bulk} = 0.1$. Images obtained from Hampton et al. (1997).

To accurately characterize $\varphi(r)$ profiles in tubes, steady state flow profiles must be achieved. The entrance length required to reach steady state $\varphi(r)$ profiles in tubes is a

complex function of flow conduit dimensions and suspension properties. Nott and Brady (1994) derived an equation to estimate the characteristic length required to reach steady state laminar flow for suspensions:

$$\frac{L}{R} \sim \frac{1}{12d(\varphi)}\left(\frac{R}{a}\right)^2 \tag{6.1}$$

where L is the length of a pipe, a the particle radius, R the radius of a tube, and $d(\varphi)$ a non-dimensional function of φ. For dense suspensions of $\varphi > 0.3$, the value $12d(\varphi) \approx 1$. The L/R required for suspensions to reach steady state laminar flow in tubes is much longer compared to Newtonian fluids.

Indirect evidence of heavy oil droplet migration in tubes can be found. Salager et al. (2001) stated that according to the Orimulsion® study, the measured field pressure drops in the pipeline were systematically lower than the ones predicted from the rheological properties measured in a Couette viscometer. Núñez et al. (1996) found that concentrated heavy O/W emulsions ($\varphi = 0.8$) in a tube flow showed evidence of a transitional flow pipe length with higher pressure drop measured for the first half of a tube compared to the second half. They also found that the difference in the pressure drop between the two halves of the tube increased as the mass flow rate increased.

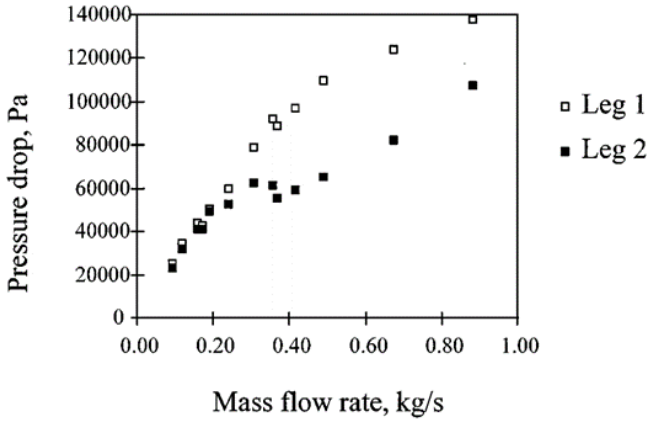

Fig. 6.2: $\Delta P\ vs. \dot{m}$ relationship for a concentrated heavy O/W emulsion ($\varphi = 0.8$). Leg 1 and leg 2 refer to the first and second half of one continuous tube with $D = 21.7\ mm$. Figure obtained from Núñez et al. (1996).

The observations made by Salager et al. (2001) and Núñez et al. (1996) showed characteristic behaviors of oil droplet migration away from the tube wall: a long transition tube length necessary to reach a steady state φ profile and a lower steady state viscosity in capillary tube viscometers compared to rotational viscometer measurements.

There are few experimentally measured φ profiles in the literature for flow of concentrated heavy O/W emulsions in capillary tubes. Gillies and Shook (1992) showed evidence of droplet migration for concentrated heavy O/W emulsions with $d \approx 120\ \mu m$ using velocity profile measurements. Heavy O/W emulsions showed lower apparent viscosities compared to the rotational viscometer measurements. Also, the tube viscometer flow of heavy O/W emulsions showed flatter velocity profiles than the velocity profiles of a homogeneous emulsion, which is evidence of droplet migration towards the center of tubes. However, Layrisse et al. (1985) and Sumner et al. (1998) demonstrated that concentrated heavy O/W emulsions with $d \approx 30\ \mu m$ showed velocity profiles very similar to Newtonian fluids with no significant variation in viscosities measured with a Couette viscometer and a tube viscometer. Direct measurements of velocity profiles of heavy O/W emulsions appeared to suggest that the mean droplet size is a critical emulsion parameter that controls droplet migration in tubes. It is not clear whether heavy O/W emulsions with a small mean droplet diameter do not show significant droplet migration in tubes or the tube length required to observe a steady state flow was not achieve in the experiments. According to Eq. 6.1, 16 times the tube length is required to achieve a steady state flow for emulsions with $d \approx 30\ \mu m$ compared to $d \approx 120\ \mu m$. All the heavy O/W emulsions were prepared with ethoxylated nonionic surfactants. Contrary to other results reported in the literature, Wyslouzil et al. (1987) showed experimental results that heavy O/W emulsions with $d \approx 5 - 10\ \mu m$ prepared

with NaOH, unlike ethoxylated nonionic surfactants, showed evidence of droplet migration in a tube viscometer.

Concentrated heavy O/W emulsions with large droplets ($d \approx 120\ \mu m$) are not stable and thus not suitable for pipeline transportation where fluid residence times can be days if not weeks. On the other hand, literature suggests that heavy O/W emulsions with small droplets ($d \approx 30\ \mu m$) do not show evidence of droplet migration in tubes, with no benefit in viscosity reduction observed from the droplet migration away from the tube wall.

Since the heavy O/W emulsions prepared in this study formed large oil droplet aggregates with aggregate sizes much larger than individual mean droplet diameters, heavy oil droplets may migrate toward the center of the tube in tube viscometers.

6.3 THEORY AND CALCULATIONS

Shear stress vs. shear rate of non-Newtonian fluids in a pipe

Capillary tube viscometers work on the principle of a pressure-driven flow. Pressure gradient vs. mean flow velocity (∇P vs. v) are the measured data that are used to calculate $\tau\ vs.\dot{\gamma}$ and $\mu\ vs.\dot{\gamma}$ relationships of the sample fluid. The equations [Chhabra and Richardson (2011)] used to calculate the $\dot{\gamma}$ and μ of the emulsions samples are defined below. The shear rate at the wall $\dot{\gamma}_w$ of a circular conduit can be derived for fluids exhibiting Newtonian behavior:

$$\dot{\gamma}_w = \frac{8v}{D} \tag{6.2}$$

where v is the mean velocity in a tube and D the tube diameter. For non-Newtonian fluids, a modification of Eq. 6.2, the Rabinowitsch-Mooney equation, can be used to quantify the $\dot{\gamma}_w$ of fluid flow in circular conduits:

$$\dot{\gamma}_w = \left(\frac{8v}{D}\right)\left(\frac{3n'+1}{4n'}\right) \tag{6.3}$$

where n' is the apparent flow behavior index. The assumptions below are made to derive Equations 6.2-3:

- Steady state laminar flow.
- Time independent fluid properties.
- No wall slippage.
- Incompressible fluid
- Negligible end effects because of large L/D

The shear stress experienced at the tube wall can be expressed as a function of the pressure gradient:

$$\tau_w = \frac{D\Delta P}{4L} \tag{6.4}$$

The tube flow parameters, apparent flow consistency index (k'), and apparent flow behavior index (n') of fluid samples can be determined from experimentally measured data of ΔP vs. v. The n' value for each data point is calculated by finding the derivative of $\ln(\tau_w)$ vs. $\ln(\dot{\gamma})$:

$$n' = \frac{d\ ln(\tau_w)}{d\ ln(\dot{\gamma})} = \frac{d\ ln(D\Delta P/4L)}{d\ ln\left(\frac{8v}{D}\right)} \tag{6.5}$$

The tube flow parameters, n and k, and yield stress of the fluid τ_w can be estimated for a range of $\dot{\gamma}_w$ by fitting the measured data of $\tau_w\ vs.\ \dot{\gamma}_w$ to the Herschel-Bulkley equation below:

$$\tau_w = \tau_y + k\dot{\gamma}_w{}^n \tag{6.6}$$

The viscosity at the tube wall is calculated using the following relationship, $\mu_w = \tau_w/\dot{\gamma}_w$.

$$\mu_w = \frac{\tau_y}{\dot{\gamma}_w} + \mathrm{k}\dot{\gamma}_w{}^{\mathrm{n}-1} \tag{6.7}$$

Wall slip correction in tube viscometers

The traditional method of characterizing wall slip with tube viscometers is to measure the rheological properties of emulsions using tubes of varying radius. The

Mooney (1931) method is used to analyze the presence and quantity of wall slip in tube viscometers. Mooney used the following expressions to characterize fluid flow with wall slip:

$$Q = Q_s + Q_{ns}, \text{ at constant } \tau_w \quad (6.8)$$

$$\frac{8v}{D} = \frac{8v_s}{D} + \frac{8v_{ns}}{D}, \text{ at constant } \tau_w \quad (6.9)$$

where Q_s is the volumetric flow rate contribution due to wall slip, Q_{ns} the volumetric flow rate contribution due to bulk fluid flow, v_s the mean velocity contribution due to wall slip, and v_{ns} the mean velocity contribution due to bulk fluid flow. The second term on the right hand side of Eq. 6.9 is constant for all D at a constant τ_w. Thus, the v_s at a constant τ_w can be calculated from the slope of $8v/D$ vs. 1/D using measured data from tube viscometers of various radii. Evaluating the v_s for a range of τ_w, the $v_s\ vs.\ \tau_w$ relationship can be measured. Wall slip corrected $\dot{\gamma}_w$ is defined as:

$$\dot{\gamma}_w = 8\left(\frac{v-v_s}{D}\right)\left(\frac{3n'+1}{4n'}\right) \quad (6.10)$$

$$n' = \frac{d\ ln(\tau_w)}{d\ ln\left(\frac{8(v-v_s)}{D}\right)} \quad (6.11)$$

The $\dot{\gamma}_w$ and μ_w of emulsions with no wall slip correction is termed the apparent shear rate at the wall $\dot{\gamma}_{w,app}$ and apparent viscosity at the wall $\mu_{w,app}$.

Alternatively, the $v_s\ vs.\ \tau_w$ relationship can be measured for heavy O/W emulsions using the method outline in Chapter 5 with smooth and rough parallel plates. The $v_s\ vs.\ \tau_w$ relationship from the parallel plate measurements can be used to correct for wall slip in a tube viscometer.

Characteristic entrance length required for steady state flow in a tube

The equation derived by Nott and Brady (1994) was used to estimate the transitional tube length required to reach a steady state flow of emulsions. Eq. 6.1 was

slightly modified by using the expression $12d(\varphi) \approx 1$ mentioned by Nott and Brady (1994):

$$\frac{L}{D} \sim \frac{1}{2}\left(\frac{D}{d}\right)^2, \varphi > 0.3 \quad (6.12)$$

where D is the dimeter of the tube and d the average dimeter of the emulsion droplets. The tube dimensions required for fully developed flow for various emulsion drop diameters of emulsions are plotted below using Eq. 6.12.

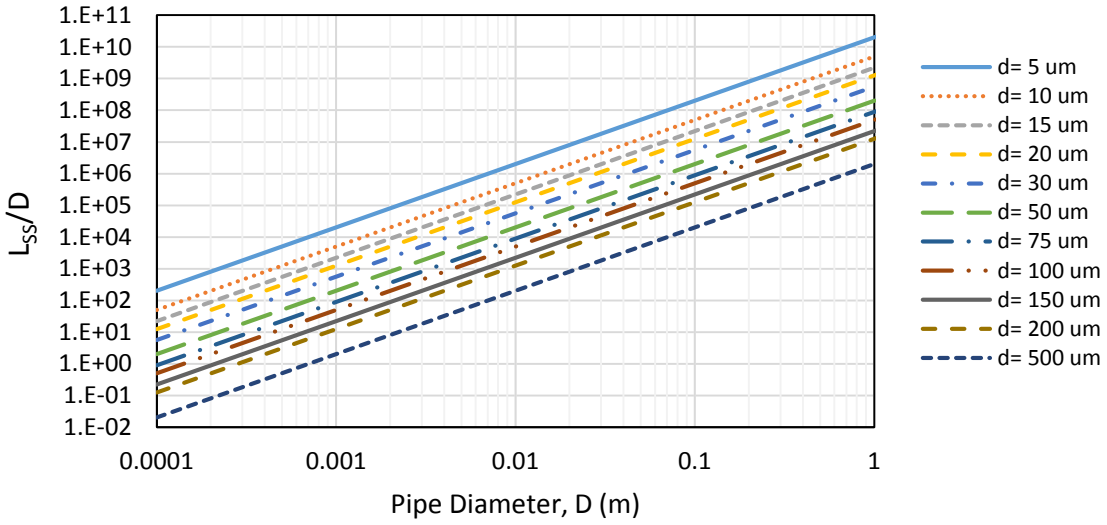

Fig. 6.3: L_{SS}/D required for suspensions to reach fully developed flow for various tube D and emulsion droplet d. Generated using Eq. 6.12.

Fig. 6.3 is used to provide a starting point for the design of tube viscometers to measure the steady state flow rheological properties of heavy O/W emulsions. The trend described by Fig. 6.3 suggested that larger L_{SS}/D values are obtained for $\uparrow D$ and $\downarrow d$. Since the heavy O/W emulsion samples prepared in this study formed aggregating structures due to the attractive interaction between the heavy oil droplets, the effective aggregate diameter is much larger than the individual droplet diameter ($d_{agg} \gg d$). This may significantly reduce the L_{SS}/D for heavy O/W emulsions depending on the d_{agg}. Fig. 6.3 also implied that for major crude oil pipelines with $D > 0.3\,m$, L_{SS} is extremely large and the flow may never reach a steady state profile. For a case of $D = 0.6\,m$ and

$d = 50\ \mu m$, a value of $L_{SS} \approx 42{,}000\ km$ is obtained from Eq. 6.12. Such large L_{SS} values are orders of magnitude longer than the length of pipelines between most pumping stations and even the length of most major pipelines.

6.4 EXPERIMENTAL SECTION

The experimental setup of tube viscometers are described in this section. The emulsion samples are prepared according to the procedure outlined in Chapter 3. The chemicals used in the emulsion formulations are also listed in Chapter 3. Two different types of tube viscometers are used for two separate experiments; (1) a single tube viscometer is used to screen various emulsion formulations and (2) a single emulsion formulation is tested with tubes of varying dimensions to quantify the effects of tube dimensions.

Tube Specifications

Stainless steel tubes (306 and 306L) and fittings were purchased from Swagelok. The dimensions of the tube viscometer used to screen emulsion formulations are listed in Table 6.1.

Table 6.1: Tube viscometer A1 dimensions

	Tube dimensions
Outer diameter (OD)	1.5875 mm
Inner diameter (ID)	0.8176 mm
Length	92.964 cm
L/ID	1137

The dimensions of the tube viscometers used to screen tube radii and lengths are listed in Table 6.2.

Table 6.2: Tube viscometer B dimensions

		Tube B1	Tube B2	Tube B3	Tube B4
Section 1	OD (mm)	1.5875	3.175	6.35	9.525
	ID (mm)	0.7035	1.419	3.141	7.036
	L (cm)	38.74	69.85	152.4	609.6
	L/ID	550	492	485	966
Section 2	OD (mm)	1.5875	3.175	6.35	
	ID (mm)	0.7071	1.417	3.163	
	L (cm)	38.74	69.85	152.4	
	L/ID	548	493	482	
Section 3	OD (mm)	1.5875	3.175	6.35	
	ID (mm)	0.7069	1.419	3.149	
	L (cm)	38.74	69.85	152.4	
	L/ID	548	492	484	
Section 4	OD (mm)	1.5875	3.175	6.35	
	ID (mm)	0.710	1.420	3.150	
	L (cm)	38.74	69.85	152.4	
	L/ID	549	493	484	
Total	OD (mm)	1.5875	3.175	6.35	9.525
	ID (mm)	0.70	1.420	3.140	7.036
	L (cm)	155	279.4	609.6	609.6
	L/ID	2200	1974	1939	966

Pressure taps are drilled into tubes to measure the effect of tube length. Drilled pressure taps eliminate possible fluid mixing that occurs when valves are used to connect separate tubes. The drilled tubes are threaded through three-way connectors to seal and connect to pressure transducers. A single straight viscometer with four sections were created with this method.

Tube Viscometer Setup

Rosemount 3051 Pressure Transmitters were connected to the inlet, outlet, and pressure taps of the tube viscometer using three way fittings to record the sectional differential pressure along the tubes. The pressure transmitters were calibrated and a range of appropriate differential pressure limits was set according to the range of emulsion flow rates. Viscosity standards (50, 100, 200, and 500 mPa*s) from NL Baroid

were injected through the tube to calibrate the tube viscometer based on differential pressure readings, flow rates, and tube dimensions. Accurate IDs of the tubes in Tables 6.1-2 are obtained from the viscosity standard calibrations. The ID of the tubes were within $\pm 5\%$ of the values reported by Swagelok.

A 500D syringe pump from Teledyne Isco was used to displace emulsion samples in a glass column through the tube viscometer at constant flow rates. Light mineral oil is used to displace the emulsion sample in the glass column. Mineral oil is inject through the top of the column because of its lighter density compared to the emulsions. The tube viscometer is filled with 0.1% NaCl water before the emulsion enters the viscometer. The steady state pressure drops are recorded for a range of flow rates. Flow rates are tested to make sure there are no leaks in the setup. Pressure drops are measured from the highest to the lowest flow rates (downward sweep of flow rates). Only steady state pressure drops are recorded. All emulsion samples are measured at a standard condition of $23℃ \pm 2$. Fig. 6.4 shows an illustration of the tube viscometer setup.

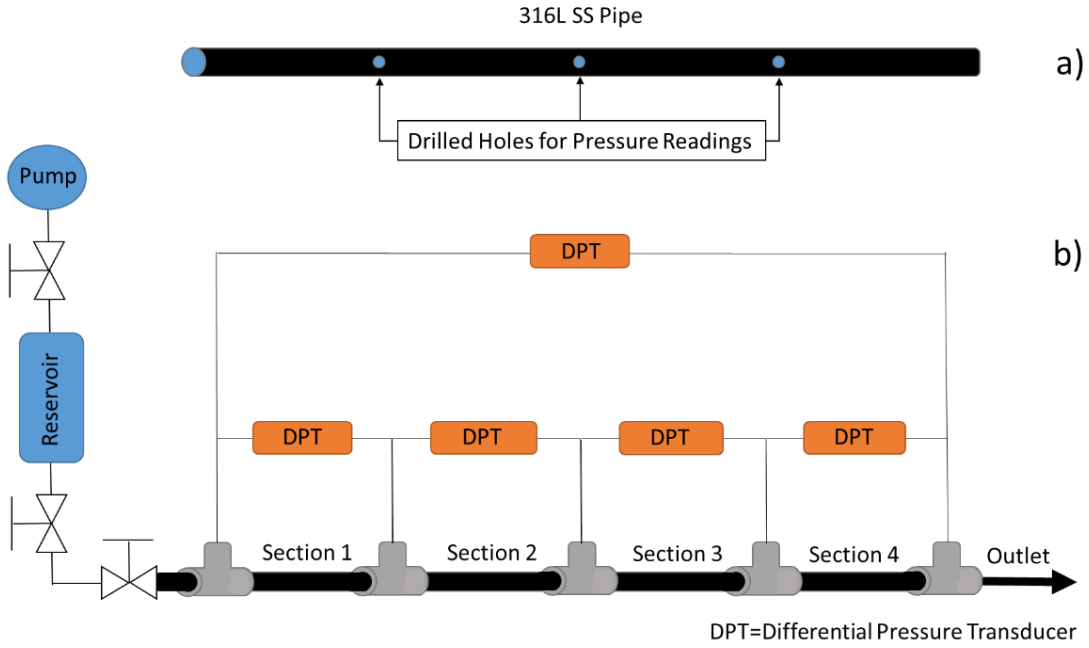

Fig. 6.4: Illustration of the tube viscometer setup. a) A 306L SS tube of a certain length has 3 small holes drilled into for pressure readings. b) The tube is threaded into three-way connectors and connected to differential pressure transducers to record the pressure gradient for four tube sections.

Tube Viscometer Cleanup Procedure

After an emulsion sample is tested, the tube viscometer and pressure lines are cleaned thoroughly using the following procedure.

1. Flush out the emulsion from the tube and pressure lines with 0.1% NaCl brine.
2. Clean out any residual crude oil present in the tube with toluene/hexane mixture.
3. Displace all the toluene/hexane in the tube and pressure lines with 0.1% NaCl brine.

6.5 Results and Discussions

The results section is divided into two sections: 1) the effect of tube dimensions and 2) the effect of emulsion formulation on the heavy O/W emulsion viscosity in Poiseuille flow.

6.5.1 Effect of Pipe Viscometer Dimensions

The four tube viscometers in Table 6.2 were setup according to the illustration in Fig. 6.4. The viscosity standard ($\mu \approx 48.5\ cP\ at\ 21$ ℃) calibration plots for the four tube viscometers in Table 6.2 are shown in Appendix (Table A6). The ΔP vs. v relationship with the calibration liquid is also used to verify the accuracy of the pressure transducers at low ΔP and v.

The heavy O/W emulsion tested has the following composition and properties.

Table 6.3: Emulsion B80: Droplet size, rheological, and wall slip properties are listed. The rheological and wall slip properties were measured using parallel plates with h=1mm at 22℃.

Emulsion Properties		Rheological Model		Wall Slip Model	
Oil Conc. (vol%)	80% Oil B	n_1	0.5	τ_{y1} **(Pa)**	0.02
Aqueous Conc. (vol %)	20%	k_1	3.16	τ_{y2E} **(Pa)**	5.25
Aqueous Composition (wt. %)	1.6% ph15EO 0.2% NaOH 0.8% NaCl	τ_{y1} **(Pa)**	0.02	τ_{y2S} **(Pa)**	2.1
		n_2	0.95	τ_{sy} **(Pa)**	0
		k_2	1.35	V_{y1} **(μm/s)**	0.25
d_{43} **(μm)**	26.7	τ_{y2} **(Pa)**	5.25	V_{y2} **(μm/s)**	1375
d_{32} **(μm)**	18.5	γ_y **(s^{-1})**	0.84	**E**	2
φ_m	0.79				

Fig. 6.5 shows the parallel plate viscosity measurements of the 80% oil B emulsion.

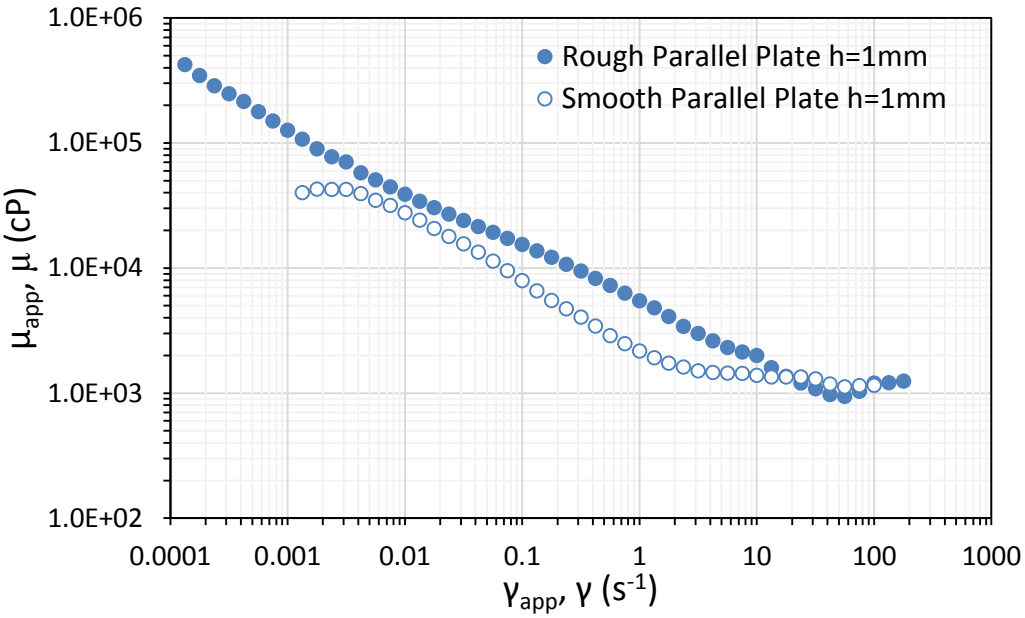

Fig. 6.5: Measured μ and $\dot{\gamma}$ (rough parallel plate) and μ_{app} and $\dot{\gamma}_{app}$ (smooth parallel plate) for 80% oil B emulsion at 22.5 ℃ $\pm$ 0.5. The subscript app indicates the presence of wall slip contributing to flow.

The 80% oil B emulsion showed the typical two-step yielding behavior observed in Chapter 5 for concentrated heavy O/W emulsions. Significant wall slip is observed at $0.003\ s^{-1} > \dot{\gamma}, \dot{\gamma}_{app}$ and $0.1\ s^{-1} < \dot{\gamma}, \dot{\gamma}_{app} < 10\ s^{-1}$. Shear thinning behavior is observed for $20\ s^{-1} > \dot{\gamma}$ and Newtonian behavior for $20\ s^{-1} < \dot{\gamma}$ with $\mu \approx 1{,}000\ cP$.

The viscosities of the same 80% oil B emulsion is measured with Tube B1-4. The measured ΔP vs. v data is presented in Appendix (A7). Fig. 6.6 shows the $\mu_{w,app}$ vs. $\dot{\gamma}_{w,app}$ calculated from the measured ΔP vs. v data for each tube viscometer and their sections. The subscript app indicates the presence of wall slip contributing to flow.

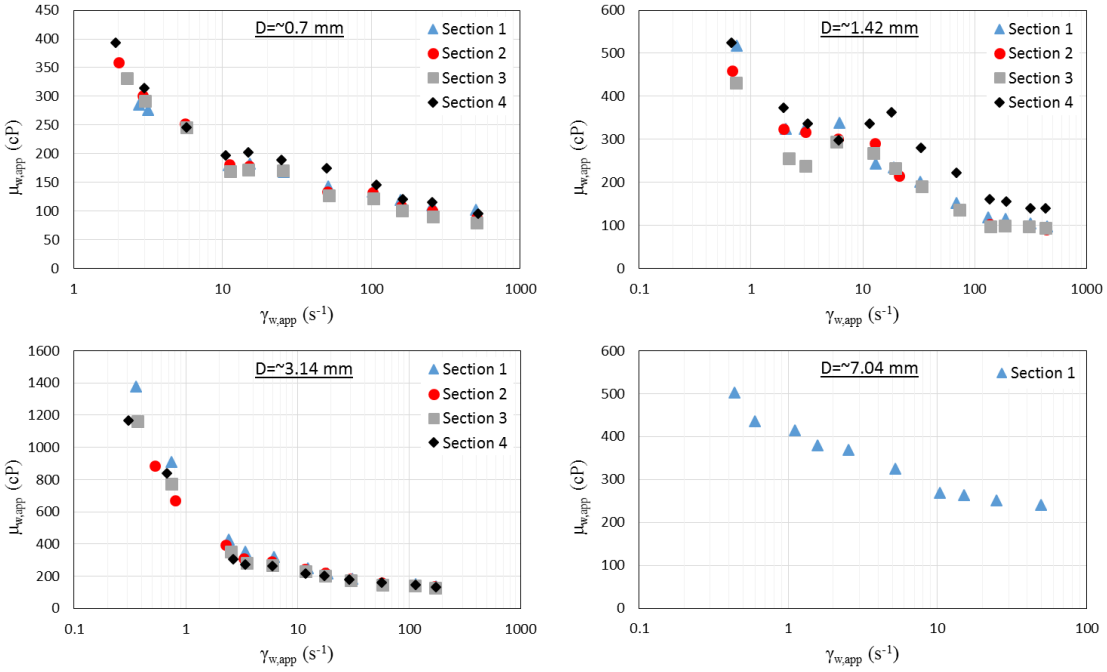

Fig. 6.6: The effect of tube viscometer length on the $\mu_{w,app}$ vs. $\dot{\gamma}_{w,app}$ relationship of 80% oil B emulsion for tubes of four different diameters. Wall slip elimination was not implemented. Measured at 23 °C $\pm$ 2.

The L/D ratio appeared to have no significant effect on the emulsion viscosity for tubes B1-B3 in increments of $L/D \approx 500$. The exception is tube B2 section 4 that showed ~50% higher viscosity at high $\dot{\gamma}_{w,app}$ than the other three sections. This is most likely an experimental error and not a property of the emulsion flow since the other two tubes showed no similar behavior. With Eq. 6.12 and $d = 20\,\mu m$, the expected L_{SS}/D values for tubes B1-4 are calculated to be ~600, ~2600, ~12,000, and ~60,000 respectively. However, the data in Fig. 6.5 indicated $L_{SS}/D \ll 500$ for tubes B1-3 and $L_{SS}/D \ll 1{,}000$ for tube B4. Attractive heavy O/W emulsions showed L_{SS}/D values that are orders of magnitude lower than what Eq. 6.12 predicted. The heavy oil droplet aggregates with $d_{agg} \gg d$ may be the reason for lower than predicted L_{SS}/D. The results imply that steady state flow profiles of heavy O/W emulsions may be achieved in major pipelines with reasonable pipe length, unlike what Eq. 6.12 predicted.

The results in Fig. 6.6 for the sections of tubes B1-4 are averaged and plotted in Fig. 6.7.

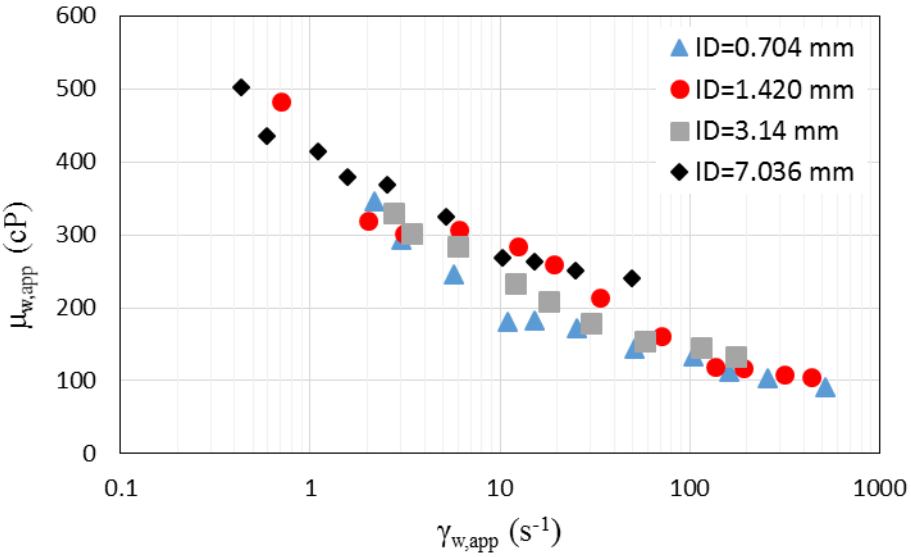

Fig. 6.7: The effect of tube viscometer diameter on the $\mu_{w,app}$ vs. $\dot{\gamma}_{w,app}$ relationship of 80% oil B emulsion. The $\mu_{w,app}$ vs. $\dot{\gamma}_{w,app}$ data were calculated based on the total length of the tube viscometers B1-4. Wall slip elimination was not implemented. Measured at 23 ℃ $\pm$ 2.

Fig. 6.7 showed up to 10-fold lower viscosities compared to the rough parallel plate measurements in Fig. 6.5. Two questions that must be answered are:

1. Is the lower viscosity measured in tube viscometers only due to wall slip or is there a contribution due to droplet migration away from the tube wall?
2. Can the wall slip velocity measurements from the parallel plate viscometers be used to correct for wall slip in tube viscometers?

The Mooney (1931) method of wall slip correction was used to analyze wall slip velocity for the 80% oil B emulsion in Fig. 6.6. Figs. 6.8-6.9 show results of the wall slip velocity analysis. The wall slip measurements from the parallel plate method is also plotted in Fig. 6.9. The mean velocity at specific τ_w values in Fig. 6.8 were calculated with the linear interpolation method between two adjacent measured data points.

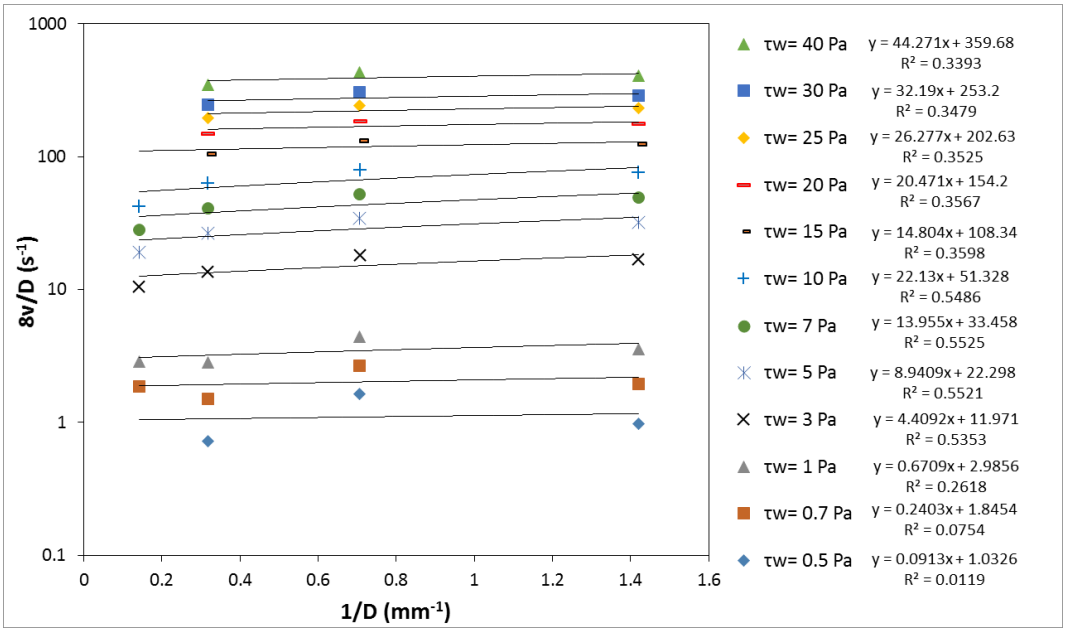

Fig. 6.8: The $8v/D\ vs.\ 1/D$ relationship based on Eq. 6.9 for the 80% oil B emulsion data in Fig. 6.7. The slopes of the linear fit lines represent $8v_s$.

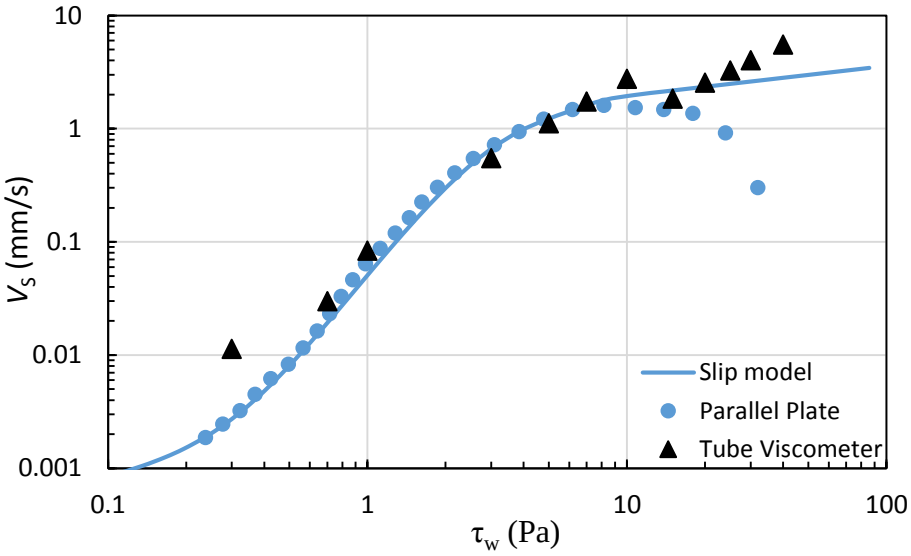

Fig. 6.9: The $v_S\ vs.\ \tau_w$ relationship plotted for the 80% oil B emulsion in Table 6.3. Blue circles are the measured slip data from rough and smooth parallel plates. Black triangles are the wall slip data extracted using the Mooney method from tube viscometer data in Fig. 6.8. The blue line is the wall slip model derived in Chapter 5.

In Fig. 6.9, $v_S\ vs.\tau_w$ measured with tube viscometers and with parallel plates (rough and smooth) showed a very good agreement and similar trends. This suggests that the $v_S\ vs.\tau_w$ relationship measured with parallel plates can be used to eliminate the wall slip effect of heavy O/W emulsions present in the tube viscometer data. A significant amount of time can be saved because characterization of slip behavior requires a fraction of the time with parallel plates compared to tube viscometers. Also, with parallel plates, accurate characterization of wall slip behavior is possible at very low shear rates and stresses whereas tube viscometers cannot be used because of unmeasurably low pressure drops. The $v_S/v\ vs.\tau_w$ relationship is plotted:

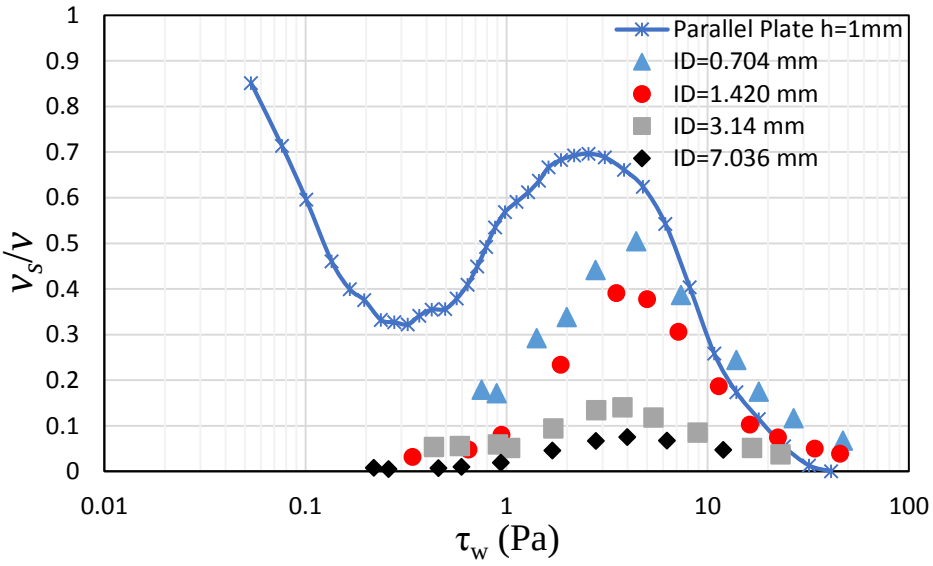

Fig. 6.10: The $v_S/v\ vs.\tau_w$ relationship for the tube viscometer and parallel plate measurements.

Fig. 6.10 showed the expected trend for $v_S/v\ vs.\tau_w$ with tube viscometers. Higher the diameter of the tubes, the less wall slip contributed to the flow of 80% oil B emulsion in tubes. The flow induced yield stress, τ_{y2}, for the emulsion is also present when measured with tube viscometers, according to the emergence of wall slip for $0.5 < \tau_w < 40\ Pa$.

Tube viscometers could not be used to accurately measure pressure drops at very low flow rates to observe wall slip at τ_w near $\tau_{y1} = 0.02\ Pa$. The contribution of wall slip to flow for tube viscometers and parallel plates showed qualitative agreements. However, the magnitude of wall slip contribution to emulsion flow between the two measurement geometries showed inconsistency when factoring in the dimension of the flow conduit. Parallel plate wall slip measurements with $h = 1mm$ should fall in between the tube viscometer measurements with $ID = 0.704mm$ and $ID = 1.42mm$. But, the tube viscometer measurements showed significantly lower v_S/v values compared to the parallel plate measurements, suggesting the bulk emulsion flow velocity in tube viscometers are significantly higher than what was predicted with the parallel plate rheological measurements.

Wall slip velocities, measured with the tube viscometers and parallel plates, are subtracted from the data in Fig. 6.7 to estimate the bulk emulsion rheological properties with no wall slip.

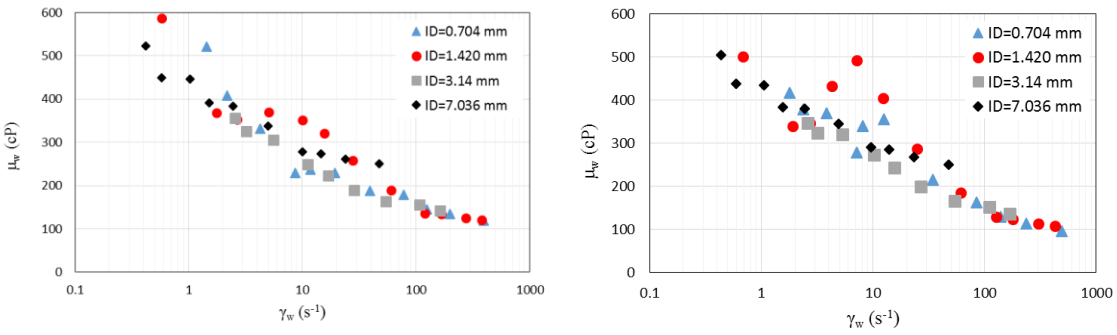

Fig. 6.11: The effect of tube viscometer diameter on the μ_w vs. $\dot{\gamma}_w$ relationship of 80% oil B emulsion. The μ_w vs. $\dot{\gamma}_w$ data were calculated based on the total length of the pipe viscometers. Wall slip velocities were subtracted from the flow rates to show no-slip bulk fluid rheological properties. Left: Mooney wall slip correction method. Right: Parallel plate wall slip correction method proposed in Chapter 5.

The μ_w vs. $\dot{\gamma}_w$ relationship with the Mooney wall slip correction method and parallel plate correction method showed comparable results. However, the parallel plate wall slip correction method resulted in a slightly more scatter for the tube with ID=1.42 mm around $\dot{\gamma}_w = 5 - 10\ s^{-1}$. For $20\ s^{-1} > \dot{\gamma}_w$, the no-slip viscosities showed up to 50% higher values compared to with-slip viscosities within the range of $\dot{\gamma}_w$ tested. For $20\ s^{-1} < \dot{\gamma}_w$, the contribution of wall slip to flow is negligible and both the slip and no slip viscosities were very similar. The wall slip resulted in lower $\mu_{w,app}$, especially for the tube viscometer with the smallest dimeters (ID=0.704, 1.42 mm).

Fig. 6.12 compares the no-slip, μ_w vs. $\dot{\gamma}_w$ parallel plate measurements to the no-slip tube viscometer measurements of the 80% oil B emulsion.

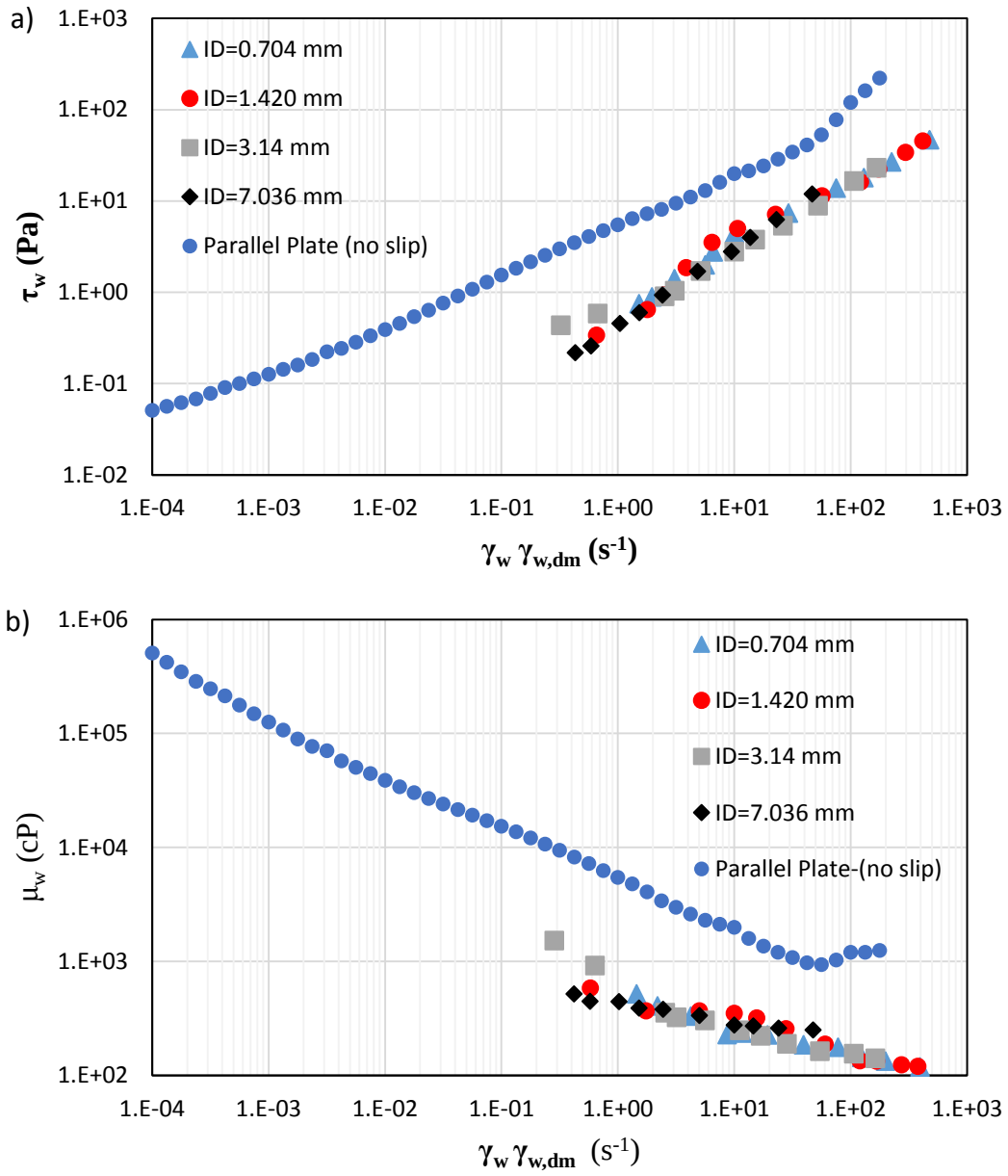

Fig. 6.12: The effect of flow types, drag flow (parallel plates) and pressure-driven flow (tubes), on the a) τ_w vs. $\dot{\gamma}_w, \dot{\gamma}_{w,dm}$ and b) μ_w vs. $\dot{\gamma}_w\, \dot{\gamma}_{w,dm}$ relationship of 80% oil B emulsion. $\dot{\gamma}_{w,dm}$ represents the wall shear rate with droplet migration in tube viscometers. Wall slip has been eliminated from both the parallel plate and tube viscometer measurements. Measured at 23 ℃ $\pm$ 2.

Even with wall slip eliminated, the μ_w vs. $\dot{\gamma}_w$ comparison in Fig. 6.12 between the two flow geometries showed a tremendous difference, with the tube viscometer data showing up to a 10-fold lower μ_w for $0.3 < \dot{\gamma}_w < 200\ s^{-1}$. The significant variation in the μ_w vs. $\dot{\gamma}_w$ relationship between the parallel plate and tube viscometer measurements was attributed to the migration of heavy oil droplets away from the tube wall caused by the inhomogeneous shear/stress field. The 80% oil B emulsion μ_w vs. $\dot{\gamma}_w$ data measured with tube viscometer is similar to the no-slip parallel plate measurements of ~70% oil B emulsion. Since the viscosity of the emulsion near the tube wall contributes ($r/R > 0.9$) the most to the emulsion flow rate, the $\varphi(r/R)$ profile in the tube viscometers for 80% oil B emulsion can be qualitatively estimated to be $\varphi \approx 0.7$ for $r/R > 0.9$ and $\varphi > 0.8$ for $r/R < 0.25$. Also, the magnitude of droplet migration did not change as the tube diameter increased ($D = 0.7 \rightarrow 7\ mm$), suggesting that droplet migration is not a function of pipe diameter.

The following equation was used to shift the $\dot{\gamma}_w$ of tube viscometer measurements with droplet migration to match that of the parallel plate measurements.

$$\dot{\gamma}/\dot{\gamma}_{w,dm} = a\sqrt{\tau_w/\rho} \tag{6.13}$$

where $\dot{\gamma}_{w,dm}$ is the wall shear rate with droplet migration, ρ the density of the emulsion, and a a fitting parameter with units of s/m. $a = 0.4$ for the 80% oil B emulsion in Fig. 6.12. The term $\sqrt{\tau_w/\rho}$ is the shear velocity, also called friction velocity, at the wall. Shear velocity is used to describe shear-related motion in moving fluids such as sediment transport in turbulent flows [Hsu et al. (2007); Le Hir et al. (2007)]. Fig. 6.13 showed the agreement between the parallel plate and tube viscometer measurements of τ_w vs. $\dot{\gamma}_w$ when Eq. 6.13 was used to correct for droplet migration in tube viscometers.

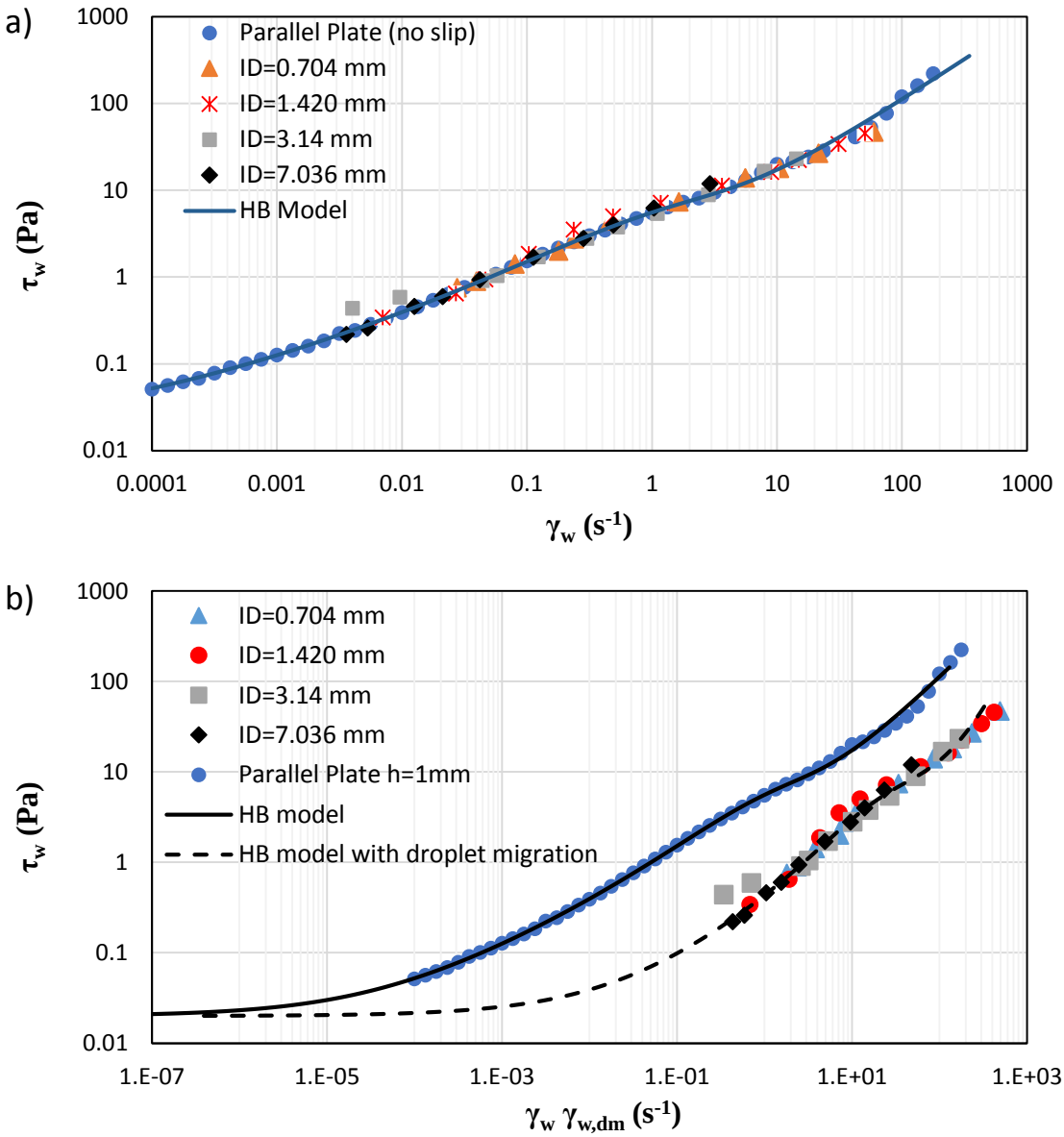

Fig. 6.13: τ_w vs. $\dot{\gamma}_w, \dot{\gamma}_{w,dm}$ measured with parallel plates and tube viscometers. $\dot{\gamma}_{w,dm}$ represents the wall shear rate with droplet migration in tube viscometers. Wall slip was eliminated. Eq. 6.13 was used to a) eliminate droplet migration from the tube viscometer measurements and b) include the effect of droplet migration to the HB model of the parallel plate measurements with $a = 0.4$.

Similar to the experiments by Wyslouzil et al. (1987), the 80% oil B emulsion showed evidence of droplet migration with small mean droplet size ($d < 30\ \mu m$). This is in contrast to the studies of Sumner et al. (1998) and Gillies and Shook (1992) that

showed that heavy oil droplets with smaller droplet diameters ($d \approx 30\ \mu m$) showed no evidence of droplet migration while with large droplet diameter ($d \approx 120\ \mu m$) showed evidence of droplet migration. Since the emulsion droplets in our study are attractive in nature and form aggregate structures with $d_{agg} \gg d$, the necessity of large mean droplet diameter for droplet migration appears to be satisfied with large droplet aggregates while still possessing the emulsion stability afforded by smaller mean droplet size.

6.5.2 Effect of Emulsion Formulation on Droplet Migration

The effect of chemical formulation on the rheological properties of heavy O/W emulsions measured with tube viscometers are presented and discussed in this section. First, the effect of oil type and oil concentration on the droplet migration in laminar tube flow is investigated. Fig. 6.14 shows the rheological properties of 80% oil A emulsion (Table 6.4) measured with parallel plates and tube viscometer. Rough parallel plate geometry was used to eliminate wall slip and the wall slip behavior characterized with the parallel plate geometry was used to eliminate wall slip in the tube viscometer.

Table 6.4: Emulsion A80: Droplet size, rheological, and wall slip properties are listed. The rheological and wall slip properties were measured using parallel plates with h=1mm at 22℃.

Emulsion Properties		Rheological Model		Wall Slip Model	
Oil Conc. (vol%)	80% Oil A	n_1	0.5	τ_{y1} (Pa)	0.3
Aqueous Conc. (vol %)	20%	k_1	7.56	τ_{y2E} (Pa)	4
Aqueous Composition (wt. %)	1.6% ph15EO 0.2% NaOH 0.8% NaCl	τ_{y1} (Pa)	0	τ_{y2S} (Pa)	1.6
		n_2	0.76	τ_{sy} (Pa)	0
		k_2	3.2	V_{y1} (µm/s)	0.005
d_{43} (µm)	21.3	τ_{y2} (Pa)	4	V_{y2} (µm/s)	1000
d_{32} (µm)	14.6	γ_y (s^{-1})	0.106	E	6
φ_m	0.76				

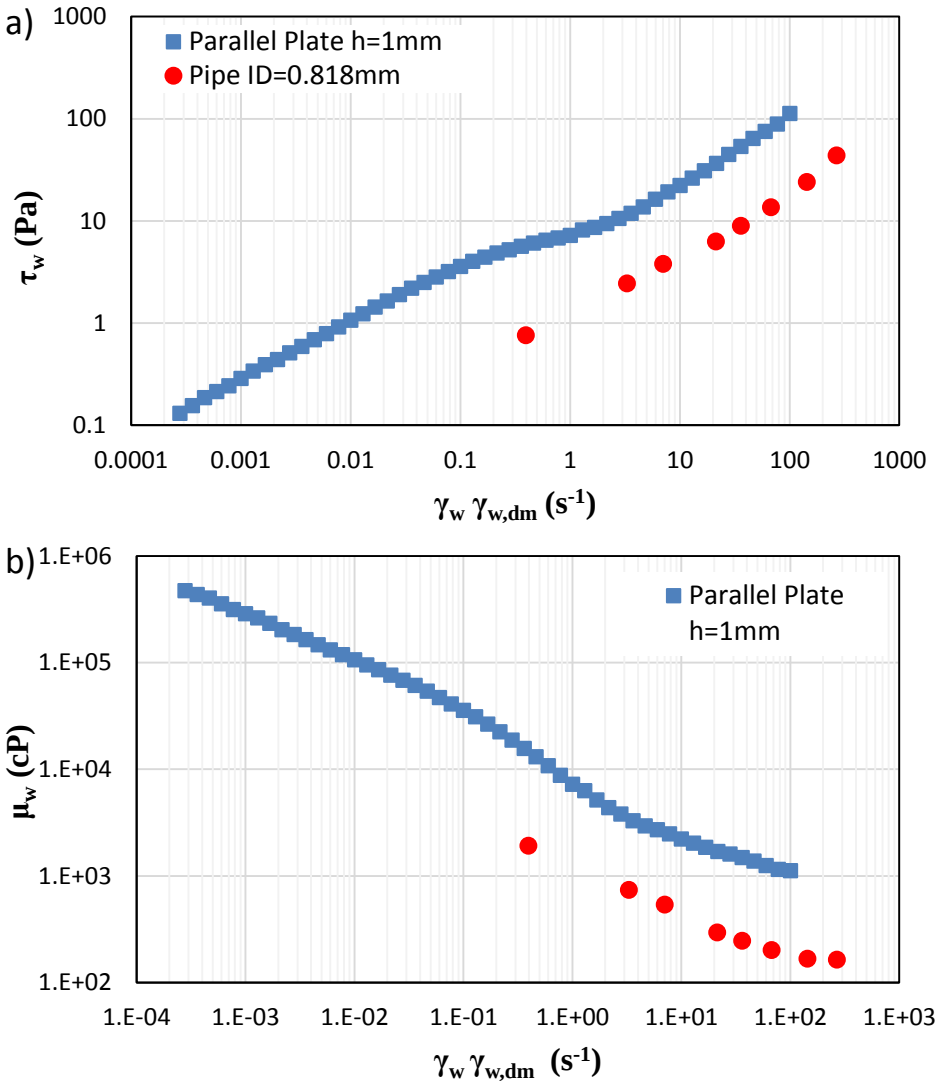

Fig. 6.14: The effect of flow types, drag-driven (parallel plates) and pressure-driven (tube), on the a) τ_w vs. $\dot{\gamma}_w, \dot{\gamma}_{w,dm}$ and b) μ_w vs. $\dot{\gamma}_{w,dm}$ relationship of 80% oil A emulsion (Table 6.4). $\dot{\gamma}_{w,dm}$ represents the wall shear rate with droplet migration in tube viscometers. Wall slip has been eliminated from both the parallel plate and tube viscometer measurements. Measured at 23 °C $\pm$ 2 with A1 tube viscometer.

The results from Fig. 6.14 are very similar to the 80% oil B emulsion behavior seen in Fig. 6.12 with up to a 10-fold decreased in the viscosity observed with the tube viscometer measurements compared to the parallel plate measurements. Droplet migration was eliminated in the tube viscometer data with Eq. 6.13

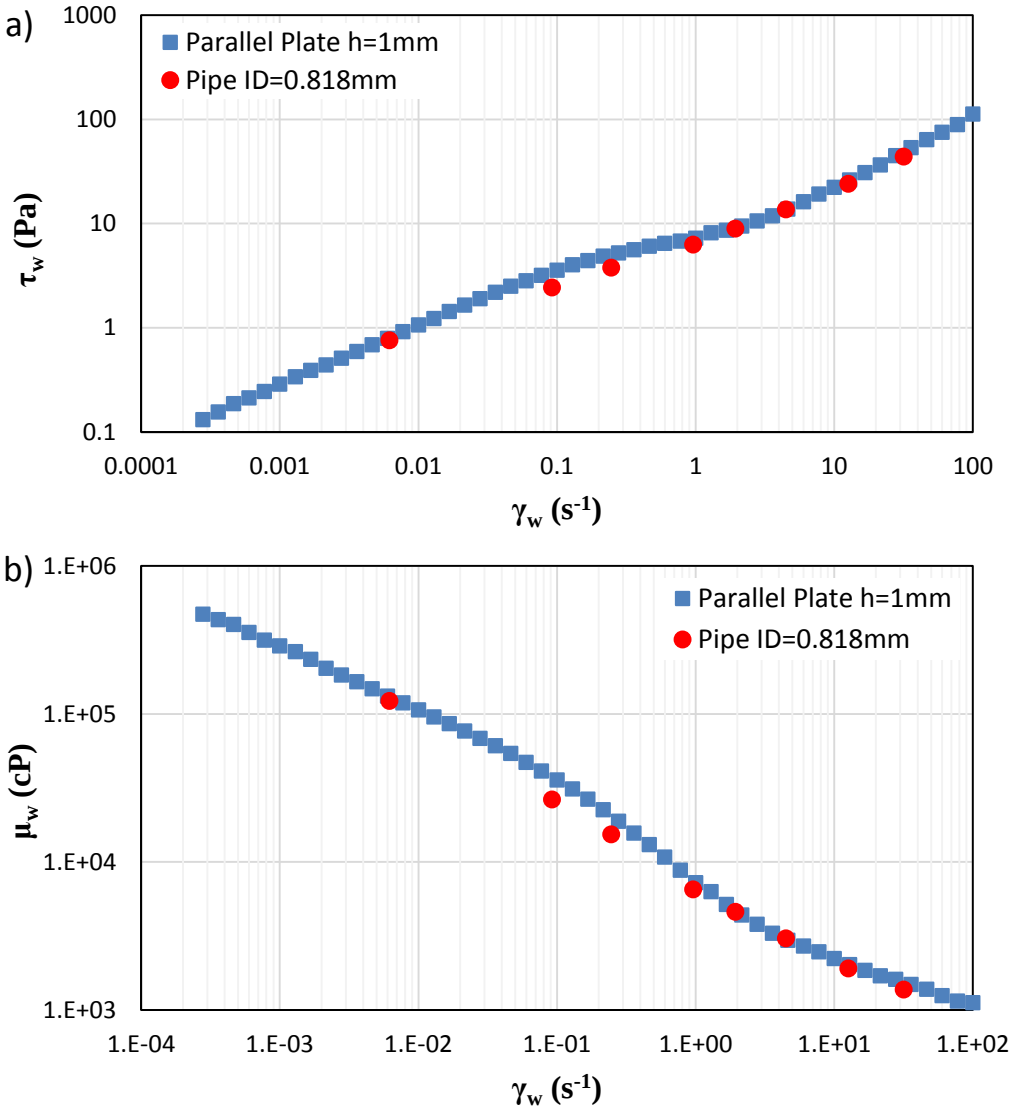

Fig. 6.15: The effect of flow types, drag-driven (parallel plates) and pressure-driven (tube), on the a) τ_w vs. $\dot{\gamma}_w$ and b) μ_w vs. $\dot{\gamma}_w$ relationship of 80% oil A emulsion (1.6% ph15EO, 0.2% NaOH, 0.8% NaCl). Eq. 6.13 was used to correct for droplet migration with $a = 0.4$. Wall slip has been eliminated from both the parallel plate and pipe measurements. Measured at 23 ℃ $\pm$ 2 with A1 tube viscometer.

The effect of oil concentration on droplet migration in tube viscometers was investigated with oil D emulsions (Table 6.5) in Fig. 6.16. Droplet migration eliminated data is shown in Fig. 6.17.

Table 6.5: Emulsion D40, D60, and D80: Droplet size, rheological, and wall slip properties are listed. The rheological and wall slip properties were measured using parallel plates with h=1mm at 22℃.

Emulsion Properties		Rheological Model		Wall Slip Model	
Oil Conc. (vol%)	40% Oil D	n_1	0.5	τ_{y1} **(Pa)**	
Aqueous Conc. (vol %)	20%	k_1	0.0075	τ_{y2E} **(Pa)**	
Aqueous Composition (wt. %)	1.6% ph15EO 0.2% NaOH 1% NaCl	τ_{y1} **(Pa)**	0	τ_{y2S} **(Pa)**	
		n_2	0.827	τ_{sy} **(Pa)**	
		k_2	0.0114	V_{y1} **(μm/s)**	
d_{43} **(μm)**	2.87	τ_{y2} **(Pa)**	0.06	V_{y2} **(μm/s)**	
d_{32} **(μm)**	1.89	γ_y **(s^{-1})**	16.9	**E**	
φ_m	0.83				
Oil Conc. (vol%)	60% Oil D	n_1	0.5	τ_{y1} **(Pa)**	0.01
Aqueous Conc. (vol %)	20%	k_1	0.113	τ_{y2E} **(Pa)**	0.3
Aqueous Composition (wt. %)	1.6% ph15EO 0.2% NaOH 1% NaCl	τ_{y1} **(Pa)**	0.01	τ_{y2S} **(Pa)**	0.12
		n_2	1	τ_{sy} **(Pa)**	0.002
		k_2	0.05	V_{y1} **(μm/s)**	1
d_{43} **(μm)**	13.6	τ_{y2} **(Pa)**	0.113	V_{y2} **(μm/s)**	1500
d_{32} **(μm)**	9.2	γ_y **(s^{-1})**	0.09	**E**	6
φ_m	0.81				
Oil Conc. (vol%)	80% Oil D	n_1	0.5	τ_{y1} **(Pa)**	0.07
Aqueous Conc. (vol %)	20%	k_1	1.39	τ_{y2E} **(Pa)**	3
Aqueous Composition (wt. %)	1.6% ph15EO 0.2% NaOH 1% NaCl	τ_{y1} **(Pa)**	0.07	τ_{y2S} **(Pa)**	1.2
		n_2	0.835	τ_{sy} **(Pa)**	0
		k_2	1.43	V_{y1} **(μm/s)**	0.65
d_{43} **(μm)**	19.8	τ_{y2} **(Pa)**	3	V_{y2} **(μm/s)**	550
d_{32} **(μm)**	14.1	γ_y **(s^{-1})**	0.62	**E**	6
φ_m	0.76				

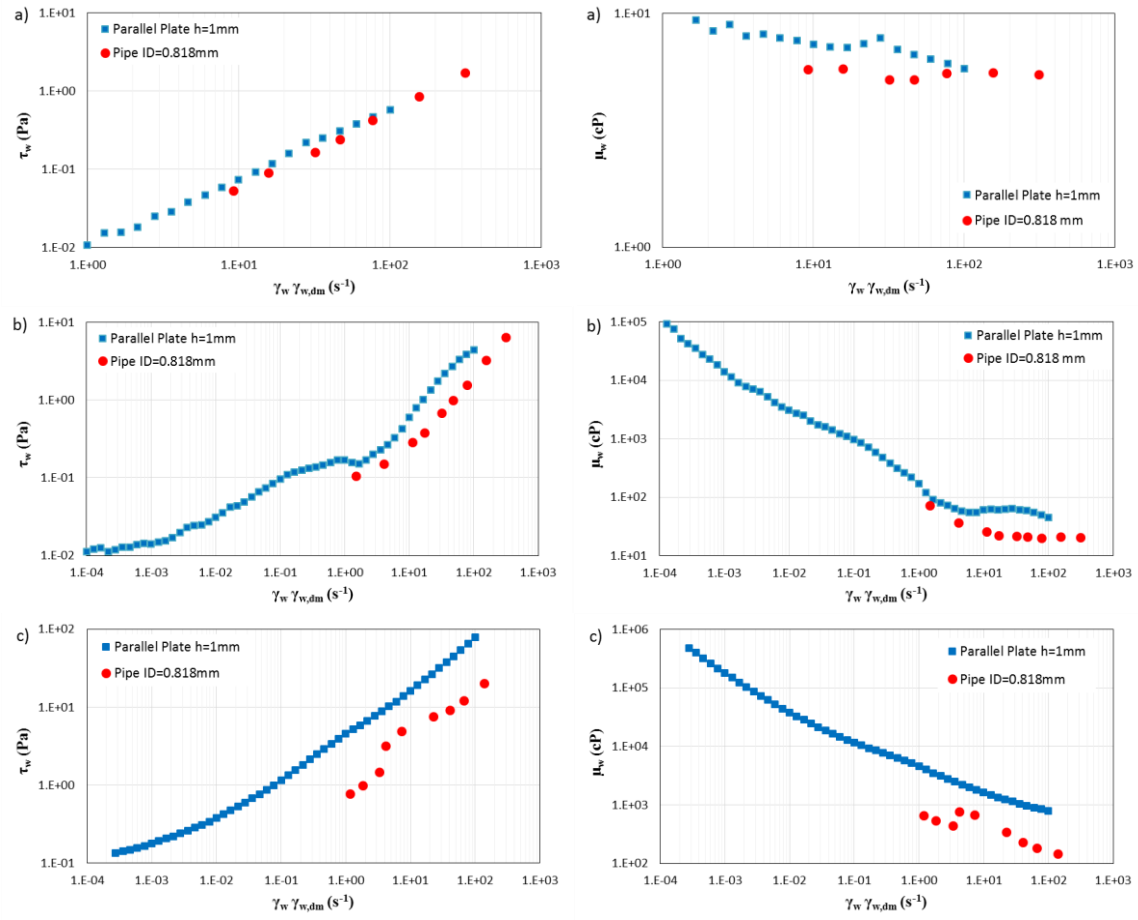

Fig. 6.16: The effect of flow types, drag-driven (parallel plates) and pressure-driven (tubes), on the τ_w vs. $\dot{\gamma}_w, \dot{\gamma}_{w,dm}$ (left column) and μ_w vs. $\dot{\gamma}_w, \dot{\gamma}_{w,dm}$ (right column) relationships of a) 40%, b) 60%, and c) 80% oil D emulsion (Table 6.5). $\dot{\gamma}_{w,dm}$ represents the wall shear rate with droplet migration in tube viscometers. Wall slip has been eliminated from both the parallel plate and tube viscometer measurements. Measured at 23 °C $\pm$ 2 with A1 tube viscometer.

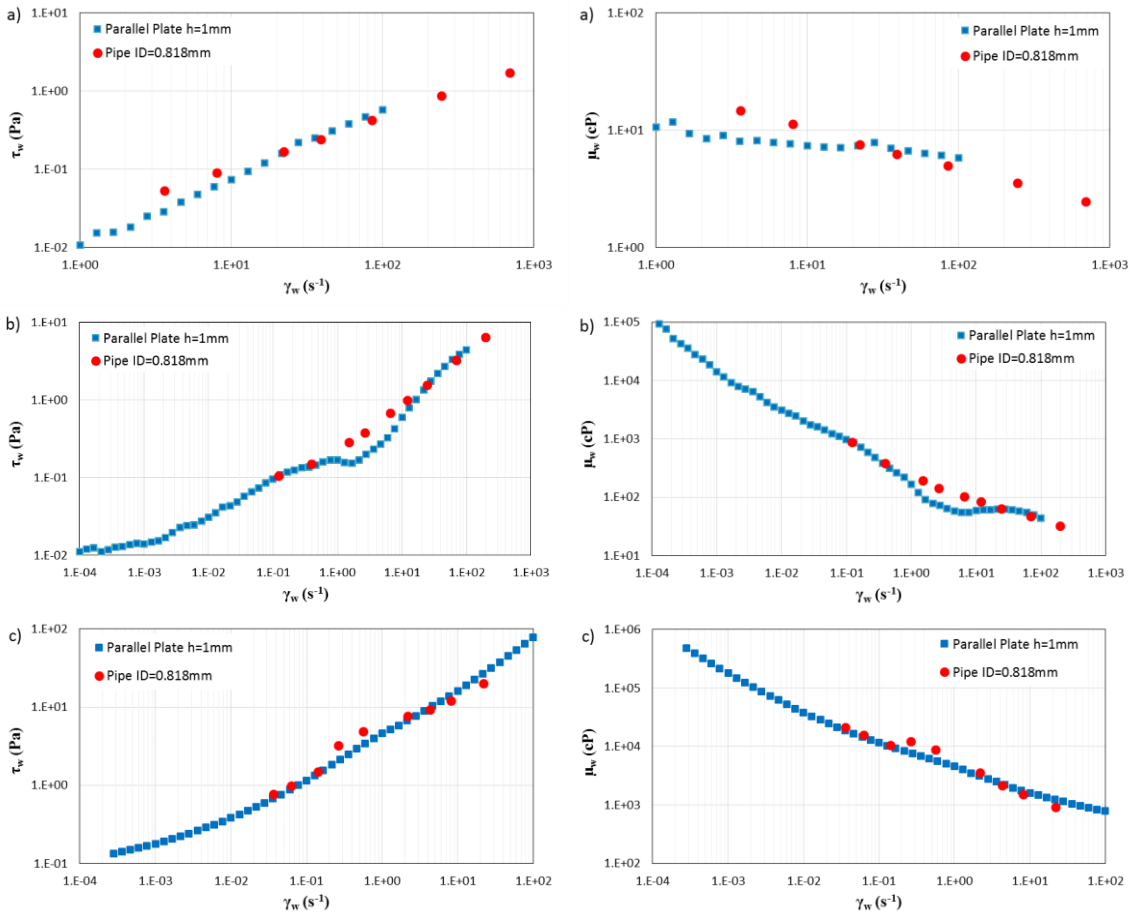

Fig. 6.17: The effect of flow types, drag-driven (parallel plates) and pressure-driven (tubes), on the τ_w vs. $\dot{\gamma}_w$ (left column) and μ_w vs. $\dot{\gamma}_w$ (right column) relationships of a) 40%, b) 60%, and c) 80% oil D emulsion (1.6% ph15EO, 0.2% NaOH, ~0.8-1.0% NaCl). Eq. 6.13 was used to correct for droplet migration with $a = 54$, $a = 6$, and $a = 1$ for 40%, 60%, and 80% oil D emulsions, respectively. Wall slip has been eliminated from both the parallel plate and tube viscometer measurements. Measured at 23 °C $\pm$ 2 with A1 tube viscometer.

Fig. 6.16 showed that 40% oil D emulsion had a very slight, if not insignificant viscosity reduction in the tube viscometer compared to the parallel plate geometry. The 60% oil D emulsion and 80% oil D emulsion samples showed up to a 3-fold, and 8-fold decrease in viscosity with the tube viscometer compared to the parallel plate geometry, respectively.

The droplet migration eliminated tube viscometer data matched well with the parallel plate viscometer data.

The Krieger-Dougherty equation is used to analyze the effect of droplet migration on viscosity reduction. Note that this is a qualitative analysis and the Krieger-Dougherty equation cannot accurately model the viscosity of concentrated heavy O/W emulsions. An assumption of a constant difference between the bulk dispersed-phase concentration and dispersed-phase concentration near the pipe wall of 0.1 was made ($\varphi_{bulk} - \varphi_{r/R=1} = 0.1$). The following viscosity ratio $\mu(\varphi_{bulk})/\mu(\varphi_{bulk} - 0.1)$ is obtained.

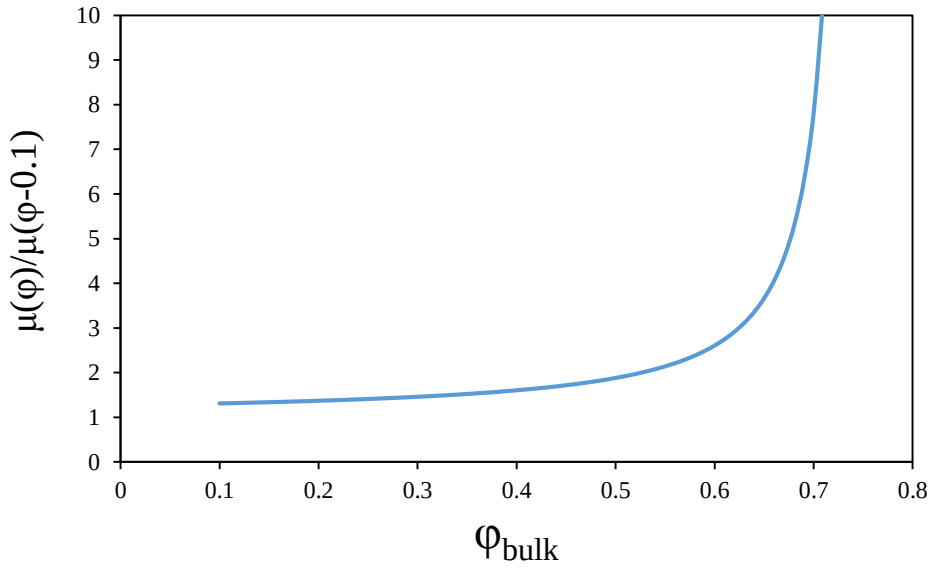

Fig. 6.18: $\mu(\varphi_{bulk})/\mu(\varphi_{bulk} - 0.1)$ vs. φ_{bulk} relationship generated with the Krieger-Dougherty equation. The $\varphi_m = 0.75$ and $\mu_c = 1\ cP$ were used.

The analysis with Fig. 6.18 agreed with the data in Fig. 6.16 that the viscosity reduction caused by droplet migration is more significant at higher φ. This is because emulsion viscosities are more sensitive to φ at $\varphi \gg 0.6$.

6.5.3 Effect of Chemical Formulation on Emulsion Viscosity

The effect of the chemical formulation used to prepare heavy oil emulsions on the emulsion viscosity is studied with a capillary tube viscometer. Capillary tube viscometer A1 was used to measure all the heavy O/W emulsions samples in this section. The heavy crude oil emulsions were prepared with the preparation method mentioned previously in Chapter 3. The composition of the emulsions are listed on the figures. The $\mu_{w,app}$ vs. $\dot{\gamma}_{w,app}$ relationships are calculated from the pressure drop data measured with the capillary tube viscometer for a sweep of flow rates. The contribution of wall slip to the emulsion flow is included in the calculated $\mu_{w,app}$ vs. $\dot{\gamma}_{w,app}$. However, wall slip is only significant for $\varphi > 0.6$ and $\dot{\gamma}_w < 25\ s^{-1}$.

6.5.3.1 Effect of heavy crude oil types and oil content on emulsion viscosity

The effect of the crude oil type and concentration on the $\mu_{w,app}$ vs. $\dot{\gamma}_{w,app}$ of emulsions are presented in Fig. 6.19. Four heavy oils are tested as well as oil concentrations from 20% to 80%.

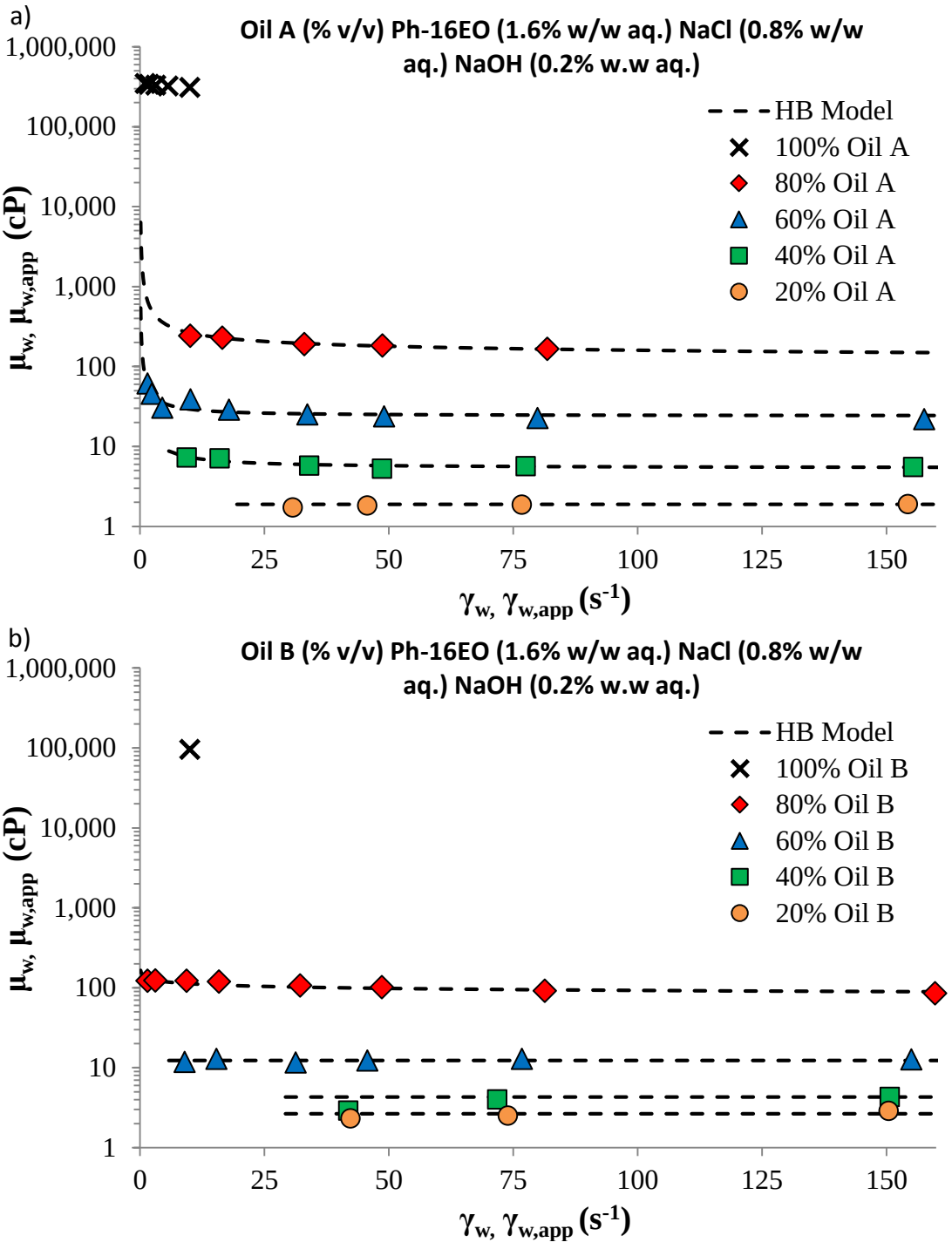

Fig. 6.19 continued.

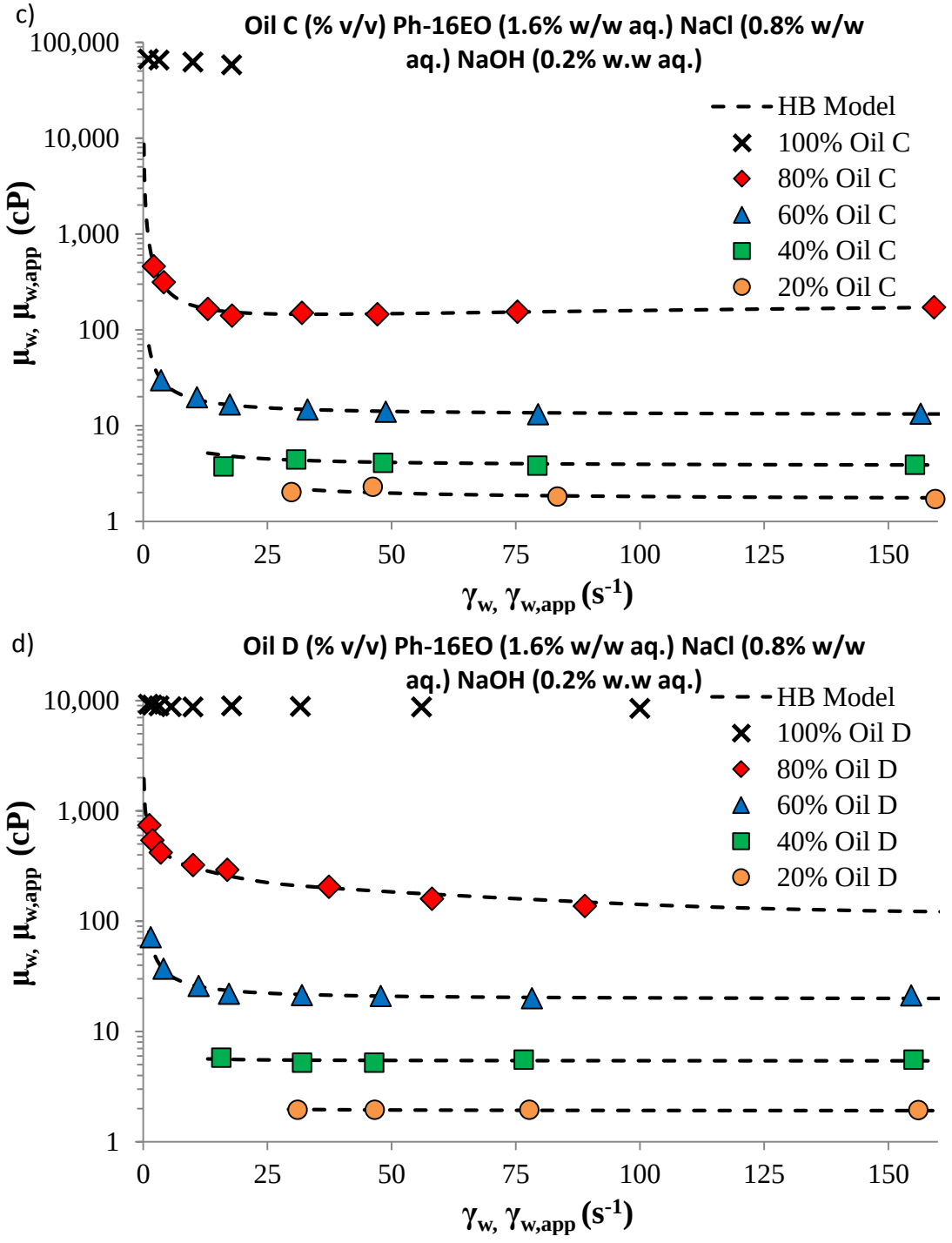

Fig. 6.19: $\mu_{w,app}$ vs. $\dot{\gamma}_{w,app}$ of 20%, 40%, 60%, and 80% emulsion and 100% oil with a) oil A, b) oil B, c) oil C, and d) oil D. Measured using the A1 tube viscometer at 23 ℃ ± 2.

The 20-40% oil emulsions showed Newtonian behavior and agreed with the viscosity calculated using the Krieger-Dougherty equation ($\varphi_m = 0.7$). The 60-80% oil emulsions showed extreme shear thinning behavior at low shear rates and weak shear thinning behavior at high shear rates. Similar results have been observed in the literature by Ahmed et al. (1999a); Nuñez et al. (2000); Romero et al. (2000, 2002). 80% O/W emulsions prepared with four different heavy oils showed up to ten times lower viscosities at $\dot{\gamma}_w > 25\ s^{-1}$ (where minimal wall slip is observed) compared to the viscosities of 80% O/W emulsions measured with the parallel plate geometry. All 80% emulsions in Fig. 6.19 showed evidence of droplet migration with lower $\mu_{w,app}$ measured with a capillary tube viscometer compared with a rotational viscometer. The crude oil concentration in the emulsions had the largest effect on the emulsion viscosity out of all variables tested, showing up to a hundred times difference in emulsion viscosities between 20% and 80% O/W emulsions.

Regardless of the fact that the heavy oil viscosities varied from 9,000 to 310,000 cP at 10 s^{-1} and 25 ℃, the emulsions prepared with different heavy oils in Fig. 6.19 showed similar viscosities at the same φ. The 80% oil D ($\mu_{oil} = 9{,}000\ cP$) emulsion showed similar emulsion viscosities compared to the 80% oil A ($\mu_{oil} = 300{,}000\ cP$) emulsion. The viscosity of heavy oils had a minimal effect on the viscosity of emulsions. On the other hand, the dilution method of transporting heavy oils requires a higher diluent volume as the oil viscosity increases. This suggests that the emulsion method of reducing heavy oil viscosity becomes economically competitive compared to the dilution method when the heavy crude oil viscosity is higher.

6.5.3.2 Effect of co-solvent types and co-solvent concentrations on emulsion viscosity

The effect of the type of co-solvents included in the chemical formulations is tested in Fig. 6.20.

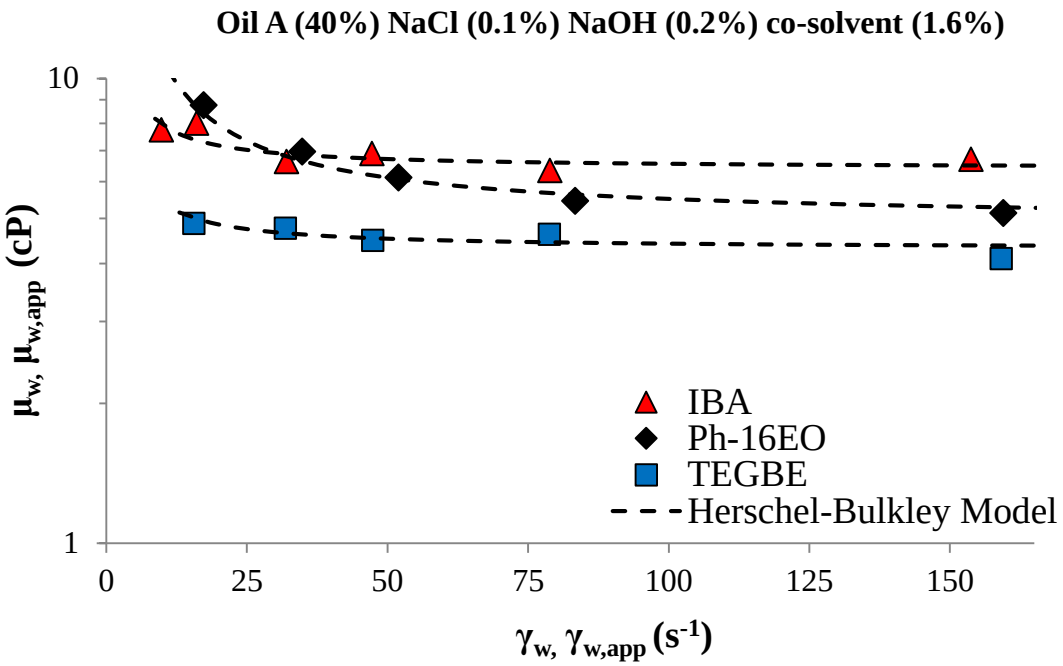

Fig. 6.20: $\mu_{w,app}$ vs. $\dot{\gamma}_{w,app}$ of 40% oil A emulsions prepared with various types of co-solvents. Measured using the A1 tube viscometer at 23 ℃ $\pm$ 2.

Fig. 6.20 showed that the heavy oil emulsions with similar viscosities can be prepared using a variety of co-solvents. The Krieger-Dougherty equation ($\varphi_m = 0.75 - 0.85$) predicted 40% O/W emulsion viscosity of $\mu \approx 4\ cP$. Emulsions in Fig. 6.20 showed slight shear-thinning behavior observed with higher $\mu_{w,app}$ than the predicted $\mu \approx 4\ cP$. This suggests that the oil droplets formed aggregate structures, increasing the effective dispersed-phase concentration $\varphi_{eff} > \varphi$. The Krieger-Dougherty equation predicted $\mu \approx 6.5\ cP$ for $\varphi_{eff} \approx 0.45 - 0.5$, implying that ~5% water is trapped within the aggregate droplet structures. The emulsion prepared with 1.6% phenol-16EO co-solvent also showed stronger shear thinning behavior compared to the emulsions prepared with IBA or TEGBE.

The effect of phenol-16EO concentration on the emulsion viscosity for 40% and 80% oil A emulsions were tested in Fig.6.21.

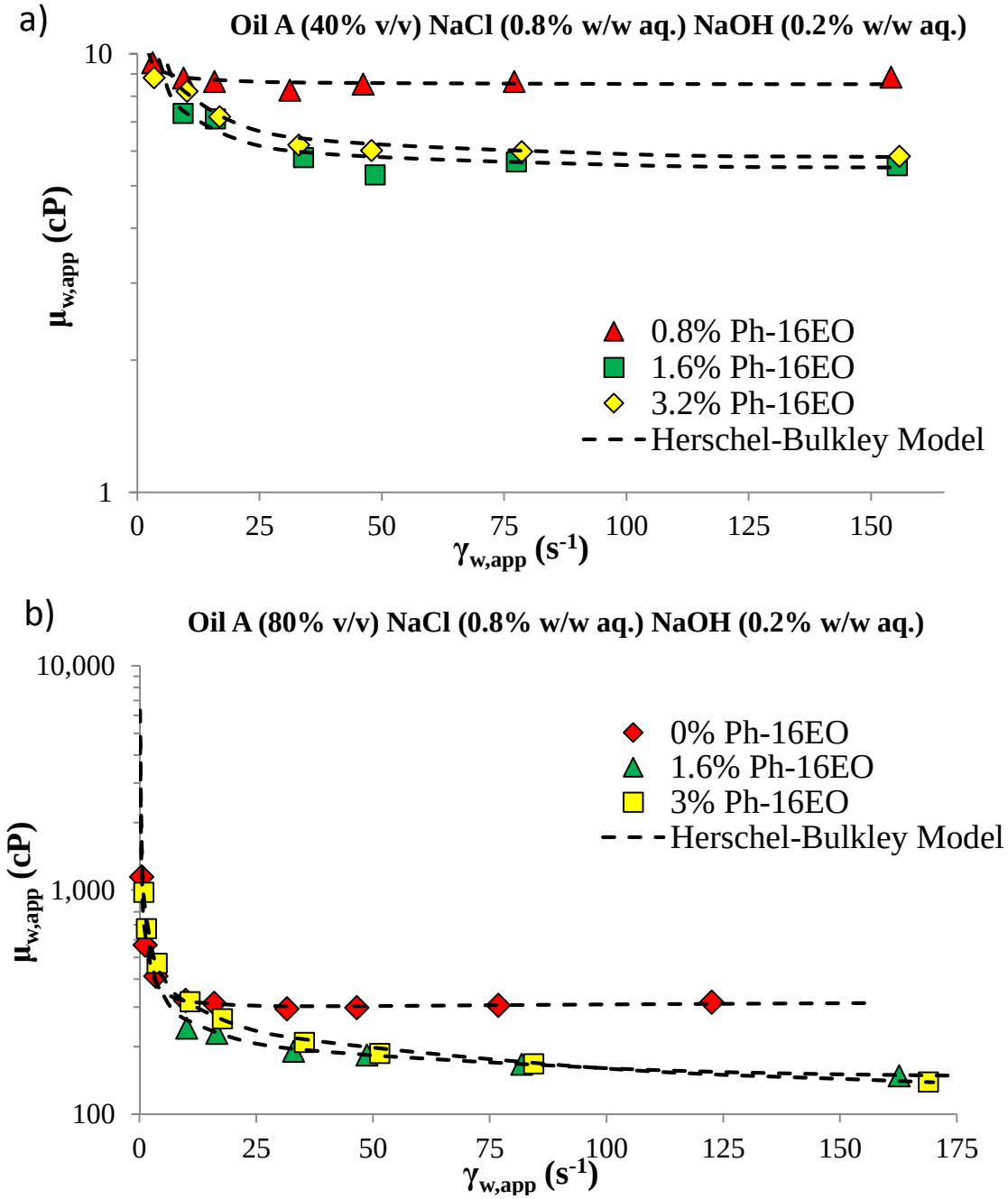

Fig. 6.21: $\mu_{w,app}$ vs. $\dot{\gamma}_{w,app}$ of a) 40% and b) 80% oil A emulsions with varying concentration of phenol-15EO co-solvent. 40% oil A emulsion with 1.6% ph15EO ($d_{32} = 1.3\ \mu m$ and $\varphi_m = 0.86$). 80% oil A emulsion with 1.6% ph15EO ($d_{32} = 16\ \mu m$ and $\varphi_m = 0.74$). 80% oil A emulsion with 3% ph15EO ($d_{32} = 15\ \mu m$ and $\varphi_m = 0.75$). Measured using the A1 tube viscometer at 23 ℃ $\pm$ 2. The 0% ph15EO for a) resulted in an extremely viscous W/O emulsion whose viscosity could not be measured.

Fig. 6.21 showed that heavy O/W emulsions prepared with higher co-solvent concentration showed lower viscosity. Emulsions prepared with 1.6% ph-15EO showed the lowest viscosity and increasing the co-solvent concentration to 3% ph-16EO resulted in negligible viscosity improvements. Only a small amount of ph-16EO co-solvent (~1.5%) decreased the $\mu_{w,app}$ of 40% and 80% oil A emulsions by 30-50% compared to the emulsions prepared with 0-0.8% ph-16EO.

Generally, the soaps generated from heavy crude oils possess low hydrophilic lipophilic balance (HLB), leading to the transition from low viscosity O/W emulsions to high viscosity W/O emulsions at a very low electrolyte concentration. Co-solvents are usually very hydrophilic and increase the HLB of soap and co-solvent mixtures compared to the HLB of soaps. The number of EOs attached to the co-solvents can be change to affect the hydrophilicity of the co-solvents with a higher EO number generally resulting in a more hydrophilic co-solvent. Table 6.6 identified whether 60% oil A emulsions prepared with different chemical formulations (0.2% NaOH, 0.1-2.4% NaCl, and 0-3% ph-xEO) formed O/W or W/O emulsions.

Table 6.6: The type of emulsions (O/W or W/O) that forms with 60% oil A emulsions prepared with 0-3% Ph-xEO, 0.2% NaOH, and 0.1-2.4% NaCl.

Co-solvent Conc.	Type of co-solvent	0.1 % NaCl	0.8% NaCl	1.6% NaCl	2.4% NaCl
0%	**No co-solvent**	O/W	W/O	W/O	W/O
1.6%	**Ph-2EO**	O/W	W/O	W/O	W/O
1.6%	**Ph-8EO**	O/W	O/W	O/W	W/O
1.6%	**Ph-16EO**	O/W	O/W	O/W	W/O
1.6%	**Ph-20EO**	O/W	O/W	O/W	W/O
3%	**Ph-15EO**	O/W	O/W	O/W	O/W

Table 6.6 showed that the emulsion inversion from O/W to W/O occurred between 0.1-0.8% NaCl for the formulation without co-solvents. However, with the addition of 1.6% phenol-8EO or higher EOs, the inversion salinity was increased to 1.6-2.4% NaCl. 60%

O/W emulsion was successfully prepared with a chemical formulation of 3% phenol-15EO, 0.2% NaOH, and 2.4% NaCl.

Fig. 6.22 showed that the number of EOs had a negligible effect on the viscosity of 60% oil A emulsions as long as the prepared emulsions are O/W. Phenol-2EO in Fig. 6.22 formed a viscous W/O emulsion whose viscosity could not be measured.

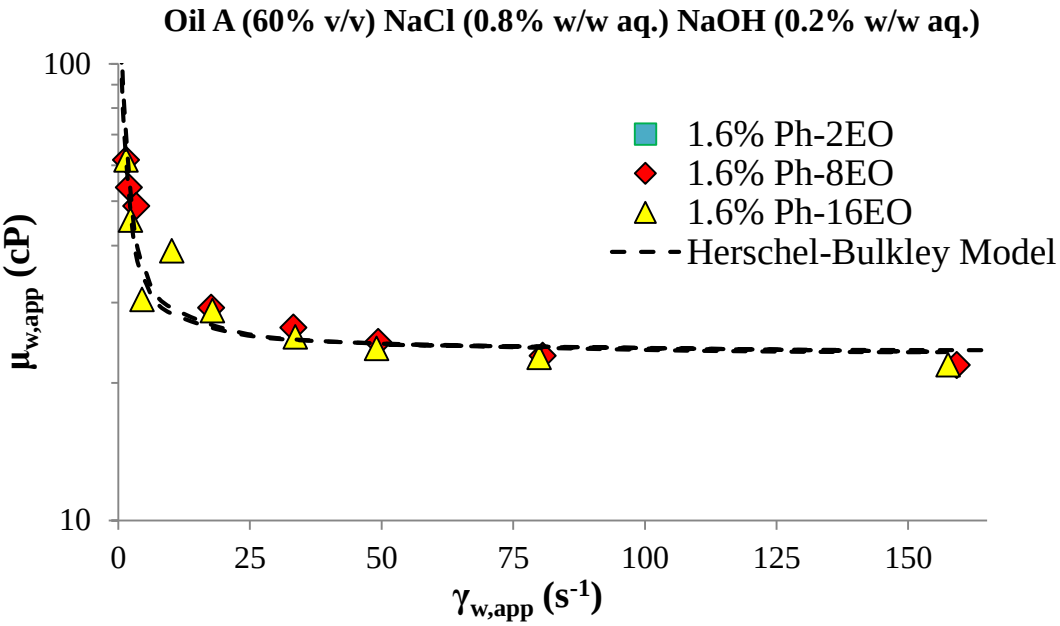

Fig. 6.22: $\mu_{w,app}$ vs. $\dot{\gamma}_{w,app}$ of 60% oil A emulsions with 1.6% phenol-xEO co-solvent. Measured using the A1 tube viscometer at 23 ℃ $\pm$ 2. The emulsion prepared with 1.6% ph-2EO formed a viscous W/O emulsion whose viscosity couldn't be measured.

The type of co-solvent, EO number, and co-solvent concentration can be optimized to prepare heavy O/W emulsions with various water sources, ranging from freshwater to softened seawater. The addition of co-solvents in the chemical formulation of heavy oil, water, and an alkali eliminated the need for a supply of very low salinity freshwater to prepare heavy O/W emulsions.

6.5.3.3 Effect of alkali type and alkali concentrations on emulsion viscosity

The effect of NaOH concentration on the viscosity of 40% and 60% oil A emulsions are shown in Fig. 6.23.

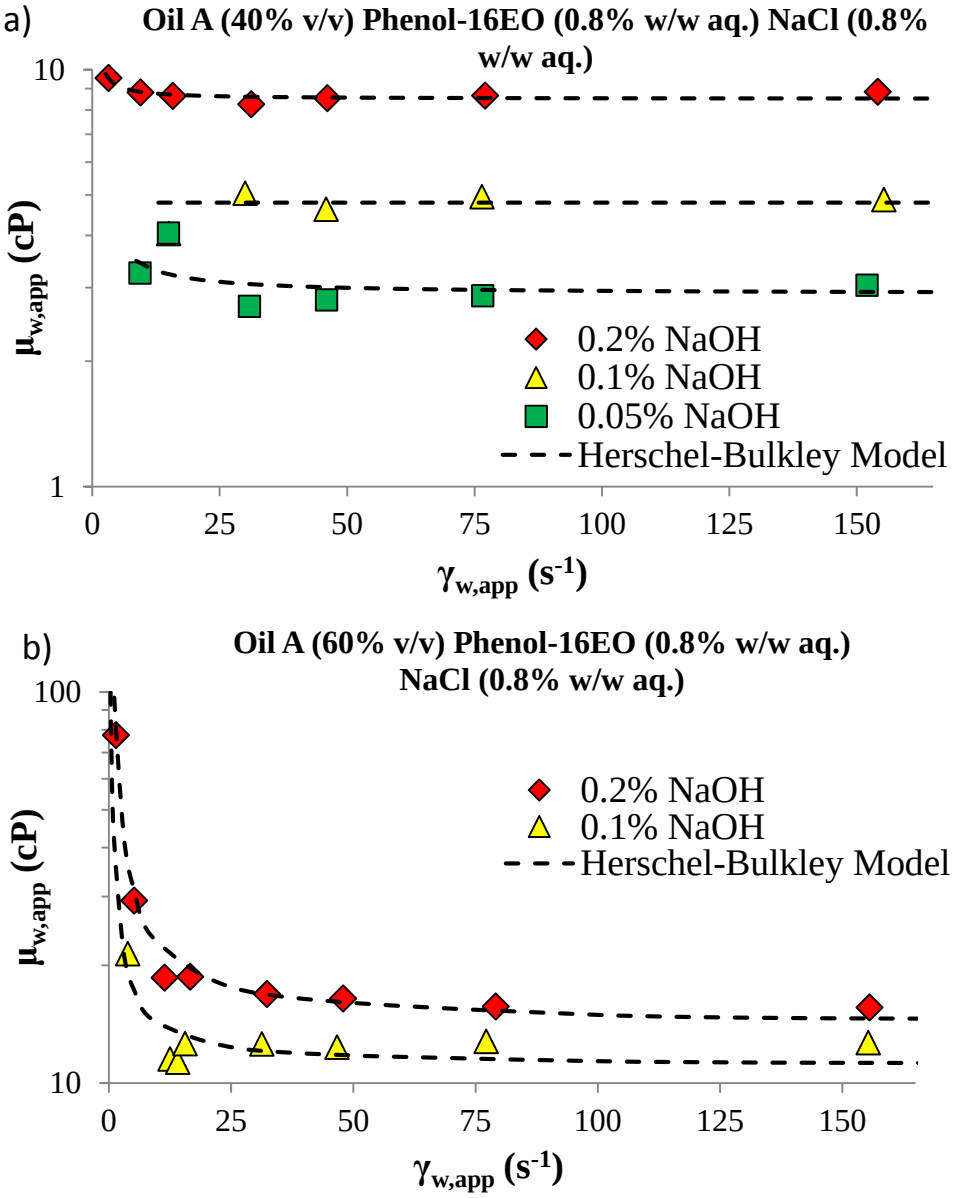

Fig. 6.23: $\mu_{w,app}$ vs. $\dot{\gamma}_{w,app}$ of a) 40% and b) 60% oil A emulsions prepared with various NaOH concentrations. Measured using the A1 tube viscometer at 23 ℃ ± 2.

NaOH concentrations of 0.05% for Fig. 6.23a and 0.1% for Fig. 6.23b were the minimum quantity of NaOH necessary to create homogenous and stable emulsions that solubilized

all the oil. Higher NaOH concentration increased the pH and resulted in a larger quantity of soap generation. Smaller oil droplets, better emulsion stability, and higher emulsion viscosities are observed with higher NaOH concentrations. Acevedo et al. (2001); dos Santos et al. n.d.; Gutierrez et al. (2003); Verzaro et al. (2002) reported similar experimental data.

Possible risks with using NaOH are the extreme sensitivity of the emulsion stability on the NaOH concentration and the small quantity needed to create low viscosity emulsions. If the pH of the emulsions is lowered because of consumption or precipitation of some OH^- ions in pipelines, emulsion phase separation could occur and lead to a plugged pipeline. Na_2CO_3 buffers at lower pH compared to NaOH [Acevedo et al. (2001)]. Fig. 6.24 demonstrated that stable 40% oil A emulsions were prepared with 0.1-0.5% Na_2CO_3. Higher concentrations of Na_2CO_3, compared to NaOH, can be used with only a small increase in the emulsion viscosity. 0.1% Na_2CO_3 was the minimum alkali needed to prepare a homogenous and stable 40% oil A emulsion.

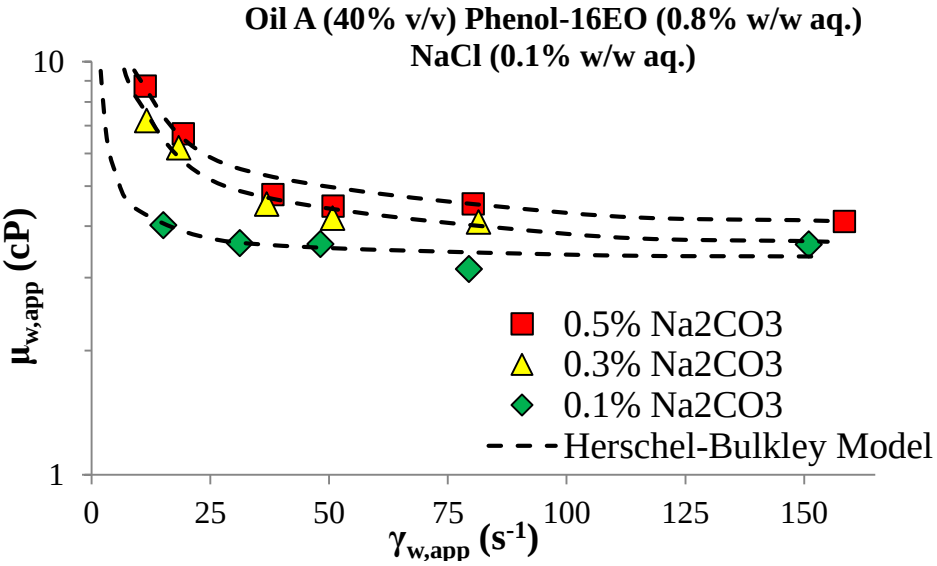

Fig. 6.24: $\mu_{w,app}$ vs. $\dot{\gamma}_{w,app}$ of 40% oil A emulsions prepared with various concentrations of Na_2CO_3. Measured using the A1 tube viscometer at 23 ℃ $\pm$ 2.

Alkalis such as potassium hydroxide, sodium bicarbonate, sodium metaborate, ammonia [Verzaro et al. (2002)], alkyl amine [Gutierrez et al. (2003)] and sodium acetate can be used to successfully prepare stable heavy O/W emulsions.

6.5.3.4 Effect of aqueous phase salinity on emulsion viscosity

The effect of salinity on the viscosity of 60% oil A emulsions is investigated in Fig. 6.25. 80% oil A emulsions showed similar trends but with higher viscosity.

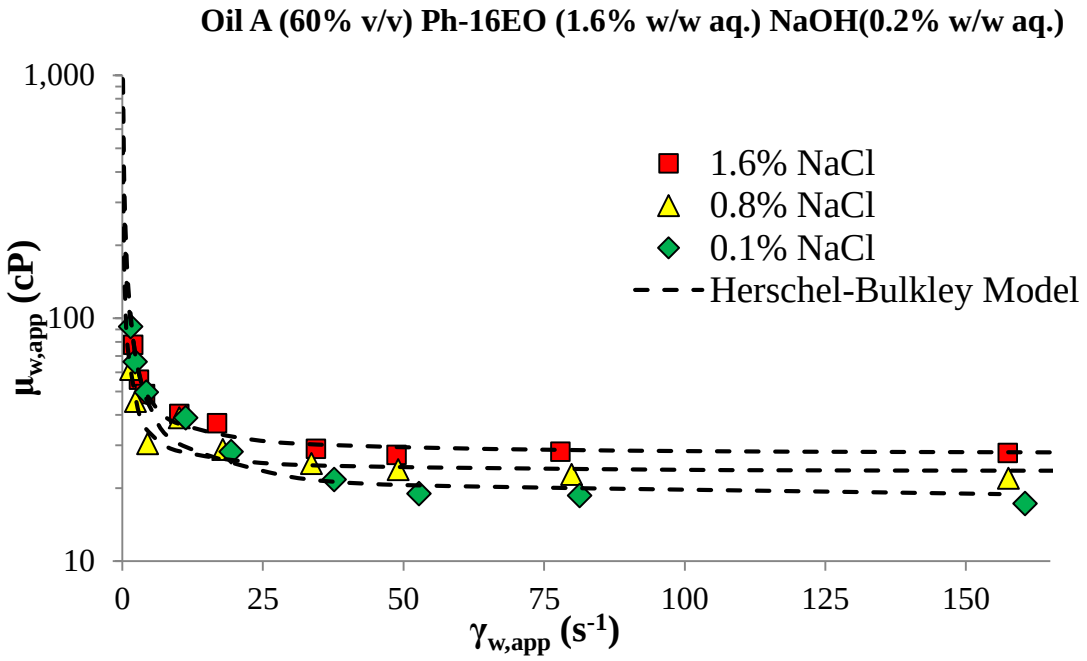

Fig. 6.25: $\mu_{w,app}$ vs. $\dot{\gamma}_{w,app}$ of 60% oil A emulsions prepared with various NaCl concentrations. Measured using the A1 tube viscometer at 23 ℃ $\pm$ 2.

The O/W emulsion viscosity increased as the NaCl concentration increased. The d_{32} of emulsions normally decrease as the NaCl concentration approaches the inversion salinity concentration of O/W to W/O emulsions (see Chapter 3). Acevedo et al. (2001); Ahmed et al. (1999b); Ashrafizadeh and Kamran (2010); Gutierrez et al. (2003) showed that the viscosity of heavy O/W emulsion increased as the d_{32} of emulsions decreased. The effect of the salinity on the viscosity of heavy O/W emulsions was found to be significant

but minor compared to the oil concentration, alkali concentration, and co-solvent concentration.

6.5.3.5 Co-solvent/natural surfactants vs. non-ionic surfactant on emulsion viscosity

Heavy O/W emulsions in the literature are often prepared with nonylphenol ethoxylate (NPE-xEO) [Ahmed et al. (1999b); dos Santos et al. (2011), n.d.; Núñez et al. (1996); Nuñez et al. (2000); Romero et al. (2002)]. The Orimulsion® was also stabilized with NPE.

The performance of the heavy O/W emulsions prepared with NPE-12EO were compared to the heavy O/W emulsions prepared with chemical formulations containing a co-solvent and an alkali. 60% oil D and 80% oil B emulsions were prepared with 1.6% NPE-12EO in the aqueous phase using the preparation procedure outline in Chapter 3. The emulsions were mixed at 75℃ because the cloud point of NPE-12EO is ~80℃ according to the supplier. The emulsions prepared with NPE showed emulsion instability. Phase separation was observed after several hours. The emulsions plugged the capillary tube viscometer several times during measurement. Heavy O/W emulsions prepared with a co-solvent and an alkali never plugged the capillary tube viscometers. Fig. 6.26 compared the viscosity measurements of emulsions prepared with NPE and emulsions prepared with a co-solvent and an alkali.

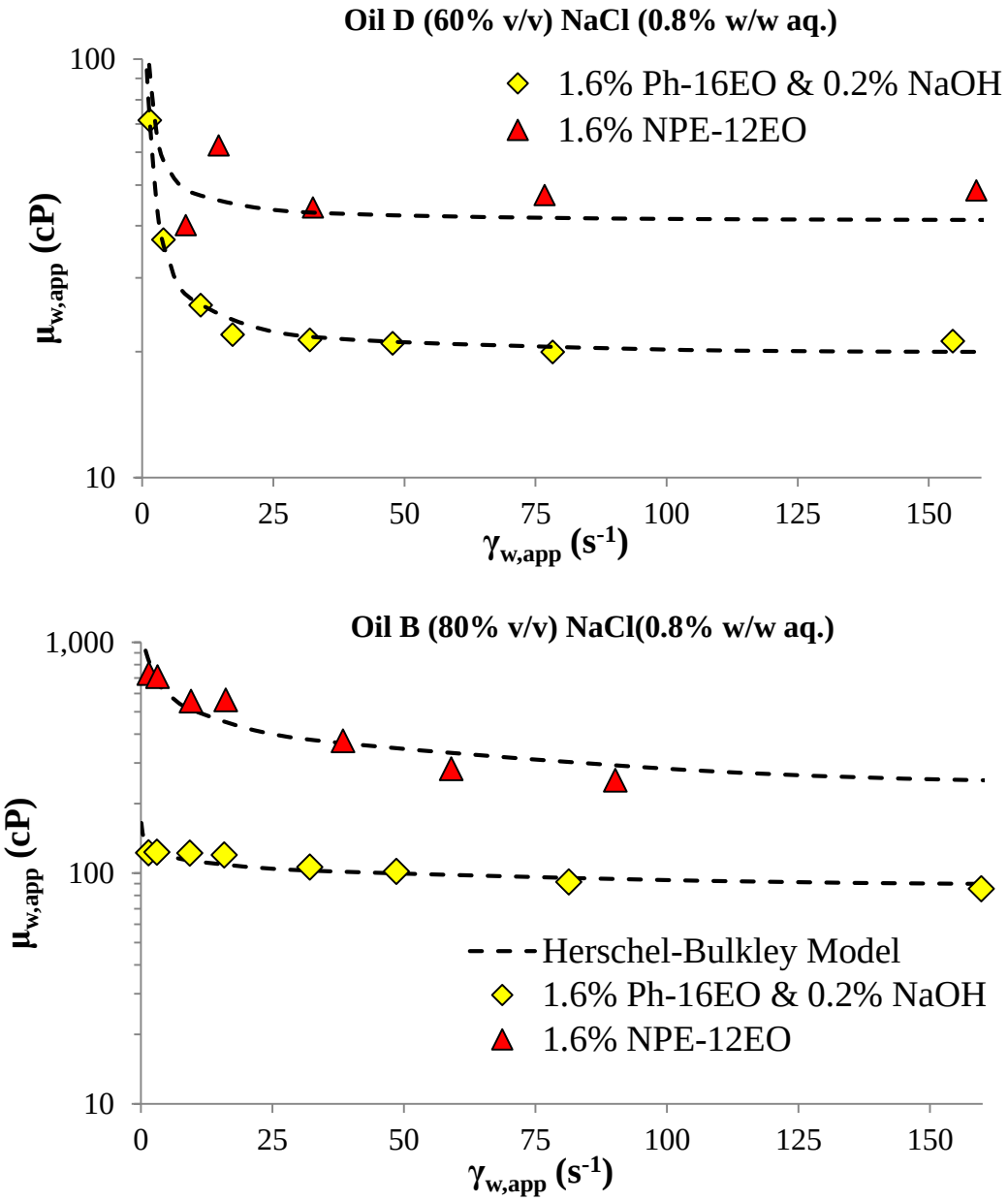

Fig. 6.26: $\mu_{w,app}$ vs. $\dot{\gamma}_{w,app}$ of a) 60% oil D and b) 80% oil B emulsions. Measured using the A1 tube viscometer at 23 ℃ $\pm$ 2.

60% oil D and 80% oil B emulsions prepared with NPE-12EO showed up to two times and six times lower $\mu_{w,app}$ compared to the emulsions prepared with phenol-16EO and

0.2% NaOH. Emulsions prepared with a co-solvent and an alkali were very stable, unlike the emulsions prepared with NPE-12EO.

6.5.3.6 Use of ethoxylated amines as both a co-solvent and an alkali

Amines are basic organic chemicals. Alkyl Amines have been used as an alternative to inorganic alkalis to prepare heavy O/W emulsions with good stability [Gutierrez et al. (2003)]. Since alkyl amines or ethoxylated alkyl amines behave as co-solvents as well as alkalis, the preparation of heavy O/W emulsions with an optimized chemical formulation may be possible with only one chemical (an alkyl amine) instead of two chemicals (a co-solvent and an alkali). Fig. 6.27 demonstrated that low viscosity oil A emulsions with good stability were prepared using various alkyl amines.

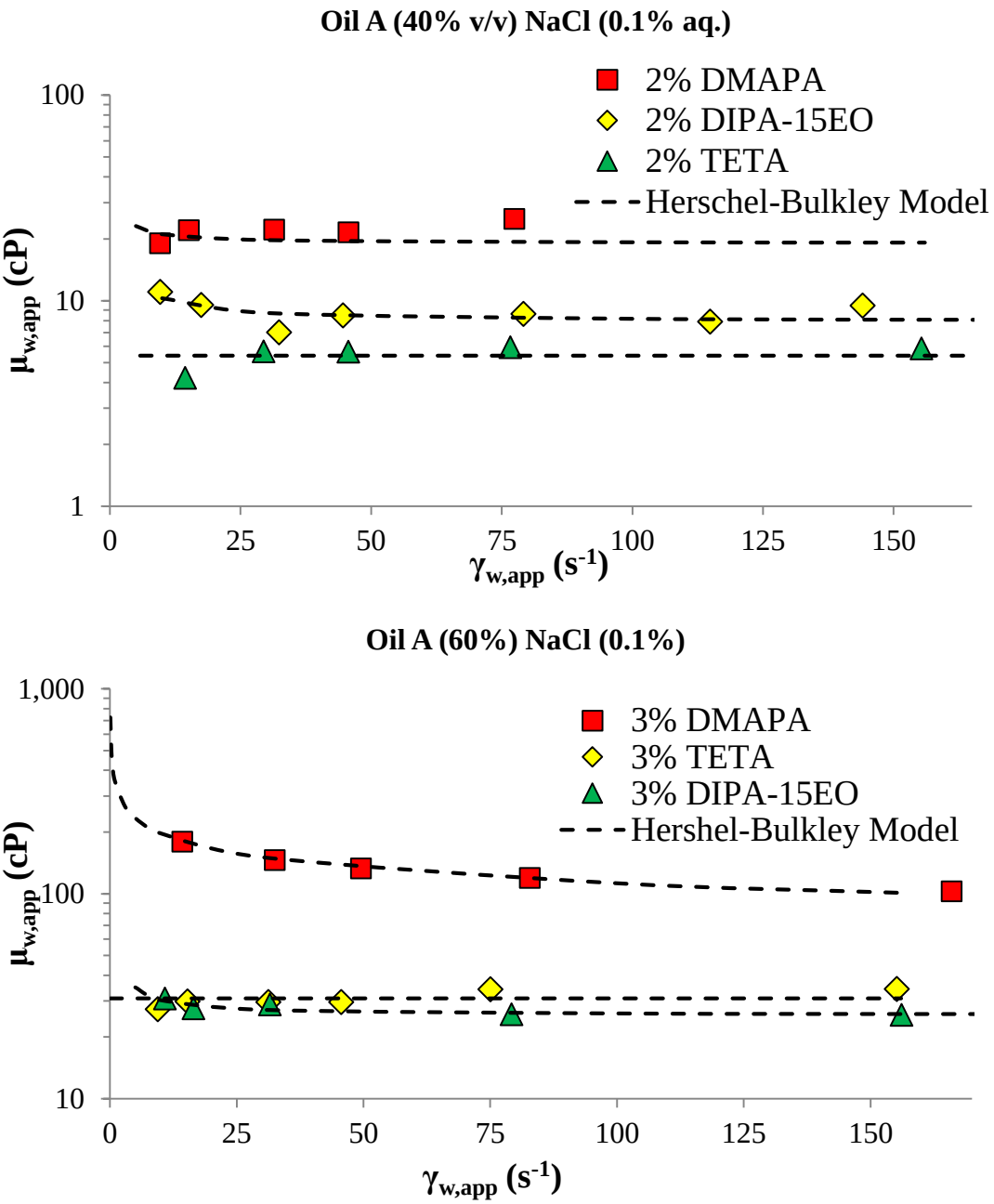

Fig. 6.27: $\mu_{w,app}$ vs. $\dot{\gamma}_{w,app}$ of 40% and 60% oil A emulsions prepared with various alkyl amines. Measured using the A1 tube viscometer at 23 ℃ $\pm$ 2.

Fig. 6.27 showed that the type of alkyl amine used made a significant difference in the viscosity of oil A emulsions. Emulsions prepared with dimethylaminopropylamine (DMAPA) showed up to two times (40% oil A emulsion) and four times (60% oil A

emulsions) higher viscosity compared to the emulsions prepared with triethylenetetramine (TETA) and ethoxylated diisopropylamine (DIPA-15EO). The photomicrographs of 60% oil A emulsions prepared with 2% TETA and 2% DMAPA showed that the droplet size distributions of the two emulsions were very similar (see Chapter 4). It may be that droplet migration of 60% oil A emulsion prepared with 3% DMAPA is minimal in the capillary tube viscometer and/or the oil droplets formed strong and large aggregate structures.

Fig. 6.28 showed the effect of oil A concentration on the viscosity of emulsions prepared with 1.5% DIPA-15EO as both an alkali and a co-solvent.

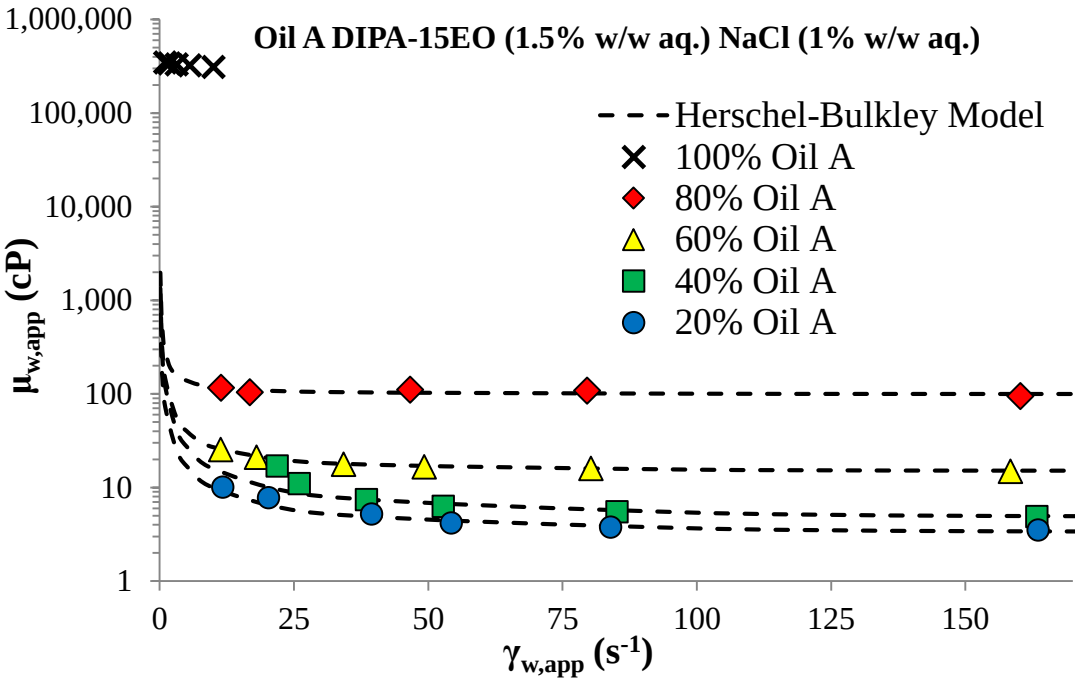

Fig. 6.28: $\mu_{w,app}$ vs. $\dot{\gamma}_{w,app}$ of 20-80% oil A emulsions prepared with 1.5% DIPA-15EO. Measured using the A1 tube viscometer at 23 ℃ $\pm$ 2.

The oil A emulsions ($\varphi \geq 0.6$) prepared with 1.5% DIPA-15EO showed noticeably lower $\mu_{w,app}$ compared to the oil A emulsions prepared with 1.6% phenol-15EO and 0.2% NaOH (see Fig. 6.19a). The difference in emulsions viscosities between Fig. 6.19a

and Fig. 6.28 may be explained by the molecular weight of the alkalis used to prepare emulsions. DIPA-15EO is a very large molecule (~760 g/mol) compared to NaOH (40 g/mol). The alkali density of 1.5% DIPA-15EO is two and half times less in terms of moles compared to 0.2% NaOH. There is a positive correlation between emulsion viscosity and alkali concentration (see Figs. 6.23 and 6.24).

Viscosity of heavy O/W emulsions prepared with DIPA-15EO and very high dispersed-phase concentrations ($\varphi > 80$) are investigated.

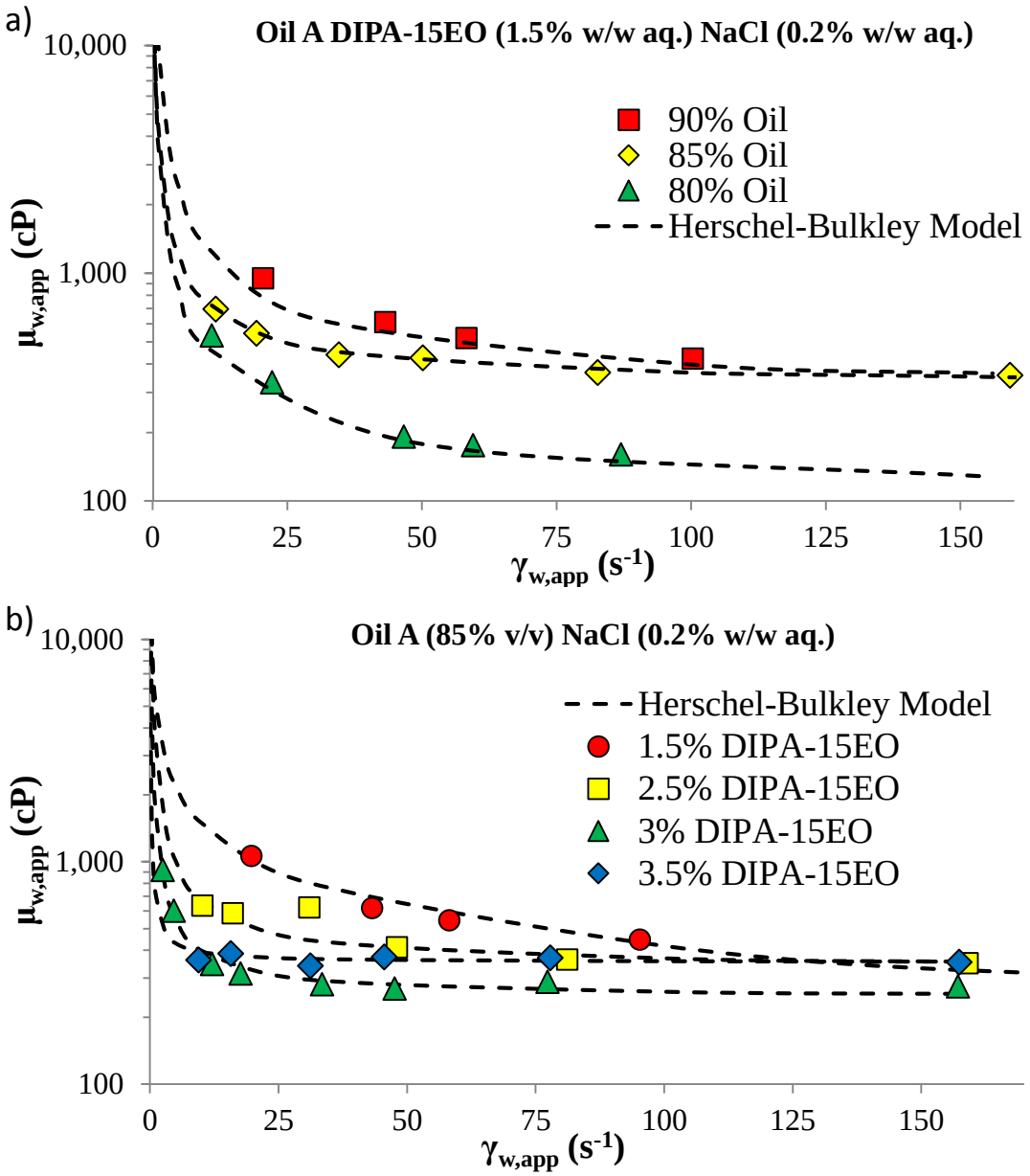

Fig. 6.29: $\mu_{w,app}$ vs. $\dot{\gamma}_{w,app}$ of a) oil A emulsions prepared with 1.5% DIPA-15EO and $0.9 > \varphi > 0.8$ and b) 85% oil A emulsions prepared with 1.5-3.5% DIPA-15EO. Measured using the A1 tube viscometer at 23 ℃ $\pm$ 2.

Stable heavy O/W emulsions with $\varphi \leq 0.9$ were prepared using 1.5% DIPA-15EO. Emulsions viscosities much higher than the pipeline limit of 350 cSt were observed for emulsions with $0.85 \leq \varphi$ (Fig. 6.29a). However, 85% oil A emulsion with $\mu_{w,app} <$

$350\ cSt$ was prepared with 3% DIPA-15EO. It may be possible that the chemical formulation used to prepare 85% oil A emulsion can be optimized further to show no-slip emulsion viscosity below the 350 cSt limit in capillary tube viscometers.

The major benefits of using alkyl amine co-solvents over conventional alkalis and co-solvents are summarized.

1. One chemical, alkyl amine, is needed to emulsify water and heavy crude oil to form O/W emulsions. The alkyl amine eliminates the use of a conventional alkali from the proposed emulsion preparation procedure, resulting in a simpler and cheaper formulation.
2. Heavy O/W emulsions with up to 85% oil concentration showed $\mu_{w,app} < 350\ cSt$.
3. Alkyl amines are known corrosion inhibitors. A small quantity (5-15 ppm) of alkyl amines in sea water significantly reduced carbon steel corrosion with the corrosion rate decreasing further with increasing amine concentration [Rihan et al. (2014)]. Since the alkyl amine concentration is at least three orders of magnitude higher than 10 ppm in the emulsion formulations used to prepare heavy O/W emulsions, the rate of pipeline corrosion due to the presence of water in heavy O/W emulsions may be reduced significantly.

6.5.3.7 Effect of temperature on emulsion viscosity

Quantifying the effect of temperature on the viscosity of heavy O/W emulsions is crucial. Pipelines are stretched over a large area of land and the pipeline temperature fluctuates daily, seasonally, and geographically. Temperature of pipelines can also be increased and pipelines insulated to operate at higher temperature similar to the Trans-Alaska Pipeline System which operated at 40^{o}C. The effect of temperature on the

viscosity of 85% oil A emulsion prepared with 1.5% DIPA-15EO is tested in Fig. 6.30. The emulsion viscosity was measured using a Couette viscometer with smooth walls.

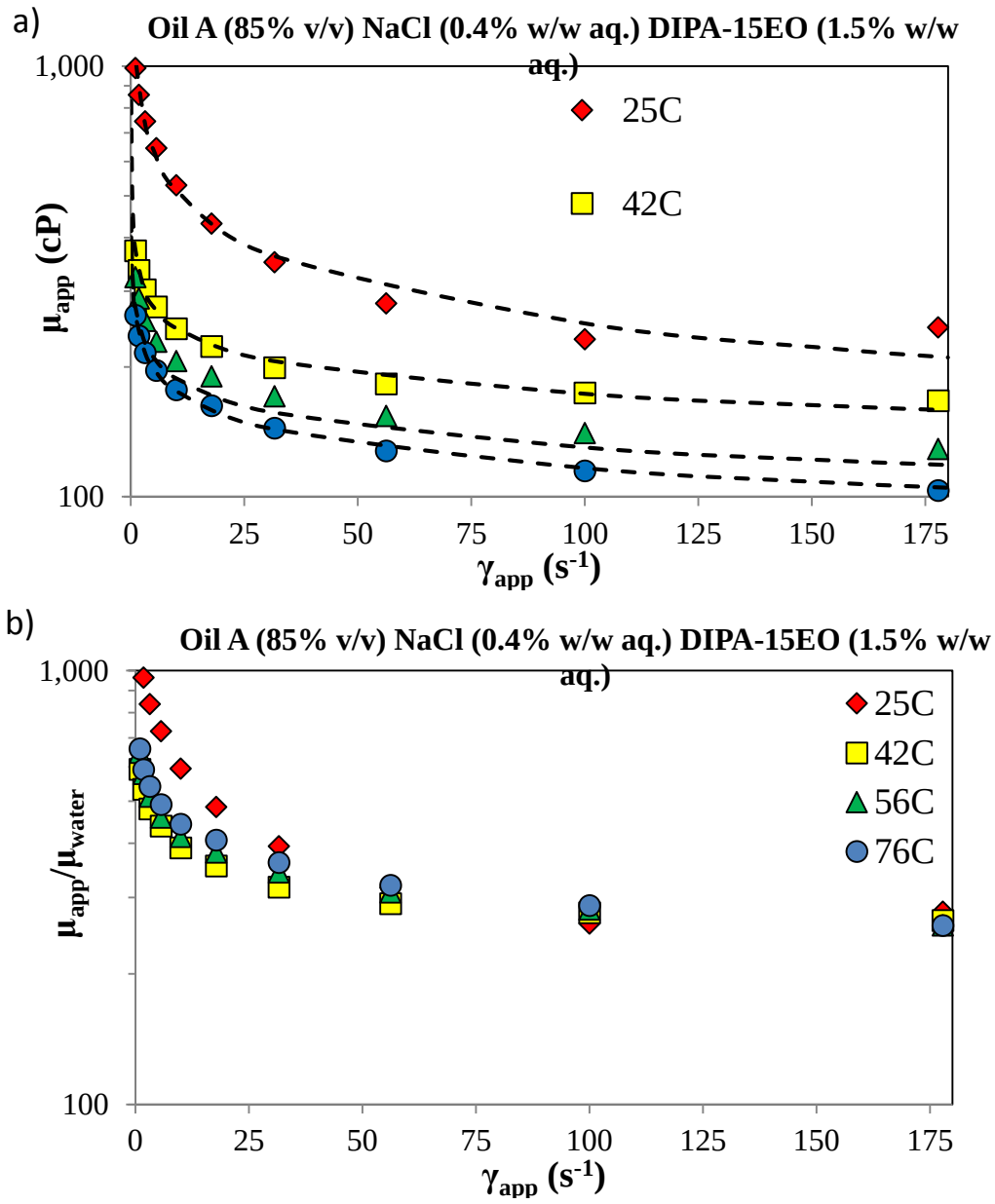

Fig. 6.30: Effect of temperature on a) μ_{app} vs. $\dot{\gamma}_{app}$ and b) μ_{app}/μ_{water} vs. $\dot{\gamma}_{app}$ of 85% oil A emulsion prepared with 1.5% DIPA-15EO. The emulsion was measured with a smooth wall Couette geometry using the ARES LS1 rheometer. The μ_{app} vs. $\dot{\gamma}_{app}$ measurements included the contributions of wall slip and possible droplet migration.

Higher measurement temperature lowered the emulsion viscosity [Abdurahman et al. (2012); Ahmed et al. (1999b); Hasan et al. (2010)]. The μ_{app} vs. $\dot{\gamma}_{app}$ of 85% O/W emulsion at various temperatures collapsed into one curve by plotting μ_{app}/μ_{water} vs. $\dot{\gamma}_{app}$. For pipelines already equipped with heating stations and insulation, the hybrid heating-heavy O/W emulsion method may be used to transport highly concentrated heavy O/W emulsions with 85-90% oil concentrations. Transport temperature only needs to be increased from 25 to 40°C to show a significant viscosity reduction of heavy O/W emulsions (Fig. 6.30a).

6.5.3.8 Emulsion Stability

Emulsion stability is an extremely important property in terms of transportation and storage. Two major process which affect the stability of emulsions are 1) creaming or sedimentation of oil droplets caused by gravity and 2) coalescence of droplets where droplets combine irreversibly to form larger droplets.

Pure layers of heavy oils caused by coalescence of oil droplets were not observed visually for most emulsions tested in this study for storage duration of weeks. Dynamic stability of heavy O/W emulsions against coalescence is shown in Chapter 5. Droplet size distribution before and after shearing were the same within the accuracy of the measurement errors. Transient viscosity measurements of heavy O/W emulsions were stable at shear rates of 0.0001-100 s^{-1} which indicate no change in the droplet size distribution of the emulsions. The only exceptions were heavy O/W emulsions that were prepared with chemical formulations very near the O/W to W/O inversion point. These emulsion samples showed good static stability but phase separation between oil and water were observed under high shear rates.

Creaming (oil droplets move to the top) and sedimentation (oil droplets move to the bottom) of heavy O/W emulsions were observed with some samples over days and

weeks. However, a few shakes of the sample vials revert the emulsions back to the original homogenous state. Most heavy O/W emulsions ($0.2 \leq \varphi \leq 0.85$) prepared in this study showed good stability against creaming/sedimentation. The only exception were the emulsions prepared with alkyl amines which showed fast sedimentation/creaming at dispersed phase of $\varphi < 0.8$.

Stoke's equation is used to analyze the good stability of heavy O/W emulsions against creaming/sedimentation. The equation only applied to emulsions with a dilute dispersed phase volume.

$$v_{stokes} = -\frac{2gR^2\Delta\rho}{9\mu_c} \tag{6.14}$$

where v_{stokes} is the velocity of creaming/sedimentation rate, g the gravity, R the radius of the droplet, $\Delta\rho$ density difference between the dispersed phase and continuous phase, and μ_c the continuous phase viscosity. The following properties of heavy O/W emulsions reduced the sedimentation/creaming rate:

1. Small density difference between water and heavy oil of $\Delta\rho < 30 - 50\ kg/m^3$
2. Small droplet diameter
3. Higher dispersed phase concentration
4. Yield stress

The presence of a yield stress for heavy O/W emulsions stabilizes emulsions against creaming/sedimentation. Tadros (2004) stated that if the yield stress is higher than the stress exerted by an emulsions droplet, sedimentation/creaming can be completely eliminated.

$$\tau_p = \frac{gR\Delta\rho}{3} \tag{6.15}$$

where τ_p is the stress exerted by an emulsion droplet. If $\tau_p < \tau_y$, creaming/sedimentation is eliminated.

Heavy oil emulsions with dispersed phase of 40% showed $\tau_y \approx 0.05\ Pa$ which is higher than $\tau_p = 9.81 m/s^2 * 200 \mu m * 50 kg/m^3/3 = 0.033\ Pa$ assuming aggregate radius of 200 μm. For this case, as long as the aggregates/clusters of oil droplets are smaller than $R < 200 \mu m$, sedimentation/creaming is eliminated. Higher the dispersed phase concentration, higher the yield stress and better stability against creaming/sedimentation is obtained. Attractive heavy O/W emulsions showed very good stability against sedimentation/creaming because of the presence of the yield stress even at small heavy oil concentrations.

6.6 CONCLUSIONS

Wall slip was observed with the flow of heavy oil-in-water emulsions in capillary tube viscometers. Wall slip velocity of heavy oil-in-water emulsions measured using the parallel plates and capillary tube viscometers agreed quantitatively as a function of wall shear stress.

The viscosity of heavy oil-in-water emulsions measured using parallel plates and capillary tube viscometers showed a larger difference at high oil concentration even with the elimination of wall slip. With a 80% heavy oil-in-water emulsion, up to ten times lower viscosities were measured with capillary tube viscometers compared with parallel plates. The lower apparent viscosity of heavy oil-in-water emulsions measured in capillary tube viscometers is attributed to the migration of oil droplet away from the tube wall due to the parabolic velocity profiles of fluids in tubes. Oil droplets travel from regions of higher shear rates (tube wall) to regions of lower shear rates (center of tube) [Hollingsworth and Johns (2006)]. A lower concentration of oil droplets near the tube wall translated to lower apparent viscosities of heavy oil-in-water emulsions compared to the bulk fluid viscosities.

Oil droplet migration of heavy oi-in-water emulsions was found to be insensitive to the diameter of capillary tube viscometers. This suggests that droplet migration may be up-scaled to major crude oil pipelines. The ratio of the shear rates experience by heavy oil-in-water emulsions in parallel plates to the wall shear rates in tube viscometers with droplet migration was found to be proportional according to $\dot{\gamma}/\dot{\gamma}_{w,dm} \sim \sqrt{\tau_w/\rho}$.

Droplet migration in capillary tube viscometers reached steady state at a much lower ratio of tube length to diameter, L_{ss}/D, than predicted based on the current theory of droplet migration in the literature. The theory proposed by Phillips et al. (1992) indicated that the hydrodynamic diffusion of large particles occurs much faster than small particles. The smaller than predicted L_{ss}/D values may be because of the properties of heavy O/W emulsions to form aggregate structures whose effective diameter is bigger compared to individual oil droplets. Small L_{ss}/D values may be integral to taking advantage of the viscosity reduction of heavy O/W emulsions caused by droplet migration in large pipelines. This is because L_{ss}/D values for large pipelines are orders of magnitude larger than the L_{ss}/D for laboratory tube viscometers. The L_{ss} value for large pipelines must be significantly smaller than the length of pipeline between pumps stations for droplet migration to occur.

Crude oil pipelines are designed and operated to transport fluids with viscosity under the maximum pipeline viscosity specification of 350 cSt. Looking at the pipeline operating shear rate range of 5-30 s^{-1}, optimized heavy O/W emulsions with oil concentrations up to $70-75\%$ showed viscosities of <350 cSt according to the parallel plate measurements. With no-slip flow and droplet migration in tube viscometers, optimized heavy O/W emulsions with oil concentrations up to $80-85\%$ showed apparent viscosities of <350 cSt. With the same pipeline operating conditions, 10% extra heavy oil can be transported in the form of emulsions in pipelines due to droplet

migration. The effect of droplet migration on the viscosity of concentrated heavy O/W emulsions is critical when formulating concentrated heavy O/W emulsions for pipeline transport.

The chemical formulation used to prepare heavy O/W emulsions affected the flow properties of emulsions in capillary tube viscometers significantly. Heavy oil types, oil concentration, co-solvents, co-solvent concentrations, alkali, alkali concentration, and salinity were screened to optimize the chemical formulation used to prepare optimized heavy O/W emulsions that showed low apparent viscosities in capillary tube viscometers. Good emulsion stability under static and dynamic conditions was another screen criteria.

Heavy oil concentration in emulsions had the largest effect on emulsion viscosity while the heavy oil viscosity had a negligible effect. Heavy O/W emulsions prepared with a co-solvent and an alkali showed lower apparent viscosity and better emulsions stability comparted to emulsions prepared with nonylphenol ethoxylate. Ethoxylated alkyl amine co-solvents are very attractive chemicals that perform the roles of a co-solvent and an alkali simultaneously. With the appropriate co-solvents, heavy O/W emulsions can be prepared with water sources up to the salinity of softened seawater. Freshwater is not necessary to form concentrated heavy O/W emulsions with low viscosity.

The rheological characterization of heavy O/W emulsions should always be performed with different measurement geometries and flow types. Rotational drag flow geometries such as parallel plates and a cone-and-plate are ideal for measuring wall slip and bulk fluid rheological properties. Pressure-driven flow in capillary tube viscometers are ideal for characterizing droplet migration and turbulent flow behavior. Care must be taken to achieve steady state emulsion flow in tube viscometers.

The apparent viscosities of 80% heavy O/W emulsions in capillary tube viscometers are up to ten times lower compared to the viscosities measured with rotational viscometers. Apparent viscosity measurements of <350 cSt were achieved for optimized heavy O/W emulsions with oil concentration up to 85% in capillary tube viscometers.

NOMENCLATURE

d	Droplet diameter
a	Droplet radius
φ	Dispersed-phase volume fraction of emulsions
R	Droplet radius
n	Flow index
k	Flow consistency index
φ_m	Maximum packing volume fraction (φ_m) of dispersed-phase possible without deformation of the spherical dispersed-phase
v	Mean velocity
Q	Mean volumetric flow rate
σ	Natural logarithm standard deviation of droplet diameter
P	Pressure
$\dot{\gamma}$	Shear rate
$\dot{\gamma}_w$	Shear rate at the tube wall
τ	Shear stress
τ_w	Shear stress at the tube wall
D	Tube diameter
L	Tube length
μ	Viscosity
Q_{ns}	Volumetric flow rate due to bulk fluid flow
Q_s	Volumetric flow rate due to wall slip
v_s	Wall slip velocity
τ_y	Yield stress

ABBREVIATIONS

O/W	Oil-in-water
W/O	Water-in-oil
HLB	Hydrophilic lipophilic balance

Chapter 7: Upscaling the Flow of Concentrated Heavy Oil-in-Water Emulsions from Laboratory to Pipelines

7.1 INTRODUCTION

The diameter of major crude oil pipelines can reach up to $1.2\ m$ and can extend thousands of miles in length. Laboratory measurements of concentrated heavy oil-in-water emulsions with tubes of such dimensions are not possible. Flow of concentrated heavy oil-in-water emulsions characterized using capillary tube viscometers with diameters of $1 - 10\ mm$ in the laboratory must be upscaled to predict flow of emulsions in major crude oil pipelines.

The rheological properties of concentrated heavy oil-in-water emulsions in capillary tube viscometers are complex and highly dependent on the tube dimensions. Two-step yielding of concentrated heavy oil-in-water emulsions translate to a two-step wall slip behavior on smooth surfaces. The contribution of wall slip to flow of emulsion decreased as the tube diameter increased. The wall slip model developed for rotational viscometers was used successfully to characterize the wall slip of concentrated heavy oil-in-water emulsion. When wall slip was eliminated, viscosity measurements of concentrated emulsions collapsed into one curve when measured with tube viscometers of varying dimensions ($D = 0.7036 - 7.035\ mm$).

After accounting for wall slip, concentrated heavy oil-in-water emulsions also showed lower apparent viscosities in capillary tube viscometers compared to viscosities measured with rotational viscometers. The lower apparent viscosities measured in capillary tube viscometers are attributed to oil droplet migration away from the tube wall due to a heterogeneous shear field. Droplet migration in tubes showed no dependence on tube diameters at steady state flow.

This chapter presents the upscaling equations used to predict the flow of heavy oil-in-water emulsions in pipelines with diameters up to $1.2\ m$. The upscaling equations accounted for wall slip, droplet migration, and transition from laminar to turbulent flow of heavy oil-in-water emulsions. Pressure gradients versus flow rates of heavy oil emulsions are compared to the flow of heavy oils and an oil with viscosity of 350 cP, the maximum oil viscosity limited by regulations for pipeline transportation. The pressure gradients in pipelines were calculated using two methods: 1) Fanning friction factor based calculations for laminar and turbulent flows, and 2) analysis of the velocity profiles of heavy oil-in-water emulsions for laminar flow.

Sensitivity analysis of pipeline dimensions and emulsion formulations was performed to identify the optimum conditions for transportation of heavy oils in an emulsified form.

7.2 THEORY AND LITERATURE REVIEW

Before equations can be derived to upscale flow measured in capillary tube viscometers to pipelines, fluid and flow vessel properties must be established as well as the boundary conditions. The assumptions used to upscale flow of heavy O/W emulsions for pipeline scale operations:

Assumptions

1. The flow is in a long, straight pipe of constant diameter.
2. Fully developed laminar and turbulent flows (steady-state flow)
3. The velocity profile is identical at any point of the length of the pipe.
4. The gravitations effects are neglected over the entire length of the pipe.
5. Incompressible fluid.
6. End-effects are neglected because of a very large L/D.

7. Constant temperature at any point of the pipe.
8. Pressure is only a function of z-direction. $(P = P(z))$

Based on these assumptions, a force balance for the flow of heavy O/W emulsions can be derived to relate pressure gradients to the pipeline radius and wall shear stress.

Force Balance

The following simplified force balance is derived according to the assumptions made and the boundary condition of $\tau = 0$ at $r = 0$.

$$\frac{\Delta P}{L} = \frac{2\tau}{r} \tag{7.1}$$

where $\Delta P/L$ is the pressure gradient, τ the shear stress, and r the radial position with $r = 0$ and $r = R$ representing the center and wall of the pipe, respectively. Shear stress distribution throughout the pipe is a linear function of radial coordinates, where shear stress is a maximum at the pipe wall and 0 at the center

$$\tau = \frac{2\tau_w r}{D} \tag{7.2}$$

where τ_w is the shear stress at the wall $(r = R)$. Thus, the pressure gradient can be related to τ_w by modifying Eq. 7.1

$$\frac{\Delta P}{L} = \frac{2\tau_w}{R} \tag{7.3}$$

There are two methods of calculating pressure gradients vs. flow rates. First method is to substitute for τ in Eq. 7.1 with an accurate rheological model $(\tau\ vs.\dot{\gamma})$ that fits the experimental data. This method can only be used for laminar flow since the velocity profiles can only be accurately estimated for this flow regime. Second method is to relate the pressure gradient experienced in a pipe to the flow velocity using the Fanning friction factor. This is a dimensionless number which represents the ratio of the local shear stress to the local flow kinetic energy density

$$f = \frac{\tau}{\rho u^2/2} \tag{7.4}$$

where f is the local Fanning friction factor, ρ the liquid density, and u the local flow velocity. Eq. 7.3 can be substituted into Eq. 7.4 to obtain the relationship between pressure gradients and flow rates:

$$\frac{\Delta P}{L} = \frac{f\rho v^2}{R} \tag{7.5}$$

where v is the average flow velocity. This method can be used for both laminar and turbulent flows as long as an accurate f is calculated.

Often, the pressure gradient, which controls the flow rate of fluids, is the limiting parameter in commercial pipeline operations. With an accurate estimation of f for both emulsions and crude oils, the pipeline performance of heavy O/W emulsions can be compared to crude oils of various viscosities using Eq. 7.5 at constant pressure gradients.

The type of flow regime, laminar or turbulent, in pipes can be predicted using the Reynolds number (Re), a dimensionless number defined as the ratio of momentum forces to viscous forces. The generalized Reynolds number for flow in a pipe is defined as:

$$Re = \frac{\rho Q D}{\mu A} \tag{7.6}$$

where Q is the volumetric flow rate, A the cross-sectional area of the pipe, and μ the viscosity of the fluid at the flow rate of Q. For Newtonian fluids, laminar flow is observed for $Re < 2{,}100$ and turbulent flow is observed for $Re > 4{,}000$. Transition from laminar to turbulent flow takes place at $2{,}100 < Re < 4{,}000$. The start and end of the transitional flow Re varies for non-Newtonian fluids. The methods used to estimate the pressure gradient vs. flow rate relationship of non-Newtonian fluids for laminar and turbulent flows is discussed below.

LAMINAR FLOW

The two methods of estimating ∇P vs. v is discussed below.

Method 1

In the literature, Eq. 7.1 was integrated to relate the velocity profile to pressure drop for Newtonian, Power Law, Bingham, and Herschel-Bulkley fluids. Since the rheology of heavy O/W emulsions is similar to Herschel-Bulkley fluids, only the Herschel-Bulkley analytical solution is discussed below. However, the solutions of the velocity profile for Newtonian, Power Law, and Bingham fluids are the limiting cases of the Herschel-Bulkley model solution where $\tau_y = 0 \,\&\, n = 1$, $\tau_y = 0$, and $n = 1$, respectively. The equivalent analytical solution of the Herschel-Bulkley velocity profile in a pipe has been developed using different methods [Cheng et al. (1968); Heywood (1980); Selby (1976); Stainsby et al. (1994)]. We used the analytical solution obtained by Stainsby et al. (1994) since it is the simplest to use. The velocity profile is given by:

$$V = V_c\,, \qquad 0 < r < r_y \tag{7.7}$$

$$V(r) = V_c\left[1 - \left(\frac{r - r_y}{R - r_y}\right)^{\left(\frac{n+1}{n}\right)}\right], \qquad r_y < r < R \tag{7.8}$$

where r_y is the radius of the plug core, V_c the velocity at $r = r_y$, n the Herschel-Bulkley flow index, and V the velocity at r.

The r_y value is given by the force balance between the yield stress and pressure gradient:

$$r_y = \frac{2\tau_y}{dP/L} \tag{7.9}$$

The critical velocity, V_c is given by:

$$V_c = \left(-\frac{1dP}{2kL}\right)^{1/n}\left(\frac{n}{n+1}\right)\left(R - r_y\right)^{\left(\frac{n+1}{n}\right)} \tag{7.10}$$

where k is the Herschel-Bulkley model fluid consistency. The average velocity is given by:

$$v = V_c\left(1 - \frac{2n\left(R - r_y\right)^2}{R^2(3n+1)} - \frac{2n(R - r_y)}{R^2(2n+1)}r_y\right) \tag{7.11}$$

The analytical solutions (Eq. 7.7-7.11) can be solve to obtain $\nabla P\ vs.\ v$ relationship for the Herschel-Bulkley rheological model.

Typical velocity profiles of Newtonian, Power Law, Bingham, and Herschel-Bulkley fluids are shown below.

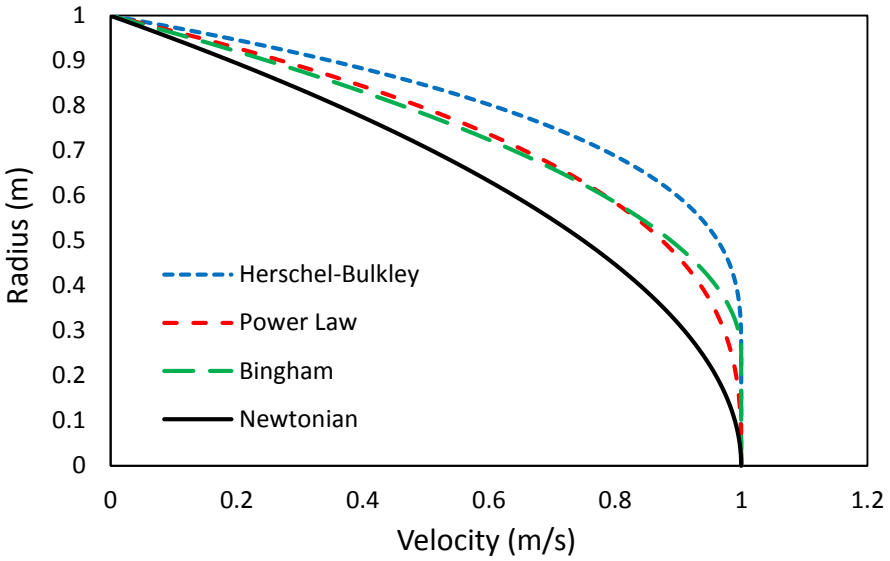

Fig. 7.1: Typical velocity profiles of Newtonian and non-Newtonian fluids. $n = 0.5$ and $\tau_y = 0.25\ Pa$. Velocity is normalized to 1 at the center of the pipe.

Method 2

The Fanning friction factor can be accurately estimated using the following relationship for laminar flow in a pipe regardless of the type of fluids, Newtonian or non-Newtonian:

$$f = 16/Re \tag{7.12}$$

Accurately calculating Re is not a trivial problem for non-Newtonian fluids. Since Eq. 7.5 is derived at the wall of the pipe, Re must be calculated with μ at the pipe wall for the volumetric flow rate of Q.

Based on the Herschel-Bulkley model, the viscosity at the pipe wall is defined as:

$$\mu_w = \frac{\tau_y}{\dot{\gamma}_w} + k\dot{\gamma}_w{}^{n-1} \tag{7.13}$$

where $\dot{\gamma}_w$ is the shear rate at the wall. The shear rate at the wall is defined as $\dot{\gamma}_w = (-\frac{du}{dr})_w$. For Newtonian fluids, $\dot{\gamma}_w = 8v/D$. However, non-Newtonian fluids have velocity profiles that differ from Newtonian fluids and $\dot{\gamma}_w \neq 8v/D$. The Rabinowitsch (1929) correction factor can be used to define the wall shear rate for non-Newtonian fluids:

$$\dot{\gamma}_w = (-\frac{dv}{dr})_w = \frac{8v}{D}\,\frac{3n'+1}{4n'} \tag{7.14}$$

where n' is the local flow index obtained from $\tau_w\, vs.\, \dot{\gamma}_{w,app}$ where $\dot{\gamma}_{app\,w}$ is the shear rate at the wall assuming Newtonian behavior ($\dot{\gamma}_{w,app} = 8v/D$). The n' value is obtained from the following equations for Herschel-Bulkley fluids [Madlener et al. (2009)]:

$$n' = \frac{\mathrm{d}\ln\tau_w}{\mathrm{d}\ln\dot{\gamma}_{w,app}}$$

$$n' = \frac{\mathrm{d}\ln(\tau_y + k\dot{\gamma}_{w,app}{}^n)}{\mathrm{d}\ln\dot{\gamma}_{w,app}} \qquad \backslash$$

$$n' = \frac{\mathrm{d}\ln(\tau_y + ke^{n\ln\dot{\gamma}_{w,app}})}{\mathrm{d}\ln\dot{\gamma}_{w,app}}$$

$$n' = \frac{\mathrm{d}\ln(\tau_y + ke^{n\ln\frac{8v}{D}})}{\mathrm{d}\ln\frac{8v}{D}}$$

$$n' = \frac{nk\left(\frac{8v}{D}\right)^n}{\tau_y + k\left(\frac{8v}{D}\right)^n} \tag{7.15}$$

Similar to Method 1, Newtonian, Power Law, and Bingham models are the limiting cases of the Herschel-Bulkley model solution where $\tau_y = 0\ \&\ n = 1$, $\tau_y = 0$, and $n = 1$, respectively. With Eqs. 7.13-15, an accurate Re of non-Newtonian fluids can be calculated. Thus, ∇P vs. v can be estimated using Eqs. 7.5-6 for laminar flow.

The most comprehensive analysis of Herschel-Bulkley fluids in laminar flow was presented by Hanks (1978). Hanks' analysis included the effects of both n and τ_y, and the critical Re where laminar flow ends. Hanks defined the generalized Reynolds number $Re = \frac{D^n v^{2-n}\rho}{8^{n-1}k}\left(\frac{4n}{3n+1}\right)^n$ to take into account the fluid consistency value n. The yield stress is accounted for with the function Ψ [Hanks (1978)]

$$f = \frac{16}{\Psi Re} \tag{7.16}$$

$$\Psi = (1+3n)^n (1-\xi_0)^{1+n} \left[\frac{(1-\xi_0)^2}{(1+3n)} + \frac{2\xi_0(1-\xi_0)}{(1+2n)} + \frac{{\xi_0}^2}{(1+n)}\right]^n \tag{7.17}$$

$$\xi_0 = \frac{\tau_y}{\tau_w} \tag{7.18}$$

where ξ_0 is the dimensionless unsheared plug radius.

TURBULENT FLOW

There exists no analytical solution to relate the f vs. Re in the literature for turbulent flow. Only semi-theoretical solutions have been derived to relate f vs. Re based on experimental data.

Newtonian Fluids

The most commonly used semi-empirical solution for turbulent flow is the Colebrook-White equation derived by Colebrook (1939) for Newtonian fluid flow in pipes of varying surface roughness.

$$\frac{1}{\sqrt{f/4}} = -2\log_{10}\left(\frac{\epsilon}{3.7D} + \frac{2.51}{Re\sqrt{f/4}}\right) \tag{7.19}$$

where ϵ is the absolute roughness of the pipe wall. Because of the implicit nature of Eq. 7.19, various numerical methods are used to solve for f. To make Eq. 7.19 easier to use, explicit solutions have been proposed to estimate the f based on the Colebrook-White equation. We used the explicit solution proposed by Cheng et al. (1968) to approximate the Colebrook-White equation for Newtonian crude oils.

$$\frac{1}{\sqrt{f/4}} = -2\log_{10}\left[\frac{\epsilon}{3.7065D} - \frac{5.0452}{Re}\log_{10}\left(\frac{1}{2.8257}\left(\frac{\epsilon}{D}\right)^{1.1098} + \frac{5.8506}{Re^{0.8981}}\right)\right] \tag{7.20}$$

Moody Diagram was created by Moody (1944) to provide a graphical representation of the Colebrook-White equation (Fig. 7.2).

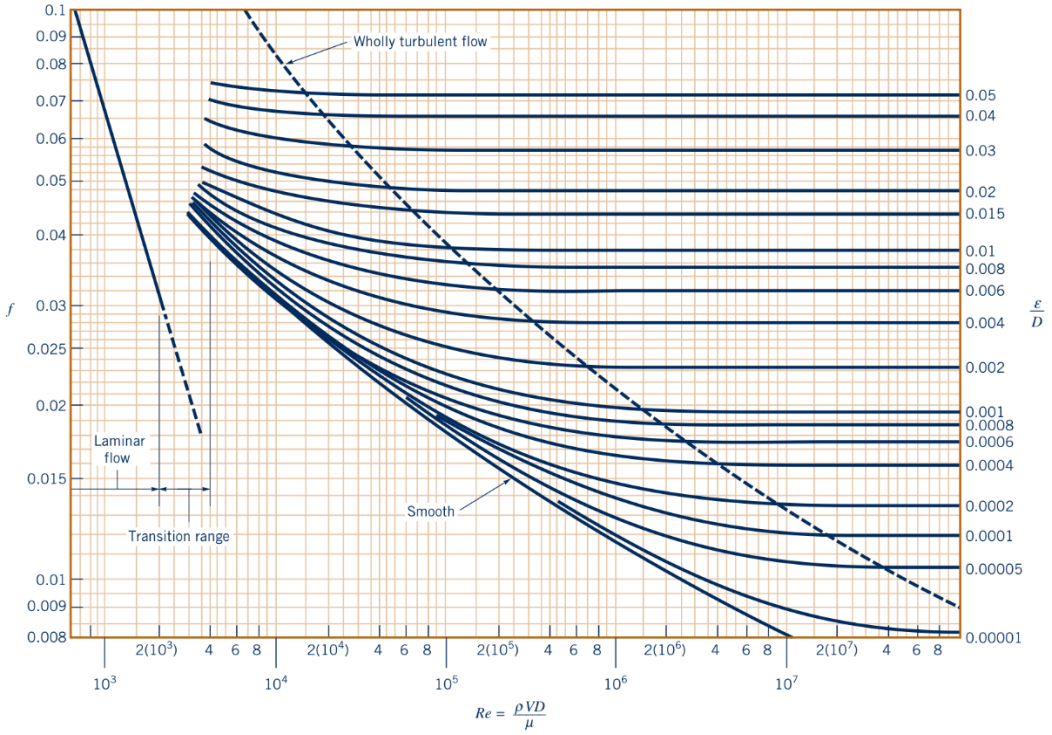

Fig. 7.2: Moody Diagram obtained from Munson et al. (1990). The friction factor on the y-axis is the Darcy friction factor which is 4 times the Fanning friction factor

Power Law Fluids

The semi-theoretical equation used to estimate the Fanning friction factor for Power Law fluids was presented by Dodge and Metzner (1959).

$$\frac{1}{\sqrt{f}} = \frac{4}{n^{3/4}} \log_{10}\left[Re\, f^{(1-\frac{n}{2})}\right] - \frac{0.4}{n^{1.2}} \qquad (7.21)$$

Eq. 7.21 accurately estimated the f of aqueous Carbopol solutions with $n = 0.36 - 0.73$ for $2{,}900 < Re < 36{,}000$ [Dodge and Metzner (1959)]. Pipe roughness was not mentioned. Graphical representation of Eq. 7.21 is shown in Fig. 7.3.

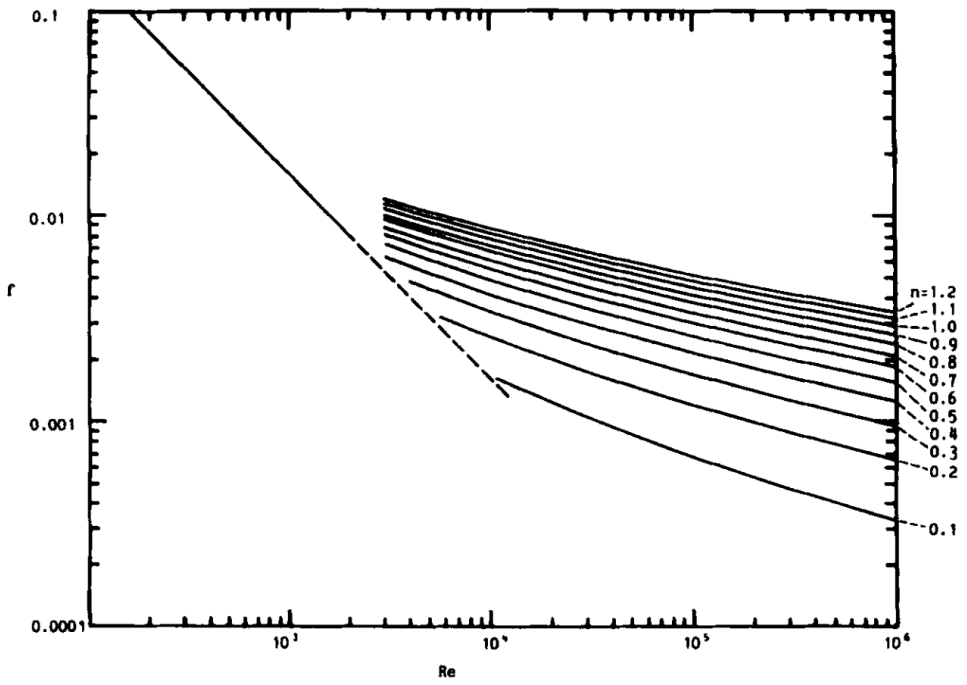

Fig. 7.3: Graphical representation of Dodge and Metzner Equation. Obtained from Garcia and Steffe (1986)

Garcia and Steffe (1986) summarized most of the correlations between f vs. Re for Power Law fluids in turbulent flow. Depending on the type of Power Law fluid, different equations appear to fit the experimental data accurately. However, there are two things that almost all the equations have in common: (1) f decreased as n decreased, and (2) the Re at which laminar flow ends and transitional flow begins increased as n decreased (see Fig. 7.3). To conclude, shear-thinning fluids show lower friction factors compared to Newtonian fluids in the turbulent flow regime.

Bingham Plastic Fluids and Herschel-Bulkley Fluids

The most comprehensive analysis of Herschel-Bulkley fluids in the turbulent flow regime was presented by Hanks (1978). Hanks equations required numerical integrations as well as implicitly solving several equations at once to calculate $f\ vs. Re$. The equations can be found in Hanks (1978) or Garcia and Steffe (1986). The graphical

representation of Hanks equation is shown for both Bingham fluids ($n = 1, \tau_y \neq 0$) and Herschel-Bulkley fluids ($n < 1, \tau_y \neq 0$). Yield stress is expressed in dimensionless Hedstrom number (He).

$$He = \frac{D^2 \rho}{k} \left(\frac{\tau_y}{k}\right)^{\frac{2-n}{n}} \tag{7.22}$$

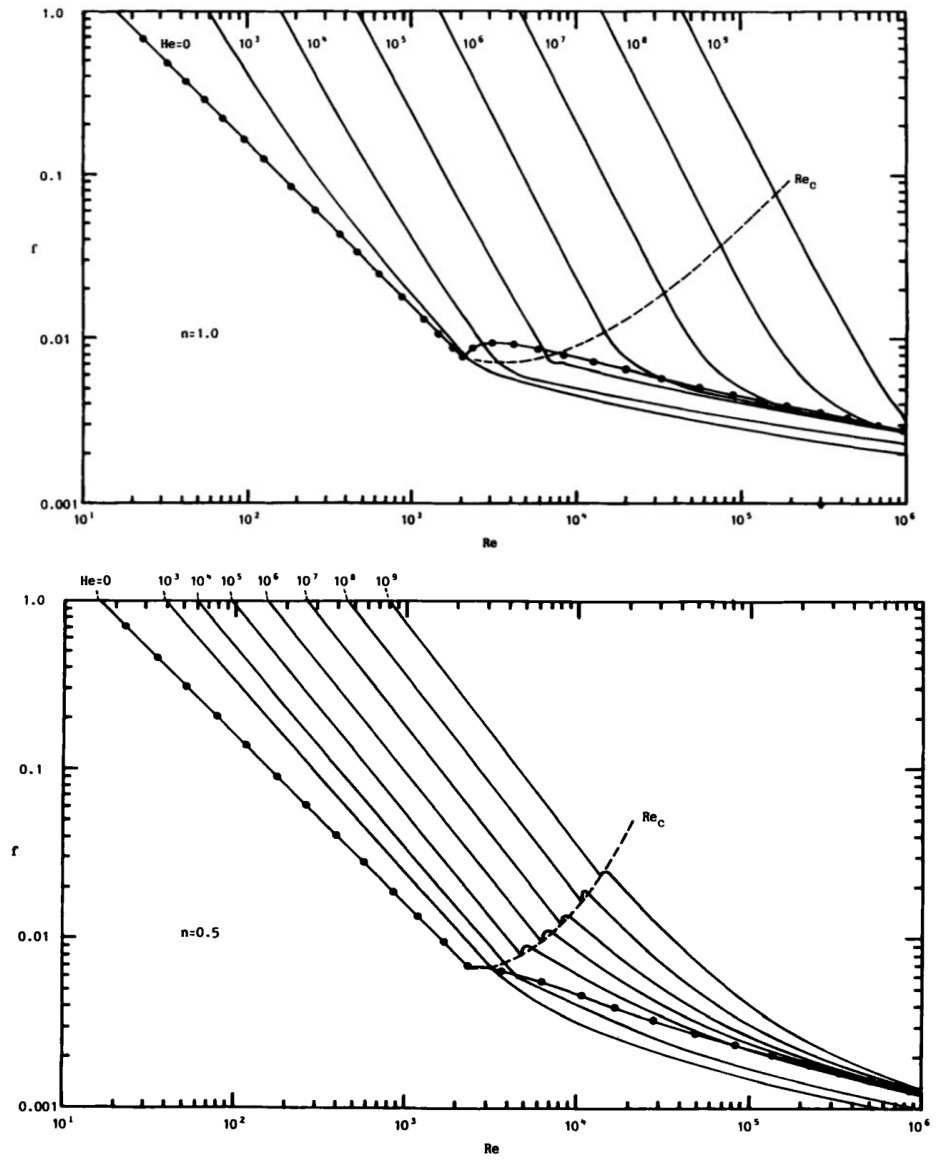

Fig. 7.4: Graphical representation of Hanks (1978) Equation. Top: Bingham fluid ($n = 1$), Bottom: Herschel-Bulkley fluid ($n = 0.5$). Obtained from Garcia and Steffe (1986)

Fig. 7.4 indicated that for laminar flow, higher He (higher τ_y) results in higher f compared to $He = 0$. For turbulent flow, $He < 10^4$ resulted in lower f and $He > 10^4$ results in higher f compared to $He = 0$. Maximum benefit in drag reduction in the turbulent regime is observed at $10^1 < He < 10^3$ compared to $He = 0$.

The lowest f is observed for turbulent flow regime of Herschel-Bulkley fluids with the lowest pipe roughness ϵ, $10^1 < He < 10^3$, and lower n values compared to Newtonian fluids.

7.3 NEW CALCULATIONS

Heavy O/W emulsions cannot be accurately modeled by a typical Herschel-Bulkley model. A combination of two Herschel-Bulkley models was necessary to accurately model the rheological property of heavy O/W emulsions (Chapter 5).

$$\tau = \tau_{y1} + k_1\dot{\gamma}^{n_1} + \left[\left(\tau_{y2} + k_2\dot{\gamma}^{n_2}\right) - \left(\tau_{y1} + k_1\dot{\gamma}^{n_1}\right)\right]\left(1 - e^{-\frac{\dot{\gamma}}{\dot{\gamma}_c}}\right) \quad (7.23)$$

where $\dot{\gamma}_c$ is the critical shear rate below which Herschel-Bulkley 1 model dominates and above which Herschel-Bulkley 2 model dominates. τ_{y1}, k_1, and n_1 represent the Herschel-Bulkley 1 model parameters for $\dot{\gamma} < \dot{\gamma}_c$. τ_{y2}, k_2, and n_2 represent the Herschel-Bulkley 2 model parameters for $\dot{\gamma} > \dot{\gamma}_c$. The velocity profile of fluids described by Eq. 7.23 has not been derived in the literature, but is necessary to calculate ∇P vs. v for laminar flow regime using Method 1. The solutions of Methods 1 and 2 are compared. Also, wall slip was included using the slip model for two-step yielding fluids (Chapter 5).

Laminar Flow Regime

Method 1

The analytical solution obtained by Stainsby et al. (1994) for Herschel-Bulkley fluids was modified to represent Eq.7.23. The velocity profile is given by:

$$V = V_{c1} + V_{c2}, \qquad 0 < r < r_{y1} \quad (7.24)$$

$$V = V_{c1}\left[1 - \left(\frac{r - r_{y1}}{r_{y2} - r_{y1}}\right)^{\left(\frac{n_1+1}{n_1}\right)}\right] + V_{c2}, \quad r_{y1} < r < r_{y2} \tag{7.25}$$

$$V = V_{c2}\left[1 - \left(\frac{r - r_{y2}}{R - r_{y2}}\right)^{\left(\frac{n_2+1}{n_2}\right)}\right], \quad r_{y2} < r < R \tag{7.26}$$

where r_{y1} is the radius of the plug core, r_{y2} the radius where the rheological model switches from Herschel-Bulkley 1 to Herschel-Bulkley 2, V_{c1} the velocity at $r = r_{y1}$, V_{c2} the velocity at $r = r_{y2}$, n_i the Herschel-Bulkley flow index, and V the velocity at r.

The r_{yi} values are given by the force balance between the yield stresses and pressure gradient:

$$r_{yi} = \frac{2\tau_{yi}}{dP/L} \tag{7.27}$$

The critical velocities, V_{ci} are given by:

$$V_{c1} = \left(-\frac{1dP}{2k_1 L}\right)^{1/n_1}\left(\frac{n_1}{n_1+1}\right)\left(r_{y2} - r_{y1}\right)^{\left(\frac{n_1+1}{n_1}\right)} \tag{7.28}$$

$$V_{c2} = \left(-\frac{1dP}{2k_2 L}\right)^{1/n_2}\left(\frac{n_2}{n_2+1}\right)\left(R - r_{y2}\right)^{\left(\frac{n_2+1}{n_2}\right)} \tag{7.29}$$

Eqs. 7.24-29 can be solve explicitly for constant ∇P at $0 \leq r \leq R$ to calculate the velocity profile of heavy O/W emulsions in a pipe ($V(r)\ vs. r$). Eqs. 7.24-26 can be numerically integrated with the cross-sectional pipe area to calculate the volumetric flow rate, Q, in a pipe at constant ∇P ($Q = 2\pi \int_0^R Vrdr$). The mean flow velocity in a pipe can be obtained with $v = Q/(\pi R^2)$.

Method 2

To obtain the Fanning friction factor using Eq. 7.12 ($f = 16/Re$), the Re value for the rheological model of heavy O/W emulsions (Eq. 7.23) must be estimated. Newtonian Re is defined as:

$$Re = \frac{\rho v D}{\mu_w} \tag{7.30}$$

where μ is the viscosity of the Newtonian fluid which is constant at any position of r. For non-Newtonian fluids, μ must be estimated at the pipe wall. Modifying Eq. 7.23 for viscosity at the pipe wall, the following expression is obtained:

$$\dot{\gamma}_w = \frac{8v}{D}\frac{3n'+1}{4n'} \tag{7.31}$$

$$\mu_w = \frac{\tau_w}{\dot{\gamma}_w} = \left[\tau_{y1} + k_1 \dot{\gamma}_w{}^{n_1} + \left[\left(\tau_{y2} + k_2 \dot{\gamma}_w{}^{n_2}\right) - \left(\tau_{y1} + k_1 \dot{\gamma}_w{}^{n_1}\right)\right]\left(1 - e^{-\frac{\dot{\gamma}_w}{\dot{\gamma}_c}}\right)\right] / \dot{\gamma}_w \tag{7.32}$$

Re for Herschel-Bulkley is obtained by substituting Eq. 7.32 into Eq. 7.30.

For $\tau_w < \tau_{y2}$

$$Re = \frac{8\rho v^2}{\tau_{y1} + k_1\left(\frac{8v}{D}\right)^{n_1}\left(\frac{3n'+1}{4n'}\right)^{n_1}}\left(\frac{3n'+1}{4n'}\right) \tag{7.33}$$

For $\tau_w > \tau_{y2}$

$$Re = \frac{8\rho v^2}{\tau_{y2} + k_2\left(\frac{8v}{D}\right)^{n_2}\left(\frac{3n'+1}{4n'}\right)^{n_2}}\left(\frac{3n'+1}{4n'}\right) \tag{7.34}$$

The n' value can be calculated with Eq. 7.15.

For a limiting case of $\tau_y = 0$, Eqs. 7.33-34 reduced to:

$$Re = \frac{\rho v^{2-n} D^n}{k(8)^{n-1}}\left(\frac{4n}{3n+1}\right)^{n-1} \tag{7.35}$$

Eq. 7.35 is not the same as the generalized Re_{DM} defined by Dodge and Metzner (1959) and Hanks (1978) for Power Law fluids. The generalized Re defined in Eq. 7.34 is related to Re_{DM} with the following expression:

$$Re = Re_{DM}\left(\frac{4n}{3n+1}\right)^{-1} \tag{7.36}$$

The Re_{DM} value is calculated according to $Re_{DM} = \rho v D/\mu$ where $\mu = \tau_w/\dot{\gamma}_{w,app}$. The shear rate $\dot{\gamma}_{w,app}$ is calculated with the assumption of Newtonian behavior. Thus, Re_{DM} value is not calculated with μ at the pipe wall. However, since experimental data presented in the literature review (Section 7.3) showed that $f = 16/Re_{DM}$ modeled the laminar flow regime very well, Eq. 7.12 is modified with the generalized Re defined in Eq. 7.34:

$$f = \frac{16}{Re}\left(\frac{3n'+1}{4n'}\right) \tag{7.37}$$

The validity of using Eq. 7.5 and Eq. 7.37 to relate $\nabla P\ vs.\ v$ (Method 2) is tested and compared to Method 1 in the next section for heavy O/W emulsions.

The effect of droplet migration on the $\nabla P\ vs.\ v$ relationship of heavy O/W emulsions are modeled using the equation proposed in Chapter 6:

$$\frac{\dot{\gamma}_w}{\dot{\gamma}_{w,dm}} = a\sqrt{\frac{\tau_w}{\rho}} \tag{7.38}$$

where $\dot{\gamma}_{w,dm}$ is the wall shear rate with droplet migration and a a fitting parameter. a can be calculated by measuring the rheological properties of heavy O/W emulsions with a rotational viscometer and a capillary tube viscometer at steady state.

Turbulent Flow Regime

Developing a $f\ vs.\ Re$ relationship for turbulent flow of heavy O/W emulsions, whose rheological properties are modeled by Eq. 7.23, is out of scope for this study. Because the heavy O/W emulsions show different velocity profiles compared to Herschel-Bulkley fluids, the method of calculating turbulent flow f proposed by Hanks (1978) for Herschel-Bulkley fluids may not be accurate. There exists no experimental data on the turbulent flow behavior of fluids that exhibit the rheological properties modeled by Eq. 7.23 in the literature to validate the accuracy of Hanks method or to propose a new relationship. The trends observed with the graphical representation of Hanks method (Fig. 7.4) can be used qualitatively to estimate whether turbulent flow $f\ vs.\ Re$ of heavy O/W emulsions may be closer to the f of laminar flow regime (lower limit of f) or the Newtonian turbulent regime (upper limit of f).

Heavy O/W emulsions may also show further drag-reducing behavior in turbulent flow regime as well as a higher Re at which laminar flow ends compared to Newtonian or Herschel-Bulkley fluids. Studies in the literature showed that a very low quantity of high molecular weight polymers (polyacrylamide, xanthan gum, etc) [Virk (1975)], long fibres

[Lee and Duffy (1976)], and surfactants [Zakin et al. (2011), (2003)] helped reduce the turbulence inside pipes, leading to lower f than expected in the turbulent flow regime. While the mechanism of drag reduction is not clear in the literature, a common structural theme for additives that show good drag reducing behavior is a larger aspect ratio of the additives (defined as the ratio of structure length to diameter) [Zakin et al. (2003)].

Virk (1975) came up with the concept of maximum drag reduction (MDR) possible with large polymer drag reducers based on experimental data. However, MDR below the Virk limit can be achieved with surfactant additives [Zakin et al. (1996)], suggesting the MDR limit is specific to the type of drag reducing additives. Pal (2007) and Omer and Pal (2013) studied the drag reduction phenomena of dispersions such as O/W emulsions, W/O emulsions, and bubbly suspensions. Both found that unstable emulsions with large droplet size showed a significant drag reduction capability and delay in laminar to turbulent transition, while surfactant stabilized emulsions with small droplet size showed a negligible drag reduction capability under turbulent flow conditions. Collins and Knudsen (1970) observed visually that large oil droplets elongate at the pipe wall (Fig. 7.5). The droplet deformation lead to a larger aspect ratio of the droplets (L/D as large or larger than 4), showing a similar structure compared to the traditional drag reducing additives such as polymers and surfactants that form thread-like cylindrical micelles under shear [Omer and Pal (2013); Pal (2007)].

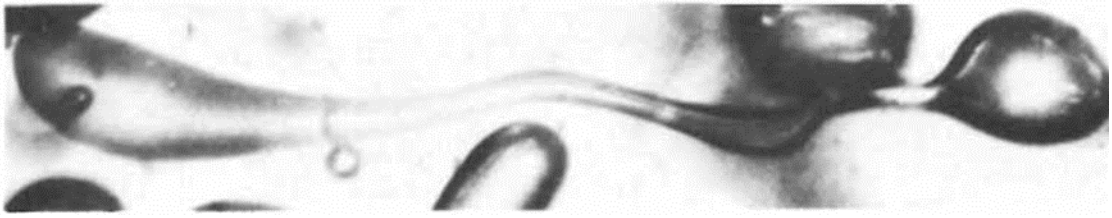

Fig. 7.5: Elongated oil droplet under shear. Obtained from Collins and Knudsen (1970)

While heavy O/W emulsions studied in our experiments show relatively small droplet size, the attraction induced aggregate structures of droplets may still be present within the range of shear rates in the pipelines. The aggregate structures may satisfy the large aspect ratio criteria of effective drag reducing additives. Aggregating suspensions such as aggregating dilute clay suspensions [Gust (1976)] have shown drag reduction behavior in the literature. Drag reduction behavior is observed with clay suspensions that formed aggregate clay structures but not with repulsive clay particles.

7.4 RESULTS AND DISCUSSION

7.4.1 Turbulent Flow Experiment

A turbulent flow experiment was conducted to observe whether heavy O/W emulsions show drag reduction capabilities. A capillary tube viscometer (L=0.15cm) was used in this turbulent flow experiment with 40% oil A emulsion. Higher oil concentration emulsions could not be measured because of the emulsions' high viscosity, which prevented turbulent regime flow rates from being achieved in the laboratory. The measurements were not corrected for entrance and exit effects and steady-state flow profiles were assumed to be achieve in the tube. The dimensions of the tube and the emulsion composition are listed in Table 7.1.

Table 7.1: Tube dimensions and emulsion composition

Capillary Tube		*Emulsion Composition*	
Diameter (mm)	1.397	*Oil volume (%)*	40% Oil A
Length (m)	0.1524	*Aqueous volume (%)*	60%
Area (m^2)	1.53×10^{-6}	*Aqueous composition (wt. %)*	1.6% Ph15EO 0.2% NaOH 0.8% NaCl

The pressure drops measured within the tube for each flow rate are listed in Table 7.2. Because of the limited pumping power, emulsion flow rate was limited to Re of

3,350. The viscosities of water and emulsion were calculated based on the laminar flow $\nabla P\ vs.\ v$. Emulsion viscosities of ~4cP was calculated for all the flow rates in the laminar regime, implying Newtonian flow behavior at high shear rates.

Table 7.2: Flow properties of water and 40% O/W emulsion in laminar and turbulent flow regimes.

DI Water at 25 °C (~0.95 cP)					40% oil A emulsion at 25 °C (~4 cP)				
v (m/s)	dP/L (Pa)	$\dot{\gamma}\ (s^{-1})$	Re	f	*v* (m/s)	dP/L (Pa)	$\dot{\gamma}\ (s^{-1})$	Re	f
0.2718	861.84	1557	395.6	0.0539	1.0728	9997.40	6144	374.7	0.0401
0.3262	1241.06	1868	474.7	0.0539	1.5983	14823.73	9153	558.2	0.0268
0.7502	1654.74	4296	1091.8	0.0136	2.0876	18960.58	11955	729.1	0.0201
0.9024	1999.48	5168	1313.3	0.0113	2.6748	23993.76	15318	934.2	0.0155
1.0873	2344.22	6227	1582.3	0.0092	3.2185	29371.67	18431	1124.1	0.0131
1.2178	2688.96	6974	1772.2	0.0084	3.6860	36404.32	21109	1287.4	0.0124
1.3646	3102.64	7814	1985.8	0.0077	4.3058	46539.61	24658	1503.8	0.0116
1.4896	3930.01	8531	2167.8	0.0082	5.5671	57226.49	31881	1944.3	0.0085
1.6527	5860.54	9465	2405.1	0.0099	6.5240	68258.10	37360	2278.5	0.0074
1.7941	7308.44	10274	2610.8	0.0105	7.4374	79289.71	42591	2597.5	0.0066
1.9463	8549.50	11145	2832.3	0.0104	8.0898	88942.37	46327	2825.4	0.0063
2.0659	9514.77	11831	3006.4	0.0103	8.3507	110316.12	47821	2916.5	0.0073
2.1746	10824.77	12453	3164.6	0.0106	9.5903	134447.77	54920	3349.4	0.0068
2.5443	14616.89	14571	3702.6	0.0104					
3.1315	21787.43	17933	4557.1	0.0103					
3.7622	30957.46	21544	5474.8	0.0101					
4.4798	41506.44	25654	6519.1	0.0096					
5.2192	55295.95	29888	7595.1	0.0094					
5.6759	64190.19	32503	8259.7	0.0092					

The $\nabla P\ vs.\ v$ data for water was used to measure the tube roughness as well as to test the accuracy of the turbulent flow setup. Based on the water flow experiment, absolute tube roughness of 4.6×10^{-9}m was measured for the stainless steel tube. The $f\ vs.\ Re$ was calculated from the $\nabla P\ vs.\ v$ data in Table 7.2 and plotted in Fig. 7.6.

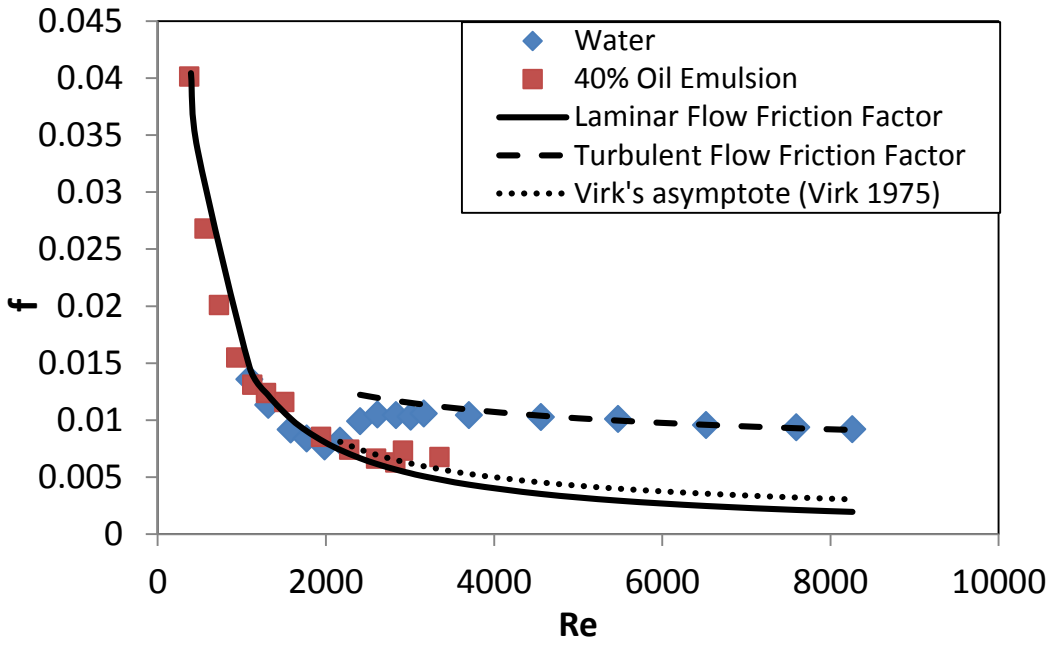

Fig. 7.6: Fanning friction factor vs. *Re* of water and 40% oil A emulsion. Solid line represents the laminar flow friction factor predicted for Newtonian fluids. Uniform dashed line represents the turbulent flow friction factor predicted using the Colebrook-While equation. Dot dashed line represents the maximum drag reduction asymptote predicted using the Virk (1975) equation.

The water $f\ vs. Re$ data showed the typical behavior for water. Laminar flow regime ended at $Re = \sim 2{,}100$ and full turbulent flow is observed at $Re = \sim 4{,}000$. 40% oil A emulsion showed delayed end to the laminar flow regime with possible drag reducing behavior observed as lower f value at $Re > 3{,}000$ compared to water data. The benefits of lower emulsion f in turbulent conditions are apparent from Fig. 7.7.

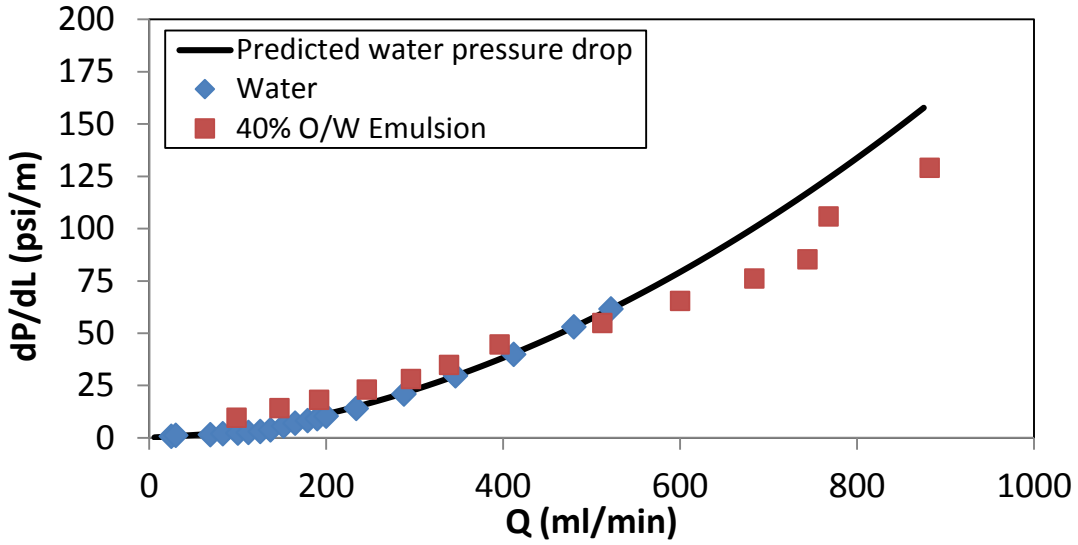

Fig. 7.7: $\nabla P\ vs. Q$ of water and 40% O/W emulsion. Colebrook-White equation was used to predict the water pressure gradient in turbulent conditions.

The lower f for 40% O/W emulsion in turbulent conditions resulted in lower ∇P for the emulsion compared to water at high flow rates. The lower ∇P of the emulsion occurred in spite of the emulsion viscosity being four times larger than the water viscosity. The turbulent flow experiment showed the benefits of the drag reduction potential of heavy O/W emulsions if tube flow conditions are in the turbulent regime.

7.4.2 Velocity Profile of Heavy O/W Emulsions

The steady-state, laminar flow velocity profiles of heavy oil emulsions were calculated according to the rheological model (Eq. 7.23). The model was fitted to the emulsion viscosity data measured with the rotational viscometer. Eqs. 7.24-29 were used to generate the $V(r)\ vs. r$ at constant ∇P values. Both cases of slip and no-slip flow of heavy O/W emulsions are investigated. Wall slip was modeled using the slip equation introduced in Chapter 5. Table 7.3 shows the rheological and wall slip model parameters of emulsions used to up-scale to crude oil pipeline dimensions.

Table 7.3: Rheological and wall slip modeling parameters of heavy O/W emulsions

Sample #	Oil	Oil Conc. (%)	Aqueous Composition (wt. %)	Rheological Properties				Wall Slip Properties				Droplet migration
				k_1, k_2 $(Pa\ s^n)$	n_1, n_2	τ_{y1}, τ_{y2} (Pa)	$\dot{\gamma}_c$ (s^{-1})	$\tau_{y1}, \tau_{y2S},$ $\tau_{y2E,}\ \tau_{sy} (Pa)$	V_1^*, V_2^* $(\mu m/s)$	C	E	a
A1	A	80%	1.6% Ph15EO 0.2% NaOH 0.8% NaCl	$k_1 = 10.53$ $k_2 = 3.8$	$n_1 = 0.5$ $n_2 = 0.67$	$\tau_{y1} = 0.53$ $\tau_{y2} = 6.2$	$\dot{\gamma}_c = 0.33$	$\tau_{y1} = 0.5$ $\tau_{y2S} = 2.5$ $\tau_{y2E} = 6.2$ $\tau_{sy} = 0.15$	$V_1^* = 0.65$ $V_2^* = 1500$	$C = 0.96$	$E = 6$	$a = 0.4$
B1	B	75%	1.6% Ph15EO 0.4% NaOH 0.8% NaCl	$k_1 = 0.34$ $k_2 = 0.26$	$n_1 = 0.5$ $n_2 = 1.0$	$\tau_{y1} = 0.008$ $\tau_{y2} = 1.5$	$\dot{\gamma}_c = 3.3$	$\tau_{y1} = 0.008$ $\tau_{y2S} = 0.6$ $\tau_{y2E} = 1.5$ $\tau_{sy} = 0$	$V_1^* = 4$ $V_2^* = 450$	$C = 0.25$	$E = 6$	
B2	B	80%	1.6% Ph15EO 0.2% NaOH 0.8% NaCl	$k_1 = 3.17$ $k_2 = 1.35$	$n_1 = 0.5$ $n_2 = 0.95$	$\tau_{y1} = 0.02$ $\tau_{y2} = 5.25$	$\dot{\gamma}_c = 0.84$	$\tau_{y1} = 0.02$ $\tau_{y2S} = 2.1$ $\tau_{y2E} = 5.25$ $\tau_{sy} = 0$	$V_1^* = 0.25$ $V_2^* = 1375$	$C = 0.8$	$E = 2$	$a = 0.4$
B3	B	80%	1.6% Ph15EO 0.2% NaOH 1.4% NaCl	$k_1 = 1.08$ $k_2 = 1.93$	$n_1 = 0.5$ $n_2 = 0.74$	$\tau_{y1} = 0.017$ $\tau_{y2} = 2.8$	$\dot{\gamma}_c = 0.8$	$\tau_{y1} = 0.017$ $\tau_{y2S} = 0.6$ $\tau_{y2E} = 2.8$ $\tau_{sy} = 0$	$V_1^* = 0.25$ $V_2^* = 275$	$C = 0.43$	$E = 6$	$a = 1.8$
D1	D	40%	1.6% Ph15EO 0.2% NaOH 0% NaCl	$k_1 = 0.2$ $k_2 = 0.15$	$n_1 = 0.5$ $n_2 = 0.51$	$\tau_{y1} = 0.05$ $\tau_{y2} = 0$	$\dot{\gamma}_c = 0.86$	$\tau_{y1} = 0.05$ $\tau_{y2S} = 0$ $\tau_{y2E} = 0$ $\tau_{sy} = 0.005$	$V_1^* = 42$ $V_2^* = 0$	$C = 0$	$E = 1$	
D2	D	50%	1.6% Ph15EO 0.2% NaOH 0% NaCl	$k_1 = 0.25$ $k_2 = 0.15$	$n_1 = 0.5$ $n_2 = 0.74$	$\tau_{y1} = 0.09$ $\tau_{y2} = 0.41$	$\dot{\gamma}_c = 1.22$	$\tau_{y1} = 0.09$ $\tau_{y2S} = 0$ $\tau_{y2E} = 0$ $\tau_{sy} = 0.005$	$V_1^* = 50$ $V_2^* = 0$	$C = NA$	$E = 1$	
D3	D	60%	1.6% Ph15EO 0.2% NaOH 0% NaCl	$k_1 = 0.76$ $k_2 = 0.65$	$n_1 = 0.5$ $n_2 = 0.86$	$\tau_{y1} = 0.19$ $\tau_{y2} = 1.9$	$\dot{\gamma}_c = 1.5$	$\tau_{y1} = 0.194$ $\tau_{y2S} = 0.76$ $\tau_{y2E} = 1.9$ $\tau_{sy} = 0.013$	$V_1^* = 10$ $V_2^* = 400$	$C = 0.43$	$E = 6$	
D4	D	70%	1.6% Ph15EO 0.2% NaOH 0% NaCl	$k_1 = 7.9$ $k_2 = 3.25$	$n_1 = 0.5$ $n_2 = 0.71$	$\tau_{y1} = 1.19$ $\tau_{y2} = 13$	$\dot{\gamma}_c = 9$	$\tau_{y1} = 1.19$ $\tau_{y2S} = 5.2$ $\tau_{y2E} = 13$ $\tau_{sy} = 0$	$V_1^* = 6.5$ $V_2^* = 1750$	$C = 0.75$	$E = 6$	
D5	D	80%	1.6% Ph15EO 0.2% NaOH 0% NaCl	$k_1 = 18.25$ $k_2 = 2.3$	$n_1 = 0.5$ $n_2 = 0.93$	$\tau_{y1} = 4$ $\tau_{y2} = 33$	$\dot{\gamma}_c = 15$	$\tau_{y1} = 4$ $\tau_{y2S} = 13.2$ $\tau_{y2E} = 33$ $\tau_{sy} = 0.2$	$V_1^* = 9$ $V_2^* = 1900$	$C = 0.8$	$E = 6$	
D6	D	85%	1.6% Ph15EO 0.2% NaOH 0% NaCl	$k_1 = 25.3$ $k_2 = 2.17$	$n_1 = 0.5$ $n_2 = 1$	$\tau_{y1} = 6.0$ $\tau_{y2} = 50$	$\dot{\gamma}_c = 16.7$	$\tau_{y1} = 6.0$ $\tau_{y2S} = 18.8$ $\tau_{y2E} = 50$ $\tau_{sy} = 0$	$V_1^* = 6$ $V_2^* = 1400$	$C = 0.725$	$E = 6$	
D7	D	40%	1.6% Ph15EO 0.2% NaOH 1% NaCl	$k_1 = 0.0075$ $k_2 = 0.011$	$n_1 = 0.5$ $n_2 = 0.83$	$\tau_{y1} = 0$ $\tau_{y2} = 0.06$	$\dot{\gamma}_c = 17$	$\tau_{y1} = 0$ $\tau_{y2S} = 0$ $\tau_{y2E} = 0$ $\tau_{sy} = 0$	$V_1^* = 0$ $V_2^* = 0$	$C = NA$	$E = 1$	$a = 54$

Table 7.3 continued.

D8	D	50%	1.6% Ph15EO 0.2% NaOH 1% NaCl	$k_1 = 0.012$ $k_2 = 0.02$	$n_1 = 0.5$ $n_2 = 0.88$	$\tau_{y1} = 0$ $\tau_{y2} = 0.03$	$\dot{\gamma}_c = 0.33$	$\tau_{y1} = 0$ $\tau_{y2S} = 0$ $\tau_{y2E} = 0$ $\tau_{sy} = 0$	$V_1^* = 0$ $V_2^* = 0$	$C = NA$	$E = 1$	
D9	D	60%	1.6% Ph15EO 0.2% NaOH 1% NaCl	$k_1 = 0.11$ $k_2 = 0.05$	$n_1 = 0.5$ $n_2 = 1$	$\tau_{y1} = 0.01$ $\tau_{y2} = 0.11$	$\dot{\gamma}_c = 0.09$	$\tau_{y1} = 0.01$ $\tau_{y2S} = 0.12$ $\tau_{y2E} = 0.3$ $\tau_{sy} = 0.002$	$V_1^* = 1$ $V_2^* = 1500$	$C = NA$	$E = 6$	$a = 6$
D10	D	70%	1.6% Ph15EO 0.2% NaOH 1% NaCl	$k_1 = 0.19$ $k_2 = 0.45$	$n_1 = 0.5$ $n_2 = 0.7$	$\tau_{y1} = 0.005$ $\tau_{y2} = 0.3$	$\dot{\gamma}_c = 0.22$	$\tau_{y1} = 0.005$ $\tau_{y2S} = 0.12$ $\tau_{y2E} = 0.3$ $\tau_{sy} = 0$	$V_1^* = 0.75$ $V_2^* = 75$	$C = 0.42$	$E = 6$	
D11	D	80%	1.6% Ph15EO 0.2% NaOH 1% NaCl	$k_1 = 1.4$ $k_2 = 1.4$	$n_1 = 0.5$ $n_2 = 0.83$	$\tau_{y1} = 0.07$ $\tau_{y2} = 3$	$\dot{\gamma}_c = 0.62$	$\tau_{y1} = 0.07$ $\tau_{y2S} = 1.2$ $\tau_{y2E} = 3$ $\tau_{sy} = 0$	$V_1^* = 0.65$ $V_2^* = 550$	$C = 0.66$	$E = 6$	$a = 0.4$
D12	D	85%	1.6% Ph15EO 0.2% NaOH 1% NaCl	$k_1 = 5$ $k_2 = 3.54$	$n_1 = 0.5$ $n_2 = 0.82$	$\tau_{y1} = 0.55$ $\tau_{y2} = 6.5$	$\dot{\gamma}_c = 0.9$	$\tau_{y1} = 0.55$ $\tau_{y2S} = 2.6$ $\tau_{y2E} = 6.5$ $\tau_{sy} = 0$	$V_1^* = 3$ $V_2^* = 750$	$C = 0.74$	$E = 6$	

Rheological and wall slip model parameters of emulsion A1 from Table 7.3 are used to generate the velocity profiles in a pipe of D=0.6 m (Fig.7.8).

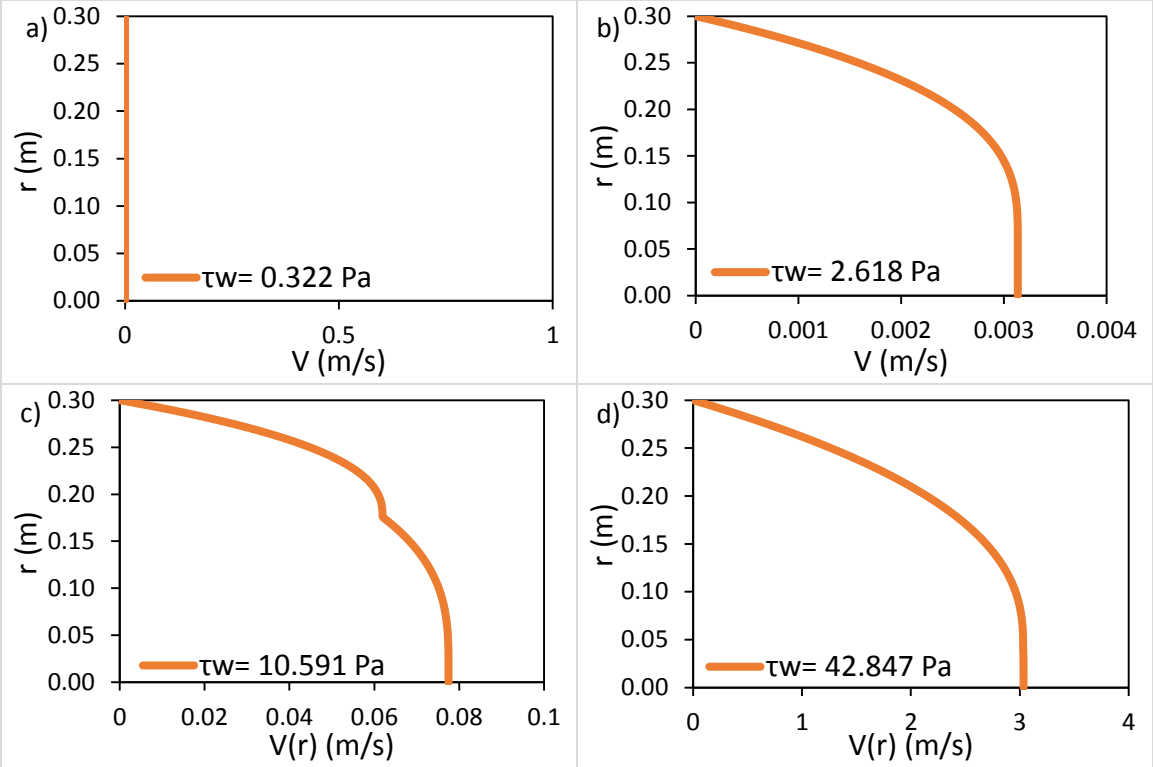

Fig. 7.8: Velocity profiles of emulsion A1 in a pipe with no wall slip (D=0.60m): a) $\tau_w < \tau_{y1}$, b) $\tau_{y1} < \tau_w < \tau_{y2}$, c) $\tau_w > \tau_{y2}$, and d) $\tau_w \gg \tau_{y2}$. See Table 7.3 for emulsion properties τ_{y1} and τ_{y2}.

The steady-state, laminar flow velocity profiles of concentrated heavy O/W emulsions transitioned through four distinct velocity profile regimes in a pipe with no wall slip. *Regime I* describes no observable flow in a pipe at $\tau_w < \tau_{y1}$, which is common for yield stress fluids (Fig. 7.8a). *Regime II* describes a typical Herschel-Bulkley fluid velocity profile in a pipe observed at $\tau_{y1} < \tau_w < \tau_{y2}$ (Fig. 7.8b). *Regime III* describes a velocity profile that is a combination of two Herschel-Bulkley models (Fig. 7.8c-d). In *Regime III*, $\tau_{y1} < \tau_w < \tau_{y2}$ is observed at $0 < r < r_{y2}$ (Herschel-Bulkley 1) and $\tau_w > \tau_{y2}$ is observed at $r_{y2} < r < R$ (Herschel-Bulkley 2), with the model transitioning from Herschel-Bulkley 1 and Herschel-Bulkley 2 at a critical shear rate, $\dot{\gamma}_c(r_{y2})$. *Regime IV* describes a velocity profile at $\tau_w \gg \tau_{y2}$ that can be approximated as a Herschel-Bulkley

fluid velocity profile. The contribution of Herschel-Bulkley 1 modeling properties to $V(r)$ is negligible at $\tau_w \gg \tau_{y2}$. The four *Regimes* describe the velocity profiles of concentrated heavy O/W emulsions in a pipe modeled using Eq. 7.23.

The presence of wall slip can complicate the velocity profiles of concentrated heavy O/W emulsions in a pipe.

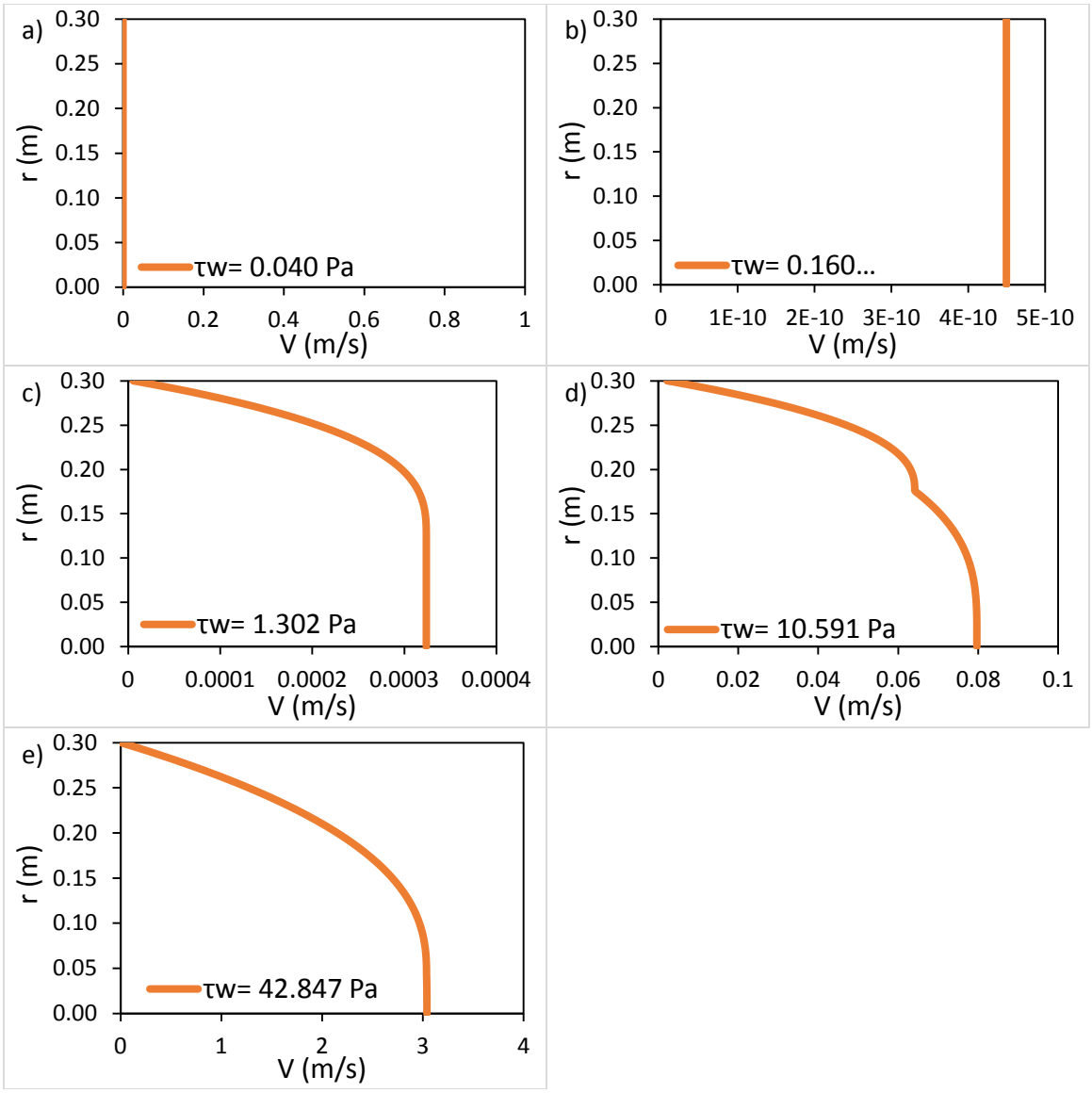

Fig. 7.9: Velocity profiles of emulsion A1 in a pipe with wall slip (D=0.60m): a) $\tau_w < \tau_{sy}$, b) $\tau_{sy} < \tau_w < \tau_{y1}$,c) $\tau_{y1} < \tau_w < \tau_{y2}$, d) $\tau_w > \tau_{y2}$, and e) $\tau_w \gg \tau_{y2}$. See Table 7.3 for emulsion A1 properties τ_{sy}, τ_{y1}, and τ_{y2}.

The laminar flow velocity profiles of concentrated heavy O/W emulsions transitioned through five distinct velocity profile regimes in a pipe with wall slip. *Slip Regime I* describes no observable flow in a pipe at $\tau_w < \tau_{sy}$ where τ_{sy} is the slip yield stress defined in Chapter 5. *Slip Regime II* describes a velocity profile of the total slip of an

emulsion in a pipe at $\tau_{sy} < \tau_w < \tau_{y1}$ (Fig. 7.9b). This flow regime does not occur if $\tau_{y1} < \tau_{sy}$. *Slip Regime III* describes a typical Herschel-Bulkley fluid velocity profile with wall slip in a pipe observed at $\tau_{y1} < \tau_w < \tau_{y2}$ (Fig. 7.9c). *Slip Regime IV* describes a velocity profile that is a combination of two Herschel-Bulkley models with wall slip (Fig. 7.9d). In *Slip regime IV*, $\tau_{y1} < \tau_w < \tau_{y2}$ is observed at $0 < r < r_{y2}$ (Herschel-Bulkley 1) and $\tau_w > \tau_{y2}$ is observed at $r_{y2} < r < R$ (Herschel-Bulkley 2), with the model transitioning from Herschel-Bulkley 1 to Herschel-Bulkley 2 at a critical shear rate, $\dot{\gamma}_c(r_{y2})$. Wall slip is significant at τ_w just above τ_{y2} (Fig. 7.9d) and slip becomes increasingly negligible as $\tau_w \gg \tau_{y2}$ (Fig. 7.9e). *Slip Regime V* describes a velocity profile at $\tau_w \gg \tau_{y2}$ that can be approximated as a Herschel-Bulkley fluid velocity profile. The contribution of Herschel-Bulkley 1 model properties to $V(r)$ is negligible at $\tau_w \gg \tau_{y2}$. The five *Slip Regimes* describe the velocity profiles of concentrated heavy O/W emulsions with wall slip in a pipe modeled using Eq. 7.23 (rheological properties) and Eq. 5.15 (wall slip properties).

The pipe velocity profiles of two-step yielding fluids, such as concentrated heavy O/W emulsions, in a steady-state laminar flow has not been described in the literature. The pipe velocity profile is based on the rotational viscometer data with no droplet migration. Since droplet migration takes some distance L_{SS} to reach steady state, the flow velocity profiles in Figs. 7.8-9 are good representations of flow start up in pipelines. Once steady state flow is achieved with droplet migration, the flow velocity profiles are different compared to Figs. 7.8-9. Droplet migration has been shown to modify the velocity profile to be more blunted similar to Herschel-Bulkley fluids [Gillies and Shook (1992)]. With droplet migration, the flow velocity profiles in Figs. 7.8-9 would look as if the heavy O/W emulsion possessed higher τ_y and lower n values. Experimental

measurements of the pipe velocity profiles of the emulsions are still needed to verify the velocity profiles in Figs. 7.8-9 and velocity profiles with droplet migration in pipes.

7.4.3 Pipe Pressure Gradient vs. Flow Rate

Laminar Flow

The integration of velocity profiles (Method 1) and using Re along with Eq. 7.37 (Method 2) to calculate $\nabla P\ vs.\ Q$ showed similar results (Section 7.3). Less than 5% error was observed for almost all samples tested as well as for all flow rates between the two methods. This verified the accuracy of the derived pipe velocity profiles as well as the new f equation for laminar flow. Either method can be used to calculate the $\nabla P\ vs.\ Q$ relationship for laminar flow of heavy O/W emulsions in a pipe. For emulsion samples that were measured using both a rotational viscometer and a capillary tube viscometer, the effect of droplet migration is added using Eq. 7.38.

Turbulent Flow

Accurate quantitative estimation of $\nabla P\ vs.\ Q$ for the heavy O/W emulsions are out of scope and capabilities of this study. The lower and upper limits of $\nabla P\ vs.\ Q$ in turbulent flow ($Re > 2{,}500$) are calculated using a laminar flow assumption with no turbulence and the Colebrook-White equation, respectively. Most concentrated heavy O/W emulsions show rheological properties of $0.5 < [n_1, n_2] < 0.8$ and $He < 10^3$. According to the Moody Diagram of Herschel-Bulkley fluids (Fig. 7.4) and the drag reduction capability of heavy O/W emulsions, the $\nabla P\ vs.\ Q$ relationship in the turbulent flow regime can be estimated to be closer to either the calculated upper or lower limit.

The limiting variable for pipeline operations is the maximum achievable ∇P. ∇P of most pipelines is controlled by the burst pressure of the pipeline, which is ~1,000-1400

psi, and the distance between the pump stations, which is ~50-100 miles. This results in a maximum ∇P of 10-25 psi/mile.

7.4.4 Effect of Pipe Radius on Pressure Gradient vs. Flow Rate

The radii of pipelines have a significant effect on the $\nabla P\ vs.\ Q$ of emulsions. 75% (B1) and 80% (B2) oil B emulsions from Table 7.3 are used in the sensitivity analysis of a pipe radius on the $\nabla P\ vs.\ Q$ of heavy O/W emulsions. The 75% oil B emulsion (B1) analysis is shown in Fig. 7.10. Droplet migration effect was not included in the calculations and wall slip had a negligible effect except for $\tau_{sy} < \tau_w < \tau_{y1}$.

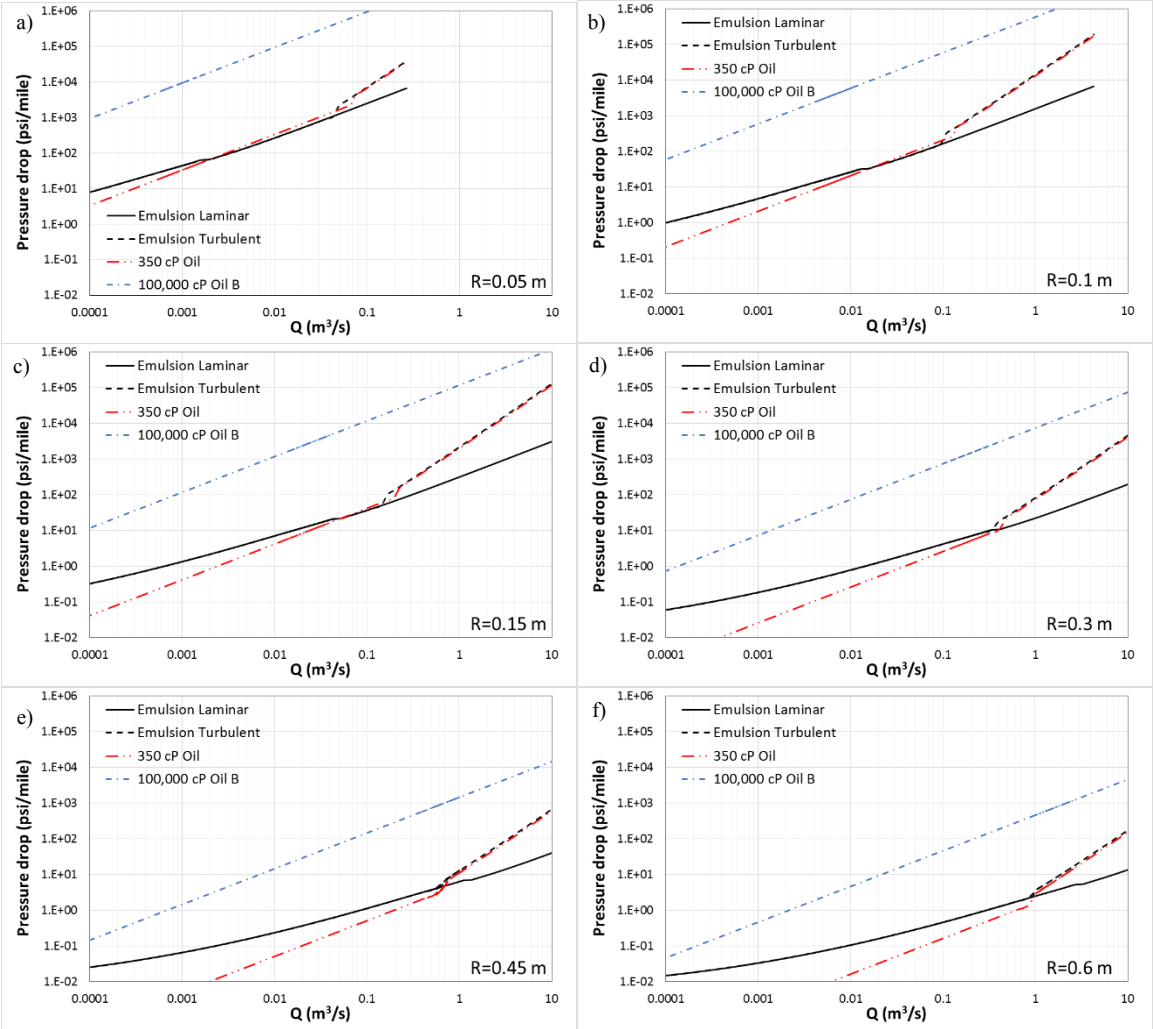

Fig. 7.10: Effect of pipe radius on ∇P $vs.$ Q of 75% Oil B emulsion (B1 from Table 7.3) at 23°C. a) R=0.05m, b) R=0.1m, c) R=0.15m, d) R=0.3m, e) R=0.45m, f) R=0.6m. Blue dashed line represents the oil B. Red dashed line represents the 350 cP reference oil. Black line represents the emulsion laminar flow. Black dashed line represents the emulsion turbulent flow assuming Newtonian behavior.

75% oil B emulsion showed significantly lower ∇P compared to heavy oil B at constant flow rates. Approximately 10-1,000 times lower ∇P are observed for the 75% oil B emulsion compared to oil B. The ∇P of 75% oil B emulsions is compared to the ∇P of 350 cP reference crude oil with a maximum operable pipeline ∇P of ~10-25 psi/mile.

1. For $R < 0.1\ m$ (Gathering lines)
    a. ∇P of 75% oil B emulsion is higher at all flow rates.

b. The maximum flow rate of 75% oil B emulsion is lower than 350 cP oil.

2. $0.15\ m < R < 0.3\ m$ (medium pipelines)
    a. At low flow rates, the ∇P of 75% oil B emulsion is higher.
    b. At moderate to high flow rates, comparable ∇P of 75% oil B emulsion is observed at 10-30 psi/mile, which is below the maximum achievable ∇P.
    c. The maximum flow rate of 75% oil B emulsion is comparable to the 350 cP oil.
3. $0.3\ m < R < 0.6\ m$ (major pipelines)
    a. At low flow rates, the ∇P of 75% oil B emulsion is significantly higher.
    b. At moderate flow rates, the ∇P of 75% oil B emulsion is slight higher or comparable.
    c. At high flow rates ($5 < \nabla P < 30\ psi/mile$), turbulent flow conditions emerge and the ∇P of 75% oil B emulsion is comparable if not lower than the 350 cP oil. The ∇P of 75% oil B emulsion in turbulent flow conditions can be found between the laminar flow curve (lower limit of ∇P) and the turbulent flow curve (upper limit of ∇P). The exact ∇P is a function of the drag reduction capability and the non-Newtonian properties of the emulsion.

For 75% Oil B emulsion (B1), very significant ∇P reductions are observed compared to heavy oil B at all pipe dimensions studied. Similar flow rates of 75% oil B emulsion are achieved compared to the 350 cP oil in laminar flow conditions for $R > 0.1\ m$. However, at low flow rates, higher ∇P are needed to transport the emulsion compared to the 350 cP oil. These ∇P are still below the maximum pipeline operating ∇P. For pipelines with large radii, higher flow rates for 75% oil B emulsion could be achieve because of the drag reduction potential of the emulsion compared to the reference oil.

The greatest benefit of transporting 75% oil B emulsion can be observed in major pipelines with $R > 0.3\ m$ operating at high flow rates compared to 350 cP oil.

75% oil B emulsion (B1) can be transported in existing crude oil pipelines (maximum transport fluid viscosity of ~350 cP) of $0.1\ m < R < 0.6\ m$. However, at low flow rates, higher utility costs are necessary to generate the extra pumping power necessary to transport the emulsion compared to the 350 cP oil.

Sensitivity analysis of different pipe radii using 80% oil B emulsion (B2) is shown in Fig. 7.11. The $\nabla P\ vs.\ Q$ of the emulsion with droplet migration effect is represented by green lines.

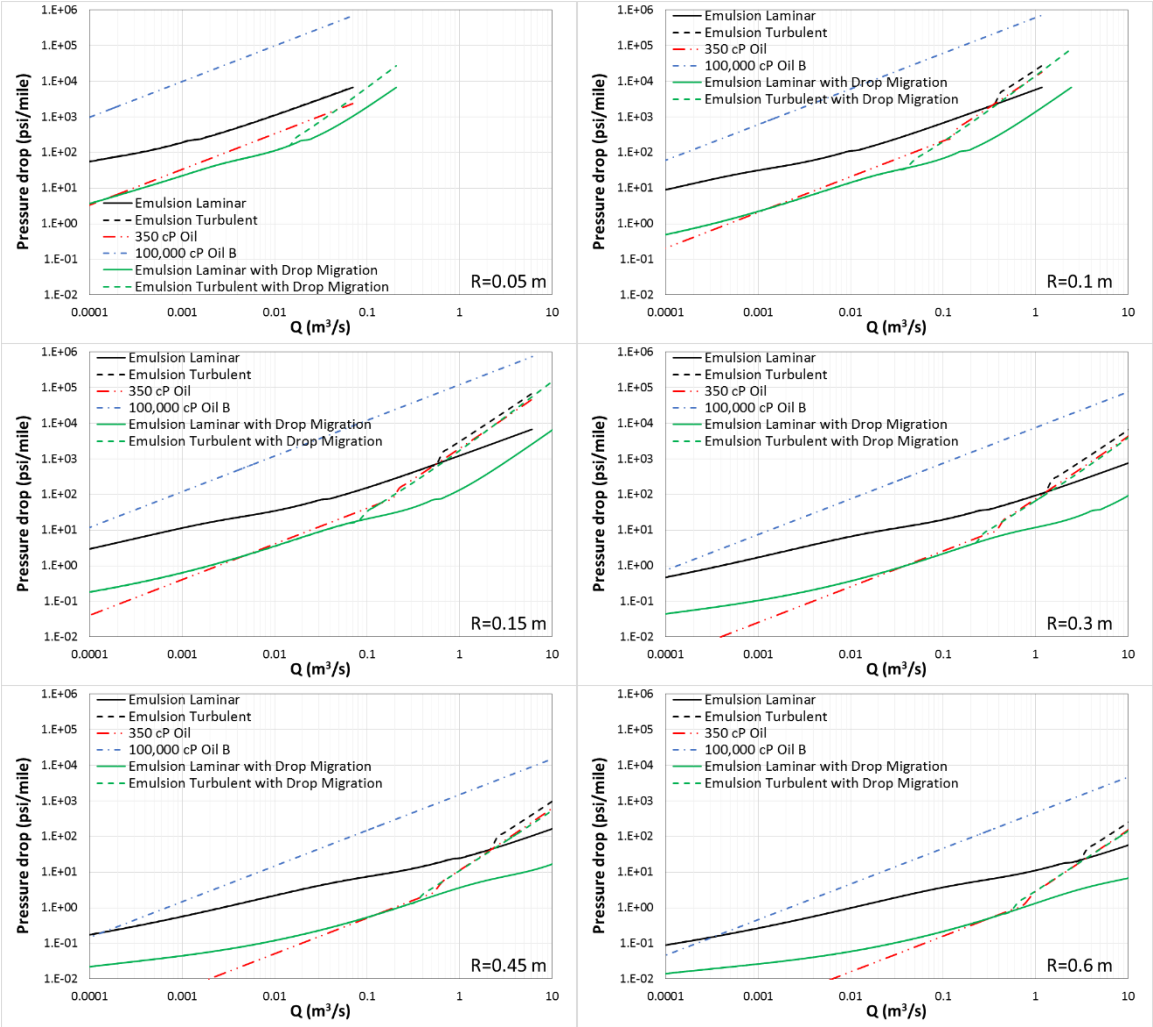

Fig. 7.11: Effect of pipe radius on $\nabla P\ vs. Q$ of 80% Oil B emulsion (B2 from Table 7.3) at 23°C. a) R=0.05m, b) R=0.1m, c) R=0.15m, d) R=0.3m, e) R=0.45m, f) R=0.6m. Blue dashed line represents the oil B. Red dashed line represents the 350 cP reference oil. Black line represents the emulsion laminar flow. Black dashed line represents the emulsion turbulent flow assuming Newtonian behavior. Green line represents the emulsion laminar flow with drop migration. Green dashed line represents the emulsions turbulent flow with drop migration.

The $\nabla P\ vs. Q$ profiles of 80% oil B emulsion (B2) without droplet migration are very similar to the profiles of 75% oil B emulsion (B1) shown in Fig. 7.10 but with higher ∇P. Compared to oil B, 10-100 times lower ∇P are observed for 80% oil B emulsion. Compared to the 350 cP reference oil, 80% oil B emulsion with no droplet migration

showed significantly higher ∇P for pipelines with any R (black lines in Fig. 7.11). With no droplet migration, optimized 75% oil B emulsion is the limit of emulsion pipeline transport and 80% oil B emulsion cannot be transported in pipelines economically. However, 80% oil B emulsion with droplet migration (green lines in Fig. 7.11) showed up to 10 times lower ∇P compared to the emulsion with no droplet migration (black lines in Fig. 7.11). 80% Oil B emulsion (B2) with steady state droplet migration can be successfully transported in existing pipelines of any R at any flow rates:

1. At low flow rates, the ∇P of 80% oil B emulsion is significantly higher but are below the $\nabla P_{max} = 10 - 20\ psi/mile$.
2. At moderate flow rates, the ∇P of 80% oil B emulsion is similar if not lower compared to the 350 cP oil.
3. At high flow rates, turbulent flow conditions emerge and the ∇P of 80% oil B emulsion is comparable if not lower compared to the 350 cP oil. The ∇P of 80% oil B emulsion in turbulent flow conditions can be found between the laminar flow curve (lower limit of ∇P) and the turbulent flow curve (upper limit of ∇P). The exact ∇P is a function of the drag reduction capability and the non-Newtonian properties of the emulsion.

Pipeline transportation of optimized heavy O/W emulsion of up to ~75% oil B is possible with existing crude oil pipelines for $R > 0.05\ m$ without accounting for the droplet migration effect on $\nabla P\ vs.\ Q$. Optimized 80% oil B emulsion cannot be transported economically in existing pipelines if droplet migration is not factored in the $\nabla P\ vs.\ Q$ calculations. However, with the droplet migration effect, pipeline transportation of optimized 80% oil B emulsion is economical with existing crude oil pipelines at all flow rates. The maximum flow rate of emulsions may also be

significantly higher than the maximum flow rate of 350 cP oil depending on the magnitude of the emulsion drag reduction in turbulent conditions.

7.4.5 Smooth vs. Rough Pipe Wall on Pressure Gradient vs. Flow Rate

Wall slip is a physical phenomenon that is controlled by the surface roughness of the flow conduit. Wall slip is completely suppressed when absolute roughness of the wall is greater than the droplet diameter ($\varepsilon > d$). This property has been used to characterize wall slip using rough and smooth surface parallel plates in Chapter 5. Does wall slip of emulsions occur in crude oil pipelines and is its effect significant on $\nabla P\ vs.\ Q$?

The average absolute surface roughness of commercial steel (carbon steel) pipelines is estimated to be ~50 μm [McDonnell (2011)]. Since almost all emulsions prepared in this dissertation showed $d_{32} < 50\mu m$, heavy oil emulsions will not slip at the pipeline wall. However, pipeline walls can be modified to reduce the surface roughness to allow wall slip to occur. Internally coated pipes have been used in the oil and gas industry worldwide, mainly to prevent pipe corrosion. The pipelines can be coated with a variety of coatings (phenolic, epoxy, urethane, and nylon) with the average absolute surface roughness of the coated pipes showing values of <1-5 μm [Farshad et al. (1999)]. Wall slip can be observed for most of the concentrated heavy O/W emulsions in this dissertation for $\varepsilon < 1 - 5\ um$. The positive effects of coating pipeline walls on emulsion pipeline operations can be split into four major improvements.

Flow Startup

A major benefit of smooth pipe walls for pipeline flow of emulsions can be observed during flow startups. Because of the yield stress of concentrated emulsions (τ_{y1}), flow does not start until $\tau_{y1} < \tau_w$ for pipelines with rough surfaces that eliminate

wall slip. Even for $\tau_{y1} < 1\ Pa$, a significant ∇P must be imposed to overcome the yield stress to start flow in long pipelines. The ∇P required to start flow can be significantly reduced with wall slip. With smooth pipe walls, flow is possible with wall slip between $\tau_{sy} < \tau_w < \tau_{y1}$ where the slip yield stress is usually $\tau_{sy} \ll \tau_{y1}$. The τ_{sy} value can also be reduced or eliminated depending on the surface coating of the pipelines [Seth et al. (2008)]. An example of the reduced ∇P necessary to start flow with and without slip is shown in Fig. 7.12.

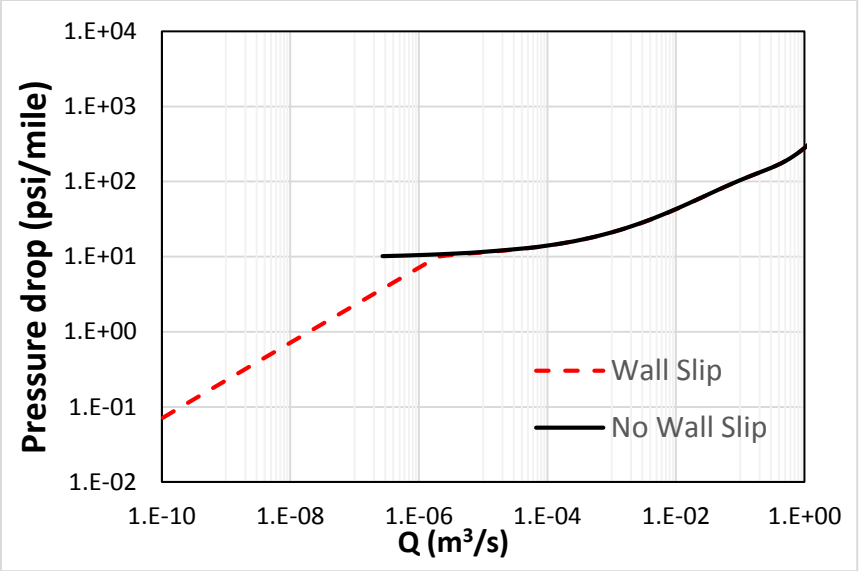

Fig. 7.12: $\nabla P\ vs.\ Q$ of 80% Oil D emulsion (D5 from Table 7.3) at 23°C. R=0.3 m. Black solid line represents flow with no wall slip and red dash line represents flow with wall slip.

The ∇P required for flow startup of emulsion D5 in a pipeline of R=0.3m reduced from $\nabla P = \sim 10\ psi/mile$ with no wall slip to $\nabla P < 0.1\ psi/mile$ with wall slip. A ∇P over 100 times lower is required for flow startup of emulsion D5 with wall slip compared to with no wall slip.

Lower Friction Factor in Turbulent Flow

Another benefit of having a smooth pipe wall over a rough pipe wall is observed if pipeline flow is in the turbulent regime. Moody's Diagram indicates that the friction factor is a function of absolute wall roughness. A smaller wall roughness leads to a lower friction factor in the turbulent flow regime. For $0.5\ um < \varepsilon < 50\ um$ and $R > 0.15\ m$, no significant change in the friction factor is observed as a result of ε for $Re < 100{,}000$. However, the effect of pipe wall roughness is more prevalent for $0.5\ um < \varepsilon < 50\ um$ and $R < 0.05\ m$ with significant reductions in the friction factor observed for lower ε for $Re < 10{,}000$.

Increased Flow Rate

Significant wall slip velocity with smooth pipe walls can be observed for concentrated emulsions near the flow induced yield stress $0.5\tau_{y2} < \tau_w < 2\tau_{y2}$. The pipe radius, emulsion rheological properties, and wall slip properties play a significant role on the contribution of wall slip to the total flow rate. The traditional view in the literature is that the contribution of wall slip to flow rate is only significant when the flow conduit diameters are very small. However, some concentrated heavy O/W emulsions prepared in this study showed that wall slip contributed significantly to the flow rate of emulsions in pipes with $R < 0.6\ m$ (see Fig. 7.13)

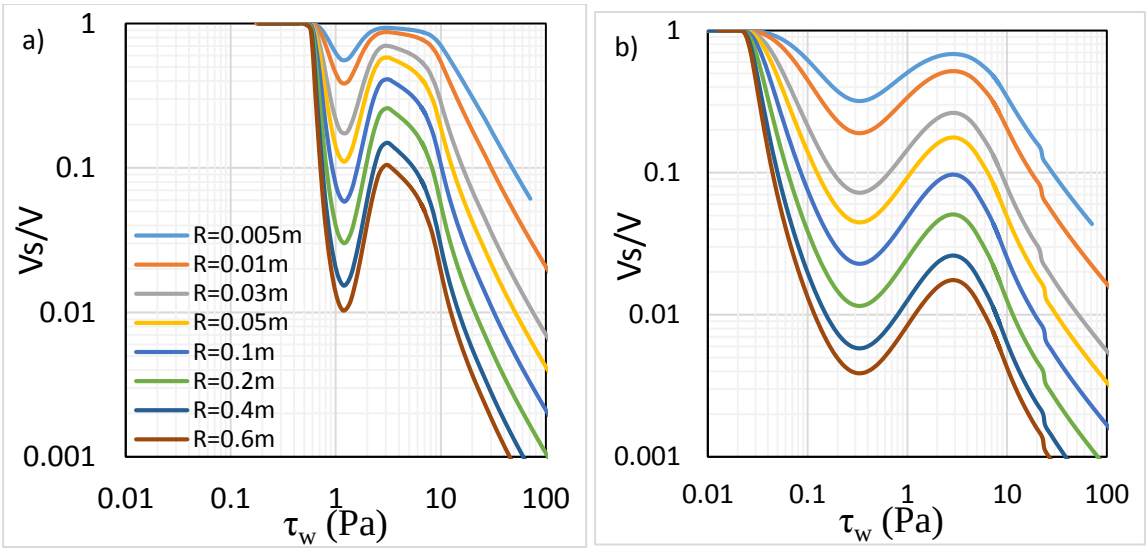

Fig. 7.13: $V_s/V\ vs.\ \tau_w$ of a) 80% oil A emulsion (A1 from Table 7.3) and b) 80% oil B emulsion (B2 from Table 7.3) at 23°C. V_s is the slip velocity and V the total mean velocity. Pipeline radii of R=0.005-0.6 m are tested.

Fig. 7.13a) showed that for emulsion A1, wall slip contributed up to 20-50% of emulsion flow with smaller pipelines ($0.05\,m < R < 0.2\,m$) and 10-20% of emulsion flow with bigger pipelines ($0.2\,m < R < 0.6\,m$). The wall slip observed at $0.5\tau_{y2} < \tau_w < 2\tau_{y2}$ occurred within the observed range of the operational ∇P of pipelines at steady state. However, emulsion B2 showed that the wall slip contributions at $0.5\tau_{y2} < \tau_w < 2\tau_{y2}$ to the emulsion flow are 5-10 times lower compared to emulsion A1. The smaller contribution of wall slip to the flow rate observed for emulsion B2 is because of the lower values of $C, V_{y2}, and\ \tau_{y2E}$ used to model wall slip.

Corrosion

A major concern with emulsion flow in existing crude oil pipelines is corrosion of pipelines caused by the continuous aqueous phase of O/W emulsions. Coating the inside of pipes would completely eliminate the corrosion concern.

The advantages of lining the inner walls of pipelines with smooth coatings (ε <1-5 μm) over commercial grade steel pipelines ($\varepsilon \approx$50 μm) for concentrated heavy O/W emulsion flow are:

1. Easier flow startup of concentrated heavy O/W emulsions due to wall slip.
2. Increased flow rate at $0.5\tau_{y2} < \tau_w < 2\tau_{y2}$ due to wall slip. Could be significant even in pipes with $R > 0.2\ m$.
3. Prevention of pipe corrosion.

The advantages of coated pipes may justify the cost of coating.

7.4.6 Effect of Oil Concentration on Pressure Gradient vs. Flow Rate

Optimizing the emulsion formulation is extremely important for transportation of concentrated heavy O/W emulsions. Figure 7.14 showed the $\nabla P\ vs.\ Q$ for oil D emulsions of φ=40-85% with aqueous composition of 1.6% phenol-15EO, 0.2% NaOH, and 0% NaCl. Constant pipeline radius of R=0.3m is used with no droplet migration effect.

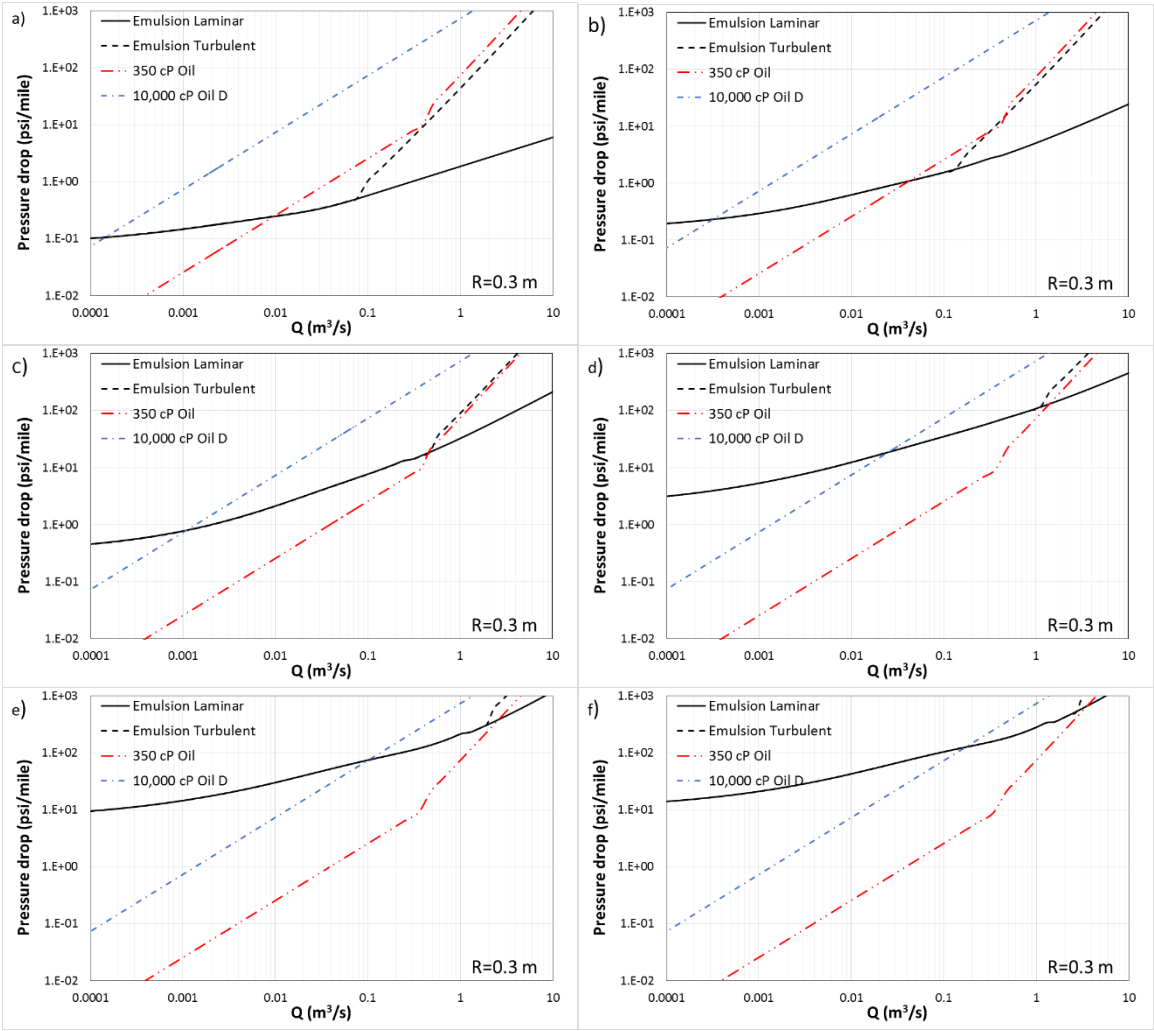

Fig. 7.14: Effect of oil concentration on $\nabla P\ vs.\ Q$ of oil D emulsion (D1-D6 from Table 7.3) at 23°C. Pipe radius of R=0.3 m is assumed for all samples. Aqueous composition of 1.6% ph15EO, 0.2% NaOH, and 0% NaCl. a) $\varphi = 0.4$ and $\varphi_m = 0.79$, b) $\varphi = 0.5$ and $\varphi_m = 0.78$, c) $\varphi = 0.6$ and $\varphi_m = 0.8$, d) $\varphi = 0.7$ and $\varphi_m = 0.73$, e) $\varphi = 0.8$ and $\varphi_m = 0.69$, f) $\varphi = 0.85$ and $\varphi_m = 0.69$.

Compared to heavy oil D, flow of oil D emulsions in a pipeline with $R = 0.3\ m$ showed lower ∇P for moderate to high flow rates and higher ∇P for low to moderate flow rates for all φ. Since oil D viscosity is approximately 10,000 cP and not as viscous as oil A and oil B, smaller improvements in flow capacity are observed for oil D emulsions.

Compared to the 350 cP reference crude oil, oil D emulsions with up to $\varphi = 60\%$ can be successfully transported in a pipeline with $R = 0.3\,m$. Oil D emulsions with $\varphi \geq 70\%$ showed significantly lower flow rates at all ∇P below $\nabla P_{max} \approx 20\,psi/mile$. The higher ∇P observed for emulsions with $\varphi > 70\%$ is because of $\varphi > \varphi_m$. The chemical formulation of oil D emulsions is modified in Fig. 7.15 to generate emulsions with higher φ_m.

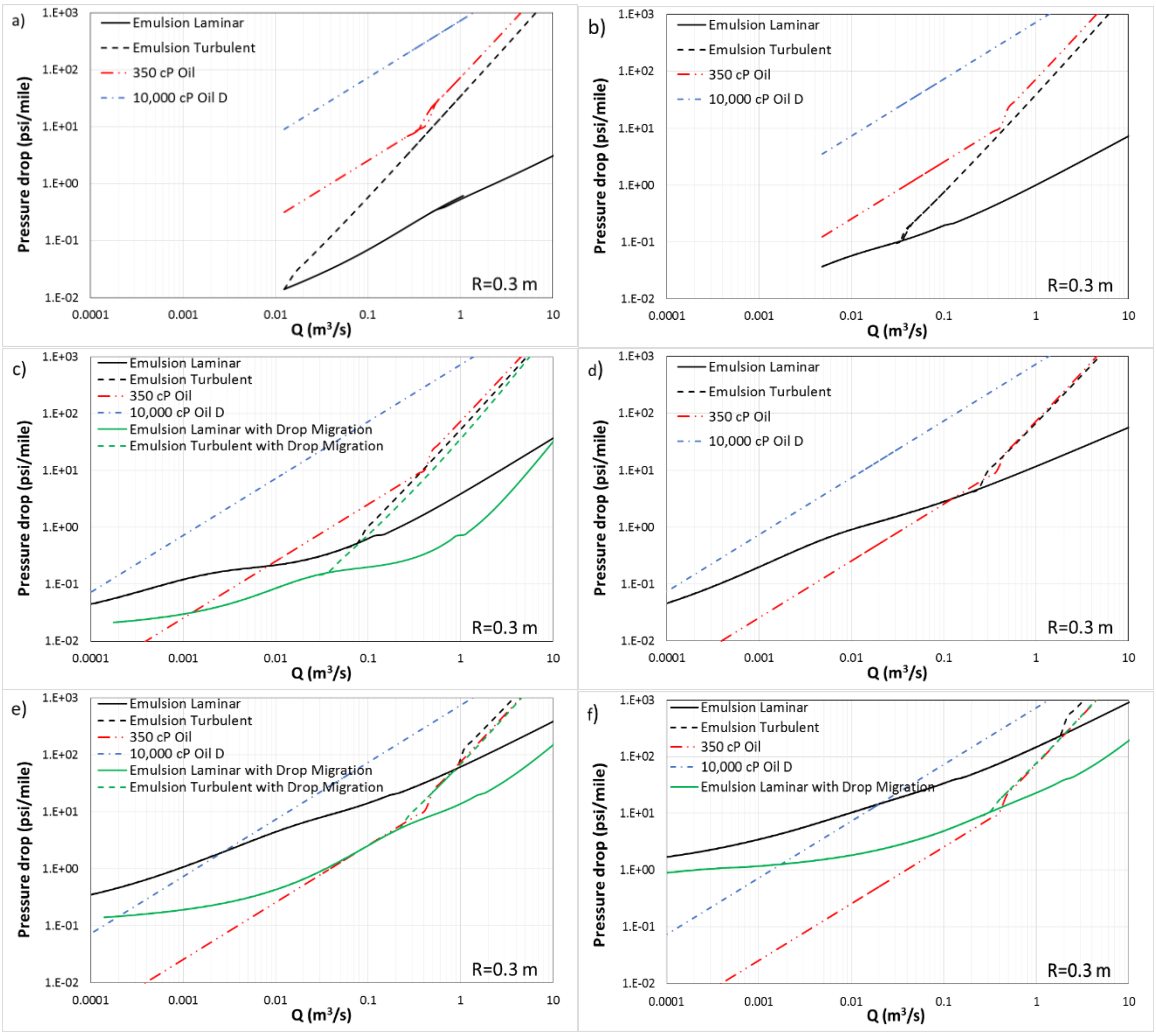

Fig. 7.15: Effect of oil concentration on $\nabla P\ vs.\ Q$ of oil D emulsion (D7-D12 from Table 7.3) at 23°C. Aqueous composition of 1.6% ph15EO, 0.2% NaOH, and 1% NaCl. a) $\varphi = 0.4$ and $\varphi_m = 0.83$, b) $\varphi = 0.5$ and $\varphi_m = 0.76$, c) $\varphi = 0.6$ and $\varphi_m = 0.81$, d) $\varphi = 0.7$ and $\varphi_m = 0.81$, e) $\varphi = 0.8$ and $\varphi_m = 0.76$, f) $\varphi = 0.85$ and $\varphi_m = 0.75$. Drop migration for φ=85% was estimated using Eq. 6.13 with $a = 0.4$.

By optimizing the salinity of the aqueous formulation used to prepare oil D emulsions, the φ_m of oil D emulsions can be increased significantly where $\varphi > \varphi_m$ is not observed until oil D emulsions are prepared with $\varphi \geq 75 - 80\%$. With the optimized chemical formulation, oil D emulsions with $\varphi \leq 75\%$ (black lines in Fig. 7.15) can be transported in a pipeline with $R = 0.3\ m$ compared to the oil D emulsions which were

not optimized with $\varphi \leq 60\%$ (black lines in Fig. 7.14). This is an improvement of extra 10-15% oil D that can be transported in a pipeline by optimizing only the salinity, without taking into account the effect of droplet migration.

With droplet migration (green lines in Fig. 7.15), significantly lower ∇P are needed for flow of emulsions compared to those with no droplet migration. Oil D emulsions with up to $\varphi = 85\%$ can be transport in pipelines ($R = 0.3\, m$) with droplet migration. An extra 10-15% oil D can be transported in an emulsified form because of the lower ∇P observed due to the droplet migration effect in pipelines.

Using the data from Figs. 7.14-15, the maximum flow rates of oil D are calculated for emulsions with φ=40-85% and NaCl=0-1%. $\nabla P_{max} \approx 15\ psi/mile$ was assumed and the ∇P of turbulent flow curves were used (dotted lines from Figs. 7.14-15). This is a conservative estimate of the maximum oil flow rates with no emulsion drag reduction assumption.

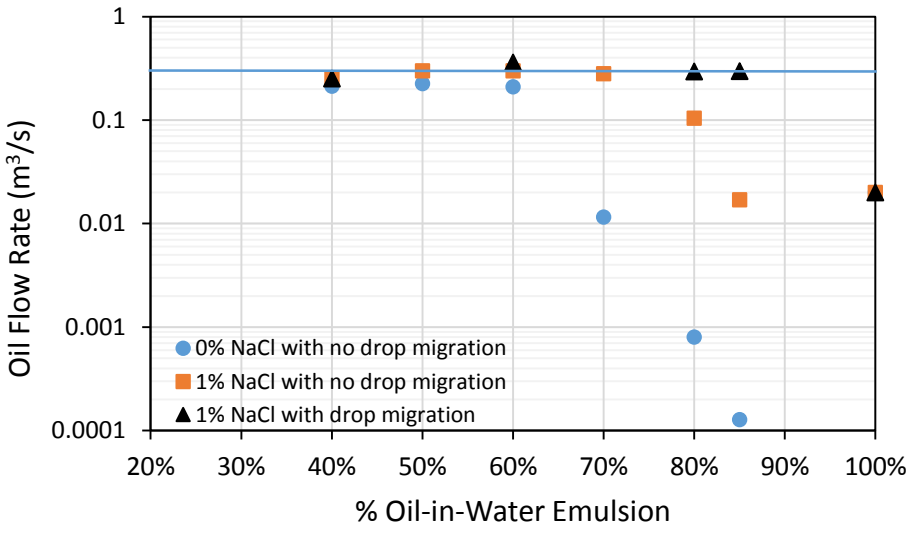

Fig. 7.16: Concentration of oil D in emulsions vs. oil D flow rate (not including the volume of water in the emulsions) is plotted. Effect of chemical formulation used to prepare oil D emulsions on the oil D flow rate is explored. Two aqueous formulations were tested. Effect of droplet migration is also tested. Pipeline radius of $R = 0.3\,m$ at 23°C. The blue line represents the oil D flow rate of diluted heavy oil with 30% diluent and a viscosity of 350 cP (volume of diluent is not included in the oil flow rate).

Both chemical formulation optimization and droplet migration are important when designing pipeline transportation of heavy O/W emulsions. The performance of pipeline transportation of emulsions are compared to pipeline transportation of 350 cP diluted heavy oil with 30% diluent in Fig. 7.16. Optimizing the chemical formulation increased the maximum concentration of oil that can be transported in an emulsified form from 60% to 70-75% O/W emulsions. Including the effect of droplet migration in pipelines further increased the maximum concentration of oil in an emulsified form that can be transported in pipelines from 70-75% to 85% O/W emulsions. With further optimization of the chemical formulation used to prepare heavy O/W emulsions in terms of the emulsion viscosity and droplet migration in pipelines, it may be possible to increase the maximum concentration of oil in an emulsified form that can be transported in pipelines to ~90% O/W emulsions. The drag reduction effect of heavy O/W

emulsions can significantly improve the maximum oil flow rates in Fig. 7.16. The improvement of the maximum flow rate depends on the magnitude of drag reduction.

The cost of chemicals is a significant concern when preparing stable heavy O/W emulsions. The chemical formulations for concentrated heavy O/W emulsions are proposed based on two sources of water, 1% NaCl brine and 2.5% NaCl brine. Higher concentrations of co-solvents are needed to prepare heavy O/W emulsions if the water source has a higher electrolyte concentration. Table 7.4 shows the estimated chemical costs for the chemical formulations used to prepare heavy O/W emulsions.

Table 7.4: Cost and quantity of chemicals in the chemical formulation used to prepare heavy O/W emulsions

Heavy O/W emulsion	Aqueous phase composition	Chemicals	NaOH	Co-solvent	Total cost
		Cost ($/lbs)	0.5	1	
80% heavy oil 20% aqueous phase	1.6% phenol-15EO 0.2% NaOH 1% NaCl brine	lbs/bbl of emulsion	0.14	1.1	
		$/bbl of emulsion	0.07	1.1	**1.20**
85% heavy oil 15% aqueous phase	1.6% phenol-15EO 0.2% NaOH 1% NaCl brine	lbs/bbl of emulsion	0.1	0.85	
		$/bbl of emulsion	0.05	0.85	**0.90**
80% heavy oil 20% aqueous phase	4% phenol-15EO 0.2% NaOH 2.5% NaCl brine	lbs/bbl of emulsion	0.14	2.8	
		$/bbl of emulsion	0.07	2.8	**2.90**
85% heavy oil 15% aqueous phase	4% phenol-15EO 0.2% NaOH 2.5% NaCl brine	lbs/bbl of emulsion	0.1	2.1	
		$/bbl of emulsion	0.05	2.1	**2.15**

The cost of alkali is negligible compared to the cost of co-solvent. For 1% NaCl brine, the chemical costs are approximately $1.00/bbl of 80-85% heavy O/W emulsions. For 2.5% NaCl brine, the chemical costs are approximately $2.90/bbl and $2.15/bbl of 80%

and 85% heavy O/W emulsions, respectively. The chemical costs are very competitive if not several times cheaper compared to the cost of diluents.

7.5 CONCLUSIONS

Successfully upscaling laboratory rheological measurements of heavy oil-in-water emulsions to flow in full scale crude oil pipelines is not simple. Using the rheological and wall slip equations developed in Chapter 5, the flow of concentrated heavy O/W emulsions in pipelines of various radii is calculated in terms of $\nabla P\ vs.\ Q$. The effect of droplet migration is modeled in pipelines using the equation developed in Chapter 6. The following conclusions have been discovered about flow of concentrated heavy O/W emulsion in pipelines:

1. Concentrated heavy O/W emulsions showed very unique velocity profiles in a pipe unlike Herschel-Bulkley fluids.
2. The $\nabla P\ vs.\ Q$ of heavy O/W emulsions in laminar flow can be calculated using two methods: 1) The velocity profile approach and 2) friction factor approach. A modified generalized Reynolds number and laminar flow friction factor equation are proposed.
3. 40% O/W emulsion showed a delayed transition from a laminar to turbulent regime as well as drag reduction capabilities. Drag reduction of heavy O/W emulsions can significantly increase the maximum flow rates of emulsions in pipelines.
4. Commercial steel pipeline surfaces have sufficient roughness to inhibit wall slip. However, a smooth pipeline surface can be created with a chemical coating, which can enable wall slip. Chemically coating the pipeline wall provides the following benefits for flow of concentrated heavy O/W emulsions in pipelines:

a. Negligible or a very small yield stress due to wall slip, resulting in easier flow startup.
b. Increased flow rate near the flow induced yield stress ($0.5\tau_{y2} < \tau_w < 2\tau_{y2}$) for some concentrated heavy O/W emulsions due to wall slip. Depending on the wall slip model parameters of the emulsions, significant improvements in flow rates can be observed for pipes with large radii ($R < 0.6\ m$). This non-negligible contribution of wall slip to emulsion flow rates in pipelines with a large radius is against the conventional theory in the literature that wall slip is only significant in flow conduits with a small radius.
c. Pipeline coatings provide a barrier between the aqueous phase and the pipeline, eliminating pipeline corrosion.

5. Optimized heavy O/W emulsions with up to 75% dispersed oil phase can be successfully transported in crude oil pipelines with the existing infrastructures (no droplet migration). With the droplet migration effect, heavy O/W emulsions with up to 85% dispersed oil phase can be successfully transported in crude oil pipelines.
6. The cost of chemicals used to prepare optimized heavy O/W emulsions is low and competitive compared to the cost of diluents.

NOMENCLATURE

ϵ	Absolute roughness of pipe wall
$\dot{\gamma}_c$	Critical shear rate
V_c	Critical velocity at r_y
A	Cross sectional area
ξ_0	Dimensionless un-sheared plug radius
φ	Dispersed-phase volume fraction of emulsions
f	Fanning friction factor
a	Fitting parameter for droplet migration equation
n	Flow index
k	Flow consistency index
ρ	Fluid density
He	Hedstrom number
n'	Local flow index
r	Local radial position in a pipe
u	Local velocity
φ_m	Maximum packing volume fraction (φ_m) of dispersed-phase possible without deformation of the spherical dispersed-phase
v	Mean velocity
Q	Mean volumetric flow rate
R	Pipe radius
D	Pipe diameter
L	Pipe length
P	Pressure
∇P	Pressure gradient
r_y	Radius of the plug core
Re	Reynolds number
$\dot{\gamma}$	Shear rate
$\dot{\gamma}_w$	Shear rate at the tube wall
$\dot{\gamma}_{w,dm}$	Shear rate at the tube wall with droplet migration
τ	Shear stress
τ_w	Shear stress at the tube wall
τ_{sy}	Slip yield stress
μ	Viscosity
v_s	Wall slip velocity
τ_y	Yield stress
Ψ	Yield stress function

Chapter 8: Conclusions and Recommendations

This dissertation addressed the rheology of colloidal suspensions with a focus on heavy oil-in-water emulsions. The study investigated whether heavy oil-in-water emulsions are a viable method of transporting heavy oils in pipelines as an alternative to the diluent method. The goal is to prepare heavy oil-in-water emulsions with as high a dispersed oil phase as possible while still maintaining low emulsion viscosity for pipeline transportability. The conclusions are split into three parts: 1) preparation method; 2) rheological characterization; and 3) flow upscaling of heavy oil-in-water emulsions. At the end, recommendations for future research are discussed.

8.1 Conclusions on Preparation of Heavy Oil-in-Water Emulsions

A new, one-step method of preparing heavy oil-in-water emulsions with the chemical formulation approach is proposed. Most heavy oils contain acidic chemical compounds which can react with an alkali to generate natural surfactants. Heavy oil and an aqueous phase composed of an alkali, electrolytes, and a co-solvent were hand mixed at an elevated temperature to prepare emulsions. Two variables, Sauter mean diameter (d_{32}) and maximum sphere packing parameter (φ_m), were calculated from the droplet size distribution of the emulsions. Previous studies have found that the viscosity of emulsions are lower when the ratio of the dispersed phase concentration to the maximum sphere packing parameter φ/φ_m is smaller and d_{32} is higher. In this study, chemical formulations were identified that produced heavy oil-in-water emulsions with high φ_m values and good stability. The following observations were identified from these experiments:

1. Stable heavy oil-in-water emulsions were prepared with four different heavy oils of varying viscosities and origins.

2. A sufficient alkali concentration is necessary to prepare homogenous emulsions that emulsified all oil. Stable emulsions were prepared with NaOH, Na_2CO_3, and alkyl amines.
3. Emulsions with $\varphi < 70\%$ showed sedimentation or creaming of oil droplets over days. However, emulsions were restored to its original homogeneous state after mildly shaking the samples a few times. Emulsions with $\varphi > 70\%$ showed stability against both coalescence and sedimentation/creaming for days if not weeks.
4. Ethoxylated co-solvents were found to be very robust chemicals that can be tailored to the salinity of the available water source to prepare heavy oil-in-water emulsions with high φ_m.
    a. Emulsions prepared with only an alkali inverted from oil-in-water to water-in-oil at very low salinity (~0.5-1% NaCl).
    b. Emulsions prepared with an alkali and a hydrophilic co-solvent increased the emulsion inversion salinity up to 2.5-3% NaCl.
5. A combination of three variables were necessary to prepare heavy oil-in-water emulsions with high φ_m
    a. A sufficient concentration of alkali
    b. A sufficient concentration of co-solvent
    c. ~75% of the Na^+ concentration necessary to reach the salinity at which point the inversion of oil-in-water to water-in-oil emulsion takes place.
6. φ_m values as high as 0.95 were measured for optimized 80% heavy oil-in-water emulsions.
7. Photomicrographs of heavy oil-in-water emulsions showed that the oil droplets are attractive in nature and formed aggregating structures.

8.2 CONCLUSIONS OF CONCENTRATED EMULSION RHEOLOGY

Heavy oil-in-water emulsions showed complex rheological properties. The type of viscometer used to measure the rheological properties of heavy oil-in-water emulsions provided different information about the rheology of emulsions.

8.2.1 Rotational Viscometer

Smooth parallel plates and roughened parallel plates were used to characterize the rheological properties of heavy oil-in-water emulsions with steady state, oscillatory, and transient measurements.

1. For moderately concentrated heavy oil-in-water emulsions ($\varphi < 0.55 - 0.65$)
    a. Only a single yield stress was observed.
    b. Wall slip was observed below and just above the yield stress.
2. For concentrated heavy oil-in-water emulsions ($\varphi > 0.60 - 0.75$)
    a. Two-step yielding behavior was observed: A traditional yield stress and a flow induced yield stress.
    b. Two-step slip behavior was observed below and just above the traditional yield stress and below and just above the flow induced yield stress.
3. A combination of two Herschel-Bulkley equations accurately modeled the rheological properties of heavy oil-in-water emulsions.
4. A wall slip equation was developed to model the two-step slipping behavior of heavy oil-in-water emulsions with measurable emulsion properties such as the yield stresses, yield strains, and mean droplet diameter.

8.2.2 Capillary Tube Viscometer

Capillary tube viscometers were used to mimic the flow of emulsions in pipelines. The following conclusions were made from the rheological measurements using the capillary tube viscometers

1. The wall slip behavior of heavy oil-in-water emulsions characterized using capillary tube viscometers agreed with the wall slip behavior characterized using parallel plates.
2. Lower emulsion viscosities were measured using the capillary tube viscometers compared to the emulsion viscosities measured using parallel plates even when wall slip was eliminated. The lower emulsion viscosities measured in capillary tube viscometers were attributed to droplet migration away from the tube wall.
3. Diameter of the capillary tube viscometer (D=0.7-7mm) had no effect on the degree of droplet migration in steady state flow of emulsions.
4. The ratio of the shear rates experience by heavy oil-in-water emulsions in parallel plates to the wall shear rates in tube viscometers with droplet migration was found to be proportional to the square root of wall shear stress divided by the fluid density $\dot{\gamma}/\dot{\gamma}_{w,dm} \sim \sqrt{\tau_w/\rho}$.
5. Droplet migration in capillary tube viscometers reached steady state at a much lower ratio of tube length to diameter, L_{ss}/D, than predicted based on the current theory of droplet migration found in the literature. This may be due to the inter - droplet attraction between the oil droplets, which leads to the formation of large aggregate structures.
6. The apparent viscosities of 80% heavy oil-in-water emulsions flowing in capillary tube viscometers were up to ten times lower compared to the viscosities measured with rotational viscometers. Apparent viscosity measurements in capillary tube

viscometers of <350 cSt were achieved for optimized heavy oil-in-water emulsions with oil concentrations up to 85%.

8.3 CONCLUSIONS ON UPSCALING FLOW OF HEAVY OIL EMULSIONS

The rheological, wall slip, and droplet migration equations were used to upscale the flow of heavy oil-in-water emulsions from laboratory viscometers to full-scale crude oil pipelines. The major conclusions about the flow of concentrated heavy oil-in-water emulsion in pipelines:

1. Unlike Herschel-Bulkley fluids, concentrated heavy oil-in-water emulsions showed unique velocity profiles in a pipe.
2. The pressure gradient versus flow rate $\nabla P\ vs. Q$ of heavy oil-in-water emulsions in laminar flow can be calculated using two methods: 1) The velocity profile approach and 2) friction factor approach. A modified generalized Reynolds number and a laminar flow friction factor equation are proposed.
3. A 40% oil-in-water emulsion showed a delayed transition from a laminar to turbulent regime as well as drag reduction capabilities. Drag reduction of heavy oil-in-water emulsions can significantly increase the maximum flow rates of emulsions in pipelines.
4. Commercial steel pipeline surfaces have sufficient roughness to inhibit wall slip. However, a smooth pipeline surface can be created with a chemical coating, which can enable wall slip. Chemically coating the pipeline wall provides the following benefits for flow of concentrated heavy oil-in-water emulsions in pipelines:
    a. Negligible or a very small yield stress due to wall slip, resulting in easier flow startup.

b. Increased flow rate near the flow induced yield stress ($0.5\tau_{y2} < \tau_w < 2\tau_{y2}$) for some concentrated heavy oil-in-water emulsions due to wall slip. Depending on the wall slip model parameters, significant improvements in flow rates can be observed for pipes with large radii ($R < 0.6\,m$). This non-negligible contribution of wall slip to emulsion flow rates in pipelines with a large radius is against the conventional theory in the literature that wall slip is only significant in flow conduits with a small radius.
c. Pipeline coatings provide a barrier between the aqueous phase and the pipeline, reducing or eliminating the risk of pipeline corrosion.

5. Optimized heavy oil-in-water emulsions with <75% dispersed oil phase can be successfully transported in crude oil pipelines with the existing infrastructures assuming no droplet migration. With the droplet migration effect, heavy oil-in-water emulsions with up to 85% dispersed oil phase can be successfully transported in crude oil pipelines.
6. The cost of chemicals used to prepare optimized heavy oil-in-water emulsions is low and competitive compared to the cost of diluents.

8.4 New Contributions to the Heavy Oil-in-Water Emulsion Technology

A significant amount of time and effort has been invested by the scientific community and oil industry to develop an economically and technically viable method of transporting concentrated heavy oil-in-water emulsions in crude oil pipelines. New research findings related to the heavy oil-in-water emulsion technology are summarized below. These new developments are expected to make the technology competitive to the dilution method of transporting heavy oils.

A summary of the heavy oil-in-water emulsion technology in the literature:

1. Pilot and commercial pipeline transportation of heavy oil-in-water emulsions
    a. Orimulsion® (70% O/W) showed apparent viscosity of 2,000 cP at 10 s^{-1} in a pipeline.
    b. Indonesian pipeline (70% O/W) showed apparent viscosity of 400 cP at 10 s^{-1} in a pipeline with D=0.5 m.
    c. Heavy O/W emulsions with $\varphi > 70\%$ resulted in extremely viscous emulsions which cannot be transported in pipelines.
2. Difficulty predicting the flow rates of heavy oil-in-water emulsions in pipelines from the laboratory viscosity measurements.

New contributions to the Technology:

1. Optimized chemical formulations developed to prepare concentrated heavy oil-in-water emulsions with low viscosity.
2. Identified that heavy oil-in-water emulsions prepared with alkali formed aggregates/clusters of oil droplets due to the attractive inter-droplet interactions.
3. Fully characterized the rheological properties of heavy O/W emulsions in a broad range of shear rates ($\dot{\gamma} = 10^{-4} - 10^{2}\ s^{-1}$).
4. Developed rheological and wall slip equations for heavy O/W emulsions that modeled flow over a broad range of shear rates ($\dot{\gamma} = 10^{-4} - 10^{2}\ s^{-1}$).
5. Identified evidence of droplet migration in capillary tube viscometers. Diameter of the capillary tube viscometer (D=0.7-7mm) had no effect on the magnitude of droplet migration in steady state flow of emulsions.
6. Developed an equation that modeled the effect of droplet migration.
7. Showed experimental evidence of the drag reduction capabilities of heavy oil-in-water emulsions.

8. Showed with upscaling calculations that optimized heavy oil-in-water emulsions with $\varphi \leq 85\%$ can be successfully transported in existing crude oil pipelines.

8.5 Recommendations for Future Research

Based on the knowledge and experience gained from this research, the following recommendations for future research are made:

1. The combinations of chemicals such as alkalis, electrolytes, surfactants, and co-solvents that can be used to prepare heavy oil-in-water emulsions are enormous. Additional tests should be done to find the optimal chemical formulations to produce concentrated heavy oil-in-water emulsions with even lower viscosity.
2. Micromechanical models have been developed that relate the rheological properties of concentrated emulsions with an unimodal droplet size distribution and repulsive droplet interactions to the physicochemical properties of the emulsion. Similar models for concentrated emulsions with a polydisperse droplet size distribution and attractive droplet interactions would be extremely valuable in terms of relating the physicochemical properties of heavy oil-in-water emulsion to their rheological properties.
3. Research on the aggregation kinetics of attractive oil droplets is necessary to fully understand the rheology of heavy oil-in-water emulsions. How do aggregates form? What is the aggregate size? How do aggregates breakup under shear?
4. Research on the droplet migration of heavy oil-in-water emulsions in pipes
    a. Measurements of velocity profiles and concentration profiles at steady state flow to confirm droplet migration.
    b. Investigate how the emulsion physicochemical properties such as heavy oil viscosity, mean droplet diameter, interfacial tension, dispersed phase

concentration, inter-droplet interactions affect the kinetics and magnitude of droplet migration.

c. Investigate the L_{ss}/D required to develop a steady state profile in terms of droplet migration in pipes for heavy oil-in-water emulsions that form larger aggregate structures. An equation must be developed to upscale L_{ss}/D measured in laboratory to crude oil pipelines. L_{ss} must be significantly smaller than the pipeline length between pumping stations to take advantage of the viscosity reduction effect of droplet migration on the flow of of heavy oil-in-water emulsions.

5. Perform turbulent flow experiments with concentrated heavy oil-in-water emulsions to quantify
   a. The stability of heavy oil-in-water emulsions in turbulent flow.
   b. The drag reduction capability of heavy oil-in-water emulsions
   c. Critical Reynolds number where laminar flow ends and transitions to turbulent flow.
6. Research on the rate of the corrosion of crude oil pipelines due to flow of heavy oil-in-water emulsions is necessary. If heavy oil-in-water emulsions corrode crude oil pipelines, solutions to eliminate corrosion of pipelines are necessary. Chemical corrosion inhibitors such as amines might be appropriate because amines can be added to the chemical formulation used to prepared emulsions in a small quantity without affecting the stability of emulsions.
7. The emulsified heavy oils must be demulsified when it reaches the refinery. An efficient and cheap method of demulsifying heavy oil-in-water emulsions must be identified. Since high pH is necessary to generate the soaps used to stabilize the emulsions, lowering the pH with acids may be an effect method of destabilizing

and demusifying the emulsions. Increasing the temperature, mixing with a small amount of diluents, and centrifuging are also expected to increase the rate of demusification.

Appendix

Table A1: Major crude oil pipeline dimensions and operating conditions in the world

Pipeline Name	Length (miles)	Diameter (inch)	Max Flow Rate (bbl/day)	Current Flow Rate (bbl/day)	Calculated Shear Rate (1/s) @ Max Flow Rate	Shear Rate @ Current Flow Rate	Velocity (miles/hr) @ Max Flow Rate	Velocity (miles/hr) @ Current Flow Rate	Reynold's # for Max Flow Rate	Reynold's # for Current Flow Rate	f	Pressure Drop (psi/mile)
Africa												
Chad-Cameroon	645	30	250,000	110,000	10.59	4.66	2.26	0.99	30077	13234	0.00595	2.84
Sumed	200	42	2,500,000	1,700,000	38.61	26.25	11.52	7.83	214832	146086	0.00397	35.26
Asia												
Caspian	940	40	1,300,000	700,000	23.24	12.51	6.60	3.55	117298	63161	0.00445	13.62
		42	1,300,000	700,000	20.07	10.81	5.99	3.22	111713	60153	0.00449	10.77
Eastern Siberia-Pacific Ocean	3,018	48	1,600,000	1,000,000	16.55	10.35	5.64	3.53	120306	75191	0.00442	8.23
Habshan-Fujairah	220	48	1,500,000	1,000,000	15.52	10.35	5.29	3.53	112787	75191	0.00447	7.33
Kirkuk Ceyhan	600	40	500,000		8.94		2.54		45115		0.00542	2.46
		46	1,100,000		12.93		4.22		86307		0.00472	5.15
Samsun-Ceyhan	340	42	1,500,000	1,000,000	23.16	15.44	6.91	4.61	128899	85933	0.00437	13.95
		48	1,500,000	1,000,000	15.52	10.35	5.29	3.53	112787	75191	0.00447	7.33
Europe												
Forties	105	36	700,000	700,000	17.17	17.17	4.39	4.39	70179	70179	0.00494	7.43
Ninian	109	36	910,000		22.31		5.71		91232		0.00468	11.90
North America												
Keystone	2,147	30	590,000		25.00		5.33		70981		0.00494	13.13
	2,000	36	1,100,000		26.97		6.90		110281		0.00451	16.75

Table A1 continued.

Trans-Alaska	800	48	2,136,000	600,000	22.10	6.21	7.53	2.12	160609	45115	0.00418	13.88
Range	100-3000	30-48	0.25-2.5 MMbbl/d	0.1-1.7 MMbbl/d	9~40	4.5-26	2-11.5	1~8				
Average					19.91	12.41	5.74	3.73	105560			11.33
Minor Pipelines												
Portland-Montreal	236	18	192,000		37.67		4.82	2.76	38498		0.00566	20.50
		24	410,000		33.93		5.78	1.55	61657		0.00510	19.99
Houma to Houston Pipeline		22	325,000	325,000	34.92	34.92	5.46	1.85	53317		0.00527	20.03
Houma to St. James, LA		18	260,000	260,000	51.01	51.01	6.52	2.76	52133		0.00531	35.24
Athabasca	335	30	345,000		14.62		3.11	0.99	41506		0.00554	5.03
Chicap	205	26	360,000		23.43		4.33	1.32	49973		0.00533	10.78

Oil viscosity of 20 cP and oil density of 800 kg/m^3 is assumed. Absolute roughness of pipeline is 50 μm. Colebrook-White equation is used to calculate the friction factor in turbulent flow.

A2 RHEOLOGY

The rheological characterization of colloidal suspensions are very challenging in terms of picking the right hardware, measurement procedures, and data analysis techniques. This section discusses in detail these issues with regards to the rheological measurements of non-Newtonian fluids such as heavy O/W emulsions.

A2.1 Types of non-Newtonian Behavior

For an incompressible and isotropic Newtonian fluid in 1D, the viscous stress can be defined as follows:

$$\tau = \mu \frac{du}{dy} \tag{A2.1}$$

where μ is the viscosity of the fluid and du/dy the shear rate, $\dot{\gamma}$, defined as the derivative of the fluid velocity that is parallel to the direction of shear. For a Newtonian fluid, μ is a constant.

Some fluids show nonlinear $\tau/\dot{\gamma}$ relationship that is a function of $\dot{\gamma}$. The shear-dependent fluid property of fluids is modeled by a Power-law model:

$$\tau = K \frac{du^n}{dy} \tag{A2.2}$$

where K is the flow consistency index and n the flow behavior index. Using Eq. A2.1, the viscosity of a Power-law fluid is modeled:

$$\mu = K \frac{du^{n-1}}{dy} \tag{A2.3}$$

Power-law fluids are grouped into three types of fluids based on the value of n.

Table. A2: Types of Power-Law Fluids

n	Type of Fluid	Effect on Viscosity
$n < 1$	Pseudoplastic (Shear-thinning)	$\downarrow \mu = \uparrow \dot{\gamma}$
$n = 1$	Newtonian (Shear-independent)	$\mu \neq \dot{\gamma}$
$n > 1$	Dilatant (Shear-thickening)	$\uparrow \mu = \uparrow \dot{\gamma}$

There are fluids that require a finite stress before they begin to flow. The finite stress required for fluid flow is termed yield stress of a fluid, τ_y. The presence of a yield stress is modeled by a modified Power-law model, Herschel-Bulkley (HB) model:

$$\tau = \tau_y + K\dot{\gamma}^n \tag{A2.4}$$

When $n = 1$ and $n < 1$, the fluids are called Bingham plastic and Bingham pseudoplastic, respectively. The viscosity of Herschel-Bulkley model is a function of shear rate and is defined as:

$$\mu = \frac{\tau_y}{\dot{\gamma}} + K\dot{\gamma}^{n-1} \tag{A2.5}$$

Figure A1 illustrates the various fluids with non-Newtonian properties as $\tau\ vs.\ \dot{\gamma}$ plot.

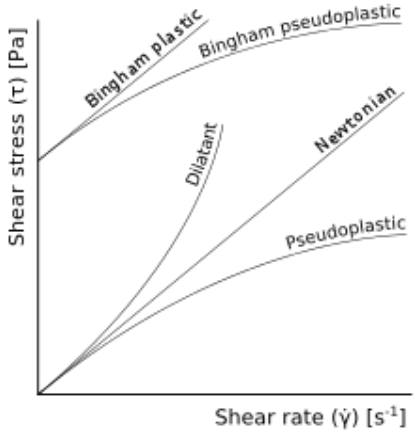

Fig. A1: Classification of non-Newtonian fluids with $\tau\ vs.\ \dot{\gamma}$ relationships.

The $\tau\ vs.\dot{\gamma}$ relationship can also be a function of time for some fluids. When τ increases or decreases as a function of time $\tau(t)$ at a constant $\dot{\gamma}$, the fluids are referred to as rheopectic and thixotropic, respectively.

Each non-Newtonian property of concentrated heavy O/W emulsions presents its own unique opportunities and challenges in flow design and optimization which are summarized in Table A3.

Table A3: Non-Newtonian properties of concentrated emulsions and the opportunities and challenges present for flow design and optimization

	Definition	Opportunities	Challenges	Characterization
Shear thinning $\boldsymbol{\mu = K\dot{\gamma}^{n-1}, n < 1}$	Viscosity decreases when subjected to higher shear rate	Lower viscosity at higher shear rate	Viscosity not constant for varying flow conduit dimensions and flow conditions	Measure $\tau = f(\dot{\gamma})$ for a wide range of $\dot{\gamma}$ and calculate $n = \ln\tau/\ln\dot{\gamma}$
Yield stress $\boldsymbol{\mu = \frac{\tau_y}{\dot{\gamma}} + K\dot{\gamma}^{n-1}}$	Finite stress is required before fluid begins to flow	Lower rate of creaming/sedimentation at rest b/w dispersed and continuous phases	Flow start up can become a challenge as well as very high viscosity at low shear rates	Measure $\tau = f(\dot{\gamma})$ for a wide range of $\dot{\gamma}$ and extrapolate τ to $\dot{\gamma} = 0$
Slip at the wall $\boldsymbol{\mu_{app} = \frac{\tau_y}{\dot{\gamma}_{app}} + K\dot{\gamma}_{app}^{n-1}}$ $\boldsymbol{\dot{\gamma}_{app} > \dot{\gamma} \rightarrow \mu_{app} < \mu}$	Finite fluid velocity is observed as a boundary condition at the flow conduit surface	Lower than expected apparent viscosity at a flow rate	Upscaling viscosity vs. shear rate for varying flow conduit dimensions is a challenge since slip is a function of effective flow conduit diameter	Measure $\tau = f(\dot{\gamma})$ for a wide range of $\dot{\gamma}$ using a roughened and smooth surface flow conduit
Thixotropy $\boldsymbol{\mu = f(\dot{\gamma}, t)}$	Viscosity is a function of time as well as shear rate	Lower viscosity is observed as the fluid is sheared longer	Flow startup can be problematic if viscosity is higher than expected	Measure $\tau = f(\dot{\gamma}, t)$ as a function of time for each shear rate until steady state τ is reached

A2.2 Measurement Geometries

There are various measurement geometries that can be used to characterize the fluid samples. The geometries can be divided into two major groups. First, flow is caused by moving one of the walls that the sample is in contact, dragging the fluid along. This is termed "drag flow." Second, the sample is forced to flow in a channel with pressure. This is termed "pressure flow." Both types of measurement geometries have their advantages and limitations. This chapter focuses on the drag flow method of characterizing emulsion properties. Chapter 6 focuses on the pressure flow method of characterizing emulsions properties which is how pipelines operate.

The most common type of device utilized to achieve drag flow in laboratories is the rotational viscometer. The three most commonly used rotational viscometer geometries are a cone-and-plate, parallel plates, and Couette (see Fig. A2 for illustrations).

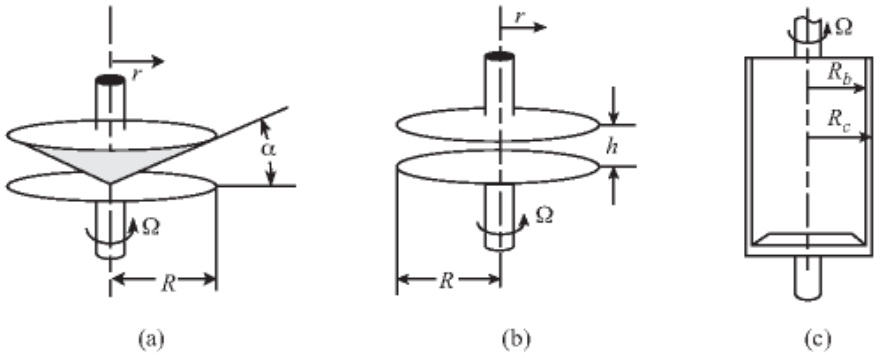

Fig. A2: Types of rotational viscometer geometries (a) a cone and plate; (b) parallel plates; (c) Couette (coaxial cylinders). Obtained from Mewis and Wagner 2011

There are two types of viscometers, stress controlled and strain controlled. For stress controlled viscometers, the torque/stress is the independent variable and strain/shear rate is the measured dependent variable. The opposite is the case for strain controlled

viscometers. Most of the experiments in the chapter have been conducted with the strain controlled procedure with a few stress controlled measurements. The general workflow is to specify the shear rates using the strain controlled rheometer as an independent variable. The torque measurements from the force transducers are recorded which is dictated by the sample rheology. Based on the dimensions of the measurement geometry, the torque measurements are converted to stresses, and the ratio of the shear stresses to shear rates yields the sample viscosity. The equations used to calculate the shear rates and stresses based on the measurement geometries, angular velocities, and torques can be found in most non-Newtonian fluid textbooks [Chhabra and Richardson (2011)]

Parallel Plates

Parallel plates are the simplest measurement geometry and the easiest to use. However, the key limitation of parallel plates is the linearly varying shear rate from zero at the center to a maximum at the edge of the plates represented by:

$$\dot{\gamma}(r) = \frac{\Omega r}{h} \tag{A2.6}$$

where $\dot{\gamma}(r)$ is the shear rate at a radial position r, Ω the angular velocity in rad/s, r a radial position, and h the gap width between plates. Shear stress also varies as a function of radial position represented by:

$$\tau(r) = \frac{T}{2\pi R^3}\left(3 + \frac{d\ln(T)}{d\ln(\dot{\gamma}(r))}\right) \tag{A2.7}$$

where $\tau(r)$ is the shear stress at a radial position r, T the torque, and R the radius of the plates. For Newtonian fluids whose viscosity is independent of shear rate, the ratio of shear stress (Eq. A2.7) and shear rate (Eq. A2.6) at the edge of the plate ($r = R$) accurately represents the viscosity. However, for non-Newtonian fluids whose viscosity is a function of shear rate, Eq. A2.7 must be modified using an appropriate correction

method to obtain accurate shear stress values. The correction method is discussed in Chapter 5.

Cone and Plate

A cone and plate geometry overcomes the limitation of parallel plates by substituting the top plate with a cone whose angle is usually $\alpha < 0.1\, rad$. The angled cone results in a shear rate that is independent of radial position and is represented by:

$$\dot{\gamma}(r) = \frac{\Omega}{\alpha} \tag{A2.8}$$

The shear stress is also independent of radial position and is represented by:

$$\tau = \frac{3T}{2\pi R^3} \tag{A2.9}$$

The homogeneous shear field of the cone and plate geometry makes it ideal for measuring non-Newtonian fluids. However, the gap width of the cone and plate geometry is fixed and cannot be varied. The gap width is also very small and not ideal for colloidal suspensions with large particles.

Couette

Couette cell is defined as an annular gap between coaxial cylinders. Couette cells are ideal for low viscosity samples because of the large surface area of the setup. The stress is represented by:

$$\tau(r) = \frac{T}{2\pi L r^2} \tag{A2.10}$$

where L is the length of the cylinders. The shear rate depends on the radial position but an average value can be estimated if the ratio of the radii of the bob to the cup is close to one; ie, the gap between the cylinders is very small.

$$\dot{\gamma}_{av} = \frac{\Omega R_{av}}{R_c - R_b} \tag{A2.11}$$

where R_{av} is the average radius of the cup and the bob, $(R_c + R_b)/2$.

The advantages, limitations and challenges of rotational measurement geometries are summarized in Table A4 below.

Table A4: Summary of the Measurement Geometry Properties

	Parallel Plates	Cone and Plate	Couette	Pipe Flow (Pressure)
Shear Rate	Shear rate dependent on the radial position	Constant shear rate independent of radius position	Shear rate dependent on the radial position	Shear rate dependent on the radial position
Sample size	Small	Small	Medium	Large
Fluid with (1) low & (2) high viscosity	(1) Good (2) Excellent	(1) Good (2) Excellent	(1) Excellent (2) Good	(1) Poor (2) Excellent
Flow Regimes	Limited to laminar flow	Limited to laminar flow	Limited to laminar flow	Laminar & turbulent flow possible
Ease of Use	Easy	Easy	Easy	Difficult
Non-Newtonian Fluid Characterization	Shear stress correction necessary	Excellent	Excellent	Shear stress correction necessary
Wall Slip Characterization	Excellent	Good	Good	Possible
Ease of loading viscous samples	Excellent	Good	Poor	Poor
Measurement Gap Change	Easy	Very difficult	Very difficult	Difficult

The choice of which measurement geometry to use must be made based on the relevant sample parameters, general measurement problems associated with colloidal suspensions, and methods utilized to eliminate or reduce the measurement problems.

A2.3 Measurement Problems

Many measurement problems are associated with colloidal suspensions. The problems have to be recognized and eliminated/reduced with proper measuring procedure

and hardware for accurate rheological characterization. Possible measurement problems are wall slip, shear banding, density difference between the dispersed and continuous phases leading to phase separation for non-colloidal size of dispersed phase, time-dependent rheological response (thixotropy or rheopexy), shear/edge fracture, and particle/aggregate size

Wall Slip

Most colloidal suspensions, especially attractive soft glasses show slip behavior on smooth surfaces. A thin layer of continuous phase forms near the flow surface as a result of geometric constraints of compress dispersed-phase particles/droplets. Meeker et al. (2004) utilized elastohydrodynamic theory to show that wall slip of soft glasses is characterized by the slip velocity or slip length proportional to the particle/droplet size. Wall slip causes the real shear rate experienced by the bulk sample to be lower than the apparent shear rate calculated from the flow conditions. Total fluid velocity is defined as:

$$v_{total} = v_{bulk} + v_{slip} \quad \text{(A2.12)}$$

where v_{bulk} is the bulk sample velocity and v_{slip} the velocity caused by wall slip. The v_{slip}/v_{total} ratio is inversely proportional to the flow conduit diameter at a constant wall shear stress. The implication of this relationship is that the wall slip contributes more to the total flow when flow diameter is small and wall slip vanishes as the flow diameter approaches infinity. Thus, wall slip must be carefully characterize when flow properties need to be estimated for flow conduit dimensions that are different compared to the viscometer geometry dimensions.

Particle/Droplet Sedimentation or Creaming

When dispersed-phase droplets/particles are small enough ($d < 1\,\mu m$), the Brownian force dominates over gravitational force and constant vertical concentration of

dispersed-phase is observed. For non-colloidal sized particle/droplets ($d > 1\,\mu m$), density difference between the dispersed-phase and continuous-phase results in a vertical concentration gradient of the dispersed-phase. The dispersed-phase droplets/particles float upward (creaming) or sink (sedimentation). For dilute suspensions, the phase separation velocity can be modeled with Stokes' Law:

$$V_s = \frac{2R^2 \Delta\rho g}{9\mu_c} \qquad \text{(A2.13)}$$

where V_s is the sedimentation/creaming velocity, R the radius, $\Delta\rho$ the density difference between the dispersed-phase and continuous phase, g the gravitational constant, and μ_c the continuous phase viscosity. Correction factors are introduced to Eq. A2.13 for more concentrated suspensions. Sedimentation or creaming colloidal suspensions contribute to the formation of a slip layer either at the top or bottom of the measurement geometry, reducing the apparent viscosity.

Shear Banding

A similar phenomenon to wall slip is termed shear banding. Shear banding refers to the coexistence of inhomogeneous flow (macroscopic bands/layers with different viscosities) within the bulk sample even with homogeneous shear rates. It has been shown to occur in complex fluids such as soft glasses and suspensions. Sample heterogeneity is the fluid property thought to be linked to the occurrence of shear banding in the literature. Similar to slip flow, shear banding flow results in lower apparent viscosity.

Shear/Edge Fracture

Shear/edge fracture is a measurement error that can occur with colloidal suspensions. This phenomenon leads to the expulsion of a sample from the gap between parallel plates or cone and plate at high shear rates. It can limit the upper shear rate at

which reliable steady state stress values can be measured. Visual inspections must be conducted to make sure no sample expulsions occur during measurements.

Time-Dependent Rheological Properties

Many colloidal suspensions have shown evidence of type-dependent rheological properties. Shear stress decreasing as a function of time (thixotropy) or increasing as a function of time (rheopexy) at constant shear rates have been observed extensively in the literature. Suitable experimental protocols must be established and used to ensure steady state flow conditions are developed before rheological measurements.

Gap Width of Measurement Geometry

The rule of thumb for colloidal suspensions rheology is to ensure that the measurement gap between the plates must be $> 10 \times$ the average particle diameter. Very narrow gap of $< 10 \times$ the average particle diameter has been shown to cause jamming between the droplets/particles, resulting in inaccurately high apparent viscosity and sample expulsion. Small gaps might also lead to the interference of aggregate formation to its full hydrodynamic size, altering the suspension rheology. Thus, measurement gap width of $\gg 10 \times$ average aggregate diameter may be necessary for attractive soft glasses that form aggregate structures. Thus, the ability to easily vary the gap width of measurement geometry becomes necessary to eliminate the effect of gap width on attractive suspension rheology.

A2.4 Selection of Measurement Geometry

When planning rheological measurements of colloidal suspensions, the appropriate choice of measurement geometry must be made based on the rich variety of measurement challenges summarized in Section A2.2.

The number one challenge, common to all measurement geometries, is how to eliminate wall slip. One of the possible solutions is to artificially create surface roughness on the measurement geometry. Roughened surfaces, with roughness larger than the largest particle diameter, have been commonly utilized in the literature to effectively eliminate the effect of slip flow, and when measured also with smooth plates, to characterize the slip behavior.

The cone and plate geometry is the preferred choice because of the constant shear rate independent of radius position, unlike the parallel plate or Couette geometries. The use of cone-and-plate makes data analysis extremely simple. However, a key problem with a cone-and-plate geometry is the inability to vary the gap size between the cone and plate. The small gap width may prove problematic because of the large particle and aggregate size of heavy O/W emulsions observed in Chapter 4. As discussed earlier, the gap width must be orders of magnitude larger than the particle or aggregate size for accurate rheological measurements. Similar problem is observed with the Couette geometry where the width between the cylinders is small and cannot be varied.

Parallel plate geometry has the most advantages and the least limitations for rheological characterization of heavy O/W emulsions based on the droplet and aggregate size of heavy O/W emulsions and the ease of varying the gap width. All three rotational viscometer geometries can be roughened. However, roughened parallel plate geometries are readily available commercially compared to the others. A minor sedimentation/creaming of samples can be tolerated with roughened parallel plates if the layer of continuous phase is thinner than the roughness of the plates. While the shear rate/shear stress is not uniform with a parallel plate geometry, shear stress data can be corrected for non-Newtonian samples after measurements with good accuracy. Using both smooth and roughened parallel plates of same dimensions would also enable the

characterization of the slip behavior of heavy O/W emulsions. Parallel plates are also the simplest geometry to load, use, and clean. A very small sample size of 1-2 ml is required for 50mm diameter parallel plates with gap width varying from 0.5-1mm.

A2.5 Rheological Measurement Techniques and Procedures

There are many rheological measurements and tests that can be performed with modern rotational viscometers on colloidal suspensions to quantify their rheological properties.

A2.5.1 Steady-State Rheology

The most common type of rheological test that is performed on any material is the steady-state measurements. Steady-state measurements are performed by increasing or decreasing the shear rate at a given rate, termed shear rate sweep. The torque values are measured and shear stress/viscosity values calculated based on the measurement geometry for each shear rate during the shear rate sweep. The end result is a curve of τ vs. $\dot{\gamma}$ or μ vs. $\dot{\gamma}$ for the range of $\dot{\gamma}$ tested. Various analysis methods can be utilized to gain valuable material properties from the τ vs. $\dot{\gamma}$ plots. Yield stress, shear-dependent flow behavior, hysteresis, and wall slip behavior are some of the information that can be obtained from steady-state measurements. Fig. A3 shows the typical flow curves of τ vs. $\dot{\gamma}$ for repulsive soft glasses; a microgel paste and a concentrated silicone oil-in-water emulsion, measured by Meeker et al. (2004).

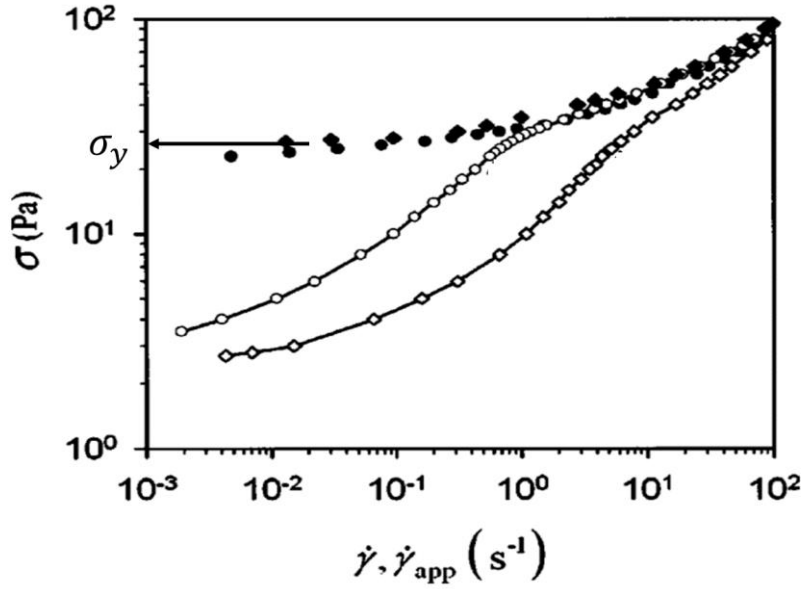

Fig. A3: Flow curves with (open symbols) and without (full symbols) wall slip for a microgel paste (circles) and a silicon oil-in-water emulsion (diamonds, R=1.5 μm, φ=0.77). Obtained from Meeker et al. (2004)

Yield Stress

In the literature, two types of yield stress measurement techniques are commonly utilized, static yield stress and dynamic yield stress methods. Static yield stress is defined as the minimum stress necessary to start flow and is more relevant for flow start-up operations. Methods of measuring static yield stress are stress/strain ramp tests and will be discussed in the transient rheology section below. Dynamic yield stress is defined as the minimum stress necessary to maintain flow and is more relevant during steady-state flow conditions. There are two commonly used methods of measuring the dynamic yield stress. First method utilizes oscillatory rheology and is discussed in the following section. Second method estimates the dynamic yield stress by fitting an appropriate rheological model to the τ vs. $\dot{\gamma}$ data.

There are two requirements for accurately measuring the dynamic yield stress with the model fitting method. First, the τ vs. $\dot{\gamma}$ data must be measured over a broad

range of $\dot{\gamma}$, with emphasis on measuring the σ to the lowest possible $\dot{\gamma}$ within the rheometer accuracy limit. The model fitting method works by extrapolating the τ to $\dot{\gamma} = 0$ from the measured τ vs. $\dot{\gamma}$ data. The extrapolated dynamic yield stress is indicated with an arrow in Fig. A3. Second, an appropriate rheological model must be determined based on the τ vs. $\dot{\gamma}$ data for dynamic yield stress extrapolation. Most soft matter materials show both yield stress and shear-thinning properties and the Herschel-Bulkley (HB) model, $\tau = \tau_y + K\dot{\gamma}^n$, has been used in the literature with great accuracy in modeling the τ vs. $\dot{\gamma}$ data.

Shear Dependent Flow Behavior

A common behavior of complex fluids is the shear dependent flow behavior. Complex fluids can show a broad range of shear dependent flow behavior ranging from shear-thinning to shear-thickening behaviors with a broad range of shear rates. Shear dependent flow behavior is linked directly to the microstructure of the complex fluids which rearrange as shear is applied. Shear dependent flow behavior is characterized with a bulk fluid flow index, n, in most rheology models where $n = 1, n < 1,$ and $n > 1$ represent Newtonian, shear-thinning, and shear-thickening behaviors, respectively. The n value can be estimated for complex fluids from the τ vs. $\dot{\gamma}$ data. The apparent flow index, n_{app}, at any shear rate can be calculated according to the expression $d\,(\ln\tau)/d\,(\ln\dot{\gamma})$. A distinction must be made between n_{app} and n because properties of complex fluids such as τ_y and wall slip can affect the n_{app} at various points, but the bulk fluid flow index, n, is independent of yield stress and wall slip.

Similar to the dynamic yield stress measurement, the n value is estimated by fitting an appropriate rheological model to the τ vs. $\dot{\gamma}$ data. The procedure utilized to measure the dynamic yield stress with the model fit method applies to n as well, especially the importance of measuring τ vs. $\dot{\gamma}$ over a broad range of $\dot{\gamma}$. Flow curves with

no wall slip in Fig. A3 showed $n \approx 0.5$ when HB model is fitted to the data, indicating shear-thinning behavior.

Hysteresis

Time-dependent flow behavior such as thixotropy/rheopexy can be inferred from performing steady-state τ vs. $\dot{\gamma}$ with both increasing and decreasing $\dot{\gamma}$, termed upward and downward sweep tests, respectively. Any indication of hysteresis with upward and downward τ vs. $\dot{\gamma}$ data is a sign of a time-dependent flow behavior of the complex fluids.

Wall Slip

Wall slip behavior of complex fluids can also be analyzed with steady-state measurements. Fig. A3 showed flow curves of same samples measured with smooth surface (slip) and roughened surface (no slip). For materials that slip, the τ vs. $\dot{\gamma}$ data measured with smooth surfaces deviated compared to the τ vs. $\dot{\gamma}$ data measured with roughened surfaces. The effect of slip appeared to be significant below and just above the τ_y of the bulk material.

Traditionally in the literature, wall slip has been characterized by using the classical method introduced by Mooney (1931) for capillary or Couette geometry. Mooney (1931) made two assumptions; (1) bulk fluid is homogeneous and a rheological model can be found that models the $\tau\ vs.\dot{\gamma}$ relationship, and (2) slip velocity is a function of wall stress τ_w only. To characterize the wall slip behavior, the shear rate of slipping materials is defined as apparent shear rate, $\dot{\gamma}_{app} = \dot{\gamma}_{slip} + \dot{\gamma}_{bulk}$ where $\dot{\gamma}_{slip}$ is the shear rate contribution of wall slip and $\dot{\gamma}_{bulk}$ the shear rate contribution of the bulk fluid without any slip. The equation $\dot{\gamma}_{app} = \dot{\gamma}_{slip} + \dot{\gamma}_{bulk}$ is modified based on the flow geometry to extract the slip velocity. Since $\dot{\gamma}_{slip}$ is a function of flow dimensions such as pipe radius and gap between plates, measuring the $\tau\ vs.\dot{\gamma}$ relationship with a measurement geometry of varying dimension makes it possible to extrapolate the slip

velocity as a function of τ. Yoshimura and Prud'homme (1988) came up with a method of extracting $\dot{\gamma}_{bulk}$ from two $\tau\ vs.\dot{\gamma}$ relationships measured using smooth parallel plates with two different gap width.

$$\dot{\gamma}_{bulk}(\tau) = \frac{h_1\dot{\gamma}_{app1}(\tau) - h_2\dot{\gamma}_{app2}(\tau)}{h_1 - h_2} \quad \text{(A2.14)}$$

where h_1 & h_2 are the two gap widths, and $\dot{\gamma}_{app1}$ & $\dot{\gamma}_{app2}$ the apparent shear rates of two gap widths.

If both smooth and roughened parallel plates of same dimensions are available, the $\dot{\gamma}_{app}$, $\dot{\gamma}_{bulk}$, and $\dot{\gamma}_{slip}$ values are easily obtained from the smooth plate measurements, rough plate measurements, and $\dot{\gamma}_{app} - \dot{\gamma}_{bulk}$ at constant τ, respectively. The contribution of slip to flow is calculated as a ratio $\dot{\gamma}_{slip}/\dot{\gamma}_{app}$ at various τ. The ratio $\dot{\gamma}_{slip}/\dot{\gamma}_{app} = 1$ represents a complete plug flow where there is no bulk fluid flow and slip is the only mechanism contributing to flow. The ratio $\dot{\gamma}_{slip}/\dot{\gamma}_{app} = 0$ represents a bulk fluid flow with no wall slip.

Flow velocity, V, can be calculated from $\dot{\gamma}$ values based on the measurement geometry used. For parallel plates, the angular velocity at the edge of the plate is calculated according to $\Omega = \dot{\gamma}h/r$ where Ω is the angular velocity, h the gap between the plates, and r the radius of the plates. Using the relationship between velocity at the edge of the plates and angular velocity, $V = \Omega r$, the following definition of flow velocity at the edge of the plates is defined, $V_{app} = 2V_{slip} + V_{bulk}$ based on the fact that slip occurs at both top and bottom plates as illustrated in Fig. A4.

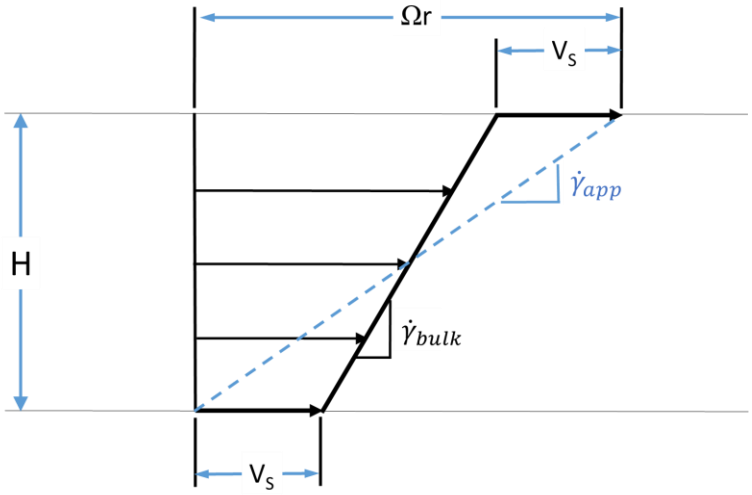

Fig. A4: Parallel plate velocity field. The velocity field is at a radius r. Modified from Yoshimura and Prud'homme (1988)

Establishing the relationship, $V_{slip}\ vs.\ \tau$, allows for one to calculate and upscale the flow of a fluid that slips at the wall to any flow geometry.

A2.5.2 Oscillatory Rheology

For complex fluids that exhibit both solid and fluid like properties, dynamic oscillatory shear tests have been becoming increasingly popular as a method of rheological analysis in the literature. Assuming solid properties are represented by an elastic solid, an investigation of colloidal suspensions with oscillatory tests have yielded additional information about the elastic (stress proportional to strain) and viscous (stress proportional to strain rate) properties of these complex materials. Instead of shearing the samples at a constant rate, dynamic oscillatory test deforms the sample with an oscillatory motion. The oscillatory motion is controlled by a sinusoidal function of sine described as follows:

$$\gamma(t) = \gamma_0 \sin \omega t \qquad \text{(A2.15)}$$

where $\gamma(t)$ is the strain as a function of time, γ_0 the strain amplitude, ω the angular frequency of oscillation, and t the time. The oscillatory shear strain imposes an orthogonal strain rate defined as:

$$\dot{\gamma}(t) = \gamma_0 \omega \cos \omega t \quad \text{(A2.16)}$$

A strain step sweep at a constant frequency or a frequency step sweep at a constant strain can be performed with the corresponding torque values measured and therefore stress values calculated. The stress response can be analyzed with various methods with the most common being a Fourier transform method. The stress to a sinusoidal strain input is represented with the assumption that the shear stress waveform contains only odd higher harmonic contributions:

$$\sigma(t, \omega, \gamma_0) = \gamma_0 \sum_{n\ odd}\{a_n(\omega, \gamma_0) \sin n\omega t + b_n(\omega, \gamma_0) \cos n\omega t\} \quad \text{(A2.17)}$$

where a_n and b_n are constants. Eq. A2.17 can be written as an expansion of τ as a function of stress response at $n = 1$ modified with an angle phase shift δ_n and with the odd higher harmonic contributions:

$$\tau(t, \omega, \gamma_0) = \sum_{n=1,odd}\{\tau_n \sin(n\omega t + \delta_n)\} \quad \text{(A2.18)}$$

Eq. A2.18 can be rewritten as components which are in-phase and out-of-phase with the sinusoidal strain input:

$$\tau(t, \omega, \gamma_0) = \gamma_0 \sum_{n\ odd}\left\{G_n'(\omega, \gamma_0) \sin n\omega t + G_n^{"}(\omega, \gamma_0) \cos n\omega t\right\} \quad \text{(A2.19)}$$

where G_n' is defined as the storage modulus, and $G_n^{"}$ the loss modulus. G_n' and $G_n^{"}$ values are materials functions (ratios of stress and strain) and represent the elastic and viscous properties of the material respectively. Fig. A5 illustrates the stress response of oscillatory measurements for purely elastic (Hookean), purely viscous (Newtonian), and viscoelastic materials.

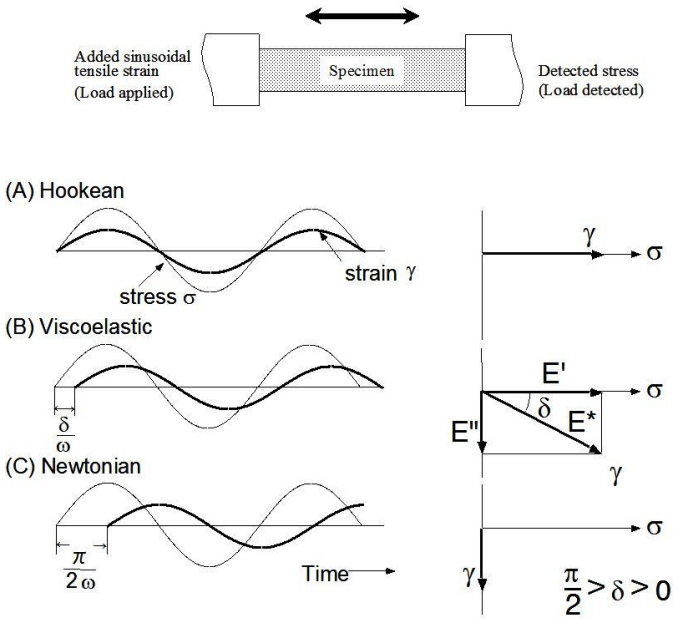

Fig. A5: Schematic illustrations the stress response to oscillatory strain input for elastic solid, viscous fluid, and viscoelastic material. Obtained from Murata (2012)

The elastic solid property, represented by G', causes the stress response by the oscillatory strain input to be in phase, showing no delay in stress response to the strain input ($\delta = 0^o$). The viscous fluid property, represented by $G"$, causes the stress response by the oscillatory strain input to be out-of-phase, showing a delay in stress response to the strain input ($\delta = 90^o$). Viscoelastic materials are a combination of elastic and viscous properties, G' and $G"$, where the stress response by the oscillatory strain input is out-of-phase with $0^o < \delta < 90^o$.

The viscoelastic properties of the material can be further grouped into two regions; linear viscoelastic region where $n = 1$ and no odd higher harmonic contributions are observed and nonlinear viscoelastic region where the odd higher harmonic contributions are present. The linear viscoelastic region is observed when G_n' and $G_n^{"}$ are only a function of ω and is independent of γ, which often occurs at small strain amplitude

values. The testing in the linear viscoelastic region is termed small amplitude oscillatory shear (SAOS) test and the stress response is represented as:

$$\tau(t,\omega) = \gamma_0[G_1'(\omega)\sin\omega t + G_1^{"}(\omega)\cos\omega t] \quad \text{(A2.20)}$$

When higher odd harmonic contributions are present (Eq. A2.19), usually at large strain amplitude values, the stress sinusoidal values are distorted and nonlinear viscoelastic region is obtained. The testing in the nonlinear viscoelastic region is termed large amplitude oscillatory shear (LAOS) test. Fig. A6 depicts an illustration of stress responses and G', $G"$ vs. γ curves for both linear and nonlinear viscoelastic regions.

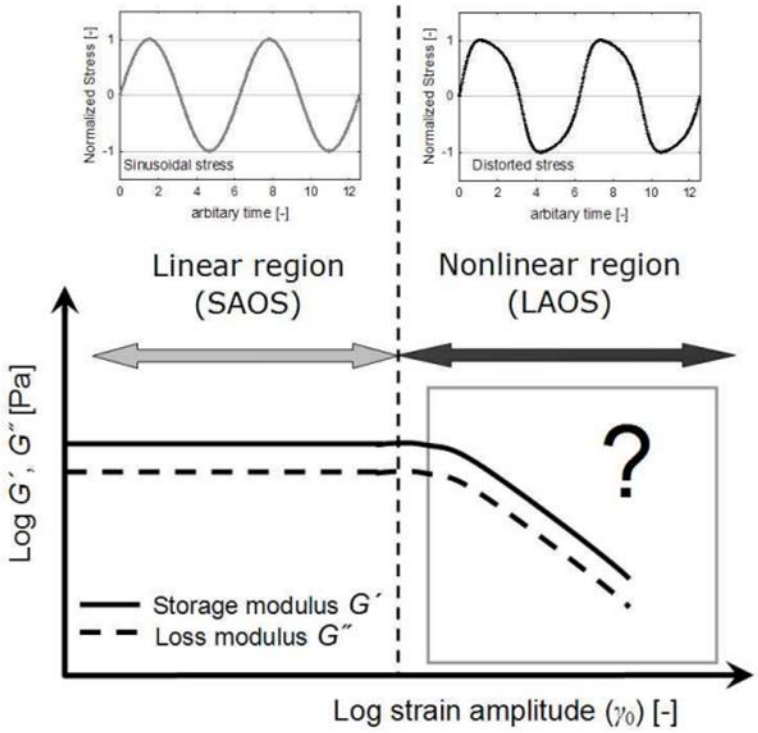

Fig. A6: An illustration of strain sweep test with a fix frequency for a viscoelastic material. The illustration indicates clear linear and nonlinear viscoelastic regions of the material. Obtained from Hyun et al. (2011).

It is important to note that most commercial rotational viscometer analysis softwares analyze the τ vs. γ data using only Eq. A2.20 and does not take into account

the stress distortion observed in the nonlinear viscoelastic region, introducing error in the G', G'' vs. γ curves at large amplitudes. The higher harmonics in stress responses were not analyzed in this study and all oscillatory measurements in this study were report with the default equation used in the commercial viscometer software (Eq. A2.20).

Small Amplitude Oscillatory Shear (SAOS)

Quantitative analysis of the viscoelastic properties of complex fluids can be performed in the linear viscoelastic region. There is a critical strain at which point the linear viscoelastic region ends and nonlinear behavior begins for strain amplitude sweep tests at constant frequency. See an example of the oscillatory strain sweep of viscoelastic material obtained from Christopoulou et al. (2009) below:

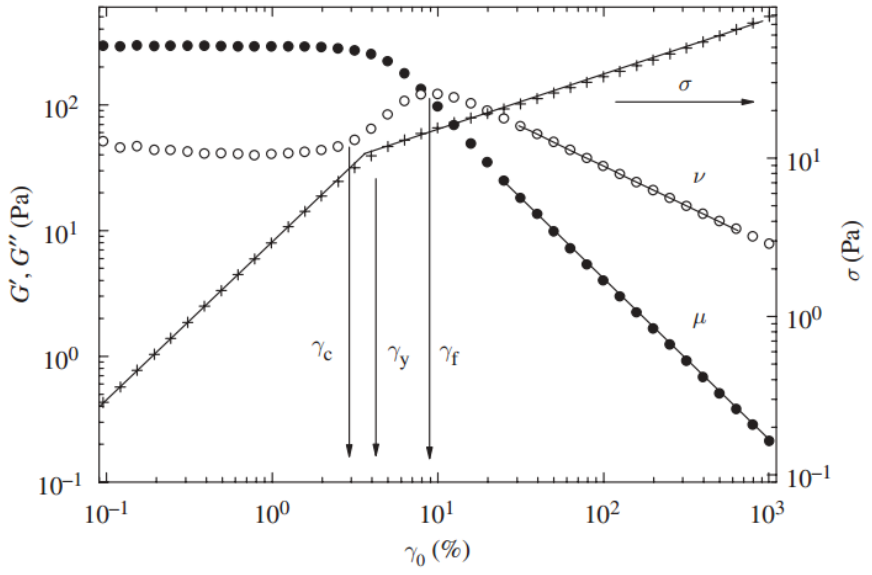

Fig. A7: Oscillatory strain sweep test of colloidal suspension solution obtained from Christopoulou et al. (2009). Vertical arrow γ_c indicates the end of the linear viscoelastic regime, γ_y indicates the yield strain, and γ_f indicates the complete liquid-like response.

There are three critical strains that indicate microstructural changes within the sample. First critical strain point, γ_c, in Fig. A7 is when either G' or G'' deviates from linearity.

Second critical strain point, γ_y, is the inflection point in stress response and represents the yield stress of the sample. The third critical strain point, γ_f, is the cross-over strain of G' and $G"$ and represents the complete transition to pure liquid-like behavior. The definition of γ_y from Christopoulou et al. (2009) is used to define the γ_y for all heavy O/W emulsions tested in this study.

Picking a fixed strain amplitude below but not too far away from γ_c, within the linear viscoelastic region, a frequency sweep can be performed to analyze the elastic properties of complex fluids. A critical parameter that can be measured from a frequency sweep, if it can be measured, is the strain and frequency independent storage modulus, G_0'. Hooke's law can be used for elastic solids with G_0' to calculate the dynamic yield stress:

$$\tau_y = G_0'\gamma_y \tag{A2.21}$$

If the G' and $G"$ curves crossover during the frequency sweep, the frequency at the crossover is defined as a critical frequency, ω_c. The inverse value of the ω_c, $1/\omega_c$ is defined as the relaxation time of the viscoelastic material.

Large Amplitude Oscillatory Shear (LAOS)

The strain sweep of material functions, G' and $G"$, can be analyzed qualitatively to provide further information about the microstructures of complex fluids under varying length and time scales. Hyun et al. (2002) outline four major types of LAOS behaviors observed with complex viscoelastic fluids.

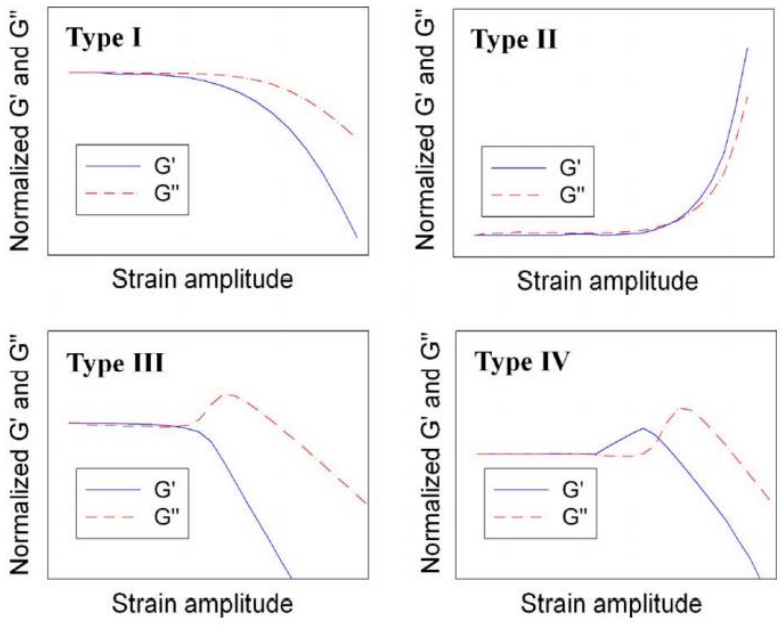

Fig. A8: Four major typical types of LAOS behavior outlined for viscoelastic materials by Hyun et al. (2002). (a) Type I: strain thinning (b) Type II: strain hardening (c) Type III: weak strain overshoot (d) Type IV: strong strain overshoot

Type I strain thinning behavior is often related to shear thinning behavior observed in steady-state shear measurements. It is commonly observed in polymer solutions and polymer melts. Type II strain hardening behavior is often related to shear induced formation of network, very similar to shear-thickening behavior observed in steady-state measurements. Type III weak strain overshoot behavior is observed commonly in soft glasses such as concentrated emulsions and suspensions. The weak strain overshoot of G" is theorized to occur because of microstructural rearrangement and/or clusters/aggregate destruction. Type IV strong strain overshoot behavior of G' and G" is observe for materials that show attractive interdroplet/interparticle interactions weaker than Type II but stronger than Type III. The behavior has been observed with associative polymer solutions.

The LAOS behavior of colloidal suspensions can be analyzed qualitatively to gather information about the interdroplet/interparticle interaction potential as well as the microstructure of the colloidal suspensions.

A2.5.3 Transient Rheology

Transient rheology is a key rheological measurement technique that measures time-dependent flow behavior of complex fluids. Stress vs. time for steady-state test and G',G" vs. time are measured with a constant shear/strain. The resultant plots can be analyzed to recover information about the static yield stress, time-dependent stress/viscosity (thixotropy/rheopexy), and microstructure of complex fluids.

Table A5: Summary of the physicochemical, rheological, and wall slip parameters of heavy oil-in-water emulsion tested in Chapter 5.

Sample Name	Oil	Oil Conc.	Co-solvent Type	Co-solvent conc.	Alkali Type	Alkali Conc.	NaCl conc	Mix Temp (°C)	d43 (um)	d32 (um)	φm	n1	k1	σy1 (Pa)	n2	k2	σy2E (Pa)	γc	σy2S (Pa)	σsy (Pa)	2Vs1 (um/s)	2Vs2	C	G0 (Pa)	γy1	γy2	wc (s)	Wt (kBT)
A80-1	A	80%	Ph15EO	1.60%	NaOH	0.20%	0.40%	96	24.3	17.3	0.79	0.5	10.5	0.53	0.67	3.8	6.5	0.33	2.6	0.15	1.3	3000	0.96	6.5	0.01	2.1	7.7	-32
A80-2	A	80%	Ph15EO	1.60%	NaOH	0.20%	0.80%	96	21.3	14.6	0.76	0.5	7.6	0.01	0.76	3.2	4	0.105	1.6	0	0.01	2000	0.96		0.01	1.85		-42
A80-3	A	80%	Ph15EO	1.60%	NaOH	0.20%	1%	96	18.22	13.8	0.75	0.5	8.1	0.187	0.78	2.8	4	0.15	1.6	0	0.1	1900	0.96	3.2	0.005	1.7	18.2	-46
A80-4	A	80%	Ph15EO	1.60%	NaOH	0.20%	1.20%	96	20	14.66	0.75	0.5	12.4	0.1	1	2.2	6	0.343	2.4	0	0.4	1700	0.95	4.5	0.0075	1.5	12.5	-55
A80-5	A	80%	Ph15EO	1.60%	NaOH	0.20%	1.60%	96	24.4	14.7	0.77	0.5	5.48	0.055	0.97	2.12	2.7	0.048	1.08	0	0.2	1200	0.95	1.8	0.015	1.6	33.3	-68.5
B80-1	B	80%	IBA-15EO	1.60%	NaOH	0.20%	0.40%	60	28.3	17.8	0.81	0.5	1.09	0.064	0.84	1.145	9	6.78	3.6	0.02	2	1000	0.13	4	0.003	0.9	0.5	-33.3
B80-2	B	80%	IBA-15EO	1.60%	NaOH	0.20%	0.40%	70	25.5	19.1	0.765	0.5	4.04	0.33	0.7	2.95	6	1.63	1.5	0	10	3200	0.84	6	0.009	2.65	1	-36
B80-3	B	80%	IBA-15EO	1.60%	NaOH	0.20%	0.40%	85	26.7	21.5	0.74	0.5	6.04	0.048	0.767	3.3	7	1.38	1.7	0	0.1	4800	0.92	2.5	0.01	2.9	6.66	-40.5
B80-4	B	80%	IBA-15EO	1.60%	NaOH	0.20%	0.40%	96	34.5	26.88	0.75	0.5	6.77	0.4	0.787	3.4	8	1.45	0.8	0	6	6000	0.98	3.5	0.025	2.9	5	-50.5
B75-5	B	75%	PH15EO	1.60%	NaOH	0.40%	0.80%	96	52.7	28.76	0.81	0.5	0.34	0.00834	1	0.26	1.5	3.3	0.6	0	8	900	0.25	0.5	0.01	1.8	1.67	-103
B80-5	B	80%	PH15EO	0.00%	NaOH	0.20%	0.00%	90	41.6	30	0.765	0.5	77.4	4.4	0.78	7.5	23	0.7										
B80-6	B	80%	PH15EO	0.00%	NaOH	0.40%	0.00%	90	30.3	15	0.8	0.5	60.16	3.9	0.97	3.55	33	0.65	13.2	2.5	0.2	1600	0.95	28	0.12	0.4	2.2	-24
B80-7	B	80%	PH15EO	0.00%	NaOH	0.60%	0.00%	90	8.1	6.8	0.73	0.5	19	2.7	0.888	5.28	35	0.189	10	1	0.6	2300	0.95	10	0.15	1	9.1	-15.5
B80-8	B	80%	PH15EO	0.00%	NaOH	0.80%	0.00%	90	6.44	5	0.745	0.5	14.76	3.71	0.756	9.2	30	0.21	10	1.5	1.25	2500	0.93	10	0.25	1.4	6.67	-15
B80-9	B	80%	PH15EO	1.60%	NaOH	0.20%	0.00%	96	46.3	33.5	0.73	0.5	45	2	0.8	4	10	0.08	2	0	40	6500	1	24	0.07	2	1.25	-27
B80-10	B	80%	PH15EO	1.60%	NaOH	0.20%	0.40%	60	152	47	0.85	0.5	1.3	0.028	0.84	1.2	5.5	2.38	0.3	0.005	1.5	6500	0.83	2.75	0.012	2.5	0.77	-89
B80-11	B	80%	PH15EO	1.60%	NaOH	0.20%	0.40%	75	27	20.1	0.77	0.5	5.9	0.067	0.779	3.33	8.5	0.96	1.2	0	0.15	6000	0.95	3.2	0.01	2.5	6.25	-38
B80-12	B	80%	PH15EO	1.60%	NaOH	0.20%	0.40%	96	30.5	23.2	0.74	0.5	9.15	0.073	0.817	3.1	11	50	2	0	0.3	6000	0.92	5.25	0.025	2.25	3.33	-43
B80-13	B	80%	PH15EO	1.60%	NaOH	0.20%	0.40%	96	39.25	26.75	0.78	0.5	6.03	0.087	0.81	3.14	8	0.83	1	0.05	0.2	5500	0.95	2.75	0.01	2.25	7.7	-51
B80-14	B	80%	PH15EO	1.60%	NaOH	0.20%	0.40%	60	20.3	11.9	0.805	0.5	1.45	0.05	0.773	1.75	4.5	1.41	1.8	0.045	0.08	1100	0.45	5	0.008	2.2	1.25	-22
B80-15	B	80%	PH15EO	1.60%	NaOH	0.40%	0.40%	96	9.75	7.7	0.88	0.5	15.5	1.09	0.83	5.28	14	0.9	4	0.2	2.5	7000	0.99	7.25	0.022	2.5	5	-20

Table A5 continued.

B80-16	B	80%	PH15EO	1.60%	NaOH	0.60%	0.40%	60	58.9	38.5	0.8	0.5	3.89	0.0288	0.777	1.1	3	1.06	?	0.02	0.04	800	0.7	2	0.005		6.67	-127
B80-17	B	80%	PH15EO	1.60%	NaOH	0.60%	0.60%	60	52.2	29.6	0.82	0.5	2.99	0.044	0.7	1.16	2.7	3.1	0.05	0.02	0.175	200	0.3	3	0.008	0.25	5	-112.5
B80-18	B	80%	PH15EO	1.60%	NaOH	0.10%	0.80%	96	59	46	0.85	0.5	18.7	1	0.81	5.75	11.4	23.5										
B80-19	B	80%	PH15EO	1.60%	NaOH	0.20%	0.80%	60	113.8	42	0.85	0.5	5.38	0.15	0.9	1.57	15	4.2	0.5	0.003	15	25000	0.99	3	0.025	2.5	3.33	
B80-20	B	80%	PH15EO	1.60%	NaOH	0.20%	0.80%	75	42	19.4	0.81	0.5	4.44	0.25	0.7954	2.35	8	1.1	1.5	0.07	2	7000	0.93	3	0.025	2.2	5.55	
B80-21	B	80%	PH15EO	1.60%	NaOH	0.20%	0.80%	96	26.7	18.5	0.79	0.5	3.16	0.0195	0.95	1.35	5.25	0.84	2.1	0	0.5	2750	0.8	2.25	0.01		4.34	
B80-22	B	80%	PH15EO	1.60%	NaOH	0.20%	0.80%	96	42	32.6	0.75	0.5	9.2	0.229	0.723	5.59	10	0.91	1	0	1.5	8000	0.97	3.25	0.01	1.85	7.69	
B80-23	B	80%	PH15EO	1.60%	NaOH	0.30%	0.80%	96	29.2	24.25	0.755	0.5	5.1	0.133	0.73	4.1	4.5	0.235	1.3	0	0.1	1550	0.9	3.5	0.005	1.85	7.69	
B80-24	B	80%	PH15EO	1.60%	NaOH	0.40%	0.80%	60	52.2	17.4	0.84	0.5	0.92	0.028	0.73	0.92	0.59	0.11	0.236					0.45	0.013	2.15	12.5	
B80-25	B	80%	PH15EO	1.60%	NaOH	0.40%	0.80%	96	26.5	21.7	0.785	0.5	4.85	0.103	0.6	6.57	3	3.1	1.2	0	0.45	1000	0.9	1.75	0.015	2.15	16.7	
B80-26	B	80%	PH15EO	1.60%	NaOH	0.40%	0.80%	96	8.8	6.6	0.94	0.5	6.44	0.055	0.759	3.3	5	0.274	2	0	0.01	1200	0.8	2	0.003	2.5	14.3	
B80-27	B	80%	PH15EO	1.60%	NaOH	0.50%	0.80%	96	23	17.3	0.82	0.5	10.7	0.146	0.55	15.1	11	12.62	0.6	0.02	0.08	3000	0.83	1	0.009	2.1	50	
B80-28	B	80%	PH15EO	1.60%	NaOH	0.60%	0.80%	60	71.1	32.8	0.84	0.5	1.26	0.0005	0.87	0.49	1.8	0.66	?	0	0.02	3000	0.84	1.5	0.015	4	0.5	
B80-29	B	80%	PH15EO	1.60%	NaOH	0.20%	1.20%	60	87.66	33.6	0.84	0.5	2	0.035	0.81	1.58	5	0.87	0.5	0	5	7000	0.94	0.85	0.01	1.85	10	
B80-30	B	80%	PH15EO	1.60%	NaOH	0.20%	1.20%	96	29.66	21.3	0.81	0.5	4.2	0.015	0.725	3.36	6.5	0.96	1.5	0	0.05	4500	0.87	3.6	0.01		2.5	
B80-31	B	80%	PH15EO	1.60%	NaOH	0.40%	1.20%	96	10.3	7.85	0.94	0.5	7.6	0.052	0.5	11.6	4.75	26.28	0.4	0	0.05	2000	0.85	8	0.0025	3.5	2.5	
B80-32	B	80%	PH15EO	1.60%	NaOH	0.20%	1.40%	60	23.55	14.9	0.8	0.5	0.97	0.01	0.72	1.55	1.8	0.276	0.26	0	0.07	950	0.77	0.8	0.004	2.25	7.7	
B80-33	B	80%	PH15EO	1.60%	NaOH	0.20%	1.40%	96	40.5	15.5	0.82	0.5	0.265	0	0.72	1.28	1.5	0.172	0.32	0	160	1300	0.85	0.3	0.004	2.5	16.7	
B80-34	B	80%	PH15EO	1.60%	NaOH	0.20%	1.40%	60	21.06	15.2	0.82	0.5	1.08	0.017	0.736	1.92	2.8	0.796	0.6	0	0.5	550	0.43	1.75	0.01	1.5	2.4	
B80-35	B	80%	PH15EO	1.60%	NaOH	0.40%	1.40%	96	17.7	14.9	0.877	0.5	21.4	0.4	0.7	8.73	18	2.02	4.75	0	0.13	6000	0.95	14	0.013	2.3	2.5	
B80-36	B	80%	PH15EO	1.60%	NaOH	0.20%	1.60%	96	44.3	31.3	0.78	0.5	6.07	0.017	1	2.77	1.05	0.06	0.42	0	0.05	150	0.9	1.1	0.01	0.3	2.5	
B80-37	B	80%	PH15EO	1.43%	NaOH	0.28%	0.00%	90	12.1	9.8	0.7	0.5	37.4	3.27	0.825	5.8	22	2.56	8.8	0.5	3	2800	0.97	37	0.11	2	0.77	
B80-38	B	80%	PH15EO	1.43%	NaOH	0.28%	0.29%	90	12.7	10.6	0.7	0.5	10.13	0.405	0.7	4.4	8	6.9	2	0.05	2	2500	0.92	8.5	0.045	2.5	2.4	
B80-39	B	80%	PH15EO	1.43%	NaOH	0.28%	0.58%	90	36.3	21.2	0.74	0.5	8.3	0.025	0.95	1.79	6	10	1.2	0	0.01	2200	0.97	4.5	0.02	2.3	5	
B80-40	B	80%	PH15EO	1.43%	NaOH	0.28%	0.87%	90	31	22.75	0.74	0.5	6	0.157	0.745	3.65	4	0.219	1.6	0	0.6	2500	0.97	6.25	0.025	2.5	4	
B80-41	B	80%	PH15EO	1.43%	NaOH	0.28%	1.16%	90	38.7	26.2	0.755	0.5	7.57	0.05	0.845	4.58	5	0.4	1.5	0	0.025	2000	0.95	7	0.055	2.1	4.2	
B85-42	B	85%	PH15EO	1.60%	NaOH	0.40%	0.80%	60	52.5	20.5	0.87	0.5	14.16	0.7	0.67	8.9	10	6.4	1.8	0.05	5	7000	0.98	8	0.03	2.5	2.5	

Table A5 continued.

D80-1	D	80%	Ph15EO	1.60%	NaOH	0.20%	0%	96	16.6	14.4	0.684	0.5	18.5	2.41	0.887	2.89	27	18.38	10.8	0	15	4500	0.8	27	0.06	1.1	0.28	-11.5
D80-2	D	80%	Ph15EO	1.60%	NaOH	0.20%	0.40%	96	15.8	13.13	0.694	0.5	5.4	0.62	0.816	2.22	9.5	5.1	3.8	0.1	4	2500	0.65	6.25	0.05	2.1	0.83	-24.5
D80-3	D	80%	Ph15EO	1.60%	NaOH	0.20%	0.80%	96	18.7	14.22	0.73	0.5	2.66	0.09	0.84	1.56	5.25	1.82	2.1	0.03	0.35	1700	0.6	2.35	0.03	2.5	2.17	-40.5
D80-4	D	80%	Ph15EO	1.60%	NaOH	0.20%	1%	96	18.98	14.15	0.78	0.5	1.51	0.029	0.835	1.37	3	1.03	1.2	0	0.5	1000	0.56	1.8	0.025	2.5	2	-47
D80-5	D	80%	Ph15EO	1.60%	NaOH	0.20%	1.20%	96	21.14	14.66	0.79	0.5	0.67	0.015	0.86	1.13	1.75	0.5	0.7	0	0.9	750	0.6	0.42	0.02	2.7	7.75	-55
D80-6	D	80%	Ph15EO	1.60%	NaOH	0.40%	0%	96	11.33	9.4	0.7	0.5	16.4	3.9	0.78	4.44	38	4.075	15.2	0	13	4500	0.8	17	0.22	1.3	0.63	-15
D80-7	D	80%	Ph15EO	1.60%	NaOH	0.40%	0.4%	96	9.84	7.13	0.735	0.5	3.57	0.49	0.8	2.24	7.5	1.31	3	0.08	3.25	2000	0.67	4.3	0.09	3.4	1.25	-18
D80-8	D	80%	Ph15EO	1.60%	NaOH	0.40%	0.60%	96	9.1	6.3	0.75	0.5	2.4	0.21	0.78	2.075	5.2	1	2.08	0.02	1.2	1350	0.62	2.7	0.07	3.8	1.82	-19
D80-9	D	80%	Ph15EO	1.60%	NaOH	0.40%	0.80%	96	10.4	7.7	0.77	0.5	1.33	0.012	0.73	1.76	3	0.44	1.2	0	0.05	1250	0.725	0.6	0.016	3.8	10	-27
D40-10	D	40%	Ph15EO	1.60%	NaOH	0.20%	0%	96	11.6	6.46	0.79	0.5	0.2	0.05	0.511	0.148	0.115	0.86		0.005	85							-5
D50-11	D	50%	Ph15EO	1.60%	NaOH	0.20%	0%	96	13.2	8.156	0.78	0.5	0.25	0.09	0.74	0.154	0.41	1.22		0.005	100							-6.3
D60-12	D	60%	Ph15EO	1.60%	NaOH	0.20%	0%	96	20.16	14.45	0.8	0.5	0.76	0.187	0.86	0.65	1.9	1.49	0.76	0.013	20	800	0.43	7.5	0.02	2.5	0.12	-11.6
D70-13	D	70%	Ph15EO	1.60%	NaOH	0.20%	0%	96	22.2	16.4	0.73	0.5	7.85	1.2	0.71	3.25	13	9	5.2	0	13	3500	0.75	13	0.07	1.8	0.38	-14
D80-14	D	80%	Ph15EO	1.60%	NaOH	0.20%	0%	96	18.5	15.56	0.69	0.5	18.84	3.95	0.93	2.3	33	15	13.2	0.2	18	3800	0.8	26	0.07	0.8	0.32	-12.5
D85-15	D	85%	Ph15EO	1.60%	NaOH	0.20%	0%	96	19.1	16.2	0.69	0.5	25.2	6	1	2.17	47	16.7	18.8	0.5	12	2800	0.725	37	0.1	0.5	0.25	-13
D40-16	D	40%	Ph15EO	1.60%	NaOH	0.20%	1%	96	2.87	1.89	0.83	0.5	0.0075	0	0.83	0.011	0.062	16.9	0									-6.3
D50-17	D	50%	Ph15EO	1.60%	NaOH	0.20%	1%	96	6.07	4.78	0.76	0.5	0.012	0	0.88	0.02	0.0305	0.325	0.0122									-15.5
D60-18	D	60%	Ph15EO	1.60%	NaOH	0.20%	1%	96	13.6	9.2	0.81	0.5	0.113	0.0015	1	0.05	0.1136	0.089	0.002					0.05	0.0345		12.5	-30.5
D70-19	D	70%	Ph15EO	1.60%	NaOH	0.20%	1%	96	21.3	12.3	0.81	0.5	0.194	0.0054	0.7	0.45	0.3	0.22	0.12	0	1.5	150	0.42	0.15	0.015	3.5	6.67	-41
D80-20	D	80%	Ph15EO	1.60%	NaOH	0.20%	1%	96	19.8	14.1	0.76	0.5	1.39	0.069	0.835	1.42	3	0.62	1.2	0	1.3	1100	0.66	1.3	0.035	2.7	3.33	-47
D85-21	D	85%	Ph15EO	1.60%	NaOH	0.20%	1%	96	20.47	14.58	0.75	0.5	5	0.55	0.818	3.53	6.5	0.9	2.6	0	6	1500	0.74	4.5	0.08	2.1	1.11	-48.5

Table A6: B1-4 tube viscometer calibration with 48.5 cP light mineral oil.

Tube #	q (ml/min)	Section 1 dP(psi)	Section 2 dP(psi)	Section 3 dP(psi)	Section 4 dP(psi)	Whole dP(psi)
B1	0.05	0.38	0.36	0.41	0.38	1.5
	0.1	0.76	0.74	0.76	0.75	3.01
	0.25	1.9	1.87	1.88	1.87	7.57
	0.5	3.81	3.72	3.75	3.75	15.17
	1.25	9.44	9.25	9.26	9.32	37.6
B2	0.1	0.11	0.09	0.08	0.08	0.36
	0.25	0.21	0.17	0.19	0.16	0.73
	0.5	0.39	0.34	0.36	0.35	1.46
	0.75	0.61	0.64	0.58	0.59	2.44
	1.25	1.02	1.05	1.01	1.02	4.13
	5	4.13	4.12	4.08	4.1	16.52
	10	8.23	8.28	8.24	8.26	33.28
B3	1.25	0.08	0.09	0.09	0.09	0.35
	2.5	0.175	0.1775	0.1825	0.19	0.73
	5	0.355	0.35	0.37	0.37	1.485
	10	0.75	0.695	0.745	0.755	2.98
	20	1.495	1.455	1.48	1.485	5.96
B4	20					0.25
	40					0.48
	60					0.75
	80					1.01

Table A7a: Pipe viscometer measured data for ID=0.704 mm

ID=0.704 mm								
Section 1	v (m/s)	dP (Pa)	8v/D (s^{-1})	τ_w (Pa)	n'	n_{avg}'	γ_w (s^{-1})	μw (cP)
	0.000129	1723.689	1.462481	0.782688		0.221854	2.744883	285.1444
	0.000214	1930.532	2.437468	0.876611	0.221854	0.453176	3.17276	276.2928
	0.000429	3102.641	4.874937	1.408839	0.684498	0.584963	5.739642	245.4576
	0.000857	4343.697	9.749873	1.972374	0.485427	0.668769	10.95711	180.0086
	0.001286	6136.334	14.62481	2.78637	0.852112	0.855378	15.24298	182.7969
	0.002144	9514.765	24.37468	4.320438	0.858644	0.813318	25.77337	167.6319
	0.004287	16202.68	48.74937	7.357268	0.767992	0.836418	51.13291	143.8852
	0.008574	30336.93	97.49873	13.77531	0.904843	0.834889	102.3192	134.6308
	0.012862	41368.54	146.2481	18.78451	0.764936	0.77934	156.6001	119.9521
	0.021436	62052.82	243.7468	28.17677	0.793745	0.834107	255.8664	110.123
	0.042872	113763.5	487.4937	51.65742	0.874469	0.874469	504.9887	102.2942
ID=0.707 mm								
Section 2	v (m/s)	dP (Pa)	8v/D (s^{-1})	τ_w (Pa)	n'	n_{avg}'	γ_w (s^{-1})	μw (cP)
	0.000127	1585.794	1.440348	0.723743		0.385083	2.015351	359.115
	0.000212	1930.532	2.400581	0.881078	0.385083	0.534791	2.922641	301.4663
	0.000424	3102.641	4.801161	1.416018	0.684498	0.596323	5.613691	252.2437
	0.000849	4412.645	9.602322	2.013892	0.508147	0.618426	11.0835	181.7018
	0.001273	5929.491	14.40348	2.706168	0.728704	0.827237	15.1555	178.5601
	0.002122	9514.765	24.00581	4.342456	0.925769	0.782719	25.6718	169.1528
	0.004244	14823.73	48.01161	6.76542	0.639668	0.819834	50.64935	133.5737
	0.008488	29647.46	96.02322	13.53084	1	0.814679	101.484	133.3298
	0.012731	38265.9	144.0348	17.46422	0.629358	0.702694	159.27	109.6517
	0.021219	56881.75	240.0581	25.96033	0.776029	0.794808	255.5518	101.5854
	0.042438	99973.98	480.1161	45.62725	0.813587	0.813587	507.6178	89.88505
ID=0.707 mm								
Section 3	v (m/s)	dP (Pa)	8v/D (s^{-1})	τ_w (Pa)	n'	n_{avg}'	γ_w (s^{-1})	μw (cP)
	0.000127	1654.742	1.441516	0.755006		0.301768	2.275364	331.8176
	0.000212	1930.532	2.402527	0.88084	0.301768	0.493133	3.019886	291.6798
	0.000425	3102.641	4.805053	1.415636	0.684498	0.561691	5.742444	246.5214
	0.000849	4205.802	9.610107	1.918973	0.438884	0.584264	11.31963	169.526
	0.001274	5653.701	14.41516	2.579603	0.729644	0.874325	14.93317	172.7432

Table A7a continued.

	0.002123	**9514.765**	**24.02527**	**4.341283**	**1.019006**	**0.812364**	**25.41258**	**170.832**
	0.004246	14478.99	48.05053	6.6063	0.605721	0.767666	51.68616	127.8156
	0.008492	27579.03	96.10107	12.58343	0.929611	0.78834	102.5516	122.7034
	0.012738	35852.74	144.1516	16.35846	0.64707	0.675471	161.466	101.3121
	0.021231	51365.94	240.2527	23.43663	0.703871	0.753535	259.898	90.17628
	0.042461	89631.84	480.5053	40.89614	0.803199	0.803199	509.9388	80.19813
ID=0.706 mm								
Section 4	v (m/s)	dP (Pa)	8v/D (s^{-1})	τ_w (Pa)	n'	n_{avg}'	γ_w (s^{-1})	μw (cP)
	0.000128	1654.742	1.448516	0.753788		0.436829	1.915381	393.5445
	0.000213	2068.427	2.414193	0.942234	0.436829	0.510896	2.991997	314.9183
	0.000426	3102.641	4.828385	1.413352	0.584963	0.568752	5.743649	246.0721
	0.000852	4550.54	9.65677	2.072916	0.552541	0.738324	10.5124	197.1876
	0.001278	6618.967	14.48516	3.01515	0.924108	0.898883	14.89252	202.4607
	0.00213	10342.14	24.14193	4.711172	0.873658	0.887061	24.91035	189.1251
	0.00426	19305.32	48.28385	8.794189	0.900464	0.868483	50.1118	175.4914
	0.00852	34473.79	96.5677	15.70391	0.836501	0.683516	107.746	145.7493
	0.01278	42747.5	144.8516	19.47285	0.53053	0.682964	161.6618	120.4542
	0.021299	65500.19	241.4193	29.83743	0.835398	0.793735	257.1034	116.0522
	0.042598	110316.1	482.8385	50.25251	0.752072	0.752072	522.6315	96.15284
ID=0.704 mm								
Total	v (m/s)	dP (Pa)	8v/D (s^{-1})	τ_w (Pa)	n'	n_{avg}'	γ_w (s^{-1})	μw (cP)
	0.000128	6618.967	1.457831	0.752179		0.336417	2.176725	345.5552
	0.000214	7860.023	2.429718	0.893212	0.336417	0.49769	3.042786	293.5507
	0.000428	12410.56	4.859436	1.410335	0.658963	0.577897	5.746783	245.413
	0.000856	17512.68	9.718872	1.990139	0.496832	0.654288	11.00269	180.8776
	0.001283	24338.49	14.57831	2.765824	0.811744	0.864528	15.14942	182.5696
	0.002139	38886.43	24.29718	4.41905	0.917311	0.827139	25.56663	172.8444
	0.004278	64810.72	48.59436	7.365083	0.736966	0.824991	51.17149	143.9294
	0.008556	122037.2	97.18872	13.86829	0.913017	0.776824	104.1691	133.1325
	0.012834	158234.7	145.7831	17.98177	0.64063	0.710769	160.6138	111.9566
	0.02139	235800.7	242.9718	26.79636	0.780908	0.795937	258.5451	103.6429
	0.042781	413685.4	485.9436	47.01117	0.810966	0.810966	514.2616	91.41489

Table A7b: Pipe viscometer measured data for ID=1.417 mm

ID=1.419 mm								
Section 1	v (m/s)	dP (Pa)	8v/D (s^{-1})	τ_w (Pa)	n'	n_{avg}'	γ_w (s^{-1})	μw (cP)
	0.000105	758.4233	0.59419	0.385177		0.497486	0.744239	517.5442
	0.000316	1310.004	1.78257	0.665305	0.497486	0.628291	2.046221	325.1384
	0.000527	1930.532	2.970949	0.980449	0.759096	0.929316	3.027442	323.854
	0.001054	4136.854	5.941898	2.100963	1.099536	0.85022	6.203589	338.6689
	0.002108	6274.229	11.8838	3.18646	0.600904	0.711496	13.08849	243.4552
	0.003162	8756.342	17.8257	4.447038	0.822087	0.794986	18.97494	234.3638
	0.00527	12962.14	29.70949	6.583017	0.767884	0.711374	32.723	201.174
	0.010539	20408.48	59.41898	10.36475	0.654865	0.624771	68.34054	151.6633
	0.021079	30819.57	118.838	15.65217	0.594678	0.70673	131.1664	119.3306
	0.031618	42954.34	178.257	21.815	0.818783	0.822366	187.883	116.1095
	0.052696	65500.19	297.0949	33.26525	0.825948	0.808853	314.6472	105.7224
	0.073775	85494.99	415.9329	43.4199	0.791758	0.791758	443.2817	97.95103
ID=1.417 mm								
Section 2	v (m/s)	dP (Pa)	8v/D (s^{-1})	τ_w (Pa)	n'	n_{avg}'	γ_w (s^{-1})	μw (cP)
	0.000106	620.5282	0.596895	0.314668		0.63093	0.684186	459.9156
	0.000317	1241.056	1.790686	0.629335	0.63093	0.747934	1.941558	324.1392
	0.000529	1930.532	2.984476	0.978966	0.864939	0.879012	3.087173	317.1075
	0.001057	3585.274	5.968952	1.818079	0.893085	0.967056	6.019787	302.0172
	0.002114	7377.39	11.9379	3.741048	1.041027	0.760615	12.87719	290.5173
	0.003171	8963.184	17.90686	4.545198	0.480203	0.580141	21.14674	214.9361
	0.005286	12686.35	29.84476	6.433204	0.680078	0.653132	33.80729	190.2905
	0.010571	19581.11	59.68952	9.929511	0.626185	0.560147	71.40725	139.0547
	0.021142	27579.03	119.379	13.98523	0.494109	0.633012	136.6815	102.3198
	0.031714	37714.32	179.0686	19.1248	0.771914	0.817403	189.0689	101.1525
	0.052856	58605.44	298.4476	29.71861	0.862892	0.854567	311.1453	95.51358
	0.073999	77910.76	417.8266	39.50826	0.846241	0.846241	436.8061	90.44806
ID=1.419 mm								
Section 3	v (m/s)	dP (Pa)	8v/D (s^{-1})	τ_w (Pa)	n'	n_{avg}'	γ_w (s^{-1})	μw (cP)
	0.000105	620.5282	0.594731	0.315049		0.523719	0.729946	431.6053
	0.000316	1103.161	1.784194	0.560087	0.523719	0.52803	2.182886	256.5809
	0.000527	1447.899	2.973656	0.735114	0.532342	0.877367	3.077566	238.8621
	0.001055	3378.431	5.947312	1.715266	1.222392	1.088769	5.826089	294.4112

Table A7b continued.

	0.002109	**6550.019**	**11.89462**	**3.325515**	**0.955146**	**0.86436**	**12.36127**	**269.027**
	0.003164	8963.184	17.84194	4.550704	0.773575	0.726826	19.51839	233.1496
	0.005273	12686.35	29.73656	6.440997	0.680078	0.653132	33.68472	191.2142
	0.010546	19581.11	59.47312	9.941539	0.626185	0.532576	72.5225	137.0821
	0.021091	26544.82	118.9462	13.47709	0.438968	0.618285	137.3049	98.15444
	0.031637	36680.11	178.4194	18.62288	0.797603	0.857464	185.834	100.2124
	0.052728	58605.44	297.3656	29.75461	0.917325	0.907854	304.9112	97.5845
	0.07382	79289.71	416.3119	40.25623	0.898383	0.898383	428.0843	94.0381
ID=1.420 mm								
Section 4	v (m/s)	dP (Pa)	8v/D (s^{-1})	τ_w (Pa)	n'	n_{avg}'	γ_w (s^{-1})	μw (cP)
	0.000106	689.4757	0.595814	0.349842		0.67534	0.667421	524.1704
	0.000317	1447.899	1.787441	0.734668	0.67534	0.718881	1.962185	374.4133
	0.000528	2137.375	2.979068	1.084511	0.762422	0.754333	3.22162	336.6352
	0.001056	3585.274	5.958136	1.819179	0.746243	0.913582	6.099035	298.2732
	0.002112	7584.233	11.91627	3.848263	1.08092	1.188193	11.44443	336.2565
	0.003168	12824.25	17.87441	6.507063	1.295466	0.990514	17.9172	363.1741
	0.005279	18202.16	29.79068	9.235831	0.685562	0.704676	32.91194	280.6225
	0.010558	30061.14	59.58136	15.25312	0.72379	0.621659	68.64664	222.1976
	0.021117	43092.23	119.1627	21.86513	0.519528	0.649053	135.2707	161.6398
	0.031675	59088.07	178.7441	29.98147	0.778578	0.758751	192.9523	155.3828
	0.052792	86184.47	297.9068	43.73026	0.738923	0.826386	313.5535	139.4667
	0.073909	117210.9	417.0695	59.47316	0.913849	0.913849	426.8991	139.3143
ID=1.420 mm								
Total	v (m/s)	dP (Pa)	8v/D (s^{-1})	τ_w (Pa)	n'	n_{avg}'	γ_w (s^{-1})	μw (cP)
	0.000106	2688.955	0.599057	0.340479		0.583011	0.706173	482.1475
	0.000318	5102.12	1.79717	0.646038	0.583011	0.66156	2.027018	318.7134
	0.00053	7446.338	2.995283	0.942866	0.740108	0.859965	3.117219	302.4702
	0.00106	14685.83	5.990566	1.859541	0.979822	0.949874	6.069598	306.3698
	0.002119	27785.87	11.98113	3.518287	0.919926	0.89397	12.33639	285.1959
	0.003179	39506.96	17.9717	5.002428	0.868013	0.78483	19.20349	260.4958
	0.005298	56537.01	29.95283	7.158798	0.701646	0.683231	33.42462	214.1774
	0.010597	89631.84	59.90566	11.34931	0.664816	0.589639	70.32854	161.3757
	0.021193	128035.6	119.8113	16.21206	0.514462	0.652646	135.7529	119.4233
	0.03179	176436.8	179.717	22.34069	0.790831	0.807846	190.4038	117.3332
	0.052984	268895.5	299.5283	34.04794	0.824861	0.845632	313.1978	108.7107
	0.074177	359906.3	419.3396	45.57186	0.866404	0.866404	435.5047	104.6415

Table A7c: Pipe viscometer measured data for ID=3.14 mm

ID=3.14 mm								
Section 1	v (m/s)	dP (Pa)	8v/D (s^{-1})	τ_w (Pa)	n'	n_{avg}'	γ_w (s^{-1})	μw (cP)
	0.000108	965.266	0.273804	0.497426		0.440573	0.360721	1378.976
	0.000215	1310.004	0.547608	0.675078	0.440573	0.412737	0.742399	909.3193
	0.000645	1999.48	1.642824	1.030382	0.384901	0.348144	2.411819	427.222
	0.001075	2344.217	2.73804	1.208034	0.311387	0.502642	3.415354	353.7069
	0.00215	3792.117	5.476081	1.954173	0.693897	0.67774	6.127038	318.9426
	0.004301	5998.439	10.95216	3.091147	0.661584	0.664101	12.33705	250.558
	0.006451	7860.023	16.42824	4.050468	0.666618	0.652788	18.61275	217.618
	0.010752	10893.72	27.3804	5.613807	0.638959	0.664766	30.83231	182.0754
	0.021503	17581.63	54.76081	9.060258	0.690573	0.813478	57.89982	156.4816
	0.043007	33646.42	109.5216	17.33885	0.936384	0.868223	113.6773	152.5268
	0.06451	46539.61	164.2824	23.98303	0.800062	0.800062	174.5461	137.4023
ID=3.16 mm								
Section 2	v (m/s)	dP (Pa)	8v/D (s^{-1})	τ_w (Pa)	n'	n_{avg}'	γ_w (s^{-1})	μw (cP)
	0.000106	896.3184	0.268291	0.465038		0.206451	0.526103	883.929
	0.000212	1034.214	0.536582	0.536582	0.206451	0.335712	0.802021	669.0371
	0.000636	1723.689	1.609746	0.894303	0.464974	0.377761	2.272629	393.5105
	0.001061	1999.48	2.68291	1.037392	0.290549	0.508765	3.330526	311.4799
	0.002121	3309.483	5.365821	1.717063	0.726982	0.7229	5.880024	292.0163
	0.004243	5446.858	10.73164	2.825999	0.718818	0.744995	11.64998	242.5755
	0.006364	7446.338	16.09746	3.863391	0.771172	0.726511	17.6124	219.3563
	0.010607	10548.98	26.8291	5.473137	0.68185	0.703728	29.65289	184.5735
	0.021214	17443.74	53.65821	9.050351	0.725606	0.800297	57.00563	158.7624
	0.042427	31991.67	107.3164	16.59827	0.874987	0.853174	111.9335	148.2869
	0.063641	44815.92	160.9746	23.25189	0.831361	0.831361	169.1379	137.4729
ID=3.15 mm								
Section 3	v (m/s)	dP (Pa)	8v/D (s^{-1})	τ_w (Pa)	n'	n_{avg}'	γ_w (s^{-1})	μw (cP)
	0.000107	827.3709	0.271741	0.427441		0.415037	0.36749	1163.136
	0.000214	1103.161	0.543482	0.569922	0.415037	0.410633	0.738492	771.7368
	0.000642	1723.689	1.630446	0.890503	0.406228	0.314041	2.520791	353.2632
	0.00107	1930.532	2.71741	0.997363	0.221854	0.453176	3.53715	281.968
	0.00214	3102.641	5.434821	1.602905	0.684498	0.720286	5.962456	268.833

Table A7c continued.

	0.004279	**5240.016**	**10.86964**	**2.707128**	**0.756074**	**0.740879**	**11.82005**	**229.0285**
	0.006419	7032.652	16.30446	3.633251	0.725684	0.727193	17.83362	203.7304
	0.010698	10204.24	27.1741	5.271776	0.728702	0.703996	30.03053	175.5472
	0.021395	16340.57	54.34821	8.441966	0.67929	0.794104	57.87107	145.8754
	0.04279	30681.67	108.6964	15.85095	0.908918	0.863428	112.9947	140.2805
	0.064186	42747.5	163.0446	22.08447	0.817938	0.817938	172.1175	128.3104
ID=3.15 mm								
Section 4	v (m/s)	dP (Pa)	8v/D (s^{-1})	τ_w (Pa)	n'	n_{avg}'	γ_w (s^{-1})	μw (cP)
	0.000107	689.4757	0.272429	0.355901		0.678072	0.304765	1167.79
	0.000214	1103.161	0.544859	0.569441	0.678072	0.504201	0.678803	838.8904
	0.000643	1585.794	1.634576	0.818572	0.330331	0.285169	2.658918	307.8591
	0.001072	1792.637	2.724293	0.925342	0.240008	0.4995	3.406729	271.6219
	0.002143	3033.693	5.448585	1.565964	0.758992	0.734743	5.940349	263.6148
	0.004286	4964.225	10.89717	2.562486	0.710493	0.760342	11.75586	217.9752
	0.006429	6894.757	16.34576	3.559009	0.810191	0.775512	17.52866	203.0394
	0.010716	10066.35	27.24293	5.196153	0.740833	0.778316	29.18279	178.0554
	0.021431	17719.53	54.48585	9.146652	0.8158	0.844879	56.98677	160.5048
	0.042863	32474.31	108.9717	16.76293	0.873959	0.834195	114.3865	146.5464
	0.064294	44815.92	163.4576	23.13356	0.794432	0.794432	174.0317	132.9273
ID=3.14 mm								
Total	v (m/s)	dP (Pa)	8v/D (s^{-1})	τ_w (Pa)	n'	n_{avg}'	γ_w (s^{-1})	μw (cP)
	0.000107	3378.431	0.273117	0.435612		0.429684	0.363743	1197.582
	0.000215	4550.54	0.546234	0.586743	0.429684	0.396244	0.754308	777.8562
	0.000644	7032.652	1.638702	0.906785	0.396244	0.268587	2.754325	329.2222
	0.001073	8066.866	2.731169	1.040136	0.268587	0.491592	3.437317	302.601
	0.002147	13237.93	5.462339	1.706889	0.714598	0.712128	6.014365	283.8021
	0.004293	21649.54	10.92468	2.791475	0.709658	0.725194	11.95963	233.4082
	0.00644	29233.77	16.38702	3.76938	0.740731	0.718327	17.99345	209.4862
	0.010734	41713.28	27.31169	5.378479	0.695922	0.711899	30.07491	178.8361
	0.021467	69085.47	54.62339	8.907828	0.727875	0.813244	57.75937	154.2231
	0.042935	128794.1	109.2468	16.60661	0.898612	0.854665	113.8911	145.8113
	0.064402	178919	163.8702	23.06967	0.810719	0.810719	173.435	133.0163

Table A7d: Pipe viscometer measured data for ID=7.04 mm

ID=7.036 mm								
Section 1	v (m/s)	dP (Pa)	8v/D (s^{-1})	τ_w (Pa)	n'	n_{avg}'	γ_w (s^{-1})	μw (cP)
	0.000214	758.4233	0.243713	0.218837		0.241008	0.43559	502.3912
	0.000429	896.3184	0.487426	0.258625	0.241008	0.532065	0.594595	434.9606
	0.000857	1585.794	0.974851	0.457568	0.823122	0.655305	1.103046	414.8219
	0.001286	2068.427	1.462277	0.596827	0.655305	0.767088	1.573275	379.3535
	0.002143	3240.536	2.437128	0.93503	0.878872	0.866837	2.530726	369.4709
	0.004287	5860.544	4.874257	1.691011	0.854802	0.787347	5.203376	324.9834
	0.008574	9652.66	9.748513	2.785195	0.719892	0.79978	10.35863	268.8767
	0.01286	13789.51	14.62277	3.97885	0.879669	0.884463	15.10031	263.4945
	0.021434	21718.49	24.37128	6.266688	0.889257	0.909434	24.97804	250.8879
	0.042868	41368.54	48.74257	11.93655	0.929611	0.929611	49.66525	240.34

References

Abdurahman, N.H., Y.M. Rosli, N.H. Azhari, B.A. Hayder, "Pipeline transportation of viscous crudes as concentrated oil-in-water emulsions," Journal of Petroleum Science and Engineering **90–91**, 139–144 (2012)

Acevedo, S., X. Gutierrez, H. Rivas, "Bitumen-in-Water Emulsions Stabilized with Natural Surfactants," Journal of Colloid and Interface Science **242**, 230–238 (2001)

Adkins, S., P.J. Liyanage, G.W.P. Pinnawala Arachchilage, T. Mudiyanselage, U. Weerasooriya, G.A. Pope, "A New Process for Manufacturing and Stabilizing High-Performance EOR Surfactants at Low Cost for High-Temperature, High-Salinity Oil Reservoirs,". Society of Petroleum Engineers (2010)

Ahmed, N.S., A.M. Nassar, N.N. Zaki, H.K. Gharieb, "Stability and Rheology of Heavy Crude Oil-in-Water Emulsion Stabilized by an Anionic- Nonionic Surfactant Mixture," Petroleum Science and Technology **17**, 553–576 (1999a)

Ahmed, N.S., A.M. Nassar, N.N. Zaki, H.K. Gharieb, "Formation of fluid heavy oil-in-water emulsions for pipeline transportation," Fuel **78**, 593–600 (1999b)

Argillier, J.-F., I. Henaut, patrick gateau, J.-P. Heraud, P. Glenat, "Heavy Oil Dilution,". Society of Petroleum Engineers (2005)

Asakura, S., F. Oosawa, "Interaction between particles suspended in solutions of macromolecules," J. Polym. Sci. **33**, 183–192 (1958)

Ashrafizadeh, S.N., M. Kamran, "Emulsification of heavy crude oil in water for pipeline transportation," Journal of Petroleum Science and Engineering, Fourth International Symposium on Hydrocarbons and Chemistry **71**, 205–211 (2010)

Baldauf, L.M., R.S. Schechter, W.H. Wade, A. Graciaa, "The relationship between surfactant phase behavior and the creaming and coalescence of macroemulsions," Journal of Colloid and Interface Science **85**, 187–197 (1982)

Balmforth, N.J., I.A. Frigaard, G. Ovarlez, "Yielding to Stress: Recent Developments in Viscoplastic Fluid Mechanics," Annual Review of Fluid Mechanics **46**, 121–146 (2014)

Batchelor, G.K., "The effect of Brownian motion on the bulk stress in a suspension of spherical particles," Journal of Fluid Mechanics **83**, 97–117 (1977)

Bécu, L., S. Manneville, A. Colin, "Yielding and Flow in Adhesive and Nonadhesive Concentrated Emulsions," Phys. Rev. Lett. **96**, 138302 (2006)

Berli, C.L.A., "Rheology and phase behavior of aggregating emulsions related to droplet-droplet interactions," Brazilian Journal of Chemical Engineering **24**, 203–210 (2007)

Bonilla, L.F., S.N. Shah, "Experimental Investigation on the Rheology of Foams,". Society of Petroleum Engineers (2000)

Bourrel, M., A. Graciaa, R.S. Schechter, W.H. Wade, "The relation of emulsion stability to phase behavior and interfacial tension of surfactant systems," Journal of Colloid and Interface Science **72**, 161–163 (1979)

Brouwers, H.J.H., "Packing fraction of particles with lognormal size distribution," Phys. Rev. E **89**, 052211 (2014)
Buckley, J.S., Mechanisms and consequences of wettability alteration by crude oils (Ph.D.). Heriot-Watt University (1996)
Buckley, J.S., K. Takamura, N.R. Morrow, "Influence of Electrical Surface Charges on the Wetting Properties of Crude Oils," SPE Reservoir Engineering **4**, 332–340 (1989)
Caenn, R., G.V. Chillingar, "Drilling fluids: State of the art," Journal of Petroleum Science and Engineering **14**, 221–230 (1996)
Chang, L.Y., "New correlation for predicting the best surfactant and co-solvent structures to evaluate for chemical EOR," (2014)
Cheng, D.C.-H., J.B. Davis, A. Scarrow, Flow of Generalised Bingham Fluids in Straight Pipelines. Warren Spring Laboratory (1968)
Chhabra, R.P., J.F. Richardson, Non-Newtonian Flow and Applied Rheology : Engineering Applications, 2nd ed. Elsevier Science, Burlington (2011)
Chirinos, M.L., A.S. Taylor, S.E. Taylor, "Preparaton of HIPR emulsions and transportation thereof,". US4934398 A (1990)
Chow, A.W., S.W. Sinton, J.H. Iwamiya, T.S. Stephens, "Shear-induced particle migration in Couette and parallel-plate viscometers: NMR imaging and stress measurements," Physics of Fluids (1994-present) **6**, 2561–2576 (1994)
Christopoulou, C., G. Petekidis, B. Erwin, M. Cloitre, D. Vlassopoulos, "Ageing and yield behaviour in model soft colloidal glasses," Philosophical Transactions of the Royal Society of London A: Mathematical, Physical and Engineering Sciences **367**, 5051–5071 (2009)
Colebrook, C.F., "Turbulent flow in pipes, with particular reference to the transition region between the smooth and rough pipe laws.," Journal of the Institution of Civil Engineers **11**, 133–156 (1939)
Collins, S.B., J.G. Knudsen, "Drop-size distributions produced by turbulen pipe flow of immiscible liquids," AIChE J. **16**, 1072–1080 (1970)
Coulaloglou, C.A., L.L. Tavlarides, "Drop size distributions and coalescence frequencies of liquid-liquid dispersions in flow vessels," AIChE J. **22**, 289–297 (1976)
Coussot, P., L. Tocquer, C. Lanos, G. Ovarlez, "Macroscopic vs. local rheology of yield stress fluids," Journal of Non-Newtonian Fluid Mechanics, Visco-plastic fluids: From theory to application **158**, 85–90 (2009)
Danov, K.D., D.N. Petsev, N.D. Denkov, R. Borwankar, "Pair interaction energy between deformable drops and bubbles," The Journal of Chemical Physics **99**, 7179–7189 (1993)
Datta, S.S., D.D. Gerrard, T.S. Rhodes, T.G. Mason, D.A. Weitz, "Rheology of attractive emulsions," Phys. Rev. E **84**, 041404 (2011)
de Souza Mendes, P.R., A.A. Alicke, R.L. Thompson, "Parallel-plate geometry correction for transient rheometric experiments," Applied Rheology **24**, 52721 (2014)

Dodge, D.W., A.B. Metzner, "Turbulent flow of non-newtonian systems," AIChE J. **5**, 189–204 (1959)
dos Santos, R.G., A.C. Bannwart, M.I. Briceño, W. Loh, "Physico-chemical properties of heavy crude oil-in-water emulsions stabilized by mixtures of ionic and non-ionic ethoxylated nonylphenol surfactants and medium chain alcohols," Chemical Engineering Research and Design **89**, 957–967 (2011)
dos Santos, R.G., A.C. Bannwart, W. Loh, "Phase segregation, shear thinning and rheological behavior of crude oil-in-water emulsions," Chemical Engineering Research and Design **92**, 1629–1636 (2014)
dos Santos, R.G., A.C. Bannwart, W. Loh, "Phase segregation, shear thinning and rheological behavior of crude oil-in-water emulsions," Chemical Engineering Research and Design n.d.
Einstein, A., "A new determination of molecular dimensions," Ann. Phys **19**, 289–306 (1906)
Evdokimov, I.N., A.P. Losev, "Effects of molecular de-aggregation on refractive indices of petroleum-based fluids," Fuel **86**, 2439–2445 (2007)
Fall, A., J. Paredes, D. Bonn, "Yielding and Shear Banding in Soft Glassy Materials," Phys. Rev. Lett. **105**, 225502 (2010)
Farr, R.S., R.D. Groot, "Close packing density of polydisperse hard spheres," The Journal of Chemical Physics **131**, 244104 (2009)
Farshad, F., T.C. Pesacret, S.R. Bikki, R.H. Davis, "Surface Roughness in Internally Coated Pipes (OCTG),". Offshore Technology Conference (1999)
Fernández-Toledano, J.C., J. Rodríguez-López, K. Shahrivar, R. Hidalgo-Álvarez, L. Elvira, F.M. de Espinosa, J. de Vicente, "Two-step yielding in magnetorheology," Journal of Rheology (1978-present) **58**, 1507–1534 (2014)
Flaaten, A., Q.P. Nguyen, G.A. Pope, J. Zhang, "A Systematic Laboratory Approach to Low-Cost, High-Performance Chemical Flooding," SPE Reservoir Evaluation & Engineering **12**, 713–723 (2009)
Fomitchev-Zamilov, M., Novel upgrading technology cuts diluent use, capital costs [WWW Document] (2015)
Fortenberry, R.P., D.H. Kim, N. Nizamidin, S. Adkins, G.W.P. Pinnawala Arachchilage, H.S. Koh, U.P. Weerasooriya, G.A. Pope, "Use of Co-Solvents to Improve Alkaline-Polymer Flooding," Society of Petroleum Engineers (2013)
Foudazi, R., I. Masalova, A.Y. Malkin, "The rheology of binary mixtures of highly concentrated emulsions: Effect of droplet size ratio," Journal of Rheology **56**, 1299 (2012)
Foudazi, R., I. Masalova, A.Y. Malkin, "Flow behaviour of highly concentrated emulsions of supersaturated aqueous solution in oil," Rheol Acta **50**, 897–907 (2011)
Frank, M., D. Anderson, E.R. Weeks, J.F. Morris, "Particle migration in pressure-driven flow of a Brownian suspension," Journal of Fluid Mechanics **493**, 363–378 (2003)

Furnas, C.C., The relations between specific volume, voids, and size composition in systems of broken solids of mixed sizes. US Department of Commerce, Bureau of Mines (1928)
Gadala-Maria, F., A. Acrivos, "Shear-Induced Structure in a Concentrated Suspension of Solid Spheres," Journal of Rheology (1978-present) **24**, 799–814 (1980)
Garcia, E.J., J.F. Steffe, "COMPARISON of FRICTION FACTOR EQUATIONS FOR NON-NEWTONIAN FLUIDS IN PIPE FLOW1," Journal of Food Process Engineering **9**, 93–120 (1986)
Gillies, R.G., C.A. Shook, "Emulsions For Short Distance Transportation Of Heavy Crude Oil: Pipeloop Test Results," Journal of Canadian Petroleum Technology **31** (1992)
Grace, H.P., "Dispersion Phenomena in High Viscosity Immiscible Fluid Systems and Application of Static Mixers as Dispersion Devices in Such Systems," Chemical Engineering Communications **14**, 225–277 (1982)
Grenard, V., T. Divoux, N. Taberlet, S. Manneville, "Timescales in creep and yielding of attractive gels," Soft Matter **10**, 1555 (2014)
Guevara, E., G. Ninez, J. Gonzalez, "[8]4 Highly Viscous Oil Transportation Methods in the Venezuelan Oil Industry," 15th World Petroleum Congress (1997)
Gust, G., "Observations on turbulent-drag reduction in a dilute suspension of clay in sea-water," Journal of Fluid Mechanics **75**, 29–47 (1976)
Gutierrez, X., F. Silva, A. Morles, D. Pazos, H. Rivas, "The Use of Amines in the Stabilization of Acidic Hydrocarbons in Water Emulsions," Petroleum Science and Technology **21**, 1219–1240 (2003)
Hamaker, H.C., "The London—van der Waals attraction between spherical particles," Physica **4**, 1058–1072 (1937)
Hampton, R.E., A.A. Mammoli, A.L. Graham, N. Tetlow, S.A. Altobelli, "Migration of particles undergoing pressure-driven flow in a circular conduit," Journal of Rheology (1978-present) **41**, 621–640 (1997)
Hanks, R.W., "Low Reynolds number turbulent pipeline flow of pseudohomogeneous slurries,", in: Proceedings of the 5 Th International Conference on Hydraulic Transport of Solids in Pipes. pp. 8–11 (1978)
Hasan, S.W., M.T. Ghannam, N. Esmail, "Heavy crude oil viscosity reduction and rheology for pipeline transportation," Fuel **89**, 1095–1100 (2010)
Havre, T.E., J. Sjöblom, J.E. Vindstad, "Oil/Water-Partitioning and Interfacial Behavior of Naphthenic Acids," Journal of Dispersion Science and Technology **24**, 789–801 (2003)
Healy, T.W., L.R. White, "Ionizable surface group models of aqueous interfaces," Advances in Colloid and Interface Science **9**, 303–345 (1978)
Heymann, L., S. Peukert, N. Aksel, "Investigation of the solid–liquid transition of highly concentrated suspensions in oscillatory amplitude sweeps," Journal of Rheology (1978-present) **46**, 93–112 (2002a)
Heymann, L., S. Peukert, N. Aksel, "On the solid-liquid transition of concentrated suspensions in transient shear flow," Rheol Acta **41**, 307–315 (2002b)

Heywood, N.I., "Pipeline design for non-Newtonian fluids,", in: Inst. Chem. Eng. Symposium Series No (1980)
Höhler, R., S. Cohen-Addad, "Rheology of liquid foam," J. Phys.: Condens. Matter **17**, R1041 (2005)
Hollingsworth, K.G., M.L. Johns, "Droplet migration in emulsion systems measured using MR methods," Journal of Colloid and Interface Science **296**, 700–709 (2006)
Hookham, P.A., Concentration and velocity measurements in suspensions flowing through a rectangular channel (phd). California Institute of Technology (1986)
Hopkins, A.B., F.H. Stillinger, S. Torquato, "Disordered strictly jammed binary sphere packings attain an anomalously large range of densities," Phys. Rev. E **88**, 022205 (2013)
Hoshyargar, V., S.N. Ashrafizadeh, "Optimization of Flow Parameters of Heavy Crude Oil-in-Water Emulsions through Pipelines," Ind. Eng. Chem. Res. **52**, 1600–1611 (2013)
Hsu, T.-J., P.A. Traykovski, G.C. Kineke, "On modeling boundary layer and gravity-driven fluid mud transport," J. Geophys. Res. **112**, C04011 (2007)
Hudson, S.D., "Wall migration and shear-induced diffusion of fluid droplets in emulsions," Physics of Fluids (1994-present) **15**, 1106–1113 (2003)
Hyun, K., S.H. Kim, K.H. Ahn, S.J. Lee, "Large amplitude oscillatory shear as a way to classify the complex fluids," Journal of Non-Newtonian Fluid Mechanics **107**, 51–65 (2002)
Hyun, K., J.G. Nam, M. Wilhellm, K.H. Ahn, S.J. Lee, "Large amplitude oscillatory shear behavior of PEO-PPO-PEO triblock copolymer solutions," Rheol Acta **45**, 239–249 (2005)
Hyun, K., M. Wilhelm, C.O. Klein, K.S. Cho, J.G. Nam, K.H. Ahn, S.J. Lee, R.H. Ewoldt, G.H. McKinley, "A review of nonlinear oscillatory shear tests: Analysis and application of large amplitude oscillatory shear (LAOS)," Progress in Polymer Science **36**, 1697–1753 (2011)
Israelachvili, J.N., "Chapter 13 - Van der Waals Forces between Particles and Surfaces,", in: Intermolecular and Surface Forces (Third Edition). Academic Press, San Diego, pp. 253–289 (2011)
Jansen, K.M.B., W.G.M. Agterof, J. Mellema, "Droplet breakup in concentrated emulsions," Journal of Rheology **45**, 227–236 (2001)
Kelessidis, V.C., R. Maglione, C. Tsamantaki, Y. Aspirtakis, "Optimal determination of rheological parameters for Herschel–Bulkley drilling fluids and impact on pressure drop, velocity profiles and penetration rates during drilling," Journal of Petroleum Science and Engineering **53**, 203–224 (2006)
King, M.R., D.T. Leighton, "Measurement of shear-induced dispersion in a dilute emulsion," Physics of Fluids (1994-present) **13**, 397–406 (2001)
Klavers, K., L. Atkins, "Global Heavy Crude Oil Outlook to 2030,". Presented at the 20th World Petroleum Congress, World Petroleum Congress (2011)

Koh, C.J., P. Hookham, L.G. Leal, "An experimental investigation of concentrated suspension flows in a rectangular channel," Journal of Fluid Mechanics **266**, 1–32 (1994)
Koumakis, N., G. Petekidis, "Two step yielding in attractive colloids: transition from gels to attractive glasses," Soft Matter **7**, 2456 (2011)
Kralchevsky, P.A., N.D. Denkov, "Analytical expression for the oscillatory structural surface force," Chemical Physics Letters **240**, 385–392 (1995)
Krieger, I.M., "Rheology of monodisperse latices," Advances in Colloid and Interface Science **3**, 111–136 (1972)
Krieger, I.M., T.J. Dougherty, "A Mechanism for Non-Newtonian Flow in Suspensions of Rigid Spheres," Transactions of The Society of Rheology (1957-1977) **3**, 137–152 (1959)
Krishnan, G.P., S. Beimfohr, D.T. Leighton, "Shear-induced radial segregation in bidisperse suspensions," Journal of Fluid Mechanics **321**, 371–393 (1996)
Laherrere, J., "Estimates of oil reserves,". EMF/IEA/IEW Meeting, IIASA Laxenburg, Austria (2001)
Lake, L.W., R.T. Johns, W.R. Rossen, G.A. Pope, Fundamentals of enhanced oil recovery. Society of Petroleum Engineers (2014)
Laurati, M., S.U. Egelhaaf, G. Petekidis, "Nonlinear rheology of colloidal gels with intermediate volume fraction," Journal of Rheology (1978-present) **55**, 673–706 (2011)
Layrisse, I., M. Rivero, I. Paterno, E. Guevara, S. Marin, J. Gonzalez, "Transportation of viscous crude oil-in-water emulsion through pipes,", in: Proceedings of the Third International Conference on Heavy Crude and Tar Sands (1985)
Lee, P.F.W., G.G. Duffy, "Relationships between velocity profiles and drag reduction in turbulent fiber suspension flow," AIChE J. **22**, 750–753 (1976)
Le Hir, P., Y. Monbet, F. Orvain, "Sediment erodability in sediment transport modelling: Can we account for biota effects?," Continental Shelf Research, Natural Coastal Mechanisms - Flume and Field Experiments on Links between Biology, Sediments and Flow **27**, 1116–1142 (2007)
Leighton, D., A. Acrivos, "The shear-induced migration of particles in concentrated suspensions," Journal of Fluid Mechanics **181**, 415–439 (1987)
Levitt, D.B., "The optimal use of enhanced oil recovery polymers under hostile conditions," (2012)
Levitt, D., A. Jackson, C. Heinson, L.N. Britton, T. Malik, V. Dwarakanath, G.A. Pope, "Identification and Evaluation of High-Performance EOR Surfactants," SPE Reservoir Evaluation & Engineering **12**, 243–253 (2009)
Lindley, D., "The Diluent Market, A Midstream Operator's Perspective," Well's Fargo Fundamental Forum (2013)
Lu, J., P.J. Liyanage, S. Solairaj, S. Adkins, G.P. Arachchilage, D.H. Kim, C. Britton, U. Weerasooriya, G.A. Pope, "New surfactant developments for chemical enhanced oil recovery," Journal of Petroleum Science and Engineering **120**, 94–101 (2014)

Madlener, K., B. Frey, H.K. Ciezki, "Generalized reynolds number for non-newtonian fluids,". EDP Sciences, pp. 237–250 (2009)
Malkin, A.Y., I. Masalova, P. Slatter, K. Wilson, "Effect of droplet size on the rheological properties of highly-concentrated w/o emulsions," Rheol Acta **43**, 584–591 (2004)
Maron, S.H., P.E. Pierce, "Application of ree-eyring generalized flow theory to suspensions of spherical particles," Journal of Colloid Science **11**, 80–95 (1956)
Martínez-Palou, R., M. de L. Mosqueira, B. Zapata-Rendón, E. Mar-Juárez, C. Bernal-Huicochea, J. de la Cruz Clavel-López, J. Aburto, "Transportation of heavy and extra-heavy crude oil by pipeline: A review," Journal of Petroleum Science and Engineering **75**, 274–282 (2011)
Masalova, I., R. Foudazi, A.Y. Malkin, "The rheology of highly concentrated emulsions stabilized with different surfactants," Colloids and Surfaces A: Physicochemical and Engineering Aspects **375**, 76–86 (2011)
Masalova, I., M. Taylor, E. Kharatiyan, A.Y. Malkin, "Rheopexy in highly concentrated emulsions," Journal of Rheology (1978-present) **49**, 839–849 (2005)
Mason, T.G., J. Bibette, D.A. Weitz, "Elasticity of Compressed Emulsions," Phys. Rev. Lett. **75**, 2051–2054 (1995)
Mason, T.G., M.-D. Lacasse, G.S. Grest, D. Levine, J. Bibette, D.A. Weitz, "Osmotic pressure and viscoelastic shear moduli of concentrated emulsions," Phys. Rev. E **56**, 3150–3166 (1997)
McDonnell, M.R., Liquid Applied Internal Flow Coatings for Oil Transmission Lines [WWW Document] 11th Pipeline Technology Conference (2011)
McGeary, R.K., "Mechanical Packing of Spherical Particles," Journal of the American Ceramic Society **44**, 513–522 (1961)
Meeker, S.P., R.T. Bonnecaze, M. Cloitre, "Slip and flow in pastes of soft particles: Direct observation and rheology," Journal of Rheology **48**, 1295–1320 (2004)
Mehrotra, A.K., R.R. Eastick, W.Y. Svrcek, "Viscosity of cold lake bitumen and its fractions," Can. J. Chem. Eng. **67**, 1004–1009 (1989)
Merhi, D., E. Lemaire, G. Bossis, F. Moukalled, "Particle migration in a concentrated suspension flowing between rotating parallel plates: Investigation of diffusion flux coefficients," Journal of Rheology (1978-present) **49**, 1429–1448 (2005)
Mewis, J., N.J. Wagner, "Current trends in suspension rheology," Journal of Non-Newtonian Fluid Mechanics, Whither Rheology? **157**, 147–150 (2009)
Meyer, R.F., E.D. Attanasi, "Heavy oil and natural bitumen-strategic petroleum resources," World **434**, 650–7 (2003)
Miadonye, A., N. Latour, V.R. Puttagunta, "A Correlation for Viscosity and Solvent Mass Fraction of Bitumen-Diluent Mixtures," Petroleum Science and Technology **18**, 1–14 (2000)
Mie, G., "Beiträge zur Optik trüber Medien, speziell kolloidaler Metallösungen," Ann. Phys. **330**, 377–445 (1908)
Møller, P.C.F., S. Rodts, M.A.J. Michels, D. Bonn, "Shear banding and yield stress in soft glassy materials," Phys. Rev. E **77**, 041507 (2008)

Moody, L.F., "Friction factors for pipe flow," Trans. Asme **66**, 671–684 (1944)
Mooney, M., "The viscosity of a concentrated suspension of spherical particles," Journal of Colloid Science **6**, 162–170 (1951)
Mooney, M., "Explicit Formulas for Slip and Fluidity," Journal of Rheology (1929-1932) **2**, 210–222 (1931)
Munson, B.R., D.F. Young, T.H. Okiishi, "Fundamentals of fluid mechanics," New York **3**, 4 (1990)
Murata, H., "Rheology - Theory and Application to Biomaterials,", in: De Souza Gomes, A. (Ed.), Polymerization. InTech (2012)
National Energy Board, "Opportunities and Challenges to 2015: An Update," (2006)
Nelson, R.C., J.B. Lawson, D.R. Thigpen, G.L. Stegemeier, "Cosurfactant-Enhanced Alkaline Flooding,". Society of Petroleum Engineers (1984)
Norman, J.T., H.V. Nayak, R.T. Bonnecaze, "Migration of buoyant particles in low-Reynolds-number pressure-driven flows," Journal of Fluid Mechanics **523**, 1–35 (2005)
Nott, P.R., J.F. Brady, "Pressure-driven flow of suspensions: simulation and theory," Journal of Fluid Mechanics **275**, 157–199 (1994)
Núñez, G.A., M. Briceño, C. Mata, H. Rivas, D.D. Joseph, "Flow characteristics of concentrated emulsions of very viscous oil in water," Journal of Rheology **40**, 405–423 (1996)
Nuñez, G.A.N., C.E. Mata, C. Blanco, M.S. Chirinos, G.A. Sánchez, T.R. Colmenares, H.J. Rivas, F.A. Silva, "Manufacture of stable bimodal emulsions using dynamic mixing,". US6903138 B2 (2005)
Nuñez, G.A., G. Sanchez, X. Gutierrez, F. Silva, C. Dalas, H. Rivas, "Rheological Behavior of Concentrated Bitumen in Water Emulsions," Langmuir **16**, 6497–6502 (2000)
Omer, A., R. Pal, "Effects of Surfactant and Water Concentrations on Pipeline Flow of Emulsions," Ind. Eng. Chem. Res. **52**, 9099–9105 (2013)
Otsubo, P.Y., R.K. Prud'homme, "Effect of drop size distribution on the flow behavior of oil-in-water emulsions," Rheola Acta **33**, 303–306 (1994)
Pal, R., "Mechanism of Turbulent Drag Reduction in Emulsions and Bubbly Suspensions," Ind. Eng. Chem. Res. **46**, 618–622 (2007)
Pal, R., "Rheology of high internal phase ratio emulsions," Food Hydrocolloids **20**, 997–1005 (2006)
Pal, R., "Viscous behavior of concentrated emulsions of two immiscible Newtonian fluids with interfacial tension," Journal of Colloid and Interface Science **263**, 296–305 (2003)
Pal, R., "Novel viscosity equations for emulsions of two immiscible liquids," Journal of Rheology **45**, 509–520 (2001)
Pal, R., "Viscosity–Concentration Equation for Emulsions of Nearly Spherical Droplets," Journal of Colloid and Interface Science **231**, 168–175 (2000a)
Pal, R., "Shear Viscosity Behavior of Emulsions of Two Immiscible Liquids," Journal of Colloid and Interface Science **225**, 359–366 (2000b)

Pal, R., "Effect of droplet size on the rheology of emulsions," AIChE J. **42**, 3181–3190 (1996)
Pauchard, V., J. Sjöblom, S. Kokal, P. Bouriat, C. Dicharry, H. Müller, A. Al-Hajji, "Role of Naphthenic Acids in Emulsion Tightness for a Low-Total-Acid-Number (TAN)/High-Asphaltenes Oil†," Energy & Fuels **23**, 1269–1279 (2008)
Perez, M., N. Zambrano, M. Ramirez, E. Tyrode, J.-L. Salager, "Surfactant-Oil-Water Systems Near the Affinity Inversion. XII: Emulsion Drop Size Versus Formulation and Composition," Journal of Dispersion Science & Technology **23**, 55 (2002)
Pham, K.N., G. Petekidis, D. Vlassopoulos, S.U. Egelhaaf, W.C.K. Poon, P.N. Pusey, "Yielding behavior of repulsion- and attraction-dominated colloidal glasses," Journal of Rheology (1978-present) **52**, 649–676 (2008)
Pham, K.N., G. Petekidis, D. Vlassopoulos, S.U. Egelhaaf, P.N. Pusey, W.C.K. Poon, "Yielding of colloidal glasses," Europhysics Letters (EPL) **75**, 624–630 (2006)
Phan-Thien, N., D.C. Pham, "Differential multiphase models for polydispersed suspensions and particulate solids," Journal of Non-Newtonian Fluid Mechanics **72**, 305–318 (1997)
Phillips, R.J., R.C. Armstrong, R.A. Brown, A.L. Graham, J.R. Abbott, "A constitutive equation for concentrated suspensions that accounts for shear-induced particle migration," Physics of Fluids A: Fluid Dynamics (1989-1993) **4**, 30–40 (1992)
Princen, H.M., "Rheology of foams and highly concentrated emulsions. II. experimental study of the yield stress and wall effects for concentrated oil-in-water emulsions," Journal of Colloid and Interface Science **105**, 150–171 (1985)
Princen, H.M., "Rheology of foams and highly concentrated emulsions: I. Elastic properties and yield stress of a cylindrical model system," Journal of Colloid and Interface Science **91**, 160–175 (1983)
Princen, H.M., A.D. Kiss, "Rheology of foams and highly concentrated emulsions: IV. An experimental study of the shear viscosity and yield stress of concentrated emulsions," Journal of Colloid and Interface Science 176–187 (1989)
Princen, H.M., A.D. Kiss, "Rheology of foams and highly concentrated emulsions: III. Static shear modulus," Journal of Colloid and Interface Science **112**, 427–437 (1986)
Rabinowitsch, B., "Über die viskosität und elastizität von solen," Z. Phys. Chem. A **145**, 1–26 (1929)
Ragouilliaux, A., G. Ovarlez, N. Shahidzadeh-Bonn, B. Herzhaft, T. Palermo, P. Coussot, "Transition from a simple yield-stress fluid to a thixotropic material," Phys. Rev. E **76**, 051408 (2007)
Rihan, R., R. Shawabkeh, N. Al-Bakr, "The Effect of Two Amine-Based Corrosion Inhibitors in Improving the Corrosion Resistance of Carbon Steel in Sea Water," J. of Materi Eng and Perform **23**, 693–699 (2014)
Rodríguez-Valverde, M.A., M.A. Cabrerizo-Vílchez, A. Páez-Dueñas, R. Hidalgo-Álvarez, "Stability of highly charged particles: bitumen-in-water dispersions," Colloids and Surfaces A: Physicochemical and Engineering Aspects, A collection

of papers presented at the International Symposium on Electrokinetic Phenomena, Cracow, Poland, August 18-22, 2003 **222**, 233–251 (2003)
Romero, N., A. Cárdenas, M. Henríquez, H. Rivas, "Viscoelastic properties and stability of highly concentrated bitumen in water emulsions," Colloids and Surfaces A: Physicochemical and Engineering Aspects **204**, 271–284 (2002)
Romero, N., A. Cárdenas, H. Rivas, "Creep compliance-time behavior and stability of bitumen in water emulsions," Journal of Rheology **44**, 1247–1262 (2000)
Rosen, M.J., J.T. Kunjappu, Surfactants and interfacial phenomena. John Wiley & Sons (2012)
Sahni, V., R.M. Dean, C. Britton, D.H. Kim, U. Weerasooriya, G.A. Pope, "The Role of Co-Solvents and Co-Surfactants in Making Chemical Floods Robust," Society of Petroleum Engineers (2010)
Salager, J.-L., M.I. Briceno, C.L. Bracho, "Heavy hydrocarbon emulsions. Making use of the state of the art in formulation engineering," Encyclopedic Handbook of Emulsion Technology **20**, 455–495 (2001)
Salager, J.-L., M. Perez-Sanchez, Y. Garcia, "Physicochemical parameters influencing the emulsion drop size," Colloid Polym Sci **274**, 81–84 (1996)
Salou, M., B. Siffert, A. Jada, "Study of the stability of bitumen emulsions by application of DLVO theory," Colloids and Surfaces A: Physicochemical and Engineering Aspects **142**, 9–16 (1998)
Sanchez, L.E., J.L. Zakin, "Transport of Viscous Crudes as Concentrated Oil-in-Water Emulsions," Ind. Eng. Chem. Res. **33**, 3256–3261 (1994)
Saniere, A., I. Hénaut, J.F. Argillier, "Pipeline Transportation of Heavy Oils, a Strategic, Economic and Technological Challenge," Oil & Gas Science and Technology **59**, 455–466 (2004)
Segovia-Gutiérrez, J.P., C.L.A. Berli, J. de Vicente, "Nonlinear viscoelasticity and two-step yielding in magnetorheology: A colloidal gel approach to understand the effect of particle concentration," Journal of Rheology (1978-present) **56**, 1429–1448 (2012)
Selby, A.J., "A method for assessing friction losses for a non-newtonian fluid, such as sewage sludge, under laminar flow conditions," THE PUBLIC HEALTH ENGINEER, VOL. 4, NO. 2, P 44-48, MARCH, 1976. 13 FIG, 2 REF. (1976)
Sentjabrskaja, T., E. Babaliari, J. Hendricks, M. Laurati, G. Petekidis, S.U. Egelhaaf, "Yielding of binary colloidal glasses," Soft Matter **9**, 4524 (2013)
Seth, J.R., M. Cloitre, R.T. Bonnecaze, "Influence of short-range forces on wall-slip in microgel pastes," Journal of Rheology (1978-present) **52**, 1241–1268 (2008)
Seth, J.R., M. Cloitre, R.T. Bonnecaze, "Elastic properties of soft particle pastes," Journal of Rheology (1978-present) **50**, 353–376 (2006)
Seth, J.R., C. Locatelli-Champagne, F. Monti, R.T. Bonnecaze, M. Cloitre, "How do soft particle glasses yield and flow near solid surfaces?," Soft Matter **8**, 140 (2012)
Seth, J.R., L. Mohan, C. Locatelli-Champagne, M. Cloitre, R.T. Bonnecaze, "A micromechanical model to predict the flow of soft particle glasses," Nat Mater **10**, 838–843 (2011)

Shao, Z., A.S. Negi, C.O. Osuji, "Role of interparticle attraction in the yielding response of microgel suspensions," Soft Matter **9**, 5492–5500 (2013)
Shewan, H.M., J.R. Stokes, "Analytically predicting the viscosity of hard sphere suspensions from the particle size distribution," Journal of Non-Newtonian Fluid Mechanics, Rheometry (and General Rheology): Festschrift dedicated to Professor K Walters FRS on the occasion of his 80th birthday **222**, 72–81 (2015)
Shukla, A., S. Arnipally, M. Dagaonkar, Y.M. Joshi, "Two-step yielding in surfactant suspension pastes," Rheol Acta **54**, 353–364 (2015)
Simpson, J.L., "Pipeline transportation of wax-laden crude oil as water suspension,". Presented at the 6th World Petroleum Congress, World Petroleum Congress (1963)
SNF Floerger, Polyacrylamide Emulsions Handbook [WWW Document] SNF Floerger (2014)
Sollich, P., F. Lequeux, P. Hébraud, M. Cates, "Rheology of Soft Glassy Materials," Phys. Rev. Lett. **78**, 2020–2023 (1997)
Spangenberg, J., G.W. Scherer, A.B. Hopkins, S. Torquato, "Viscosity of bimodal suspensions with hard spherical particles," Journal of Applied Physics **116**, 184902 (2014)
Speight, J.G., High Acid Crudes. Gulf Professional Publishing (2014)
Stainsby, R., R.A. Chilton, S.C. Thompson, "Prediction of the headlosses in non-Newtonian sludge pipelines using CFD,", in: Proc. 2nd CFDS Int. User Conf. pp. 259–272 (1994)
Stokes, J.R., W.J. Frith, "Rheology of gelling and yielding soft matter systems," Soft Matter **4**, 1133 (2008)
Sumner, R.J., K.B. Hill, C.A. Shook, "Pipeline Flow of Heavy Crude Oil Emulsions," Journal of Canadian Petroleum Technology **37** (1998)
Tadros, T., "Application of rheology for assessment and prediction of the long-term physical stability of emulsions," Advances in Colloid and Interface Science, Emulsions, From Fundamentals to Practical Applications **108–109**, 227–258 (2004)
Taghavifar, M., "Enhanced heavy oil recovery by hybrid thermal-chemical processes," (2014)
Takamura, K., R.S. Chow, "The electric properties of the bitumen/water interface Part II. Application of the ionizable surface-group model," Colloids and Surfaces **15**, 35–48 (1985)
Taylor, G.I., "The viscosity of a fluid containing small drops of another fluid," Proceedings of the Royal Society of London. Series A, Containing Papers of a Mathematical and Physical Character 41–48 (1932)
Taylor, S.D., J. Czarnecki, J. Masliyah, "Refractive index measurements of diluted bitumen solutions," Fuel **80**, 2013–2018 (2001)
Tolosa, L.-I., A. Forgiarini, P. Moreno, J.-L. Salager, "Combined Effects of Formulation and Stirring on Emulsion Drop Size in the Vicinity of Three-Phase Behavior of Surfactant−Oil Water Systems," Ind. Eng. Chem. Res. **45**, 3810–3814 (2006)

Verzaro, F., M. Bourrel, O. Garnier, H.G. Zhou, J.-F. Argillier, "Heavy Acidic Oil Transportation By Emulsion In Water," Soceity of Petroleum Engineers (2002)
Virk, P.S., "Drag reduction fundamentals," AIChE J. **21**, 625–656 (1975)
Wasan, D.T., A.D. Nikolov, F. Aimetti, "Texture and stability of emulsions and suspensions: role of oscillatory structural forces," Advances in Colloid and Interface Science, Emulsions, From Fundamentals to Practical Applications **108–109**, 187–195 (2004)
Wu, X., J. Czarnecki, N. Hamza, J. Masliyah, "Interaction Forces between Bitumen Droplets in Water," Langmuir **15**, 5244–5250 (1999)
Wylde, J.J., D. Leinweber, G. Botthof, A.P. Oliveira, C. Royle, C. Kayser, "Heavy oil transportation: Advances in water-continuous emulsion methods," World Heavy Oil Congress **WHOC12-333** (2012)
Wyslouzil, B.E., M.A. Kessick, J.H. Masliyah, "Pipeline flow behaviour of heavy crude oil emulsions," The Canadian Journal of Chemical Engineering **65**, 353–360 (1987)
Yarranton, H.W., J.C. Okafor, D.P. Ortiz, F.G.A. van den Berg, "Density and Refractive Index of Petroleum, Cuts, and Mixtures," Energy Fuels **29**, 5723–5736 (2015)
Yoshimura, A., R.K. Prud'homme, "Wall Slip Corrections for Couette and Parallel Disk Viscometers," Journal of Rheology (1978-present) **32**, 53–67 (1988)
Zaki, N., T. Butz, D. Kessel, "Rheology, Particle Size Distribution, and Asphaltene Deposition of Viscous Asphaltic Crude Oil-in-Water Emulsions for Pipeline Transportation," Petroleum Science and Technology **19**, 425–435 (2001)
Zakin, J.L., B. Lu, H.-W. Bewersdorff, "Surfactant Drag Reduction," Reviews in Chemical Engineering **14**, 253–320 (2011)
Zakin, J.L., J. Myska, Z. Chara, "New limiting drag reduction and velocity profile asymptotes for nonpolymeric additives systems," AIChE J. **42**, 3544–3546 (1996)
Zakin, J.L., Y. Qi, Y. Zhang, "Recent Experimental Results on Surfactant Drag Reduction," 729–734 (2003)
Zaki, N.N., "Surfactant stabilized crude oil-in-water emulsions for pipeline transportation of viscous crude oils," Colloids and Surfaces A: Physicochemical and Engineering Aspects **125**, 19–25 (1997)
Zhou, Z., J.V. Hollingsworth, S. Hong, H. Cheng, C.C. Han, "Yielding Behavior in Colloidal Glasses: Comparison between "Hard Cage" and "Soft Cage,"" Langmuir **30**, 5739–5746 (2014)
Zong, Y., G. Yuan, C. Zhao, C.C. Han, "Differentiating bonding and caging in a charged colloid system through rheological measurements," The Journal of Chemical Physics **138**, 184902 (2013)